



# The role of the neuroepithelial-glia niche in *Drosophila* larval neurogenesis: a transcriptomic analysis

*Doctoral Thesis presented by*  
**Pol Ramon-Cañellas**

**- 2019 -**

*Thesis Director*

Javier Morante Oria, PhD

*Doctoral Program in Neuroscience*







# The role of the neuroepithelial-glial niche in *Drosophila* larval neurogenesis: a transcriptomic analysis

*Doctoral Thesis presented by*

**Pol Ramon-Cañellas**

**- 2019 -**

*Thesis Director:*

**Javier Morante Oria, PhD**

*Doctoral Program in Neuroscience*

*Neuroscience Institute – UMH-CSIC*





Sant Joan d'Alacant, 7<sup>th</sup> January 2019

To whom it may concern,

The doctoral thesis introduced hereafter under the title “The role of the neuroepithelial-glia niche in *Drosophila* larval neurogenesis: a transcriptomic analysis” has been developed by myself, Pol Ramon Cañellas. This thesis is in a conventional compendium format of experimental studies undertaken at the Neuroscience Institute of Alicante during the doctoral course in neuroscience of the Miguel Hernández University.

Yours sincerely,

Pol Ramon Cañellas



Sant Joan d'Alacant, 7<sup>th</sup> January 2019

To whom it may concern,

The doctoral thesis introduced hereafter under the title “The role of the neuroepithelial-glia niche in *Drosophila* larval neurogenesis: a transcriptomic analysis” has been developed by myself, Pol Ramon Cañellas. This thesis includes the following publication, of which I am the first author, and I declare that the publication has not been used and will not be used in any other thesis in agreement with my thesis director Javier Morante:

Ramon-Cañellas, P., Peterson, H.P., and Morante, J. (2019). “ From Early to Late Neurogenesis: Neural Progenitors and the Glial Niche from a Fly’s Point of View ”. *Neuroscience* 399, 39–52. Forefront Review. DOI: 10.1016/j.neuroscience.2018.12.014.

Yours sincerely,

Pol Ramon Cañellas

Dr. Javier Morante Oria





Sant Joan d'Alacant, 7 de enero de 2019

D. Javier Morante Oria, Científico titular del Consejo Superior de Investigaciones Científicas (CSIC),

AUTORIZO la presentación de la Tesis Doctoral titulada “The role of the neuroepithelial-glial niche in *Drosophila* larval neurogenesis: a transcriptomic analysis” y realizada por D. Pol Ramon Cañellas, bajo mi inmediata dirección y supervisión como director y tutor de su Tesis Doctoral en el Instituto de Neurociencias (CSIC-UMH) y que presenta para la obtención del grado de Doctor por la Universidad Miguel Hernández.

Y para que conste, a los efectos oportunos, firmo el presente certificado.

Dr. Javier Morante Oria



Sant Joan d'Alacant, 7 de diciembre de 2019

D. Miguel Valdeolmillos López, Catedrático y Director del programa de doctorado en Neurociencias del Instituto de Neurociencias de Alicante, centro mixto de la Universidad Miguel Hernández (UMH) y de la Agencia Estatal Consejo Superior de Investigaciones Científicas (CSIC),

CERTIFICO:

Que la Tesis Doctoral titulada “The role of the neuroepithelial-glia niche in *Drosophila* larval neurogenesis: a transcriptomic analysis” ha sido realizada por D. Pol Ramon Cañellas, bajo la dirección de D. Javier Morante Oria como director, y doy su conformidad para que sea presentada a la comisión de Doctorado de la Universidad Miguel Hernández.

Y para que conste, a los efectos oportunos, firma el presente certificado.

Dr. Miguel Valdeolmillos López





*Als meus pares, esposa i família tota*



# **ACKNOWLEDGEMENTS / AGRAÏMENTS**

---







**M**oltes són les persones a les que he d'estar agraït i que durant aquest llarg procés d'una manera o altre, m'han ajudat a seguir endavant. A totes elles, i ja em disculpo anticipadament per si me'n descuidés alguna, mil gràcies.

No voldria començar aquest apartat sense mostrar la meva infinita gratitud a les dues persones que avalen i saben de primera mà l'esforç que ha requerit arribar fins aquí. Primerament, a la persona que m'ha anat dia a dia animant durant els més ja de 30 anys de la meva vida, la meva mare. És gràcies a la seva perseverança i sacrificis què ara mateix em trobo en aquest punt d'inflexió personal i professional tant important i, reconeixent que no és tant freqüent en mi com m'agradaria fer visible, li estic eternament agraït. I un afegit a aquesta última frase, no tinc paraules suficients per agrair a l'Ale, la meva dona, aquella persona que ha viscut (i sofert) tot aquest llarg procés de tesis, la capacitat d'alçar-me en els moments complicats recorrent a les seves infinites virtuts innates, i relativitzant i posant en primer lloc les coses importants de la vida. A ambdues, gràcies.

Es de agradecido también seguir con quien me dio la oportunidad de embarcarme profesionalmente en el ámbito de la investigación científica, el Dr. Javier Morante. Partiendo de un proyecto ambicioso para resolver dudas del funcionamiento de nuestro órgano más fascinante, el cerebro, he aprendido a desarrollar de manera autónoma una línea científica a partir de una idea, agudizando mi capacidad de proyectar soluciones de una manera que, de seguro, me va a resultar de gran valor en un futuro profesional, a la vez que personal. Gracias Javier.

Al unísono, mi más sincero agradecimiento a la Dra. María Domínguez. Ella es la que, aparte de aportarme su amplia experiencia profesional y empujes científicos, la que me facilitó la logística acogiéndome en su laboratorio como otro de sus doctorandos y pasando de ser mi laboratorio de acogida a convertirse, simplemente, en mi laboratorio.

Eso me lleva a acordarme de mis compañeros de trabajo, amigos al inicio y confesores al final. Así puedo nombrar al Dr. Tobias Reiff como aquel que lo ejemplifica. Como persona voluntariosa que es (y alemán!), estuvo dispuesto a compartir no solo detalles de rutina en un laboratorio de investigación básica, sino también de vitalidad en otros muchos ámbitos esenciales para compaginar la vida personal con el trabajo. A él le dejé mi más sentido de admiración y todo se puede resumir con un Danke schön! Continuando con los miembros de más experiencia profesional, otro que tengo que agradecerle su incesante buena disposición a dar de una manera gratuita alegría, buenrollismo y simpatía con un simple "...y jamás volveré a hacerlo", es argentino, carnívoro confeso y defensor de la pequeña política (pero que muy pequeña). El Dr. Nahuel Villegas es sin duda aquél que se queda con mi parte divertida. También desde el otro lado del charco la Dra. colombiana Diana Vallejo me ha aportado el buen hacer y la exquisitez experimental, así como una parte comprensiva a la vez que resolutiva. Ella se queda con mi tranquilidad. I finalment, i no per això menor, és la comprensió que m'ha aportat la compatriota Dra. Dolors Ferrés en els moments més convulsos d'un període inquietant que ens ha tocat viure lluny de la nostra terra. Afegint-hi, a més, el seu profund coneixement en l'àmbit *Drosophila*

que m'ha sabut transmetre d'una manera clara y profunda i és per això que ella és l'experiència en majúscules.

Siguiendo en el labo, pero ya entrando en el terreno de estudiantes de doctorado pioneros y según mi perspectiva temporal, nos encontramos a doctores eméritos tales como la Dra. Verónica Miguela. Ella me enseñó los pequeños detalles para empezar a rodar con las moscas así como recordándome esa parte friki que en algún momento pasó a formar parte de mi más profundo ser. Yo le devuelvo esa admiración por lo japonés y esa cultura "cómica". El Dr. Zeus Antonello fue ese ser italiano mitológico que al principio lo puse en el saco de leyendas urbanas ya que pasaban los meses y por allí no aparecía nadie con ese nombre, mientras me decían que con la tesis debajo el brazo estaba surcando los mares a lo Sandokán...y tal que así fue! Una vez a puerto y bajado del Olimpo, me demostró su parte guerrera e inconformista, a la que se la devuelvo muy agradecido. En versión culinaria, el primer plato fuerte es al recordarme de la Dra. Irene Gutiérrez...tanto que decir! Sin tiempo a mencionarlo todo, en ella vi una evolución metamorfofísica en la que al final, salió una *Drosófila* lista para volar continentes (o subida a una bicicleta) con sus conocimientos fundamentados en la experiencia trabajada y las buenas artes (marciales). Siempre querré seguir, y agradecerle, su manera metódica de hacer una buena ciencia fundamentada, por encima de todo, en ser una buena compañera. El segundo plato principal, y aunque a él no le gustaría serlo, no puede ser otro que el ya Dr. Sergio Juárez. Tal vez sea el hecho de empezar casi a la par por el que se haya convertido en un amigo del que te sientes a gusto andando a su lado y de los que te alegras por sus éxitos. Siempre pisando fuerte científicamente, su determinación en hacer ciencia me ha llevado a ser un espectador de lujo de cómo desarrollarse dentro de este mundo sea en congresos, "retreats" o en el mero día a día. Y sin embargo el éxito no será lo que le otorgo (porque no lo necesita), sino mi amistad más sincera.

Y con los que temporalmente siguen mis pasos en la carrea predoctoral llega el postre. Y ese se lo comerá Lucía García, no literalmente (que por su saque bien podría), sino por la parte dulce que está implícita. Ella ha sido como aquella hermana menor que la ves crecer y pasar por cada fase de la vida, en este caso científica, y que estas atento a que todo le pueda ir bien. Y además todo eso con mucha alegría vigorosa (aunque otras veces tocaba tristeza...) que han animado esas tardes que ya no decían nada. Sin duda, a ella le daría todo lo mejor, porque bien se lo merece. Otro que tiene estilo, en este caso de café italiano, es Roberto Santoro. Aquellas muecas que te siguen el rollo y no saber bien si es que te ha entendido o no capito...me hacían sonreír también. Por eso, a él le doy mi sonrisa para que nunca la pierda (aunque probablemente termine haciéndolo, por eso también le he dejado otra de repuesto). Finalmente, a la última incorporación al "labo team" Juan Carranza, con un movimiento más del sureño y con flow, que le viene bien para saber moverse por el laboratorio. Y a él le dejaría mi legado en formato de experiencia, para que su futuro sea más presente.

Otras partes muy importantes de mi transcurso en el instituto los he podido compartir con compañeros y confidentes. En todo laboratorio hay un principio, y ese tiene el nombre de Noelia García, que entre nosotros dos nos lo hacíamos todo más fácil, mucho más fácil. A ella le delego

la bondad. Y también hay una fase final, o una historia más reciente, en la que Hannah Payette Peterson se me unió como escudera para tomar aire entre experimentos (in)finitos. Sin duda su aportación en mi parte final de la tesis es impagable, y por eso se merece mi *social network* y, porque no, mi sufrido sentido del humor. *Thanks for nothing a lot!* Asimismo, en esta línea quiero acordarme de Mari Consuelo M-M, la más veterana y voluntariosa técnico que no le da miedo enfrentarse a nuevos retos de la vida moderna. Ella es, por definición, la sabiduría que no se la dejo, sino que se la pido. Esther Ballesta, es un nombre propio que brilla por su profesionalidad, a la vez que humanidad. Y no busca la excelencia, sino que la encuentra sin buscarla, fruto pues de un trabajo muy bien hecho. Gracias por guiarme en lo molecular y dejarme tu destreza, la que ahora te devuelvo. También agradezco a Laura Mira, Irene Oliveira y Alicia Sánchez, el equipo de las moscas y que sin ellas, no hay ciencia en *Drosophila*, literalmente. Además, la primera aportando su incesante perspectiva de lo positivo, la segunda su carácter afable para quien lo quiera recibir (y alguna que otra receta deliciosa) y la tercera su buenas palabras. A vosotras, os dejo vuestra buena predisposición en su gran medida con la que me a habéis ayudado. Otras son las que en un mayor o menor tiempo, han pasado por la rutina del laboratorio y a las que me gustaría recordar y darles un gracias: Virginie Roure, Flora Stephano, Cristhian Faustor, Aitana Romero, Lourdes Díaz y Ernesto Saez. Finalmente, también se merece muchas palabras de agradecimiento Rosa Sánchez, nuestra secretaria y aliviadora de peso burocrático. De las muchas veces que me ha ayudado se ve que es pieza fundamental para el buen funcionamiento del engranaje científico. Muchas gracias por todo el tiempo compartido, a ti mi más sentido reconocimiento.

Así mismo, muchos han sido los Investigadores Principales (a.k.a. PI) del instituto que en algún momento de necesidad han respondido de manera positiva a mis cuestiones algunas meramente de rutina de laboratorio, otras más profundas y que me han permitido avanzar en momentos de estancamiento procesal. Especialmente a los de la Unidad de Neurobiología del Desarrollo, y más específicamente a los de la Unidad de *Drosophila*, Dr. Luís García-Alonso, Dr. Francisco Tejedor y Dra. Ana Carmena, estos tres sumamente importantes como expertos del ámbito. Es aquí donde también tengo que agradecer a sus respectivos laboratorios por crear un ambiente de cooperación (y comprensión), en especial a los *Drosophileros* que, por lo que nos acarrea, muchos momentos de respiro y fraternidad nos hemos dado. Que quede dicho pues, a Rafael Susín, Kat Gers-Barlag, Ana María de Torres, Sandra Manzanero, y en especial a Maribel Franco, muy agradecido!

Es de justicia agradecer el buen trabajo de todo el personal del instituto, desde administración hasta conserjería, pasando por los servicios de cultivos, imagen, taller, ilustración, lavado y limpieza; así como buen funcionamiento del instituto en gran medida gracias a la profesionalidad de Maite García. Además de sus dos directores que durante mi estancia he visto ponerse al frente con buena determinación, Dr. Juan Lerma y Dr. Salvador Martínez. Es en este punto donde quiero hacer una mención especial al técnico que probablemente me ha sufrido durante un mayor tiempo, Antonio Caler, y a la vez ayudado por igual. Miles y miles de horas entre ensayos/errores para mejorar mis resultados llevan a su equivalente acercamiento al lado más

humano del trabajo. Mitad técnico y mitad buena persona, le debo agradecer su especial interés en que las cosas me salieran como lo deseado. Así pues, esa mera capacidad de escuchar siempre con una carcajada, aunque la cosa no fuera para tal, de muy buen grado le brindo la satisfacción de mi trabajo bien hecho. In this line, I will never forget my stay in Germany. My time at GeneCore was a quality leap in my research work and an acquisition of new knowledge for me too. I have much to thank for that stage the boss, Dr. Vladimir Benes, that his ability to manage the work group from its most human and integrating side, made me feel part of a laboratory with a human factor also very high. To all of them, Jelena Pistolic, Dinko Pavlinic, Rajna Hercog, Bianka Baying, Nayara de Azevedo, Ferris Jung, Anja Telzerow, Jürgen Zimmermann, and Tomi Baehr-Ivacevic on the “wet lab”, and Jonathan Landry, Jan Provaznik, and Tobias Rausch on the *in silico* lab, as well as the EMBL administrative staff, thank you very much!

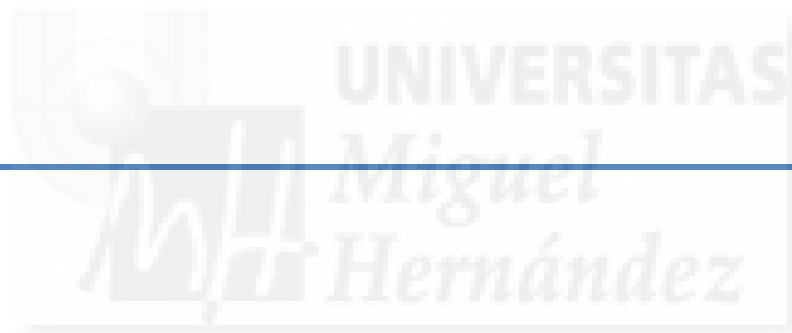
También una parte muy importante durante estos años de tesis doctoral, aunque de manera más indirecta, es el rol que ha fraguado la familia y los amigos. Todos ellos, me han ayudado en ir seccionando esta etapa y complementarla con vivencias personales y vitales, que son de tanto valor para mí. Ahora que este trayecto llega a su final, intentaré de alguna manera optimizar el tiempo para devolvérselo en forma de agradecimiento.

Para concluir, sólo me queda por mencionar que en todo proceso de vivencia y aprendizaje, y más intensamente como es el de una tesis doctoral, se produce un desprendimiento personal de cualidades junto con el de nueva adquisición, que son fruto de la convivencia humana. Al final uno da, otros reciben, pero como el “Boomerang” (canción de Els Manel), para que lo dado esté siempre de vuelta se necesita la pericia de un profesional. En resumidas, lo bueno que se pege, mientras que lo malo...uno tiene que ser capaz de desecharlo. Así pues, decirles a todas esas personas que me han ayudado en esta bonita etapa de mi vida en ser mejor en cualquier aspecto...G-R-A-C-I-A-S!!

A tots vosaltres, eternament agraït.

*“(...). I en acabat, que cadascú es vesteixi  
com bonament li plagui, i via fora!,  
que tot està per fer i tot és possible.”*

Poema *Ara mateix* de **Miquel Martí i Pol**.



## **INDEX**



<b>ACRONYMS AND ABBREVIATIONS .....</b>	<b>I</b>
<b>ABSTRACT / RESUMEN.....</b>	<b>V</b>
<b>INTRODUCTION.....</b>	<b>1</b>
1. Neurogenesis across species.....	3
2. <i>Drosophila melanogaster</i> for studying brain development.....	4
2.1. The fly in science.....	4
2.2. Design approach using cutting-edge techniques in <i>Drosophila</i> .....	4
2.2.1. <i>The Gal4/UAS system</i> .....	4
2.2.2. <i>Cell sorting by fluorescent flow cytometry</i> .....	6
2.2.3. <i>Transcriptome sequencing for gene expression analysis</i> .....	7
2.3. Life cycle of <i>Drosophila melanogaster</i> .....	8
2.4. The larval central nervous system .....	10
2.5. Neuronal progenitors in larva fruit fly .....	10
3. Organ growth control .....	14
3.1. Intrinsic factors of the temporal patterning.....	14
3.2. Extrinsic factors in cell niches .....	14
4. Glia as progenitor niche interactor .....	15
4.1. Different types of glia in the larval central nervous system.....	15
4.2. Glial niche.....	17
5. Deficiencies in neuronal development results in brain injuries.....	17
5.1. Intrinsic defects provokes severe brain injuries .....	17
5.2. Dysregulated cells have a direct impact in precursors niches and cause the development of brain disorders.....	18
5.3. Relevance of optic lobe surface-associated cortex glia in the stem cell niche ...	18
<b>OBJECTIVES / OBJETIVOS .....</b>	<b>21</b>
<b>MATERIALS AND METHODS.....</b>	<b>27</b>
1. Fly genetics .....	29
1.1. <i>Drosophila</i> husbandry .....	29
1.2. Establishment of recombinant lines .....	29
1.3. Supplementary fly methodologies.....	30
1.3.1. <i>LexA/LexAop system</i> .....	30
1.3.2. <i>FLP-Out clonal analysis</i> .....	30
1.3.3. <i>Coupled MARCM analysis</i> .....	30

1.4. Image acquisition .....	30
2. Immunohistochemistry and image analysis .....	31
2.1. Immunohistochemistry procedure .....	31
2.2. Microscopy image capture and processing .....	31
3. Flow cytometry .....	32
3.1. Tissue dissociation into individual cell.....	32
3.2. Fluorescence-activated cell sorting.....	32
4. Cell culture.....	32
4.1. Cell culture procedure .....	32
4.2. Staining of cultured cells .....	32
4.3. Microscopy image capture and processing.....	32
5. RNA extraction, retrotranscription and quantitative PCR.....	33
5.1. RNA extraction .....	33
5.2. Total mRNA quantification and quality determination .....	33
5.3. Retrotranscription and quantitative PCR.....	33
6. RNA sequencing.....	34
6.1. cDNA library preparation.....	34
6.2. cDNA quantification and library quality .....	34
6.3. RNA sequencing and data quality control.....	35
7. Bioinformatics analyses .....	35
8. Gene validation.....	35
9. Climbing assay .....	36
10. Larval age determination .....	36
10.1. Measurement of developmental timing .....	36
10.2. Larva size measurements .....	36
10.3. Jaws assay.....	36
11. Feeding assay .....	36
<b>RESULTS.....</b>	<b>37</b>
1. Glial niche characterisation in a <i>Drosophila</i> larval brain .....	39
1.1. Assess <i>c855a</i> -Gal4 as larval brain driver for neuroepithelial cells .....	39
1.2. Identification of <i>cg25c</i> -Gal4 driver in optic lobe-specific surface-associated cortex glia .....	42
2. Fluorescent cell sorting of optic lobe niche populations for transcriptomics .....	48



3. Niche transcriptome sequencing and bioinformatics analysis of gene expression .....	52
3.1. Massively-parallel cDNA sequencing and quality control .....	52
3.2. Sequences indexing and mapping .....	55
3.3. Differential gene expression between samples .....	57
3.3.1. <i>Data exploration and representation</i> .....	57
3.3.2. <i>Differential expression analysis 1: Cell type approach</i> .....	59
3.3.3. <i>Differential expression analysis 2: Stage approach</i> .....	62
4. Identification of glial and neuroepithelial extrinsic cues from candidate genes.....	69
4.1. Genetic <i>in vivo</i> validation of top-hit genes .....	69
4.2. Genes involved in unusual phenotypes at pupal and adult stages .....	71
4.3. Genes involved in unusual phenotypes at larval stages .....	75
5. Characterization of octopamine receptors and their implication in brain growth.....	84
5.1. The impact of the octopamine receptor in mushroom bodies (Oamb) in development.....	85
5.2. The impact of the octopamine $\beta$ 1receptor (Oct $\beta$ 1R) in development .....	89
5.3. The impact of the octopamine $\beta$ 3 receptor (Oct $\beta$ 3R) in development .....	92
5.4. Signalling pathway underlying octopamine modulation in the brain .....	96
<b>DISCUSSION</b> .....	<b>99</b>
1. Characterization of the neuroepithelial-glial niche and its separation by FACS technique .....	101
2. Niche transcriptome sequencing and bioinformatics analysis of gene expression .....	102
3. Validation of top-hit genes .....	103
4. The octopamine receptors in the cells of the niche.....	108
<b>CONCLUSIONS / CONCLUSIONES</b> .....	<b>115</b>
<b>APPENDIX I / <i>Supplementary figures</i></b> .....	<b>125</b>
<b>APPENDIX II / <i>Supplementary tables</i></b> .....	<b>147</b>
<b>BIBLIOGRAPHY</b> .....	<b>159</b>





**ACRONYMS AND ABBREVIATIONS**

---



## Symbols

4-TU	4-thiouracil
5-HT	5-hidroxitriptamina or serotonin
5-HT2B	5-hydroxytryptamine receptor 2B
7-AAD	7-aminoactinomycin D
$\beta$ -Gal	$\beta$ -galactosidase
$\beta$ -ME	$\beta$ -mercaptoethanol
$\mu$ g	microgram
$\mu$ m	micrometre

## A

AEL	after egg laying
ALG	astrocyte-like glia
aos	argos

## B

bark	bark beetle
baz	bazooka
BBB	blood-brain-barrier
Burs	bursicon

## C

Cam	calmodulin
CaMKII	calcium/calmodulin-dependent protein kinase II
Cas3	caspase 3
CB	central brain
CG	cortex glia
cg25c	cytogenic location polytene chromosome band 25C
CNS	central neural system
CPC	common progenitor cell
crb	crumbs

## D

Damb	dopamine receptor in mushroom bodies
DDC	DOPA decarboxylase
DE-Cad	<i>Drosophila</i> E-cadherin
Dh44-R1	diuretic hormone 44 receptor 1
dILPs	<i>Drosophila</i> insulin-like peptides
DIP	dpr-interacting protein
Dlg-1	disc large-1
dpr	defective proboscis extension response

## E

ed	echinoid
EG	ensheathing glia
eg	epithelial glia
EGFR	epidermal growth factor receptor
Elav	embryonic lethal abnormal vision

## F

FACS	fluorescent-activated cell sorting
Fas	fasciclin
FB	fat body
flp	flippase
FSC	forward scatter
fz	frizzled

## G

GC	guanine-cytosine
GEF	rho guanine nucleotide exchange factor
GFP	green fluorescent protein
GMC	ganglion mother cell
GO	gene ontology
GOF	gain-of-function
GPC	glia precursor cell
GPCR	G protein-coupled receptors

## H

HA	hemagglutinin
HTS	high throughput-sequencing

## I

IL	instar larval
ine	inebriated
INP	intermediate neural precursor
InR	insulin-like receptor
IPC	inner proliferation centre

## J

JH	juvenile hormone
----	------------------

## L

L2 and L3	second and third instar larval stage
Lawf PC	lamina wide-field precursor cell
LexAop	lexA operator sequence
LF	lamina furrow
Lgr	leucine-rich repeat-containing G protein-coupled receptor
LOF	lack-of-function
LPC	lamina precursor cell

## M

MAPK	mitogen-activated protein kinases
MARCM	mosaic analysis with a repressible cell marker
MB	mushroom body
meg	medulla glia
mew	multiple edematous wings
mg	marginal glia
mir	microRNA
mm	millimetres
Mmp2	matrix metalloproteinase 2
mng	marginal glia
MPC	migrating progenitor cell
MPS	massively-parallel sequencing
mtt	mangetout
mys	mysospheroid

## N

NA	noradrenaline
nAChR $\alpha$ 3	nicotinic acetylcholine receptor $\alpha$ 3
NB	neuroblast
NEC	neuroepithelial cell
NG	neuropil glia

**NGS** next generation sequencing  
**Nrx-IV** neurexin IV  
**NSC** neural stem cell

## O

**OA** octopamine  
**Oamb** octopamine receptor in mushroom bodies  
**Octβ1R** octopamine β1 receptor  
**Octβ3R** octopamine β3 receptor  
**OL** optic lobe  
**O/N** overnight  
**OPC** outer proliferation centre  
**otk** off-track

## P

**PBS** phosphate-buffered saline  
**Pburs** partner of bursicon  
**PCA** principal components analysis  
**PFA** paraformaldehyde  
**PG** perineural glia  
**PH3** phospho-histone 3  
**ppMAPK** phospho-p44/42 MAPK  
**prc** pericardin  
**ptc** patched  
**Ptp69D** protein tyrosine phosphatase 69D

## Q

**qPCR** quantitative polymerase chain reaction

## R

**repo** reversed polarity  
**RFP** red fluorescent protein  
**RG** ring gland  
**RNAi** RNA interference  
**RNA-seq** RNA sequencing

## S

**santa-maria** scavenger receptor acting in neural tissue and majority of rhodopsin is absent

**scRNA-seq** single-cell RNA sequencing  
**SEM** standard error of mean  
**SG** surface glia  
**sg** satellite glia  
**SIFaR** SIFamide receptor  
**SPG** subperineural glia  
**Spi** spitz  
**SSC** side scatter  
**stan** starry night

## T

**tβh** tyramine β hydroxylase  
**TA** tyramine  
**TAAR** trace amine-associated receptor

**Ten-a** tenascin accessory  
**TF** transcription factor  
**TGF-α** transforming growth factor α  
**Tig** tiggrrin  
**TOR** target of rapamycin

## U

**UAS** upstream activation sequence  
**UPRT** uracil phosphoribosyltransferase

## V

**vkg** viking  
**Vmat** vesicular monoamine transporter

**VNC** ventral nerve cord

## W

**wg** wingless  
**wls** wntless  
**wnt** wingless/integrated

## Y

**YFP** yellow fluorescent protein

UNIVERSITAS

**ABSTRACT / RESUMEN**

---







## **Abstract**

Adequate neuronal development is essential for communication between organs and, consequently, for the vital functions of animals. Neurogenesis is a process by which neurons are generated from stem cells (SCs) or other progenitor cells, and it is during the initial stages of development of an organism when this process is most active. SCs of the nervous system are derived from neuroepithelial cells (NECs), which are rapidly and symmetrically amplified during the early stages of embryonic development in order to increase the number of SCs. Regulation of proliferation and the transition from NECs to SCs is extremely important. Alterations in the control of this process can have serious consequences for the final size of the adult brain. These problems can lead to brain diseases such as hyper- and hypoplasia, microcephaly and tumour generation, among others, which can also lead to severe neurodegenerative diseases. Previous studies have shown that internal dysregulation of progenitor cells can be caused by factors from their environment, in other words, from a cellular niche. The environment created by other cells close to the progenitors can influence, via extrinsic factors, the intrinsic factors that promote the transition from NECs to SCs.

Studies done by our laboratory using *Drosophila melanogaster* as a model for brain development have described a glial niche that controls neurogenesis in larval stages. In this research, a type of glial cell defined by the expression of the microRNA *miR-8*, the homolog of *miR-200* in vertebrates, was identified and characterized, and it was determined that it control the neuroepithelium-stem cell transition by regulating the TGF- $\alpha$ /EGFR pathway. The similarity between the NEC-neuroblast transition (the fruit fly neuronal SC) and the NEC-radial glia transition (the mammalian neuronal SC) evidence a conservation in the cellular elements that control the neurogenesis. In addition, this aspect highlights that deregulation of gliogenesis, the generation of glial cells, may have side effects on the formation of neuronal cells and can cause the development of gliomas which are one of the most common and aggressive tumours related to glia in the central nervous system (CNS).

The aim of this doctoral thesis is to contribute to the knowledge of the mechanisms that regulate brain maturation and early neurogenesis through the aforementioned glial niche. However, at the beginning of this study, the laboratory identified a new marker for niche glial cells (*cg25c*<sup>+</sup>) that was more specific than the one used before (*miR-8*<sup>+</sup>). Consequently, the first part of my work focuses on characterizing this new marker, along with the marker for NECs (*c855a*<sup>+</sup>), using the Gal4/UAS expression system and fluorescence microscopy techniques. To address the main objective of this thesis, I used a multidisciplinary genetic approach that includes several state-of-the-art techniques. Firstly, I carried out the precise separation of the two brain cell populations using fluorescence-activated cell sorting (FACS). Then, I sequenced each population's transcriptome (RNA-seq) and analysed them bioinformatically during a stay in the laboratory of Dr. Vladimir Benes (EMBL-Heidelberg, Germany).

The 151 genes obtained from the bioinformatics screening are related to ligands and receptors (or other intercellular signalling molecules) and are potentially differentially expressed at different larval ages. The genes were validated *in vivo* using the binary Gal4/UAS system and transgenic fly lines for regulating the gain (UAS) and loss (RNAi) of function of these genes. From the validation, I found 51 genes that function both as ligands and receptors in different signalling pathways involved in, for example, tissue growth (*EGFR*, *Spitz*, *Argos*, *Echinoid*, and

*Crumbs*), synapses (*Neurexin-IV* and *Inebriated*), oncogenes (*Ret oncogene*), integrins (*Myospheroid* and *Tiggrin*), the Hedgehog pathway (*Patched*) or the Wnt pathway (*Wnt2*, *Wg*, *Pebble*, and *Off-track2*). In addition, I found other molecules involved in the neurotransmission of nerve impulses (*Inebriated*), serotonin (*5-HT2B*), acetylcholine (*nAChRalpha3*) and glutamate (*Mangetout*), among others. These 51 genes were identified as producing anomalies during development, including malformations of the CNS, when under- or overexpressed in the niche cells. The analysis of the genes whose altered expression produced the most interesting anomalies allowed me to identify a series of genes that are important for organism development. Individuals with altered expression of these genes undergo delay or arrest at a specific larval stage, which can cause differences between body and brain size and result in lethality.

There is a group of receptors among those genes that is associated with the signalling pathway of the octopamine (OA) neurohormone, which is equivalent to noradrenaline in mammals. The characterization of these receptors (*Oamb*, *Octβ1R* and *Octβ3R*) by histochemical techniques enabled me to define the impact they have on the cells of the niche, on their progeny (neurons and neural circuits) and on other tissues (imaginal discs, fatty tissue, ring gland, etc.), as well as the signalling pathways by which receptors cause a deregulation of the cell cycle that ultimately affects the whole organism's growth. The receptors of the OA pathway have been commonly studied in octopaminergic neural circuits, where the production of OA itself has also been described. Studies in epithelial cells from the oviduct of *Drosophila* have demonstrated the function of the OA receptors *Oamb* and *Octβ3R*, which control the secretion of activity effector molecules in other nearby cell types to establish an epithelial niche. Although a function of this type of receptors in insect glial cells has been hypothesized for years, few evidences are found on this subject. For instance, some studies in *Drosophila* show that astrocytes of the CNS have *Oct-TyrR* receptors and stimulate the activity of multiple sensory behaviours through internal regulation of  $Ca^{2+}$ . Thus, the findings obtained in this doctoral thesis can provide new conclusions about the role of the OA pathway in the glial niche that controls the brain growth and the development of the organism.

## Resumen

Un desarrollo neuronal adecuado es esencial para la comunicación entre órganos y, en consecuencia, para las funciones vitales de un ser vivo. La neurogénesis es un proceso mediante el cual las neuronas se generan a partir de células madre u otras progenitoras, y es durante las etapas iniciales de desarrollo de un organismo cuando este proceso es más activo. Las células madre del sistema nervioso derivan de células neuroepiteliales, las cuales se amplifican de forma rápida y simétrica durante los primeros estadios del desarrollo embrionario con el objetivo de aumentar el repertorio de dichas células madres. La regulación correcta de la proliferación y transición de célula neuroepitelial a célula madre es un proceso de extrema importancia en el que alteraciones en su control puede acarrear graves consecuencias en el tamaño final del cerebro adulto. Esos problemas pueden dar lugar a enfermedades cerebrales tales como hiperplasia e hipoplasia cerebral, microcefalia o generación de tumores, entre otras, que a la vez pueden derivar en enfermedades neurodegenerativas severas. Estudios anteriores han demostrado que la desregulación interna de las células progenitoras puede ser causada por factores procedentes de su entorno, es decir, de un nicho celular. El ambiente creado por otras células próximas a las progenitoras puede controlar, mediante factores extrínsecos, a factores intrínsecos que promueven la transición de célula neuroepitelial a célula madre.

Trabajos realizados en nuestro laboratorio utilizando *Drosophila melanogaster* como modelo de desarrollo cerebral han descrito un nicho glial que controla la neurogénesis en etapas larvianas. En esta investigación se identificó y caracterizó un tipo de célula glial definido por la expresión del microRNA *miR-8*, el homólogo de *miR-200* en vertebrados, y se determinó que controlaba la transición neuroepitelio-célula madre mediante la regulación de la vía de TGF- $\alpha$ /EGFR. La similitud entre la transición neuroepitelio-neuroblasto (célula madre del cerebro de la mosca de la fruta) y la transición neuroepitelio-glía radial (célula madre del cerebro de mamífero) evidencia una conservación en los elementos celulares que controlan la neurogénesis. Además, este hecho pone de relieve que una desregulación en la gliogénesis, la generación de células gliales, tenga efectos colaterales en la formación de células neuronales pudiendo desarrollar gliomas, es decir, tumores relacionados con la glía los cuales son uno de los tumores más comunes y agresivos del sistema nervioso central.

El objetivo de esta tesis doctoral es contribuir al conocimiento de los mecanismos que regulan la maduración cerebral y la neurogénesis temprana mediante el nicho glial mencionado anteriormente. No obstante, al inicio de este estudio el laboratorio identificó un nuevo marcador para las células gliales del nicho (*cg25c*<sup>+</sup>) que era más específico que el utilizado hasta el momento (*miR-8*<sup>+</sup>). En consecuencia, la primera parte de mi trabajo se ha centrado en la caracterización de éste nuevo marcador, junto con el de las células neuroepiteliales (*c855a*<sup>+</sup>), utilizando el sistema de expresión Gal4/UAS y técnicas de microscopia de fluorescencia. Para abordar el objetivo principal de la tesis he utilizado una aproximación genética multidisciplinar que incluye varias técnicas de vanguardia. Primeramente, separé las dos poblaciones celulares del cerebro de manera precisa mediante la técnica de separación celular por fluorescencia (FACS). Seguidamente, secuencié su transcriptoma (RNA-seq) y lo analicé bioinformáticamente durante una estancia en el laboratorio del Dr. Vladimir Benes (EMBL-Heidelberg, Alemania).

Los 151 genes obtenidos que están relacionados con ligandos y receptores (u otras moléculas de señalización intercelulares) y que potencialmente tienen una expresión diferencial en distintas edades larvales, han sido validados mediante un cribaje *in vivo* utilizando el sistema binario Gal4/UAS y líneas de moscas transgénicas para regular la ganancia (UAS) y falta (RNAi) de función de esos genes. Ahí encontré 51 genes que funcionan tanto de ligandos como receptores en diferentes vías de señalización y que están implicadas, por ejemplo, en crecimiento tisular (*EGFR*, *Spitz*, *Argos*, *Echinoid* y *Crumbs*), en las sinapsis (*Neurexin-IV* e *Inebriated*), como oncogenes (*Ret oncogene*), como integrinas (*Myospheroid* y *Tiggrin*), vía de Hedgehog (*Patched*) o vía de Wnt (*Wnt2*, *Wg*, *Pebble* y *Off-track2*); además de otras moléculas con actividad en la neurotransmisión de impulsos nerviosos (*Inebriated*), de serotonina (*5-HT2B*), de acetilcolina (*nAChRalpha3*) o de glutamato (*Mangetout*), entre otros. Estos 51 genes fueron identificados por producir anomalías durante la etapa de desarrollo incluidas malformaciones en el sistema nervioso central, debido a una expresión disfuncional en las células del nicho. El análisis de esos genes con anomalías más interesantes me ha llevado a identificar una serie de genes que producen una desregulación del desarrollo del organismo por el que experimenta un retraso o arresto en un estadio larval concreto produciendo diferencias entre el tamaño corporal y el del cerebro, que termina finalmente en letalidad.

Entre esos genes, se encuentran un grupo de receptores asociados con la vía de señalización de la neurohormona octopamina, un equivalente a la noradrenalina de los mamíferos. La caracterización de estos receptores (*Oamb*, *Octβ1R* y *Octβ3R*) mediante técnicas histoquímicas me ayudó a definir el impacto que tienen tanto en las células del nicho, en su progenie (neuronas y sus circuitos neuronales) o en otros tejidos (discos imaginales, tejido graso, glándula anular, etc.), así como las vías de señalización por las que causan una desregulación del ciclo celular que deriva a una afectación sistémica del crecimiento del organismo. Los receptores de la vía de octopamina han sido comúnmente estudiados en circuitos neuronales octopaminérgicos donde también está descrito que ocurre la producción de esa neurohormona. Estudios en el oviducto de *Drosophila* han evidenciado la función de receptores de octopamina, tales como *Oamb* y *Octβ3R*, en células epiteliales que controlan la secreción de moléculas efectoras de actividad en otras células próximas, formando un nicho epitelial. Aunque desde hace años se ha hipotetizado una función de este tipo de receptores en las células gliales de los insectos, pocas evidencias se encuentran sobre este tema. Algunas investigaciones en *Drosophila* demuestran que, por ejemplo, los astrocitos del sistema nervioso central tienen receptores *Oct-TyrR* que, a través de una regulación interna del  $Ca^{2+}$ , estimula la actividad de múltiples comportamientos sensoriales. De esta forma, los hallazgos obtenidos en esta tesis doctoral pueden aportar nuevas conclusiones sobre la función de la vía de la octopamina en el nicho glial que controla el crecimiento del tejido cerebral y el desarrollo del organismo.



---

## **INTRODUCTION**



# 1. Neurogenesis across species

The suitable development of an organism's brain, from flies to mammals, is essential for proper communication between organs and the vital functions they execute (Droujinine and Perrimon, 2016). Furthermore, the fact that neural circuits conserve their functions between species shows their importance. A relevant example of an evolutionarily conserved function is the role that the brain has in regulating body size and obesity-linked behaviours (Beshel et al., 2017; Vallejo et al., 2015).

The human brain has been seen as unique due to its considerable size and complexity, and humans' cognitive ability has long been thought to result from the brain's large cerebral cortex. However, measurements of brains across species have revealed that larger brain size does not translate to greater numbers of neurons; indeed, human brains are differentiated by their efficient, space-saving layout which allows them to have a high proportion of neurons for their size (Herculano-Houzel, 2009). Studies of the developing brain and neurogenesis can provide important insights into the efficiency of brain formation.

In mammal's brain development, there are two main periods described during corticogenesis: first, a proliferative stage with symmetric cell division and later a neurogenic phase when asymmetric cell division takes place. This transition to neurogenesis is due to a temporal transcription identity during diverse developmental times independently of the cell-cycle (Delaunay et al., 2017; Okamoto et al., 2016) and it has been observed between different species of animals (Jacob et al., 2008; Rossi et al., 2017; Wang et al., 2013). An example of an evolutionarily conserved mode of cell division in neurogenesis is seen in the generation of neural stem cells (NSCs) before neuron birth. In the ventricular zone of the mammalian brain cortex, NSCs which are also known as radial glia, are produced from neuroepithelial cells (NECs; Borrell and Götz, 2014; Fietz et al., 2010). Similarly, in the optical brain region of *Drosophila melanogaster* (from now on referred to as *Drosophila*), NECs delaminate into neuroblasts (NBs, the NSCs in *Drosophila*) which asymmetrically divide to produce neurons or glia (Homem et al., 2015).

At present, the neurogenic similarities within species, as well as their particularities, have emerged from massive genome analysis to clarify the molecular processes that take place (Gerstein et al., 2014; Gulden and Šestan, 2014; van de Leemput et al., 2014; Llorens et al., 2011; Lui et al., 2014; Wang et al., 2013). Therefore, in this thesis I take advantage of transcriptomics to first overview the expression profile of the progenitor NECs, and another brain cell type, glia; and then explain their possible roles in a dysregulated microenvironment in the *Drosophila* central neural system (CNS).

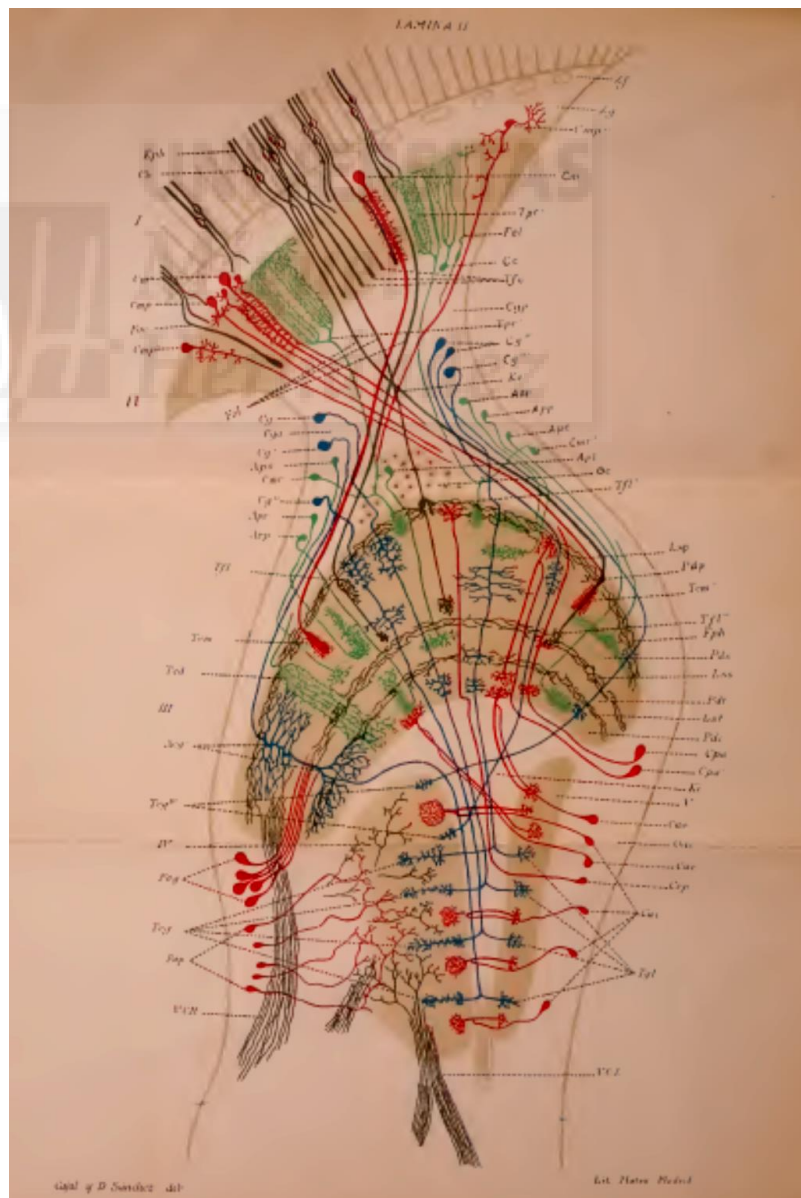


Figure 1. Schematic drawing of retina and optic centres of the bluebottle fly (*Calliphora vomitoria*). Lamina II of Cajal and Sánchez, 1915.

## **2. *Drosophila melanogaster* for studying brain development**

### **2.1. The fly in science**

Insects have been an important animal model in modern neuroscience for years (Koniszewski et al., 2016). At the beginning of the 20<sup>th</sup> century, flies were very useful for Santiago Ramon y Cajal in his histological studies of the CNS (Cajal, 1909). He benefitted from insects of the order Diptera such as the bluebottle fly (*Calliphora vomitoria*) and the pale giant horse fly (*Tabanus bovinus*) to depict brain cells' physical characteristics (Cajal and Sánchez, 1915; Figure 1). The use of *Drosophila* as a model organism in the research of several Nobel laureates in physiology and medicine reflects the impact that this invertebrate has on basic research. Their discoveries gave new insight into the role played by chromosomes in heredity (1933, Thomas H. Morgan), the production of mutations by means of X-ray irradiation (1946, Hermann J. Muller), the genetic control of early embryonic development (1995, Edward B. Lewis, Christiane Nüsslein-Volhard and Eric F. Wieschaus), odour receptors and the organisation of the olfactory system (2004, Richard Axel), the activation of innate immunity (2011, Jules A. Hoffmann), and molecular mechanisms controlling the circadian rhythm (2017, Jeffrey C. Hall, Michael Rosbash and Michael W. Young). This last award is especially significant because it shows the essential role that the fruit fly plays within brain research.

For more than a century, research in developmental biology and neuroscience employing *Drosophila* as a model organism has also added to scientists' knowledge of vertebrate biology due their evolutionary conserved similitudes (Bellen et al., 2010; Terriente and Pujades, 2015; Urbach, 2007). Fundamental principles of function and organisation of the nervous system are preserved between fruit flies and mammals due to the fact that about 60% of genes are shared between the two species. As a result, around 75% of known human diseases have equivalent genes in fruit flies (Reiter et al., 2001) and up 50% of fly proteins have homologs in mammals. For these reasons, flies are commonly used for research on human diseases such as cancer, neurodegeneration and microcephaly (Jaiswal et al., 2012; Pandey and Nichols, 2011; Villegas et al., 2018; Yamamoto et al., 2014).

### **2.2. Design approach using cutting-edge techniques in *Drosophila***

The fruit fly CNS has provided interesting insights via research carried out through cutting-edge systems of molecular and genetic manipulation. The many tools available for use in fruit flies are helpful for overcoming initial technical difficulties and for furthering biological knowledge. For instance, techniques adapted for use in flies, such as CRISPR/Cas9 (Gratz et al., 2013), have allowed scientists to better determine cells' profiles during the process of development (Du et al., 2017). Along this line, refined staining methodologies (Manning and Doe, 2017) also allow researchers to characterise whole circuits during different stages of development.

More knowledge of cells' properties leads to a better understanding of themselves when they are studied within a particular context, that is, a niche. For example, the glia-neuron interactions within a microenvironment are characterised using BAC (Bacterial Artificial Chromosome) transgenic flies (Banerjee et al., 2017). Other methods use cell-specific fluorescence to isolate populations and reveal niche interactions with deep analysis of their transcriptome (Berger et al., 2012). The process followed in this thesis is the fluorescence-activated cell sorting (FACS) followed by next generation sequencing (NGS) and ending with a genetic validation taking advantage of the Gal4/UAS system. The principles of all those techniques are explained below.

#### **2.2.1. The Gal4/UAS system**

Elementary work in *Drosophila* takes advantage of the broad *in vivo* methodologies available which are genetically sophisticated but also simple to use. Since the 1990s, the targeted gene expression Gal4/UAS system (Brand and Perrimon, 1993) has been employed by laboratories working with *Drosophila* due its accessible procedure and the multiple genetic adaptations that the technique admit. The mechanisms consist of an endogenous or exogenous specific gene, called a promoter, which encodes the yeast transcriptional activator Gal4. Later on, the Gal4 protein binds an upstream activation sequence (UAS) and then drives the expression of a target gene, called a reporter. When the promoter is tissue- or cell-specific, activation of the reporter allows for the visualisation of the precise pattern of expression of the promoter.



Use of the system in *Drosophila* (Figure 2) requires two different transgenic flies: one with the Gal4 gene under the control of a tissue-specific enhancer (Figure 2, in red) and a second with the target transgene under the control of a UAS sequence (Figure 2, in green). After crossing parental flies from each line with those of the other, the progeny will inherit both transgenes on each allele. That means that cells in which the driver gene is expressed will produce the Gal4 protein as well as the reporter gene of interest (Figure 2, in purple).

In order to characterise the driver's transgene location, researchers often use as the reporter gene any of a huge variety of fluorescent proteins available or LacZ sequence and other fused proteins which can be tagged with antibodies. In addition, the Gal4-UAS system is also used to investigate the consequences of the malfunctioning of a gene from specific cells. The gain or lack of function (GOF or LOF, respectively) is revealed when using reporter mutant flies or RNAi lines. To further refine the expression pattern of the target gene, the Gal80 can be introduced, which negatively regulates the Gal4 transgene expression. This protein has been also modified to be thermosensitive which means that can be temporally activated at 18 °C and inactivated at 29 °C (Gal80<sup>ts</sup>; Lee and Luo, 1999; Matsumoto et al., 1978; McGuire et al., 2003).

The continual advances in developing genetic tools for *Drosophila* (Awasaki and Lee, 2011; Venken et al., 2011) have brought related systems such as the FLP-out system (Ito et al., 1997; Struhl and Basler, 1993) and the GeneSwitch (Osterwalder et al., 2001). In addition, other complementary mechanisms can be used at the same time: the LexA/LexAop (Lai and Lee, 2006), the Q system (Potter et al., 2010) or the mosaic analysis with a repressible cell marker (MARCM) analysis (Lee and Luo, 1999) with all its variations (Lai and Lee, 2006; Pfeiffer et al., 2010; Potter et al., 2010; Yu et al., 2009). Currently, the tools mentioned here in combination with the large number of gene drivers generated for the brain (Jenett et al., 2012; Manseau et al., 1997) have extended the power of the Gal4/UAS system making it the most powerful tool for the fruit fly.

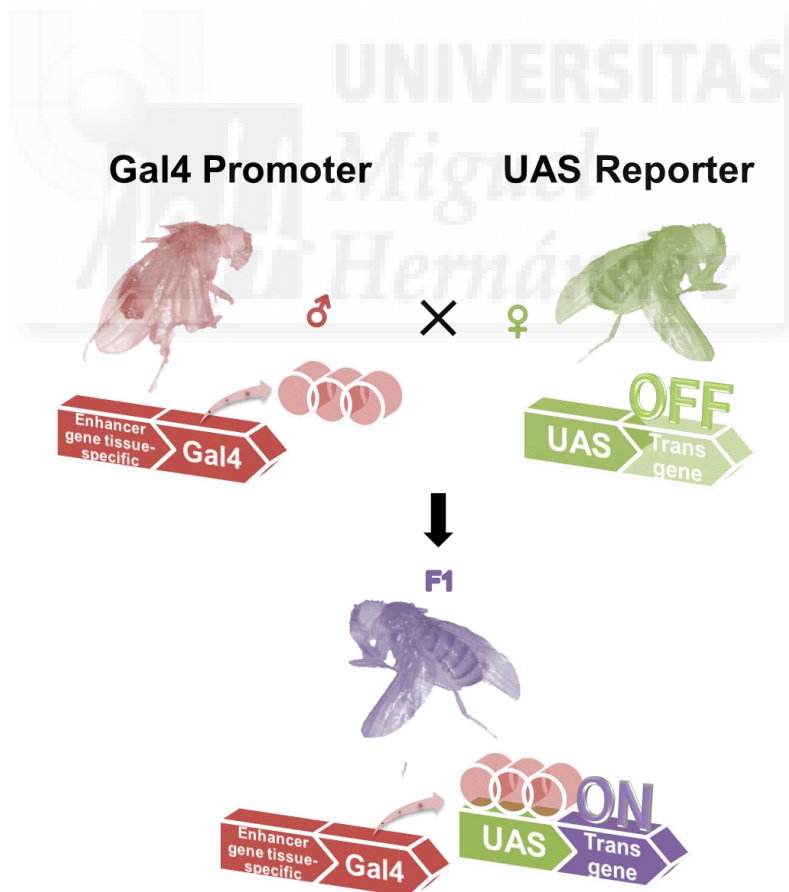


**Figure 2. Schematic representation of the Gal4/UAS system in flies.** In red, one parental fly carrying the Gal4 gene under the control of a tissue-specific enhancer. In green, the other parental transport the inactivated target transgene under the control of a UAS sequence. In purple, the target gene is transcriptionally activated in the progeny when the Gal4 proteins attach to the UAS region. Adaptation of Figure 1 from Brand and Perrimon, 1993.

### 2.2.2. Cell sorting by fluorescent flow cytometry

The isolation of individual *in vitro* cells in order to separate them into populations has been used to study the group characteristics through the cells' transcriptome (Gay et al., 2014). Profiling stem cells and rare cell types from fresh tissues in *Drosophila* has been a challenge. Several methods are used to isolate these cells, such as the 4-thiouracil (4-TU) mRNA tagging (Miller et al., 2009; Syed et al., 2017a), RNA co-immunoprecipitations (Kunitomo et al., 2005; Roy et al., 2002) and nuclei tagging isolation (INTACT; Steiner et al., 2012). However, the characteristics of the cells being isolated are important and need to be taken into consideration when selecting the methodology. Recent studies for purifying fly cells have concluded that FACS sorting is a suitable technique for the profile type of our cells of interest (Berger et al., 2012; Dutta et al., 2013; Korzelius et al., 2014; May Lim et al., 2012; Tauc et al., 2014). The method (Harzer et al., 2013) consists of selecting fluorescent cells, and for that, the Gal4/UAS system enables this type of technique for the *Drosophila* research model. Previously to sorting, the methodology requires a soft enzymatic and mechanic dissociation of the tissue into single cells; then, the cells go through a computational fluorescent sorting in order to be isolated and selected into groups of interest.

The fundamental principles of the high-throughput sorting involve the use of a sophisticated instrument which selects cells via electrically charged drops (Figure 3). First, the mixture of cells is distributed into individual cells which remain into single drops. Next, several lasers excite the cell's fluorescence, which gives information about the size of the cell and its nucleus. The wavelengths of light emitted from the cells pass by coloured filters and are then distinguished by a photomultiplier detector. Single or double positive or negative charges, as well as no-charge, are next applied to the drops by a computer analysis through an electrical wire depending on the criteria of selection. Finally, charged cells pass through deflection plates where they are distributed into collection vials via the use of attractive and repulsive forces. Apart from fluorescence information, the apparatus also retain information about the nucleus (side scatter, SSC) and cell (forward scatter, FSC) size in order to have more criteria with which to differentiate cells within the sample. Thus, cells are grouped into each fluorescent population.

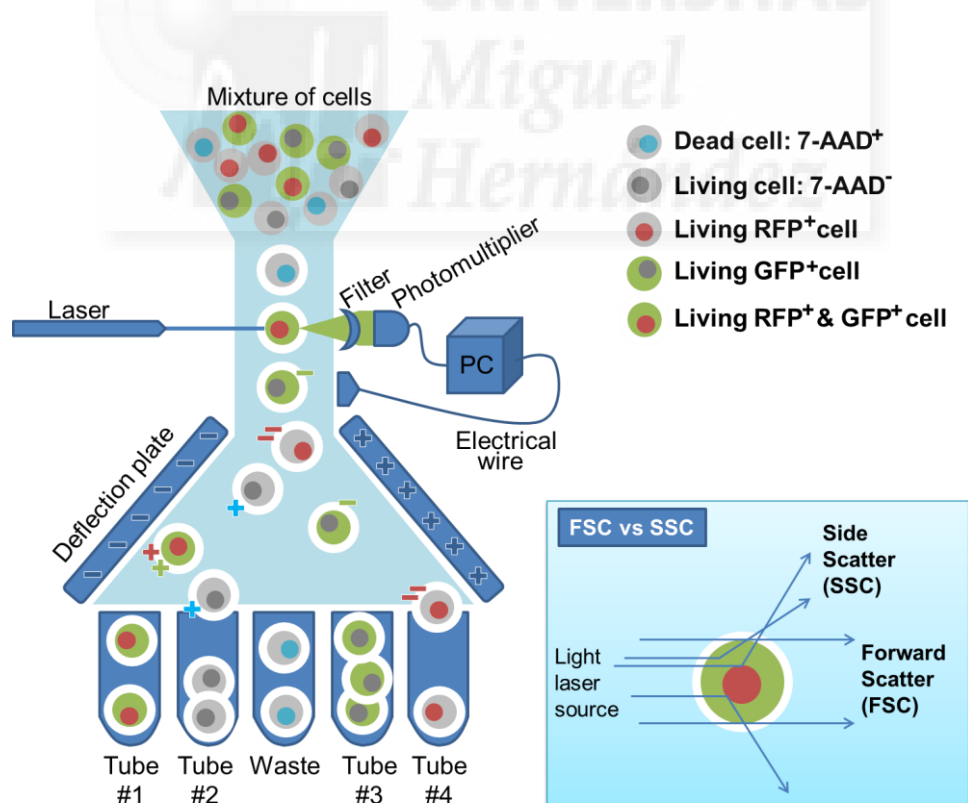


**Figure 3. Schematic representation of the FACS system.** A mixture of cells is sorted. The cells are separated into individual drops. A laser excites the fluorophores, which differentiates cell size (FSC) and nucleus size (SSC), as indicated in the highlighted box. The wavelength is filtered by a colour filter and received by a photomultiplier. A computer analyses the signal and, through an electrical wire, charges the drops depending on each cell's properties. A deflection plate distributes each cell into the corresponding tube: dying cells stained with the nuclear fluorescent 7-AAD are discarded (waste); living cells with no fluorescence (tube #2) are collected for negative control; cytosolic green fluorescence (tube #3) and nuclear red fluorescence (tube #4) are collected for positive controls; the double fluorescent cells for red nuclear and green cytosolic (tube #1) are selected for analysis of their transcriptome.

### 2.2.3. Transcriptome sequencing for gene expression analysis

The genus *Drosophila* is considered a powerful tool for genetic research (*Drosophila* 12 Genomes Consortium et al., 2007), as mentioned in previous sections. The four chromosome pairs of the species *D. melanogaster* (Figure 4A) enable studies of the impact of mutations within pathways and complex networks (Keightley et al., 2009). Moreover, the entire fruit fly genome was sequenced in the year 2000 (Adams et al., 2000) and was found to be ~180Mb in size, of which 118-120 Mb are euchromatic, and contain almost 14,000 coding genes (Adams et al., 2000; *Drosophila* 12 Genomes Consortium et al., 2007). These genome characteristics make the fly user-friendly for genetic studies.

The mapping of all the genes in the genome has allowed researchers to go further in the development of Omics technology, such as genome-wide fluorescent protein localisation (Sarov et al., 2016) and transcriptomics. Sequencing RNA (RNA-seq) has become a common method of obtaining a very robust genome read-out and is widely used to reveal which *Drosophila* developmental genes are shared across species (Gerstein et al., 2014) and which are related to human disease-associated genes (Reiter et al., 2001). The high throughput-sequencing (HTS) technology is also employed in gene expression studies to compare different temporal patterns (Liu et al., 2015; Syed et al., 2017a) or ligand and receptor interactions between diverse cell population (Tan et al., 2016). The continued advances in the technology during recent years has led to next generation sequencing (NGS) methodologies which enable researchers to perform RNA-seq from single cells (scRNA-seq) from a broad range of protocols (Ziegenhain et al., 2017) which improve upon single-cell technologies used up until now (Hoppe et al., 2014). One of the main purposes for scRNA-seq is to discover different cell profiles between subtypes (Bifari et al., 2017; Llorens-Bobadilla et al., 2015; Macosko et al., 2015; Zeisel et al., 2015). However, apart from the high cost of achieving powerful results, this technique presents substantial technical variation in sensitivity, accuracy and precision, due to the very small amount of starting material (Brennecke et al., 2013; Kolodziejczyk et al., 2015; Wagner et al., 2016). Thus, considering that my thesis goal is compare gene expression by time conditions and that scRNA-seq does not provide substantial data but enlarge the raw data, I opted to use the standard RNA-seq workflow.

In transcriptome analysis (Figure 4B), a high-quality starting material (homogenous animal genotype, protocols of RNA extraction, sample purity, etc.) is as important as an accurate design of the entire process. Among all the sequencing platforms, Illumina® is the most established one in the field (Reuter et al., 2015), so its working pipeline is followed in this thesis. One of the first steps in the creation of cDNA libraries is the RNA purification which is done by isolating mRNA or depleting ribosomal RNA (which constitutes ~80% of the total RNA). Another valuable step is adding barcodes (unique sequence identifiers) to the sample fragments in order to localise them when multiple libraries are pooled together in the sequencer. Another important factor to keep in mind is to strand specifically or not the library fragments (Zhao et al., 2015). This element, which is incorporated into the fragments for example using the dUTP method (Levin et al., 2010; Parkhomchuk et al., 2009), adds original strand information of directionality and therefore is important for identifying antisense transcripts as well as accurate annotation of genes, including overlapping transcripts, which directly impact gene expression levels.

This type of massively-parallel cDNA sequencing (MPS) needs to consider two other issues for the experiment run. The read depth, or the amount of sequencing needed, is determined by the nature of the sample and the goals of the study. The higher number of reads performed, the higher number of genes with low expression are covered (low expression does not necessarily mean that a gene is functionally less important). Also, the sequencing depth is influenced by a second issue, to single or paired ends which means read once or twice each fragment. For instance, a sequencing depth of 50 million reads per sample performing single ends means 25 million reads per sample when performing paired ends. This means that with the same cost, we obtain fewer reads per fragment, although doing paired ends is useful in the determination of isoforms. In this thesis, I am interested in discovering novel elements and strong quantifications of known transcripts, so a single end sequencing with an average of 40 million reads per library is suitable.

Finally, the gene expression profile is obtained by bioinformatic data mining. Proper indexing and mapping as well as reporting a differential expression are highly important parts of the RNA-seq pipeline. All in all, the techniques mentioned in this section constitute the fundamental workflow of the present thesis. Each one was set up and used to eventually achieve the project objectives.

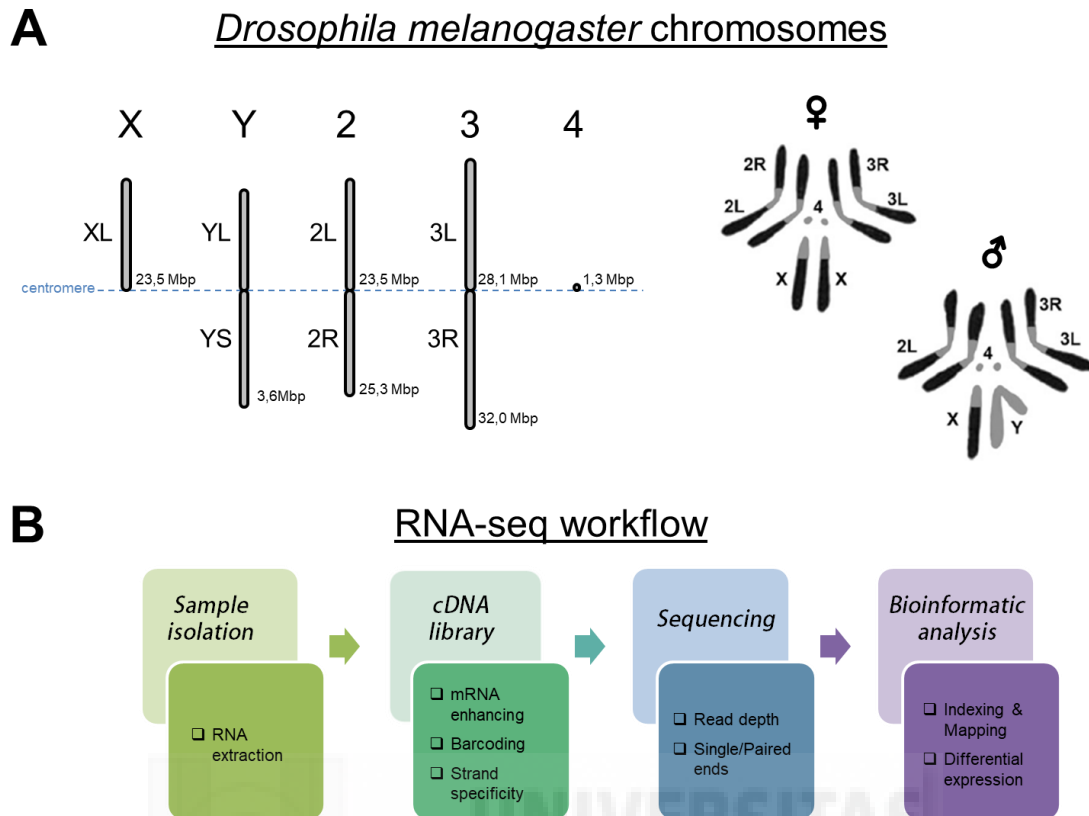


**Figure 4. Genetics and transcriptomics for *Drosophila melanogaster*.** (A) The four chromosomes that exist in the fruit fly (adapted from Carvalho, 2002 and Kaufman, 2017). (B) Pipeline used in high throughput sequencing and its main phases.

### 2.3. Life cycle of *Drosophila melanogaster*

Nowadays, fruit flies at all developmental stages are used in scientific research. The short life cycle of *Drosophila* is advantageous compared with other more complex animal models. While experiments in flies commonly take days, weeks or a few months at most, the same experiments in mice last several months or years. Flies are grown for around 10 days at 25 °C to generate adults which live for at least 10 weeks (Figure 5A).

Studies of early development use *Drosophila* from the early embryo until the late larval stage where the two waves of neurogenesis take place, respectively. The first neurogenic phase, during the embryogenesis of fertilised eggs, has been extensively studied for morphogenetic patterning and cell lineage studies (Baumgardt et al., 2007, 2009; Bivik et al., 2015; Landgraf and Thor, 2006). As the morphologies of the organs vary from larva to adulthood (Figure 5B,C), the examination of primary imaginal discs and other tissues, such as the brain, provides deep insights into organogenesis during the second wave of neurogenesis. It is during the larval period when provides knowledge of the development of neural circuits as well as the ability of a generic cell lineages to develop into several different lineages (Kim et al., 2009; Lee, 2017). Moreover, the switch from the proliferative to the neurogenic stage described in a specific region of the brain, takes place between the second and third instar larval (IL) stages (Apitz and Salecker, 2014; Egger et al., 2007; Li et al., 2013; Morante et al., 2013). For this reason, in this thesis I use both stages to identify changes in neurogenesis.

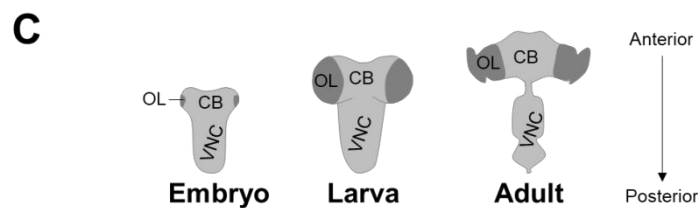
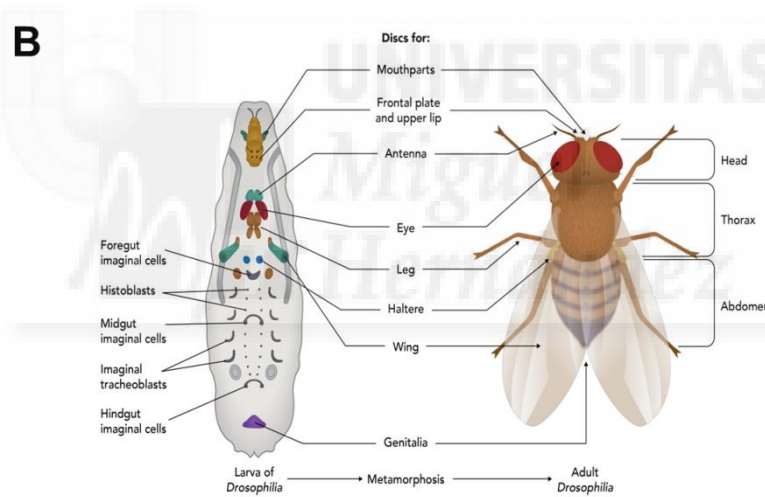
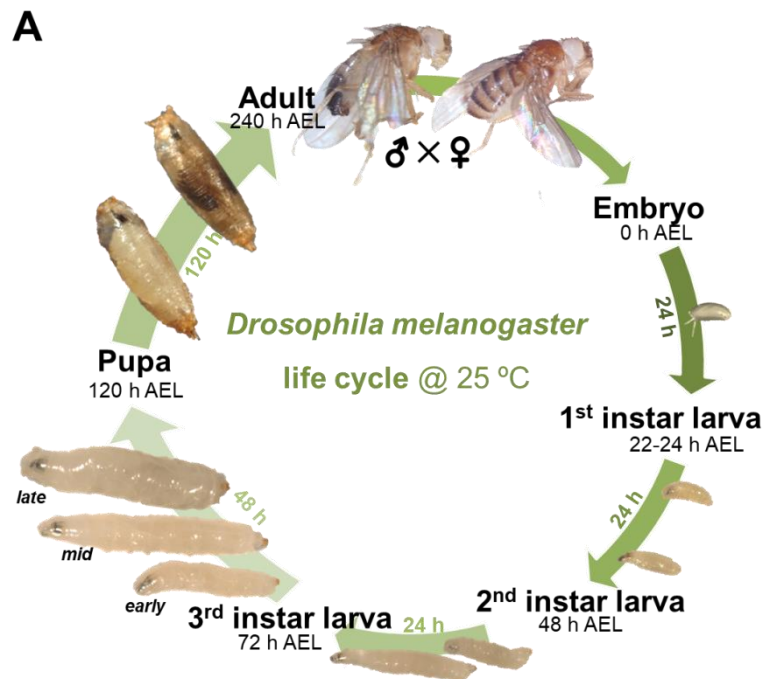


**Figure 5. *Drosophila melanogaster* life cycle and organ development. (A)** After an embryo is fertilised, 22-24 hours of development at 25 °C is needed until the egg hatches. Then, a larva is born and begins a maturation process of 96 hours during which the larva moults several times. The 1<sup>st</sup> instar larval (IL; a.k.a. L1) stage lasts for 24 hours, from 22-24 hours after egg laying (AEL) until 48 hours AEL. The 2<sup>nd</sup> IL (a.k.a. L2) stage is a period of another 24 hours which spans from 48 to 72 hours AEL. The 3<sup>rd</sup>-IL (a.k.a. L3) stage is the longest period in larval development, and it starts at 72 hours AEL and lasts for 48 hours in total; during this time, the larvae pass through three different development periods of 16 hours each, known as early, mid and late. At 120 hours AEL, when a pre-pupa is formed, a pupa metamorphosis period of 96 hours begins, and the adult fly is ready to eclose at 240 hours AEL. The cycle starts again when adult flies mate. **(B)** A huge variety of structures in adult flies are formed from the larval imaginal discs (image by Emily Roberts, Answers in Genesis). **(C)** *Drosophila* CNS development in an embryo, larva and adult fly (adapted from Sousa-Nunes et al., 2010). Three major areas can be distinguished at each development period: the ventral nerve cord (VNC), the central brain (CB) and the optic lobe (OL).

## 2.4. The larval central nervous system

The *Drosophila* CNS has been used from their youth to adulthood as a model for developmental studies of tissue complexity and connectivity (Technau, 2008). During this development process, the brain compartmentalises into regions (Figure 5C) differentiated by origin, temporal and type of expansion and function (Hartenstein et al., 2015). The three main regions are the ventral nerve cord (VNC), which is analogous to the spinal cord in vertebrates, the central brain (CB), owing special structures essential for olfactory learning and memory, and the optic lobe (OL), which is entirely destined to the vision sense (Figure 6). Each of those regions contains different types of progenitors, and their progeny acquire region-specific patterning that modify the progenitors' behaviour in a feedback loop (Arendt and Nübler-Jung, 1999; Guillermin et al., 2015; Lee et al., 1999; Pereanu et al., 2010; Ramon-Cañellas et al., 2019).

The OL, due to the exclusive and the large brain size dedication to only one of the senses, reveals the importance of vision for flies (Morante and Desplan, 2008; Néric and Desplan, 2016). The complexity for this special region is shown by the diversity of neurogenic patterns that come from two proliferative regions (Figure 6): the outer proliferation centre (OPC) and the inner proliferation centre (IPC; Apitz and Salecker, 2014; Ngo et al., 2017; Pinto-Teixeira et al., 2018; Yoon et al., 2018). Both contain a unique type of progenitor cells, the NECs, which lead to NB and the subsequent types of lineage cells. This thesis is centred on the area of proliferation located in the OPC of the larval OL.

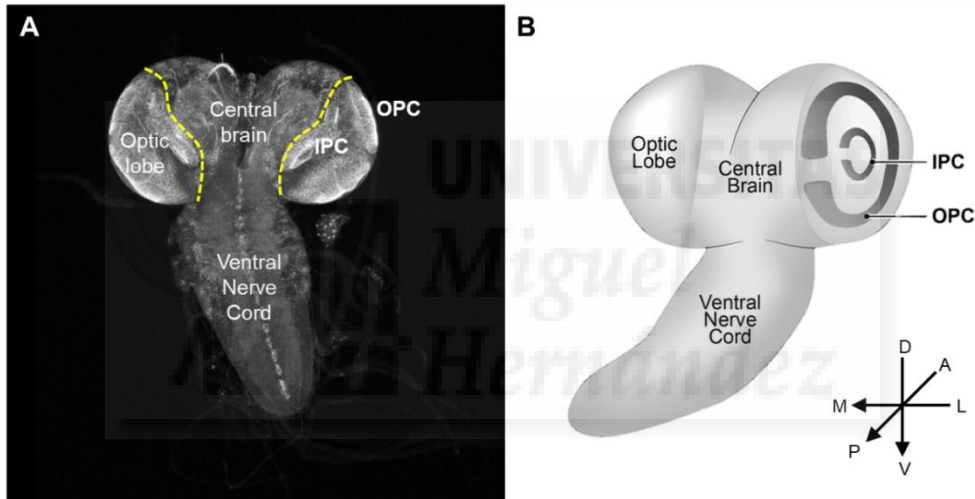


**Figure 6. *Drosophila melanogaster* late larval brain.** Confocal image (A) and schematic representation (B) of the fruit fly central nervous system in a late-3<sup>rd</sup> instar larva (adapted from Figure 2 of Ramon-Cañellas et al., 2019). Three main areas are distinguished: the ventral nerve cord, the central brain and the optic lobe. Within the brain optic lobe, two proliferation zones where neuroepithelial cells reside can be identified: the outer proliferation centre (OPC) and the inner proliferation centre (IPC). The different neuronal regions are identified with respect to three axes: anterior-posterior (A-P), dorsal-ventral (D-V) and lateral-medial (L-M).

## 2.5. Neuronal progenitors in larva fruit fly

*Drosophila* NBs, which are the equivalent of human radial glial cells, are widely used for studying brain development due to their multipotency as stem cells. Although they are present from embryonic stages until adulthood (Ramon-Cañellas et al., 2019), NBs modify their properties during larval stages. A transition takes place when they change from a proliferative phase into a differentiative phase in order to cause the OL to expand in size and function. This switch is due to the change in progenitors' cell division from symmetric to asymmetric (Ceron et al., 2001; Egger et al., 2007).

As mentioned, depending on the cells' origin, the NBs can be distinguished during larval stages within the three main brain regions: NBs of the CB (Figures 7A and 8A), which originally delaminate from the embryonic procephalic neuroectoderm, NBs of the VNC (Figures 7C and 8C), which delaminate from their embryonic VNC neuroectoderm, and lastly NBs of the OL (Figures 7B and 8B), which recently has also been identified that a small set of progenitors delaminates from the late embryonic optic placode (Hakes et al., 2018) although the vast majority are originated from the OL larval neuroepithelium.

During the late embryogenic stage, NBs of the VNC are responsible for the tissue growth until they enter into quiescence (Ulvklo et al., 2012). During larval stages, these NBs, categorised as type I (Figure 7C), exit from quiescence and give rise to ganglion mother cells (GMCs) which generate neurons or glia (Figure 8C).

The CB accommodates a hundred of Type I NBs per lobe (Figure 7A). Type II NBs, of which there are eight per lobe, have also embryogenic origin (Álvarez and Díaz-Benjumea, 2018) and are like the neural progenitors of the human outer sub-ventricular zone that divide asymmetrically to generate intermediate neural precursors (INPs) before their division to form GMCs (Bayraktar and Doe, 2013; Figure 8A). Another type of progenitors, mushroom bodies (MB) NBs, is also found in the central brain, with four cells per hemisphere (Figure 7A). MBs are special because are generated in the embryonic stage and continuously dividing during the rest of development without entering into quiescence (Kunz et al., 2012). The cell division mode of MBs is similar to that of type I NBs (Figure 8A), and generates the adult centres for cognitive and associative olfactory functions (Lee et al., 1999). Finally, five antennal lobe (AL) NBs per hemisphere dividing in a Type I division mode (Figure 8A) are the responsible of the adult olfactory system in *Drosophila* (Das et al., 2013; Jefferis et al., 2001; Lin et al., 2012; Figure 7A).

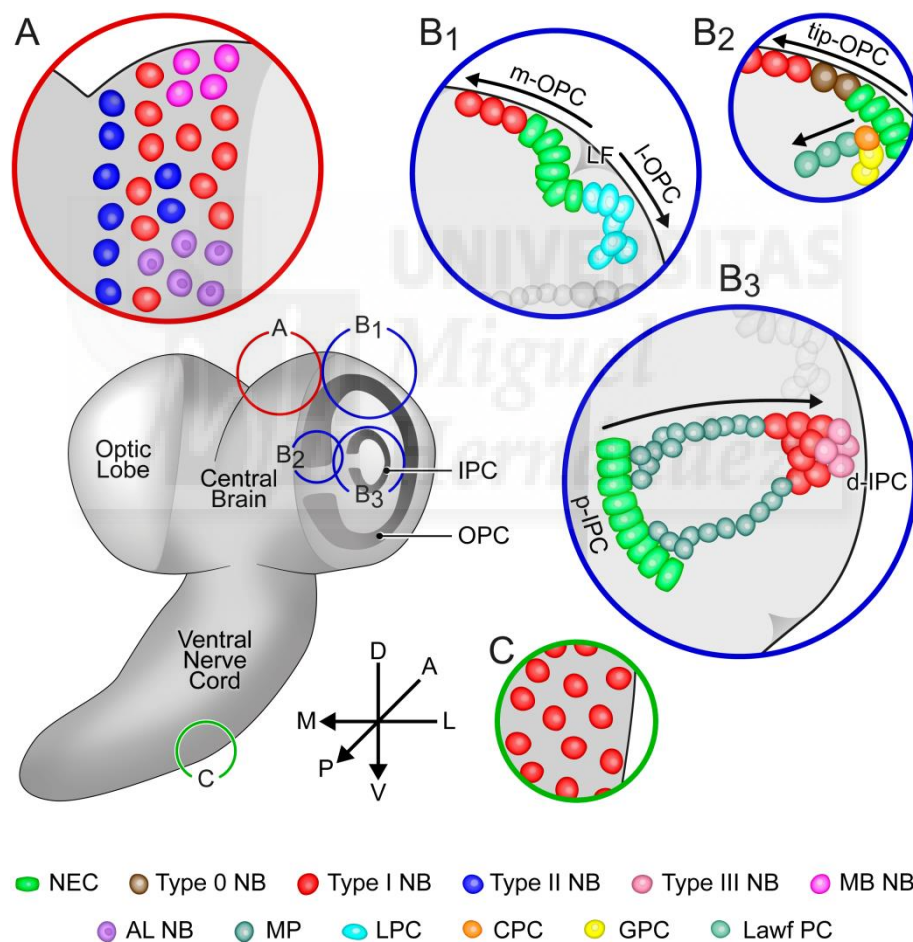


**Figure 7. Neural progenitors within the different regions of a larval brain.** A schematic representation of the neural progenitors described in the central nervous system of larval *Drosophila* (Figure 2 of Ramon-Cañellas et al., 2019). **(A)** The central brain, encircled in red, contains four types of neuroblasts (NBs): type I (hundreds cells per hemisphere), type II (8 cells per hemisphere), antennal lobe (AL) NBs (5 cells per hemisphere) and mushroom bodies (MB) NBs (4 cells per hemisphere). **(B)** The optic lobe, encircled in blue, is more complex in its variety of progenitor cells types. **B1** shows the outer proliferation centre (OPC) where neuroepithelial progenitors (NECs) delaminate into type I NBs and equally lamina precursor cells (LPCs). From a different point of view, **B2** shows the tip-OPC where type 0 NBs give rise to type I NBs and, also in this location, the common progenitor cells (CPCs) which, at the same time, lead to lamina wide-field precursor cells (Lawf PCs) and glial precursor cells (GPCs). **B3** shows the inner proliferation centre (IPC) where NECs delaminate into migrating progenitors (MPs), which first differentiate into type I NBs and later into type III NBs. **(C)** The ventral nerve cord, encircled in green, display the single NB type found there: type I. All perspectives are frontal views except for **B2** which is a dorsal view (for a precise viewpoint look at figures of Ngo et al., 2017). Lamina furrow (LF), medial-OPC (m-OPC), lateral-OPC (l-OPC), proximal-IPC (p-IPC), distal-IPC (d-IPC).

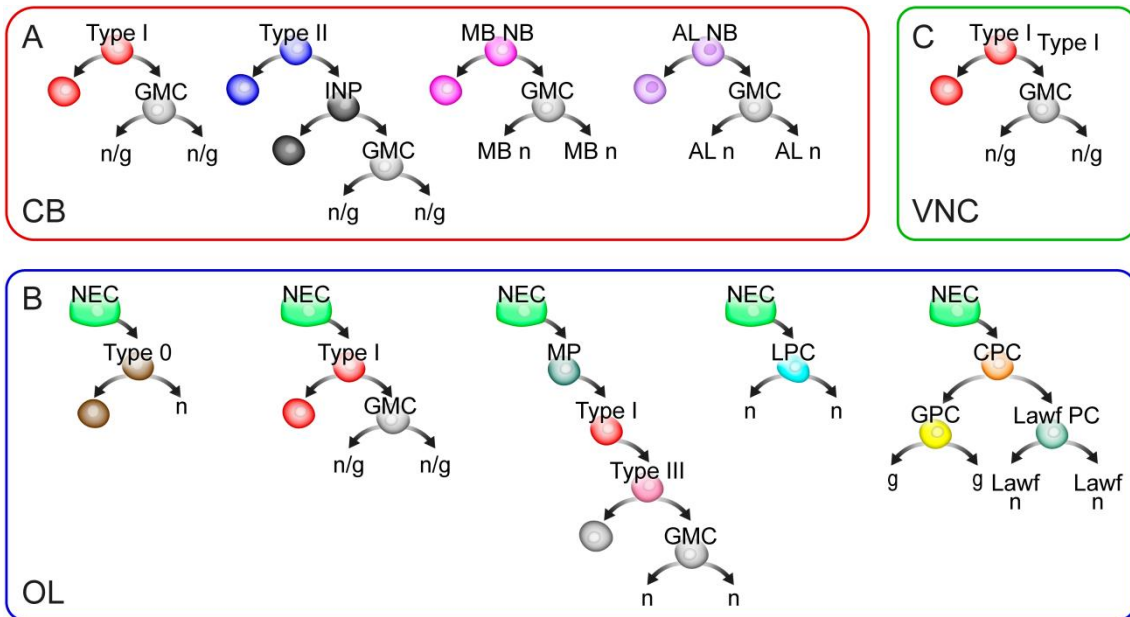


**Figure 8. Neural progenitor cell division modes and progeny in the *Drosophila* larval brain.** Representation in cascade of all types of neuroblasts (type 0, I, II and III) and cell progenitors defined in the central neural system of the larval fruit fly (Figure 3 of Ramon-Cañellas et al., 2019). The model illustrates the type of cell division (symmetric or asymmetric) that takes place by indicating the offspring generated. The progenitors are grouped by the brain region in which they are found: bordered in red (A), the central brain (CB); bordered in blue (B), the optic lobe (OL); and bordered in green (C), the ventral nerve cord (VNC). Neuroepithelial cell (NEC), neuroblast (NB), ganglion mother cell (GMC), intermediate neural progenitor (INP), mushroom body (MB), antennal lobe (AL), migrating progenitor (MP), lamina precursor cell (LPC), common progenitor cell (CPC), glia precursor cell (GPC), lamina wide-field precursor cell (Lawf PC), neuron cell (n), glial cell (g).

Due to the wide variety of progenitors in the OL, determined by their position, function and regulation, the OL is considered a “mini-cortex” model and needs to be described in detail (Doe, 2017; Homem and Knoblich, 2012; Ramon-Cañellas et al., 2019). The vast majority of the OL NBs, unlike the rest of the NSCs found in the *Drosophila* brain, delaminate from NECs in the early-2<sup>nd</sup> IL stage (Figures 7B and 8B). Before this period, NECs divide symmetrically to proliferate and expand, and when they reach the early-2<sup>nd</sup> IL stage they switch into an asymmetric division mode to produce NBs (Egger et al., 2007). Notably, this particular differentiation mode resembles that which occurs in the mammalian forebrain. Characterisation of the fly OL reveals that its four ganglia originate from the two neuroepithelial proliferative zones (Figure 6): the OPC produces medulla and lamina neurons while the IPC gives rise to lobula and lobula plate neuropil (Hofbauer and Campos-Ortega, 1990; Meinertzhagen and Hanson, 1993). Despite this, evidence shows that there exists an interrelationship between the two proliferative areas to properly establish all ganglia (Suzuki et al., 2016).

The IPC (Figure 7B-3) consists of three regions defined on their location: surface (s-IPC), proximal (p-IPC) and distal (d-IPC). NECs from the p-IPC divide asymmetrically and delaminate into migrating progenitors (MPs), which migrate from the p-IPC to d-IPC (Apitz and Salecker, 2015). This EMT-like mechanism resembles the move of radial glia-like cells from the meninges to the neonatal cortex in mice in order to functionally integrate (Bifari et al., 2017). When the MPs reach the d-IPC, a series of proneural factors causes them to first develop into type I NBs and later shift to type III NBs, which are characterised by their symmetric cell division to form GMCs and end their multipotency (Apitz and Salecker, 2018; Mora et al., 2018; Pinto-Teixeira et al., 2018; Figure 8B).

The neuroepithelia of the OPC (Figure 7B-1) is divided by the lamina furrow (LF), which separates the medial domain (m-OPC) from the lateral domain (l-OPC). On the medial side mostly medulla neurons are generated while on the lateral side lamina ganglia are produced, although these areas also differ in their distinct forms of neurogenesis (Apitz and Salecker, 2014). In the first region, the m-OPC, NECs proliferate in a symmetric mode until in the transition zone they arrest in the G1 phase of the cell cycle (Reddy et al., 2010); later, when they exit arrest, NECs divide asymmetrically to produce type I NBs (Figure 8B). A series of temporal transcription factors (TFs), including



Homothorax (Hth), Klumpfuss (Klu), Eyeless (Ey), Sloppy-paired (Slp), Dichaete (D) and Tailless (Tll), trigger differentiation of ganglion mother cells (GMCs) and act together with Notch-dependent asymmetric cell division for the control of differentiation of its neuronal progeny (Figure 9A). The tip of the OPC (tip-OPC; Figure 7B-2) is a particular area (Bertet et al., 2014) where *Distalless* (*Dll*)<sup>+</sup> NBs divide asymmetrically to directly generate a single neuron and because of this they are categorised as type 0 NBs. At certain point, these NBs give rise to type I NBs which express a unique series of TFs, including *Ey*, *Slp* and *D*, that generate neuronal diversity not only for the medulla but also for the lobula, lobula plate and adult CB (Figure 8B). Also described in the tip-OPC (Figure 7B-1), common progenitor cells (CPCs) delaminate from NECs and later become glial precursor cells (GPCs) or Lawf precursor cells (Lawf PCs; Figure 8B). None of these precursors express NB profiles and their neuroglial differentiation process resembles, in many ways, that of their vertebrate counterparts (Chen et al., 2016). In another region of the OPC, the I-OPC (Figure 7B-1), there exists a type of progenitor called lamina precursor cells (LPC), which do not present a NB profile and undergo mitosis in the G2 phase to symmetrically produce lamina neurons (Huang et al., 1998; Figure 8B).

In this thesis, the region of interest is the OPC of the brain lobes (Figure 9). It is here where the first progenitor cells, the NECs, start the differentiation process which ends in neurogenesis. For this reason, any dysregulation in this region and of the process which occurs there may have an irreparable impact on the development of the CNS.

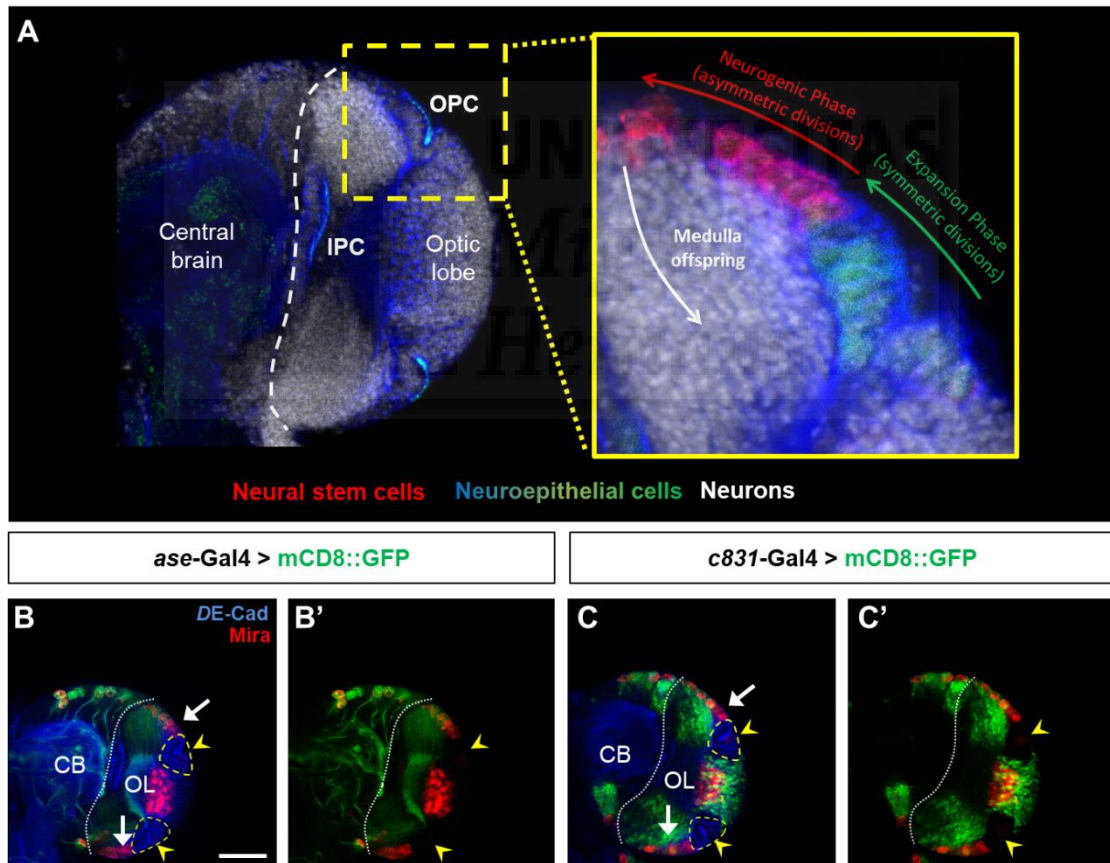


**Figure 9. The outer proliferation centre in the larval brain optic lobe of the fly.** Confocal images delineating the neuroepithelial proliferative area. (A) The lobes of the central nervous system are divided into the central brain (CB) and the optic lobe (OL). In the OL there exist two progenitor areas: the inner (IPC) and the outer (OPC) proliferation centres. In the OPC reside neuroepithelial cells (NECs) which first expand through symmetric divisions and later switch to asymmetric cell division to begin medulla neurogenesis. (B-B', C-C') Neuroblasts (NBs) and their progeny (in green) are shown when NB promoters, such as *ase-Gal4* (B-B') or *c831-Gal4* (C-C'), drive the expression of stable fluorescent reporters like *UAS-mCD8::GFP*. This reveals the OPC areas (yellow arrowheads) where NECs are found and neighbouring with NBs (white arrows). Images were taken from late-3<sup>rd</sup> instar larvae. Scale bars represent 50  $\mu$ m in (B).

### **3. Organ growth control**

A vast number of different types of neurogenesis are involved in the shaping of different brain areas. Therefore, it is essential to understand the roles that progenitors play in organ modelling, which basically depend on three factors: the cell's identity (previously explained), intrinsic timer patterning, and the location or immediate environment.

Moreover, proper development of the neural progenitors is necessary for the correct functioning of organs. NSCs' multipotency arises from their ability to proliferate and differentiate, which gives rise to neuronal diversity in response to both intrinsic and extrinsic cues (Doe, 2017; Kohwi and Doe, 2013; Morante et al., 2013; Syed et al., 2017b). Although nowadays intrinsic cues are more widely studied than extrinsic cues (Paridaen and Huttner, 2014; Tiberi et al., 2012), deeper knowledge of both types of cues is still necessary to fully understand the modulation of brain development within different progenitor niches.

#### **3.1. Intrinsic factors of the temporal patterning**

The development of NSCs across species has shown that depends mainly on their temporal internal circumstances (Jacob et al., 2008; Ramon-Cañellas et al., 2019; Rossi et al., 2017; Wang et al., 2013). Genetic signalling, whether either active or absent, and the interaction between genes determine the cells' life cycle. In this context, temporal patterning of NBs was first observed in an embryonic *Drosophila* VNC and later on also detected in the larval OL (Doe, 2017).

As mentioned, during larval stages type I NBs of the m-OPC expand through six sequentially expressed TFs (Hth, Klu, Ey, Slp, D and Tll; Li et al., 2013; Suzuki et al., 2013). NBs of the tip-OPC express a reduced series of those TFs: Ey, Slp and D (Bertet et al., 2014). Later, Notch binary fate choice controls the neural diversity of the NB progeny. Previously in this region, the switch of NECs from proliferative to differentiative stages is controlled by a complex network of temporally regulated genes from the Fat-Hippo / Notch / EGFR pathway (Reddy et al., 2010; Yasugi et al., 2010) or JAK/STAT signalling (Ngo et al., 2010; Suzuki et al., 2013; Yasugi et al., 2008). More factors are also involved, such as the spindle orientation of the cells (Egger et al., 2010) or the microRNA miR-7 (Caygill and Brand, 2017).

The IPC also contains examples of proneural factor expression that define different progenitors' profiles. When the MPs arrive at the d-IPC, they differentiate into type I NBs that first consecutively express D and Ase (Ase) producing C and T neurons. Later on, these NBs initiate a temporal window of the TFs Tll, Atonal (Ato) and Dac where the Ato lead to generate C- and T-neurons (Apitz and Salecker, 2015). Here, two models for the T-neurons production have been postulated. The first model relay in Notch-dependent divisions of Ato<sup>+</sup> NBs that produce symmetrically T4 and T5 neurons (Apitz and Salecker, 2018; Pinto-Teixeira et al., 2018). The second one, is symmetric cell division of NBs, type III NBs, that ensures those neurons and Ato regulated those amplification (Mora et al., 2018; Pinto-Teixeira et al., 2018).

Those examples shows that progenitors throughout brain regions share similarities as well as differences in neurogenesis regulation (Colonques et al., 2011). For instance in the CB, the differentiation of MBs is controlled by opposing temporal gradients which guide a varied neuronal fate (Liu et al., 2015). In definitive, the inside mechanisms of progenitor cells determine their behaviour and its implication in organ shaping.

#### **3.2. Extrinsic factors in cell niches**

Apart from temporal cues, extrinsic cues resulting from the environment in which progenitors reside are another evolutionarily conserved factor of patterning that modifies their behaviour. Although some of these spatial cues originating in NSC microenvironments have been recently identified in *Drosophila* (Syed et al., 2017b), further studies need to be done on this subject.

In a systemic context, larvae raised on a diet without amino-acids have continually dividing MB NBs, which perturbs the natural temporal patterning of their lineages (Lin et al., 2013). In this way, dietary amino-acids incorporated to the organism contribute, via the target of rapamycin (TOR) pathway of the fat body (FB), to the postembryonic reactivation of quiescent NBs in the VNC and CB (Chell and

Brand, 2010; Sousa-Nunes et al., 2011). In early larval stages, nutrition cues regulate symmetric division of NECs via insulin/PI3K/TOR signalling. However, in late larval stages, progenitors become unresponsive to dietary nutrients and their proliferation starts to be orchestrated by the steroid hormone Ecdysone via Delta/Notch signalling (Lanet et al., 2013). Ecdysone, produced outside of the CNS, acts as hormonal cue on TFs when down-regulate Chinmo/Imp and next activates Syncrip/Broad/E93 (Dillard et al., 2018; Syed et al., 2017a).

In brief, these examples show the importance of external inputs for progenitors that create a microenvironment known as the niche (Maurange and Gould, 2005). One step further is the need to understand how extrinsic cues regulate temporal cues for neural progenitor identity (Syed et al., 2017b). Definitively, only the full integration of both types of cues into a niche can reveal precisely how progenitors generate such neural diversity (Erclik et al., 2017).

## **4. Glia as progenitor niche interactor**

In the nervous system, the glia is without doubt the most abundant cell type together with neurons. Nonetheless, in early era of brain science they were dismissed as merely scaffolding for neurons and thought to perform a passive task in the nervous system. Fortunately, several discoveries on the last scientific period changed that theory and revealed that glial cells have an active and essential role in brain function and development. Thus, the number of studies has risen and nowadays glia is thoroughly considered in neuroscience from *Drosophila* to vertebrates (Freeman and Doherty, 2006; Lopez-Atalaya et al., 2018; Ou et al., 2014).

### **4.1. Different types of glia in the larval central nervous system**

Glial cells of the fruit fly are genetically similar to glia in mammals, and also express typical TFs such as the gene *gcm* (glial cell missing), which is responsible for glial cell fate (Freeman et al., 2003). In the *Drosophila* CNS, a small set of progenitors differentiate into glial cells (Figure 8). Those progenitors are called glioblasts or neuroglioblasts depending on whether they uniquely produce glia or both neurons and glia, respectively. Those multipotent cells delaminate from the post-gastrulated embryo neuroectoderm and their number increases during the 3<sup>rd</sup> IL stage due to a combination of two mechanisms: the continued division of neuroglioblasts (Larsen et al., 2009) and the division of differentiated glia (Colonques et al., 2007). Finally, the glial diversity in the adult brain depends on their progenitor's early patterning during embryonic and larval stages. Therefore, extensive knowledge of glial development is crucial to fully understand their structure and function in a mature brain (Awasaki et al., 2008).

Glia in the CNS are classified into three main groups defined by their characteristics and function, which are described below (Freeman, 2015; Hartenstein, 2011; Ramon-Cañellas et al., 2019; Stork et al., 2012).

The first main group is the surface glia (SG). This population is located on the most outer part of the brain and enwraps the entire CNS, serving as the gateway for molecules within the haemolymph (the analogous fluid in insects to blood). The SG are divided into perineural glia (PG), which serve as the first physical and chemical barrier for great molecules, and subperineural glia (SPG), which use septate junctions to communicate among themselves and function as a conserved blood-brain-barrier (BBB; DeSalvo et al., 2011; Stork et al., 2008; Figure 10). SPG also use adherent or gap junctions to maintain contact with other underlying cells or glial subtypes. PG cells are small in size and have an elongated cell body whilst SPG are big and have an even nucleus. In each brain hemisphere, there are hundreds of PG cells and only around ~20 SPG cells (Figure 10A,B).

A second principal glial cell type, called cortex glia (CG), is located underneath the SG (Figure 10). In each OL of the brain there are around ~140 CG cells that enwrap cell bodies of the NBs, GMCs and neurons and their function is to act as trophic supporters (Morante et al., 2013; Figure 10A,B). Although this glial subtype is pointed out as a relevant mediator between the outer and the inner environments of the brain, it is the least-studied glia cell type.

Lastly, the third main glial type is neuropil glia (NG) which is located between the cortex and the neuropil (dense region composed mostly of axons and dendrites). Although is the most diversified

population due to the wide range of molecular markers and structures, it is divided into two subtypes depending on their location: ensheathing glia (EG) and astrocyte-like glia (ALG, also known as reticular glia; Figure 10). Both glial subtypes communicate with neuronal axons and specifically, EG enwrap regions of the neuropil while ALG act in pruning and synaptic formation for neural remodelling (Omoto et al., 2015).

As mentioned before, the complexity of the residing cells in the OL not only concerns to progenitor cells but also to glia and for that it is necessary to special heed into its different subtypes of glia (Chotard and Salecker, 2007; Huang and Kunes, 1996; Figure 10B). A subtype of surface-associated CG differentiated by its expression of the microRNA *miR-8* ensheathes the neuroepithelium of the OPC but also CB lineages (Morante et al., 2013; Figure 3A,B). Satellite glia (sg) is also a CG subtype which enwraps cell bodies but, in this case, of lamina neurons. Two subtypes of NG, medulla glia (meg) and medulla neuropil glia (mng), are originated in the GPC region of the OPC and move to the edges of the medulla neuropil. Marginal glia (mg) and epithelial glia (eg), also subtypes of NG, have their origin in the GPC area and share lineage with lawf neurons (Chen et al., 2016). Next, both subtypes move to below (mg) and above (eg) the lamina plexus, where photoreceptor axons projecting from the eye imaginal discs reach them (Chotard and Salecker, 2007). All in all, the broad range of glial behaviour, the existence of glia throughout the whole CNS, and the complexity of glial development firmly indicate that the glial role in brain control through niches is essential, and for this reason glia are evolutionarily conserved across species (DeSalvo et al., 2011; Stork et al., 2008).

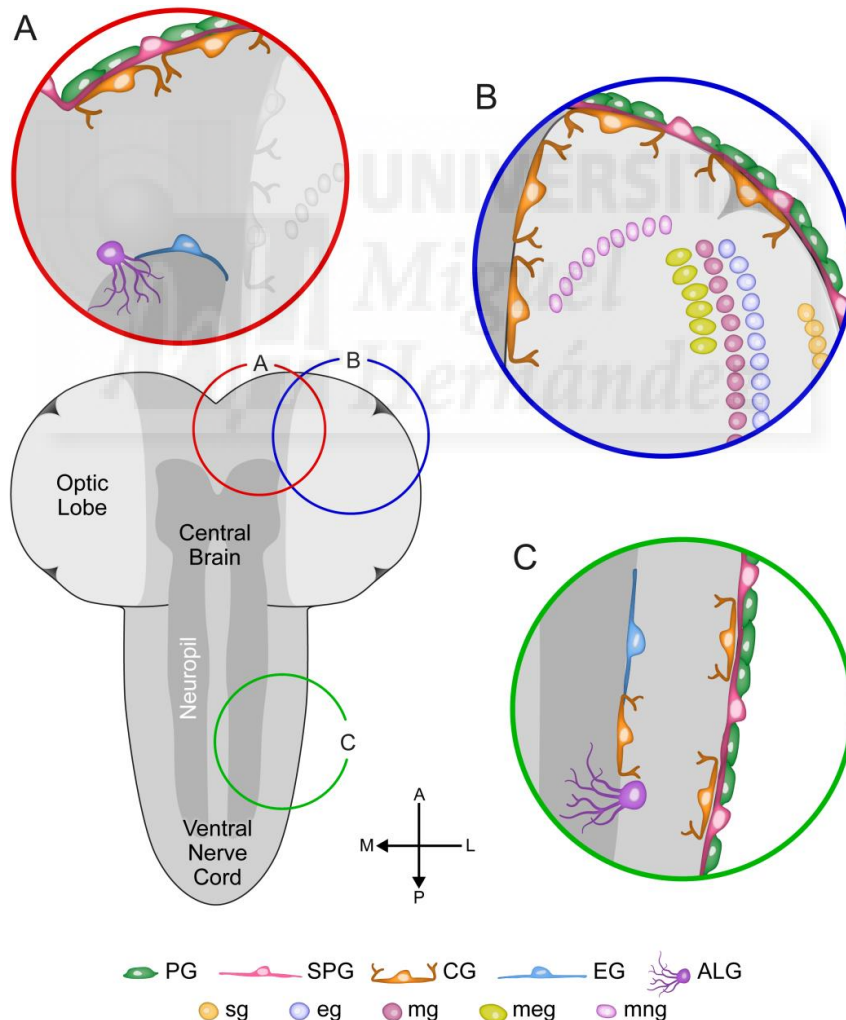


**Figure 10. Glial cell types in the *Drosophila* larval brain.** Schematic model of the different glial cell types described in the central nervous system of the larval fruit fly (Figure 4 of Ramon-Cañellas et al., 2019). (A) In the central brain, encircled in red, the outer surface glia are divided into perineural glia (PG) and subperineural glia (SPG). Below are located the cortex glia (CG). Finally, the neuropil glia are divided into Astrocyte-like glia (ALG) and ensheathing glia (EG). (B) In the optic lobe, encircled in blue, the PG and SPG are the most external layers of glia. CG are located underneath them. Around the different ganglia, various types of NG are located: medulla glia (meg), medulla neuropil glia (mng), marginal glia (mg), epithelial glia (eg) and satellite glia (sg). (C) In the ventral nerve cord, encircled in green, there are the same glial types as in the central brain.

## 4.2. Glial niche

Nowadays, it is clear that the NSC microenvironment affects progenitor development and behaviour (Morrison and Spradling, 2008; Siegenthaler and Pleasure, 2011). There is no doubt that extrinsic cues received by NSCs are required to be correctly interpreted to generate the adequate intrinsic response. However, exist little detailed data about those interactions and the surrounding cells. Due to the fact that glia are large in number and have many different subtypes, in addition to their location close to proliferative zones, it has recently been accepted that glia do substantially interact with neurons (Fernandes et al., 2017; Huang et al., 1998; Liu et al., 2017; Nave et al., 2017; Rossi and Fernandes, 2018), although deeper knowledge of precursors cells is needed.

Studies have shown that the sub-ventricular zone of an adult mammalian brain receives external BBB inputs from diffusible morphogens, the cerebrospinal fluid and the blood (Dani and Lehtinen, 2016; Silva-Vargas et al., 2016). Likewise, in a developmental fly brain, the task of the SG layer as analogous to that of the BBB enhances the importance of its membership in a progenitor microenvironment known as the neurovascular niche (Otsuki and Brand, 2017). There is some clear evidence that SG develop other tasks in niches, such as the SPG's role in tissue growth. SPG are polyploid, an attribute which is necessary to preserve BBB integrity as well as the SPG cells' proper growth and that of the brain at large (Unhavaithaya and Orr-weaver, 2012). Other studies suggest that SPG communicate directly with NBs through Dlp and Gbb signals, which results in key cues for brain development (Kanai et al., 2018). Altogether, this shows how active glia are within microenvironments, indicating that more functions are belong to those cells and are not assigned yet.

Previously, I explained about hormones and dietary nutrients as extrinsic cues; such signals are also processed by glia. For instance, when dietary amino-acids activate FB signalling, they also provoke a glial release of *Drosophila* insulin-like peptides (dILPs), which reactivate quiescent NBs (Chell and Brand, 2010; Sousa-Nunes et al., 2011). Recently, it was discovered that NBs can enter into quiescence in the G2 cell cycle phase. The exit from quiescence of those NBs arrested in G2 is induced by dILPs from the BBB glia, and these NBs demonstrate a quicker regeneration response than those arrested in G0 (Otsuki and Brand, 2018). Another example of the dILPs action from glia can be found in the fly visual system retinotopy. Photoreceptors act on EG, and through dILPs they induce LPC progenitors to differentiate into neurons of the lamina (Fernandes et al., 2017; Rossi and Fernandes, 2018). In the end, the glial function as a lipid reservoir is evolutionarily conserved and therefore glia can also perform functions such as energy transfer in axonal myelination and synapses (Liu et al., 2017; Nave et al., 2017).

The communication between cells is bidirectional, and this has an impact on the niche as well. Progenitors also send signals, which induce glial remodelling and an adaptation of the microenvironment to their needs. Firstly, the activation of the P12k/Akt pathway via nutritional cues in NSCs produces a growth of membrane processes. Later, the NSCs exit quiescence to resume proliferation and at this point in time they send signals to glia in order to resume neurogenesis (Spéder and Brand, 2018).

All the novel discoveries here discussed, reinforce the idea that glia have a decisive role in essential development process across distinct brain regions. Notwithstanding, more efforts are needed in the field to elucidate the specific relationship between niche cells.

## **5. Deficiencies in neuronal development results in brain injuries**

There is no doubt that a dysregulation of important TFs which control the transition from progenitors to neuronal lineage cells may lead to brain diseases (Saini and Reichert, 2012). Furthermore, the environment where NSCs are located is extremely important to homeostasis neurogenesis processes from early development to adulthood and fix it in case of malfunctioning (Doherty et al., 2009).

### **5.1. Intrinsic defects provokes severe brain injuries**

Temporal patterning and the role that sequentially expressed TFs play in neurogenesis are already highlighted in previous sections. However, the vital importance of the correct functioning of this

mechanism is made clear when the natural series of TFs expressed is disrupted. This molecular interruption results in loss of neural and glial identity as well as the formation of malignant tumours (Narbonne-Reveau et al., 2016). Other genes expressed in precursor cells are found to be relevant not only for neuronal differentiation but also for control of orthologues of disorders such as Down syndrome (Shaikh et al., 2016). Appropriate gene expression for compartmentation of NECs and distribution through early developmental stages is important and thus conserved from invertebrates to vertebrates, and this gene expression also has effects on the development of other tissues (Gold and Brand, 2014). All these examples clearly show the relevance of temporal patterning for proper neural fate and organ growth.

## **5.2. Dysregulated cells have a direct impact in precursors niches and cause the development of brain disorders**

The CNS in vertebrates, although it does not regenerate in totality, does react to injury with responses from glial cells to help repair the damage (Alunni and Bally-Cuif, 2016). For instance, while in a neuroinflammatory state that may evolve into a neurodegenerative disease, microglia is activated to serve a neuroprotective role. It has been demonstrated that this process is switched on when the ligand-receptor interaction, CD200-CD200R, is absent between neurons and microglia as well as astrocytes (Dentesano et al., 2014). There is evidence that this response is evolutionarily conserved from invertebrates to vertebrates. Under normal circumstances, the NG of the larval fruit fly act as axonal enwrapment, neurotransmitter recyclers or modulators of neural activity. However, under the circumstances of an injury, *Drosophila* NG repair and regenerate via phagocytosis, cleaning-up of cell debris, stimulation of proliferation and enwrapment of progenitors and their progeny in a protective manner (Kato et al., 2017).

Therefore, a dysfunction in glia and their non-autonomous effects on progenitor niches may create harsh issues in the fruit fly CNS. Recently, it has been demonstrated in larva that depletion in the glial lineage-specific *wdr62*, which is the second most commonly mutated gene in primary microcephaly, provokes a loss of NB population. The consequences of this imbalance are significant, and decrease the volume of the entire brain resulting in microcephaly (Lim et al., 2017). NECs, as brain progenitors of different populations, physically constrain the dividing cells in order to organise growing tissue. However, errors in cell polarity of this progenitor have a strong effect on their offspring, including glia, that may result in tumorigenesis (McCaffrey and Macara, 2011).

In summary, taking into consideration that significant advances have already been made in knowledge of progenitor niches and the role of glia in the control of neural development, there is still much more to be understood in this field. Thus, combining new studies in mammals and new discoveries in *Drosophila*, a powerful model organism, scientists may shortly be able to interpret the specific function of each neural progenitor and other niche cells such as glia within the distinct brain microenvironments.

## **5.3. Relevance of optic lobe surface-associated cortex glia in the stem cell niche**

The similarity of the fly OL to the mammalian cortex makes it an exceptional area of the brain that must be studied in depth. It has been reported that the expression, or lack thereof, of glial ligands can have profound implications for NECs and thus, as former progenitors, can also affect the development of the OL brain in larva. An example of this is the non-autonomous impact that the release of the protein Serrate in SPG provokes in the NEC Notch signalling pathway (Perez-Gomez et al., 2013). Another example of the glial repercussion on progenitor cells described in the OL arises from previous investigations in my laboratory. Those observations revealed that *miR-8*<sup>+</sup> surface-associated CG release a transforming growth factor (TGF- $\alpha$ )-like ligand, named Spitz (Spi), which acts on the epidermal growth factor receptor (EGFR) in neuroepithelium (Figure 11). The presence or absence of this ligand results in a modification of the subsequent neurogenesis that alters the size of the fly brain (Morante et al., 2013). This discovery is the basis of the present thesis, which attempts to go further and investigate novel glial signalling in the neuroepithelial niche.

In conclusion, and considering the active role of glia in progenitor niches shown here in different examples, I am going to address both types of signalling: glia-to-NECs and the resulting feedback. In the same vein, those signalling relationships are needed to be dealt with first per separate, and later put both in common in order to have an accurate picture of the two-way interrelationship.

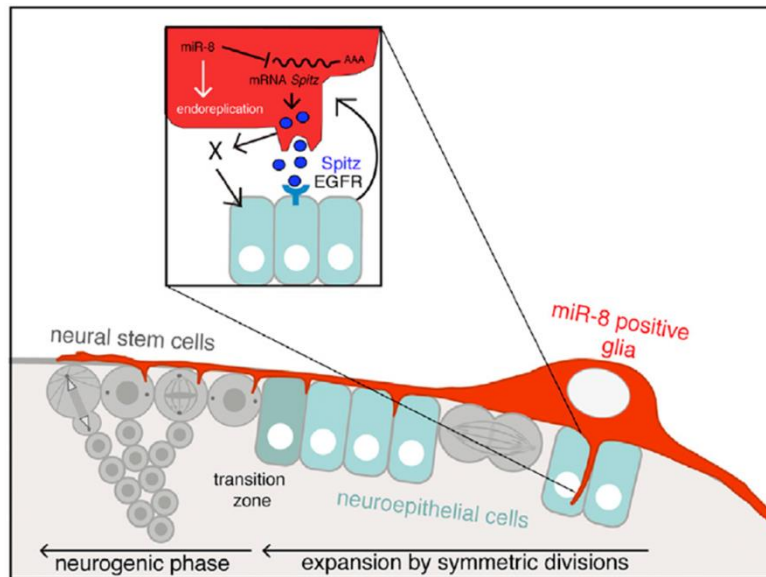


**Figure 11. Model of interactions between glial *miR-8*, Spitz expression and neuroepithelial EGFR for OPC neurogenesis.** The conserved microRNA *miR-8* increases cells' endoreplication in an autocrine manner, provoking an expansion of glial size and the ensheathing of neuroepithelium. *miR-8* also inhibits translation of the protein Spitz, whose normal function, once released, is to act in the EGFR of NECs. Thus, glia regulates neuroepithelial expansion and neuroblast transition in a paracrine manner. Feedback signalling also regulates glial cells via *rho* and *aos*. Adapted from Figure 9D Morante et al., 2013.









**OBJECTIVES / OBJETIVOS**

---



## Principal objective:

The general objective is expanding current knowledge of the functions of glial cells, specifically during early-maturing brain development where the suitable functioning of neuronal precursor cells is necessary for the proper growth of nervous tissue. Therefore, I use vanguard genomic techniques to undertake a massive genetic approach to discern genes involved in development which are important in the *Drosophila melanogaster* brain. Finally, I attempt to identify new signalling pathways and control mechanisms in the glial-neuroepithelial niche in the larva where the second wave of neurogenesis takes place and in which malfunctions would result in neurodegenerative or tumoural illnesses.

## Specific objectives:

1. Characterisation of the glial niche and the Gal4-drivers specific to neuroepithelial (*c855a*-Gal4) and glial (*cg25c*-Gal4) cells.
2. Separation and precise collection of genomic material from each cell population using the identification and fluorescent-associated cell sorting (FACS) technique.
3. Massive parallel sequencing of the genomic material using the next generation RNA sequencing (RNA-seq) technique and subsequent bioinformatics analysis of the transcriptome.
4. Identification of new glial and neuroepithelial interactive factors (receptors, ligands, transmembrane or secreted proteins, etc.) through a massive genetic validation of candidate genes looking for gain- and loss-of-function.
5. Characterization of the most phenotypically interesting genes identified in the niche as well as possible novel signalling and communication pathways that regulate brain growth.



## Objetivo principal:

El objetivo general es ampliar el conocimiento actual sobre las funciones que se le atribuyen a las células gliales y más específicamente en el desarrollo del cerebro inmaduro dónde es necesario un adecuado funcionamiento de las células precursoras neuronales para el propio crecimiento del tejido nervioso. Para ello, me he ayudado de técnicas genómicas de vanguardia para realizar un abordaje genético masivo y discernir aquellos genes implicados que son importantes en el cerebro de *Drosophila melanogaster*. Finalmente, me propongo identificar nuevas rutas de señalización y mecanismos de control derivados del nicho glía-neuroepitelio en larva que es cuando tiene lugar la segunda etapa de neurogénesis y por el que un mal funcionamiento puede derivar en enfermedades neurodegenerativas o tumorales.

## Objetivos específicos:

1. Caracterización del nicho glial y de los “drivers” Gal4 específicos de células neuroepiteliales (*c855a*-Gal4) y gliales (*cg25c*-Gal4) que los identifica.
2. Separación y obtención precisa del material genómico procedente de cada población celular utilizando la técnica de identificación y separación asociada a células fluorescentes (FACS).
3. Secuenciación masiva en paralelo del material genómico mediante la técnica de secuenciación de RNA de segunda generación (RNA-seq) y posterior análisis bioinformático del transcriptoma.
4. Identificación de nuevos factores gliales y neuroepiteliales de interacción (receptores, ligandos, proteínas transmembranales o secretadas, etc.) mediante una validación genética masiva de genes candidatos a través de su ganancia y falta de función.
5. Caracterización de los genes fenotípicamente más interesantes que han sido identificados en el nicho, así como las posibles vías de señalización y comunicación inéditas reguladores del crecimiento cerebral.





**MATERIALS AND METHODS**

---





# 1. Fly genetics

## 1.1. *Drosophila* husbandry

Flies were bred and kept on standard *Iberian* fly food at 25 °C and on a 12-hour light/dark cycle unless otherwise indicated. A copy of each stock was stored at 18 °C. The crosses where the thermosensitive allele Gal80 suppressor (*tub::Gal80<sup>ts</sup>*) controls transgene expression were first kept at 18 °C for transgene repression and then shifted to 29 °C for its activation. *w<sup>1118</sup>* or *y<sup>1</sup>w<sup>1118</sup>* fly lines were used as a wild-type strain unless otherwise indicated.

Flies for the Gal4/UAS binary system: *c855a-Gal4*, *cg25c-Gal4*, *mir-8<sup>NP5427</sup>-Gal4*, *NP2222-Gal4*, *NRT-Gal4*, *NP2776-Gal4*, *NP6293-Gal4*, *repo-Gal4*, *ase-Gal4*, *c831-Gal4*, *engrailed-Gal4*, *ppl-Gal4*, *lsp2-Gal4*, *phm-Gal4*, *Oamb-Gal4*, *Octβ1R-Gal4*, *Octβ3R-Gal4*, *tβh-Gal4*, UAS-H2B::RFP, UAS-mCD8::RFP, UAS-H2B::YFP, UAS-stinger::GFP, UAS-mCD8::GFP, UAS-destabilised-GFP (gift from Dr. Gary Struhl, Columbia University, NY, USA), UAS-HA::UPRT, UAS-*Dcr2*, UAS-*rpr*, UAS-*spitz*::GFP, UAS-*spitz*-RNAi, UAS-*cg25c*-RNAi, UAS-*viking*-RNAi, and UAS-*rpr*-IR.

Flies for the *lexA/lexAop* system: *repo-lexA*, and *lexAop-myr::GFP* (from Janelia Farm Collection, Howard Hughes Medical Institute, Ashburn, VA).

Other transgenic flies: *miR-8::lacZ*, *Viking::GFP*, *PPO1<sup>A</sup>,2<sup>A</sup>,3<sup>1</sup>* triple-mutant (from Dr. Lemaitre, Global Health Institute, Lausanne), *tub::Gal80<sup>ts</sup>*, *repo::Gal80* and *tsh::Gal80*.

A detailed description of the transgenic lines and stocks used in this project can be consulted in FlyBase (FB2018\_03, released Jun 19, 2018). The transgenic lines (UAS, TRIP RNAi, GD and KK) used for gene validation of the RNA-seq top-hits were obtained from Bloomington *Drosophila* Stock Centre (BDSC; Indiana University, Bloomington, IN, USA) and Vienna *Drosophila* Resource Centre (VDRC; Vienna Biocenter, Vienna, Austria) and the lines that resulted in abnormal phenotypes are described in Appendix II (Table S6).

## 1.2. Establishment of recombinant lines

*Drosophila*'s power of recombination allows for the combination of different alleles in the same chromosome. However, this recombination only occurs in females and their rate of recombination is dependent on the distance between genes. In order to carry out recombination, F1 heterozygous female virgins were selected and crossed again with males having balancer chromosomes to obtain the final recombinant stock. All stocks generated are available for my current lab and listed below (Table 1).

**Table 1. Genotype of recombinant fly stocks.**

chr. I	chr. II	chr. III
<i>y<sup>1</sup>w<sup>122</sup></i>	; <i>cg25c-Gal4 / CyO</i>	; <i>repo-lexA, lexAop-myr::GFP / TM6B</i>
<i>y<sup>1</sup>w<sup>122</sup></i>	; <i>cg25c-Gal4, tsh::Gal80</i>	; TM2 / TM6B
<i>y<sup>1</sup>w<sup>122</sup></i>	; <i>cg25c-Gal4, UAS-H2B::YFP / CyO</i>	; TM2 / TM6B
<i>y<sup>1</sup>w<sup>122</sup></i>	; <i>cg25c-Gal4, UAS-stinger::GFP / CyO</i>	; TM2 / TM6B
<i>y<sup>1</sup>w<sup>122</sup></i>	; <i>cg25c-Gal4, UAS-stinger::GFP / CyO</i>	; UAS-H2B::RFP / TM6B
<i>y<sup>1</sup>w<sup>122</sup></i>	; <i>cg25c-Gal4, UAS-stinger::GFP / CyO</i>	; UAS-mCD8::RFP / TM6B
<i>y<sup>1</sup>w<sup>122</sup></i>	; <i>cg25c-Gal4, UAS-stinger::GFP / CyO</i>	; UAS-HA::UPRT / TM6B
<i>y<sup>1</sup>w<sup>122</sup></i>	; <i>cg25c-Gal4, UAS-destabilised-GFP / CyO</i>	; TM2 / TM6B
<i>y<sup>1</sup>w<sup>122</sup></i>	; <i>cg25c-Gal4, UAS-destabilised-GFP / CyO</i>	; UAS-H2B::RFP / TM6B
<i>y<sup>1</sup>w<sup>122</sup></i>	; <i>cg25c-Gal4, UAS-mCD8::GFP / CyO</i>	; UAS-H2B::RFP / TM6B
<i>y<sup>1</sup>w<sup>122</sup></i>	; <i>cg25c-Gal4, lexAop-myr::GFP / CyO</i>	; <i>repo-lexA / TM6B</i>
<i>y<sup>1</sup>w<sup>122</sup></i>	; <i>Sp / CyO</i>	; <i>c855a-Gal4, UAS-destabilised-GFP / TM6B</i>
<i>y<sup>1</sup>w<sup>122</sup></i>	; <i>UAS-mCD8::RFP / CyO</i>	; <i>c855a-Gal4, UAS-destabilised-GFP / TM6B</i>
<i>y<sup>1</sup>w<sup>122</sup></i>	; <i>Sp / CyO</i>	; <i>c855a-Gal4, UAS-H2B::RFP / TM6B</i>
<i>y<sup>1</sup>w<sup>122</sup></i>	; <i>UAS-H2B::YFP / CyO</i>	; <i>c855a-Gal4, UAS-H2B::RFP / TM6B</i>
<i>y<sup>1</sup>w<sup>122</sup></i>	; <i>UAS-destabilised-GFP / CyO</i>	; <i>c855a-Gal4, UAS-H2B::RFP / TM6B</i>
<i>y<sup>1</sup>w<sup>122</sup></i>	; <i>UAS-mCD8::GFP / CyO</i>	; <i>c855a-Gal4, UAS-H2B::RFP / TM6B</i>
<i>y<sup>1</sup>w<sup>122</sup></i>	; <i>UAS-HA::UPRT / CyO</i>	; <i>c855a-Gal4, UAS-H2B::RFP / TM6B</i>
<i>y<sup>1</sup>w<sup>122</sup></i>	; <i>UAS-stinger::GFP / CyO</i>	; <i>c855a-Gal4, UAS-mCD8::RFP / TM6B</i>

$y^1w^{122}$	; lexAop-myr::GFP / CyO	; c855a-Gal4, UAS-mCD8::RFP, <i>repo</i> -lexA / TM6B
$y^1w^{122}$	; c831-Gal4, UAS-stinger::GFP / CyO	; UAS-H2B::RFP / TM6B
$y^1w^{122}$	; c831-Gal4, UAS-stinger::GFP / CyO	; UAS-mCD8::RFP / TM6B
$y^1w^{122}$	; c831-Gal4, UAS-mCD8::GFP / CyO	; UAS-H2B::RFP / TM6B

### 1.3. Supplementary fly methodologies

The traditional Gal4/UAS system (Brand and Perrimon, 1993) was used in combination with other related systems of transgene expression.

#### 1.3.1. LexA/LexAop system

This system is similar to the Gal4/UAS system and may be used together as a dual expression (Lai and Lee, 2006). In this system, the promoter transgene drives the expression of a LexA sequence (LexA::VP16 or LexA::GAD). When the LexA gene is translated, the protein binds to another transgene LexA operator sequence (LexAop) which finally activates the reporter gene. The LexA driver expression can be suppressed by the Gal80ts protein. Modified forms of the initial methodology expand the capacity of this technique (Du et al., 2017).

#### 1.3.2. FLP-Out clonal analysis

This system is based on complex transgenes carrying the Gal4/UAS system. Using the yeast protein Flippase (*flp*), a site-specific recombinase, gives the FLP-FRT recombination capacity to a FLP-out cassette that labels a subset of Gal4-positive cells. The FLP-out activation can be generated by either Gal4-FLP-out or UAS-FLP-out (Ito et al., 1997; Struhl and Basler, 1993). In my experiments, the hsp70 promoter was driven the expression of the *flp* gene ( $y^1w^{1118}$ -hsp::*flp*; Act::FRT- $y^+$ -FRT::Gal4, UAS-GFP; UAS-H2B::RFP/TM6B) and this leads to express also another RNAi gene of the experiment (UAS-*Xgene*-RNAi). Therefore, the recombinase was activated when L1 larvae were heat-shocked at 37 °C for 10 min and express fluorescence in cells that were undergoing division. Larvae were fixed in the late 3<sup>rd</sup> instar (120 h after egg laying (AEL)) and their brains were dissected. The cells expressing the reporter gene were visualized under a confocal microscope after immunostaining with standard protocols.

#### 1.3.3. Coupled MARCM analysis

Clonal analysis using coupled-MARCM (Potter 2010), an upgrade of the traditional mosaic analysis with a repressible cell marker technique (Lee and Luo, 1999), enables the labelling of both progeny cells from a dividing cell with different colours. This technique uses the promoter of the ubiquitous gene *tubulin* (*tub*) to drive the expression of the yeast repressor proteins GAL80 (repressor of GAL4) and QS (repressor of QF). In my experiments, transgenic larvae ( $y^1w^{1118}$  tub-QS13F FRT19A/tub-GAL80 hsp-FLP FRT19A; QF-ET40 QUAS-mtdTomato/+; c558a-GAL4 UAS-GFP/UAS-Fas2-RNAi<sup>34084</sup>) were heat-shocked at 37 °C for 1 h during the 1<sup>st</sup> instar (24-48 h AEL) to induce twin clone formation. Therefore, in the same mitotic recombination event in the X chromosome, twin clones were labelled with two different colours: the control cell clone in red, and the mutant cell clone expressing the Fas2 RNAi in green. Finally, larvae were fixed in the late 3<sup>rd</sup> instar (120 h AEL) and brains were dissected, immunostained with standard protocols, and mounted to be visualized under a confocal microscope.

### 1.4. Image acquisition

Images of *Drosophila* larvae and adult flies were captured with an optical microscope Zeiss Axiophot using a MicroPublisher 5.0 camera (QImaging) and the corresponding software QCapture (QImaging). Several specimens were used to obtain a representative organism.

## 2. Immunohistochemistry and image analysis

### 2.1. Immunohistochemistry procedure

Immunohistochemistry staining was used to evaluate the effects of genetic manipulation in larval fly tissues (CNS, ring-glands, imaginal discs and fat body). First, larvae were dissected in cold phosphate-buffered saline (PBS) and fixed in 4% paraformaldehyde (PFA) for 20 minutes (Morante and Desplan, 2011). Later, they were incubated overnight with primary antibodies (Table 2) and stained for 3 h with secondary antibodies (Table 3). Different staining was used to identify certain cell types: anti-repo for glial cells; anti-Moody- $\beta$  for SPN glia; anti-DE-Cad, anti-Dlg1 and anti-Patj for neuroepithelia; anti-elav for neurons; and anti-mira for neuroblasts. Also commonly used were anti-PH3 to identify proliferative mitotic cells, anti-MAPK for proliferative cells via EGFR, and anti-Cas3 for apoptotic cells. Other antibodies used were anti- $\beta$ -Gal, anti-GFP, anti-DsRed and anti-HA to identify reporter expression. To show intracellular lipid droplets, 45 minutes of staining with Nile Red (Invitrogen, dilution 1:500) was performed. All cell nuclei were counterstained with DAPI (Invitrogen, 0,3  $\mu$ g/ml). Finally, tissues were mounted in Vectashield (Vector Labs) and maintained their three-dimensional structure (Morante and Desplan, 2011).

**Table 2. Primaries antibodies.**

Antigen	Host Specie	Source	Working Dilution
$\beta$ -Galactosidase ( $\beta$ -Gal)	rabbit	Cappel	1:10000
Caspase 3 (Cas3)	rabbit	Upstate	1:500
DE-Cadherin (DE-Cad)	rat	DSHB	1:50
Disc large 1 (Dlg1)	mouse	DSHB	1:100
DsRed	rabbit	Clontech	1:500
Embryonic lethal abnormal vision (Elav)	rat	DSHB	1:50
GFP	rabbit	Abcam	1:1000
Hemagglutinin (HA)	mouse	Sigma-Aldrich	1:500
Hemagglutinin (HA)	rabbit	Abcam	1:500
Miranda (Mira)	mouse	(Ohshiro et al., 2000)	1:50
Moody- $\beta$	rat	From U. Gaul	1:200
Patj	rabbit	(Bhat et al., 1999)	1:2000
Phospho-Histone 3 (PH3)	rabbit	Sigma-Aldrich	1:2000
Phospho-p44/42 MAPK (MAPK)	rabbit	Cell Signaling Technology	1:500
Reversed polarity (Repo)	mouse	DSHB	1:50

**Table 3. Secondary antibodies.**

Antigen	Fluorophore	Source	Working Dilution
mouse	Alexa 488	Thermo Fisher Scientific	1:500
mouse	Alexa 555	Thermo Fisher Scientific	1:500
mouse	Alexa 633	Thermo Fisher Scientific	1:200
mouse	Alexa 647	Thermo Fisher Scientific	1:200
rabbit	Alexa 488	Thermo Fisher Scientific	1:1000
rabbit	Alexa 555	Thermo Fisher Scientific	1:1000
rabbit	Alexa 647	Thermo Fisher Scientific	1:500
rat	Alexa 488	Thermo Fisher Scientific	1:500
rat	Alexa 555	Thermo Fisher Scientific	1:500
rat	Alexa 647	Thermo Fisher Scientific	1:200

### 2.2. Microscopy image capture and processing

Images of *D. melanogaster* larval tissues (CNS, ring glands, imaginal discs and fat body) were obtained using mainly a Leica TCS SP2 confocal microscope. Pictures of larval brains were taken in horizontal view unless otherwise indicated. Routinely, images of dimensions 1024x1024 pixels were acquired using a 20x dry objective and stacks within intervals of 1  $\mu$ m in Z axis in LCS software. Files were saved in .tiff format. Detailed images of areas of tissue preparation were obtained with the superresolution microscope Zeiss LSM880 Elyra PS.1. Larval full brain multiview light sheet fluorescence images were obtained with Zeiss Lightsheet Z.1. The Z reconstruction for a movie of cell-specific drivers in both microscopes was done with ZEN Black software. Image analysis (maximum projection images of Z-stacks, channels merge and videos) was carried out using ImageJ open source image-processing software (Schneider et al., 2012).

### **3. Flow cytometry**

#### **3.1. Tissue dissociation into individual cell**

For transcriptome profiling, larval brain cells first need to be disaggregated and isolated. Transgenic larvae of late L2 stage (64-to-72 h AEL at 25 °C) and late L3 stage (104-to-120 h AEL at 25 °C) expressing GFP or RFP fluorescence under the control of either a neuroepithelial driver (*c855a-Gal4*) or glial driver (*cg25c-Gal4*) were collected. Then, they were dissected under a stereomicroscope and brain lobes were collected in tubes with cold PBS. From this moment, tissue disaggregation was carried out following an adapted protocol for FACS (Harzer et al., 2013). Finally, the reagent 7-aminoactinomycin D (7-AAD, Merck, 0,025 µg/ml) was added several minutes before the sorting in order to enable exclusion of dying cells.

#### **3.2. Fluorescence-activated cell sorting**

After the cells were properly dissociated, they passed by a FACS sorting apparatus (FACSaria™ III, BD; Figure 3). The strategy followed was gating cell populations which were plotted in scatter graphs (Figure S3). Firstly, plotting events in the side scatter area (SSC-A) and the forward scatter area (FSC-A, log) was allowing to obtain a population (P1) from which debris and dead cells as well as cell clusters were discarded. Then, SSC width versus height excluded cells by complexity, isolating a second cell population (P2). Next, FSC width versus height removed cells by size and separated out a third population (P3). At this point, signals from cells excited with fluorescent lasers were needed. The laser phycoerythrin (PE-Cy5, log) determined 7-AAD<sup>+</sup> cells which indicated that were dying or had compromised membranes; this allowed for their remove and the plotting of the subset of events that consists only of individual living cells (P4). Next, the 488-nm (GFP FITC-A, log) and the 555-nm (RFP PE-Texas Red-A, log) lasers consecutively or separately grouped the double fluorescent population of interest. Finally, 35.000 sorted cells were collected in cooled 1,5 ml RNase-free tubes which were containing PBS for cell culture or lysis buffer for RNA extraction. Per larval brain, I was able to sort ~55 NECs and ~75 glial cells at late L2 stage and respectively ~290 and ~175 at late L3 stage.

### **4. Cell culture**

#### **4.1. Cell culture procedure**

Larval brain fluorescent cells in suspension before and after sorting by FACS (Harzer et al., 2013) were cultured in Schneider's *Drosophila* medium (Invitrogen) which was supplemented with 10% heat-inactivated fetal bovine serum (FBS, Merck), 0,02 mg/ml of insulin (Merck), 2% penicillin-streptavidin (Merck), 20 mM of l-glutamine (Merck) and 0,04 mg/ml of l-glutathione (Merck). Cells were settled for 1 hour at 25°C in an incubator without humidity nor ambient CO<sub>2</sub> (adapted from Ceron et al., 2006).

#### **4.2. Staining of cultured cells**

Cells in culture were immediately stained for 1h to label their nuclei. Dying cells were identified with DAPI (Invitrogen, 0,3 µg/ml) whereas living cells (as well as dying cells) with the membrane permeable Hoechst 33342 (Invitrogen, 1 mg/ml).

#### **4.3. Microscopy image capture and processing**

Pictures of cultured cells were taken 1 hour after staining treatments with a fluorescent inverted Leica DM IRB microscope using a 40x objective and LAS v4.3 Leica software.

## **5. RNA extraction, retrotranscription and quantitative PCR**

### **5.1. RNA extraction**

Different extraction protocols are used to extract RNA from FACS sorted cells depending on the final purpose of the RNA.

To quantify mRNA levels by quantitative polymerase chain reaction (qPCR), sorted cells were collected in 750  $\mu$ l of TRIzol (Invitrogen) and frozen at -80 °C until downstream application. The RNeasy Mini kit (Qiagen, ref. #74106) was used under manufacturer standards protocol for total RNA purification. A DNase treatment was applied to eliminate remaining DNA (TURBO DNA-free kit, Applied Biosystems, ref. #AM1907) and sample's concentration was performed with RNeasy MiniElute Cleanup kit (Qiagen, ref. #74204). The final RNA was eluted in RNase-free water, frozen with liquid nitrogen and stored at -80 °C until use.

Sorted cells used for next generation sequencing were directly collected in cold 1,5 ml tubes containing 200  $\mu$ l of RLT lysis buffer with  $\beta$ -mercaptoethanol ( $\beta$ -ME), quickly frozen with liquid nitrogen and stored at -80 °C until use. The process for RNA purification was similar to that which was previously described, however this time the RNeasy Micro RNA kit (Qiagen, ref. #74004) was used following the manufacturer's protocol. RNA samples were stored as previously described.

### **5.2. Total mRNA quantification and quality determination**

The total amount of RNA present in the samples was necessary to be determined. The spectrophotometer NanoDrop® ND-1000 was used for samples of an estimated amount of 100-to-3.000 ng/ $\mu$ l. For samples whose estimated concentration was lower, the fluorometer Qubit® 2.0 (Invitrogen) was needed. For samples containing around 1-100 ng/ $\mu$ l of RNA, the Broad Range (BR) assay kit (Invitrogen, ref. #Q10210) was used; for samples containing between 250 pg/ $\mu$ l and 100 ng/ $\mu$ l, the RNA High Sensitivity (HS) kit (Invitrogen, ref. #Q32852) was used.

It was also necessary to assess the quality of the RNA samples using the 2100 Bioanalyzer (Agilent Technologies). A range of 50-to-5.000 pg/ $\mu$ l was measured using chips from the RNA 6.000 Pico kit (Agilent Technologies).

Additionally, the integrity of the high concentration RNA samples was measured by electrophoresis on a denaturing formaldehyde agarose gel. First, the gel was prepared with 1% agarose, 10% 10X MESA running buffer and 25  $\mu$ l of RedSafe™ Nucleic Acid staining reagent (iNtRON Biotechnology). Second, 1  $\mu$ g of sample and 2  $\mu$ g of RNA Millennium™ molecular weight markers (Ambion) were prepared by adding 1X NorthernMax® formaldehyde load dye (Life Technologies) and incubating for 15 minutes at 70 °C. The samples and markers were loaded into a gel full covered with 1X MESA running buffer and electrophoresis was run in the dark at 80 V for 1,5 hours. Finally, the gel was visualised using a UV transilluminator Alphamager™ 2200 system (Alpha Innotech Corporation). Note that *Drosophila* rRNA is an exception to eukaryotic norms in that its 28S band splits into two fragments of similar weight as the 18S band; thus, one large unique band is detectable and the RIN value is not available.

### **5.3. Retrotranscription and quantitative PCR**

1 $\mu$ l of RNA was retrotranscribed to cDNA with SuperScript III Reverse Transcriptase (Invitrogen) and Oligo(dT) Primers (Invitrogen). Standard real-time PCR (qPCR) was performed with 10 ng of template cDNA, Power SYBR Green PCR Master Mix (Applied Biosystems) and gene-specific primers (Table 4) read on 7500 Real-Time PCR System (Applied Biosystems) with the conditions: 10 minutes at 95 °C followed by 40 cycles of 15 seconds at 95 °C and 40 seconds at 60 °C. Rp49 primers of *Drosophila* endogenous ribosomal protein expression levels were used for the normalisation of results. Triplicate samples per each condition as well as technical triplicates were performed and the relative gene expression was normalised by  $\Delta$ Ct analysis. The gene primer design was done using the Primer Quest® tool (IDT, <http://www.idtdna.com/PrimerQuest/Home/Index>). The data is shown as mean  $\pm$  standard error of mean (SEM), and was statistically analysed with repeated ANOVAs, considering a P-value of < 0,05 to be statistically significant.

Table 4. Primers pairs for qPCR.

Gene	Forward sequence (5' to 3')	Reverse sequence (5' to 3')
<i>rp49</i>	TGTCCTTCCAGCTTCAAGATGACCATC	CTTGGGCTTGCGCCATTTGTG
<i>rfp_1</i>	GACTACTTGAAGCTGTCTTCC	CGCAGCTTCACTTGTAGAT
<i>rfp_2</i>	TGAGGTCAAGACCACCTACA	CTGTTCCACGATGGTGTAGTC
<i>gfp_1</i>	GAACCGCATCGAGCTGAA	TGCTTGTGGCCATGATATAG
<i>gfp_2</i>	GCACAAGCTGGAGTACAACCTA	TGTTGTGGCGGATCTTGAA
<i>cg25c</i>	GATCGCGGGAGCGTTAGTC	TCACGGAGTCCTGAATCGAAC
<i>repo</i>	TCGCCACCTATGTGACCAAG	CGGCGCACTAATGTAICTCG
<i>DE-Cad</i>	GAATCCATGTCGGAAAATGC	GTCCTGGCGCTGATAGTCA
<i>mira</i>	CCCAATTGGAGCTGGACAACA	GGTGTTCACAGCAGAGAGG
<i>elav</i>	CGCACCATTGGAGCAATAAT	AGGCAATGATAGCCCTTGTGG

## 6. RNA sequencing

Total mRNA from 12 FACS sorted samples was processed. The samples belong to four conditions, neuroepithelial or glial and late-L2 IL or late-L3 IL, with three biological replicates per each condition. All the steps of this technique were performed at the Genomics Core Facility (Gencore) of the European Molecular Biology Laboratory (EMBL) in Heidelberg, Germany and supervised by the head of the facility, Dr. Vladimir Benes.

### 6.1. cDNA library preparation

1 ng of total RNA of each sample was processed. Such low amount of input requires a high yield of high quality library which was performed using the NEBNext® Ultra™ II directional RNA library prep kit for Illumina® (New England BioLabs, ref. #E7760) which uses the dUTP method (Levin et al., 2010; Parkhomchuk et al., 2009) for strand-specificity. The library preparation workflow was divided into two parts: first, the cDNA synthesis from the original total RNA; and second, the library construction from the purified double-stranded cDNA (ds cDNA). The first part consisted of ribosomal RNA removal by poly(A) mRNA enrichment with magnets, mRNA fragmentation and random priming, first strand synthesis, second strand synthesis using the dUTP method, and ds cDNA clean-up. The second part consisted of an end repair and dA-tailing, adaptor ligation (dilution 1:300), uracil excision for strand-specificity, clean-up the smaller fragments, 20 cycles of PCR amplification incorporating barcodes to enable multiplexing (Table 5) and enriched library by a clean-up. Then, samples were ready for cluster generation and sequencing.

Table 5. Barcodes/Index sequences for pooling and multiplexing.

<i>c855a</i> <sup>+</sup> late L2	Index Seq. (5' to 3')	<i>cg25c</i> <sup>+</sup> late L2	Index Seq. (5' to 3')
<b>Sample 1:</b>	GATCAG	<b>Sample 4:</b>	CGATGT
<b>Sample 2:</b>	ACAGTG	<b>Sample 5:</b>	GCCAAT
<b>Sample 3:</b>	ATCACG	<b>Sample 6:</b>	TAGCTT

<i>c855a</i> <sup>+</sup> late L3	Index Seq. (5' to 3')	<i>cg25c</i> <sup>+</sup> late L3	Index Seq. (5' to 3')
<b>Sample 7:</b>	TTAGGC	<b>Sample 10:</b>	TGACCA
<b>Sample 8:</b>	ACTTGA	<b>Sample 11:</b>	CTTGTA
<b>Sample 9:</b>	GGCTAC	<b>Sample 12:</b>	CAGATC

### 6.2. cDNA quantification and library quality

To continue with the procedure, it was necessary to determine the concentration and quality of the cDNA library. Firstly, the concentration was measured with the fluorometer Qubit® 2.0 (Invitrogen) using the dsDNA High Sensitivity (HS) kit (Invitrogen, ref. #Q32854) able to detect samples of around 0,2 ng/μl and 100 ng/μl. Then, the quality of the cDNA samples was assessed with the 2100 Bioanalyzer (Agilent Technologies). An estimated range of 0,5-to-50 ng/μl was measured by chips from the DNA 1.000 kit (Agilent Technologies).

### 6.3. RNA sequencing and data quality control

A concentration of 4nM was used for cluster amplification and 1,8 pM was loaded onto a last generation Illumina® sequencer NextSeq 500 High using a read length cycle of 1 x 85 bp (+ 7 bp for barcodes) single-end sequencing run (Flow Cell ID #HFWJ2BGX3) with demultiplexing. The output data was given in FASTQ files.

The quality control of the sequencing run was performed with MultiQC v1.0 software (Ewels et al., 2016) using the tool FastQC v0.11.5 (created by Dr. Simon Andrews, Babraham Institute, Cambridge, UK). This allowed for the visualisation of quality reports of the sample sequences, which gave valuable information such as barcode distribution, general statistics (sequence length, total reads counts or duplicate reads), GC content, adapter content, overrepresented sequence and Phred quality score. Note that Phred logarithmic value (Ewing and Green, 1998) was the most valuable statistic and was obtained with the following equation:  $q = -10 \times \log_{10}(p)$ , where  $q$  is the Phred value and  $p$  is the estimated error probability for the base-call.

In order to manage raw data from the RNA-seq I used command-lines, small programs that perform specific functions, through the software MobaXterm (Mobatek®), a toolbox for remote computing.

To visualise sequenced reads, the *Drosophila melanogaster* reference genome sequences (FASTA files) and annotations (GTF files) were first downloaded from the Ensemble Project database (EMBL-EBI, Cambridge, UK). Afterwards, the tool STAR v2.4.2a (Spliced Transcripts Alignment to a Reference) generated the genome indexes (Dobin et al., 2013) and used them for mapping sequenced reads (FASTQ files) to the reference genome. Also, the reads within the gene were transformed by this tool to a total of counts per gene. The output data (BAM files) were used in the IGV v2.4.4 program (Interactive Genome Viewer) for visualising the transcript expression pattern of the samples (Robinson et al., 2011; Thorvaldsdóttir et al., 2012).

## 7. Bioinformatics analyses

Differential expression analysis was done with the free R programming language (GNU project) with the software RStudio v3.4.0 under the interface RStudio Server Spinoza v1.1.456 (GBCS-EMBL). A mix of command-lines and packages (or libraries) from CRAN or Bioconductor v3.6 (Gentleman et al., 2004; Huber et al., 2015) open source projects was used for data processing (Table S1).

The Gene Ontology (GO) analysis was performed using R programming language (Table S1). The FlyBase.org webpage together with several on-line tools and platforms were used to test the data in the different GO experiment steps. For GO hierarchy: Superfamily v1.75 (<http://supfam.org/SUPERFAMILY/>; Fang and Gough, 2013; Gough et al., 2001), QuickGO (<https://www.ebi.ac.uk/QuickGO/>; EMBL-EBI) and AmiGO2 (<http://amigo.geneontology.org/amigo/>; GO Consortium, 2017; GO Consortium et al., 2000). For molecular interaction, networks and pathways visualisation: BioMart (<https://www.ensembl.org/biomart>; Ensembl EMBL-EBI), Reactome (<https://reactome.org/>; Fabregat et al., 2018) and Cytoscape v3.6.0 (Cytoscape Consortium, NIGMS). For protein-protein interactions: STRING v10.5 ([www.string-db.org](http://www.string-db.org); SIB, CPR-NNF, EMBL). For Venn diagrams: Venny v2.1.0 (<http://bioinfogp.cnb.csic.es/tools/venny/>; Oliveros, 2009) and Venn diagrams from BEG (<http://bioinformatics.psb.ugent.be/webtools/Venn/>; VIB-UGent).

## 8. Gene validation

The function of the 151 candidate genes discovered in the bioinformatics analysis were validated in niche cells. The validation was performed using the Gal4/UAS system to overexpress (UAS lines) and underexpress (RNAi lines) those genes in NECs (*c855a-Gal4*) and glia (*cg25c-Gal4*). Each gene was tested with two to five different mutant lines from BDSC and VDRC stocks centres. Genes with abnormal phenotypes in development (e.g. temporal stage mismatch, organ development, cell cycle death or premature lethality) were separated and re-tested (Table S6). Finally, those genes that were biologically interesting were analysed in detail in order to understand the functional relevance for the brain niche cells.

## **9. Climbing assay**

A group of 10 newborn (from 0-24 h AEL) flies, 5 males and 5 females, were transferred into a new tube with fresh food where they stayed for 24 h (three vials per genotype). Then, every 2-3 days, the climbing activity of each group was tested during a total of 16 days. The flies were transferred into a new 15 cm-tall tube without being anaesthetised with CO<sub>2</sub>. After allowing flies to recover for a while, the tube was tapped five times to send the flies to the bottom and then they were allowed to begin climbing the sides of the tube. This process was performed five times in a row and recorded on video with a Logitech webcam and the CyberLink YouCam 5 software. Then, after the first 5 seconds of climbing, the average height climbed for each fly (in cm) was annotated. Three replicate trials were carried out for each condition, and wild-type flies were used as controls. Adult flies with abnormal phenotypes in climbing the tube walls demonstrated locomotor deficiencies that were produced by dysfunctional genes; these dysfunctions may lead to neurodegenerative diseases.

## **10. Larval age determination**

### **10.1. Measurement of developmental timing**

Flies were allowed to mate and lay eggs for 6 hours at 25 °C and then transferred to a fresh tube. The progeny were grown at 25 °C until desired stage of development and their age was measured in hours AEL, when adult flies are removed from the tube.

### **10.2. Larva size measurements**

Larvae grown for developmental time measurements were collected from tubes and frozen at -80 °C for several hours to several days in order to immobilize them and make photographing easier. The larvae were then photographed in a standard fashion using a Leica MZ16 FA fluorescence stereomicroscope (model MSV269, Leica Microsystems) at zoom 7,12x and a MicroPublisher 5.0 camera (model MP5.0-RTV-R-CLR-10-C, QImaging). The photos were captured using the software QCapture Pro (Roper Technologies). All pictures were taken with a scale bar for a length (L) and width (W) measurements and the larval volume (V) of 15 larva in triplicate per condition was calculated according to the following formula:  $V=(4/3)\pi(L/2)(W/2)^2$  (Vallejo et al., 2015).

### **10.3. Jaws assay**

The larvae used for the larval size assay were then dissected in distilled water to obtain the jaws, which were cleaned of as much tissue as possible. The jaws were then mounted on slides in drops of glycerol in the same order in which the larvae were previously photographed so as to enable the comparison of each larva's overall size with its own mandible. Once mounted, the larval jaws were photographed at zoom 40x using a Leica DM4000 B microscope (Leica Microsystems), a QICAM 12-Bit Fast 1394 digital camera (model QIC-F-M-12, QImaging), and the software NeuroLucida Version 2018 (MBF Bioscience). The larval age in *Drosophila* was determined by the size of the jaws and the number of teeth of 15 larvae in triplicate per condition (Alvarez et al., 2017; Jakobs et al., 2017; Roberts, 1998).

## **11. Feeding assay**

Tubes with standard Iberian fly food were heated in the microwave until the food liquefied, and then ~50µl of blue food colouring was added and mixed into the food in each tube. After cooling, adult flies were placed in the tubes and allowed to reproduce. The larvae that hatched from these crosses were then photographed at different stages using a Leica MZ16 FA fluorescence stereomicroscope (model MSV269, Leica Microsystems) at zoom 7,12x and a MicroPublisher 5.0 camera (model MP5.0-RTV-R-CLR-10-C, QImaging).





## **RESULTS**



# 1. Glial niche characterisation in a *Drosophila* larval brain

## 1.1. Assess *c855a*-Gal4 as larval brain driver for neuroepithelial cells

It is important to properly characterise niche cells. In this thesis, I focus on the area that delimitates the outer proliferation centre (OPC) from the optic lobe (OL) in which occurs cell proliferation. During recent years, the *c855a*-Gal4 promoter has been thoroughly used in the fruit fly to study neuroepithelial precursor cells (Egger et al., 2007, 2010; Gold and Brand, 2014; Guillermin et al., 2015; Morante et al., 2013; Perez-Gomez et al., 2013; Reddy et al., 2010; Wang et al., 2013).

Originally, the transposable element *c855a* is inserted in the 3<sup>rd</sup> chromosome (Manseau et al., 1997). A meticulous description of its expression in *Drosophila* (Hrdlicka et al., 2002) did not note any signalling in the embryo. In female adult flies, however, *c855a*-Gal4 is perceived in the posterior terminal cells and the columnar cells of ovaries. In males, it is associated with the seminal vesicle that connects the testis to the seminal duct and with the muscle cells that ensheath the testis. During larval stages, the driver is localized in *DE-Cad*<sup>+</sup> cells identified as the epithelium (Figure 12). For example, in imaginal discs, the peripodial membrane of eye-antennal disc (Figure 12B) and leg discs are perceived as well as the central anterior/posterior boundary of wing discs, but not in haltere discs. Simultaneously in the central neural system (CNS), OPC and inner proliferation centre (IPC) neuroepithelial cells (NECs; Figure 12A) within each larval stage are also shown with the driver (Chen et al., 2014; Egger et al., 2007; Wang et al., 2011).

In order to identify the cells in which the *c855a*-Gal4 driver is active in the larval brain, I used conventional fluorescent proteins under the control of a UAS reporter transgene (Figure 13). I observed that both nuclear (Figure 13A,B) and membranaral (Figure 13C,D) fluorescence undergo the phenomenon of *Lineage Perdurance*. This type of inheritance happens when a very stable protein (the nucleus has high perdurance while the membrane has moderate) is expressed in progenitor cells and inherited by offspring during neurogenesis. Thus, the protein will remain present even if the mRNA encoding is absent. The fluorescent cells visible by the *c855a*-Gal4 expression (Figure 13) indicate both, a present expression for some cells as well as a past synthesis of histones and transmembrane glycoprotein for other cells. Therefore, classical fluorescent proteins highlight not only the NECs but also all the optic lobe progeny (Figure 13B',D').

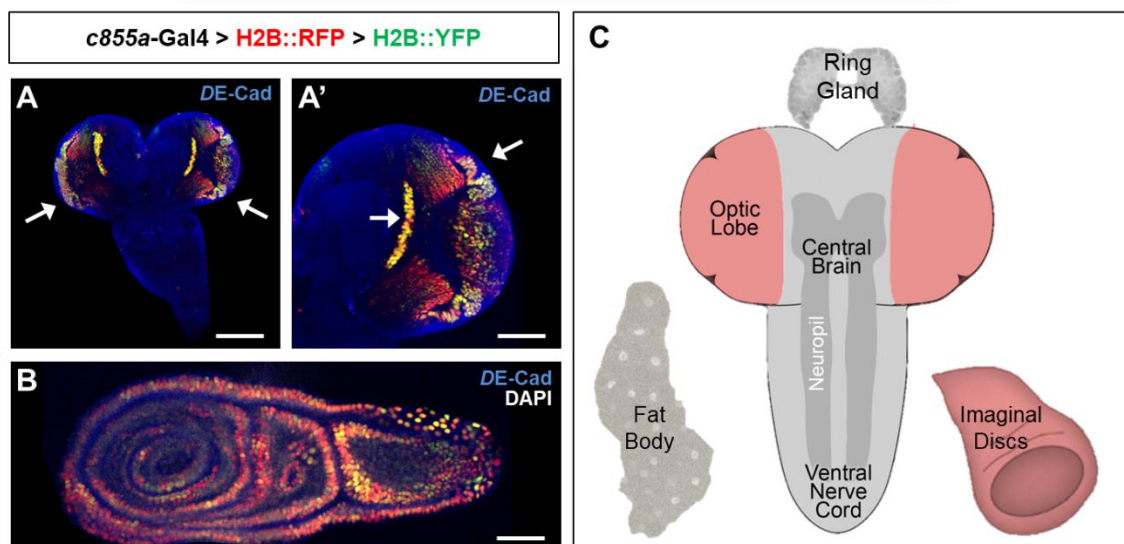


**Figure 12. *c855a*-Gal4 driver expression pattern in *Drosophila* larvae corroborates specificity for imaginal discs and the brain's optic lobe.** Confocal images show that the driver *c855a*-Gal4 expression is region-specific during larval stages. (A-C) There are two tissues highlighted when *c855a*<sup>+</sup> cells express the nuclear fluorescent markers UAS-H2B::RFP (red) and UAS-H2B::YFP (green): the optic lobe (A-A') and imaginal discs (B). Epithelial cells (arrows) from these two regions stained with anti-*DE-Cad* antibody (blue) are precursor cells of these tissues. (C) Schematic representation of the areas in which *c855a*-GAL4 is expressed in larvae (red): the eye-antennal, wing and leg imaginal discs (Hrdlicka et al., 2002) and the proliferative centres of the brain optic lobe (Egger et al., 2007). Images were taken from late 3<sup>rd</sup>-instar larvae. Scale bars represent 150  $\mu$ m in (A) and 50  $\mu$ m in (A' and B).

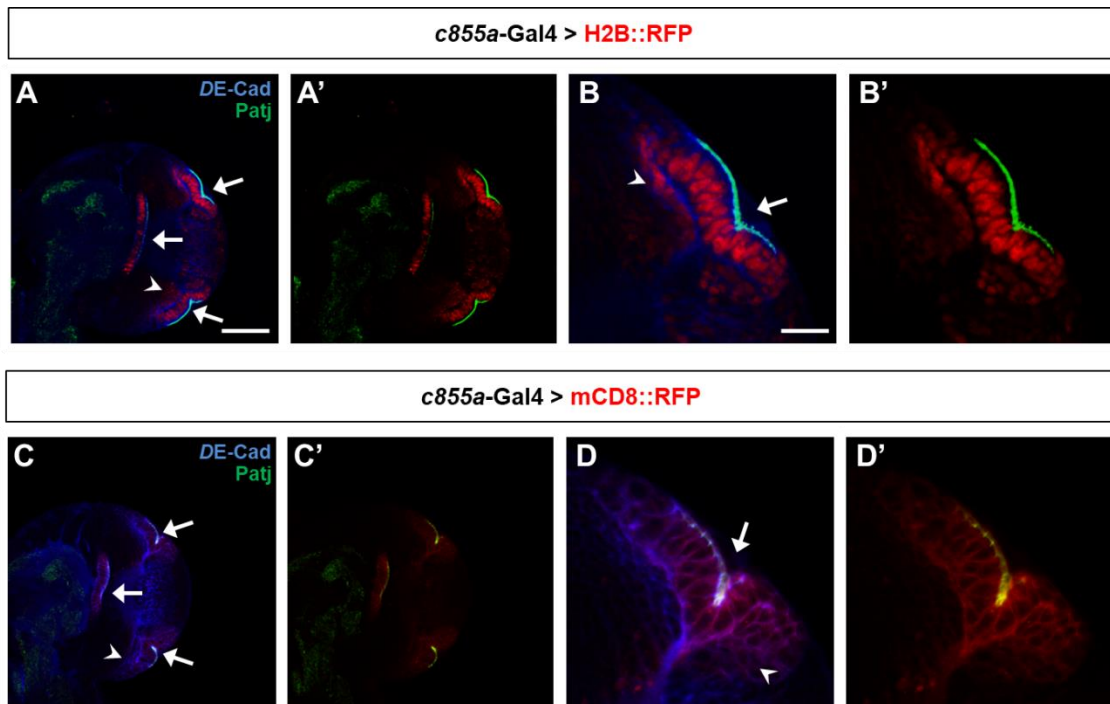


**Figure 13. Fluorescence perdurance for the *c855a-Gal4* driver marks neuroepithelia and its progeny.** Microscope images show that the Gal4 expression is inherited by the progeny of neuroepithelial cells (NECs) as indicated by commonly used nuclear (histone) and membrane (transmembrane glycoprotein) fluorescent proteins. (A-D) NECs stained with anti-DE-Cad antibody (blue) and anti-Patj antibody (green), on their apical zones, are some of the cells highlighted with fluorescence expression (red). A nuclear UAS-H2B::RFP (A-A',B-B') or a membrane UAS-mCD8::RFP (C-C',D-D') reporter are not able to distinguish cells which currently express the promoter (arrows) from their progeny (arrowheads) due to the phenomenon of perdurance. Images were taken from late 3<sup>rd</sup>-instar larvae. Scale bars represent 50  $\mu\text{m}$  in (A) and 20  $\mu\text{m}$  in (B).

To solve the problem of *c855a-Gal4* fluorescent signal persistence in cell progeny, I tested an unstable form of GFP (Lieber et al., 2011). The transgene generated with a short half-life coding sequence of the fluorescent protein under the control of a reporter (UAS-destabilised-GFP) indicates only current *c855a-Gal4* expression. The destabilised-GFP reporter has been found to show a far more accurate signal of transcriptional activity than those produced by commonly used fluorescent proteins (Atkins et al., 2013; Karandikar et al., 2014). In my experience, using the *c855a-Gal4* promoter to drive expression of the destabilised-GFP protein (Figure 14) highlights the NECs residing in the proliferative centres of the larval *Drosophila* optic lobe (Figure 14A,B) but not their descendent stem cells (Figure 14C,D). All in all, working with the short-lived fluorescence reporter allowed me to uniquely identify the neuroepithelium and not its offspring (Figure 14E,F), therefore resolving the lineage perdurance issue.

Finally, it was necessary to characterize *c855a-Gal4* expression throughout larval development (Figure 15). In order to confirm the pattern I observed with the destabilised-GFP in a late 3<sup>rd</sup>-IL (Figure 14), I took advantage of the short-lived expression of the enzyme uracil phosphoribosyltransferase fused together with hemagglutinin (UAS-HA::UPRT). This enzyme (Miller et al., 2009) will be activated in the neuroepithelium when new mRNA is synthesized. I observed that the enzyme is expressed in all NECs in late 3<sup>rd</sup>-IL (Figure 15A,B). Although expression is uniform at this stage, it is varied earlier in development. The *c855a* driver is distinctly activated in different NECs in early 3<sup>rd</sup>-IL. This may be because the driver is intermittently expressed or because its expression varies depending on at which point each cell is in the cell cycle (Figure 15C,D).

**Figure 14. *c855a-Gal* exclusively highlights the neuroepithelium with an unstable fluorescent protein.** Confocal images reveal the neuroepithelial-specific signal that marks the *c855a-Gal4* driver with short-lifespan fluorescence (Lieber et al., 2011) and resolves the issue of lineage perdurance. (A-A',B-B') The unstable fluorescence expression (green) highlights neuroepithelial cells (NECs; arrows) marked with anti-DE-Cad antibody (blue) and anti-Patj antibody (red), on their apical zone. (C-C',D-D') Otherwise, the neuroblasts tagged by anti-Mira antibody (in red, arrowheads) generated are not labelled with the destabilised-GFP. (E-E',F-F') The lineage perdurance phenomenon caused by common fluorescence (UAS-CD8::RFP) is solved with the new fluorescent protein because it uniquely tags NECs (arrows) and not their offspring (arrowheads). Images were taken from late 3<sup>rd</sup>-instar larvae. Scale bars represent 50  $\mu\text{m}$  in (A) and 20  $\mu\text{m}$  in (B).

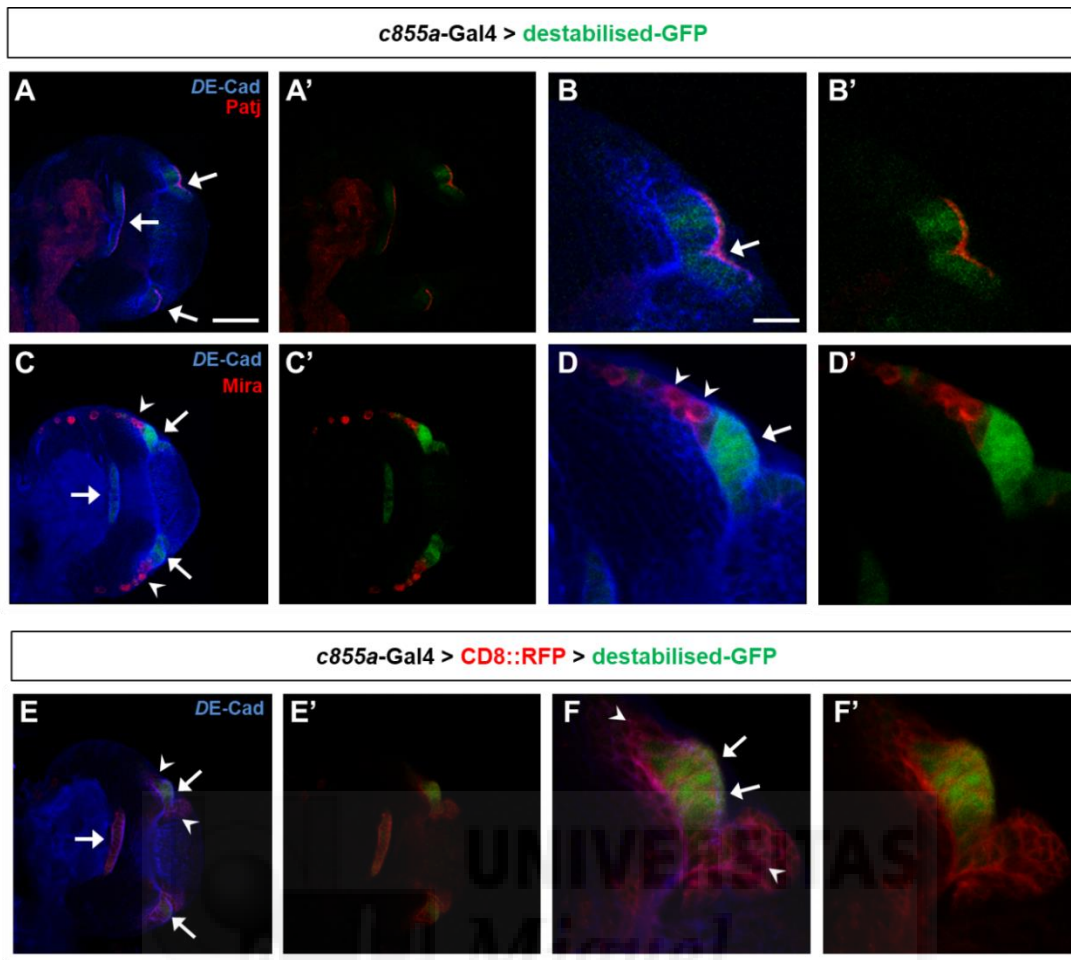
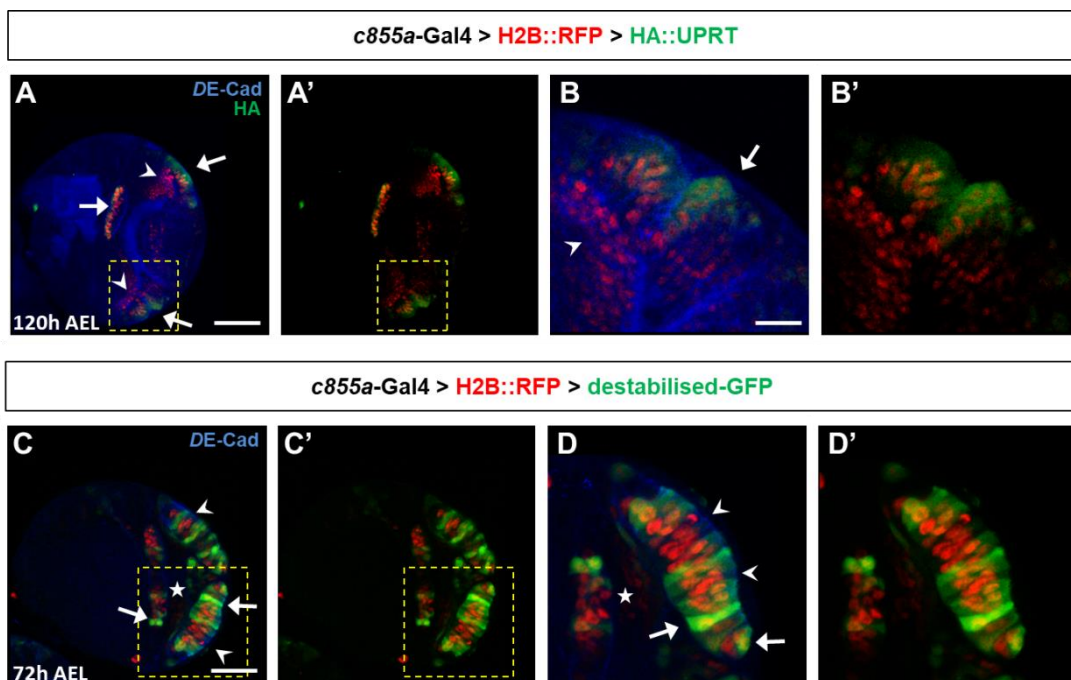


**Figure 15. c855a-Gal promoter is differentially expressed in neuroepithelial cells during larval development.** Confocal images reveal that the driver *c855a-Gal4* is not equally expressed in each brain cell in consecutive larval stages. **(A-A',B-B')** In late 3<sup>rd</sup> instar larvae (120 h AEL), the promoter drives equal expression of the UPRT enzyme (UAS-HA::UPRT; Miller et al., 2009) in neuroepithelial cells (in green, arrows) but not in their progeny (arrowheads) as described with the destabilised-GFP (see Figure 14). By contrast, in earlier stages **(C-C',D-D')** such as early 3<sup>rd</sup>-instar larvae (84 h AEL), patchwork expression of short-lived markers of *c855a-Gal4* (arrows and arrowheads) indicates that the driver is either intermittently expressed or that cells are at the different moments of the cell-cycle and have not all begun to express the driver. The asterisk marks the neuroepithelial offspring. The yellow box in **(A-A')** and **(C-C')** indicates the magnified OPC. Scale bars represent 50  $\mu$ m in **(A)**, 20  $\mu$ m in **(B)** and 35  $\mu$ m in **(C)**.



## 1.2. Identification of *cg25c*-Gal4 driver in optic lobe-specific surface-associated cortex glia

During recent years, a significant effort has been made to develop new techniques to characterise the glia in the *Drosophila* CNS (Awasaki and Lee, 2011). Along these lines, the aim of this thesis is to identify the glial component in the neuroepithelial microenvironment where neurogenesis takes place. Initially, the *mir-8*-Gal4 driver was used for identifying the OL surface-associated cortex glia (CG) of the larval brain, as previously described by our laboratory (Morante et al., 2013). This microRNA driver not only identifies CG cells but also cells of the fat tissue of the larva. The observation of this fact led us to test a collagen driver, *cg25c*-Gal4, which marks the same fat body (FB) cells (Figure 16C) and simultaneously marks glial cells of the CNS (Figure 16B).

In vertebrates and their conserved *Drosophila* homologs, collagen proteins are widely known to be an important part of the extracellular matrix known as the basement membrane. The basement membrane principal matrix protein is collagen type IV which comprises 50% of the basement membrane and has critical implications in tissue organization and developmental processes (Isabella and Horne-Badovinac, 2016; Monson et al., 1982; Natzle et al., 1982; Rodriguez et al., 1996). In the fly there exist different types of collagen type IV proteins which are identified by their structure: the gene *cg25c* (originally known as *DCg1*) encodes a  $\alpha$ 1-chain protein and has human homologs *COL4A1*, *COL4A3* and *COL4A5* (Monson et al., 1982); *viking* (*vkg*) encodes a  $\alpha$ 2-chain and has *COL4A2*, *COL4A4* and *COL4A6* as human homologs (Rodriguez et al., 1996; Yasothornsrikul et al., 1997); finally, the *pericardin* (*prc*) gene encodes a protein that has an  $\alpha$ -chain and has *COL1A1* and *COL1A2* as human homologs, though it contributes to heart formation rather than the basement membrane (Chartier et al., 2002).

In *Drosophila*, the gene locus of *cg25c* (cytogenic location polytene chromosome band 25C) is on the left side of the 2<sup>nd</sup> chromosome (Lindsley and Zimm, 1992), adjacent to *vkg* but in the opposite orientation (Figure 16A). *cg25c* (originally known as *DCg1*) has been found to be expressed in the FB throughout the entire fly life-cycle and where the protein is going to be secreted (Broadie et al., 2011; Le Parco et al., 1986; Pastor-Pareja and Xu, 2011; Rodriguez et al., 1996; Figure 16C). In the embryo, *cg25c* is also expressed in the hemocytes of the hemolymph (Broadie et al., 2011; Knibiehler et al., 1987; Rodriguez et al., 1996) and located, but not expressed, in the basement membrane, the gut and the ventral nerve cord (VNC) neuropil (Broadie et al., 2011; Mirre et al., 1992). Although originally studies did not observe expression in the larval CNS (Mirre et al., 1992; Le Parco et al., 1986), others do detected expression on there (Rodriguez et al., 1996) that I observed to be within the VNC and OL regions but not the central brain (CB) in 3<sup>rd</sup>-IL (Figure 16B). All things considered, I am able to affirm that during the L3 stage the driver *cg25c*-Gal4 is expressed in the VNC and OL areas of the brain as well as in the FB tissue (Figure 16D).

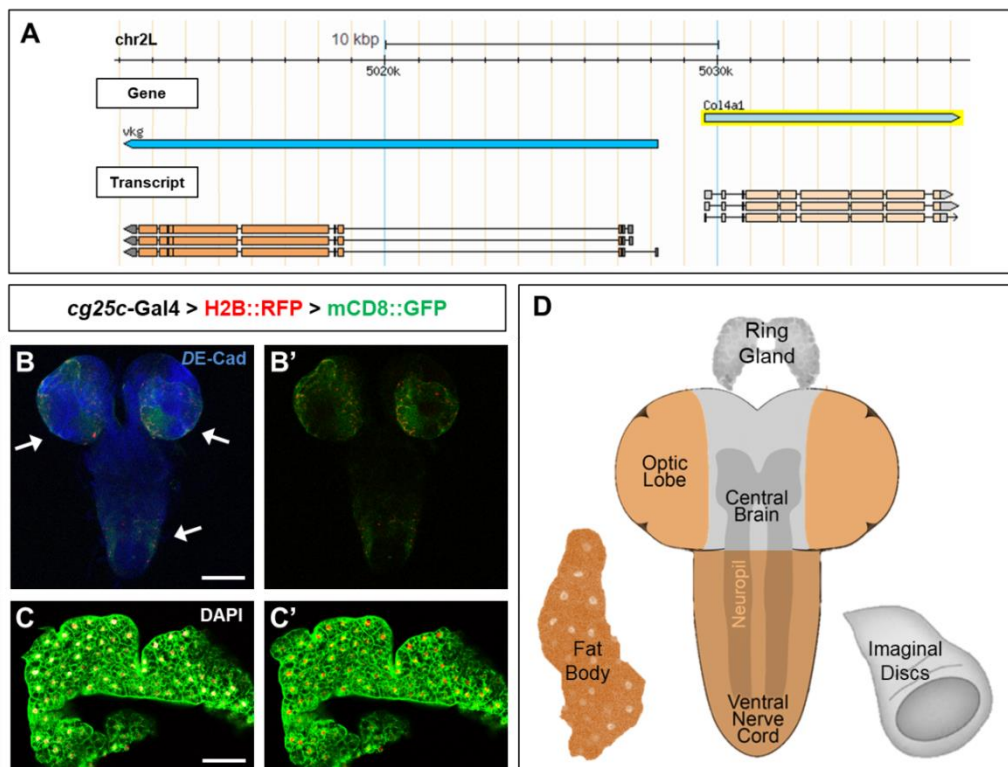


**Figure 16. *cg25c*-Gal4 driver expression in tissues during the L3 stage.** (A) Gene and transcript identification of *Drosophila* collagen IV *cg25c* (highlighted in yellow) and *viking* (adapted from Gbrowse2 online tool at FlyBase.org). (B-B', C-C') Confocal images show areas of *cg25c*-Gal4 promoter expression (arrows) in the brain and fat body identified by fluorescence (H2B::RFP and mCD8::GFP). (D) Schematic representation of the *cg25c*-Gal4 driver expression zones in larvae (orange) which are the fat body (Pastor-Pareja and Xu, 2011) and the central nervous system, specifically in the optic lobe and the ventral nerve cord. Images were taken from late 3<sup>rd</sup>-instar larvae. Scale bars represent 150  $\mu$ m in (B,C).

The first observation about the relevance of *cg25c*<sup>+</sup> cells is that an induction of their death under the ectopic expression of the apoptotic gene *reaper* (*UAS-rpr*; Nordstrom et al., 1996) affects the entire organism and causes lethality in premature larval stages (data not shown). A second observation about the *cg25c*<sup>+</sup> cells is that they are located close to the basement membrane of the brain and FB (Figures 16B,C and S1), as revealed by the Vkg protein (*Vkg::GFP*) that surrounds those tissues (Morin et al., 2001). This information leads us to consider the possible contribution that the *cg25c*<sup>+</sup> cells that we are working with, may make in the extracellular matrix as collagen type IV proteins in an auto-, para- or endocrine manner (Isabella and Horne-Badovinac, 2016). Unfortunately, down-regulating the expression of both proteins (*UAS-cg25c*-RNAi and *UAS-vkg*-RNAi) in the *cg25c*<sup>+</sup> cells with RNA interference does not appear to affect the whole larva or the tissue (data not shown). However, when the down-regulation is FB-specific (*pp1*-Gal4) for both collagen IV proteins, there are clear phenotypic effects: near-complete lethality in the pupal stage and the few adults that do emerge from pupae are smaller and not well-formed (data not shown). In the end, these observations point to a special role of the cells which express the gene *cg25c* in larval development.

In this thesis, the goal is to reveal novel extrinsic factors in the previously described *mir-8*<sup>+</sup> glia niche of the OL larval brain (Morante et al., 2013). Thus, it is important to characterise the similarities and differences between the *mir-8*-Gal4 and the *cg25c*-Gal4 drivers in that tissue. Experimental observations carried out via fluorescence show that both are expressed in the larval lobe but with the particularity that *cg25c*<sup>+</sup> cells are localised only in the OL instead of in both lobe regions, the OL and the CB, as is the case with *mir-8*<sup>+</sup> cells (Figure 17A-D). In addition, both groups of cells share a similar architecture (Figure 17B,D) as well as the fact that they both colocalise with classical glial antibodies (Figure 17E,F), but not with neuronal (Figure S2A,C), lead to the conclusion that the *cg25c*-Gal4 promoter is expressed in cells that express the *mir-8*-Gal4 driver and are located specifically in the optics region of the brain lobe.

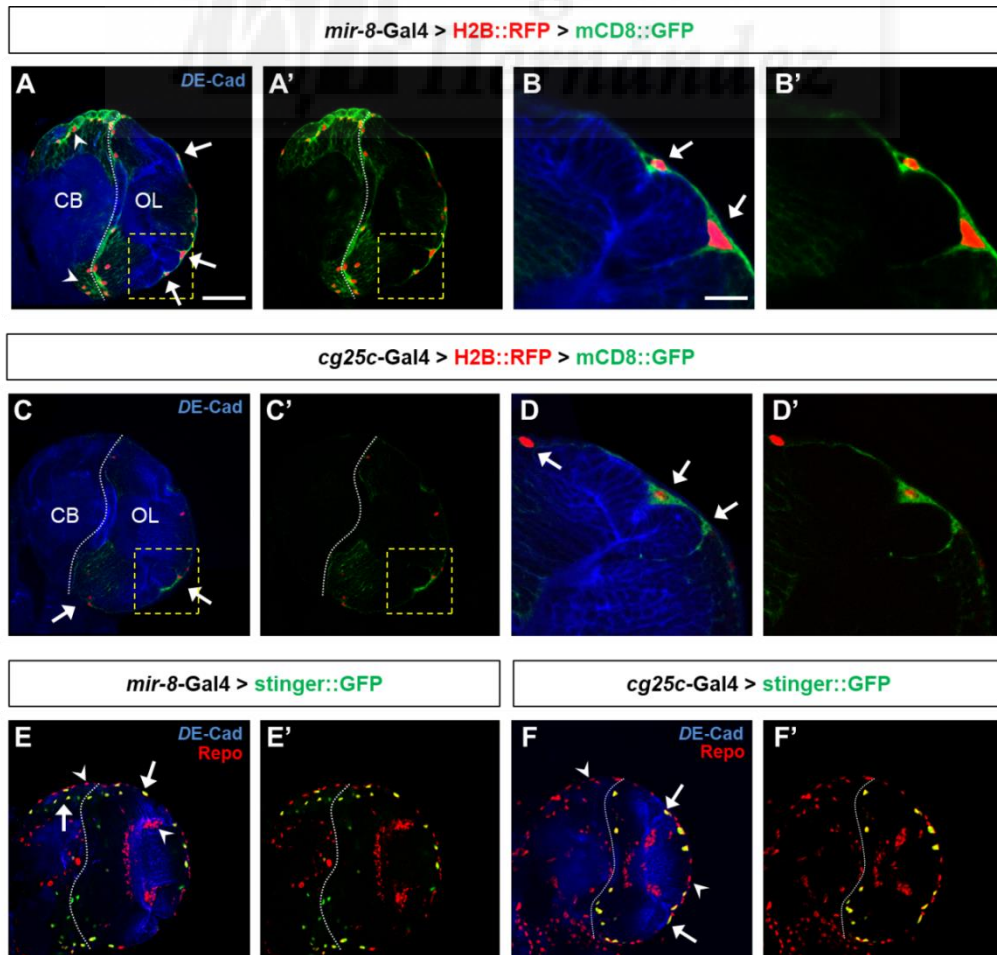


**Figure 17. The promoter *cg25c*-Gal4 is expressed in similar *mir-8*-Gal4 glial cells but is optic lobe-specific.** Confocal images show that both drivers tag lobe glia but the collagen driver is expressed in the optic lobe (OL) area while the *mir-8*<sup>+</sup> cells also label the central brain (CB). The driver *mir-8*-Gal4 (**A-A'**,**B-B'**) is shown to be located within the entire lobe, the OL (arrows) and the CB (arrowheads), when expressing a nuclear and a fluorescent effector (UAS-H2B::RFP and UAS-mCD8::GFP). However those proteins report that the expression for the *cg25c*-Gal4 driver (**C-C'**,**G-G'**) is OL-specific (arrows). (**E-E'**,**F-F'**) The cells expressing green nuclear fluorescence (UAS-stinger::GFP) as driven both promoters are also marked in red by the glial anti-Repo antibody (arrows); at the same time, not all the lobe glial cells (arrowheads) express both drivers. Neuroepithelial cells and brain neuropil are stained with anti-DE-Cad antibody (blue). Images were taken from late 3<sup>rd</sup>-instar larvae. The yellow box in (**A-A'**) and (**C-C'**) indicates the magnified OPC. Scale bars represent 50  $\mu$ m in (**A**) and 20  $\mu$ m in (**B**).

The similar areas of expression in the OL of the promoters *mir-8*-Gal4 and *cg25c*-Gal4 lead to the question of whether or not cells expressing these promoters are located in exactly the same place. Microscope images in which these cell types were marked by a strong nuclear fluorescent protein (UAS-stinger::GFP; Barolo et al., 2000) confirm that both are found in the OPC alongside the neuroepithelia (Figure 18A,B). Not only are those glial cells close to the neuroepithelia but they also ensheath the apical parts of NECs, assuming that their membranes enter into physical contact (Figure 18C,D). These observations endorse the idea of a glial-neuroepithelial niche in the OPC area, where neurogenesis starts and the novel OL-specific *cg25c*-Gal4 driver is active.

Using a *miR-8*::lacZ enhancer trap line I confirmed that *miR-8*<sup>+</sup> cells which are located in the OL, and specifically in the OPC, but not in the CB are the same cells that express the *cg25c*-Gal4 promoter (Figure 19). With this experiment I am able to categorise the *cg25c*<sup>+</sup> cells as an OL-specific subset of *miR-8*<sup>+</sup> cells.

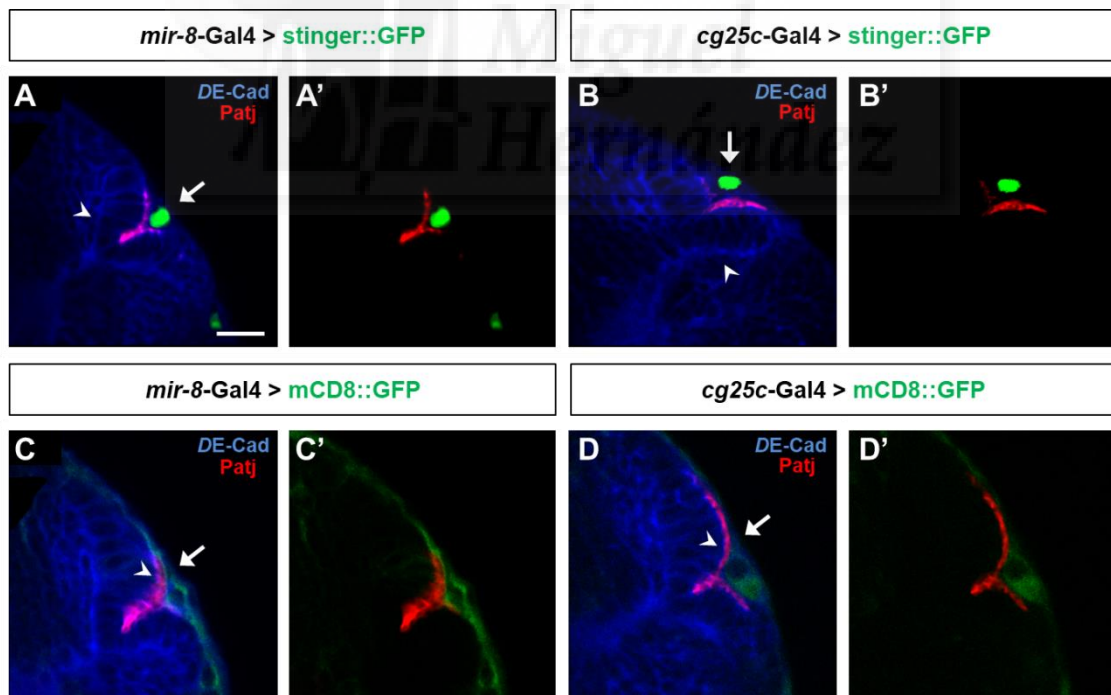


**Figure 18. Both *cg25c*<sup>+</sup> cells and *miR-8*<sup>+</sup> cells are located in the outer proliferation centre of the optic lobe.** Green nuclear fluorescent protein expression (UAS-stinger::GFP) under the control of the *mir-8*-Gal4 (**A-A'**) and *cg25c*-Gal4 (**B-B'**) drivers reveals the expression (arrows) of these drivers in the outer proliferation centre (OPC); neuroepithelial cells (NECs; arrowheads) of the optic lobe are marked with anti-DE-Cad antibody (blue) and anti-Patj antibody (red), in their apical zones. In addition, *miR-8*<sup>+</sup> (**C-C'**) and *cg25c*<sup>+</sup> (**D-D'**) cell membranes (UAS-mCD8::GFP, arrows) are physically in contact with the membranes of NECs of the OPC (arrowheads). Images were taken from late 3<sup>rd</sup>-instar larvae. Scale bar represents 20  $\mu$ m in (**A**).



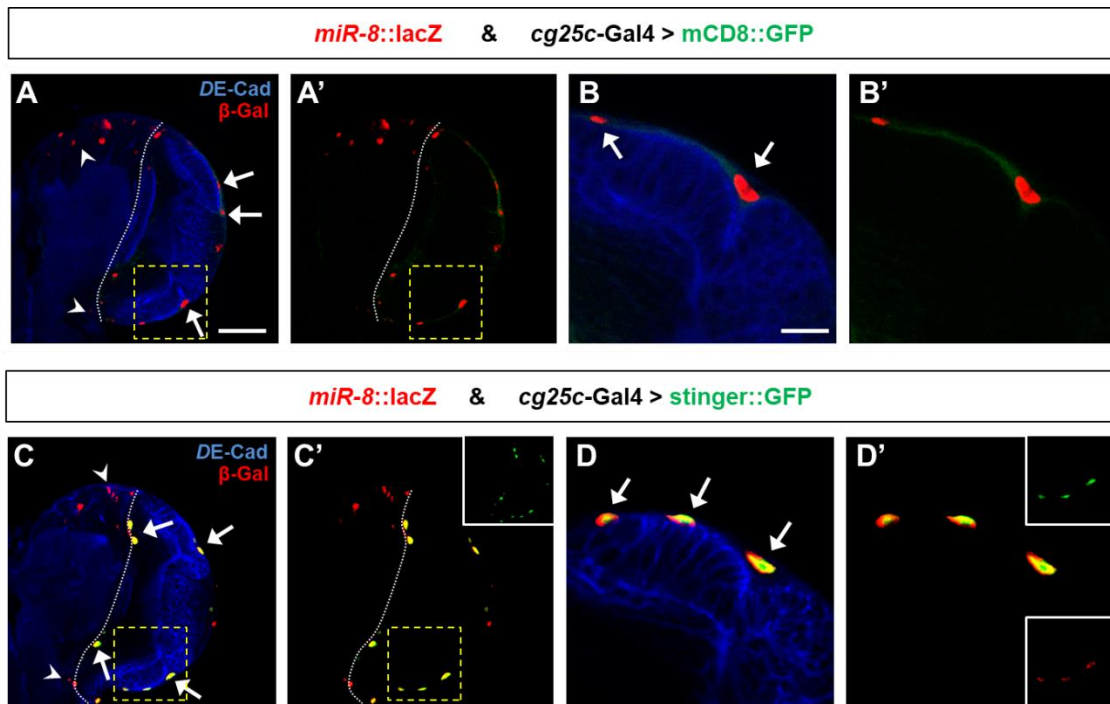


**Figure 19.** Cells expressing the *cg25c-Gal4* driver are an optic-lobe specific subset of *miR-8*<sup>+</sup> cells. *miR-8::lacZ* (red) labels lobe glial cells (A-A', C-C'), including those in the OPC (B-B', D-D'), when stained with an antibody for the protein β-Galactosidase. Only cells located in the optic lobe (arrows), but not in the central brain (arrowheads), express both *miR-8* (red) and *cg25c* (green) drivers simultaneously (yellow). Neuroepithelial cells and neuropil are marked with anti-*DE-Cad* antibody (blue). Images were taken from late 3<sup>rd</sup>-instar larvae. The yellow box in (A-A') and (C-C') indicates the magnified OPC. Scale bars represent 50 μm in (A) and 20 μm in (B).

Not many years ago, *miR-8*<sup>+</sup> cells of the brain were identified as surface-associated CG (Morante et al., 2013). Thus, as we have identified *cg25c*<sup>+</sup> cells as a *miR-8*<sup>+</sup> glia subset (Figure 19), cells expressing the novel driver ought also to belong to the same type of glia. Confocal images show first that the collagen IV driver for glial cells in the lobe (Figure 20B), like the *miR-8* promoter (Figure 20A), is expressed in cells under the anti-Moody-β antibody for subperineural glia (SPG; Bainton et al., 2005; Schwabe et al., 2005). Secondly, when *cg25c*<sup>+</sup> cells express cytosolic fluorescence (UAS-destabilised-GFP) and these cells are stained with the glial anti-Repo antibody, these cells appear to be beneath other glial cells, some of which have large nuclei as do the *cg25c*<sup>+</sup> cells (Figure 20C). The glia located above the *cg25c*<sup>+</sup> cells are identified as surface glia (SG), with the perineural glia (PN) subtype having small nuclei and the SPN subtype having large nuclei (DeSalvo et al., 2011; Morante et al., 2013; Stork et al., 2008). These observations are also apparent in early stages of development, when *cg25c*<sup>+</sup> glial cells are situated underneath other glial cells with large nuclei (Figure 20E,F). Taking this into consideration, the *cg25c*<sup>+</sup> glia cells located in the OPC zone of a larval brain are classified as surface-associated CG (Figure 20D).

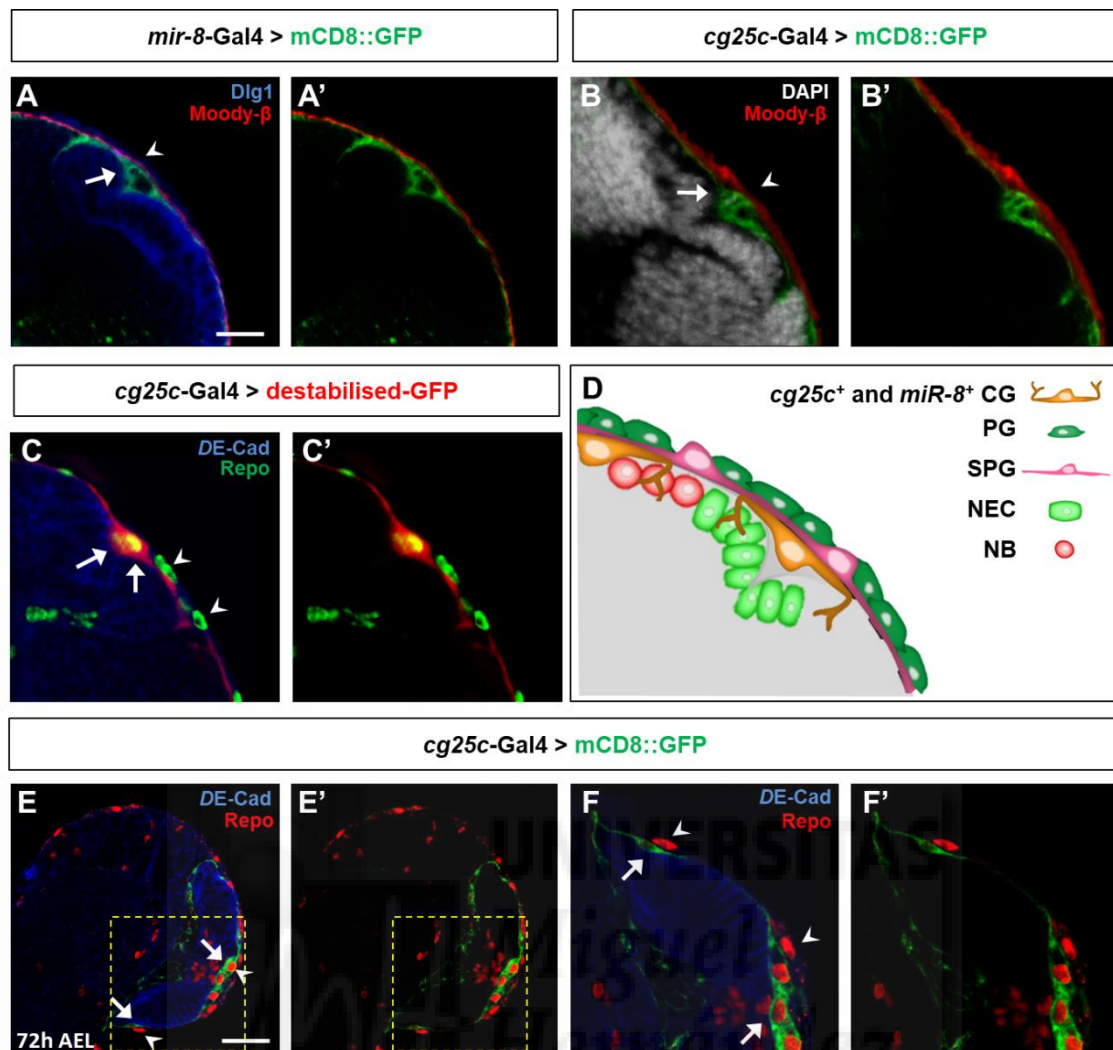


**Figure 20. *cg25c*<sup>+</sup> cells are classified as surface-associated cortex glia based on their location underneath surface glia of the larval optic lobe.** (A-A') Green fluorescent (UAS-*mCD8::GFP*) *mir-8*<sup>+</sup> cells (arrows) of the outer proliferation centre (OPC) are located between neuroepithelial stem cells (NECs) and subperineural glia (SPG, arrowheads) marked with the antibody for Moody-β (in red, Morante et al., 2013). (B-B') Likewise, *cg25c*<sup>+</sup> cells (arrows) are visualized between SPG (arrowheads) and NECs. (C-C') Staining with a glial antibody for Repo (green) shows that cells with the *cg25c-Gal4* driver for green fluorescent protein (UAS-*destabilised-GFP*) have large nuclei (arrows). Above *cg25c*<sup>+</sup> cells are other glial cell types (arrowheads) that resemble surface glia. NECs and neuroepithelial cells (NECs) of the OPC. In early stages (E-E', F-F'), such as early 3<sup>rd</sup>-instar larva (IL), the *cg25c-Gal4* driver is also expressed (arrows) in cells underneath other more superficial glial cells (arrowheads). Images were taken from late 3<sup>rd</sup>-IL in (A-C') and early 3<sup>rd</sup>-IL (E-F'). The yellow box in (E-E') indicates the magnified OPC. Scale bars represent 20 μm in (A) and 35 μm in (E).

As *cg25c*<sup>+</sup> glial cells have proven to be a subset of *mir-8*<sup>+</sup> glia specific to the OL, we speculate that these *cg25c*<sup>+</sup> glia have a similar role in the OPC niche to that of *mir-8*<sup>+</sup> glia. It has been determined that *mir-8*<sup>+</sup> glial cells control neuroepithelial expansion and neuroblast (NB) transition (and hence OL neurogenesis) in the brain lobes (Morante et al., 2013). This process is mediated by the TGF-α, known as *spitz*, which is released by *mir-8*<sup>+</sup> glial cells and acts on the EGFR of the NECs downstream in the signalling pathway. Experimentally, when *mir-8*<sup>+</sup> cells inhibit the expression of the endogenous *spitz* (UAS-*spitz-RNAi*), it blocks the proliferation of NECs and NBs, which decreases the size of the brain (Figure 21B). In addition, an overexpression of TGF-α induces the opposite effect: the overproduction of NBs and expansion of the neuroepithelia cause enlargement of the brain (Figure 21C).

We might expect to observe similar effects on the brain when the *cg25c*<sup>+</sup> cells are modified under the same conditions. Surprisingly, when the ligand Spitz is down-regulated (Figure 21A,E), the result is an expansion of NECs which causes a drastic increase in brain size. Unlike in the case of *miR-8*<sup>+</sup> cells, in which brain overgrowth is triggered by the overproduction of Spitz, the increase in brain size observed in *cg25c*<sup>+</sup> cells does not involve an increase in the number of NBs nor glial cells, though there is an augmentation of the neuropil. Interestingly, both the OL and the CB are increased in size, despite the fact that the *cg25c*-Gal4 driver is not expressed in the CB. Overall, though these results leave some unanswered questions about this signalling pathway regulated by the OL counterpart of the *miR-8*<sup>+</sup> cells, there is no doubt that *cg25c*<sup>+</sup> glia plays a role in OPC neurogenesis. Thus, going forward, my thesis focuses on finding the possible signals controlling neurogenesis that are released by the two niche partners: OL surface-associated CG and the neuroepithelium.

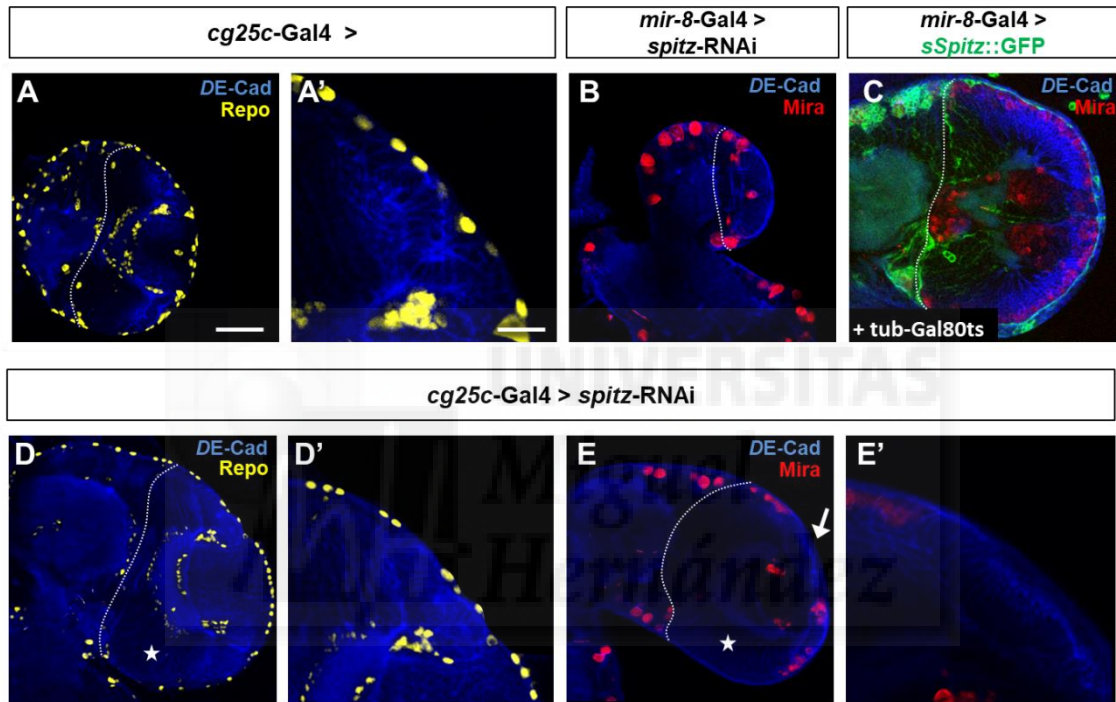


**Figure 21. A dysfunction in *cg25c*<sup>+</sup> glia has a different impact than one in *miR-8*<sup>+</sup> glia in the outer proliferative centre of the larval optic lobe. (A-A')** Control brain carrying the *cg25c*-Gal4 driver without expressing any transgene. **(B)** Inhibition of Spitz expression (UAS-*spitz*-RNAi) in *miR-8*<sup>+</sup> glial cells blocks proliferation of neuroblasts (NBs), labelled in red by the antibody anti-Mira, via the neuroepithelium, marked in blue by anti-DE-Cad antibody (Morante et al., 2013). **(C)** Larvae raised at 18 °C and moved to 29 °C during the L3 stage to overexpress Spitz (UAS-*sSpitz*::GFP) in *miR-8*<sup>+</sup> glial cells produce an overproliferation of neuroepithelial cells and thus an overproduction of NBs (Morante et al., 2013). However, when Spitz is down-regulated in the *cg25c*<sup>+</sup> glial subset, the result is an overproduction of the neuroepithelium **(D-D')** without any effects on NB production **(E-E')**. Images **(B,C)** are adapted from Figure 7 of (Morante et al., 2013). Images were taken from late 3<sup>rd</sup>-instar larvae. Scale bars represent 50 µm in **(A)** and 20 µm in **(A')**.

## 2. Fluorescent cell sorting of optic lobe niche populations for transcriptomics

In this study, the identification of a specific driver for OPC surface-associated CG cells (*cg25c-Gal4*) and the use of this driver along with the driver already identified for NECs (*c855a-Gal4*; Egger et al., 2007) allowed us to isolate cellular RNA. In order to achieve this, it is necessary to precisely separate the material from each population; at present, there exist a range of methodologies for that purpose, as mentioned in the introduction. Originally, several trials were done with the 4-TU mRNA tagging technique (Miller et al., 2009). However, the nature of glial cells made it difficult to obtain enough quantity of sample with which to proceed (data not shown).

Consequently, due to the capacity to tag *Drosophila* cells by fluorescence, the technique eventually used was fluorescent activated cell sorting (FACS). The technique (Harzer et al., 2013), as mentioned in the introduction, consists of a soft enzymatic and mechanical dissociation of larval brains into single cells followed by a computational fluorescent sorting in order to isolate the cells of interest.

Initially, it was mandatory to establish a stock in which both populations were separately tagged. Previous experiences with characterising the *c855a-Gal4* driver made it clear that short-life span GFP (UAS-destabilised-GFP) was required in order to avoid the perdurance phenomenon of that promoter (Figures 13 and 14). In addition, as other techniques take advantage of dual fluorescence tagging to enhance robustness of identified cells (Antonello et al., 2015; Toledano et al., 2012), I simultaneously used nuclear fluorescence (UAS-H2B::RFP). Although the driver *cg25c-Gal4* for surface-associated CG cells does not have the perdurance handicap, I also used the same strategy of dual labelling. To summarize, using the ability of recombination in flies I established the following genotype for sorting: *c855a-Gal4>UAS-H2B::RFP>UAS-destabilised-GFP* to identify NECs and *cg25c-Gal4>UAS-H2B::RFP>UAS-destabilised-GFP* for glial cells (Figure 22).

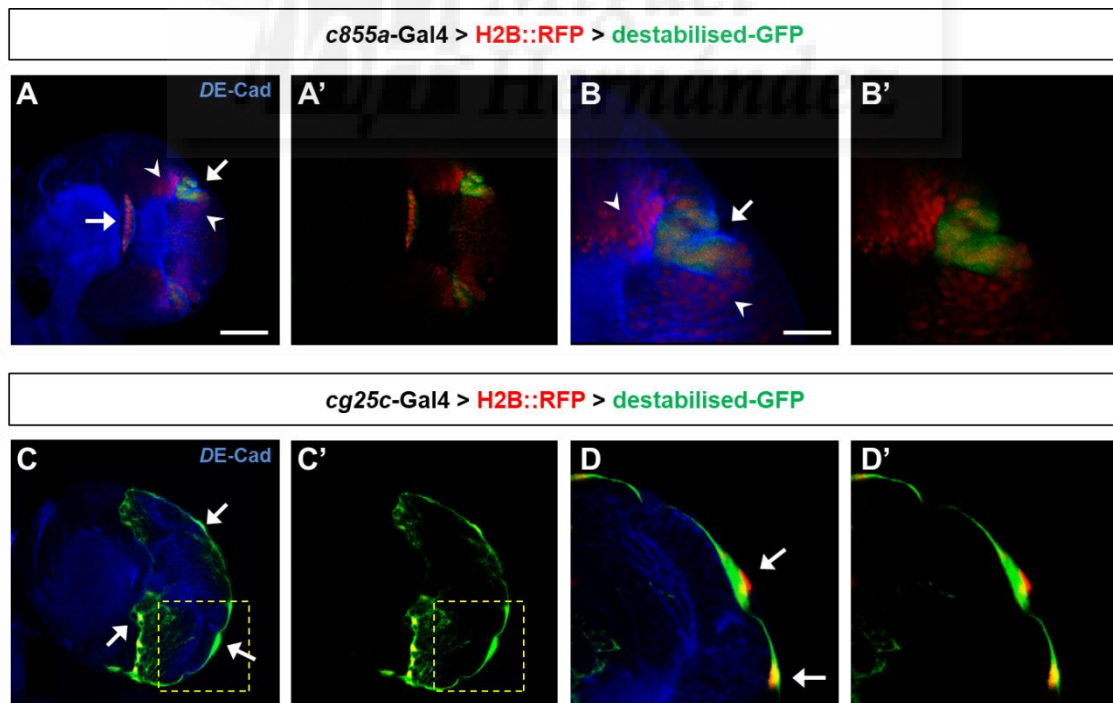


**Figure 22. Neuroepithelial and glial cells dual fluorescent stocks used for sorting.** Double-fluorescent stocks marked with red nuclear (UAS-H2B::RFP) and green cytosolic (UAS-destabilised-GFP) fluorescence are used for FACS technique. **(A-A',B-B')** Neuroepithelial cells (arrows) expressing the *c855a-Gal4* promoter are identified by combining a nuclear (red) and a short-lived (green) fluorescent protein and separating these dual-fluorescent cells from the neuroepithelial lineage, which displays the perdurance phenomenon (arrowheads). **(C-C',D-D')** For consistency, the same combination of fluorescent markers under the expression of the *cg25c-Gal4* driver is used to identify glial cells (arrows). The yellow box in **(C-C')** indicates the magnified OPC. Images were taken from late 3<sup>rd</sup>-instar larvae. Scale bars represent 50  $\mu\text{m}$  in **(A)** and 20  $\mu\text{m}$  in **(B)**.

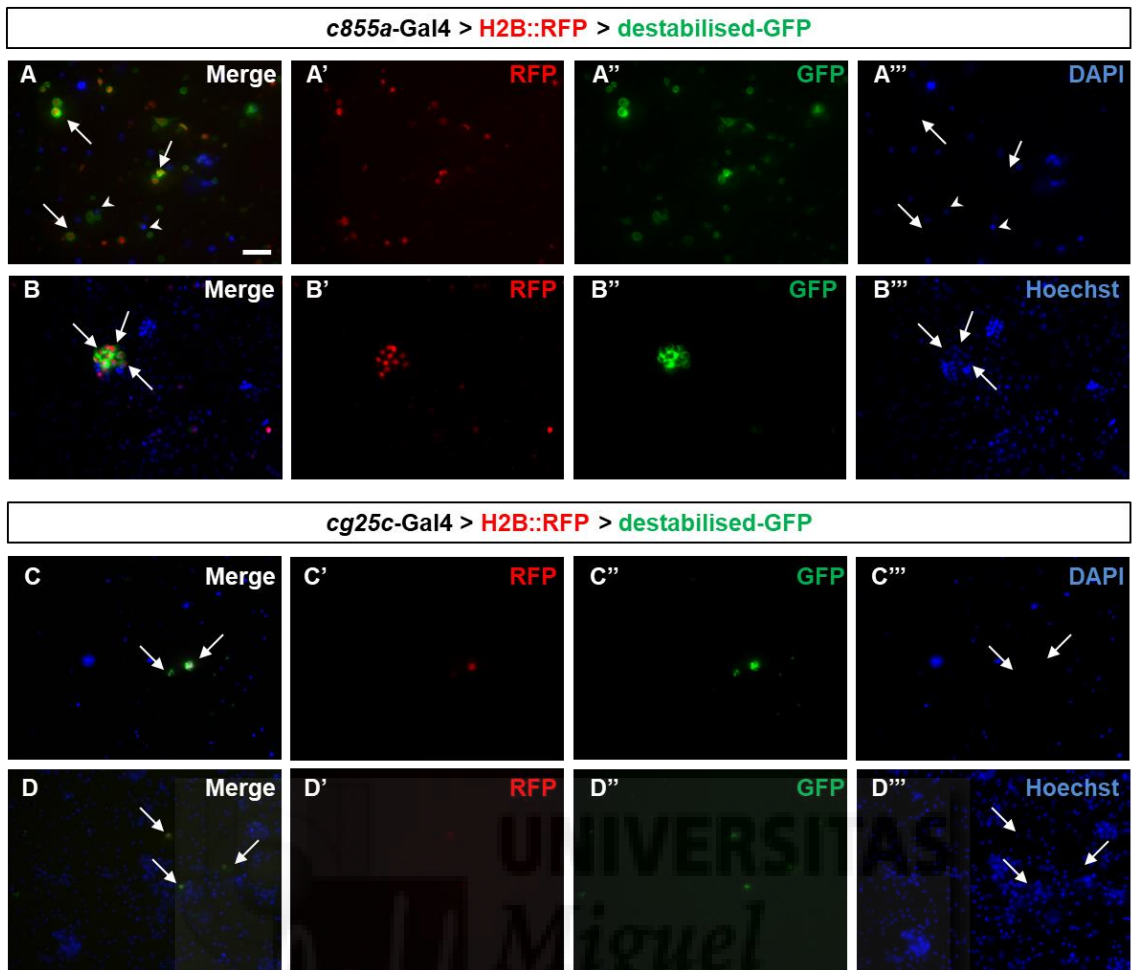


**Figure 23. Cells in culture from disaggregated larval brains before sorting.** Microscope images of cultured double-fluorescent cells (UAS-H2B::RFP and UAS-destabilised-GFP) before being sorted by FACS. After enzymatic and mechanical dissociation of tissue, the majority of *c855a*<sup>+</sup> double-positive cells are alive (arrows), which is shown by the fact that they do not colocalise with DAPI (**A-A'''**) but do with the permeable Hoechst 33342 (**B-B'''**); cells which are dead (arrowheads) display both markers. (**C-C'''**,**D-D'''**) Although *cg25c*<sup>+</sup> cells are fewer in number and have an arborisation-like shape, they also survive (arrows) the tissue digestion process. Images were taken 1 h after disaggregation treatments from cells of late 3<sup>rd</sup>-instar larval brains. Scale bar represents 50  $\mu$ m in (**A**).

Sorting following the FACS technique requires that tissues disaggregate into individual cells. The first step was dissecting larvae to collect the CNS and, simultaneously, discard those tissues where *c855a-Gal4* and *cg25c-Gal4* drivers are also expressed (Figures 10 and 14). In addition, it is crucial in *cg25c*<sup>+</sup> CNS to remove the VNC region from the brain due to driver's expression pattern. Although the neuroepithelial driver is not present in that CNS region, the step was also done in *c855a-Gal4* samples for FACS efficiency. At this point in the process, I adapted the FACS methodology to optimise it for the particular cells I was testing (Harzer et al., 2013). Tissues were incubated with an enzymatic mix (Papain and Collagenase I) and mechanically disaggregated. To ensure that this step was effective, I checked the cells' viability by growing some samples in culture. The samples were stained with DAPI, which fluorescently labels cell nuclei with compromised membranes, as well as with Hoechst 33342, which permeates functional membranes and intercalates the DNA. This experiment revealed that most of the double-fluorescent cells were negative for DAPI staining and positive for Hoechst 33342, meaning that both cell populations were living (Figure 23). The results together indicate that the tissue disaggregation step for larval brains was ready to be used in the FACS methodology.

The basis for sorting by fluorescence, as mentioned in the introduction, requires the proper gating of events from the entire population of mixed cells. Once debris, cell clusters and dying cells are removed, the living cells are ready to be separated by fluorescence (Figure S3). Driver autofluorescence (Figure S4) and signal overlapping of the fluorescent reporters (Figure S5) were

discarded. A lack of positive results when testing for dual-fluorescence in the nucleus (Figure S7) and a combination of nuclear and membranal fluorescence (Figure S8) indicated the need to use unstable GFP with the neuroepithelial driver. As mentioned before, the full recombinant genotype for the NECs was *c855a-Gal4 > UAS-H2B::RFP > UAS-destabilised-GFP* and, although the glial driver is not inconvenient to use in any of the fluorescent versions (Figures S6, S7 and S8), the same genotype combination was used for glia in order to be consistent across cell types (*cg25c-Gal4 > UAS-H2B::RFP > UAS-destabilised-GFP*).

At this point, the FACS technique was sufficiently adapted to my niche-specific cells. After gating all the events and separating the living cells, the fluorescence shows which cells belong to each population (Figure 24). The final percentage of double-fluorescent cells for neuroepithelia (0,5%) reveals that ~290 cells per larval brain are isolated while the percentage double-fluorescent of glial cells (0,3%) shows that ~175 are isolated per larval brain.

It is important to properly control the cell separation; for this reason, part of the collected cells were cultured (Figure 25). This shows that all the *c855a*<sup>+</sup> cells are dual-fluorescent and alive, and the *cg25c*<sup>+</sup> cells, although lower in number, are also living. Via this process, the niche cells are correctly separated and ready to have their RNA extracted.

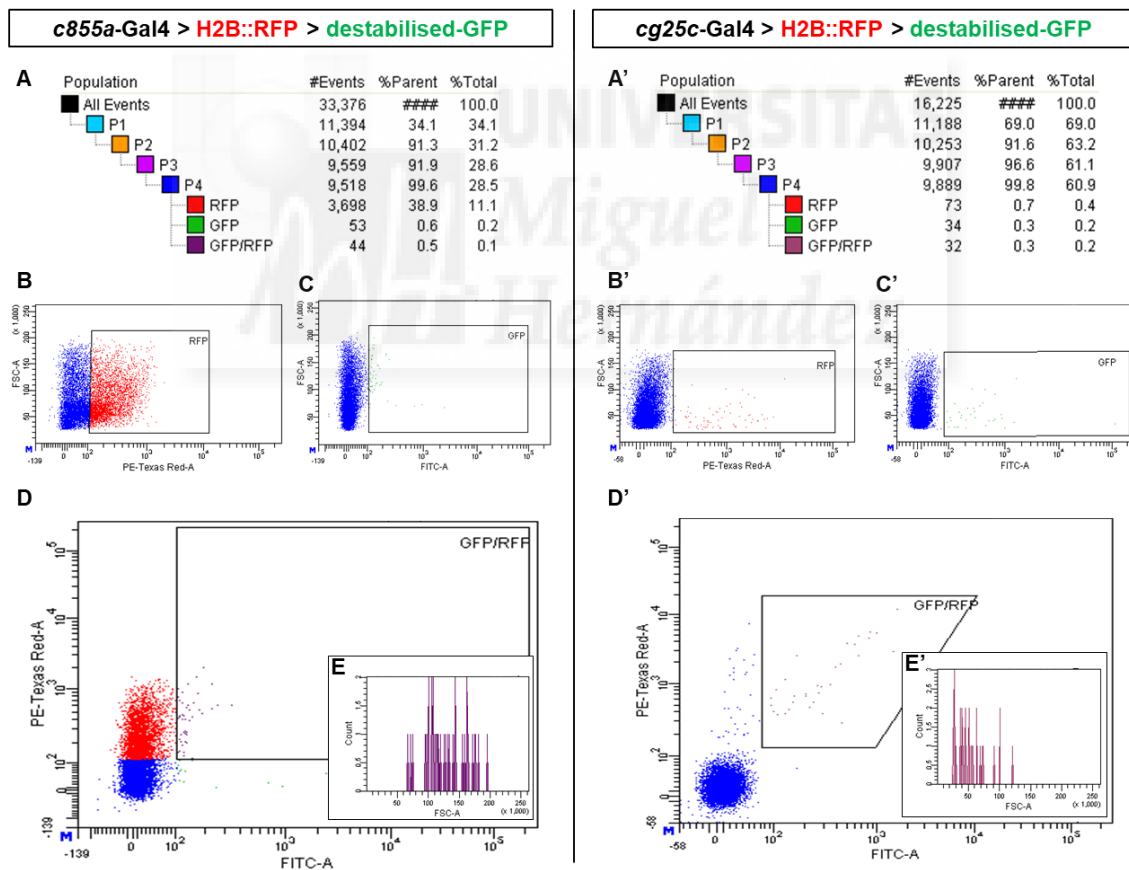


**Figure 24. FACS sorting of neuroepithelial and glial dual-fluorescent cells from late L3 larval brains.** Fluorescent cell sorting for which the neuroepithelial *c855a-Gal4* and the glial *cg25c-Gal4* promoters are driving fluorescent expression for red (UAS-H2B::RFP) and green (UAS-destabilised-GFP). Gating (A,A') the nuclear reporter UAS-H2B::RFP (B,B') and the cytosolic reporter UAS-destabilised-GFP (C,C') for the neuroepithelial driver *c855a-Gal4* (D) and the glial driver *cg25c-Gal4* (D') enables the separation of each population of the niche (E,E'). The percentage of double-fluorescent neuroepithelial cells (0,5%) means that around ~290 per larval brain are isolated, and ~175 glial cells (0,3%) are isolated. Therefore, nuclear and cytosolic double-labelling is suitable for both drivers. Graph axes are the same as in Figure S3.

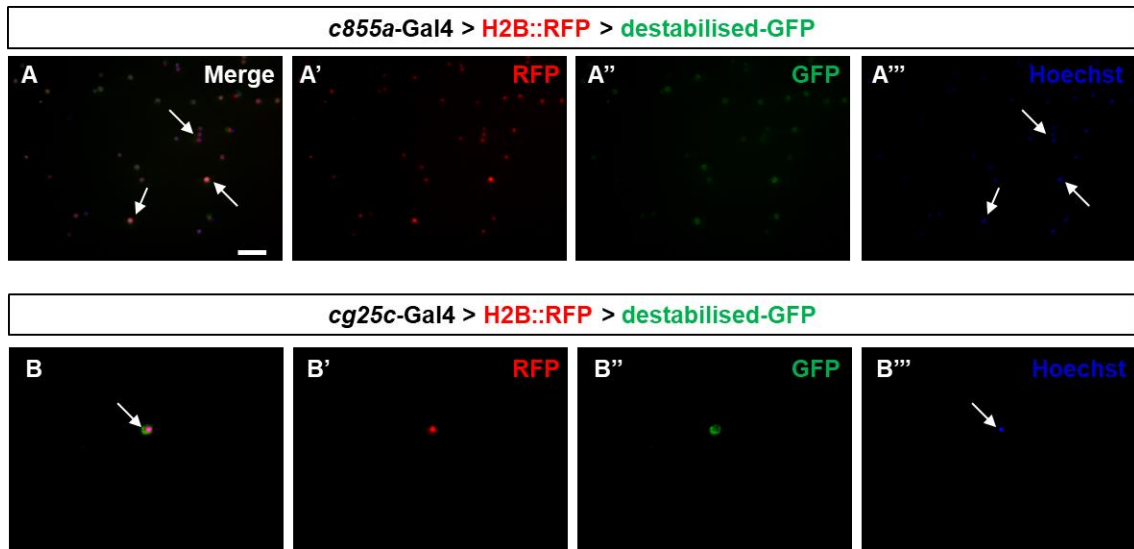


**Figure 25. Double-positive cells in culture from sorted larval brains.** Microscope images of cultured double-fluorescent cells (UAS-H2B::RFP and UAS-destabilised-GFP) after being sorted by FACS. **(A-A''')** All the sorted *c855a*<sup>+</sup> cells are double-fluorescent (arrows indicate examples) and marked with the permeable Hoechst 33342. **(B-B''')** Although *cg25c*<sup>+</sup> cells (arrows) are fewer in number they are also double-positive and survive the sorting process. Images were taken 1 h after FACS sorting. Scale bar represents 50  $\mu$ m in **(A)**.

For transcriptome analysis in a particular larval stage, it is necessary to know information about gene expression in previous stages in order to compare expression levels. Therefore, apart from the FACS experiments previously done in late L3 brains, I needed also to obtain the niche cells from late L2 stage larvae. Thus, the same isolating approach was followed because it is also suitable for this early stage (Figure 26). However, in this situation, the L2 cell rate of survival is lower (~15% of the initial events) when compared with that of the L3 stage cells (~50-60% of the initial events). Due to both this complication and the fact that L2 larvae have not yet undergone a great OL expansion, fewer cells can be collected per brain: ~55 *c855a*<sup>+</sup> cells and ~75 *cg25c*<sup>+</sup> cells.

After finishing FACS sorting and obtaining cells from niche populations at each larval stage, the next step is to extract the cells' mRNA with extraction kits as indicated in the section *Materials and Methods*. Interestingly, unlike in other eukaryotes, the integrity of *Drosophila* RNA cannot be evaluated using the conventional ratio for integrity. When fly RNA is run on electrophoresis gels, the ribosomal RNA 28S band splits into two bands of similar molecular weight which migrate similarly to the 18S RNA, resulting in the appearance of one unique band. Thus, the common ratio for integrity, RIN (28S:18S), is not suitable for giving the integrity value even though the fragment is intact (Figure S9). For this reason and also due to the low amount of sample obtained, the most suitable technique for measuring the samples' quality and quantity is working with RNA chips of the Bioanalyzer systems. All FACS samples were correctly validated using this technique (Figure S10) before proceeding to the next step, RNA-sequencing.

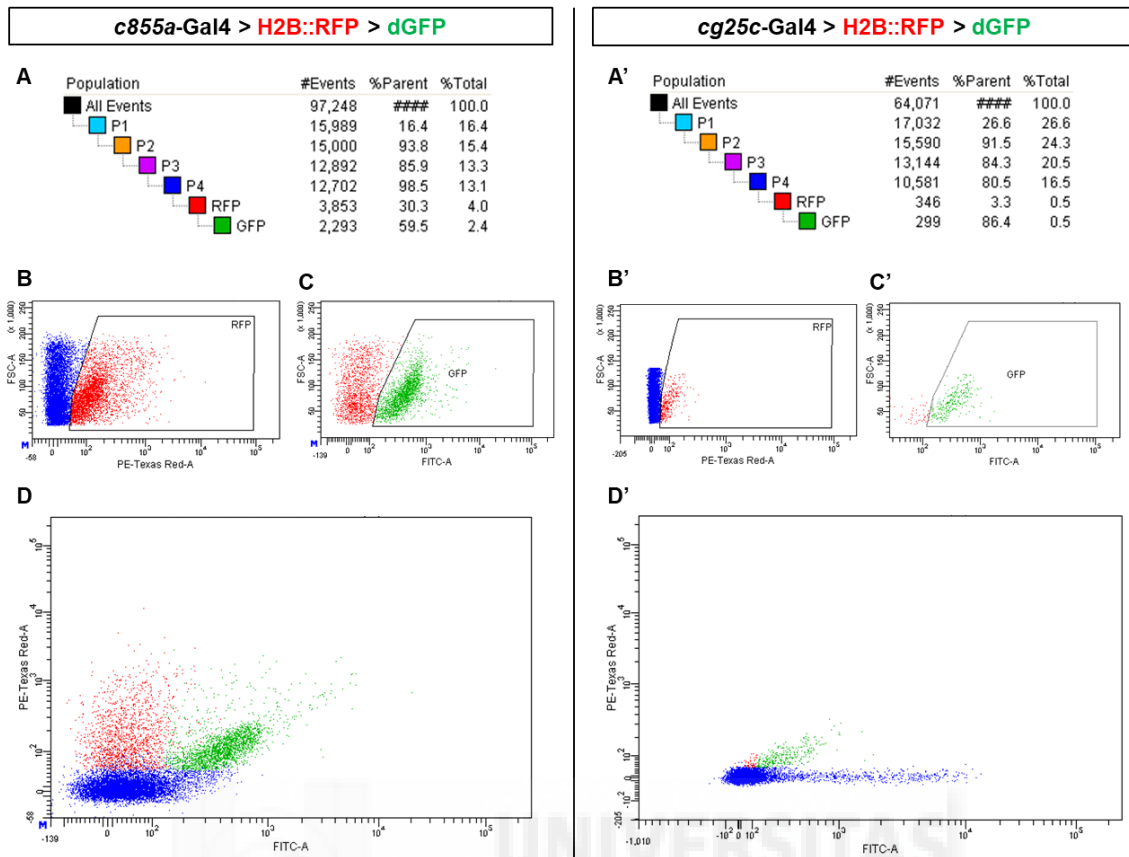


**Figure 26. FACS sorting of neuroepithelial and glial dual-fluorescent cells from late L2 larval brains.** Fluorescent cell sorting for which the neuroepithelial *c855a*-Gal4 and the glial *cg25c*-Gal4 promoters drive fluorescent expression of red (UAS-H2B::RFP) and green (UAS-destabilised-GFP). Gating (**A,A'**) the nuclear reporter UAS-H2B::RFP (**B,B'**) and the cytosolic reporter UAS-destabilised-GFP (**C,C'**) for the neuroepithelial driver *c855a*-Gal4 (**D**) and the glial driver *cg25c*-Gal4 (**D'**) are possible to separate each population of the niche in early stages. The fact that larvae in the late L2 stage have not yet undergone the neurogenic phase as well as the low percentage of cell survival (~15%) decreases the total number of double-fluorescent isolated cells to ~55 neuroepithelial cells and ~75 glial cells per larval brain. Apart from this minor inconvenience, the double nuclear and cytosolic labelling is suitable for both niche drivers. Graph axes are the same as in Figure S3.

### 3. Niche transcriptome sequencing and bioinformatics analysis of gene expression

#### 3.1. Massively-parallel cDNA sequencing and quality control

To effectively perform a transcriptome analysis, it is very important to begin with high quality samples. My samples have four conditions differing in the niche population (*c855a*<sup>+</sup> and *cg25c*<sup>+</sup>, hereafter referred to as neuroepithelium and glia respectively) and the larval developmental stage (late 2<sup>nd</sup>-IL and late 3<sup>rd</sup>-IL, hereafter referred to as L2 and L3 respectively). Per each condition, three biological replicates are used. Thus, the concentration (despite being very low) and quality of the twelve samples were evaluated (Figure S10) and considered appropriate for processing through the following steps. I carried out the transcriptome sequencing and bioinformatics analysis in the Genomics Core Facility (Gencore) of the European Molecular Biology Laboratory (EMBL) in Heidelberg, Germany, supervised by the head of the facility, Dr. Vladimir Benes.

Such a low input amount needs to be processed with the next generation of high-yield preparations kits to obtain a high quality cDNA library. It is important to note from the second-generation library construction protocol that it keeps the directionality of the original RNA fragments. This characteristic is derived from the dUTP method (Levin et al., 2010; Parkhomchuk et al., 2009) for strand-specificity which consists of labelling the second strand of cDNA using dUTP which allows its destruction downstream in the process. Thus, the cDNA library only contains a single strand providing the



original directionality for each transcript. This gives me the possibility to accurately quantify the expression levels of coding overlapping transcripts (Zhao et al., 2015) and enhances the value of the massively-parallel cDNA sequencing (MPS) experiment. All 12 samples in the library had suitable concentrations and quality (Figure S11) and were thus ready to be pooled and sequenced.

The average concentration and fragment length of the 12 samples (Figure S11) were used for pooling together in a final concentration of 4nM. Then, a cluster concentration of 1,8 pM was loaded into the NextSeq 500 High sequencer from Illumina, which sequenced a read length cycle of 85 bp and an extra 7 bp for barcodes, with single-ends. Finally, a demultiplexing process was needed to identify each sample's transcript, and the output information about sequenced reads of each sample was given in FASTQ files. FASTQ files, which are plain text files similar to FASTA files, contain extra information within the sequence format encoding their quality.

At this point, it is important to analyse the RNA-seq quality control to understand the sort of data one is dealing with. The quality control is performed with the software MultiQC (Ewels et al., 2016) and the tool FastQC using each sample's FASTQ files. The outgoing report uses different approaches (Figures 27 and S12) to overview quality information about the twelve sequenced samples. The first data to check is barcoding distribution within the more than five hundred million sequences of my cDNA library from which the 98,78% of them were assigned to their original sample (Figure 27A). General statistics from each sample are grouped together in a table (Figure 27B) giving important information such as the 85 bp average sequence length and the average percentage of guanine-cytosine (GC) content which maintains the natural 2:1 ratio (Keightley et al., 2009). The volume of sequencing run data generated is revealed in a total of sequences per sample which is between 37,1 and 53,4 million reads (Figure 27B,C). In a pair ends sequencing for *Drosophila*, between 80 to 90 million reads cover the 93% of the genome and arrives to a plateau state (Daines et al., 2011); thus, as the present experiment is performed in single ends, it is suitable to use between 40 to 50 million reads, as it was done. It is also important to consider the duplicate reads, which represent more than 82% of each sample; this may be a consequence of highly expressed genes or a small amount of starting material (Figure 27B,C). All of this information illustrates what kind of data I have and indicates that the sequencing was carried out properly.

Additional information is also useful to further understand each sample sequence. The Phred quality score is a logarithmic property which defines a base-calling error probability (Ewing and Green, 1998); it is the most important statistic to be considered. In my data (Figure 27D), the high mean quality score per each nucleotide (a Phred over 31) and the relative stability across the sequence length (it is not unusual for the quality of nucleotides to drop progressively with time due to sequencing chemistry degradation) indicate that the chance of error is minimal and a bias in library quality based on position read can be dismissed. Phred is also used to measure the sequence quality within each sample (Figure 27E). Displaying the Phred value of my sample sequences and plotting the number of reads (counts) shows a tiny subset of reads which have universally poor quality (red and beige zones). However, this may be caused by the poor image quality at the edges of the sequencer field of view and only represents a very small percentage of the total sequences. Overall, the vast majority of the reads have a very good quality score of over 28 (green zone). Thus, the Phred quality information suggests that the output data from RNA-seq are generally fairly robust.

Within the twelve samples, their sequences' base position shows that the four DNA bases are proportionally distributed in each position (~25% of reads) because the library was randomly created (Figure S12). The bias in the beginning of the reads, in the first 12 bp of each run, is attributed to priming using random hexamers and is omitted because it neither denotes any individually biased sequences nor affects the downstream analysis. It is also important to know the GC percentage of the sequence; as a random library, all samples share a roughly typical distribution of GC content which may be compared with a normal distribution containing a central peak of overall GC content (Figure 27F). Other information such as base N content in each position (<0,1%), which indicates insufficient confidence calls, suggests that the sequencer performed effectively (data not shown). In terms of top overrepresented sequences (Figure 27G), nearly all of the samples present some of them but mostly represent <1% of the total possibly explained by PCR overamplification which is frequent in low input libraries; additionally this also could mean a narrow diversity of sequences. The other possible reason for sequence overrepresentation is the adapter content, but their accumulative performance in the green zone graph (Figure 27H) discards that bias and, at the same time, the necessity for the sequences to be trimmed.

On the whole, the various methods used to evaluate the quality of the RNA-seq output data suggest that the sequencing was successful. Going forward, I will discuss the bioinformatics analysis as well as neuroepithelial and glial transcriptome expression.

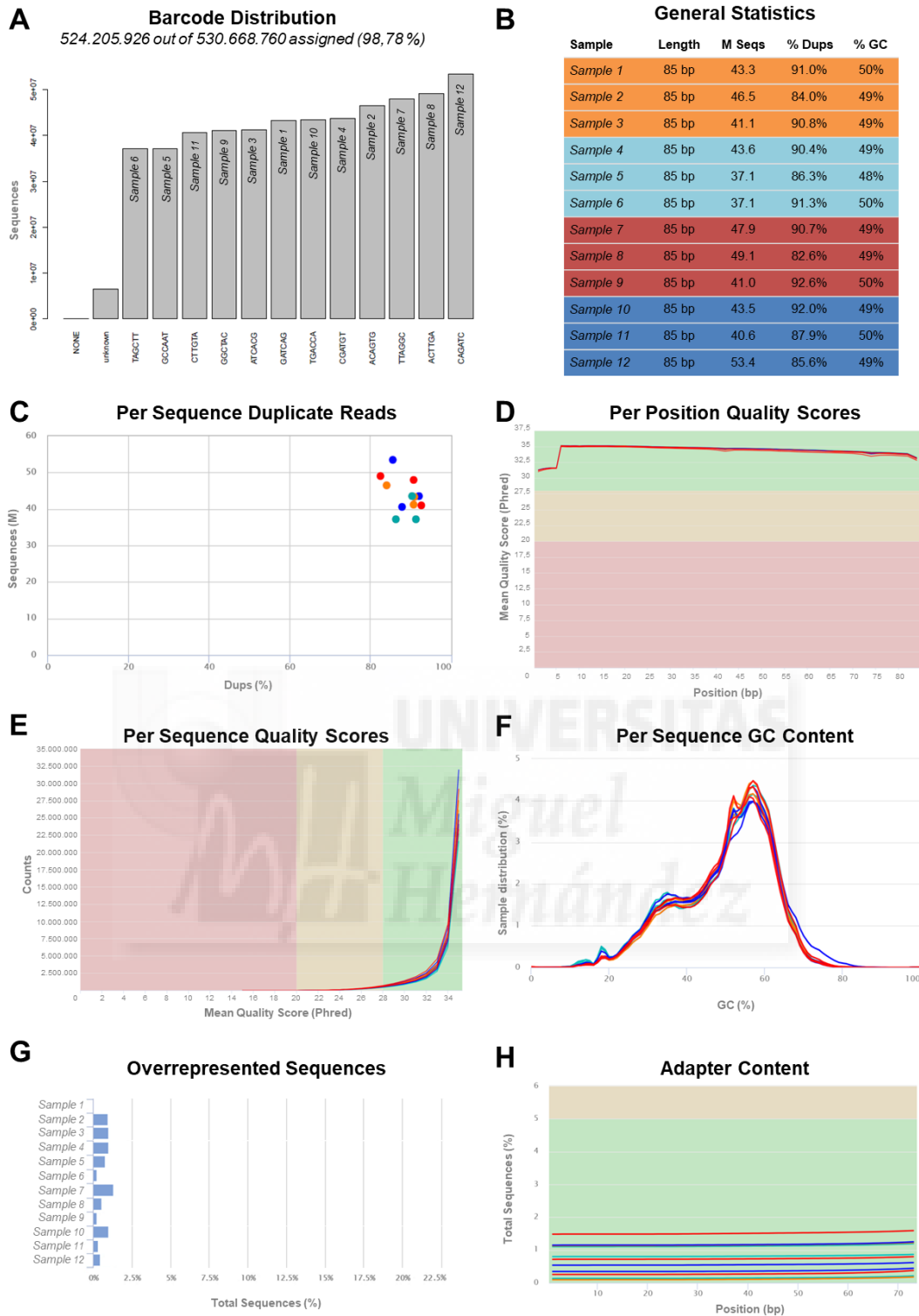


**Figure 27. RNA sequencing quality control.** Quality report of each of the samples sequenced. (A) Illumina barcode distribution shows 98% demultiplexing success. (B) The table of general statistics gives information about the average sequence length in bp (Length), the total sequences in millions of reads (M Seqs), the percentage of duplicate reads (Dups), and the average percentage of guanine-cytosine content (GC). (C) Percentage of sequence duplicates reads (Dups) plotted against sequence counts in millions of reads. (D) Mean quality values (Phred score) across all bases at each position are the most valuable statistic; when this score is over 30 it indicates a low probability of reading mistakes. (E) Quality scores per each sequence reveal that the majority of the counts are high quality (score over 28) and thus, the data is reliable. (F) The percentage of guanine-cytosine content in a sequence forms a nearly normal distribution with a central peak. (G) Top overrepresented sequences per sample shows a possible bias due to PCR overamplification or the adapters (H); however, the graph of adapter content shows that the accumulative adapters are in a green zone and thus do not interfere with the output data. Graphics made in MultiQC software. The samples plotted follow the colour legend from (B). The coloured background of some graphs shows high (green), medium (beige) and low (red) quality zones. Sample data are represented by colours depending on their condition of origin: neuroepithelium-L2 (orange), glia-L2 (light blue), neuroepithelium-L3 (red) and glia-L3 (dark blue).

### 3.2. Sequences indexing and mapping

In order to manage raw data acquired from high-throughput sequencing experiments, it is necessary to run programs in the classical way using command-lines, which are small programs that perform specific functions. Therefore, from then on, I used command-lines following a classical data mining work-flow (Love et al., 2015) and the software MobaXterm, a toolbox for remote computing, as an intuitive interface.

Aligning the short sequencing reads to a reference genome, knowing as mapping, allows for visualisation of the transcript expression pattern of my samples. Finding a read sequence within the reference genome is computationally demanding and thus software-specific indexes are generated. The *Drosophila melanogaster* genome of reference is obtained from the Ensembl Project database. The tool used for both indexing and mapping is STAR (Dobin et al., 2013), and the program used for alignment visualisation is IGV (Robinson et al., 2011; Thorvaldsdóttir et al., 2012).

When the 12 samples sequenced are aligned with the fruit fly reference genome (Figure 28A,B), in almost all of the libraries more than 85% of the reads corresponded, with the exception of the *Sample 11* in which ~71% matched. However, it must be said that all those sequences were fully mapped on the length. All of these statistics support the strength of the sequencing run.

A view of the fragments aligned with the fly reference genome reveals the gene coverage as well as detailed nucleobases paired within the exons (Figure S13). Besides that, fragment visualising gives new insights of the biological replicates and a more specific overview of the transcript expression pattern of my samples (Figure 29). Thus, I detect alignments in neuroepithelial genes (*DE-Cad* and *patj*) in those samples which belong to *c855a*<sup>+</sup> transcripts for both stages, late-L2 IL (Figure 29A) and late-L3 IL (Figure 29C). However, typical genes from NBs (*mira*), neurons (*elav*) or glia (*repo* and *cg25c*) were not identified. In the same way, triplicates from *cg25c*<sup>+</sup> present fragments in glial genes but not for other cell type genes (Figure 29B,D). In conclusion, the mapping performance can be also taken as a quality control because highlights a good execution of the RNA-seq as well as confirms a proper cell identity of the original samples.

Once the mapping and its quality control is done, it is necessary to extract the number of aligned reads per gene. Transcript quantification also depends on the reference genome. STAR also produces this step transforming the overlapped reads into counts and identifying them with a gene for differential expression calling (data not shown).

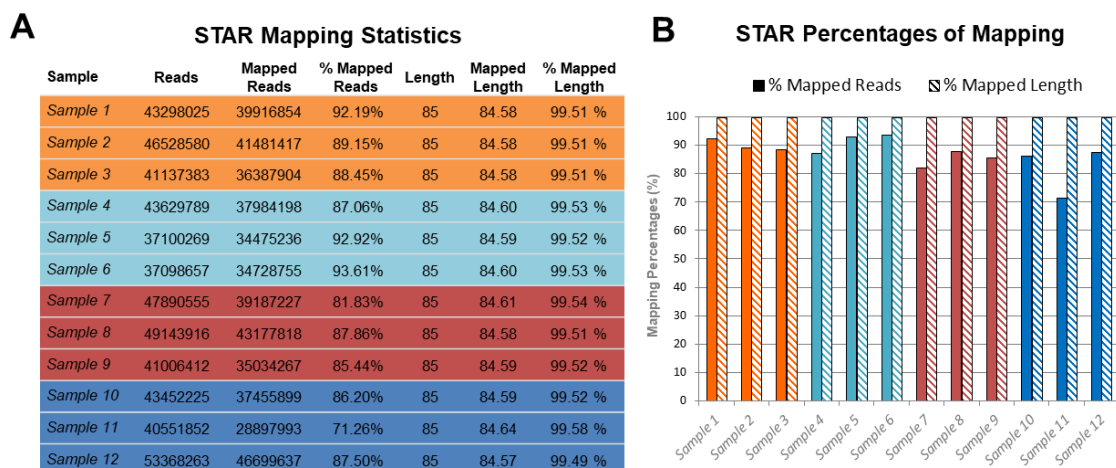


**Figure 28. Indexing and mapping reads from sequences with *Drosophila melanogaster* reference genome.** The sequenced samples were aligned using STAR software. Except *Sample 11*, all the reads were >85% mapped; the sequences all together were almost fully mapped in length. STAR output data is presented in a table of statistics (A) and in a bargraph of percentages (B). Sample colours by condition are the same as in Figure 27.

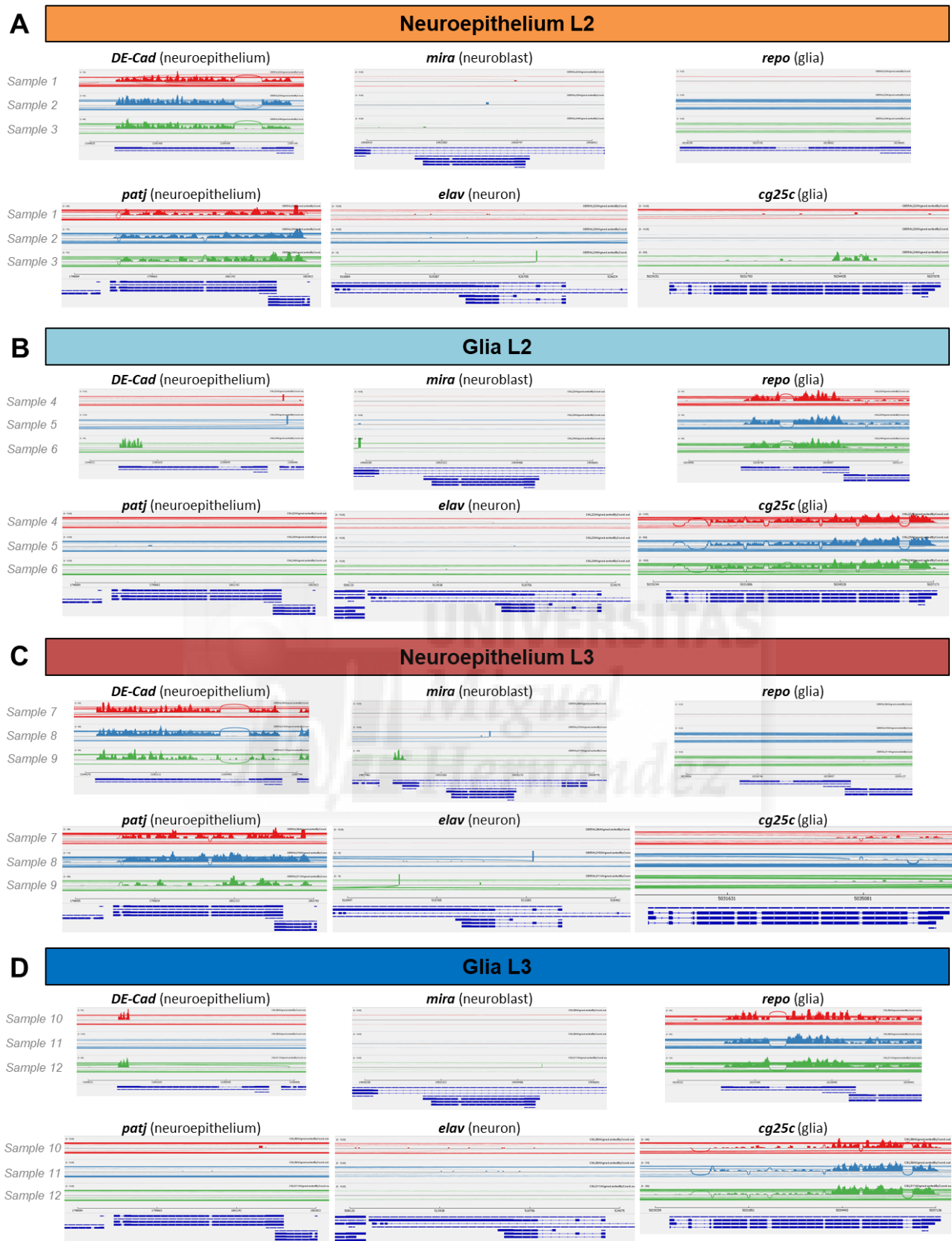


**Figure 29. Visualising mapped genes reveals data quality.** Sashimi representations from IGV software shows that biological triplicates share similar patterns of reads alignment and reveals also characteristic genes from each samples condition. Reads from neuroepithelial samples either late-2<sup>nd</sup> IL (A) or late 3<sup>rd</sup> IL (C) reflect alignment in genes specifics for this cell type such as *DE-Cad* or *patj* but not for neuroblasts (*mira*), neuronal (*elav*) or glial (*repo* and *cg25c*) genes. Likewise, glial samples in an earlier (B) or later (D) stage expose glial genes but neuroepithelial, neuroblast or neuronal genes. Sample colours by condition are the same as in Figure 27.

### 3.3. Differential gene expression between samples

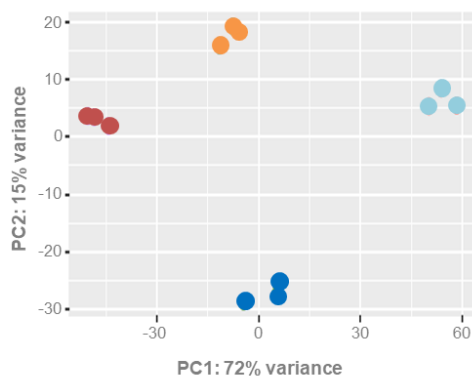
A detailed understanding of differential gene expression over time requires careful management of the high-throughput data. Once this point, the command-lines in R programming language are very useful for data mining, which is an important part of this thesis. R is a free software environment for statistics and plotting from the GNU project. I ran the user interface called RStudio which allows for the tracking of scripts, managing of R packages and viewing of datasets all in one interface. The packages of functions are provided by the projects CRAN and Bioconductor (Gentleman et al., 2004; Huber et al., 2015) and that ones I used are detailed in Appendix II (Table S1). After converting reads into counts (Anders et al., 2015), the differential expression of genes between samples is going to be run with the package DESeq2 (Love et al., 2014) which provides analysis based on the negative binomial distribution.

#### 3.3.1. Data exploration and representation

Firstly, data preparation is important; so tables and matrices allow plotting and help to explore the counts per each sample's gene. The first step is to normalise counts with the sequencing depth, because long genes can have more counts but low expression and thus normalising helps to stabilise the variance through the mean. To observe the transformation effect, I plotted the biological replicates between each other. This visualisation may use the  $\log_2$  normalised count values (Figure S14) but the low counts genes are significantly variable on this common logarithmic scale. However, the  $rlog$  (regularised-logarithm) transforms the values, minimising the variation with low count genes which contribute with irrelevant information about differential expression. Thus, when plotting  $rlog$  values between two replicates (Figure 31), most gene counts fall along the diagonal and very few are far from it. Taking advantage of the third replicate, these counts should be corrected.

A sample-to-sample distance representation helps to visualise overall similarities between samples. The  $rlog$ , apart from contributing to computing the distance between samples, is also used here to plot the principal components analysis, known as PCA. In short, PCA consist on finding the first and the second component (PC1 and PC2 respectively) that explains most of the differences between samples; thus when those components are plotted on each axis of the graph, the samples are projected into a bidimensional plane. Within my samples (Figure 30A), the PC1 explains 72% of the variance and the PC2 15%; this suggests that both principal components refer to cell type and stage condition, respectively. The graph also shows that triplicates are nicely clustered together while the different conditions are far away from each other. It is fair to say that, ideally, the two glial conditions should be closer on the graph although, at the same time, they differ sufficiently from the neuroepithelial groups. Another possible representation of sample-to-sample distance is a heat map of  $rlog$ -transformed data (data not shown). However, I used instead an improved measurement known as the Poisson distance (Witten, 2011) that takes into consideration the inherent variance structure of counts. In this representation (Figure 30B), it is easy to distinguish each triplicate grouped together as expected, meaning that the similarity between triplicates per each condition is very high.

**A** Principal Component Analysis



**B** Sample-to-sample Poisson Distance

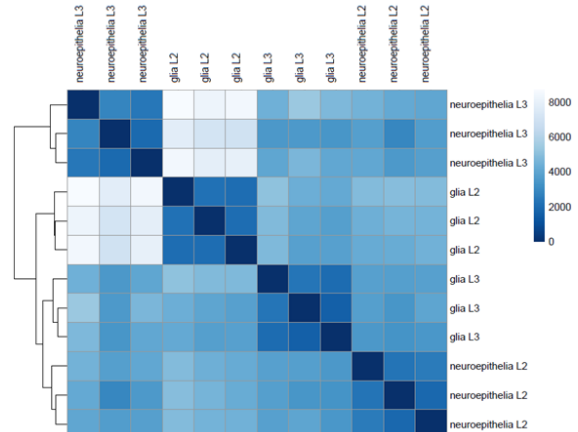


**Figure 30. Sample-to-sample distance visualisation.** Different representations are used to reveal the differences and similarities within samples. **(A)** The principal component analysis graph separates the samples into the two components which differ most. The x-axis represents the direction along which samples differ the most (PC1) while the y-axis the second most (PC2); on both are notated the percentages of the variance. **(B)** Sample-to-sample distance calculated using the Poisson method and represented in a heat map shows the similarities and differences between samples and the four conditions (neuroepithelium/glia and L2/L3). Sample colours in **(A)** by condition are the same as in Figure 27.

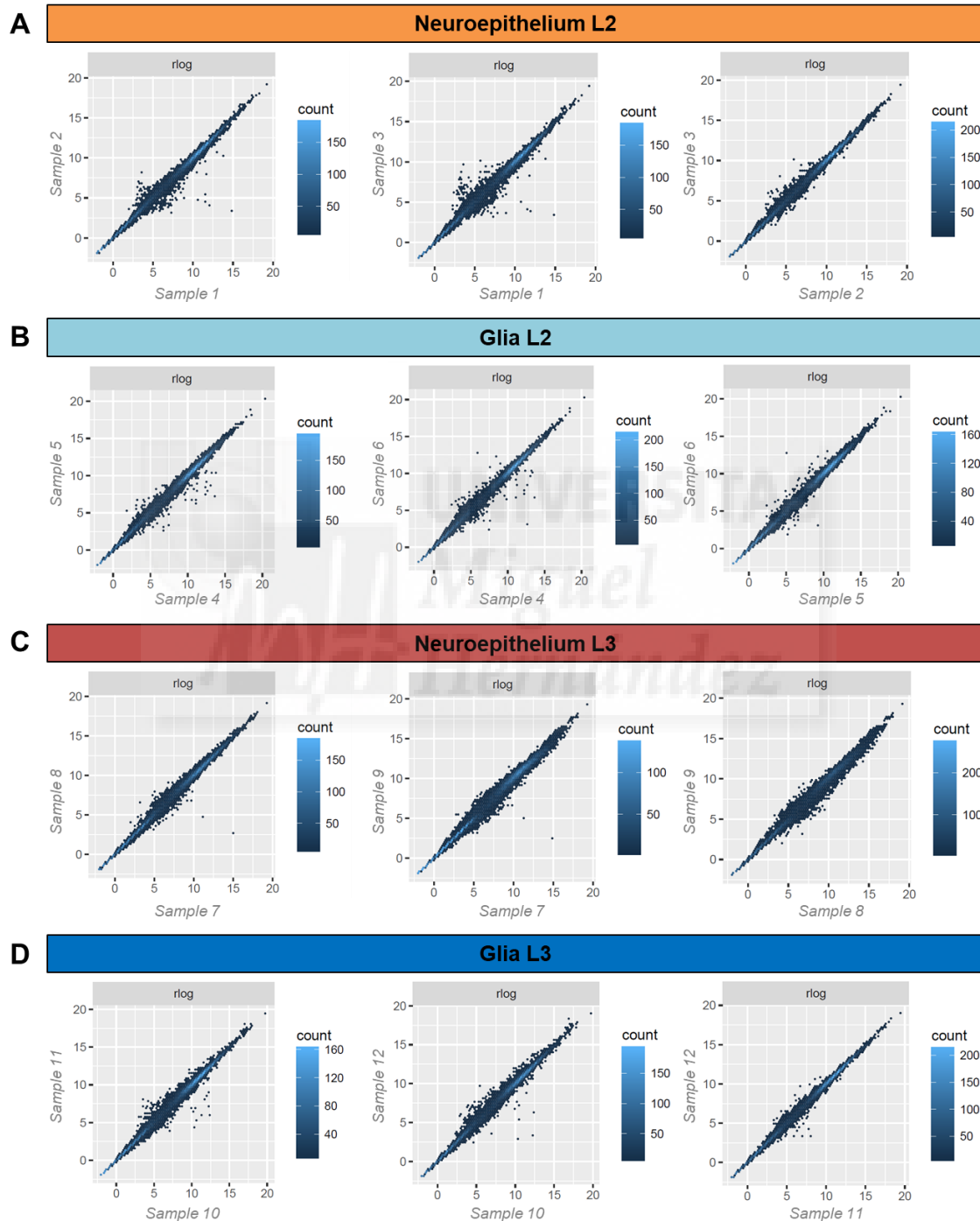


**Figure 31. Scatterplot of transformed counts among two replicates from the same condition.** Plotting *rlog* transformed avoids low counts, which are irrelevant for differential expression, but still shows higher counts. **(A-D)** Biological replicates from different larval periods are shown for neuroepithelium and glia. Sample colours by condition are the same as in Figure 27.

### 3.3.2. Differential expression analysis 1: Cell type approach

Once the RNA-seq data is verified as reliable, it is time to begin the analysis of the differential expression between conditions. Using my data, different approaches may be utilised to handle this step. The first method I used (Figure 33A) was comparing gene expression between the different cell types (neuroepithelium versus glia) from the same stage. This allowed me to determine cell-type specific as well as stage specific genetic markers. However, the main information from this approach which is relevant for me is the expression of classical genes per each cell type. Determining the expression levels of known genes from each condition acts as a control that affirms the accuracy of the expression levels measured for the genes in each sample.

As previously stated, I first removed from the raw data those genes that were not expressed at all; from the 13.068 genes in the *Drosophila* genome, those with 0 counts were discarded and we ended up with 12.379 genes in L2 and 11.885 genes in L3. Then, the function DESeq is used to perform different steps. These steps can be summarised in the estimation of size factors that controls the differences in the sequencing depth of the samples, the estimation of dispersion values for each gene, and finally fitting in a generalised linear model. Using neuroepithelial genes as a reference (serving as glia precursors), the output results give the estimated  $\log_2$  fold changes (Log2FC) and the p-value per gene. However, a multiple testing correction is needed to overcome the false positive that results from the calculation of a p-value even when  $p\text{-value} < 0,01$ . This correction is named the Benjamini-Hochberg adjustment and calculates per each gene an adjusted p-value (p-adjusted) which takes into account the false discovery rate (FDR). Then, a probability of  $p\text{-adj} < 0,1$  is considered acceptable. This results in 5.481 statistically significant genes in the L2 stage from which 2.908 are more expressed in glia and 2.573 are more expressed in NECs. In the L3 stage, from the 3.349 statistically significant genes there are 2.007 genes belonging to glia and 1.342 genes to NECs (table of Figure S15A).

As mentioned before, the normalisation of data is crucial to identify and remove systematic sources of variation and this allows comparisons to be made between stages. Plotting histograms of normalised counts with the previous p-adj criteria (Figure 32A) is useful to see their frequencies and thus exclude genes with very small counts. Another useful visualisation that allows one to see which genes must be excluded is the minus average of estimated coefficients (MA-plot; Dudoit et al., 2002). Plotting the Log2FC against the mean of normalised counts by size factor (Figure 32B), comparing the different stages. As  $p\text{-adj} < 0,1$ , the red plots identify genes which are below this threshold and thus are excluded for the analysis, while genes containing enough significant information remain.

With this data, I examined the expression of classical neuroepithelial and glial markers (Figure 33B-D). The number of normalised counts are visualised briefly, plotting the amount of expression for particular gene markers in each condition (Figure 33B) which is also detailed separately within their replicates (Figure 33C). Those values are interpreted clearly in a Log2FC gene expression graph (Figure 33D), which presents the expression of typical neuroepithelial makers such as *DE-Cad*, *patj* and *dlg1* for NECs and specific glial markers such as *repo* and *cg25c* for glial cells. Note that Log2FC values for NECs are negative because they are used as a reference to which expression in glia may be compared, meaning that they need to be considered for their absolute value.

Finally, merging the differentially expressed cell-type genes in distinct stages in a Venn diagram and plotting them in expression graphs as well as clustering in heat maps allows for the determination of which genes are cell specific markers as well as which are temporally specific markers (Figure S15). Although this part of the analysis is not the main objective of the thesis, the potential marker genes here mentioned are already unified by its Gene Ontology (GO; data not shown) and, if desired later on, could be tested *in vivo* and more knowledge could be gained from this point of the study.

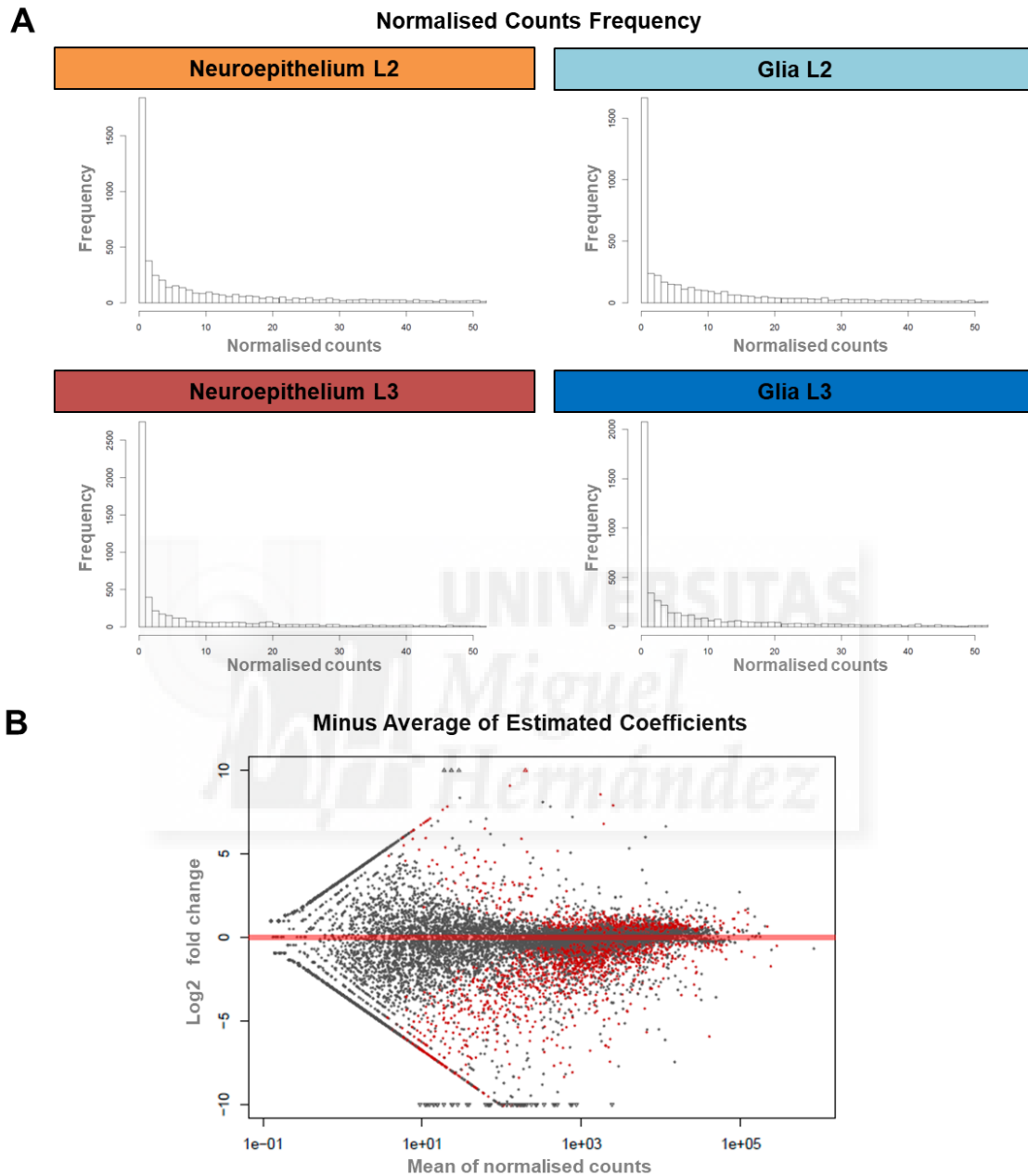


**Figure 32. Normalised counts allows for the exclusion of low significance genes.** These graphs follow the criteria of  $p\text{-adj} < 0.1$ . **(A)** Histograms of normalised count frequency identify the values with small amounts of fragments. **(B)** The minus average graph, which plot genes by mean of normalised counts versus  $\text{Log}_2\text{FC}$ , identifies in red the genes under the threshold and, thus, those that will be removed from the analysis. Sample colours in **(A)** by condition are the same as in Figure 27.



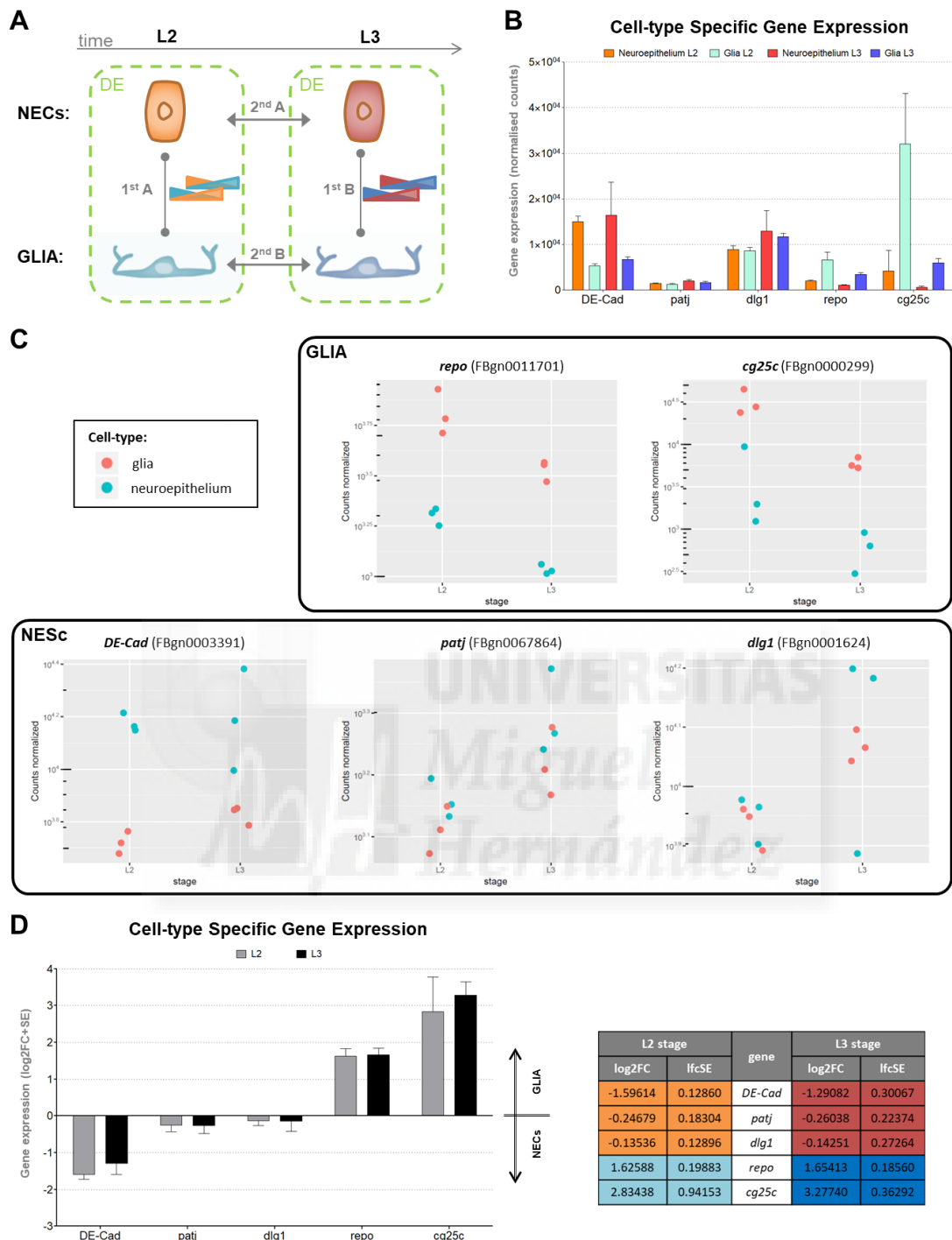


**Figure 33. Cell type differential expression approach reveals typical markers of each cell population. (A)** Schematic representation of the first differential expression (DE) approach defined by larval cell type of the same stage. Circled in green, two separated DE per gene are performed between neuroepithelial (NECs) and glia cell types depending on larval developmental time. This gives us information about different cell markers between both cell types in L2 (1<sup>st</sup> A) and L3 (1<sup>st</sup> B) stage. Also, a gene comparison between the different stages of NECs (2<sup>nd</sup> A) and glia (2<sup>nd</sup> B) may give specific time markers. **(B)** Gene expression in the number of normalised counts shows the total amount of fragments per condition from the genes that are markers for NECs (*DE-Cad*, *patj*, *dlg1*) and glial cells (*repo*, *cg25c*). **(C)** Plotting the number of normalised counts in each sample shows the dispersion of cell markers between replicates. **(D)** The Log2FoldChange value shows the specific genes differentially expressed in their appropriate cell type; as expression levels in the neuroepithelium are used as a reference, the positive values belong to glia and the negative to NEC expression. Sample colours by condition are the same as in Figure 27.

### 3.3.3. Differential expression analysis 2: Stage approach

The objective of the second approach is to find which genes are differentially regulated at two distinct points in time and, later on, determine their molecular partners in the niche cell types. To achieve this, differential expression analysis (Figure 34A) was performed comparing different larval stages (L2 versus L3) per each group of cells (neuroepithelium and glia). The procedure used for this approach is generally the same as in the previous section, with the addition of an extensive GO analysis and an *in vivo* validation further on.

Therefore, in this case, from the 13.068 genes of the *Drosophila* genome, there were 12.059 genes in NECs and 12.253 genes in glia that had counts aligned. When applying the differential expression method to normalised counts, expression at the L2 stage was used as a reference for previous expression levels. Hence, the output data gave positive Log2FC values for the genes up-regulated in L3 and negative values for those down-regulated in this stage. After applying the p-value correction to  $p\text{-adj} < 0,1$ , the number of statistically significant genes in neuroepithelium was 2.471 from which 933 genes were up-regulated and 1.538 genes down-regulated (Figure 34B). When the correction was applied to glia, 4.663 genes were found, out of which 2.070 genes were up-regulated in L3 versus L2 and 2.593 of which were down-regulated (Figure 34B).

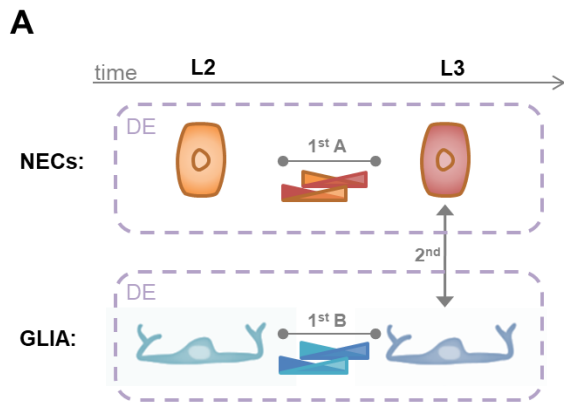
Afterward, the four condition lists containing the differentially expressed genes were merged in a Venn diagram (Figure 34B). Plotting the expression of the genes which are pooled together, it is possible to visualise the up- and down-regulated genes at the L3 stage specifically in each cell type (Figure 34C) in addition to genes that NECs and glia share (Figure 34D). This information is highlighted in a heat map which allows for the identification of relative expression between each original sample (Figure 34E,F).

The main objective of this thesis is to unveil the potential molecular partners derived from this RNA-seq data. At this point and in order to effectively do this, GO enrichments are needed, and in the present study I used the package “mgsa” in R for modelling the analysis. The model-based gene set analysis (MGSA, Bauer et al., 2010) does not analyse each set in isolation as do classical methods; instead, it considers the overlap, which reduces the number of redundant sets. Once the differential expression of a group of genes is fitted into the model for an estimate probability  $> 0,1$ , the tool gives as results the different GO numbers based on biological process (BP), cellular component (CC) and molecular function (MF).

Three *in silico* screenings have been applied to the group of genes from the Venn diagram (Figure 34B) to indicate the genes that are top hits. The first screening is to find the expressed genes which are up-regulated uniquely in each cell type and have molecular partners from the other niche cell type that may interact. Thus, this trial workflow (Figure 35A) consists of GO filtering in series (Figure 35B and Table S2) combined with the interactive molecular partners and ending in a manual selection of the interesting genes. From the initial 1.318 glial-specific up-regulated genes and 195 NEC-specific genes, a total of 18 and 17 target genes were obtained for glia and NECs respectively, which are also molecular partners with each other. Overall, this screening identifies a total of 35 unique genes (Figure 35C) which are then evaluated with an *in vivo* validation presented in the next chapter.

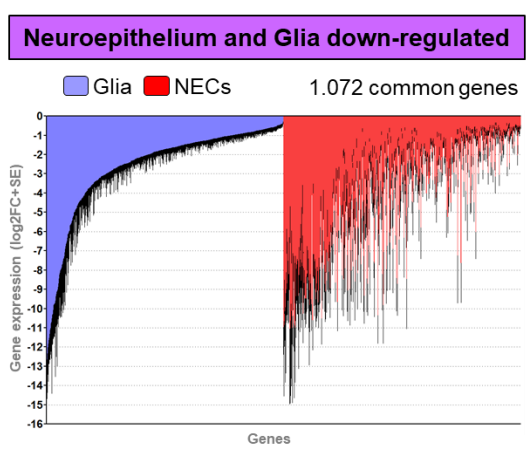
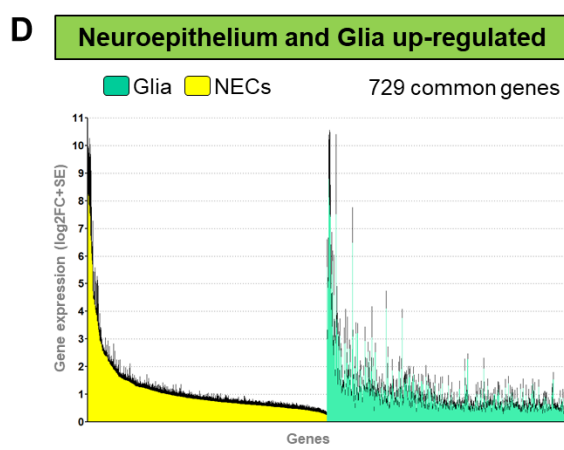
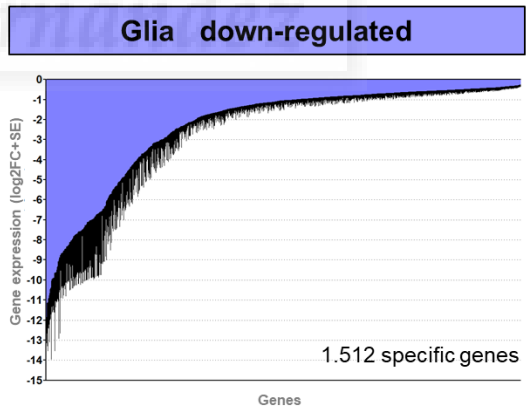
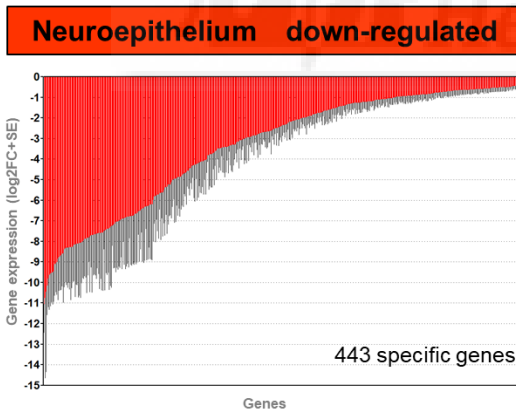
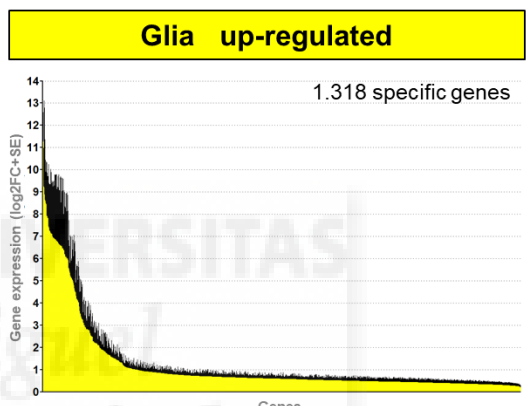
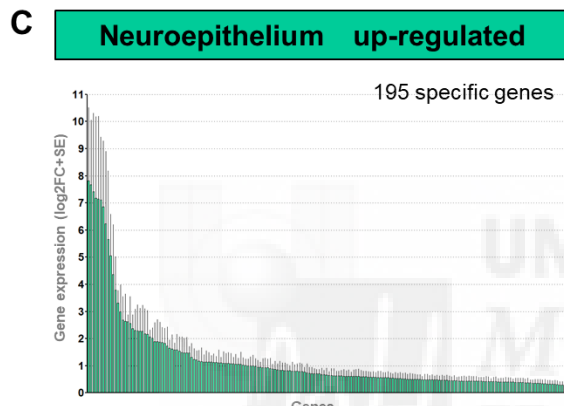
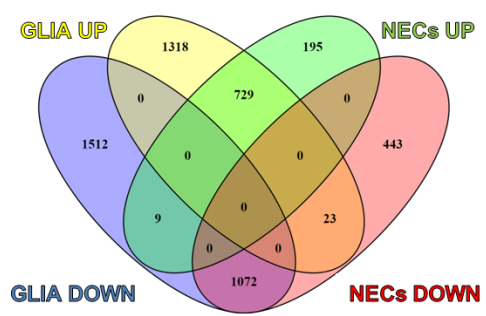
The second screening (Figure 36A) was performed with the 729 genes up-regulated that were common in both NECs and glia. Two consecutive GO filterings (Figure 36B and Table S3) produced a list of 39 top-hit up-regulated genes. Later, we found their up- or down-regulated molecular partners for the other cell type in the niche. This procedure revealed 35 interactive genes for neuroepithelium and 46 genes for glia. However, as the lists contain some shared genes among them, the partner lists contribute with 27 genes of a total of 66 unique genes from this second screening (Figure 36C). From those final 66 genes, 50 genes needed to be validated *in vivo* in NECs and 61 genes in glial cells (Figure 36D).

The third and last screening of this section was performed with the genes that were down-regulated in L3 in both niche cell types (Figure 37A). From the 1.072 genes on the list, 68 top-hit genes were identified after parallel GO filtering (Figure 37B and Table S4). The next step was to find the independently regulated molecular partners for top-hit genes. This procedure found 9 neuroepithelial genes and 12 glial genes which may interact with the genes down-regulated in both cell types in L3 larvae. As with the cellular partners in the second screening, some genes were shared and thus there was a total of 10 unique genes from a final list of 78 top-hit genes (Figure 37C). The final list contained 73 genes that needed to be tested in NECs and 77 in glial cells (Figure 37D).

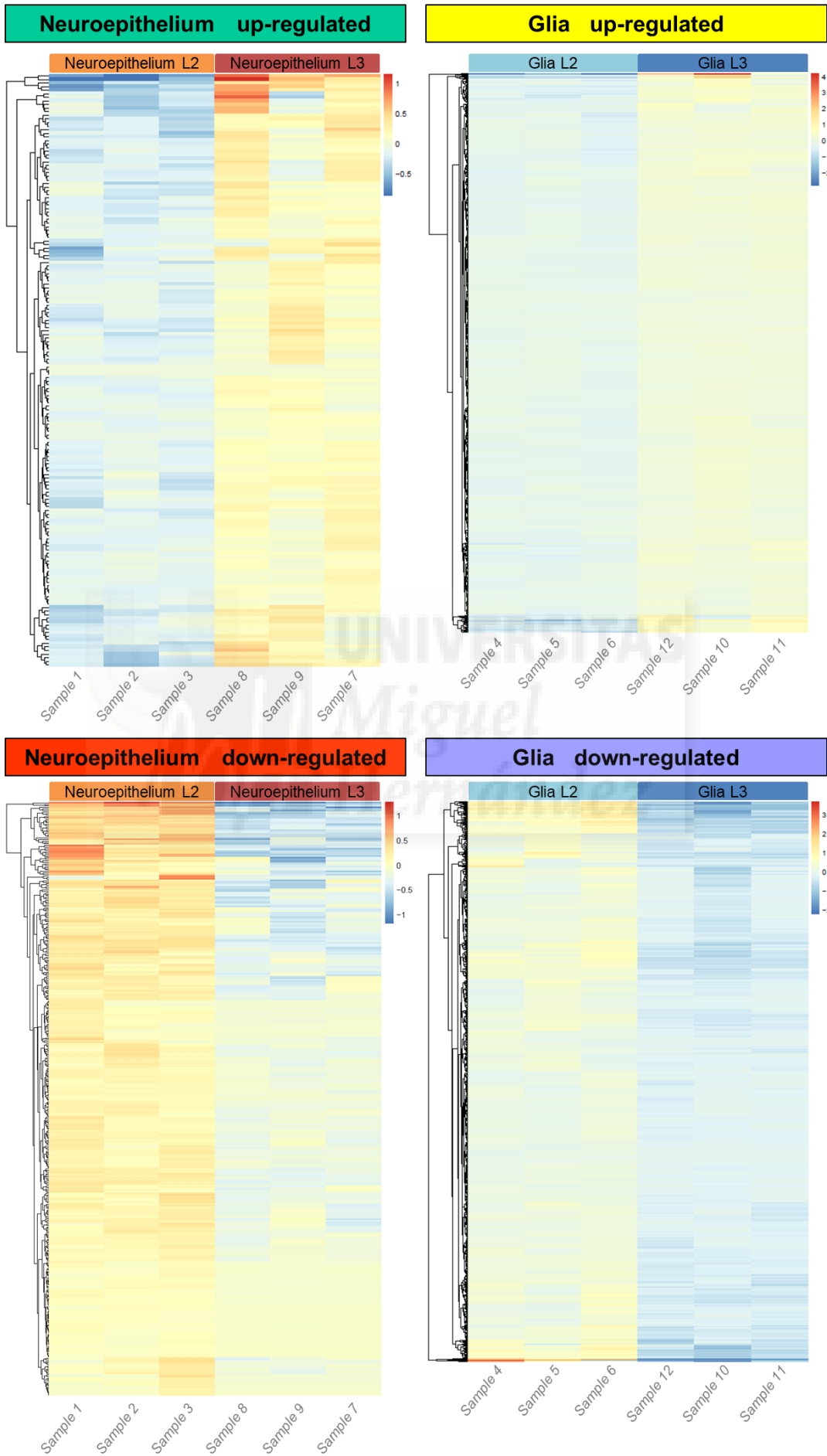


**B** Grouping DE genes by condition

Condition	Number of DE genes	Total genes per cell type	Overall number of unique genes
NECs L2	1.538	2,471	5,301
NECs L3	933		
Glia L2	2,593	4,663	
Glia L3	2,070		



E



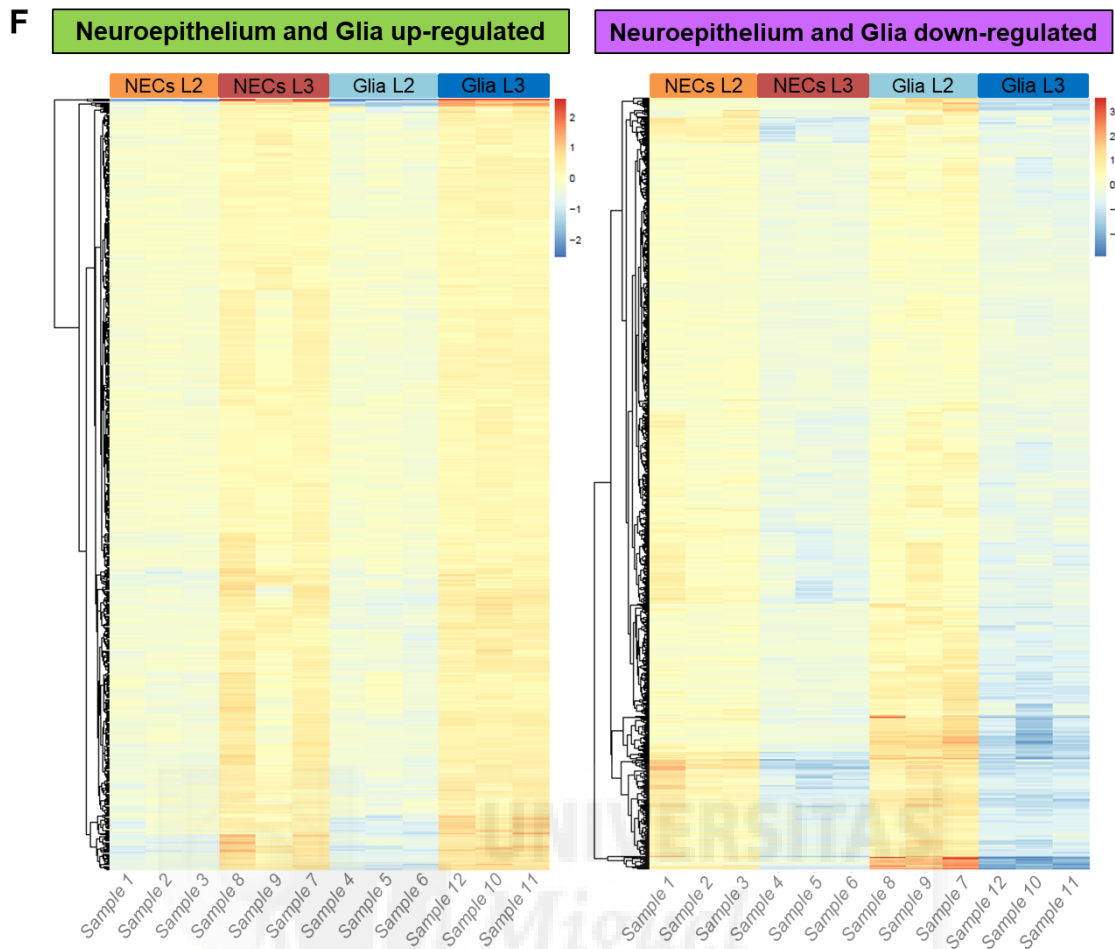
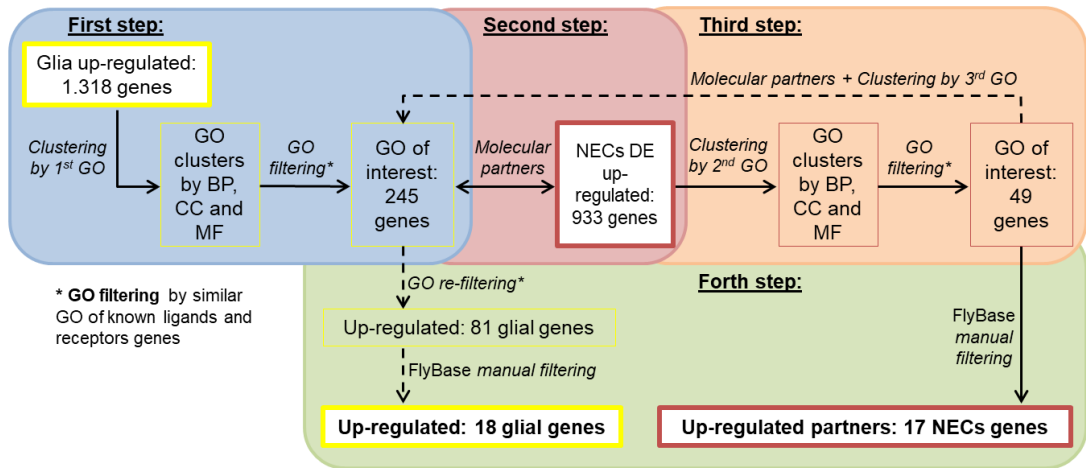


**Figure 34. Stage differential expression approach shows cell-type-specific grouped genes.** (A) Schematic representation of the second differential expression (DE) approach defined by larval stage of the same cell type. Circled in purple, two separate DE measurements per gene are carried out in L2 and L3 stage per each cell type: neuroepithelial (NECs) and glia. This gives us information about the change in gene expression over time for NECs (1<sup>st</sup> A) and glia (1<sup>st</sup> B). Finally, a gene comparison between both cell types (2<sup>nd</sup>) reveals their molecular partners. (B) Venn diagram shows all possible relationships between the four conditions of differential gene expression. (C) Gene expression per each condition shows top specifically expressed genes which are up- or down-regulated (positive and negative values, respectively). (D) Gene expression per stage shows common specific genes which are potentially up- or down-regulated. (E,F) Gene clustering in heat maps of Venn diagram groups reveals the genes with the highest variance of relative *rlog*-transformed values across samples. Sample colours by condition are the same as in Figure 27. Grouped genes colours are the same as in Venn diagram (B).

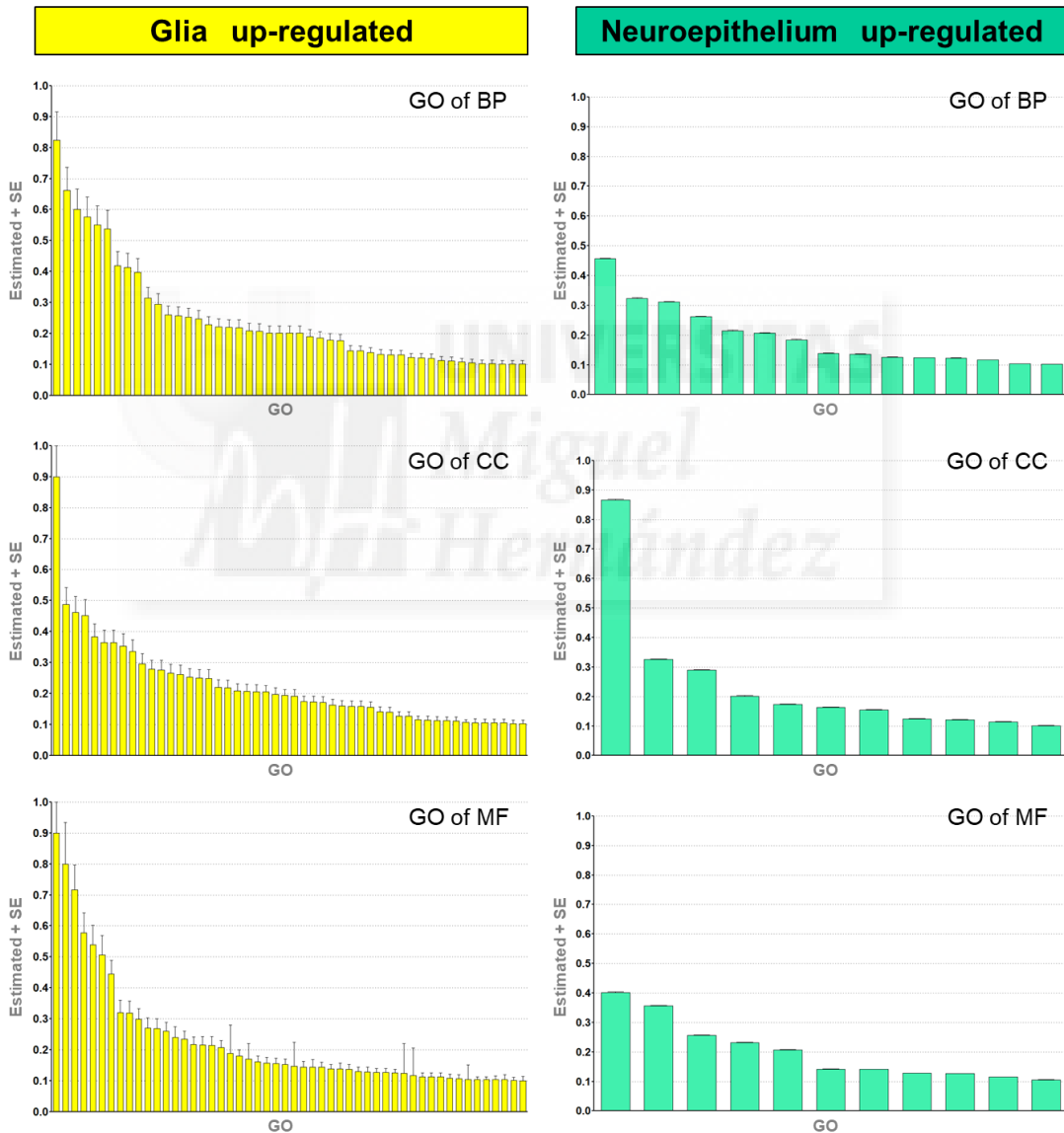
**Figure 35. Screening 1 workflow enables identify top-hit up-regulated genes for glia and neuroepithelium molecular partners.** (A) The screening 1 workflow consists of four steps. First, the glia up-regulated gene list (1,318 genes) underwent a GO analysis clustered by biological process (BP), cellular component (CC) and molecular function (MF) which obtained the group of target genes. The second step was acquiring their molecular partners from the other cell type niche. The third step was GO filtering those partners to obtain a partner list of genes; then, the group of target genes was also re-filtered by GO. The last step was to filter manually using FlyBase.org to achieve the list of 18 top-hit glial genes and 17 neuroepithelial genes. GO filtering were performed according GO similarities of known ligands and receptors genes (e.g. BP: development or signalling; CC: membrane or cell periphery; MF: receptor or molecule binding) and are annotated in Table S2. This pipeline was also performed starting with a list of genes up-regulated in NECs (195 genes) and following basically the same process, adding one extra gene in each top-hit list. (B) Graphical representation of GO groups by BP, CC and MF from glia and NECs up-regulated gene lists for the first filtering step. (C) Venn diagram shows the final top-hit lists where the 18 glial and 17 neuroepithelial up-regulated genes are unique. Sample colours by condition are the same as in Figure 27. Grouped genes colours are the same as in Figure 24B Venn diagram.

**A**

**Screening 1: Glia up-regulated GO workflow**



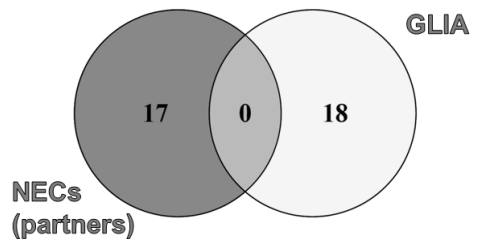
**B**



**C**

**Screening 1 top-hit list**

List	Number of genes	Overall number of unique genes
Glia up-regulated	18	35
NECs up-regulated (partners)	17	



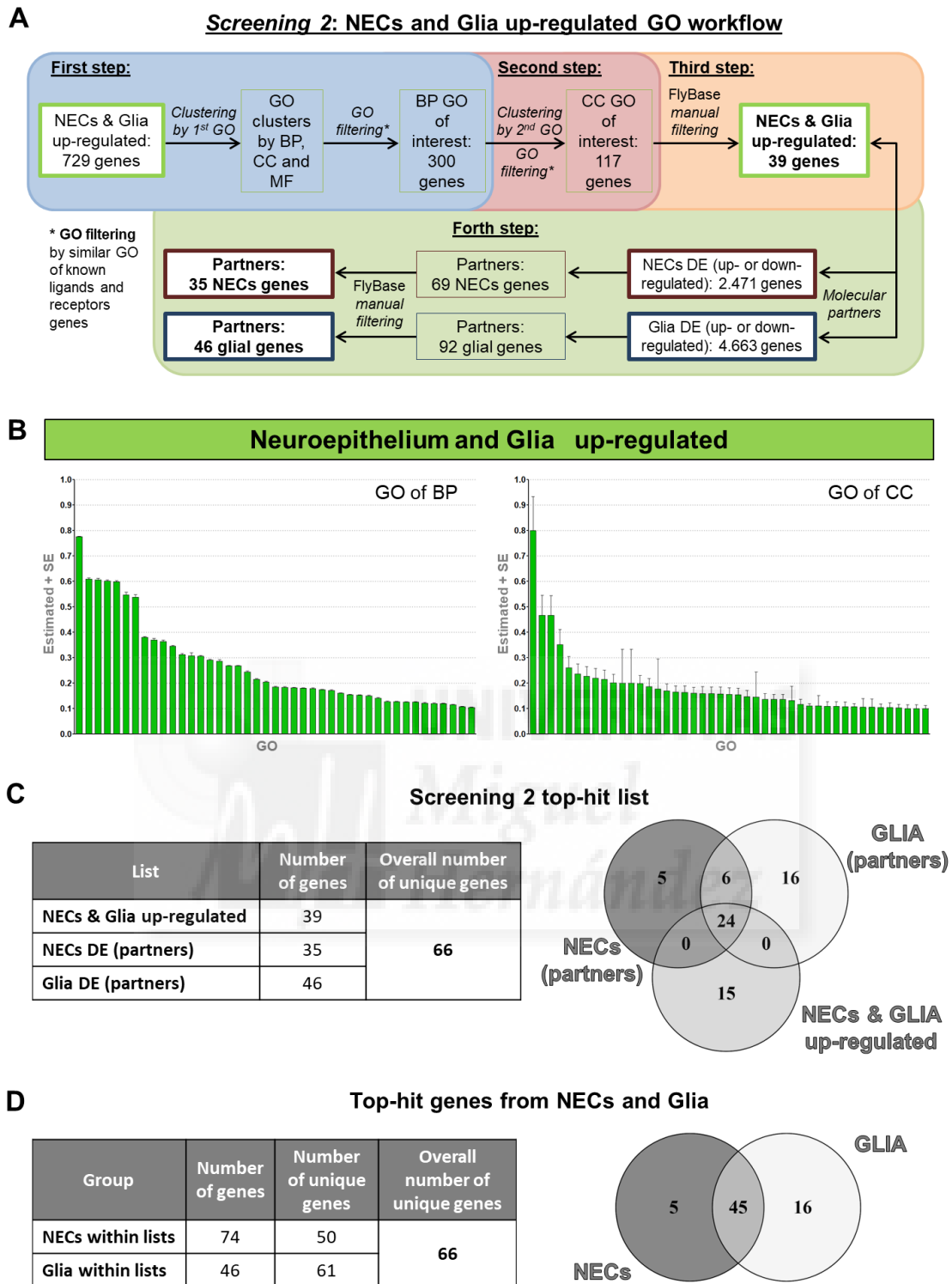
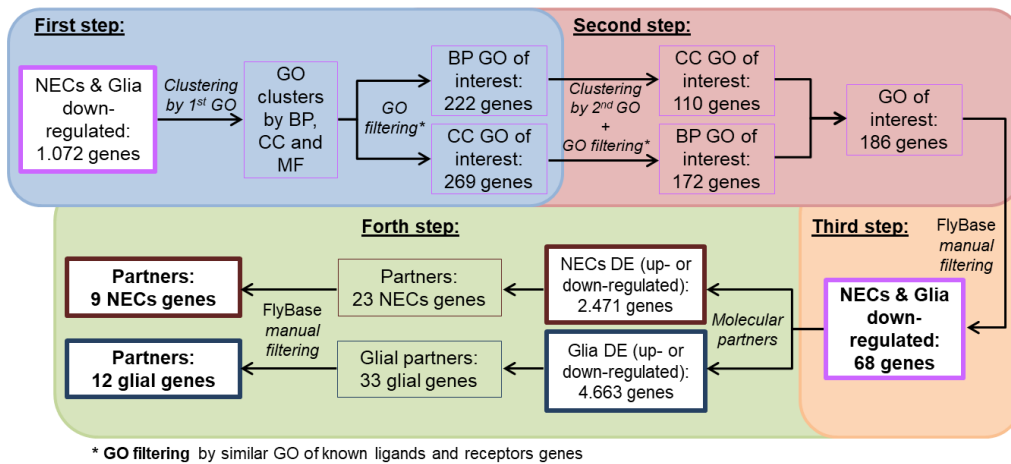
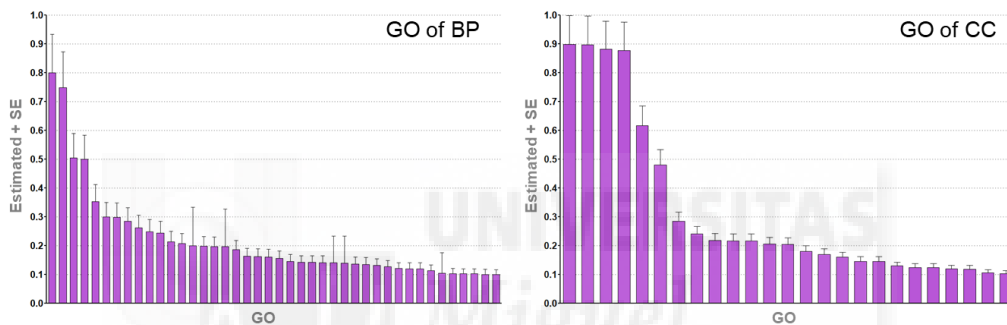


**Figure 36. Screening 2 workflow enables identify top-hit genes up-regulated in both neuroepithelium and glia and also their molecular partners. (A)** Screening 2 workflow consists of four steps. First, the list of genes up-regulated in both NECs and glia (729 genes) underwent a GO analysis clustered by biological process (BP) which obtained the group of target genes. Second, the target genes were re-filtered by the cellular component (CC) GO clustering, reducing the target gene list. The third step was filtering manually using FlyBase.org to achieve the list of 39 top-hit genes per each type of niche cell. The last step was to acquire the genes' molecular partners from the other cell type of the niche; thus, 35 neuroepithelial and 39 glial top-hit genes were added to the final list. GO filtering were performed according GO similarities of known ligands and receptors genes (e.g. BP: development or signalling; CC: membrane or cell periphery; MF: receptor or molecule binding) and are annotated in Table S2. **(B)** Graphical representation of GO groups by BP and CC for the first and the second filtering steps respectively from glia and NECs common up-regulated gene list. **(C,D)** Venn diagrams show the final top-hit lists from which 39 are common up-regulated genes for niche cells from a total of 66 unique genes. Sample colours by condition are the same as in Figure 27. Grouped genes colours are the same as in Figure 24B Venn diagram.

### A Screening 3: NECs and Glia down-regulated GO workflow

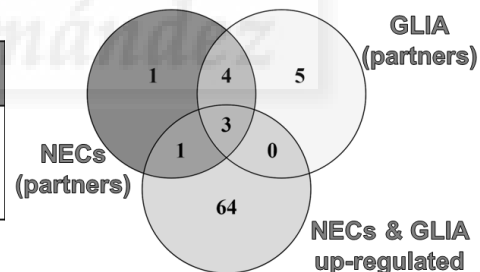


### B Neuroepithelium and Glia down-regulated



### C Screening 3 top-hit list

List	Number of genes	Overall number of unique genes
NECs & Glia down-regulated	68	78
NECs DE (partners)	9	
Glia DE (partners)	12	



### D Top-hit genes from NECs and Glia

Group	Number of genes	Number of unique genes	Overall number of unique genes
NECs within lists	77	73	78
Glia within lists	80	77	

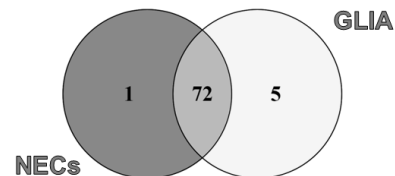


**Figure 37. Screening 3 workflow enables identify top-hit genes that are down-regulated in both neuroepithelium and glia and also their molecular partners.** (A) The screening 3 workflow consists of four steps. First, the list of genes down-regulated in both NECs and glia (1.072 genes) underwent a GO analysis clustered by biological process (BP) and cellular component (CC) in parallel which obtained each group of target genes. The second step was re-filtering the target genes conversely, that is to say CC and BP GO clustering respectively, reducing the target gene list. The third step was filtering manually using FlyBase.org to achieve the list of 68 top-hit genes per each type of niche cell. The last step was to acquire each gene's molecular partners from the other niche cell type; thus, 9 neuroepithelial and 12 glial partners' top-hit genes were added to the final list. GO filtering were performed according GO similarities of known ligands and receptors genes (e.g. BP: development or signalling; CC: membrane or cell periphery; MF: receptor or molecule binding) and are annotated in Table S2. (B) Graphical representation of GO groups by BP and CC for the first filtering step of gene list down-regulated in both NECs and glia. (C,D) Venn diagrams show the final top-hit lists from which 68 are genes down-regulated in both types of niche cells from a total of 78 unique genes. Sample colours by condition are the same as in Figure 27. Grouped genes colours are the same as in Figure 24B Venn diagram.



After performing three different screenings, I ended up with 35 genes from the first screening (Figure 35), 66 genes from the second screening (Figure 36), and 78 genes from the third screening (Figure 37). Those final lists share some genes, as shown in a Venn diagram (Figure 38A), and thus the numbers of new genes added in the second and third screening are, respectively, 45 and 71 genes. Therefore, the overall number of top-hit genes on the stage approach is 151 unique genes, of which 125 were later validated in NECs and 139 in glial cells (Figure 38B and Table S5). It is worthy of mention that other screening workflows may be performed using the RNA-seq data and for this reason the new screenings carried out enlarge the final top-hit list of genes.

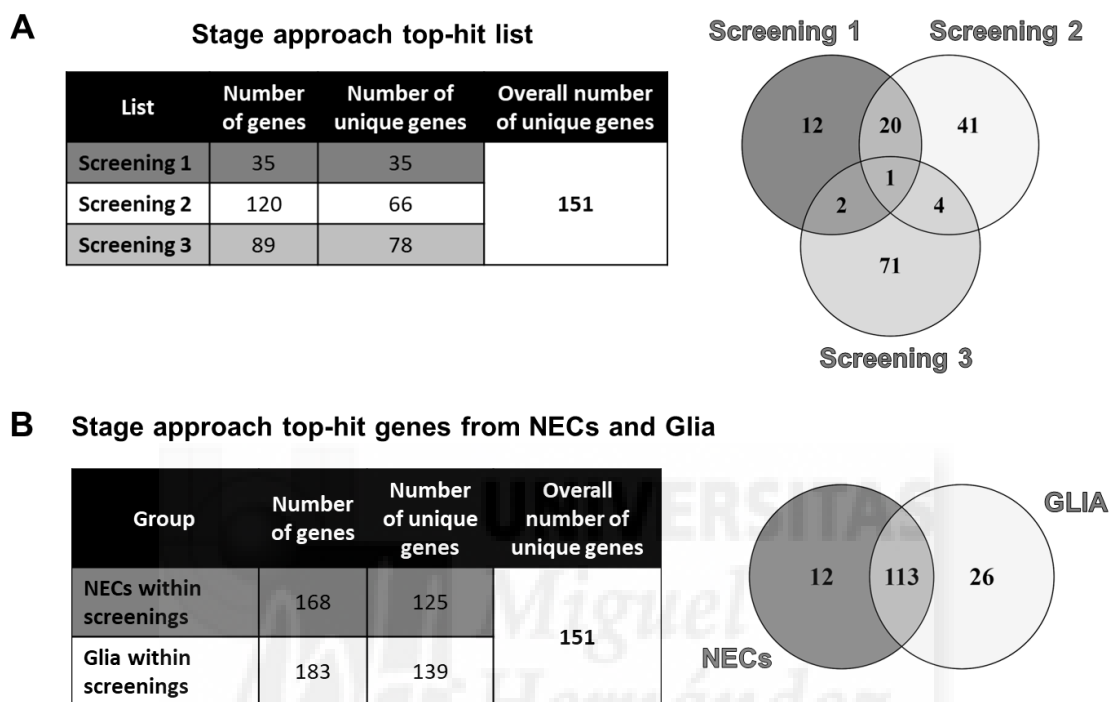


**Figure 38. Top-hit genes for neuroepithelium and glia from all the screenings of the stage approach.** Venn diagrams show (A) the final top-hit genes from each of the three screenings carried out in which a total of 151 unique genes were found. From those top genes (B) 125 are differentially expressed in NECs and 139 in glial cells. Their expression levels are summarised in Table S5. The run was performed in Venny 2.1.0. software.

## 4. Identification of glial and neuroepithelial extrinsic cues from candidate genes

### 4.1. Genetic *in vivo* validation of top-hit genes

The bioinformatics analysis of the RNA-seq data has narrowed the differentially expressed genes examined from thousands to specifically 151 genes (Figure 38 and Table S5). After completing this analysis, I proceeded to the validation of these top-hit genes in order to test whether they are functionally relevant or not. Due to the nature of *Drosophila*, massive genetic validations are highly efficient in terms of time, resources and accuracy in detecting significant developmental abnormalities as a result of gene activity defects (Villegas et al., 2018; Yamamoto et al., 2014). In this thesis, the candidate genes (receptors, ligands, transmembrane or secreted proteins, etc.) were analysed via gain of function (GOF; UAS lines) or lack of function (LOF; RNAi lines) mutant flies. Each up- or down-regulation of a gene was tested with two to five different mutant lines from BDSC and VDRC stock centres, resulting in a total of ~650 crosses. When a dysfunction in the progeny was detected, the line was separated for re-testing. Finally, the genes affecting biological processes of interest were further analysed with the goal of revealing important niche cell functions.

Up- or down-regulation of approximately one third of the top-hit genes (34%, 51 of 151 genes) caused development deficiencies (e.g. temporal stage mismatch, problems with organ development, cell cycle death or premature lethality; Figure 39A). These phenotypes resulting from changes in expression levels of these genes were observed in multiple fly lines for each gene during the validation (Table S6). Some of the abnormal phenotypes were produced by dysregulated genes in *c855a*<sup>+</sup> cells and others in *cg25c*<sup>+</sup> cells (Figure 39B). Interestingly, some of the genes expressed in both cell types displayed the same abnormal phenotype when up- or down-regulated in each cell type while others displayed different phenotypes, as shown below. Moreover, the malfunctions of those 51 genes may have implications in any stage of the fly's life cycle: in larvae, pupae or adult flies (Figure 39C). Although all the phenotypes found for the genes examined are mentioned next, due to space constraints and the nature of some phenotypes (e.g. lethality), it is not possible to show all of the data and thus, only relevant phenotypes are presented below in figures.

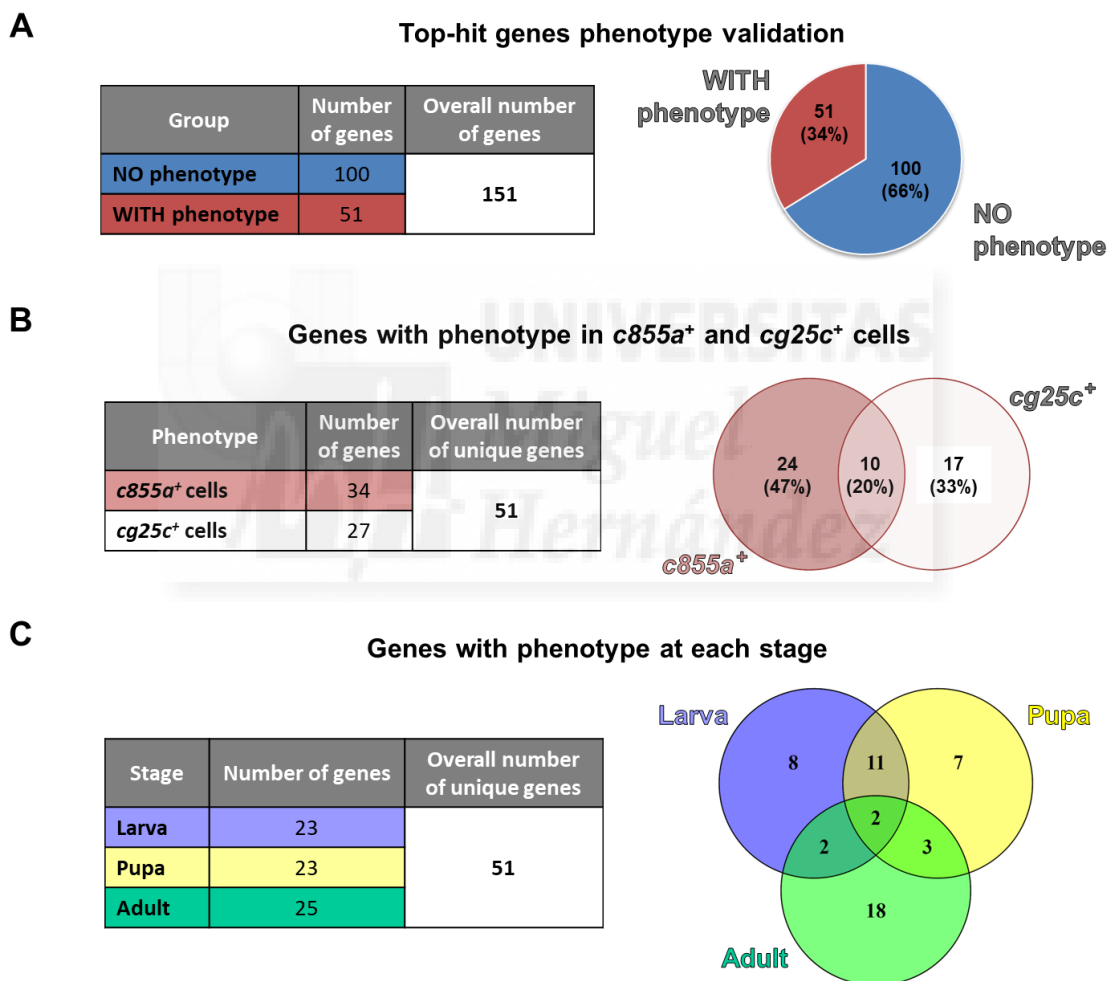


**Figure 39. *In vivo* validation of top-hit genes from RNA-seq.** Validation reveals abnormal phenotypes resulting from GOF or LOF of genes (phenotypes include lethality, temporal mismatch, anomalous organ development, cell death, etc.). (A) About a 34% of the genes tested (51 of 151 genes; Table S6) had impacts on *Drosophila* development when their expression levels were altered. The rest, 66% of the genes (100 of 151 genes), caused no apparent negative effects on the fly's life cycle when up- or down-regulated. (B-C) Venn diagrams show the genes for which altered expression caused abnormal phenotypes. These genes may play important roles in either *c855a*<sup>+</sup> or *cg25c*<sup>+</sup> cells, or both (B), and in any of the developmental stages (C).

## 4.2. Genes involved in unusual phenotypes at pupal and adult stages

Despite the fact that defects in pupa and adult were not the main goal of this thesis, malfunctions of the genes studied in niche cells reveal that these genes are also relevant during those developmental stages.

Out of the 51 genes found in the validation, up- or down-regulation of 23 of these genes caused dysfunctions at the pupal stage (Figure 39C). Genes found by the validation in *c855a*<sup>+</sup> cells (Figure 40A) almost all present lethality or semi-lethality in pupa (Figure 40A') when their expression is down-regulated with RNAi. Examples of this are *5-hydroxytryptamine receptor 2B (5-HT2B)*, one of the five serotonin receptors in *Drosophila* (Blenau et al., 2017; Clark et al., 2004); *Insulin-like receptor (InR)*, required in the TOR pathway for PG proliferation (Avet-Rochex et al., 2012); and *wntless (wls)*, a transmembrane protein required for Wingless/Integrated (Wnt) protein secretion (Bartscherer et al., 2006). The involvement in lethality of the genes *ptc*, *Oamb*, *Octβ3R*, and *nAChRα3* will be discussed in the next section. In contrast, overexpression of the gene *wingless (wg)*, a ligand of the Wnt/Wg signalling pathway (Couso et al., 1994), causes lethality. Another interesting gene is *ebi*, which modulates EGFR pathway in development (Dong et al., 1999); underexpression of this gene causes lethality in pupa in females only, since males do emerge as adults flies. Finally, apart from the lethality phenotype resulting from underexpression of the gene *echinoid (ed)*, which is a cell adhesion molecule that cooperates with DE-Cad and participates in various signalling pathways including EGFR, Hippo and Notch pathways (Rawlins, 2003; Spencer and Cagan, 2003; Wei et al., 2005; Yue et al., 2012), causes greater pupa volume; this is also the case for the gene *dpr10*, which will be explained further on. Additionally, defective expressed genes in *cg25c*<sup>+</sup> cells can cause not only lethality in pupal stages but also may lead to abnormal organ sizes during development (Figure 40A-A'). The phenotypes resulting from dysregulation of the genes *dpr5*, *Egfr*, *mys*, *Octβ1R* and *Tig* in a glial context will be discussed below.

I detected 25 genes whose down-regulation with RNAi provoked developmental abnormalities features in adulthood (Figure 39C). When *c855a*<sup>+</sup> cells (Figure 40B) lack a proper expression of the gene *bark beetle (bark)*, a transmembrane scavenger receptor-like protein (Hildebrandt et al., 2015), the adult fly is unable to unfold its wings (Figure 40B'). This phenotype is the same when the gene down-regulated is *Pburs (Partner of Bursicon)*, a protein which dimerises with *Burs* to form a neurohormone which acts in the *Lgr2* receptor to unfold the wings (Luo et al., 2005; Mendive et al., 2005). Apart from defects in wing development, I also observed defects in climbing the tube walls when gene expression was down-regulated in *c855a*<sup>+</sup> cells. A climbing assay revealed that when a gene was not present, for example, the seven-pass transmembrane protein *starry night (star)* (Organisti et al., 2015), fruit fly climbing ability decreased beginning in early adulthood; however, the lack of expression of other genes such as *argos (aos)*, *multiple edematous wings (mew)* and *frizzled (fz)* result in increased overall movement of the flies (Figure 41B). Due to the fact that climbing experiments are time-consuming and defects in adulthood are not the focus of this thesis, other genes in *c855a*<sup>+</sup> cells including *egr*, *Inx3*, *Mmp2*, *otk*, *Ten-m* and *Wnt4* remain to be tested.

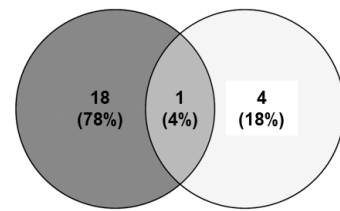
Down-regulation of genes in niche counterpart *cg25c*<sup>+</sup> cells (Figure 40B) also causes deficiencies in adult flies (Figure 40B'). Abnormal curly and coarsed wings were detected when the neuropeptide receptor *SIFamide (SIFaR)* (Hewes and Taghert, 2001; Jørgensen et al., 2006) was underexpressed. An unusual swollen abdomen developed when *bazooka (baz)*, a gene which is related to epithelial cells (Morais-de-Sá et al., 2010) and NBs (Wodarz et al., 1999), was underexpressed. Finally, down-regulating genes such as *tenascin accessory (Ten-a)*, a teneurin transmembrane protein (Mosca and Luo, 2014), and *protein tyrosine phosphatase 69D (Ptp69D)*, a transmembrane receptor tyrosine phosphatase (Hakeda-Suzuki et al., 2017), both of which are involved in synapse organisation, caused organism malfunctioning. These defects lead to a premature decrease in climbing activity from the very beginning of adulthood, that is to say, a neurodegenerative phenotype (Figure 41B'). As previously mentioned, some genes for *cg25c*<sup>+</sup> cells which are defective in adult fly climbing are also remain to be analysed (*Dscam4*, *Ptp99A*, *Sec8*, *sns* and *trio*).

It is remarkable that the same gene produces different phenotypes at different moments in development depending on in which cell-type the gene is down-regulated. One example is the neurotransmitter transporter *inebriated (ine)* (Luan et al., 2015); when down-regulated in *c855a*<sup>+</sup> cells, it causes lethality in pupa (Figure 40A-A') while its down-regulation in *cg25c*<sup>+</sup> cells results in incorrect wing development in the adult fly (Figure 40A-A'). Another example is the gene *mangetout (mtt)*, a G-protein coupled receptor (Brody and Cravchik, 2000) which, when down-regulated in *c855a*<sup>+</sup> cells, leads to lethality for half the larvae at the late L3 stage and up to 15-days of arrest for the other half; conversely, down-regulation in *cg25c*<sup>+</sup> cells of the *mtt* gene provoke the presence of some crystal cells, which are immune reactive hemocytes (Meister and Lagueux, 2003; Rizki and Rizki, 1959), in the abdomen of adult flies (Figure 40B-B').

Crystal cells not only appear in adulthood but also during larval stages. Down-regulation of *Egfr* in *cg25c<sup>+</sup>* cells shows crystal cells in both larval and adult stages (Figure 40B-B' and 43A-A'). The lack of that transmembrane tyrosine kinase receptor function (Buchon et al., 2010) also causes semilethality in pupal stages (Figure 40A-A'). Thus, the abnormal expression of this gene results in different phenotypes depending on the stage of fly's life. *Tiggrin* (*Tig*) is another gene for which down-regulation in *cg25c<sup>+</sup>* cells causes a phenotype in larva that is preserved throughout development (Figure 40). A lack of this integrin ligand and extracellular matrix protein (Fogerty et al., 1994) leads to significantly longer larvae and pupae and adult flies with elongated abdomens (Figure 41A-A'). Other fly lines of *Tig*, apart from showing the same previous phenotype in larva and pupa, present lethality in pupa when that gene is down-regulated.

### A Cell-type dysfunctional genes in pupa

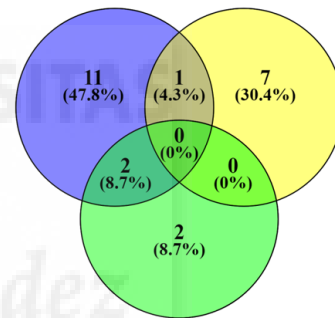
Defect	Number of genes	Dysfunctional gene lines	Overall genes
<i>c855a<sup>+</sup></i> cells	19	5-HT2B, aos, bark, Burs, dpr10, ebi, ed, Fas2, ine, InR, mys*, nAChR $\alpha$ 3, Nr $x$ -IV, Oamb, Oct $\beta$ 3R, otk2, ptc, wg, wls	23
<i>cg25c<sup>+</sup></i> cells	5	dpr5, Egfr, mys*, Oct $\beta$ 1R, Tig	



\*Same line

### A' Phenotypes in pupa

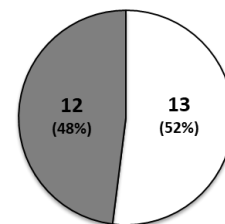
Defect	Number of genes	Phenotypical gene lines	Overall genes
Lethal	14	5-HT2B, aos, ed*, Fas2, ine, mys, nAChR $\alpha$ 3, Nr $x$ -IV, Oct $\beta$ 1R, Oct $\beta$ 3R, otk2, ptc**, Tig*, wg	23
Semilethal	8	bark, Burs, ebi, Egfr, InR, Oamb, ptc**, wls	
Size	4	dpr5, dpr10, ed*, Tig*	



\*Same line / \*\*Different lines

### B Cell-type dysfunctional genes in adult flies

Defect	Number of genes	Dysfunctional gene lines	Overall genes
<i>c855a<sup>+</sup></i> cells	12	aos, bark, egr, fz, Inx3, mew, Mmp2, otk, Pburs, stan, Ten-m, Wnt4	25
<i>cg25c<sup>+</sup></i> cells	13	baz, Dscam4, Egfr, ine, mtt, Ptp69D, Ptp99A, Sec8, SIFaR, sns, Ten-a, Tig, trio	



### B' Phenotypes in adult flies

Defect	Number of genes	Phenotypical gene lines	Overall genes
Abdomen	2	baz, Tig	25
Climbing	17	aos, Dscam4, egr, fz, Inx3, mew, Mmp2, otk, Ptp69D, Ptp99A, Sec8, sns, stan, Ten-a, Ten-m, trio, Wnt4	
Crystal cells	2	mtt, Egfr	
Wings	4	bark, ine, Pburs, SIFaR	

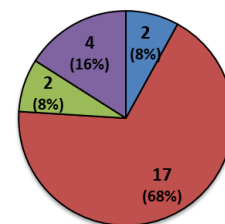


**Figure 40. Gene clusters by dysfunctional cell-type and different phenotypes presented in pupal and adult stages.** From the 51 top-genes for which down- or up-regulation caused abnormal phenotypes, 23 genes are important for normal development in pupa and 25 genes in adult *Drosophila*. (**A-A'**) During pupal stage, besides a few differences in size, dysregulation of almost all genes in *c855a<sup>+</sup>* or *cg25c<sup>+</sup>* cells results in lethality. (**B-B'**) The adult flies present crystal cells and defects in wings or abdominal development and in climbing when there is a dysfunction in *c855a<sup>+</sup>* or *cg25c<sup>+</sup>* cells.

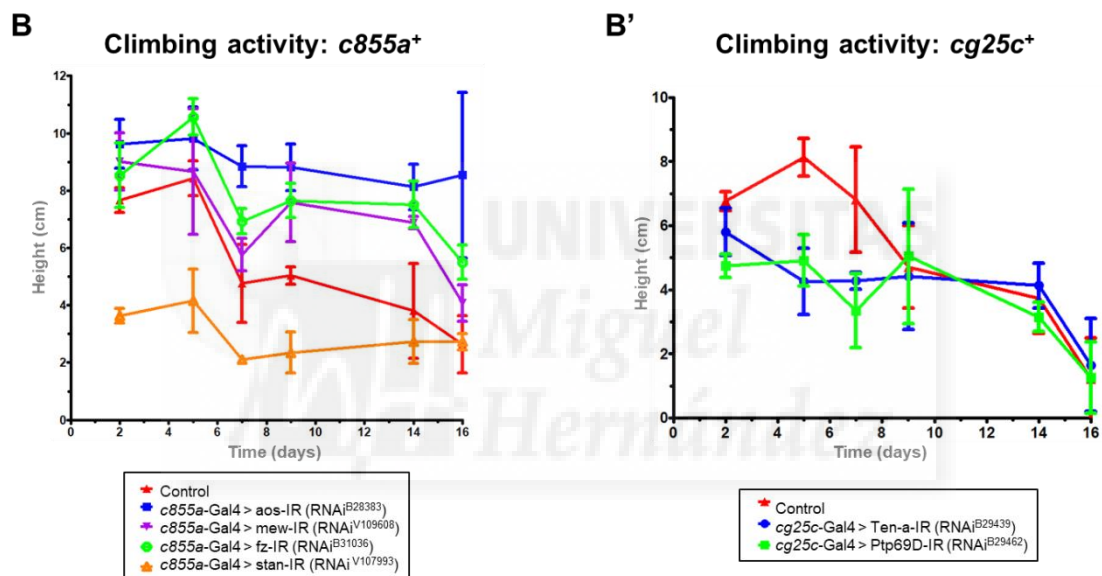
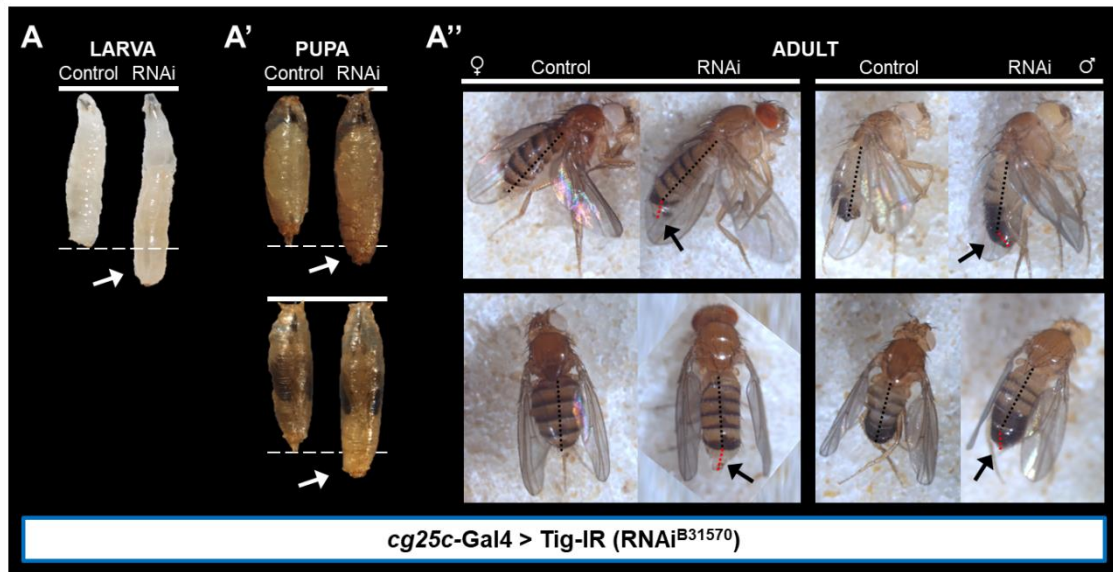
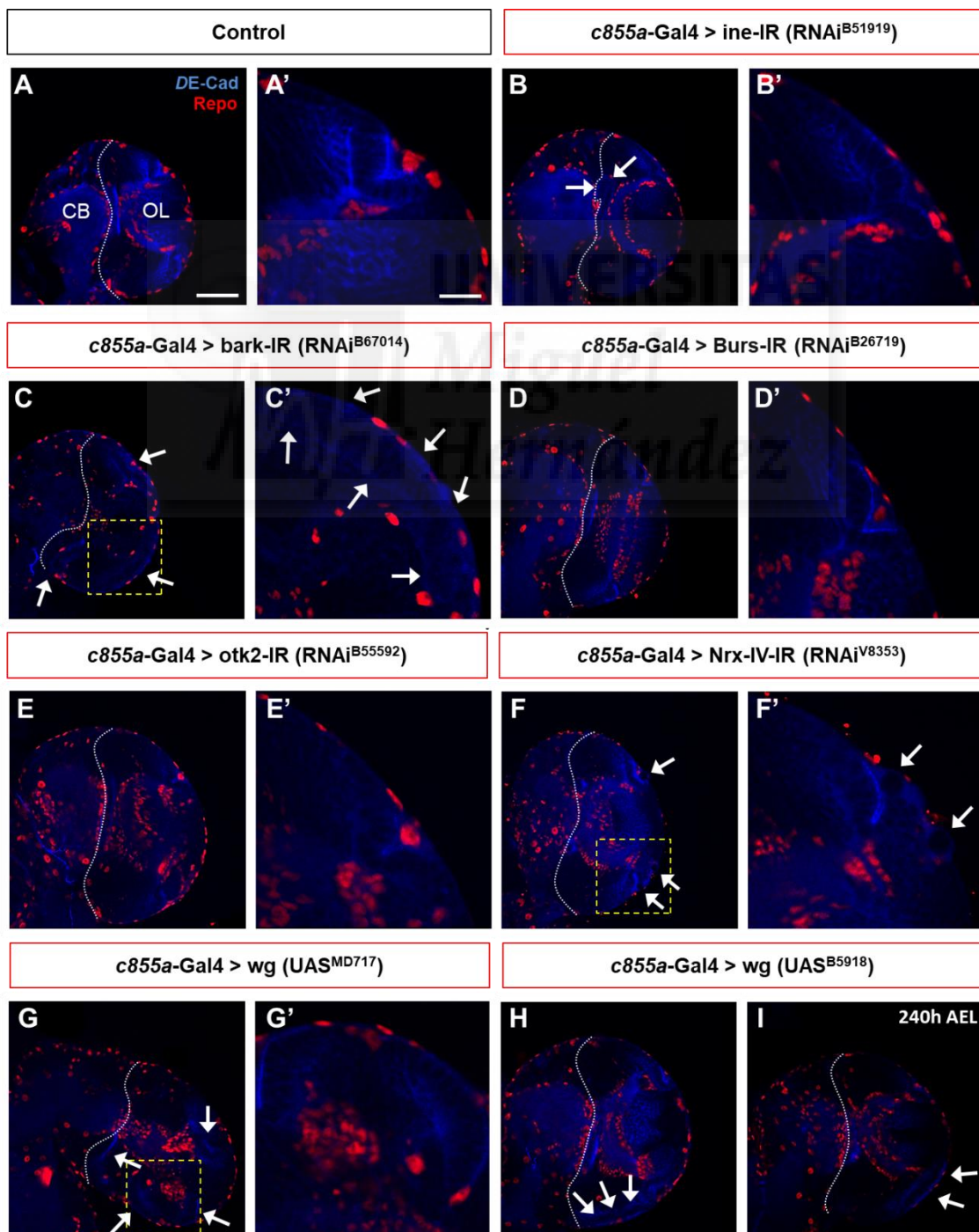


**Figure 41. Down-regulated niche genes with abnormal phenotype in pupa and adult fly.** Genes that result in defects in pupal and adult stages when are underexpressed in *c855a*<sup>+</sup> and *cg25c*<sup>+</sup> cells. (A-A'') Some of them present defects in size, such as the gene *tiggrin* (*Tig*), which results in longer larvae (A) and pupae (A'), and also longer abdomens in adult flies (A'') when down-regulated in *cg25c*<sup>+</sup> cells. (B-B') Down-regulation of other genes in *c855a*<sup>+</sup> (B) and *cg25c*<sup>+</sup> (B') cells cause abnormal climbing activity in adult flies.

As previously mentioned, the deregulation of some of the niche genes tested caused lethality in the pupal stage. Therefore, the subsequent step is to find out whether this fatal phenotype may be caused during the larval stages and before pupariation. Notably, dysfunctional genes in *c855a*<sup>+</sup> cells cause abnormal brain formation in late larva (Figure 42). For instance, a LOF of the genes *ine* and *bark* induces NEC overproliferation that results in aberrant structuring of the proliferative centres, although the overall brain size is not affected (Figure 42B,C). In contrast, down-regulation of other genes can increase the overall brain size. This is the case with *Bursicon* (*Burs*; Figure 42D-D'), which partners with *Pburs* to form a neurohormone (Dewey et al., 2004; Honegger et al., 2002), and *off-track2* (*otk2*; Figure 42E-E'), a transmembrane co-receptor of Wnt signalling pathway (Linnemannstöns et al., 2014). Down-regulation of another transmembrane protein, *Neurexin IV* (*Nrx-IV*), which is critical for septate junctions formation in epithelia (Bhat et al., 1999; Slovakova and Carmena, 2011), also results in an enlarged brain phenotype along with holes or bubbles in the surface of the brain (Figure 42F-F'). Down-regulation of the gene *aos*, an antagonist regulator of EGFR which directly competes with *spi* (Freeman, 2002; Jin et al., 2000; Klein et al., 2004; Morante et al., 2013), also results in a phenotype of NEC overproliferation which causes enlarged brains (Figure 42J-J'). An extreme version of this phenotype, with uncontrolled NEC overproliferation and

massive brain size, is observed when the gene *wg* is overexpressed (Figure 42G-I). The effects of the driver *c855a*-Gal4 in epithelial cells are not only seen in the brain but also in other organs. Down-regulation of *Fasciclin 2* (*Fas2*), an immunoglobulin which also inhibits EGFR signalling in development (Grenningloh et al., 1991; Mao and Freeman, 2009), causes not only an enlarged brain (Figure 42K-K') but also overproliferation of *c855a*<sup>+</sup> cells in imaginal discs that enlarge this tissue (Figure 42L). However, randomly labelled clones in OL NECs null for *Fas2* using the coupled MARCM technique (Lee and Luo, 1999; Potter et al., 2010), which allow for visualisation of both sets of sister clones with different fluorescent reporters (GFP and RFP), revealed no effect in NEC twins nor in their offspring (NBs, GMCs and neurons), and therefore, is not affecting the OPC size (Figure 42M).

Overall, the validation has shown that down-regulation of some genes expressed in niche cells results in deleterious developmental phenotypes. However, more in-depth analysis of those phenotypically interesting genes is needed in order to comprehensively characterise their role in development.



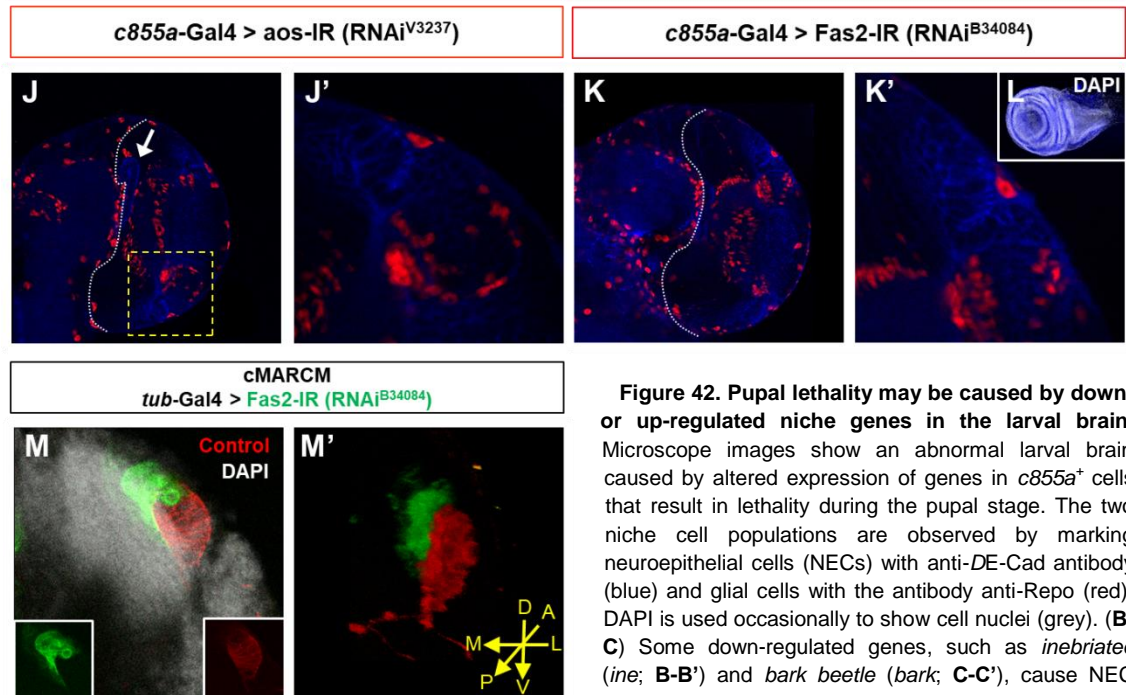


**Figure 42. Pupal lethality may be caused by down- or up-regulated niche genes in the larval brain.** Microscope images show an abnormal larval brain caused by altered expression of genes in *c855a*<sup>+</sup> cells that result in lethality during the pupal stage. The two niche cell populations are observed by marking neuroepithelial cells (NECs) with anti-DE-Cad antibody (blue) and glial cells with the antibody anti-Repo (red). DAPI is used occasionally to show cell nuclei (grey). (**B-C**) Some down-regulated genes, such as *inebriated* (*ine*; **B-B'**) and *bark beetle* (*bark*; **C-C'**), cause NEC overproliferation which induces abnormal folding in the

proliferative centres (arrows), although this does not affect the brain size. (**D-M**) However, other down-regulated genes, for instance *Bursicon* (*Burs*; **D-D'**) and *off-track2* (*otk2*; **E-E'**), do affect the brain, increasing its size. Underexpression of *Neurexin IV* (*Nrx-IV*; **F-F'**) makes holes or bubbles appear on the surface of the brain (arrows). Also, the overexpression of the gene *wingless* (*wg*; **G-G',H,I**) causes NEC overproliferation (arrows) and massive brains, as does the down-regulation of *argos* (*aos*; **J-J'**). Finally, the underexpression of *Fasciclin 2* (*Fas2*) not only affects the size of the brain (**K-K**) but also other organs (**L**) where the *c855a*-Gal4 driver is expressed. (**M-M'**) However, the cMARCM technique does not reveal how exactly this gene affects NECs when affected (green) and unaffected (red) twin cell lineages are compared. Images were taken from late-3<sup>rd</sup> instar larva at 120 h AEL, except (**I**) which phenotype are presenting 240 h AEL of delay. The coordinate axes indicate anterior-posterior (A-P), lateral-medial (L-M), and dorsal-ventral (D-V) directions. The yellow box in (**C**), (**F**), (**G**), and (**J**) indicates the magnified OPC. Scale bars represent 50  $\mu$ m in (**A**) and 20  $\mu$ m in (**A'**).

### 4.3. Genes involved in unusual phenotypes at larval stages

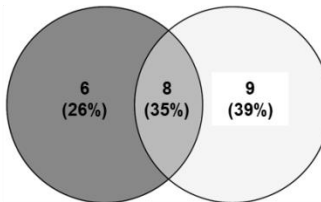
Larval development is crucial for proper maturation of tissues necessary in adulthood; thus any genetic defect during this stage may result in dysfunctional organogenesis for the adult fruit fly.

The validation of the top-hit genes reveals 23 genes (out of the 51 for which phenotypes were observed) which, when down- or up-regulated, caused dysfunctions in larval stages (Figure 39C). From those 23, 6 genes are important for *c855a*<sup>+</sup> cells, 9 genes for *cg25c*<sup>+</sup> cells, and 8 genes for both cell types (Figure 43A). Among these genes, I observed various unusual phenotypes such as increased larvae size, arrest transition between stages, premature wandering, delay in pupariation, appearing of immune crystal cells, as well as lethality (Figure 43A'). It is important to emphasise that the gene *spi* is among the 23 larval genes that, when deregulated, causes a defective phenotype and, in addition, *spi* is detected in glia (Figure 43A-A'). These consolidate the RNA-seq analysis and bioinformatics workflow (Table S5).

Previously, we have seen an example of differences in larval size when a depletion of the gene *tig* in *cg25c*<sup>+</sup> cells results in longer larvae (Figure 41A). Deficiencies in the expression of the gene family *defective proboscis extension response* (*dpr*) also have impacts on the larval size, increasing the whole larval and pupal volume. *Dpr* immunoglobulin forms a complex with *dpr-interacting proteins* (*DIPs*) that have been found to be important in neuron synapses (Carrillo et al., 2015; Howell and Hobert, 2016; Pipes et al., 2001; Tan et al., 2016). In this case, down-regulation of the genes *dpr5* in *cg25c*<sup>+</sup> cells and *dpr10* in *c855a*<sup>+</sup> cells causes increased body size (Figure 43A').

## A Cell-type dysfunctional genes in larva

Defect	Number of genes	Dysfunctional gene lines	Overall genes
<i>c855a</i> <sup>+</sup> cells	14	<i>crb</i> , <i>dpr2</i> <sup>*</sup> , <i>dpr10</i> , <i>ed</i> <sup>**</sup> , <i>mtt</i> , <i>mys</i> <sup>*</sup> , <i>nAChRα3</i> , <i>Nrx-IV</i> <sup>**</sup> , <i>Oamb</i> <sup>**</sup> , <i>Octβ1R</i> <sup>*</sup> , <i>Octβ3R</i> <sup>*</sup> , <i>ptc</i> , <i>unc-5</i> , <i>wg</i> <sup>*</sup>	23
<i>cg25c</i> <sup>+</sup> cells	17	<i>Dh44-R1</i> , <i>dpr2</i> <sup>*</sup> , <i>dpr5</i> , <i>ed</i> <sup>**</sup> , <i>Egfr</i> , <i>mys</i> <sup>*</sup> , <i>Nrx-IV</i> <sup>**</sup> , <i>Oamb</i> <sup>**</sup> , <i>Octβ1R</i> <sup>*</sup> , <i>Octβ3R</i> <sup>*</sup> , <i>Ret</i> , <i>santa-maria</i> , <i>spi</i> , <i>Tig</i> , <i>trio</i> , <i>wg</i> <sup>*</sup> , <i>Wnt2</i>	



\*Same line / \*\*Different lines

## A' Phenotypes in larva

Defect	Number of genes	Phenotypical gene lines	Overall genes
Arrest	8	<i>Dh44-R1</i> <sup>*</sup> , <i>dpr2</i> <sup>*</sup> , <i>mtt</i> <sup>*</sup> , <i>mys</i> <sup>*</sup> , <i>nAChRα3</i> <sup>*</sup> , <i>Oamb</i> <sup>**</sup> , <i>Octβ1R</i> <sup>*</sup> , <i>Octβ3R</i> <sup>*</sup>	23
Crystal cells	6	<i>Dh44-R1</i> <sup>*</sup> , <i>Egfr</i> , <i>mys</i> <sup>*</sup> , <i>Oamb</i> <sup>**</sup> , <i>Octβ1R</i> <sup>*</sup> , <i>spi</i> <sup>*</sup>	
Delay	9	<i>ed</i> , <i>Nrx-IV</i> , <i>Octβ1R</i> <sup>*</sup> , <i>ptc</i> , <i>santa-maria</i> , <i>trio</i> , <i>unc-5</i> , <i>wg</i> , <i>Wnt2</i>	
Lethal	10	<i>Dh44-R1</i> <sup>*</sup> , <i>crb</i> , <i>dpr2</i> <sup>*</sup> , <i>mys</i> <sup>*</sup> , <i>nAChRα3</i> <sup>*</sup> , <i>Oamb</i> <sup>**</sup> , <i>Octβ1R</i> <sup>*</sup> , <i>Octβ3R</i> <sup>*</sup> , <i>Ret</i> , <i>spi</i> <sup>*</sup>	
Semilethal	2	<i>mtt</i> <sup>*</sup> , <i>Oamb</i> <sup>**</sup>	
Others	5	<i>dpr2</i> <sup>*</sup> & <i>Octβ1R</i> <sup>*</sup> (premature wandering), <i>dpr5</i> & <i>dpr10</i> (bigger), <i>Tig</i> (longer)	

\*Same line / \*\*Different lines

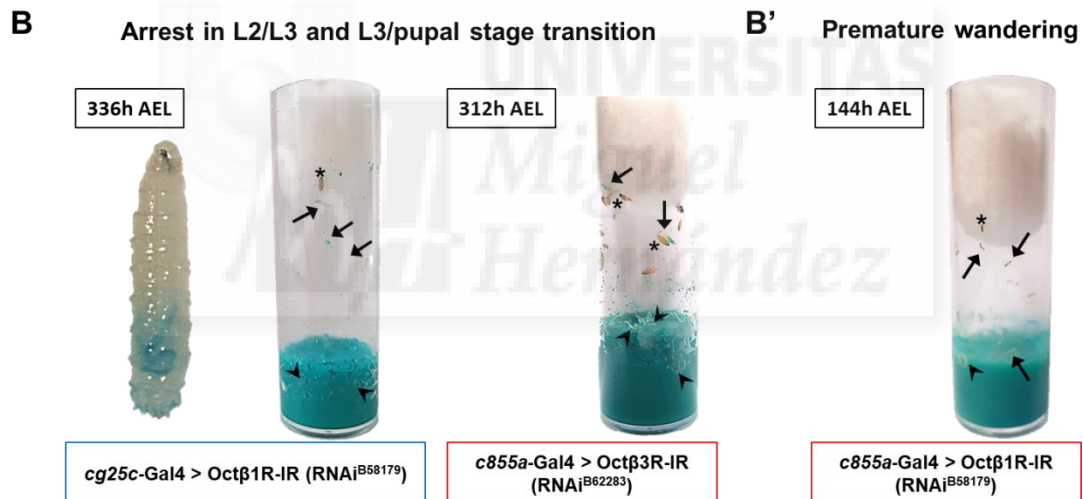


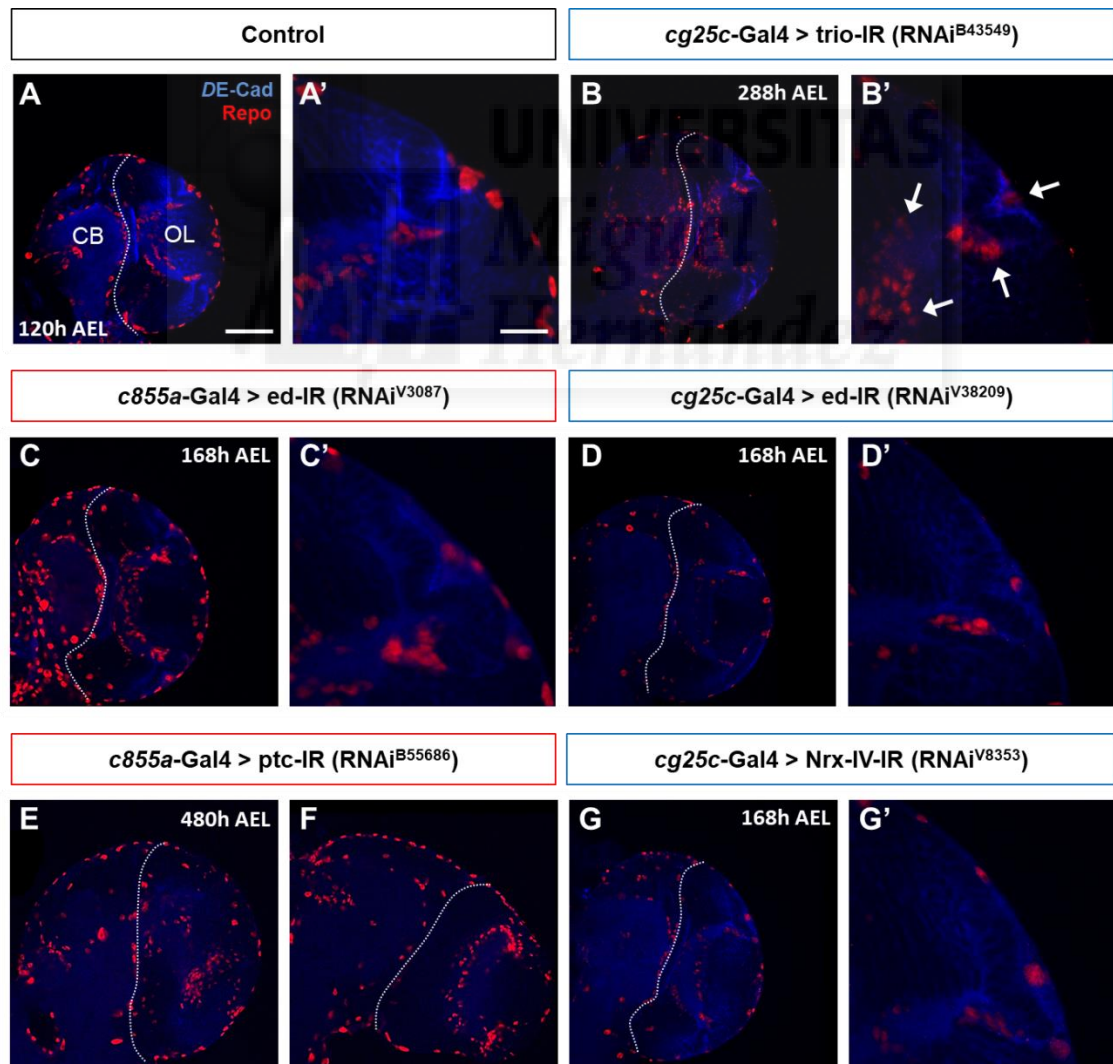
**Figure 43. Gene clusters by dysfunctional cell-type and different phenotypes presented in larval stages.** The 51 top genes whose altered expression levels cause abnormal phenotypes present 23 that are important for larval development. (A-A') Dysfunction in *c855a*<sup>+</sup> or *cg25c*<sup>+</sup> cells in this stage results in various phenotypes including differences in size, premature wandering, presence of crystal cells, delay in pupariation, arrest in stage transition and lethality. (B-B') Feeding assay allows for the detection of food intake during abnormal larval behaviour due to a lack of gene function. (B) For example, I observe problems in the transition from L2 to L3 stages (arrowheads) or from L3 (arrows) to pupa (asterisk). (B') Another example is to detect ingestion of food in larvae that display premature wandering.

A delay in pupariation may be between 2 and 7 days, up to a maximum of 15 days. This delay is found to be caused by altered gene expression in both niche cell types, neuroepithelial and glia, and this fact impacts the proliferation of brain cells that finally affects the lobe size (Figure 44). Down-regulation of genes in *c855a*<sup>+</sup> cells results in bigger brains, as it is presented right away. Additionally, down-regulation of the gene *unc-5*, which encodes a repulsive netrin receptor that directs motor axon guidance and glial migration out of the CNS (Freeman et al., 2003; Long et al., 2016), results in the presence of some holes or bubbles in the tissue surface (Figure 44H-H'). Underexpression of the gene *patched* (*ptc*), a transmembrane receptor involved in Hedgehog signalling pathway at imaginal discs (Chen and Struhl, 1996), produces a blurred-like massive lobe and also big proliferative centres (Figure 44E,F) that results in pupal lethality. Down-regulation of the gene *ed* in both niche cell types



results in a developmental delay which are equal in number of days that finally results in a larger brain (Figure 44C,D). However, the case of this gene is unusual because the number of glial cells in affected brains seems to be higher when the defect is in *c855a*<sup>+</sup> cells (Figure 44C-C') and lower when it is in *cg25c*<sup>+</sup> cells (Figure 44D-D').

Down-regulated genes in *cg25c*<sup>+</sup> cells also produce abnormal brain phenotypes. The gene *trio* encodes GEF, which acts in several pathways including BMP and Abl tyrosine kinase pathways (Ball et al., 2010; Liebl et al., 2000); a LOF of the gene provokes the disruption of glial nuclei, although it does not affect brain size (Figure 44B-B'). A bigger brain is observed when expression of the gene *Nrx-IV* is depleted (Figure 44G-G'); this gene has been described as critical in midline glia (Banerjee et al., 2017; Slovakova and Carmena, 2011). Aside from differences in size, down-regulation of the *Wnt* oncogene analog 2 (*Wnt2*), a member of the conserved Wnt family of powerful molecules (Sidow, 1992), causes overproliferation of brain NECs that additionally are found ectopically (Figure 44I,J). Not only down-regulation but also overexpression of genes in *cg25c*<sup>+</sup> cells can result in enlarged brain phenotypes. *Wg*, which was previously mentioned to cause pupal lethality when up-regulated in *c855a*<sup>+</sup> cells (Figure 42G-I), also causes a phenotype of delay when overexpressed. Under the same characteristics, GOF of the gene *scavenger receptor acting in neural tissue and majority of rhodopsin is absent* (*santa-maria*; Wang et al., 2007) causes larval delay and enlarged brains (Figure 44K-K').



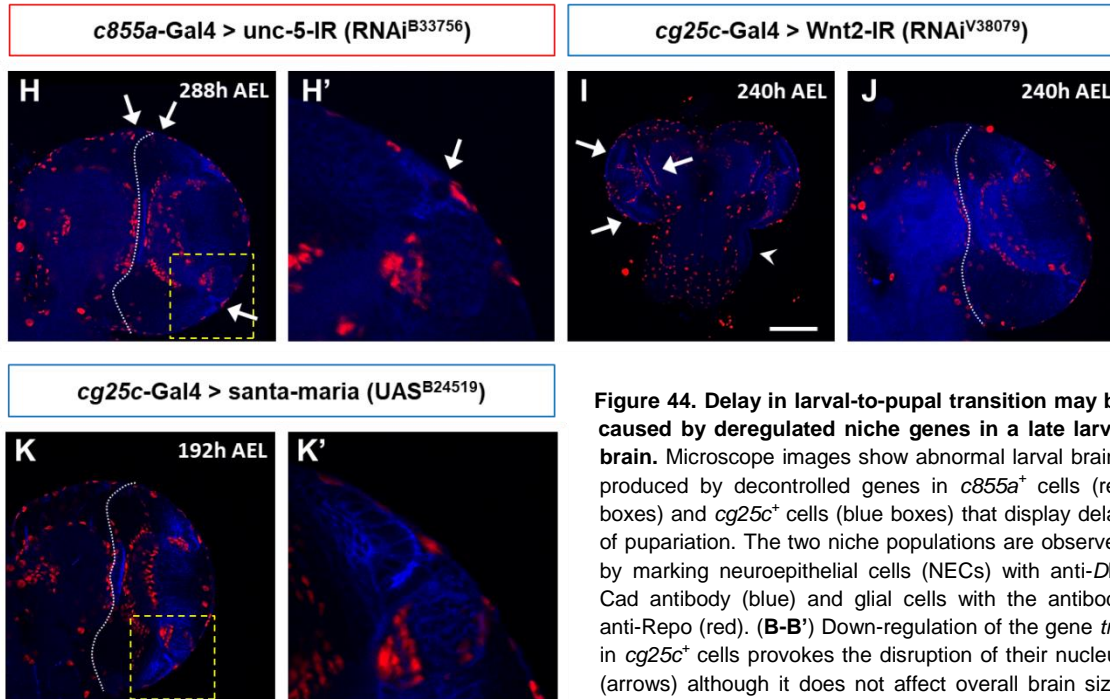


**Figure 44. Delay in larval-to-pupal transition may be caused by deregulated niche genes in a late larval brain.** Microscope images show abnormal larval brains produced by decontrolled genes in *c855a*<sup>+</sup> cells (red boxes) and *cg25c*<sup>+</sup> cells (blue boxes) that display delay of pupariation. The two niche populations are observed by marking neuroepithelial cells (NECs) with anti-DE-Cad antibody (blue) and glial cells with the antibody anti-Repo (red). (B-B') Down-regulation of the gene *trio* in *cg25c*<sup>+</sup> cells provokes the disruption of their nucleus (arrows) although it does not affect overall brain size. (C-K) However, other dysregulated genes do affect the

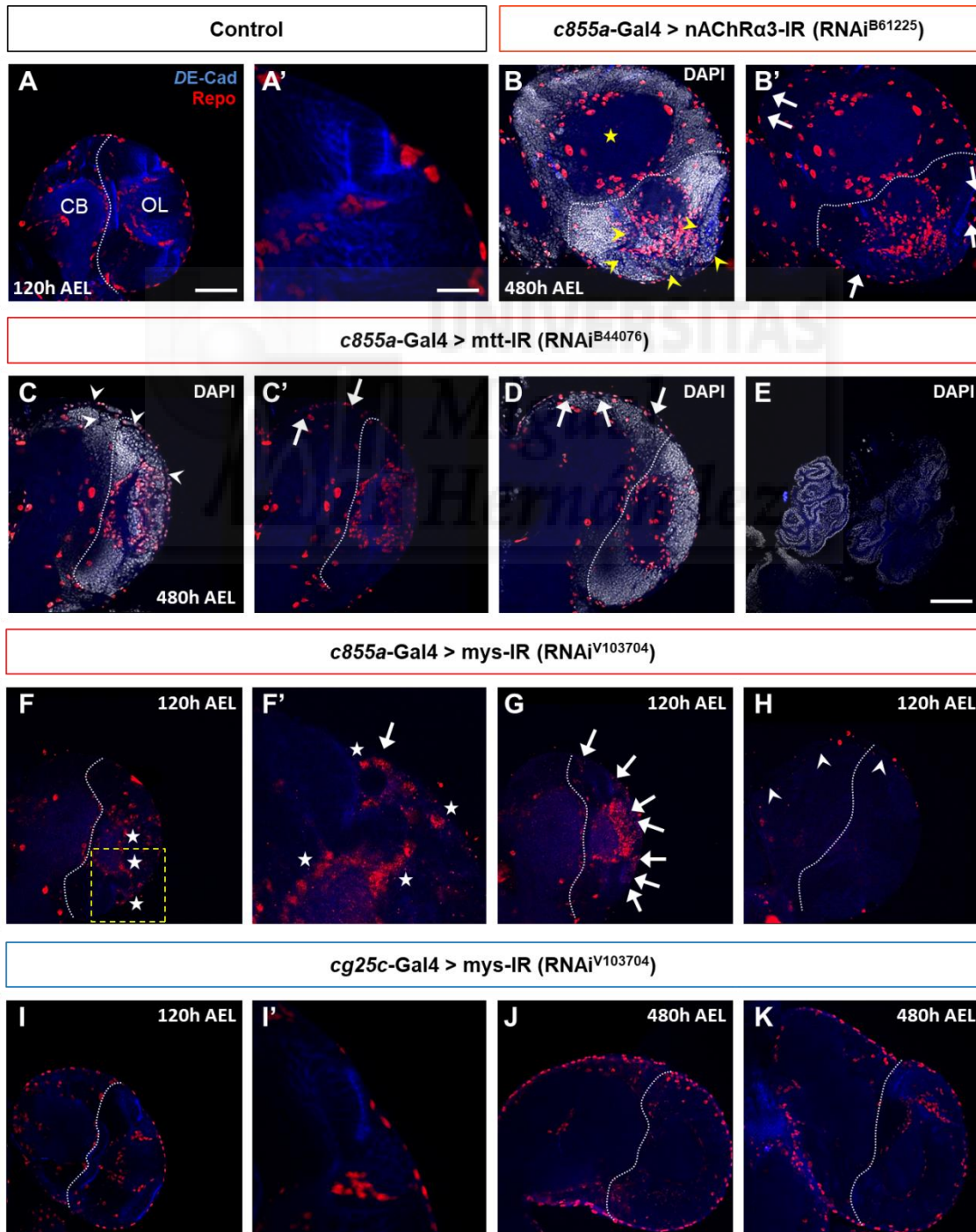
brain, enlarging its size. This phenotype is seen when in *cg25c*<sup>+</sup> cells there is a down-regulation of the genes *echinoid* (*ed*; D-D') which appears to cause decreased numbers of glial cells; and also underexpression of *Neurexin IV* (*Nrx-IV*; G-G') and *Wnt oncogene analog 2* (*Wnt2*; I,J) which additionally cause an overproliferation of brain NECs (arrows), also ectopically (arrowhead). An overexpression of the gene *scavenger receptor acting in neural tissue and majority of rhodopsin is absent* (*santa-maria*; K-K') also causes enlarged brains. Down-regulation of some genes in *c855a*<sup>+</sup> cells results in bigger brains: the LOF of *ed* (C-C') additionally seems to increase the number of glial cells, LOF of *patched* (*ptc*; H-H') produces blurred-like proliferative centres, and LOF of *unc-5* (H-H') causes holes or bubbles to appear in the surface of the brain (arrows). Images were taken from late-3<sup>rd</sup> instar larva at maximum time of delay. The yellow box in (H) and (K) indicates the magnified OPC. Scale bars represent 50  $\mu$ m in (A), 20  $\mu$ m in (A') and 100  $\mu$ m in (I).

Lethality among the different larval stages was also observed. It is interesting that some genes induce larval lethality at very early stages, that is to say, during the 1<sup>st</sup> IL (data not shown). For instance, this occurs when the gene for the transmembrane protein *crumbs* (*crb*), which is related with epithelial morphogenesis and growth control via the Hippo pathway (Chen et al., 2010; Tepaß and Knust, 1990), is overexpressed in *c855a*<sup>+</sup> cells. This also occurs when the *Ret* oncogene, which is a cell surface receptor expressed in embryonic neuronal precursor cells (Sugaya et al., 1994), is overexpressed in *cg25c*<sup>+</sup> cells.

In addition to lethality in early larval stages, dysregulation of some genes was also observed to cause lethality at very late larval stages, at the time of transition to the pupal stage. This happens when expression of the *nicotinic Acetylcholine Receptor  $\alpha$ 3* (*nAChRa3*) reported in *Drosophila* (Schulz et al., 1998), and *mtt* (which is explained above) are down-regulated in *c855a*<sup>+</sup> cells. Both genes are partially lethal at the transition from larva to pupa, since half of the larva with the down-regulated gene arrest at the late L3 stage for a maximum of 15 days. The brains of these larvae arrested at L3 have a phenotype of overproliferation of NECs and a resulting enlarged brain (Figure 45B-D). The brains of those with reduced *nAChRa3* expression have massive CB, unstructured neuroepithelial overproliferative centres that increase the number of glial cells, and also holes or bubbles in the brain surface (Figure 45B-B'). Reduced *mtt* expression leads these brain holes or bubbles to scratches observed between cells bodies (Figure 45C-D); in addition, overproliferative NECs are also visible in imaginal discs where they cause an amorphous structure and increase the imaginal discs volume (Figure 45E).

The validation also revealed an interesting gene, *mysospheroid* (*mys* a.k.a. *betaPS*), whose down-regulation caused similar phenotypes in both niche cell types. *Mys* encodes one of two integrin  $\beta$  subunits that dimerise and form a transmembrane receptor which acts in cell adhesion and macrophages migration (Beumer et al., 1999; Comber et al., 2013; Estrada et al., 2007). *Mys* LOF in *c855a*<sup>+</sup> cells results in lethality at the transition from larva to pupa; a slightly different phenotype occurs when the LOF is in *cg25c*<sup>+</sup> cells: half of the larva arrest development and the other half enter

the pupal stage but die during it. When *mys* is down-regulated in both cell types, the size of the brain is normal at 120 h AEL. At this moment, the defective larva in *c855a*<sup>+</sup> cells for that gene show brains that present holes or bubbles which evolve into scratches and, in addition, disrupted glial nuclei are visible (Figure 45F-H). Dysfunctional larva in expression of *mys* in *cg25c*<sup>+</sup> cells show late L3 brains that have extra neuroepithelium in their proliferative centres (Figure 45I-I') and that, after 15 days of developmental arrest and continued proliferation, causes a huge increase in brain size and glial cell number, also glia from the surface (Figure 45J). At this time of the arrest I also observed a longer VNC as well as a massive size of the ring gland (RG; Figure 45K); however, the imaginal discs are very small (data not shown). The phenotype also produces lack of lipid droplets in the OL and also an abnormal presence in the RG (Figure 45K). Those arrested larvae also have crystal cells, indicating an innate immune response (data not shown).



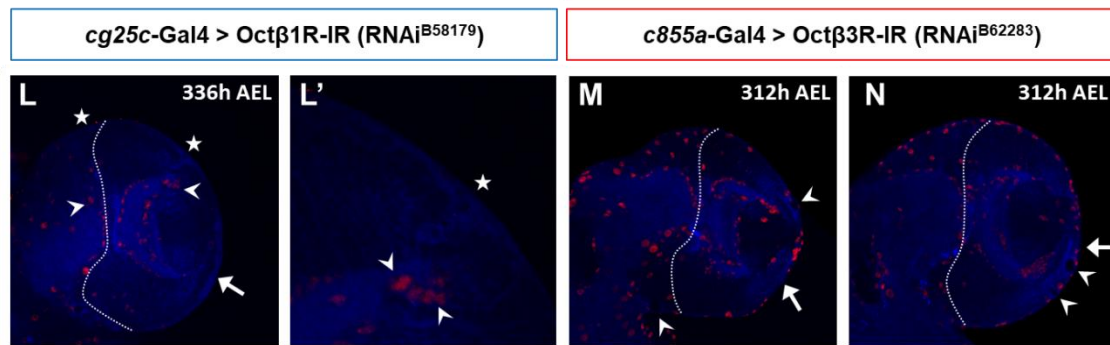


**Figure 45. Arrest in late L3 stage as well as lethality in larval-to-pupal transition may be caused by dysregulated niche genes in the brain.** Microscope images show abnormal larval brains produced by genes down-regulated in *c855a*<sup>+</sup> cells (red boxes) and *cg25c*<sup>+</sup> cells (blue boxes) that result in strong unusual phenotypes in late larval development. The two niche populations are observed by marking neuroepithelial cells (NECs) with anti-*DE-Cad* antibody (blue) and glial cells with the antibody anti-*Repo* (red). DAPI is used occasionally to show cell nuclei (grey). **(B-K)** Down-regulated genes in niche cells provoke overproliferation of NECs. A dysregulation of *nicotinic Acetylcholine Receptor α3* (*nAChRa3*; **B-B'**) in *c855a*<sup>+</sup> cells causes an enlargement of the brain lobes, mainly of the central brain (asterisk), and causes holes or bubbles in the surface (arrows) and an apparent increase in the number of glial cells. In addition, NECs of the proliferative centres appear to be unstructured (arrowheads). Also in *c855a*<sup>+</sup> cells, a dysfunction of the gene *mangetout* (*mtt*) causes enlarged brains (**C-D**) as well as holes or bubbles in the surface (arrows) that develop into scratches (arrowheads); NECs of the imaginal discs (**E**) overproliferate resulting in abnormal growth. Although the down-regulation of the gene *mysospheroid* (*mys*) in niche cells does not affect the brain in size, LOF in *c855a*<sup>+</sup> cells (**F-H**) also provokes holes or bubbles in the surface (arrows) that develop into scratches (arrowheads) as well as the disruption of the glial nuclei (asterisks) and a decrease in number of glia. In contrast, LOF in *cg25c*<sup>+</sup> cells (**I-K**) increases the number glial cells and causes an enlarged brains and ring gland, and longer ventral nerve cord (asterisks); there is no presence of lipid droplets (nile red; hash) within optic lobes and neither in the ring gland. **(L-N)** Finally, down-regulation of two receptors for octopamine results in bigger brains with NEC overproliferation (arrows). LOF of *octopamine β1 receptor* (*Octβ1R*) in *cg25c*<sup>+</sup> cells (**L-L'**) provokes a loss of glial cells and also surface glia (asterisks) but not neuropil glia (arrowheads) in brain lobes. Underexpression of *octopamine β3 receptor* (*Octβ3R*) in *c855a*<sup>+</sup> cells (**M-N**) causes holes or bubbles in the surface of the brain (arrowheads). Images were taken from late-3<sup>rd</sup> instar larva at 120 h AEL or at maximum time of arrest. The yellow box in **(F)** indicates the magnified OPC. Scale bars represent 50 μm in **(A)**, 20 μm in **(A')** and 150 μm in **(K and E)**.

Tissue regeneration needs to be coordinated with development, and a mismatch between the two processes may result in a phenotype of life cycle arrest (Garelli et al., 2012; Jaszczak and Halme, 2016; Juarez-Carreño et al., 2018; Rewitz et al., 2013; Vallejo et al., 2015). As shown above, the larval arrest may take place before the transition from larva to pupa. As another example, arrest at this stage occurs when the *diuretic hormone 44 receptor 1* (*Dh44-R1*; Johnson et al., 2004) is down-regulated in *cg25c*<sup>+</sup> cells; in this case, late L3 larva arrest for several days until they present crystal cells and die (data not shown). Interestingly, I observed that this arrest may be produced earlier in the larval period during the molt from L2 to L3 stages (Figures 46, 47 and S16). Phenotypes caused by down-regulation of several interesting genes in both niche cell types were identified: *dpr2*, which causes a premature wandering phenotype that rapidly becomes lethal (Figure 43A'), and genes of the octopamine (OA) receptor family (*Oamb*, *Octβ1R* and *Octβ3R*) which cause arrest and then lethality. Due to unusual sizes of the larva presenting this arrested phenotype, more characterisation of their developmental stage is needed, as is revealed later.

As previously mentioned, down-regulation of the gene *dpr2* in both niche cell types causes arrest. At 168 h AEL, larvae arrested due to underexpression of *dpr2* in *c855a*<sup>+</sup> cells show clear deficiencies in size: they have L2-like length though greater than L2 width (Figures 46A and S16). This results in a volume which is similar to an early L3 control larva of ~76 h AEL (Figure 46B-B'). Finally, observation of the larval jaws, which is the most unbiased method of determining *Drosophila* larval stage (Alvarez et al., 2017; Jakobs et al., 2017; Roberts, 1998), reveals that they are arrested in the L3 stage (Figure 46C). Additionally, feeding assays show that jaws are functional since larvae continue feeding (Figure 46D). In contrast, down-regulation of *dpr2* in *cg25c*<sup>+</sup> cells causes larval arrest for 216 h AEL; after this amount of time, the larvae have early L3-like length and width (Figures 46A and S16). As a result, these larvae have a volume similar to that of an early L3 control larva of ~78 h AEL (Figure 46B-B'). Lastly, these *dpr2* deficient larvae have jaw characteristics that indicate that the arrested stage is L3 (Figure 46C). All in all, LOF of the gene *dpr2* in both cell types (Figure 46E) produces arrest in the 3<sup>rd</sup>-IL according to jaws (Figure 46C), with a similar early L3 larval volume comparable to that of control larvae between ~76 and ~78 h AEL (Figure 46B-B') but with different length to width ratios (Figures 46A and S16).

Other interesting larval arrested phenotypes are produced by altered expression of a group of genes that encode OA receptors. OA is a hormone related with noradrenaline (NA; a.k.a. norepinephrine) that functions as neurotransmitter but in invertebrates also functions as a neurohormone and neuromodulator (Chen et al., 2013; Ohhara et al., 2012). The validated OA genes whose over- or under-expression caused observable phenotypes are *octopamine receptor in mushroom bodies* (*Oamb*), *octopamine  $\beta$ 1 receptor* (*Oct $\beta$ 1R*), and *octopamine  $\beta$ 3 receptor* (*Oct $\beta$ 3R*).

Overexpression in *c855a*<sup>+</sup> cells of the first gene mentioned, *Oamb*, causes a phenotype of arrest in the early L3 stage that ends in lethality (Figure 43A-A'); a down-regulation of this receptor also results in lethality for almost all individuals, but in pupal stages (Figure 40A-A'). Down-regulation of *Oamb* in *cg25c*<sup>+</sup> cells results in larval arrest for up to 266 h AEL (Figure 46); these arrested larvae also have crystal cells (Figure 46A). These abnormal larvae have size similar to early L3 control larvae (Figures 46A and S16) but their volume is more like of late L2 control larvae at ~70 h AEL (Figure 46B-B'). However, the jaw characteristics of these abnormal larvae reveal that they are arrested in the L3 stage (Figure 46C). In summary, when the *Oamb* receptor is up-regulated in *c855a*<sup>+</sup> cells and down-regulated in *cg25c*<sup>+</sup> cells, the same arrested phenotype is observed in both.

The second OA receptor gene is *Oct $\beta$ 1R*. Down-regulation of this gene's expression in *c855a*<sup>+</sup> cells produces premature wandering and lethality due to the fact that larvae stay up on tube walls at up to 144 h AEL without feeding (Figure 43B'). When those abnormal larvae are compared with control larvae, they have L2-like length but L3-like width (Figures 46A and S16). This leads to a larval volume similar to that of late L2 control larvae at ~68 h AEL (Figure 46B-B'). However, the jaw assay demonstrates that the abnormal larvae belong to the 3<sup>rd</sup> IL stage (Figure 46C). When *Oct $\beta$ 1R* is down-regulated in *cg25c*<sup>+</sup> cells, some of the larvae are arrested in the late L3 stage up to 336 h AEL, feeding and presenting crystal cells, while the rest of the larvae reach the pupal stage but die (Figure 43B). The brains of these larvae arrested in L3 are bigger and have overproliferative neuroepithelia. Interestingly, *cg25c*<sup>+</sup> cells, as well as SG cells, are not observed unlike those NG cells of the lobes (Figure 45L-L'). Thus, defects of *Oct $\beta$ 1R* in both niche cell types cause arrest phenotypes in stage transition that end in lethality.

The last of OA receptors validated is *Oct $\beta$ 3R*. Underexpression of this gene in *c855a*<sup>+</sup> cells results in some larvae arresting at the late L3 for 312 h AEL while the rest of the larvae reach the pupal stage but die (Figure 43B). The larvae have larger brains with overproliferative neuroepithelia as well as holes or bubbles in the brain surface (Figure 45M,N). Down-regulation of *Oct $\beta$ 3R* in *cg25c*<sup>+</sup> cells causes arrest of larvae at the transition between L2 and L3 stages, according to their size (Figures 46A and S16). This is also reflected by their larval volume, which resembles the volume of a ~71 h AEL control larva that is also around that L2 to L3 stage transition (Figure 46B-B'). Nevertheless, their jaw characteristics suggest that those larvae are already in the 3<sup>rd</sup> IL stage (Figure 46C). Thus, for *Oct $\beta$ 3R* I came to the same conclusion as for *Oct $\beta$ 1R*.

As mentioned earlier, the arrested phenotype may be as a result of lack of coordination between development and tissue regeneration (Garelli et al., 2012; Jaszczak and Halme, 2016; Juarez-Carreño et al., 2018; Rewitz et al., 2013; Vallejo et al., 2015). The results shown above suggest that the niche cells of the brain may have a role in arrest and is mismatched with the larval developmental age.

Larval brain images taken at 360 h AEL with *dpr2* down-regulated in both niche cell types shows L3-like lobes (Figure 47C,D). However, the phenotype of the CNS that results from underexpression of *dpr2* in *c855a*<sup>+</sup> cells resembles a mid L3 brain of ~88 h AEL based on its size and the structure of the proliferative centres; it additionally has holes or bubbles in the brain surface (Figure 47C,C'). In contrast, down-regulation of *dpr2* in *cg25c*<sup>+</sup> cells results in larvae with an early L3-like brain similar to that expected at ~88 h AEL (Figure 4D,D'). In both cases, the brains are normal in terms of estimated age size, and shows cell proliferative activity in NECs (Figure 47C,D).

The cases where the OA receptors tested were down-regulated, the brains present features from a late L2 stage of ~64 h AEL (Figure 47E-H), but at the same time they differ in size. A normal L2-like brain occurs when there is overexpression of *Oamb* in *c855a*<sup>+</sup> cells after 288 h AEL arrest (Figure 47E,E'); however, when *Oamb* is down-regulated in *cg25c*<sup>+</sup> cells for 336 h AEL, the brain becomes massive (Figure 47F,F'). In the other OA receptors (*Oct $\beta$ 1R* and *Oct $\beta$ 3R*), the size is normal for a 144 h AEL brain with underexpression of *Oct $\beta$ 1R* in *c855a*<sup>+</sup> cells (Figure 47G,G'); but a 312 h AEL brain is enlarged when there is underexpression of *Oct $\beta$ 3R* in *cg25c*<sup>+</sup> cells (Figure 47H,H'). All in all, dysfunctions in OA receptors cause arrested larval phenotypes which remain at the L3 developmental stage. In addition, these abnormal larvae also present differences in size and in volume, which resemble those of late L2 larva between ~68 to ~71 h AEL (Figures 46 and S16). A lack of coordination within organs is also apparent, since brains resemble those of earlier larval

stages (Figure 47). Therefore, due to the peculiarities of these initial results, the OA receptor family is going to be addressed in depth in the next section.

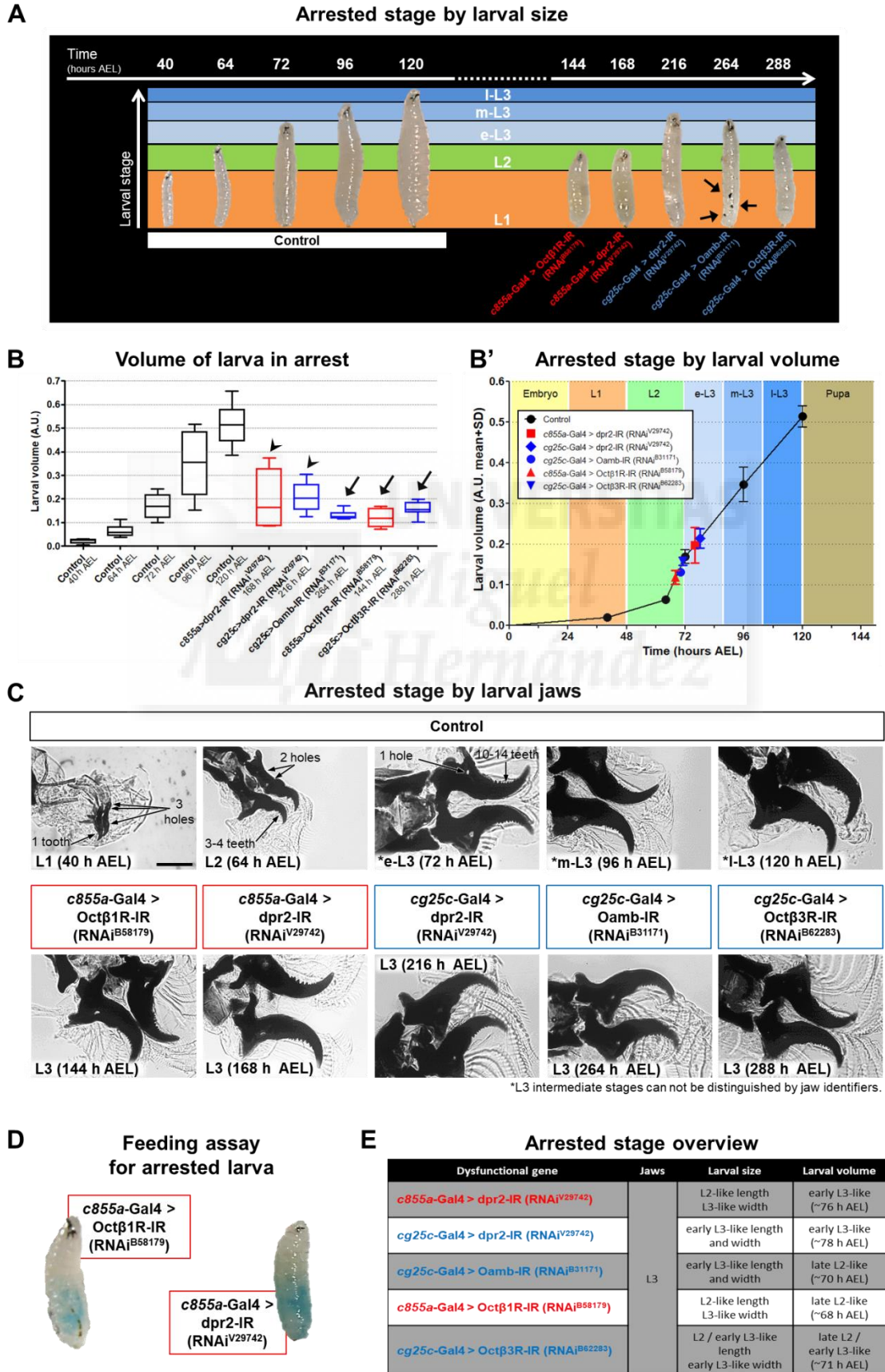
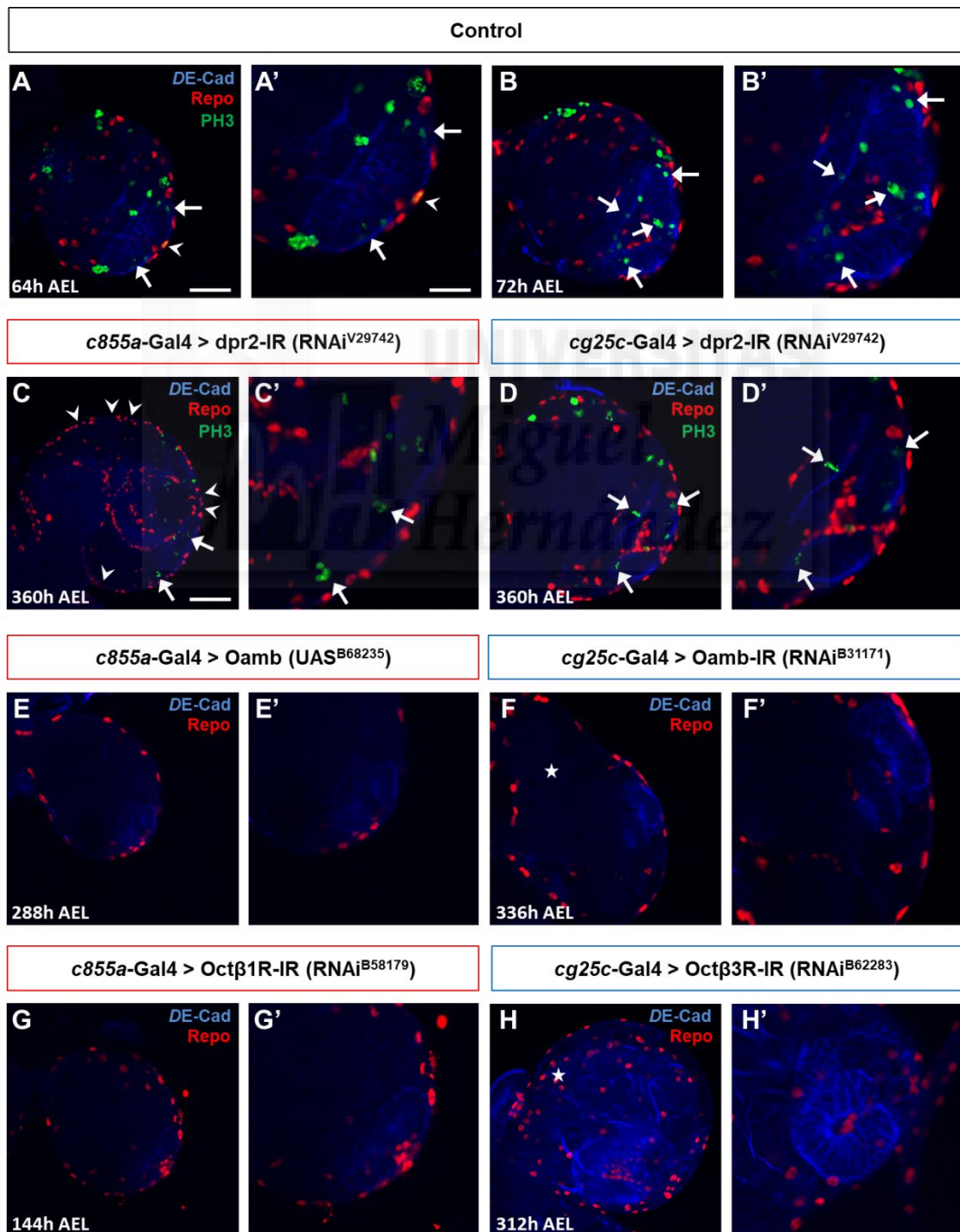


**Figure 46. Dysfunctional genes with arrested phenotype in larval stage.** Down-regulation of the genes *defective proboscis extension response 2* (*dpr2*) and octopamine receptors (*Oamb*, *Octβ1R* and *Octβ3R*) in *c855a*<sup>+</sup> (data in red) and *cg25c*<sup>+</sup> (data in blue) cells provoke arrest during larval development. (A) Different size phenotypes are detected in arrested larva: underexpression of *dpr2* and *Octβ1R* in *c855a*<sup>+</sup> cells produce defects in length; underexpression of *dpr2*, *Oamb* and *Octβ3R* in *cg25c*<sup>+</sup> cells cause retain in overall size, and larvae may even present crystal cells (arrows). (B-B') Measurements in length and width reveal a similar larval volume (B) for larvae with defective *dpr2* in both cell-types and also within down-regulated octopamine genes. This data shows that their larval volumes are late L2 / early L3-like (B'), regardless of the overall time spent in arrest. (C) The jaw identifiers of the arrested phenotypes reveal that all larvae are in the L3 stage. Scale bar represents 100 μm. (D) The feeding assay shows a normal food intake during abnormal developmental behaviour. (E) Table summarising the characterisation of the arrested phenotypes.



I

### Arrested stage overview

Dysfunctional gene	Brain like
<i>c855a-Gal4 &gt; dpr2-IR (RNAi)<sup>V29742</sup></i>	Normal mid L3-like (~88 h AEL)
<i>cg25c-Gal4 &gt; dpr2-IR (RNAi)<sup>V29742</sup></i>	Normal early L3-like (~72 h AEL)
<i>c855a-Gal4 &gt; Oamb (UAS)<sup>B08230</sup></i>	Normal L2-like (~64 h AEL)
<i>cg25c-Gal4 &gt; Oamb-IR (RNAi)<sup>B31171</sup></i>	Bigger L2-like (~64 h AEL)
<i>c855a-Gal4 &gt; Octβ1R-IR (RNAi)<sup>B58179</sup></i>	Normal L2-like (~64 h AEL)
<i>cg25c-Gal4 &gt; Octβ3R-IR (RNAi)<sup>B62283</sup></i>	Bigger L2-like (~64 h AEL)

down-regulation of the gene *defective proboscis extension response 2* (*dpr2*) in *c855a*<sup>+</sup> cells (C-C') results in a mid L3-like brain with emerging holes or bubbles in the brain surface (arrowheads); *dpr2* down-regulation in *cg25c*<sup>+</sup> cells (D-D) causes the brain to be early L3-like. There is NEC proliferation (arrows) in both niche cell phenotypes. (E-H) Dysfunctional octopamine receptors in niche cells provoke brain arrest at an L2-like stage. Normal L2-like brains are observed when there is overexpression of the *Octopamine receptor in mushroom bodies* (*Oamb*; E-E') and underexpression of the *Octopamine β1receptor* (*Octβ1R*; G-G') in *c855a*<sup>+</sup> cells, whereas underexpression of *Oamb* (F-F') and of *Octopamine β3 receptor* (*Octβ3R*; H-H') in *cg25c*<sup>+</sup> cells enlarge the L2-like brain (asterisk). (I) Table summarising the characterisation of the arrested brain phenotypes. Images were taken at maximum time of arrest. Scale bars represent 35 μm in (A), 20 μm in (A') and 50 μm in (C).

**Figure 47. Arrest in L2 to L3 stage transition may be caused by deregulated niche genes in the brain.** Microscope images show abnormal larval brains caused by altered expression of genes in *c855a*<sup>+</sup> cells (red boxes) and *cg25c*<sup>+</sup> cells (blue boxes) that causes arrest between late L2 and early L3 larval development. The two niche populations are observed by marking neuroepithelial cells (NECs) with anti-DE-Cad antibody (blue) and glial cells with the antibody anti-Repo (red). NECs (arrows) and glial (arrowheads) proliferation (green) are shown using the antibody against PH3. (C-D) A

## 5. Characterization of octopamine receptors and their implication in brain growth

The RNA-seq analysis of neuroepithelial and glial cells provided novel possible roles for the cell niche. Some of the most interesting phenotypes observed are those that affect the ability of the fly to undergo transitions between different stages of development (Figures 45, 46 and 47); in particular, many of these phenotypes are of larval growth arrest. Among the validated genes that induce larval arrest, there is a group of OA receptors that stand out: *Oamb*, *Octβ1R* and *Octβ3R*. These genes encode protein receptors for the OA hormone (Erspamer, 1948). In humans, OA is a member of the endogenous trace amines which are agonist of trace amine-associated receptor (TAAR; Borowsky et al., 2001; Bunzow et al., 2001; Zucchi et al., 2006). In insects, OA is related with tyramine (TA) and functions as a neurohormone, neuromodulator and neurotransmitter; its function is analogous to that of NA in mammals (Hauser et al., 2006; Ohhara et al., 2012). OA has been investigated in *Drosophila* in studies of learning, memory and many other behaviours during development of the fruit fly (Kim et al., 2013; Li et al., 2016; Sujkowski et al., 2017; Zhou et al., 2008). Several OA receptors have been described in *Drosophila* and classified depending on similarities in their structure and signalling properties with vertebrate adrenergic receptors (Evans and Maqueira, 2005). Therefore, there are two α-adrenergic-like receptors (*Oamb* a.k.a. *Octa1R*, and *Octa2R*), three β-adrenergic-like receptors (*Octβ1R*, *Octβ2R*, *Octβ3R*), and one tyramineric receptor (*Oct-TyrR*; Han et al., 1998; Maqueira et al., 2005; Qi et al., 2017; Robb et al., 1994).

From the validation in dysfunctional *c855a*<sup>+</sup> and *cg25c*<sup>+</sup> cells, other G protein-coupled receptors (GPCRs) for the insect biogenic amines present some type of phenotype but not arrest (e.g. *5-HT2B* and *nAChRa3*; Jørgensen et al., 2006; Figures 40 and 45B). Apart from *Oamb*, *Octβ1R* and *Octβ3R* arrested phenotypes, other receptors for OA (*Octa2R*, *Octβ2R* and *Oct-TyrR*) were also tested due to the fact that they were differentially expressed in the bioinformatic analysis (Table S5). However, their validation did not reveal any abnormal phenotypes resulting from altered expression of these genes.

As previously mentioned, the development of organisms is close related with tissue regeneration and, thus, the arrested phenotypes observed may be associated to a lack of coordination among both (Garelli et al., 2012; Jaszczak and Halme, 2016; Juarez-Carreño et al., 2018; Rewitz et al., 2013; Vallejo et al., 2015). Therefore, as the OA receptors are hormone receptors, the role of OA-related genes has also been analysed in several tissues besides the larval CNS. It is important to note that the data presented next was recently collected and thus, in some cases, due to time constraints, more experiments are needed to further explore and clarify the findings.



## 5.1. The impact of the octopamine receptor in mushroom bodies (Oamb) in development

*Oamb* was the first cloned OA receptor to be studied in *Drosophila* (Han et al., 1998). This receptor was originally identified in mushroom bodies (MBs; Han et al., 1998) and, interestingly, its function there is highly linked with the dopamine receptor (*Damb*; Han et al., 1996; Himmelreich et al., 2017).

I previously described the abnormal larval phenotypes caused by altered *Oamb* expression in niche cells. As a reminder, up-regulation of *Oamb* in *c855a*<sup>+</sup> causes larval arrest in the early L3 stage, and these abnormal larvae have normal-appearing L2-like brains (Figures 43A,A' and 47E,E'); down-regulation causes lethality in the pupal stage (Figure 40A,A'). *Oamb* overexpression in *cg25c*<sup>+</sup> cells does not produce any phenotype but down-regulation results in early L3 arrest for several days (Figure 46). The latter phenotype also exhibits a massive L2-like brain (Figure 47F,F'), which is interesting to further characterise (Figure 48).

Hence, immunostainings were used to observe L2-like brains from L3 arrested larvae due to down-regulation of *Oamb* in *cg25c*<sup>+</sup> cells. First, I was interested to know whether the increment in size of the L2-like brain involves cell proliferation. Confocal images verified an increase in mitotic cells in the entire brain (Figure 48E,E'). Later, I wanted to know whether the *cg25c*<sup>+</sup> cells used the EGFR pathway to stimulate this growth, as occurs in the signalling between NECs and OL *miR-8*<sup>+</sup> glial cells (Morante et al., 2013) and because the *cg25c*<sup>+</sup> cells are a subset of *miR-8*<sup>+</sup> glia. However, in this case, the brain overgrowth phenotype is not caused by mitogens which activate EGFR (Figure 48F,F') and thus may be triggered by other signals, for example from Wnt, Notch, or Hippo pathways, to trigger cell proliferation (Duronio and Xiong, 2013). Neither NECs nor NBs seem to be altered in number (Figure 48G,G'). However, it is very interesting that there is a group of a few neurons in each lobe that are harmed and undergo apoptosis (Figure 48H,H').

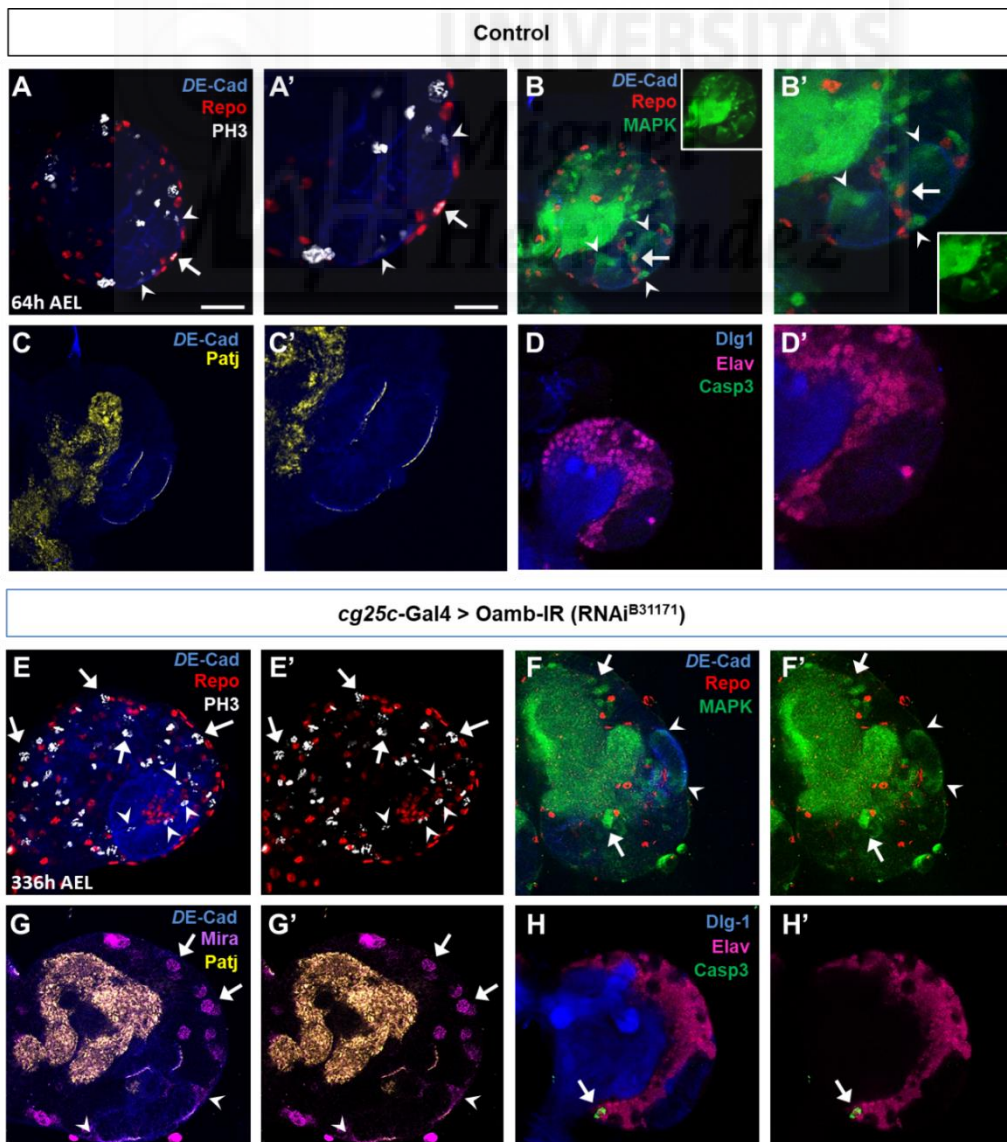


**Figure 48. Characterisation of the phenotype of *cg25c*<sup>+</sup> cells defective in *Oamb* at the larval stage arrested.** Microscope images show cell behaviour in abnormal larval brains from larvae arrested between late L2 and early L3 stages of development; this phenotype is caused by a down-regulation of the *Oamb* receptor in *cg25c*<sup>+</sup> cells. The two niche populations are observed by marking neuroepithelial cells (NECs) with the antibodies anti-DE-Cad (blue), anti-Dlg1 (blue) and anti-Patj (yellow); and glial cells with the antibody anti-Repo (red). (A-D) In control brains, neuroblasts (NBs) are tagged with an anti-Mira antibody (purple) and neurons with an anti-Elav antibody (pink); NEC (arrowheads) and glial (arrows) proliferation is shown using the anti-PH3 (white) and anti-MAPK (green) antibodies, and apoptosis is marked with the antibody against Casp3 (green). (E-H) Brains with abnormal phenotypes show an increase in cell proliferation and mitosis (E-E') in the lobe (arrows) as well as in NECs (arrowheads) but not via the MAPK pathway (F-F'). NBs from the central brain (arrows) and the optic lobe (arrowheads) do not seem to be affected (G-G'), but there is cell death of a very small set of neurons (arrow; H-H'). Images were taken at maximum time of arrest. Scale bars represent 35  $\mu$ m in (A) and 20  $\mu$ m in (A').

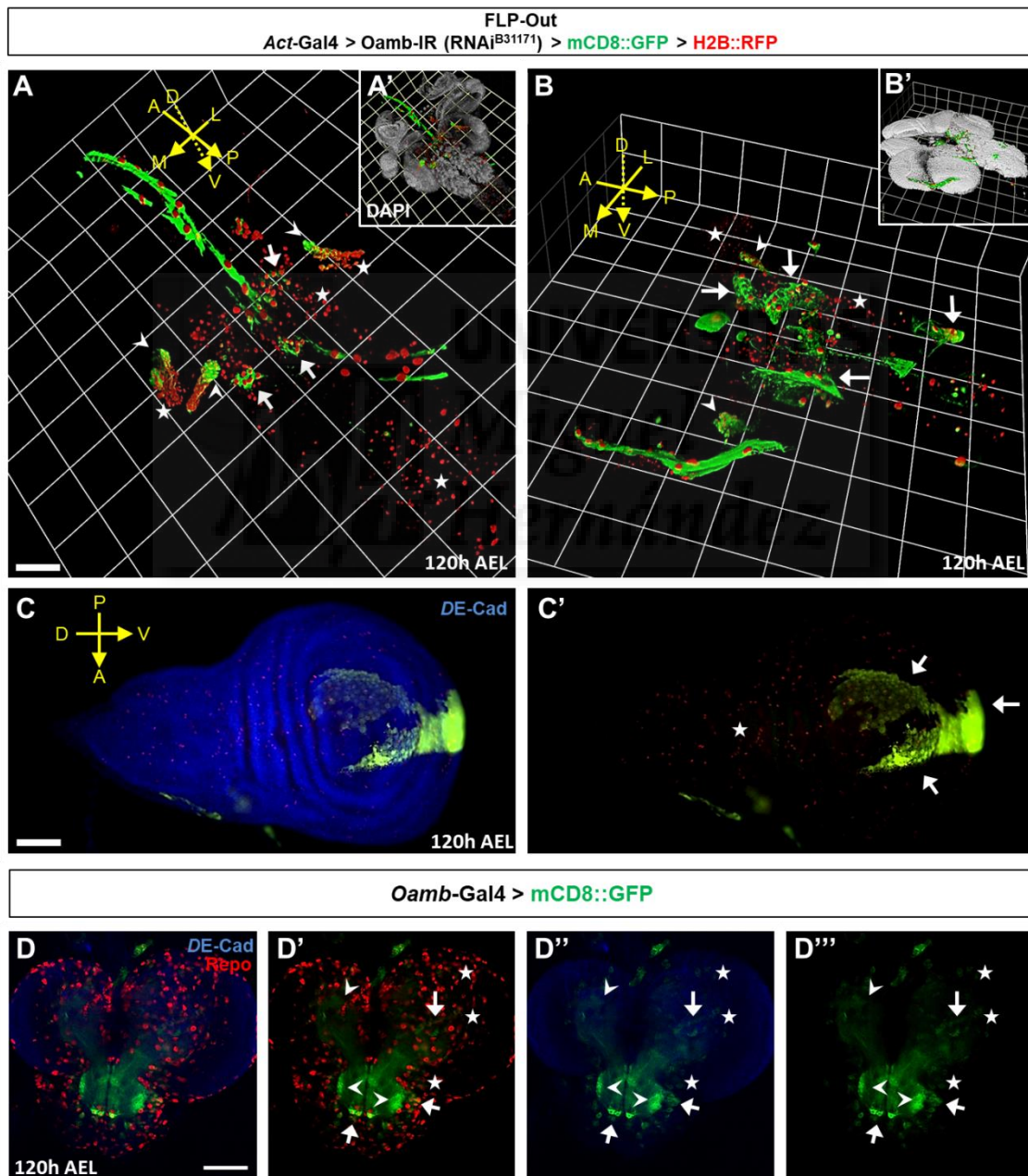


**Figure 49. Characterisation of the *Oamb* receptor during larval stages.** (A-C) Microscope images show cell behaviour when there is a down-regulation of *Oamb* using the FLP-Out clonal analysis. This system uses the gene *actine* to drive the expression of membranar (UAS-mCD8::GFP) and nuclear (UAS-H2B::RFP) fluorescent proteins in recombined cells. (A-A',B-B') Underexpression of the receptor *Oamb* in cells of the brain reveals that it does not affect the integrity of cells with large nuclei and arborisation-like shapes (arrows) that resemble glia, nor does it affect cells that

resemble optic lobe progenitors (arrowheads). However, simultaneously, LOF also cause cell death (asterisks) in other glial cells (big nuclei) and neurons (small nuclei) of any part of the brain. (C-C') In imaginal discs, epithelial cells (arrows) and their offspring from the wing pouch seem not to be affected by a depletion of the *Oamb* receptor, but also there is death of other cells (asterisks). (D-D'") The driver of *Oamb* (*Oamb-Gal4*) triggering the membranal green fluorescent protein (UAS-mCD8::GFP) expression reveals that the receptor is expressed in glial cells (arrows) as well as in other cells (arrowheads) of the central brain and ventral nerve cord; some of those cells may be *cg25c*<sup>+</sup> glial cells from the medial side of the OL (asterisks). Epithelial cells were stained with an anti-DE-Cad antibody (blue), glial cells with an anti-Repo antibody (red) and the nuclei of cells with DAPI (grey). Images were taken from late-3<sup>rd</sup> instar larva. The coordinate axes indicate anterior-posterior (A-P), lateral-medial (L-M), and dorsal-ventral (D-V) directions. Scale bars represent 100  $\mu$ m in (A), 150  $\mu$ m in (C), and 85  $\mu$ m in (D').

---

This last finding of dead neurons in the arrested phenotype lead me to use a FLIP-Out technique to see the behaviour of the different cell types when the expression of *Oamb* was diminished therein (Figure 49A-C). In the CNS (Figure 49A,B), there are cells that resemble glia (big nuclei and arborisation-like shape) as well as OL progenitors which are not affected by a down-regulation of *Oamb*. In contrast, other CNS cells lack the GFP expression that suggests they are dead; the majority of those cells have small nuclei and may indicate they are neurons. This cell death was also shown in imaginal discs cells although not in epithelial cells and their offspring from the wing pouch (Figure 49C,C').

In order to reveal the *Oamb* receptor expression pattern among the CNS cells, an antibody anti-Repo staining was carried out, and showed that in late L3, some of those cells are glia while others are not (Figure 49D-D'"). Moreover, due to confocal images, I speculated that some of the glial cells may be *cg25c*<sup>+</sup> from the medial side of the OL. The expression at the L2 stage remains to be addressed.

To determine in which CNS glial type the *Oamb* expression is important, I depleted it using different Gal4 drivers. The results reveal that *Oamb* expression is not important in some types of glia such as CG (*NP2222-Gal4* and *NRT-Gal4*), SPG (*NP2776-Gal4*) and PG (*NP6293-Gal4*). However, fly larvae have abnormal arrested phenotypes when *Oamb* is underexpressed using a larval pan-glial driver (*repo-Gal4*) which arrest in early L3, or the driver for *miR-8*<sup>+</sup> cells (*mir-8-Gal4*) which arrest in late L2. Both arrest phenotypes end in lethality during the larval stage.

A general *Oamb* depletion in glial cells (*repo-Gal4*) arrests larvae for up to 180 h AEL; these arrested larvae resemble early / mid L3-like larvae in size (Figures 50A and S17). However, the arrested larvae when are compared with controls have volumes that would be expected of mid L3 larvae at around ~92 h AEL (Figure 50B,B'). Finally, the jaw features of these abnormal larvae confirm that they are arrested at the L3 stage (Figure 50C). The development of larvae *Oamb* defective in *miR-8*<sup>+</sup> cells stay in arrest for up to 168 h AEL and their size resembles that of a late L2 control larva in length and width (Figures 50A and S17). In addition, volume measurements reveal that their volume resembles that of a mid L2 control larva at ~66 h AEL (Figure 50B,B'). This is consistent with their jaws, which have characteristics of L2 larvae (Figure 50C). I also verified that their brains were arrested at this stage (Figure 50F), and additionally had lengthened VNCs (Figure 50E). Although it is promising that the phenotype with *Oamb* deficiencies in *miR-8*<sup>+</sup> cells resembles in many aspects that one with deficiencies in *cg25c*<sup>+</sup> cells, the main difference is that the *miR-8*<sup>+</sup> defective phenotype cause arrest before the L2-to-L3 larval transition and the *cg25c*<sup>+</sup> defective phenotype after it (Figures 50 and S17). In essence, it is encouraging that two glial drivers (*repo-Gal4* and *mir-8-Gal4*), where *cg25c*<sup>+</sup> glial cells from the niche belong, evoke arrested phenotypes using the OA receptor *Oamb*.

Finally, I wondered whether the *Oamb* receptor may interfere locally in other tissues and be the reason of the differences of age development among larval size, volume, jaws and brain that are observed along the different arrested phenotypes. Down-regulation in the RG (*phm-Gal4*) provokes arrest in half of the larvae at the early L3 stage that are wandering up the tube walls, while the other half of the larvae undergo arrest at the late L3 stage for ~480 h AEL (data not shown). The down-regulation of *Oamb* in FB cells (*isp2-Gal4*; Lazareva et al., 2007) does not cause any abnormal phenotype; however, using another driver for FB cells (*ppl-Gal4*; Colombani et al., 2003) causes small sizes of the individuals in larva, pupa and adult but not lethality nor arrest (data not shown). This is possibly explained because even though *ppl-Gal4* driver is used as FB-specific, it is also expressed in few CB neurons and it has little expression in wing disc, salivary glands and intestine. In addition, the phenotype difference may also be explained by a different time expression between both FB drivers used. Interestingly, an overexpression of this OA receptor in *ppl*<sup>+</sup> cells causes arrest in half of the larvae at the early L3 stage (data not shown).

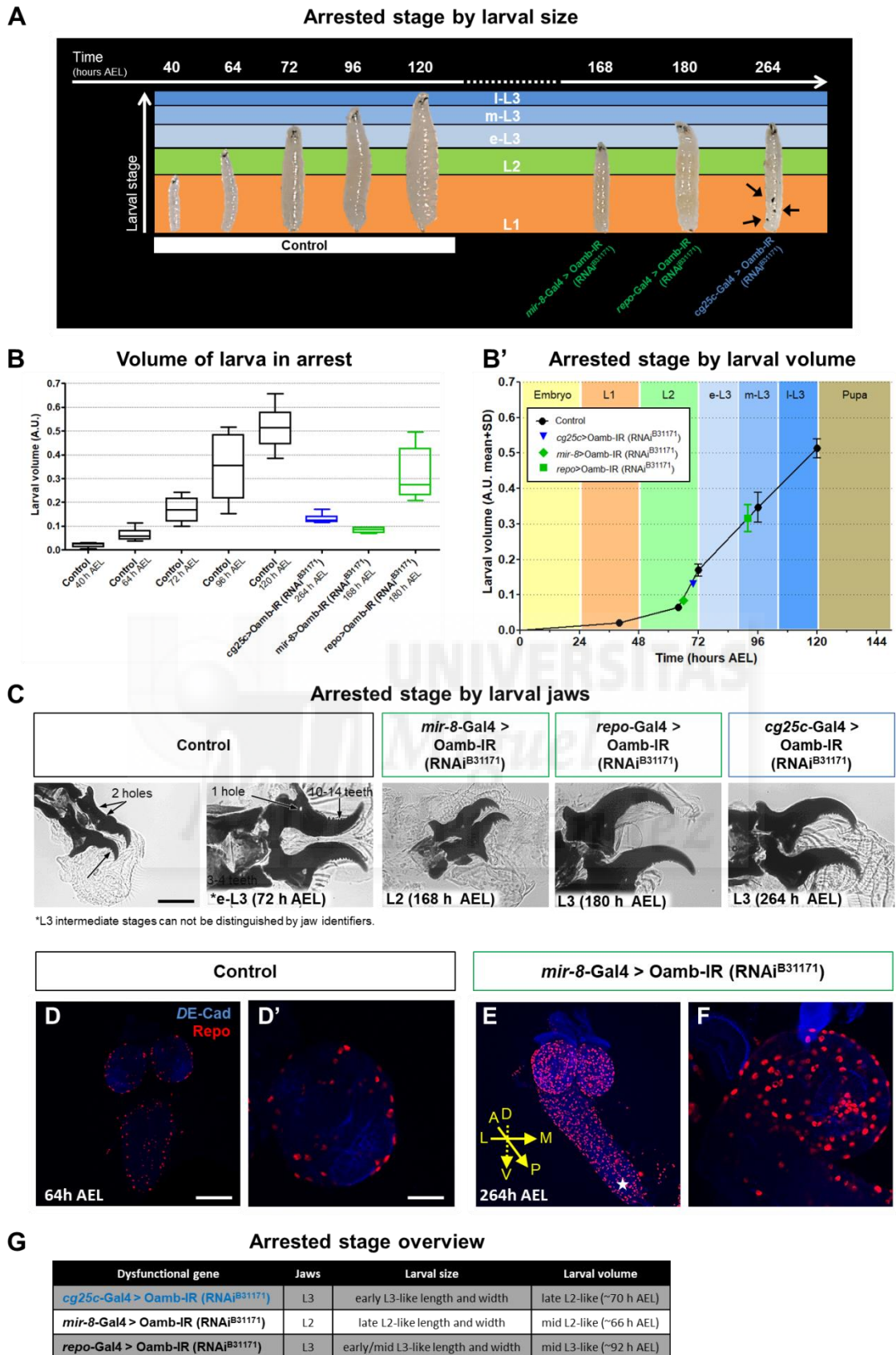


**Figure 50. Drivers for glia with down-regulated *Oamb* produce arrested phenotypes in larval stage.** Down-regulation of the receptor *Oamb* in *mir-8*<sup>+</sup> and *repo*<sup>+</sup> glial cells (data in green) cause arrest during larval development; as is the case in *cg25c*<sup>+</sup> cells (data in blue). (A) Abnormal larvae arrest at different sizes and developmental stages depending on which cell type is affected by *Oamb* underexpression; thus, altered expression in *mir-8*<sup>+</sup>, *repo*<sup>+</sup> and *cg25c*<sup>+</sup> cells causes arrest at different stages and for different amounts of time. (B-B') Measurements in length and

width reveal similar larval volumes (**B**) for organisms with defects in *cg25c*<sup>+</sup> cells and *miR-8*<sup>+</sup> cells but different for *repo*<sup>+</sup> cells. This data shows that the larval volumes are mid L2-like for larvae affected in *miR-8*<sup>+</sup> cells, late L2 / early L3-like for those affected in *cg25c*<sup>+</sup> cells, and mid L3-like for larvae affected in *repo*<sup>+</sup> cells (**B'**), regardless of their overall time of arrested. (**C**) The jaw identifiers of the arrested phenotypes reveal that larvae with *Oamb* underexpression in *miR-8*<sup>+</sup> cells are arrested in the L2 stage whereas the larvae with *Oamb* down-regulated in *cg25c*<sup>+</sup> and *repo*<sup>+</sup> cells are in the L3 stage. (**D-F**) Confocal images show the two niche cell populations by marking neuroepithelial and glial cells with the antibodies anti-DE-Cad (blue) and anti-Repo (red), respectively. (**E-F**) *Oamb* LOF in *miR-8*<sup>+</sup> cells of larvae at maximum time of arrest cause L2-like brains and longer ventral nerve cords (asterisk). (**G**) Table summarising the characterisation of the phenotypes in arrest. The coordinate axes indicate anterior-posterior (A-P), lateral-medial (L-M), and dorsal-ventral (D-V) directions. Scale bars represent 100  $\mu\text{m}$  in (**C**), 75  $\mu\text{m}$  in (**D**), and 35  $\mu\text{m}$  in (**D'**).

## 5.2. The impact of the octopamine $\beta$ 1receptor (*Oct $\beta$ 1R*) in development

The *Drosophila Oct $\beta$ 1R*, together with the rest of the  $\beta$ -adrenergic-like receptor family, was first characterised in neurons from the adult CNS (Maqueira et al., 2005). Briefly, as explained before, the underexpression of this receptor in *cg25c*<sup>+</sup> cells produces arrest at L3 in half of larvae and enlarged brains which, apart from presenting overproliferation of NECs, show loss of *cg25c*<sup>+</sup> glial cells and lobe SG but not of NG (Figures 43B and 45L,L'). *Oct $\beta$ 1R* down-regulation in the other niche cell type, *c855a*<sup>+</sup> cells, causes arrest at the early L3 stage and premature wandering behaviour (Figures 43B' and 46); however, affected larvae have normal L2-like brains in size (Figure 47G,G'). More detailed characterisation of these brains shows apparently normal NBs (Figure 51D,D') but a clear inactivation of overall lobe cell proliferation via the mitogen-activated protein kinases (MAPK) pathway (Figure 51C,C'), which may explain why brains appear to be of normal size even after being arrested for several days.

Clones created with the FLIP-Out technique (Figure 51E,F) shows that some neurons (cells with small nuclei) from any part of the CNS do not appear to be affected by *Oct $\beta$ 1R* dysfunction, though others are. In addition, cells of any CNS region with large nuclei and arborisation-like shapes, which resemble glia (SG and other inner glia), are not affected when *Oct $\beta$ 1R* is down-regulated. This is in conflict with the brain phenotype observed when *Oct $\beta$ 1R* is down-regulated in *cg25c*<sup>+</sup> cells (Figure 45L,L'); for this reason a Gal4 validation using different larval drivers for glial cells was performed. Firstly, down-regulating *Oct $\beta$ 1R* in SG (*NP2776-Gal4* for SPG and *NP6293-Gal4* for PG) does not cause any abnormality in organism development. Secondly, using the driver *NRT-Gal4* for down-regulate *Oct $\beta$ 1R* in CG cells, did not show any phenotype; however, using the *NP2222-Gal4* driver remains arrested in early L3 stage (Figures 52 and S18). This is explained because the driver *NRT-Gal4* it has been shown that marks CG cells from the VNC (Bailey et al., 2015) while *NP2222-Gal4* marks CG cells in the entire CNS (Avet-Rochex et al., 2012); thus, the dysfunctional CG cells which promote the arrest phenotype are those in the brain. Down-regulation of *Oct $\beta$ 1R* using the *mir-8-Gal4* driver also causes arrest in early L3 (data not shown). Unfortunately, at this moment in time, the pan-glial driver *repo-Gal4* larval phenotype has not yet been tested and therefore more experiments are needed.

A broad characterisation of the brain *NP2222*<sup>+</sup> CG dysfunction shows that arrested larvae up to 336 h AEL have L1-like length but L3-like width (Figures 52A and S18). This small body size results in a volume similar to that of an early L2 control larva at ~50 h AEL (Figure 52B,B'). However, it is interesting to see that these abnormal larvae have jaws equivalent to those of L3 stage larva (Figure 52C,C'). All in all, these findings suggest that brain glia plays a role in stage transition via *Oct $\beta$ 1R*.

Another characteristic assessed for *Oct $\beta$ 1R* were the tissues related with a down-regulation of this receptor. Normal development is observed when *Oct $\beta$ 1R* is not expressed in FB cells (*lsp2-Gal4*); however, using another FB driver (*ppl-Gal4*) truncates this normality. This may be explained by the different cells that express *ppl* or the difference temporal expression, as mentioned before. Thus, underexpression of *Oct $\beta$ 1R* in *ppl*<sup>+</sup> cells arrests larva up to 212 h AEL at a size similar to that of an early L3 control larva in length and width (Figures 52A and S18). This results in a volume similar to that of a late L2 control larva at ~70 h AEL (Figure 52B,B'). However, these larvae have jaws that confirm that they are arrested in the L3 stage (Figure 52C,C'). Finally, mention that due to time constraints, it has not yet been possible to test *Oct $\beta$ 1R* in RG cells.

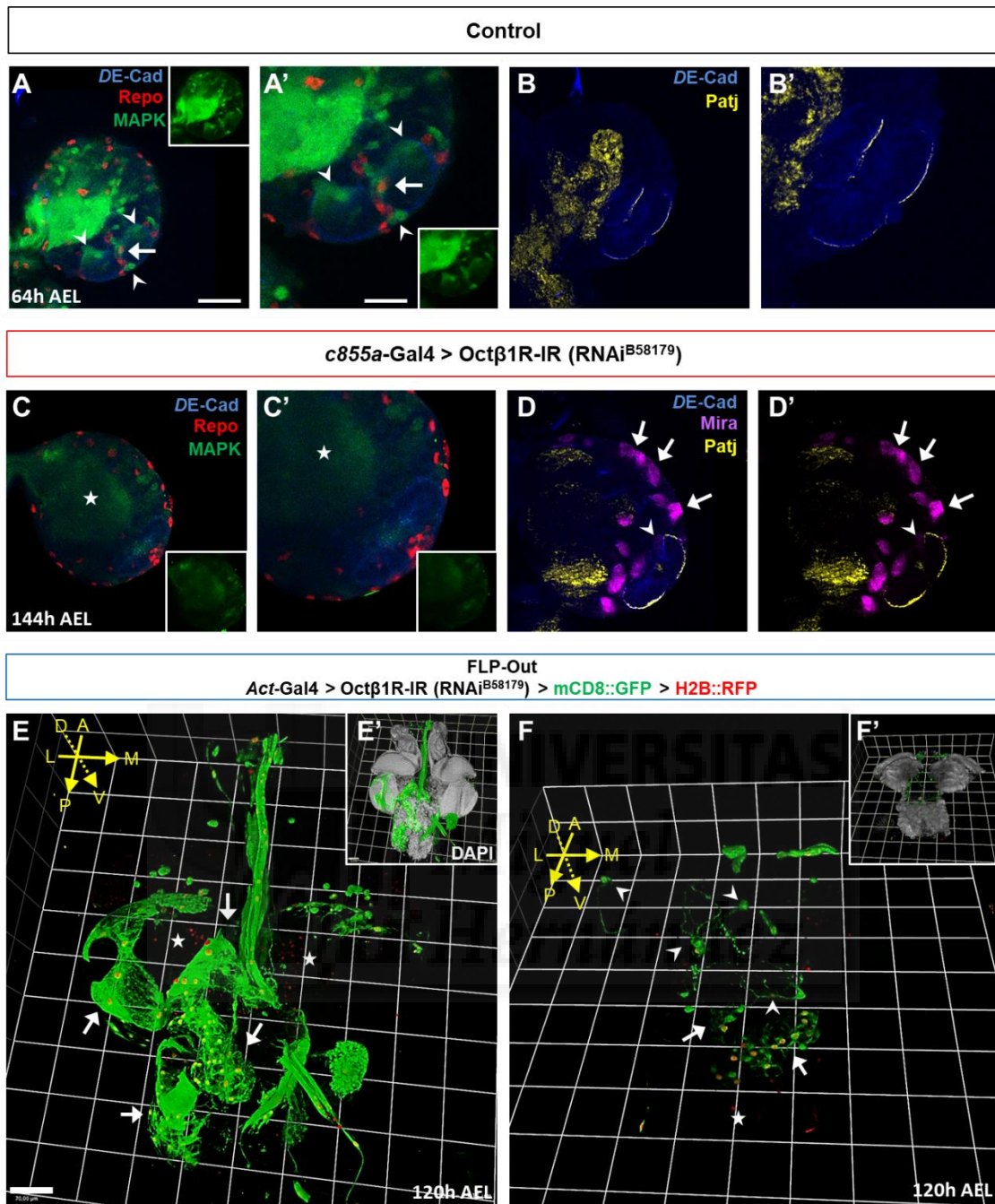


**Figure 51. Characterisation of the phenotypes caused by down-regulation of *Octβ1R* during larval stages.** Microscope images show cell behaviour when the *Octβ1R* is down-regulated. (A-D) The two niche cell populations are observed by marking neuroepithelial cells (NECs) with the antibodies anti-DE-Cad (blue) and anti-Patj (yellow) and glial cells with the antibody anti-Repo (red). Neuroblasts (NBs) are tagged with the anti-Mira antibody (purple) and proliferation is shown using the antibody against MAPK (green). Images were taken at maximum time of arrest. (A-B) NECs (arrowheads) and glia (arrows) of control brains were compared with (C-D) brains from larvae arrested between late L2 and early L3 stages of development, which was caused by down-regulation of *Octβ1R* in *c855a*<sup>+</sup> cells. There is a lack of cell proliferation via the MAPK pathway (C-C') within the lobe (asterisk), although NBs from the central brain (arrows) and the optic lobe (arrowheads) do not seem to be affected (D-D'). (E,E'-F,F') Late 3<sup>rd</sup>-instar larval tissues show cell response when there is a down-regulation of *Octβ1R* using FLP-Out clonal analysis. This system uses the gene *actine* to drive the expression of membranal (UAS-mCD8::GFP) and nuclear (UAS-H2B::RFP) fluorescent proteins in recombined cells. Images reveal that *Octβ1R* LOF does not affect the integrity of some cells with big nuclei and arborisation-like shapes (arrows) that resemble glia, nor does it affect some other cells that resemble neurons (arrowheads) throughout the entire CNS. However, LOF does appear to cause cell death (asterisks) in neurons (small nuclei) throughout the brain. The nucleus of the cells are stained with DAPI (grey). The coordinate axes indicate anterior-posterior (A-P), lateral-medial (L-M), and dorsal-ventral (D-V) directions. Scale bars represent 35 μm in (A), 20 μm in (A') and 75 μm in (E').

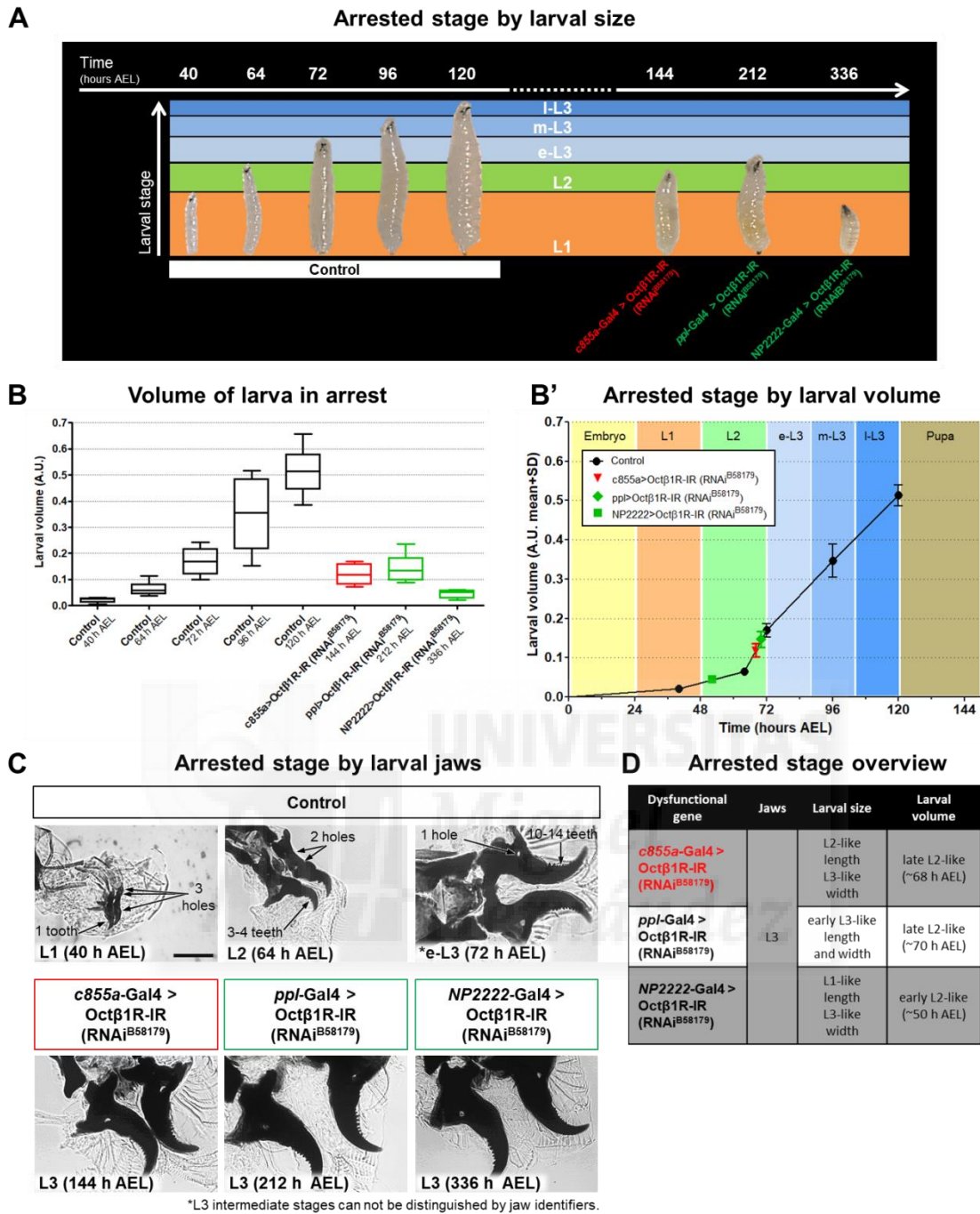


**Figure 52. Different drivers with a dysfunctional *Octβ1R* produce arrested phenotype in larval stage.** Down-regulation of the receptor *Octβ1R* in *ppl*<sup>+</sup> fat body cells and *NP2222*<sup>+</sup> cortex glial cells (data in green) and in *c855a*<sup>+</sup> neuroepithelial cells (data in red) causes arrest during larval development. **(A)** Arrested larvae display different size phenotypes: underexpression of *Octβ1R* in *c855a*<sup>+</sup>, *ppl*<sup>+</sup> and *NP2222*<sup>+</sup> cells causes holding in length but not in width at different stages and for different amounts of time. **(B-B')** Measurements in length and width reveal a similar larval volume **(B)** for larvae with defects in *c855a*<sup>+</sup> cells and *ppl*<sup>+</sup> cells but different volume for those with defects in *NP2222*<sup>+</sup> cells. These data show that larval volumes are early L2-like for organisms with *Octβ1R* down-regulation in *NP2222*<sup>+</sup> cells and late L2-like for those which *Octβ1R* down-regulation is in *c855a*<sup>+</sup> and *ppl*<sup>+</sup> cells **(B')**, regardless of their overall time arrested. **(C)** Jaws of all arrested larvae indicate that they are at the L3 stage. Scale bar represent 100 μm. **(D)** Table summarising the characterisation of the phenotypes in arrest.

### 5.3. The impact of the octopamine $\beta$ 3 receptor (*Oct $\beta$ 3R*) in development

*Oct $\beta$ 3R*, like the rest of *Drosophila*  $\beta$ -adrenergic-like receptor family, is a GPCR that increases cyclin AMP levels when coupled with OA (Maqueira et al., 2005). In short, down-regulation of *Oct $\beta$ 3R* in both niche cells causes arrest in larval stages for more than 300 h AEL. Underexpression of *Oct $\beta$ 3R* in *c855a*<sup>+</sup> cells results in arrest in half of the larvae at late L3 stage (Figure 43B); these larvae also have larger brains and exhibit NEC overproliferation (Figure 45M,N). In contrast, when the *Oct $\beta$ 3R* down-regulation is in *cg25c*<sup>+</sup> cells, the larval arrest occurs at early 3<sup>rd</sup> IL (Figure 46), but the brain resembles a larger version of that of an L2 control larva (Figure 47H,H'). Further characterisation of this arrested brain did not show increased proliferation when mitotic cells were tagged (Figure 53D,D') nor when the MAPK pathway was stained (Figure 53E,E'). Although the number of NBs is apparently high (Figure 53F,F'), more in-depth characterisation of this brain phenotype is needed.

I was also interested in investigating the behaviour of the different CNS cell types when the receptor *Oct $\beta$ 3R* is underexpressed (Figure 54A,B). The FLIP-Out technique revealed that a lack of *Oct $\beta$ 3R* expression in neurons (axonal cells with small nuclei) caused cell death in some of them but not in others. Similarly, the integrity of glial cells (cells with arborisation-like shape with large nuclei) seems to be partially affected, probably depending on the glial subtype. NECs from the brain also appear to be unaffected, as well as are epithelial cells from the imaginal discs, although some cells from this organ die. Additionally, cells from other organs such as the RG appear not to be influenced by *Oct $\beta$ 3R* down-regulation.

Later on, the cells expressing *Oct $\beta$ 3R* were analysed and the receptor expression pattern characterised using its Gal4 line and fluorescent proteins as reporters (Figure 54C-F). This experiment showed that in late L2 brains, the receptor is expressed in neurons of the VNC and CB but also in other cells that resemble glia, some of them very close to the OL (Figure 54C,D). Interestingly, the receptor expression in the 3<sup>rd</sup>-IL stage (Figure 54E,E') is high in the OL region and in cells that resemble glia, which may be fortunately *cg25c*<sup>+</sup> cells; also, there is expression of *Oct $\beta$ 3R* in the VNC and CB, in some cells that may be glia though this remains unclear. Images from L3 imaginal discs display some epithelial cells which express *Oct $\beta$ 3R* (Figure 54F,F'). Additionally, in both stages there are some cell nuclei highlighted, meaning that the expression of the *Oct $\beta$ 3R* is dependent on time but not cell-type.

Therefore, the next step was to analyse which of the cells of the CNS that express *Oct $\beta$ 3R* have an important function for growth and development. Down-regulation of *Oct $\beta$ 3R* in SG (*NP6293-Gal4* for PG and *NP2776-Gal4* for SPG) clarifies that this misexpression is not relevant for those cells. However, while the CG driver which is VNC-specific (*NRT-Gal4*) presents a normal development phenotype when the receptor is underexpressed; the other driver for CG, which is expressed in CG of the whole CNS (*NP2222-Gal4*), arrests the development of the larva (Figures 55 and S19). This suggests that the CG involved in this phenotype are from the lobes. In addition, another lobe glial driver (*mir-8-Gal4*) was also observed that phenotype that arrests at the larval stage (Figures 55 and S19). Experiments with the pan-glial driver *repo-Gal4* still need to be done.

I went to study in detail in the two glial drivers for which larvae arrest for 264 h AEL when *Oct $\beta$ 3R* is underexpressed (Figures 55 and S19). Down-regulation of the receptor in *mir8*<sup>+</sup> cells causes arrest, resulting in larvae with early L3-like width but L2-like length (Figures 55A and S19). These abnormal larvae have a volume similar to mid L2 control larva of ~65 h AEL (Figure 55B,B'). However, their jaws reveal that they arrest at the L3 stage (Figure 55C). The other glial driver which leads to abnormal phenotype is the *NP2222-Gal4* for CG. In this case, larvae arrest at a variety of different sizes, and half reach the pupal stage but then die (Figure 55A); a part of the larvae in arrest are smaller than the others (Figures 55A and S19). The larval volume reveals that the smallest arrested larvae have mid L2-like volume similar to that of a control larva of ~62 h AEL, whereas the bigger ones are similar in volume to mid/late L3 larvae of ~103 h AEL (Figure 55B,B'). Despite this, the jaw characteristics of these abnormal larvae reveal that both are arrested in the L3 stage (Figure 55C). All in all, when the OA receptor *Oct $\beta$ 3R* is downregulated in glial cells, including *cg25c*<sup>+</sup> glia, it causes larval arrest in the 3<sup>rd</sup> instar (Figures 55 and S19). Interestingly, these phenotypes cause different body sizes and volumes in larvae. For this reason, it is important to know at which stage of development are the larval internal organs when these larvae are arrested, which may provide a deeper understanding of these phenotypes.

Aside from those CNS phenotypes, I wanted to know if other tissues respond to an *Oct $\beta$ 3R* down-regulation. Thus, using the driver *phm-Gal4* and *isp2-Gal4*, I showed that *Oct $\beta$ 3R* depletion in RG cells and FB cells, respectively, are irrelevant for this receptor function. However, underexpression of *Oct $\beta$ 3R* in *pp1*<sup>+</sup> cells does cause arrest in half of larvae in the early L3 stage for ~168 h AEL (data not



shown). Due to similarities with *Octβ1R* for FB drivers, in this case, the interpretation in *Octβ3R* may be the same.

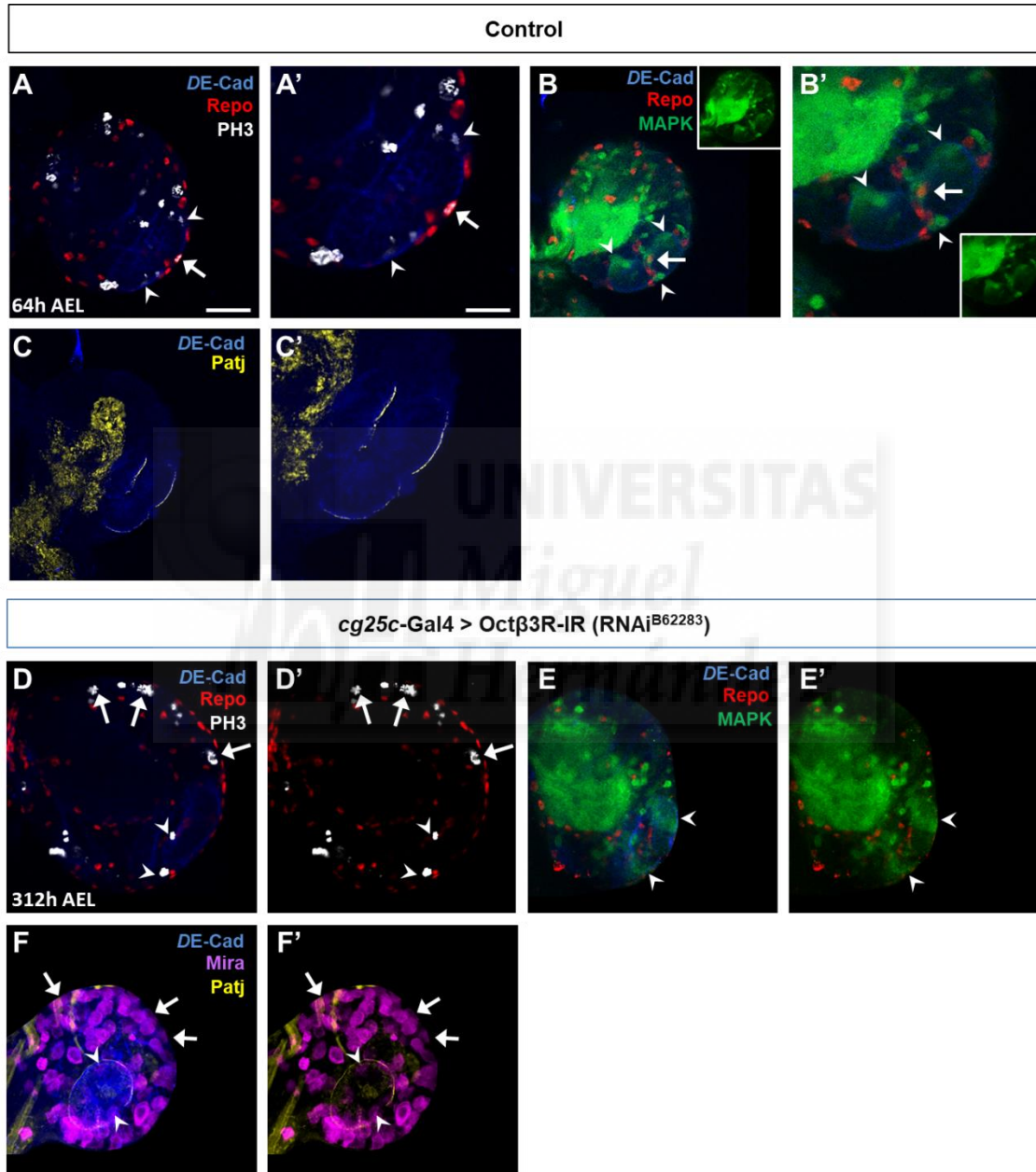


**Figure 53. Characterisation of the phenotype of *cg25c*<sup>+</sup> cells deficient in *Octβ3R* expression at the larval stage arrested.** Microscope images show cell behaviour in abnormal larval brains which is caused by a down-regulation of the *Octβ3R* receptor in *cg25c*<sup>+</sup> cells; images are from larvae arrested between late L2 and early L3 stages of development. The two niche populations are observed by marking neuroepithelial cells (NECs) with the antibodies anti-*DE-Cad* (blue) and anti-*Patj* (yellow), and glial cells with the antibody anti-*Repo* (red). **(A-C)** Control brains with NEC (arrowheads) and glial (arrows) proliferation tagged with the antibodies against PH3 (white) and anti-MAPK (green). **(D-F)** Brains with abnormal phenotypes show normal ratios of cell proliferation and mitosis **(D-D')** in the lobe (arrows) as well as in NECs (arrowheads) and also normal levels of MAPK pathway activation **(E-E')**. Neuroblasts in the central brain (arrows) and the optic lobe (arrowheads) stained with anti-*Mira* antibody (purple) are apparently more numerous than normal **(F-F')**. Images were taken at maximum time of arrest. Scale bars represent 35 μm in **(A)** and 20 μm in **(A')**.

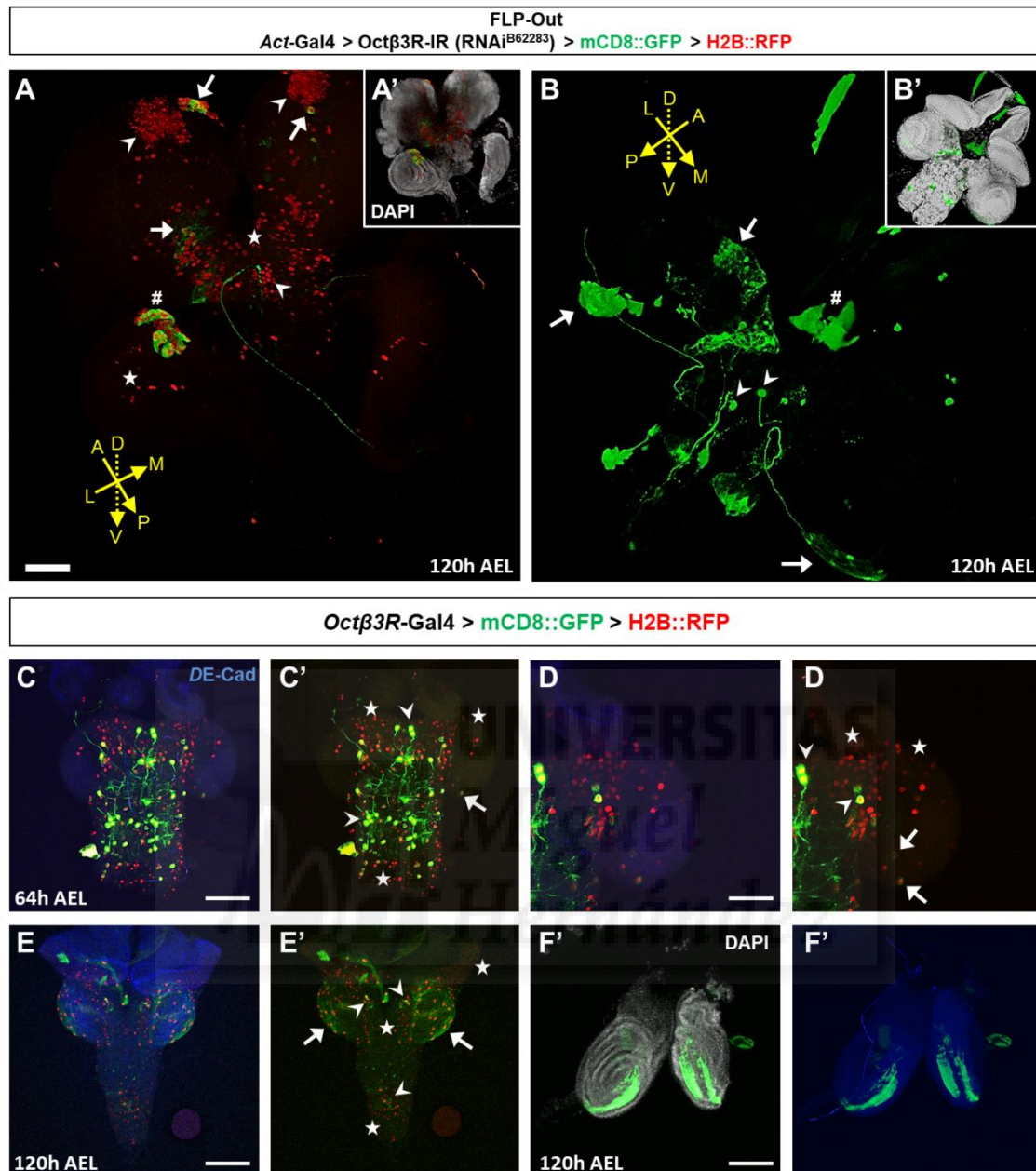


**Figure 54. Characterisation of the *Octβ3R* receptor during larval stages.** (A,A'-B,B') Microscope images show cell behaviour when there is a down-regulation of *Octβ3R* using the FLP-Out clonal analysis. This system uses the gene *actine* to drive the expression of membranar (UAS-mCD8::GFP) and nuclear (UAS-H2B::RFP) fluorescent proteins in recombined cells (note that nuclear fluorescence is not present in (B-B')). *Octβ3R* LOF in cells of the brain does not appear to affect the integrity of cells with large nuclei and arborisations that resemble glia (arrows), nor other cells that resemble progenitors or neurons (arrowheads). Cells (hash) of the imaginal discs (A) and the ring gland (B) do not seem to be affected either. However, LOF in the brain also causes cell death (asterisks) in other types of glia (large nuclei) and neurons (small nuclei) as well as in other tissues. Images were taken from late-3<sup>rd</sup> instar larva. (C-F) The driver for *Octβ3R* when express the same fluorescent reporter genes previously mentioned, reveal its expression pattern. (C,C'-D,D') In L2 stage brains, the *Octβ3R* receptor is expressed throughout the central nervous system, primarily in neurons (arrowheads) but also glial cells, some of them close to the optic lobe (arrows). (E-E') In L3 stage brains, the expression is detected mainly in glia of the optic lobe that are *cg25c*<sup>+</sup> (arrows), but also in other cells throughout the entire CNS (arrowheads). (F-F') There is expression in epithelial cells of the imaginal discs as well. The nuclear perdurance phenomenon reveals that the receptor expression throughout development takes place through the time within different cells (asterisks). Epithelial cells were stained with an anti-DE-Cad antibody (blue) and the nucleus of the cells with DAPI (grey). The coordinate axes indicate anterior-posterior (A-P), lateral-medial (L-M), and dorsal-ventral (D-V) directions. Scale bars represent 150 μm in (A) and (E), 75 μm in (C), 35 μm in (D), and 100 μm in (F).

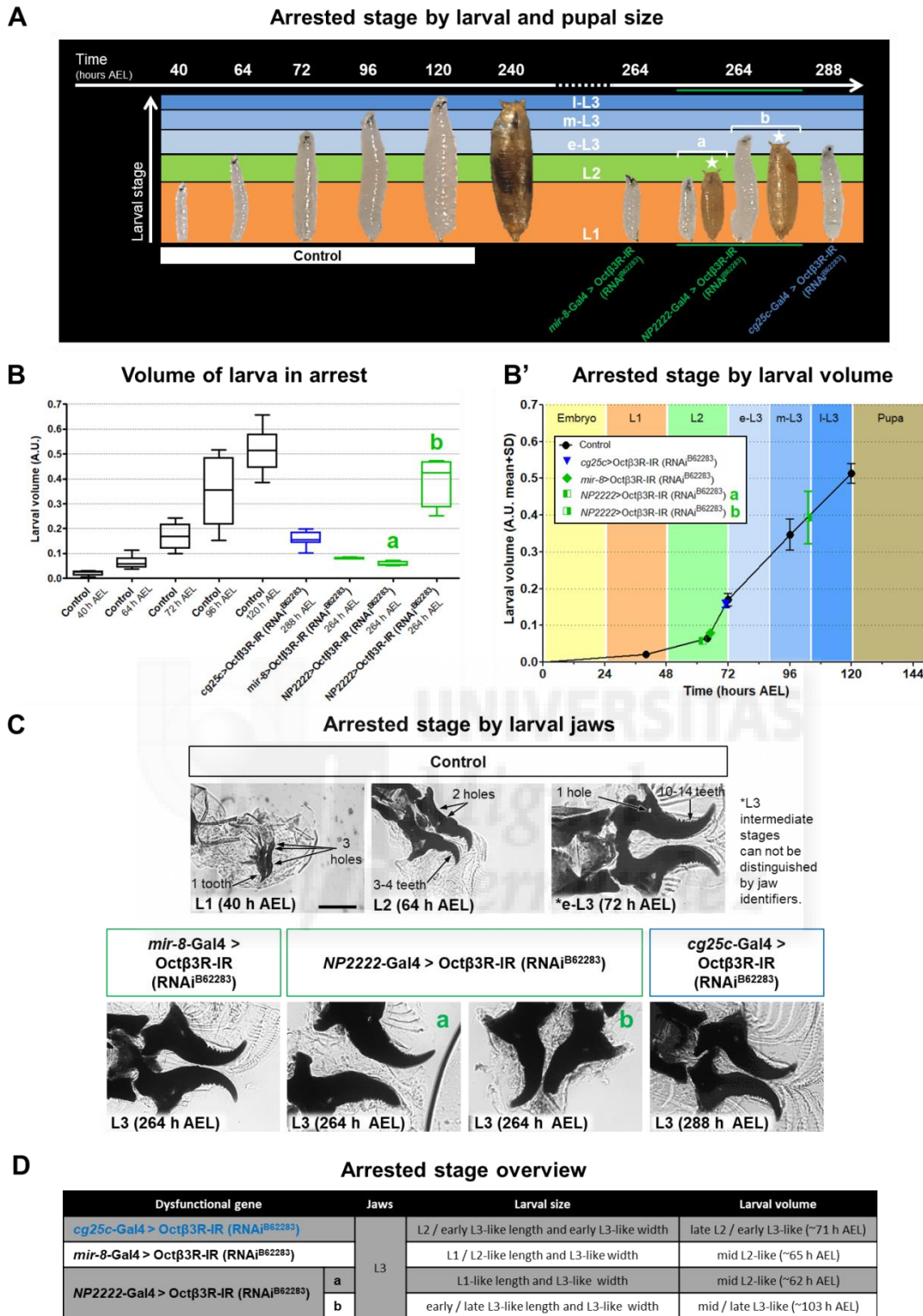


**Figure 55. Drivers for glia with down-regulated *Octβ3R* produce arrested phenotype in larval stage.** Down-regulation of the receptor *Octβ3R* in *miR-8*<sup>+</sup> and *NP2222*<sup>+</sup> glial cells (data in green) and in *cg25c*<sup>+</sup> cells (data in blue) causes arrest during larval development. **(A-a,A-b)** The driver *NP2222* cause arrest into two different larval times (**a** and **b**) and, in addition, some of these larvae make the transition to pupa (asterisks) but die in this stage. **(A)** Different phenotypes of size are present among arrested larvae: malfunction of *Octβ1R* in *NP2222*<sup>+</sup>, *miR-8*<sup>+</sup> and *cg25c*<sup>+</sup> cells causes retention in length but not in width at different larval stages and for different amounts of time. **(B-B')** Measurements in length and width reveal a similar larval volume **(B)** for *Octβ3R* down-regulation in *miR-8*<sup>+</sup> cells and *NP2222*<sup>+</sup>-**a** cells but different for *NP2222*<sup>+</sup>-**b** cells. These data show that their larval volumes are mid L2-like for *miR-8*<sup>+</sup> and *NP2222*<sup>+</sup>-**a** larvae, late L2-like for *cg25c*<sup>+</sup> larvae, and mid/late L3-like for *NP2222*<sup>+</sup>-**b** larvae **(B')**, regardless of their similar overall time arrested. **(C)** The jaw identifiers of the arresting phenotypes reveal that all larvae are at the L3 stage. Scale bar represent 100 μm. **(D)** Table summarising the characterisation of the phenotypes in arrest.

## 5.4. Signalling pathway underlying octopamine modulation in the brain

The focus until now has tended to be on the OA receptors and their role in *Drosophila* development. Thus, efforts have been directed towards characterisation of *Oamb*, *Octβ1R* and *Octβ3R*, whose down- or up-regulation in cells from the CNS, especially glia and NECs, mainly results in larval arrest phenotypes. Although still much remains to be done to profile OA receptors, the OA<sup>+</sup> cells and their signalling pathways in the larval brain are also interesting to address.

In that regard, I wanted to visualise which cells produce the ligand of the OA receptors and its expression pattern during larval stages. In order to do this, I used a driver for the key enzyme that synthesises OA known as *tyramine β hydroxylase* (*tβh*; (Monastirioti et al., 1996), a monooxygenase which regulates many fly functions such as olfactory learning and memory, aggression and locomotor activity, among others (Saraswati et al., 2004; Schwaerzel et al., 2003; Zhou et al., 2008). Confocal images using the driver *tβh-Gal4* and fluorescent reporters (Figure 56) reveal that, in the 2<sup>nd</sup>-IL stage, the majority of *tβh*<sup>+</sup> cells resemble neurons due to their small nuclei and axons; however, there are some *tβh*<sup>+</sup> cells that, because of their shape and the size of their nuclei, may be glia belonging to the tip of the VNC and close to the OL (Figure 56A,B). A similar expression pattern as the previous stage is shown in late L3 CNS, although there may be some expression in epithelial cells in the imaginal discs (Figure 56C). In addition, this experiment shows the nuclei of CNS cells which expressed the enzyme at some point during development but not at the moment of staining (Figure 56).

OA can autoregulate its own release through OA receptors expressed in octopaminergic cells (Koon and Budnik, 2012; Koon et al., 2011; Robb et al., 1994). The question is whether the niche cells may express the enzyme and thus, function in a cell autonomous (autocrine) manner. However, down-regulation of the *tβh* enzyme in *c855a*<sup>+</sup> and *cg25c*<sup>+</sup> cells does not affect development. The vesicular monoamine transporter (*Vmat*), which is in charge of transport and release of DA, serotonin (5-HT), and OA (Chen et al., 2013; Greer et al., 2005), is used to identify monoaminergic cells (Croset et al., 2017) and it has also been described in *Drosophila* blood-brain-barrier (BBB) glia in adult brains (DeSalvo et al., 2011, 2014). Unfortunately, when *Vmat* expression was down-regulated either in *cg25c*<sup>+</sup> glia or *c855a*<sup>+</sup> NECs, there was no abnormal developmental phenotype observed. Therefore, *tβh* and *Vmat* experiments suggest that none of the niche cells function in a cell autonomous manner for OA receptor signalling.

As mentioned before, OA is a member of the trace amines family, and the receptors of this family maintain such a close connection that OA receptors respond to different trace amines and other neuromodulators (Qi et al., 2017; Robb et al., 1994). Likewise, the synthesis of different aminergic molecules is interconnected and thus one molecule may influence the molecular pathway of others (Roeder, 2005; Vömel and Wegener, 2008). Considering this, I was wondering whether synthesis of other neuromodulators in the studied niche cells may interfere with OA synthesis in a non-cell autonomous (paracrine) manner. Tyrosine is the source for dopamine and OA synthesis in the biosynthetic pathway of tyramines. Thus, down-regulating the key enzyme to produce dopamine, *DOPA decarboxylase* (*DDC*; Livingstone and Tempel, 1983), may interfere with OA production in a compensatory manner (Roeder, 2005; Vömel and Wegener, 2008). Unfortunately, as with the *tβh* enzyme, down-regulation of *DDC* in the niche cells (*c855a*<sup>+</sup> and *cg25c*<sup>+</sup>) does not lead to abnormal phenotypes in fruit fly growth. All in all, the experiments completed indicate that neuroepithelial and glial cells do not play a role in regulation of OA synthesis. However, more knowledge is needed on this topic.

The next step was examining the OA receptor signalling pathway within the niche cells. Studies show that OA receptors stimulate intracellular accumulation of cAMP and Ca<sup>2+</sup> (Balfanz et al., 2005; Han et al., 1998). Research along these lines have brought more knowledge of their intracellular signalling describing the role that the enzyme *calcium/calmodulin-dependent protein kinase II* (*CaMKII*) has in the secretion of downstream effectors in epithelial cells from the oviduct (Lee et al., 2009; Lim et al., 2014). The calcium-binding messenger protein *Calmodulin* (*Cam*) interacts with *CaMKII* and is an active part of the calcium signal transduction pathway (GuptaRoy et al., 1996; Xu et al., 1996). Also in epithelial follicle cells, octopaminergic signalling regulates enzymatic *matrix metalloproteinase 2* (*Mmp2*) activity via intracellular Ca<sup>2+</sup> (Deady and Sun, 2015).

Therefore, the intracellular signalling analysis and the implication of *Mmp2*, *CaMKII*, and *Cam* proteins in OA receptors was performed using the Gal4/UAS system. Firstly, down-regulation of the gene *Mmp2* in both niche cells did not have any consequence in *Drosophila* development. However, up-regulation of that gene in both cell types causes lethality in the L1 stage (data not shown). Secondly, neither underexpression nor overexpression of *CaMKII* in *cg25c*<sup>+</sup> niche cells has been shown to affect growth. Nevertheless, in *c855a*<sup>+</sup> cells not *CaMKII* underexpression but overexpression arrest half of larvae at the early L3 larval stage (data not shown). Finally, the

underexpression of the protein *Cam* in *cg25c<sup>+</sup>* cells results in normal fruit fly growth. However, when *Cam* is underexpressed in *c855a<sup>+</sup>* cells, larvae arrest in the L3 stage for several days (Figures 57 and S20); this stage of arrest is confirmed by their jaw characteristics (Figure 57B). This larval phenotype resembles late L3 control larvae in length and width (Figures 57A and S20), and exhibits a larval volume typical of this stage despite being arrested for up to ~118 h AEL (Figures 57C,C'). All in all, these exciting discoveries about OA receptors and their signalling pathways in a neuroepithelial-glia context have proved to be a highly interesting challenge that will be discussed next.

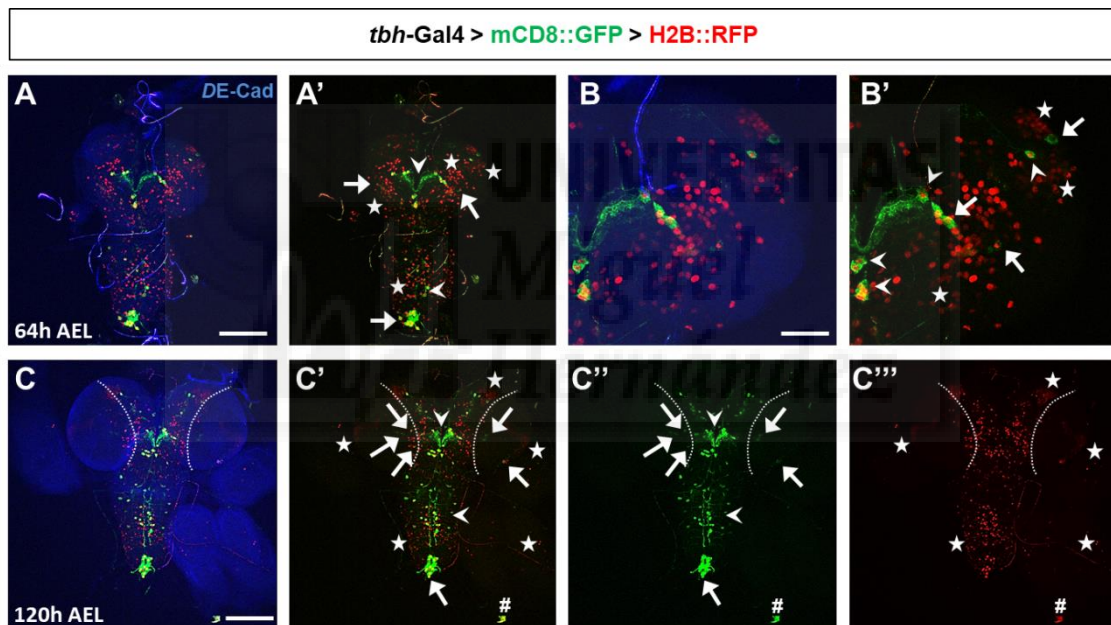


**Figure 56. Characterisation of the *tβh<sup>+</sup>* cells which synthesise octopamine in larval stages.** The driver for *tβh*, a key enzyme in octopamine synthesis, drives expression of membranous (UAS-mCD8::GFP) and nuclear (UAS-H2B::RFP) fluorescent proteins to reveal the expression pattern of *tβh*. (**A,A'-B,B'**) In L2 stage brains, the enzyme is expressed throughout the central nervous system in cells of which the majority remain neurons (arrowheads), but also in some glial cells, some of them close to the optic lobe (arrows). (**C-C'''**) In L3 stage brains, the expression is very similar to that of the previous stage and, in addition, expression is detected in epithelial cells of the imaginal discs (hash). The nuclear perdurance phenomenon reveals that the receptor expression throughout development takes place within different cells (asterisks). Epithelial cells were stained with anti-DE-Cad antibody (blue). Scale bars represent 75 μm in (**A**), 35 μm in (**B**), and 150 μm in (**C**).

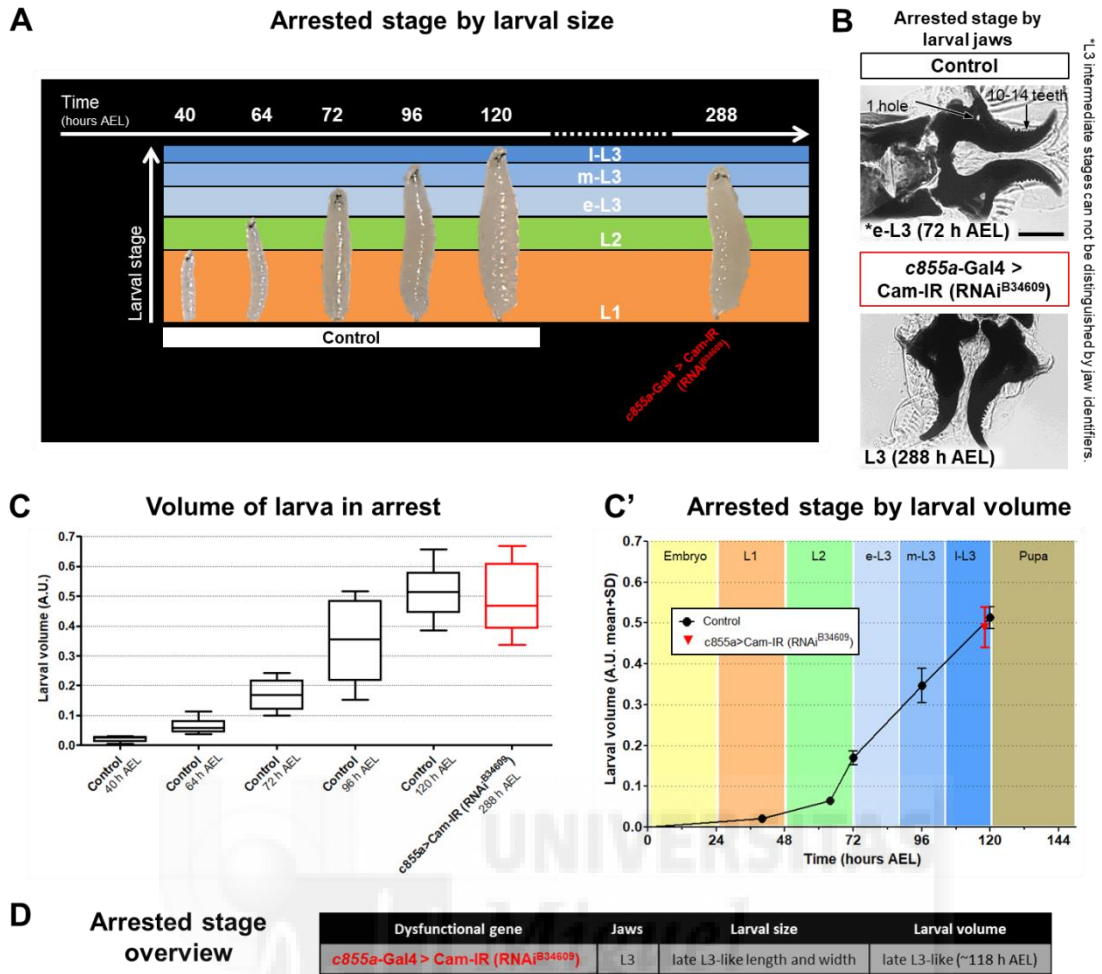


**Figure 57. Characterisation of the OA receptor signalling pathway in larvae. (A-D)** In *c855a*<sup>+</sup> cells, down-regulation of the gene *calmodulin* (*Cam*; data in red), a downstream signal of octopamine receptors, causes arrest during larval development. **(A)** Underexpression of *Cam* in *c855a*<sup>+</sup> cells causes retention of larval size at late L3-like stage for ~288 h AEL. **(B)** The jaw identifiers of the arrested phenotype reveal that larvae are arrested in the L3 stage. **(C-C')** Measurements in length and width reveal a volume similar to that of late L3 control larvae. **(D)** Table summarising the characterisation of the phenotype in arrest. Scale bar represent 100  $\mu$ m in **(B)**.



**DISCUSSION**





# 1. Characterization of the neuroepithelial-glia niche and its separation by FACS technique

A correct neurogenesis at early ages of the development of an organism is fundamental for a proper growth of both the vital organs and the whole organism (Droujinine and Perrimon, 2016; Garelli et al., 2012; Jaszczak and Halme, 2016; Juarez-Carreño et al., 2018; Rewitz et al., 2013; Vallejo et al., 2015). That is why the regulation pathways of neurogenesis are conserved from insects to mammals (Delaunay et al., 2017; Jacob et al., 2008; Rossi et al., 2017; Wang et al., 2013). In recent years several research groups have shown the importance of glial cells in forming a microenvironment capable of controlling both neurogenesis and neuronal functions (Huang et al., 1998; Liu et al., 2017; Otsuki and Brand, 2017; Ou et al., 2014; Ramon-Cañellas et al., 2019; Siegenthaler and Pleasure, 2011). This regulation is done through extrinsic cues that are received by neuronal progenitor cells and that modify their intrinsic cues (Morante et al., 2013; Morrison and Spradling, 2008; Otsuki and Brand, 2018). Different works have shown that the interaction of glia with the different types of neural stem cell (NSCs) can be through insulin/IGF-like peptides, TGF- $\beta$  proteins, and other molecules, (Chell and Brand, 2010; Fernandes et al., 2017; Kanai et al., 2018; Rossi and Fernandes, 2018) and bidirectional (Spéder and Brand, 2018). In addition, deficiencies in glial cells, for example down-regulation of *wdr62*, can alter the production of NSCs and contribute to brain diseases such as microcephaly (Lim et al., 2017). Studies in our laboratory and others, have shown that this glial niche also exists with the neuroepithelial cells (NECs) that give rise to the neuroblasts (NBs; Morante et al., 2013; Perez-Gomez et al., 2013). Deregulations in the *miR-8*<sup>+</sup> surface-associated cortex glia (CG) of the release of the ligand *spi*, a TGF $\alpha$ -like protein that binds to the EGFR of the NECs, cause modifications in the neuroepithelia that affects the neurogenesis and the larval brain growth (Morante et al., 2013). Although there are several evidences of NEC-glia communication, this relationship has not been studied exhaustively. For this reason, this doctoral thesis aims to identify key genes of development in both cell types and thus, expand knowledge about this neuroepithelial-glia niche.

First of all, it was necessary to well define the two populations of the niche: the NECs and the glial cells of the larval brain, when the second stage of neurogenesis occurs (Apitz and Salecker, 2014; Egger et al., 2007; Li et al., 2013; Morante et al., 2013; Ramon-Cañellas et al., 2019). The brain niche that I am interested is specifically located in the outer proliferation centre (OPC) of the optic lobe (OL). Additionally, in this thesis it was necessary to observe two different moments of the larval development, when occurs the switch from a proliferative neuroepithelium to a neurogenic stage (Delaunay et al., 2017; Homem et al., 2015; Jacob et al., 2008; Rossi et al., 2017; Wang et al., 2013). These two periods of development occurs from the late 2<sup>nd</sup> instar to the 3<sup>rd</sup> instar, and thus, both times were analysed in order to compare the genetic expression in each larval time. The *Drosophila*'s Gal4/UAS system in, combined with fluorescent proteins, is an essential technique used to characterize both populations.

*c855a*-Gal4 is the driver commonly used to mark exclusively the NECs of the larval brain (Egger et al., 2007; Gold and Brand, 2014; Morante et al., 2013) although it is also expressed in epithelial cells of the imaginal discs (Hrdlicka et al., 2002). As I observed by immunohistochemistry, the expression of the *c855a*-Gal4 driver in NECs is constant in the 3<sup>rd</sup> instar. However, the expression in the 2<sup>nd</sup> instar is intermittent or varies depending on at which point each NEC is in the cell cycle. At this moment, it would be useful to apply the G-TRACE technique (Evans et al., 2009) to identify the transient expression pattern of *c855a*-Gal4 in each larval stage.

As mentioned, the glial cells that are part of the larval niche studied are *miR-8*<sup>+</sup> (Morante et al., 2013). We also knew that the *mir-8*-Gal4 driver marks fat body (FB) cells as well (Hyun et al., 2009). Then, we observed that the driver *cg25c*-Gal4, which encodes the type IV collagen in *Drosophila* FB that is the main component of the tissue basement membrane including the central nervous system (CNS; Brodie et al., 2011; Isabella and Horne-Badovinac, 2016; Monson et al., 1982; Natzle et al., 1982; Le Parco et al., 1986; Pastor-Pareja and Xu, 2011), is also expressed in larval CNS cells which seemed to be the *miR-8*<sup>+</sup> glial cells. Although originally it was stated that there was no expression of the gene *cg25c* in the larval CNS (Mirre et al., 1992; Le Parco et al., 1986), this expression was later observed (Rodriguez et al., 1996) and, as I showed, occurs in the ventral nerve cord (VNC) and OL regions. The identification of *cg25c*<sup>+</sup> cells close to the extracellular matrix of the CNS suggests a possible contribution of these cells in the formation of the tissue basement membrane in an auto-, para- or endocrine manner, like the FB cells do (Isabella and Horne-Badovinac, 2016). However, this contribution is not highly important since a down-regulation of the gene *cg25c* (or other genes that encode extracellular matrix proteins such as *vkg*; Rodriguez et al., 1996; Yasothornsrikul et al., 1997) in the *cg25c*<sup>+</sup> cells does not affect the development of the organism; if those proteins are negatively regulated in FB cells, then do produce developmental abnormalities (Pastor-Pareja and Xu, 2011). On the other hand, I showed that the premature death of *cg25c*<sup>+</sup> cells also causes premature death of the larva in the 1<sup>st</sup> instar and, therefore, those cells are important for larval development. So, an

exhaustive characterization of the driver *cg25c*-Gal4 showed that *cg25c*<sup>+</sup> cells of the CNS are glia and, furthermore, confirmed also that those in the brain belong to a subset of the *miR-8*<sup>+</sup> surface-associated CG that are specific to the OL. Despite this, it is interesting to observe that a different behaviour in their signalling pathways as for example happens with the gene *spi*, a TGF- $\alpha$  ligand that acts on EGFR of the NECs (Morante et al., 2013). Down-regulation of *spi* in *miR-8*<sup>+</sup> cells disable the proliferation of NECs and NBs and cause a smaller size of the larval brain (Morante et al., 2013); by contrast, I observed that when the down-regulation of *spi* occurs in the *cg25c*<sup>+</sup> subset, it triggers just the opposite phenotype and leads the development of a huge larval brain. Although, the functional *miR-8*<sup>+</sup> cells from the central brain (CB) may suggest a role in that region in the dysfunctional *cg25c*<sup>+</sup> phenotype, is not clear the cause of the massive OL neuropil and neuroepithelium without increasing the number of NBs. These phenotypes between *miR-8*<sup>+</sup> and *cg25c*<sup>+</sup> cells are interestingly opposed and a more precise characterization is needed to reveal the cause of this behaviour. Also, these experiments confirm the relevant role that *cg25c*<sup>+</sup> cells have in the development of the larval brain.

To isolate the cells from the neuroepithelial-glia niche, I used the FACS technique (Harzer et al., 2013) which uses the fluorescence emitted by fluorescent proteins expressed in the cells. In differentiated cells, such as the *cg25c*<sup>+</sup> glial cells, the result of separating using nuclear or membranal fluorescent protein is equivalent and suitable in both cases. However, in progenitor cells such as *c855a*<sup>+</sup> NECs I observed that these types of fluorescent proteins evoke to the phenomenon of *Lineage Perdurance*, which will mark their lineage (NBs, neurons and glia) even when there is no mRNA expression. Despite this, I found a way to solve it using an unstable fluorescent protein (destabilised-GFP; Lieber et al., 2011) under the control of the neuroepithelial driver. This short-lived protein presents a more precise expression signal of the gene driver, unlike the traditional ones, and this mark only the NECs and solving the phenomenon of the *Lineage Perdurance*. I combined the unstable GFP (UAS-destabilised-GFP) with a stable nuclear marker of different fluorescence (UAS-H2B::RFP) to avoid false positives due to the methodology. This combination of fluorescence was used equally in the two stocks with the drivers of each population. The use of a dual fluorescent labelling, as indicated also in other techniques (Antonello et al., 2015; Toledano et al., 2012), gives robustness and precision to the FACS technique to identify and isolate cells from the neuroepithelial-glia niche. The separation by FACS, apart from used in L3 brains, was also used in brains of the L2 stage in which I observed a lower rate of cellular survival suggesting a greater sensitivity of these cells to the technique due to the larval age.

## **2. Niche transcriptome sequencing and bioinformatics analysis of gene expression**

The pursuit of new relevant genes in the interaction between the cells of the studied niche can be done through a transcriptomic analysis. This approach requires first, a transcriptome sequencing (RNA-seq) and later, a bioinformatic study; I did both tasks during a stay in the laboratory of Dr. Vladimir Benes (EMBL-Heidelberg, Germany). To obtain valuable information of the genetic expression it is required to use samples with high standards of purity and integrity which give robustness to the data. These features were confirmed in the populations separated by FACS using primary cultures, in the mRNA samples extracted from these populations by the Bioanalyser, in the cDNA libraries sequenced also by Bioanalyser, and finally, in the bioinformatic data through the sequencing values obtained (barcoding distribution, Phred scores, nucleotide distribution, guanine-cytosine content, duplicate reads, adapter content, overrepresented sequencing, etc.; Daines et al., 2011; Ewels et al., 2016; Ewing and Green, 1998; Keightley et al., 2009). Although all these features have been well discussed along with their representation graphics, it is important to highlight the Phred quality score because is the most important RNA-seq statistic to be considered. Phred score, which defines a base-calling error probability (Ewing and Green, 1998), reveals an adequate performance in features such as each nucleotide from sequences and each sequence read; although it also shows a small subset of reads with poor quality which represents a very small percentages of the total sequences, and which could be the result of poor image quality at the edges of the sequences field. Despite the fact that my initial samples contained a low input amount of mRNA, using high-yield kits in quantities much lower than those previously used by the host laboratory, I managed to maintain the maximum information of the original RNA fragments such as the directionality for each transcript (Levin et al., 2010; Parkhomchuk et al., 2009) which allows to accurately quantify the expression levels of coding overlapping transcripts (Zhao et al., 2015) and enhances the value of the sequencing.

The first important step of the bioinformatic analysis are indexing and mapping reads from the sequenced raw data to the *Drosophila melanogaster* genome of reference (Dobin et al., 2013; Love et al., 2015). This process was successful, obtaining in most of the sequenced samples more than 85% of mapping, with the exception of a sample that was ~ 71%; all those sequences were fully mapped on the length. In addition to that, the visualization of the aligned fragments (Robinson et al., 2011; Thorvaldsdóttir et al., 2012) shows: on the one hand, in NEC samples from both stages, late-L2 IL (hereafter referred to as L2) and late-L3 IL (hereafter referred to as L3), genes typically expressed in these cells such as *DE-Cad* and *patj*, as well no presence of typical genes from NBs (*mira*), neurons (*elav*) or glia (*repo* and *cg25c*); on the other hand, triplicates from *cg25c*<sup>+</sup> present fragments in glial genes but not for other cell type genes. So, the set of these results support the strength of the sequencing run.

Once I extracted the exact number of aligned reads for each gene (Anders et al., 2015) I obtained the differential gene expression between groups of samples (Love et al., 2014). Then, I did the exploration and the transformation of the data for normalising the counts with the sequencing depth, which means to stabilise the variance of the genes and their expression through the mean. This transformation may be done with the *log2* normalised count values, but instead I used the *rlog* since it transforms the values minimizing the variation with low count genes which contribute with irrelevant information about differential expression. The representation of these standardised data allowed me to know more in detail each group and their sample-to-sample distance. Firstly, scatterplot of transformed counts shows that, in case a gene varied a lot in expression between two biological replicates, the third replicate corrected it. Secondly, in the principal components analysis (PCA) visualisation, the PC1 explains the 72% of the variance which may refer to cell type, while the PC2 explains the 15% of the variance which may refer to stage. Lastly, a heat map of *rlog*-transformed data improved by the Poisson distance, which considers the inherent variance structure of counts (Witten, 2011), also showed how each group replicates were similar to each other, while the groups save differences between them .

The analysis of the gene differential expression between conditions I undertook through two approaches, cell type approach and stage approach, depending on what conditions the comparison of expression was made. In the first approach, the cell type approach, I compared the expression of the genes between NECs and glia from the same stage, taking as reference the neuroepithelium since it is a precursor cell. The analysis of gene expression (Log2FC+SE) and its subsequent refinement (p-adj; Dudoit et al., 2002) allowed me to observe statistically significant and specific markers for both cell type and stages, although that is not the main objective of my thesis. The relevance of this approach was to determine the expression of classical genes from the two cell types in each condition: *DE-Cad*, *patj* and *dlg1* in NECs samples, and *repo* and *cg25c* in glial samples; thus, the expression levels measured for the genes in each sample was again shown the accuracy of the RNA-seq and bioinformatic analysis.

In the second approach, the stage approach, I compared the differential gene expression of the different larval stages (L2 versus L3) in each cell type, taking as reference the L2 stage as a level of previous expression. As in the previous approach, I performed an analysis and refinement of the data that led to determine a total of 5.301 unique genes differently expressed. Using a Venn diagram, gene expression graphs and heat maps, I discerned among those genes which ones were up- and down-regulated in L3 in each cell type both specifically and shared. At this point, I performed three *in silico* screenings from the different gene clusters generated; the workflows I used were based on their gene ontology (GO; MGSA, Bauer et al., 2010) from biological process (BP), cellular component (CC) and molecular function (MF), as well as their molecular partners, in order to find those genes that encode both membrane and secreted proteins that may be functional relevant in signalling pathways. It is possible to perform other types of screenings and workflows, apart from those I used in this thesis, which together would provide new information on the RNA-seq data. In the end, combining the three *in silico* screenings which I performed, I narrowed the differentially expressed genes from thousands to specifically 151 top hit genes which were up- and down-regulated in NECs, glia, and both.

### **3. Validation of top-hit genes**

The 151 differentially expressed genes in the top hit list needed to be validated *in vivo* to verify whether they have a relevant function in the niche cells. Therefore, I carried out a massive genetic validation, which is a very common resource in *Drosophila*, in order to detect problems in development due to gain-of-function (GOF) and lack-of-function (LOF; Villegas et al., 2018;

Yamamoto et al., 2014). Using the drivers *c855a*-Gal4 and *cg25c*-Gal4 together with over- and under-expression fly lines (UAS and RNAi) I was able to observe through more than ~650 crosses that 51 of 151 top-hit genes (34%) show some type of development deficiencies such as temporary stage mismatch, problems with organ development, cell cycle death or premature lethality. It is important to emphasize that the gene *spi*, previously discussed about its abnormal brain phenotype when it is down-regulated in *cg25c*<sup>+</sup> cells, is among the 23 larval genes with glial phenotype. This case consolidates the RNA-seq analysis and the bioinformatics workflow of the screening performed. Note that due to time constraints and complexity of the interrelations between genes, all genes presented in this thesis are not deeply studied. Therefore, I will contextualize those genes that have shown phenotypes mentioning their possible roles but they undoubtedly need to be adequately examined.

As expected, some validated genes that exhibit abnormal phenotypes in the development had previously been related by other research work with the cell types tested, although I observed some particularities in my validation. For example, I detected an overexpression of the gene *crb* in *c855a*<sup>+</sup> cells that causes lethality in L1. The expression of this gene is required for the development of epithelial tissues and, as previous studies shown, mutants for this gene die during the 1<sup>st</sup> larval stage (Chen et al., 2010; Tepas and Knust, 1990). Therefore, it would be interesting to know which tissue, the brain or imaginal discs, is the one that produces that fatal phenotype. Another example is the developing phenotype caused by down-regulation of the gene *Tig* in the *cg25c*<sup>+</sup> cells which generate significantly longer larvae and pupae (and also pupa lethality for some RNAi lines) as well as adult flies with elongated abdomens. This bigger body size has already been observed in mutants of *Tig* (Bunch et al., 1998). The fact that *Tig* has been described as having a role in the extracellular matrix, together with Collagen IV, and being expressed in FB cells of the embryo (Fogerty et al., 1994), suggests that this abnormal size is due to the FB *cg25c*<sup>+</sup> cells; however, it would be also interesting to know the function, if there is any, of the glial part of the *cg25c*-Gal4 driver.

In the validation, I observed that the deregulation of a large number of molecules related to Wg/Wnt signalling pathway in the niche cells cause abnormalities in the development of *Drosophila*. The gene *wg* is related to cell-cell interactions from vertebrates to invertebrates (Couso et al., 1994; Yin et al., 2018) and also required in the development and patterning of the nervous system (Kerr et al., 2014; Patel et al., 1989). I observed that *wg* overexpression in the *c855a*<sup>+</sup> cells cause pupal lethality, and that may be as a result of late L3 deregulation of the NECs which develops massive brains. However, it must be considered that the *c855a*-Gal4 driver is also expressed in imaginal discs where *wg* activity has been described (Couso et al., 1994; Struhl and Basler, 1993). *Wg* overexpression produces larval delay when it occurs in *cg25c*<sup>+</sup> cells; and this is aligned with other studies where they have described *wg* activity regulated and secreted by glial cells (Kerr et al., 2014). Down-regulation of *wls* in *c855a*<sup>+</sup> cells causes half of the pupae to die. *Wls* is required for Wnt signalling (Bartscherer et al., 2006) and it has also been described that *wls* regulates *wg* but, as I mentioned above, *wg* is secreted by glial cells in the context of neuromuscular junction (Kerr et al., 2014). *Wnt2* is a member of the conserved Wnt family (Sidow, 1992). When *wnt2* is down-regulated in *cg25c*<sup>+</sup> cells causes larval delay whose brain is larger and the overproliferative NECs are additionally observed ectopically. It has been described that *Wnt2* interacts with *wls* (Herr and Basler, 2012); however, the lack of literature on *Wnt2* expression in the glia and the FB makes this phenotype attractive to study in detail. Down-regulation in *c855a*<sup>+</sup> cells of *otk2*, a receptor of the Wg/Wnt signalling pathway, causes an increase in the larval brain size that may be the cause of pupal lethality. *Otk2* is co-expressed with *otk* during larval development in imaginal discs as well as in the brain, and especially in the OL (Linnemannstöns et al., 2014). Because *otk2* is poorly studied in *Drosophila* and the evidence of its expression in *c855a*<sup>+</sup> tissues, it is very interesting to find the explanation for my experimental observed phenotype. Note that *otk2* interacts with *Wnt2* (Linnemannstöns et al., 2014) and in my tests they are expressed in *c855a*<sup>+</sup> and *cg25c*<sup>+</sup> cells respectively; since the down-regulation in both cell types causes an enlarging brain phenotype, this may indicate interaction in the studied niche. In addition, as Wg/Wnt signalling pathway has been related to the development of several illness such as Huntington disease (Dupont et al., 2012) and cancer (Yin et al., 2018), it is of great interest to understand the role of the studied niche cells.

Another signalling pathway well represented is EGFR pathway (Freeman, 2002; Malartre, 2016). The lack of this transmembrane tyrosine kinase receptor function (Buchon et al., 2010) causes the appearance of crystal cells in both larval and adult stages, as well as lethality in half of the pupae. The *egfr* is necessary for the survival of glial cells in both embryos and adults (Hidalgo et al., 2001; Lee and Sun, 2015), and has been shown to respond to an injury in the larval VNC (Kato et al., 2011). One of the EGFR agonists is *spi* which down-regulated in *cg25c*<sup>+</sup> cells produces crystal cells and lethality in larvae. In these larvae I observed a brain overgrowth phenotype that is opposite to that when expressed by *miR-8*<sup>+</sup> cells (Morante et al., 2013). This may be due to a compensatory effect of the *spi* signal either by agonist/antagonist signalling or by the CG part of the CB, that when the expression is absent in those cells the compensatory phenomenon may not occur. It would be

very interesting to come to discern this phenotype. A *spi* antagonist that competes directly to regulate EGFR signalling is *aos* (Jin et al., 2000; Klein et al., 2004; Morante et al., 2013). Down-regulation in *c855a*<sup>+</sup> cells of this gene results in a phenotype of NEC overproliferation which causes enlarged brains and the death in pupa. Unregulated growth may be understood because NECs cannot regulate EGFR in an autocrine manner through *aos*. Due to the *c855a*-Gal4 driver, the imaginal discs expression must also be considered (Pallavi and Shashidhara, 2003) as well as the possible role that these cells may have in both the phenotype and the niche. Note that previously the *miR-8*<sup>+</sup> glial cells of the niche were observed to control the release of *aos* (Morante et al., 2013); unfortunately, it is necessary to test that gene in the *cg25c*<sup>+</sup> cells, and thus to know whether these cells also release *aos*, as would be expected. The receptor *Fas2* is also known to bind EGFR and inhibit the pathway signalling (Malartre, 2016; Mao and Freeman, 2009). In my experiments, I observed that when *Fas2* is down-regulated in *c855a*<sup>+</sup> cells causes not only an enlarged brain but also overproliferation of those cells in imaginal discs that enlarge this tissue; these organisms die in pupa. The phenotypes in both tissues are accordingly a continued signal stimulation of growth pathways in epithelial cells, where it has previously been described to express *Fas2* (Gomez et al., 2012). Finally another interesting gene is *ebi*, which modulates intracellularly EGFR pathway in development (Dong et al., 1999). Underexpression of this gene in *c855a*<sup>+</sup> cells causes lethality in pupa in females only, since males do emerge as adult flies. This suggests that *ebi* is expressed in NECs, like *Egfr* (Morante et al., 2013); however, as this molecule regulates many other pathways, a deeper study is required to properly explain the phenotype observed.

The participation of *ed* in various signalling pathways, including EGFR (Spencer and Cagan, 2003), Hippo and Notch pathways (Rawlins, 2003; Spencer and Cagan, 2003; Yue et al., 2012), also makes their study very interesting. When *ed* is underexpressed in both niche cells causes larval delay in equal number of days, which also ends in pupa lethality when the dysfunction occurs in *c855a*<sup>+</sup> cells, and finally in both cases results in larger brains. However, apparently its action on glia is different: it increases the number of glial cells when *ed* is down-regulated in *c855a*<sup>+</sup> cells, but however decreases them when the disorder is in *cg25c*<sup>+</sup> cells. *Ed* has been associated as an adhesion molecule in epithelial cells (Laplante, 2006) and, recently, also as extrinsic cue secreted by larval brain CG that acts on progenitor cells (Ding et al., 2016; Syed et al., 2017b). Especially this last study shows that lack of glial *ed* stimulates NBs growth and proliferation which is actually the brain phenotype I observed; also the glial niche established with progenitors where both express *ed* may also occur in the niche studied in this thesis.

Studies reveal that the gene *Bark* is related to the maturation of septate junctions in developing epithelial cells (Hildebrandt et al., 2015). This is consistent with what I observed: down-regulation of *Bark* in *c855a*<sup>+</sup> cells induces overproliferation of NECs that deconstruct OL proliferative centres in late L3, although maintains a normal brain size; this may cause the lethality in pupa. I also observed that some RNAi lines of *Bark*, did not affect the development in pupa but, however, the adult fly is unable to unfold its wings. This other phenotype may be related to the *c855a*<sup>+</sup> epithelial cells from the imaginal wing disc and their development. Another gene which is critical for septate junctions formation in epithelia is *Nrx-IV* (Bhat et al., 1999). I observed that its down-regulation in *c855a*<sup>+</sup> cells affects brain size and produces holes or bubbles, and therefore both abnormalities may be important in pupal lethality. A down-regulation in *cg25c*<sup>+</sup> cells also affects the brain size which, in addition, delays the larva-pupa transition. This is in agreement with other studies that linked *Nrx-IV* with glial cells, either through neurons or blood-brain-barrier (BBB) function (Banerjee et al., 2017; Baumgartner et al., 1996; Slovakova and Carmena, 2011). Therefore, *Nrx-IV* is expressed in the glial cells and when it loses its function, it causes a similar enlarged brain phenotype.

The gene *ptc* down-regulated in *c855a*<sup>+</sup> cells causes large proliferative centres and brains which may be the cause of pupal lethality. However, the function that *ptc* of *c855a*<sup>+</sup> cells from discs may play must be considered since it is described that *ptc* acts on the wing imaginal discs through the Hedgehog signalling pathway (Chen and Struhl, 1996). Half of the larvae with *nAChRa3* down-regulated in *c855a*<sup>+</sup> cells arrest in late L3 and the other half die in the larva-pupa transition. The brains of those arrested larvae present massive CB, unstructured neuroepithelial overproliferative centres that increase the number of glial cells, and also holes in the brain surface. The *nAChRa3* gene encodes a subunit of the nicotinic receptor for the excitatory neurotransmitter acetylcholine of neurons from the insect CNS (Gaudet et al., 2011; Schulz et al., 1998). However, other nicotinic subunits, such as  $\alpha 7$  which was originally thought to be only in neurons, have been shown to be also expressed in epithelial cells (Li and Wang, 2006; Wang et al., 2001). Therefore, the results observed open the possibility that NECs are also those that have nicotinic receptors functional and important for the CNS growth.

The validation led me to find genes with anomalous developmental phenotypes which were not previously related to the niche cells. For example, I visualized lethality in L1 due to overexpression of the *Ret* oncogene in *cg25c*<sup>+</sup> cells. The expression of this gene have reported in precursors cells, that

is to say, epithelial cells and NBs of the embryonic CNS (Sugaya et al., 1994); however, there is no evidence of the function that it may have in glial cells. In the adulthood, down-regulation of the gene *SIFaR* in *cg25c*<sup>+</sup> cells causes abnormal curly and coarsened wings. Since this gene has been described as a neuropeptide receptor (Hewes and Taghert, 2001; Jørgensen et al., 2006), it would be interesting to know the reason of the phenotype observed and its relation with *SIFaR* in glial pathways. Also in adult flies, an unusual swollen abdomen was developed when *baz* was underexpressed in *cg25c*<sup>+</sup> cells. Although this gene is related to NBs (Wodarz et al., 1999), epithelial cells (Morais-de-Sá et al., 2010), and specifically NECs of OL proliferation centres (Perez-Gomez et al., 2013), there are no indications of the possible glial role and, for that reason, it would be interesting to study it in this cell type.

*Pburs* dimerises with *Burs* to form a neurohormone which acts in the *Lgr2* receptor to unfold the wings in the adult fly (Luo et al., 2005; Mendive et al., 2005); it is the lack of *Burs* which is described to cause the phenotype (Dewey et al., 2004). However, I observed that down-regulation of *Pburs* in *c855a*<sup>+</sup> also cause abnormal wings development. Therefore, this evidence suggests that on this occasion the dimerization is truncated due to the lack of *Pburs*, probably in cells of the imaginal wing discs. Studies have shown that both *Pburs* and *Burs* are also expressed in the L3 CNS (Dewey et al., 2004; Honegger et al., 2002; Luo et al., 2005). Note that down-regulation of *Burs* in *c855a*<sup>+</sup> cells increases the brain size and, in this case, that NECs deregulation may be the cause of the pupal death. All in all, since the heterodimer *Burs/Pburs* is a neurohormone, it would be expected that their expression in *c855a*<sup>+</sup> cells would have effects in other parts of the organism and, thus, it is interesting to examine deeper that niche role.

Down-regulation of *trio* in the *cg25c*<sup>+</sup> cells cause delay and, in the brain, provokes the disruption of glial nuclei. This gene encodes GEF which acts in BMP and Abl tyrosin kinase pathways, and is associated with neuronal growth phenotypes in the embryonic CNS (Ball et al., 2010; Liebl et al., 2000). Thus, more experiments are needed to carry out a *trio* role hypothesis in *cg25c*<sup>+</sup> cells. Down-regulation of the gene *unc-5* in *c855a*<sup>+</sup> cells results in bigger brains which present some holes or bubbles in the tissue surface. These abnormal brains may cause the delay in half of the larvae. *Unc-5* gene encodes a repulsive netrin receptor which is described in glial cells to direct the motor axon guidance (Freeman et al., 2003; Long et al., 2016); however, there are no evidences that *Unc-5* have a role in NECs of the CNS nor in the imaginal discs. Overexpression of the gene *santa-maria* in *cg25c*<sup>+</sup> cells causes late L3 larval delay and enlarged brains. In the glia of fly heads, this receptor introduces into the cell the carotenoids which induce the formation of vitamin A (Wang et al., 2007). The little research on this receptor and once shown to be in glial cells, are sufficient arguments to study its importance in the larval brain niche.

I observed that the same gene can give similar anomalies in the same organs even when it is expressed in different cells; but at the same time with different nuances in the development of the organism. This is the case of *Nrx-IV*, discussed above, where its down-regulation in both NECs and glia produces an increase in brain size, that is to say, they cause a similar organ growth phenotype; however, their phenotypes in the development of the organism are different.

The *mtt* gene also causes different phenotypes depending on which niche cell is down-regulated. Dysfunctions in *c855a*<sup>+</sup> cells it causes overproliferation of the NECs that increase brain size and also cause holes or bubbles and scratches between cells bodies. This deregulation cause late L3 semi-arrest, larva-pupa transition death and pupal death. In addition, overproliferative NECs are also visible in imaginal discs where they cause an amorphous structure and increased tissue volume. Conversely, down-regulation of *mtt* in *cg25c*<sup>+</sup> cells emerge the presence of some crystal cells in the abdomen of adult flies; this shows an activation of the innate response of the immune system which is mediated by FB cells (Khadiolkar et al., 2017; Meister and Lagueux, 2003; Wang et al., 2014). Recent studies have suggested that Collagen IV protein has an important role in the modulation of immunity (Kiss et al., 2016). Therefore, this set of facts point out that it is the *cg25c*<sup>+</sup> of the FB responsible for this phenotype. However, the *mtt* gene, which encodes a G-protein coupled receptor, has been little studied and the information is confusing. For example, some studies have described *mtt* as a metabotropic glutamate receptor (Brody and Cravchik, 2000; Gaudet et al., 2011) and others, however, refute such function (Mitri et al., 2004). At this moment, the shallow study of the phenotypes observed along with the little information of the *mtt* gene does not allow me to postulate a possible role for that gene in the observed phenotype; therefore, it would be very interesting to deepen its function in both niche cell types.

The underexpression of the gene *mys*, which encode an integrin  $\beta$  subunit that dimerise and form a transmembrane receptor (Estrada et al., 2007), in both niche cell types cause lethality in pupa. In addition, dysfunctions in the *cg25c*<sup>+</sup> cells arrest half of the larvae in late L3 arrest which present crystal cells. As I discussed earlier, these crystal cells may be a consequence of the role that FB *cg25c*<sup>+</sup> plays in the immunological innate response (Khadiolkar et al., 2017; Meister and Lagueux,

2003; Rizki and Rizki, 1959; Wang et al., 2014); additionally, the gene *mys* is related to the migration of hemocytes (Comber et al., 2013; Huelsmann et al., 2006). The larval brains in both phenotypes are affected. On the one hand, LOF in *c855a*<sup>+</sup> cells causes holes or bubbles which evolve into scratches and, in addition, disruption of the glial nuclei. This consequence in the brain may be because *mys* is involved in cell-cell interaction and cell survival, as well as epithelial morphogenesis (Delon and Brown, 2009). On the other hand, LOF in *cg25c*<sup>+</sup> cells implies NECs overproliferation that causes a massive brain size and, consequently, an increase in glial cells. Several studies describe *mys* for being involved in the growth and its alteration causes severe morphological aberrations, also in the epithelium (Beumer et al., 1999; Delon and Brown, 2009). In addition, I observed this lack of *mys* in CNS *cg25c*<sup>+</sup> cells causes an elongation of the VNC probably caused by the glial subset located on there. There is a research work that also described this aberrant CNS phenotype caused by dysfunctional *mys* and determined to be due to glial cells (Meyer et al., 2014), as in my observations. Other studies show that the glial cells of the brain in *Drosophila* store lipid droplets which contain neutral lipids for neurons (Liu et al., 2015a, 2017), and this is related to the absence of lipid droplets that I observed in this phenotype. However the role of OL *cg25c*<sup>+</sup> glia in all those observations still remains to be determined. Furthermore, it is interesting the consequences that a lack of *mys* in *cg25c*<sup>+</sup> cells has in other tissues of the larvae, such as massive size of the ring gland (RG) but very small imaginal discs. This is another evidence of how an altered gene expression in one of the two cells of the niche has implications for their partner as well as in other larval tissues. Note that *mys* interact with *Ret* (Soba et al., 2015), another gene that is expressed in the cells of the niche and that gives the abnormal developmental phenotype explained above.

Down-regulation of the gene *ine*, which encode a neurotransmitter transporter (Soehnge et al., 1996), also causes different phenotypes depending on the niche cell in which the dysregulation occurs. On the one hand, underexpression in *c855a*<sup>+</sup> cells induces NEC overproliferation that results in aberrant structuring of the proliferative centres, although the overall brain size is not affected, and it causes lethality in pupa. Studies reveal that *ine* is expressed in the epithelial cell membrane and regulates water homeostasis (Luan et al., 2015). On the other hand, dysregulation of this gene in *cg25c*<sup>+</sup> cells results in incorrect wing development in the adult fly. This receptor is also described to act in peripheral glia that control motor neuron excitability in late larvae (Yager et al., 2001). The set of information about the *ine* gene suggests that it may have a role in the phenotypes found; however, a thorough analysis is necessary.

The serotonin receptor *5-HT2B* when down-regulated in *c855a*<sup>+</sup> cells causes lethality in pupa. In *Drosophila*, serotonin receptors are widely expressed in the CNS (Yuan et al., 2005, 2006) and also 5-HT2B has been defined in neurons of the adult CNS (Gnerer et al., 2015). However, the gene *5-HT2B* (Blenau et al., 2017; Clark et al., 2004) has only been shown to be expressed at the human lung epithelium (Königshoff et al., 2010; Mann and Oakley, 2013). Therefore, the role that *5-HT2B* may play in NECs and in the *Drosophila* development is still veil. Down-regulation of another peptide hormone receptor in *c855a*<sup>+</sup> cells produce semi-lethality in pupa. Studies have shown that the gene *InR*, required in the TOR pathway (Avet-Rochex et al., 2012), controls the embryonic CNS (Fernandez et al., 1995) and the growth of both the larval imaginal discs (Chen et al., 1996) and the adult CNS (Murillo-Maldonado et al., 2011). Thus, the phenotype that I observed may be due to the *InR* function of the *c855a*<sup>+</sup> in both the imaginal discs and the CNS; a more in-depth study is needed. The diuretic hormone receptor *Dh44-R1* (Hewes and Taghert, 2001; Johnson et al., 2004) down-regulated in *cg25c*<sup>+</sup> cells cause late L3 larval arrest which present also crystal cells and die. This neuropeptide receptor is expressed in adult CNS neurons controlling the circadian locomotor activity and starvation (Cannell et al., 2016; King et al., 2017; Yang et al., 2018); and also in the embryonic CNS midline cells which consist in neurons and glia (Fontana and Crews, 2012). Since *Dh44-R1* is a receptor still little studied, it would be very interesting to know how that receptor influences the *cg25c*<sup>+</sup> glial cells, the innate response and the development of *Drosophila*.

Interestingly, in the validation I detect a group of genes from the *dpr* family which are expressed on the cell surface mainly on neurons (Nakamura et al., 2002; Tan et al., 2016). Down-regulation of the genes *dpr5* in *cg25c*<sup>+</sup> and *dpr10* in *c855a*<sup>+</sup> causes an increase in both larval and pupal size. Studies defined that these molecules are expressed in both larval and pupal CNS, especially in the VNC but also in the OL (Carrillo et al., 2015; Howell and Hobert, 2016; Pipes et al., 2001; Tan et al., 2016). I observed a very interesting phenotype when there is a *dpr2* defect in the niche cells. In both cases, there is an L3 arrest phenotype that promotes premature wandering and causes prompt death of the larvae. When *dpr2* is down-regulated in *c855a*<sup>+</sup> cells it causes small and fat larvae with a mid L3 brain. However, when that gene is underexpressed in *cg25c*<sup>+</sup> cells, larvae have a similar volume to mid L3 but early L3-like brain. Therefore, the mismatch between tissue regeneration and larval development that ends in an arrest phenotype, is due to the lack of coordination between both processes, as other studies indicate (Garelli et al., 2012; Jaszczak and Halme, 2016; Juarez-Carreño et al., 2018; Rewitz et al., 2013; Vallejo et al., 2015). Although the set of phenotypes observed are very interesting, few studies refer to those genes and, therefore, a more exhaustive analysis is

required to well characterize their niche functions. Other genes that give an arrest phenotype are those that encode for the octopamine (OA) receptors *Oamb*, *Octβ1R*, and *Octβ3R*, and the characterization I carried out is explained in the following section.

Apart from defects in development, I also observed that certain dysfunctional genes in cells of the niche may cause abnormal adult phenotypes in climbing the tube walls. Thus, down-regulation of certain genes in *c855a<sup>+</sup>* cells (*stan*, *aos*, *mew*, and *fz*) and in *cg25c<sup>+</sup>* (*Ten-a*, and *Ptp69D*) may lead to neurodegenerative diseases that cause locomotor deficiencies; however, a deeper study is required.

In summary, *in vivo* validation shows that there is an interaction between the cells of the studied niche since a deregulation in any of those cell types has effects on the other partner that influence the development of both internal organs and the entire organism. Apart from describing functions of genes already known, I have also contextualized functions of other genes in cell types that had not previously been described. At the same time, I also highlight genes whose function was different depending on which cell type is expressed, as well as related genes, families of genes and several signalling pathways. In addition, the validation also discover genes that their abnormal function in NECs leads to pupal death, and that this may be due to a deregulation in larval brain progenitors that promotes phenotypes of CNS enlargement. Finally, I also observed in the niche cells the expression of receptors for neuropeptides, neuromodulators and neurohormones that play an important role for the normal development of the organism, especially the family that I will discuss on below.

#### **4. The octopamine receptors in the cells of the niche**

In the *in vivo* validation, I identify a few genes from the OA receptor family (Evans and Maqueira, 2005; Han et al., 1998; Maqueira et al., 2005; Qi et al., 2017; Robb et al., 1994), the insect neurohormone and neurotransmitter equivalent to the role of NA in mammals (Borowsky et al., 2001; Bunzow et al., 2001; Erspamer, 1948; Hauser et al., 2006; Ohhara et al., 2012; Zucchi et al., 2006), which provide new possible roles for the cells of the studied brain niche. Currently, the use of HTS technology has already illustrated the potential of neuropeptides, neuromodulators and neurotransmitters, together with their receptors, in other cell profiles (Croset et al., 2017; Davis et al., 2018; Shih et al., 2018) as well as in certain types of glia (Davis et al., 2018; Ma et al., 2016). The OA receptors that I observed to present interesting development abnormality are *Oamb*, *Octβ1R* and *Octβ3R*. Deregulations in the expression of these three receptors, both in NECs and glia of the studied niche, produce arrest phenotypes in the L2-to-L3 larval transition and stop of the CNS growth. Other research studies have shown that an abnormal development of the organism is closely related to a lack of coordination with its organs (Garelli et al., 2012; Jaszczak and Halme, 2016; Juarez-Carreño et al., 2018; Rewitz et al., 2013; Vallejo et al., 2015). Next, I will discuss the evidences that I have found so far about this issue and those three receptors, as well as their signalling pathway in the cells of the niche.

The *Oamb* receptor was the first to be cloned in *Drosophila* and its expression was described in mushroom body (MB) neurons of the adult brain for the control of appetitive olfactory learning (Han et al., 1998; Kim et al., 2013; Schwaerzel et al., 2003; Shih et al., 2018). Researchers have shown via RT-PCR that the RNA expression of *Oamb* is high in L3 brain but very low or even not detected in other organs such as the intestine, trachea, FB, salivary glands, or malpighian tubules (El-Kholy et al., 2015). In the transcriptome analysis I performed, *Oamb* appears to be down-regulated at L3 stage in both brain NECs and glia. This may indicate that in L2 stage, or around that stage transition moment, *Oamb* expression is even higher. That speculation gives sense of the arrested phenotype showed in the niche cells I following discuss.

I observed that in *c855a<sup>+</sup>* cells, up-regulation of *Oamb* causes early L3 arrest but its brain has the appearance of a normal L2-like brain; conversely, down-regulation of the receptor causes lethality in the pupal stage. That difference of phenotypes depending on whether *Oamb* is up- or down-regulated in the *c855a<sup>+</sup>* cells may be, respectively, due to the acquisition of a new temporal trait because of the unnatural larval expression in those cells (GOF at inappropriate time), and the importance in those cells of the natural expression of *Oamb* in pupa (LOF). One way to address the behaviour of a cell type when *Oamb* is down-regulated would be using the FLP-Out genetic technique. There I observed how the OL progenitors seem not to be altered by that underexpression but their neural lineage is affected; the same happens in the imaginal discs with the epithelial cells and their offspring. The fact that a cell is not affected by the decrease in that expression may be because the process that is transferring the OA signal is not important for the cell itself, although it



would affect the secretion of important signals for other cells. A second possible explanation that may clarify that it would be the summative and alternative function of other receptors that ends up converging in the same transmission signal (Lim et al., 2014). Although several research studies have described the presence of the *Oamb* receptor in *Drosophila* epithelium (Faisal et al., 2014; Lee et al., 2003, 2009; Lim et al., 2014), I observed the expression pattern of *Oamb-Gal4*, which uses a Trojan exons method (Diao et al., 2015; Lee et al., 2018) and did not perceive any signal in NECs of L3 brain. Even so, before reaching any conclusion it is necessary to observe the expression of the *Oamb* driver in the late L2 stage (64h AEL), which is when the phenotype occurs, as well as the imaginal discs expression in both stages. For that reason the G-TRACE technique (Evans et al., 2009) may help to identify the expression pattern of *Oamb*<sup>+</sup> cells both in larval time and in the lineage profile.

On the other hand, I observed that down-regulation of *Oamb* in *cg25c*<sup>+</sup> cells results in early L3 arrest larvae which present crystal cells and develop massive L2-like brains. As previously mentioned, crystal cells may show an activation of the innate response of the immune system which is mediated by FB cells, or also due to the role of *Oamb* in haemocytes since the presence of OA receptors was described in those immune cells (Khadilkar et al., 2017; Meister and Lagueux, 2003; Rizki and Rizki, 1959; Roeder, 2005; Wang et al., 2014); a deeper study is necessary in this issue. In the enlarged L2-like brains, I observed an increase of the mitotic cells, although not via EGFR pathway. Then, the brain overgrowth phenotype may be triggered by other signals such as Wnt, Notch, or Hippo pathways that activate cell proliferation (Duronio and Xiong, 2013). Neither NECs nor NBs seem to be altered in number, although it would provide useful information the observation of the proneural wave start through the proneural protein Lethal of scute which is a OPC signal of the NECs to NBs transition (Yasugi et al., 2008). However, I detected a very interesting group of a few neurons in each lobe that are harmed and undergo apoptosis. The FLP-Out technique for underexpressing *Oamb* in different cell types indicates that the integrity of the brain glial cells is not affected; at the same time, it also suggests that it does affect CNS cells with large nuclei that could be glia, and other cells with smaller nuclei that may belong to neurons. This could indicate that the glial cells, whether their integrity is affected (brain area) or not (VNC area) by the *Oamb* down-regulation, have a direct communication with other brain cells, such as neurons, which may be affected by a glial dysfunction. The *Oamb* expression pattern in the L3 CNS reveals that is expressed in glial cells in both the VNC and the CNS, as well as some medial OL that may be *cg25c*<sup>+</sup>; in addition, I observed other non-glial cells that also express that OA receptor and among which there would be the MB neurons (El-Kholy et al., 2015; Shih et al., 2018). Although years ago was described that OA affected the glial cells of insects (Schofield and Treherne, 1985), recent studies in *Drosophila* have shown that certain types of glia express OA receptors: astrocyte-like glia (ALG) of the larval CNS express *Oct-Tyr* receptor (Ma et al., 2016), and lamina glia express *Oamb* in the adult OL (Davis et al., 2018). However, as I mentioned before, it is necessary to observe that cells that express *Oamb* in earlier stages such as late L2 (64h AEL), which is the moment when the CNS would be arrested on this dysfunction.

Using surface glia (SG) drivers, I discarded that *Oamb* is important for both perineural (PG) and subperineural glia (SPG). I also did not perceive any abnormal phenotype with *Oamb* down-regulation using CG drivers. Although *cg25c*<sup>+</sup> OL cells are CG in the brain, this lack of phenotype could be attributed to the different larval time expression of these drivers which is not the important expression moment for *Oamb*. Nonetheless, other glial drivers provoke the larval arrest phenotype when *Oamb* is down-regulated. *Repo-Gal4* arrests larvae at early/mid L3, while *mir-8-Gal4* arrests larvae at late L2 as well as their CNS with the peculiarity that the VNC is enlarged. This enlarged VNC may be attributed to the LOF of *Oamb* in the *mir-8*<sup>+</sup> glial cells of that region. Although a down-regulation of the receptor in the *mir-8*<sup>+</sup> and *cg25c*<sup>+</sup> cells causes arrest in larval stages, it is interesting to observe they do it in late L2 and early L3, respectively; these phenotypes suggest a role of the *mir-8*<sup>+</sup> cells of the CB in the L2-to-L3 transition. Despite these arrest phenotypes occur in slightly different larval times, probably due to their moment of expression, it is encouraging that the *cg25c*<sup>+</sup> cells belong to both glial drivers. The *lsp2-Gal4* driver and according to other studies (El-Kholy et al., 2015) I discarded that the part of the *cg25c*<sup>+</sup> and *mir-8*<sup>+</sup> cells of the FB is responsible for the observed arrest. Even so, I appreciated that another FB driver (*ppl-Gal4*) causes abnormalities in the development (small sizes of the individuals) when *Oamb* is down-regulated, but neither arrest nor lethality, which may be explained because that driver is also expressed in few CB neurons, wing disc, salivary glands and intestine (El-Kholy et al., 2015). On the other hand, the overexpression of *Oamb* receptor in *ppl*<sup>+</sup> cells causes arrest in half of the larvae at the early L3 stage; this phenotype may also be explained by the non-FB cells role or the non-natural expression of FB cells (GOF at inappropriate tissue). Others FB-specific drivers, such as *F30-Gal4* (Colombani et al., 2003), should be tested to provide information on this tissue. In any case, to discard the possible action of the *cg25c*<sup>+</sup> cells from the FB (as well as the *mir-8*<sup>+</sup> FB cells) on the dysfunctional *Oamb* phenotype, is convenient to test them with *repo-Gal80* in order to inhibit the glial expression. In addition, the driver *tsh-Gal80* will be useful for me to check the possible role of those VNC *cg25c*<sup>+</sup> cells (Gao et al., 2013; Ma et al., 2016). Finally, *Oamb* down-regulation in other tissues, such as the RG, also arrests

larvae in early L3 and premature wandering up the tube walls. Research studies have shown the expression of OA receptors in that endocrine organ (Ohhara et al., 2012) although there is no information indicating a possible role in these cells through *Oamb*. In brief, it is interesting to observe how both niche cell types result in a similar type of arrest depending on whether there is an *Oamb* GOF or LOF in those cells. For all these reasons, *Oamb* is an extremely important receptor for the niche cells and must be continue studying in depth.

The second OA receptor detected in the *in vivo* validation was *Octβ1R* (Evans and Maqueira, 2005; Maqueira et al., 2005). Whereas some of the OA receptors show a very broad expression profile, *Octβ1R* is restricted to a very few organs (El-Kholy et al., 2015). Studies show that the RNA expression of the *Octβ1R* gene is very high in fly heads (CNS) but lower in the rest of the body (muscle and trachea; El-Kholy et al., 2015; Maqueira et al., 2005; Ohhara et al., 2012); in larva, the expression of the receptor is also high in L3 CNS but undetectable in other organs (intestine, trachea, FB, and malpighian tubules; El-Kholy et al., 2015; Koon and Budnik, 2012; Ohhara et al., 2012). This data suggests that during development, *Octβ1R* is mainly working in the CNS but additionally may play functional roles in other tissues of the organism. Furthermore, the transcriptome analysis I performed shows *Octβ1R* down-regulation in L3 compared to L2 stages; this is also in agreement with the whole body mRNA expression pattern shown in other studies (Ohhara et al., 2012). When *Octβ1R* is down-regulated in both cells of the niche causes larval arrest phenotypes. Specifically, underexpression of that receptor in the *c855a*<sup>+</sup> cells provokes arrest at early L3 stage and premature wandering behaviour. The early L3 arrested larvae have a normal L2-like brain in size with any signal of proliferation via MAPK pathway that may explain the normal size of the brain, even after being arrested for several days. Although I would personally test the *Octβ1R*-Gal4 driver both in late L2 and in late L3, other works show clearly that in late L3 brains there is expression of the receptor in the OPC NECs, and the IPC to a lesser extent, even though they do not focus in their study (El-Kholy et al., 2015; Ohhara et al., 2012). Therefore, it is proper to characterize that brain more in detail using immunostainings for NECs (anti-DECad and anti-Patj) as well as the behaviour of other lineage cells such as neurons (anti-Elav) while observing both proliferation (anti-PH3) and cell death (anti-Casp3). Clones created by the FLIP-Out technique showed some neurons any part of the CNS do not appear to be affected by *Octβ1R* dysfunction, though others are. This is explained by studies where the expression of this receptor was observed in neurons of the CNS of both larval and adult, including those of the MB (El-Kholy et al., 2015; Koon and Budnik, 2012; Koon et al., 2011; Shih et al., 2018). Finally, the possible role of the *c855a*<sup>+</sup> cells of the imaginal discs must be taken into account since other research have described *Octβ1R* expression in this tissue (Koon and Budnik, 2012; Ohhara et al., 2012).

On the other hand, when *Octβ1R* is underexpressed in *cg25c*<sup>+</sup> cells causes arrest at L3 in half of larvae. Those arrested larvae have enlarged brains which present NECs overproliferation, indicating a direct impact on their niche partner. This may be somehow connected by the fact that the NECs also express *Octβ1R* (El-Kholy et al., 2015; Ohhara et al., 2012). Then, a decrease in the receptor of the *cg25c*<sup>+</sup> cells evoke more OA availability for receptors of other CNS cells (*Octβ1R* is highly expressed in both CB and VNC, and in some OL cells including NECs; El-Kholy et al., 2015; Koon and Budnik, 2012; Ohhara et al., 2012) that could indirectly deregulate the OA pathway of those cells. It is interesting to note that those enlarged L3 brains show loss of *cg25c*<sup>+</sup> glial cells and lobe SG but not of neuropil glia (NG). However, when I examine the behaviour of the cells glial in the FLIP-Out clones down-regulated in *Octβ1R*, they seem not to be affected. I deepened in this conflict using different larval drivers for glial cells. Down-regulating *Octβ1R* in SG (PG and SPG) does not cause any abnormality in fly development, neither in *NRT*<sup>+</sup> CG cells. Interestingly, down-regulation of *Octβ1R* in *NP2222*<sup>+</sup> CG cells does arrest larvae in early L3 stage although their size is L1-like length but L3-like width. A possible explanation may be because the driver *NRT*-Gal4 has been demonstrated to mark CG cells from the VNC (Bailey et al., 2015) while *NP2222*-Gal4 marks CG cells of the entire CNS (Avet-Rochex et al., 2012); thus, the dysfunctional CG cells which promotes the arrest phenotype are those in the brain. Down-regulation of *Octβ1R* in *miR-8*<sup>+</sup> cells causes early L3 arrest, consolidating the possible role of OL *cg25c*<sup>+</sup> cells. All in all, these findings suggest that the brain glia plays a role in stage transition via *Octβ1R*, although it would be convenient to carry out some more experiments on this matter especially in their brains characterization. On the other hand, it was also necessary to test the possible role of *cg25c*<sup>+</sup> cells from the FB. A normal development is observed when *Octβ1R* is underexpressed in FB cells (*Isp2*-Gal4); however, using another FB driver (*ppl*-Gal4) arrests larvae in early L3. This may be explained by the different cells that express the gene *ppl* or also by the temporary expression difference, as mentioned before, since other studies have not observed any expression in the FB (El-Kholy et al., 2015). As in the case of *Oamb*, the use of *F30*-Gal4 as FB-specific driver (Colombani et al., 2003) would be helpful in this issue. Apart from FB, as previously mentioned, *Octβ1R* is described to have lower expression in other tissues. Because I observed the larval arrest phenotype with the down-regulation of *Oamb* in the RG, along with the description of *Octβ3R* expression in that tissue (Ohhara et al., 2012), it would also be interesting to observe the *Octβ1R* behaviour in the RG although its expression has not been

detected so far (Ohhara et al., 2012). Finally, due to time constraints, as I mentioned it was possible to test the *Octβ1R*-Gal4 expression profile by myself which, together with the G-TRACE technique (Evans et al., 2009), may be decisive in the characterization of that OA receptor in larva. *Octβ1R* is described as antagonist of *Octβ2R* on synaptic growth (Koon and Budnik, 2012; Koon et al., 2011) as well as required for increasing locomotor speed which enhance climbing in adult flies (Sujkowski et al., 2017) through inhibition of cAMP production (Koon and Budnik, 2012; Maqueira et al., 2005). These functions, together with the ability of *Octβ1R* of autoregulation through activating retrograde signals (Koon and Budnik, 2012), make this receptor very interesting for understanding its function in the cells of the studied niche.

*Octβ3R* (Evans and Maqueira, 2005; Maqueira et al., 2005) was the third OA receptor highlighted in the *in vivo* validation that I performed. In adults, this receptor is high expressed in fly heads, primarily in the CNS, but also in other tissues of the body, although in low expression (El-Kholy et al., 2015; Maqueira et al., 2005; Ohhara et al., 2012; Shih et al., 2018). In larva, its expression is also detected in the CNS, as well as in other tissues such as imaginal discs, RG, midgut, malpighian tubules, and reproductive organs (El-Kholy et al., 2015; Ohhara et al., 2012). Down-regulation of *Octβ3R* in both cell types of the studied niche causes larval arrest. Like the other OA receptors examined, *Octβ3R* is down-regulated in L3 on the transcriptomic analysis I performed, which means that it is more expressed in L2 than in L3 stage. This is in accordance with the mRNA expression changes observed in the whole larva by other labs (Ohhara et al., 2012).

On the one hand, down-regulation of *Octβ3R* in *c855a*<sup>+</sup> cells results in arrest in half of the larvae at late L3 stage. Their brains are larger and also present overproliferation of NECs. The FLIP-Out technique reveals that when there is a down-regulation of *Octβ3R* in NECs, this brain cells are not affected. The expression pattern using a Gal4 driver for that receptor did not show any expression in the NECs, neither in late L2 brains nor in L3. Nevertheless, the use of other *Octβ3R*-Gal4 lines that differ in the intronic region of the cloned receptor may reveal the expression in those cells, as other studies have indicated such variety between drivers (Koon and Budnik, 2012). The driver *Octβ3R*-Gal4 showed expression in both VNC and CB neurons in L2 stage although it is not so clear in L3. This suggests that *Octβ3R* may be important for neuronal signalling in early larval stages rather than in final stages. Using the FLIP-Out technique, I observed that some of these neurons were damaged while others were not, suggesting a greater sensitivity of this cell type than others when processing octopaminergic signals. This is not surprising since studies on *Octβ3R* demonstrate great importance in several neuronal types (El-Kholy et al., 2015; Maqueira et al., 2005; Shih et al., 2018). Since *Octβ3R* has been described in epithelial cells of non-nervous larval organs (Faisal et al., 2014), it is important to considerate the possible role of *c855a*<sup>+</sup> epithelial cells from the imaginal discs. In the FLIP-Out experiment, I observed that the epithelial cells of this tissue are not affected by underexpression of *Octβ3R*; however, some other cells die. My observations together with those of other laboratories (El-Kholy et al., 2015; Ohhara et al., 2012) of the L3 expression of *Octβ3R* in the *c855a*<sup>+</sup> cells of the imaginal discs leads me to postulate an important role of them in the observed phenotype, and because of the connection between organs cause the arrested CNS (Roeder, 2005). However, despite not observing expression in NECs, it can not be discarded that is their own underexpression of *Octβ3R* what causes overproliferation of them and has an effect on the observed phenotype.

On the other hand, when *Octβ3R* is down-regulated in *cg25c*<sup>+</sup> cells, larvae arrest at early L3 and present a larger L2-like brain with a higher number of NBs which suggesting an impact of *cg25c*<sup>+</sup> cells on them. I observed through the Flip-Out technique that there were glial cells whose integrity was preserved when there was a down-regulation of *Octβ3R*; however, others were possibly affected due to the glial subtype they belong. The expression pattern of *Octβ3R*-Gal4 shows in L2 some cell close to OL that may be glia. Anyway, in L3 I clearly observed that the receptor expression is mainly located in the cortical layer of the OLs, which is confirmed also by other articles (Ohhara et al., 2012). I strongly propose that these cells are glia and, in addition, they reminiscent of *cg25c*<sup>+</sup> cells suggesting the role of *Octβ3R* in those niche cells. However, as in those studies I mentioned before (Ohhara et al., 2012), I observed in the L3 VNC and CB other cells that expressed the receptor. For that reason, I analysed which glial cell type of the CNS that express *Octβ3R* have an important function for growth and development. Down-regulation of *Octβ3R* in SG (PG and SPG) shows normal development and thus, it was discarded that this receptor is important in that glial type. Interestingly, I observed that the *NRT*<sup>+</sup> CG, which is specific for VNC, did not present any abnormality in the development; nevertheless, the *NP2222*<sup>+</sup> CG of all the CNS does. This suggests that the CG involved in this phenotype are from the lobes. Down-regulation of *Octβ3R* in *NP2222*<sup>+</sup> cells arrest larvae in L3. Unusually, I observed variety in size (mid L2-like and mid L3-like) and also half of the larvae reach to pupae but then die. I also detected arrest in early L3 when *Octβ3R* is down-regulated in *miR-8*<sup>+</sup> cells which although they are similar to early L3 larva in width, their length is like L2 larva. All in all, when the receptor *Octβ3R* is downregulated in glial cells, including *cg25c*<sup>+</sup> glia, it causes larval arrest in the 3<sup>rd</sup> instar and, therefore, it would be suitable to perform a

characterization of their brains. Aside from those CNS glial phenotypes, it is also important to know the role of *Octβ3R* may have in the *cg25c<sup>+</sup>* cells of the FB. The *lsp2<sup>+</sup>* cells indicate that this receptor is not important for the development in that tissue; however, in *ppl<sup>+</sup>* cells it does cause early L3 arrest in half of the larvae. As in the case of *Oamb* and *Octβ1R*, that phenotype may be explained by the non-FB cells that express the *ppl* gene and, additionally, may be helpful the use of another specific FB receptor such as *F30-Gal4* (Colombani et al., 2003). Even so, my observations along with that of other studies (El-Kholy et al., 2015) suggest that there is no expression of *Octβ3R* in FB cells; likewise, other research neither observe significant changes in the FB of defective *Octβ3R* flies (Li et al., 2017). For all the above, I postulate that the cells that may cause the phenotype of larval arrest due to an underexpression of *Octβ3R* in *cg25c<sup>+</sup>* cells are the OL glia.

Lastly, the *Octβ3R* behaviour in the RG was also interesting to observe since other studies detected expression on this tissue during larval stage and mainly in the prothoracic gland region which is the site for Ecdysone production (Ohhara et al., 2012). In addition, the biogenic amines, and among them OA, have been shown to stimulate the synthesis of Juvenile hormone (JH) that together with Ecdysone ensure the proper growth of the larva (Goodman and Granger, 2005; Granger et al., 1996; Hiruma and Kaneko, 2013). Interestingly, these two hormones are antagonistic: JH is constantly expressed in larva until the moment of promoting metamorphosis in the 3<sup>rd</sup> IL, while ecdysone increases its expression by promoting larva-to-larva molt and growth until the body reaches the critical weight necessary to begin the metamorphosis (Jaszczak and Halme, 2016). Unfortunately, underexpression of *Octβ3R* in RG cells does not cause any abnormality in development. Also the cells of the RG appear not to be influenced by *Octβ3R* down-regulation on the FLIP-Out experiment. However, it is very interesting to follow the hypothesis that connects both the OA and its receptors with Ecdysone and JH for the control of growth between the larval molts. Finally, mention that as other β-adrenergic-like OA receptors, *Octβ3R* play a significant role in the fly climbing (Sujkowski et al., 2017); and for that it would be helpful supplement the current data with other genetic techniques available in *Drosophila*, such as the G-TRACE (Evans et al., 2009), to defining precizing the role of that receptor in larval development.

After examining the role of OA receptors, I was interested to observe the OA signalling pathway (Erspamer, 1948; Huang et al., 2016; Livingstone and Tempel, 1983; Roeder, 2005; Schwaerzel et al., 2003; Vömel and Wegener, 2008) and the effects it may generate on the niche cells. Examining OA presence along fly stages, a high expression in both larval and adult CNS are detected (Busch and Tanimoto, 2010; Busch et al., 2009; Denno et al., 2015; Monastirioti et al., 1995; Roeder, 2005; Selcho et al., 2014; Zhou et al., 2008) enhancing the importance of OA in the stage and tissue of my interest. Using the driver of the enzyme that catalyses OA biosynthesis, *tβh-Gal4* (Monastirioti et al., 1996), I studied the OA expression pattern which seems to be expressed by different cells of the CNS during the larval development (L2 and L3) Thus, although the vast majority of *tβh<sup>+</sup>* cells of the CNS appear to be neurons mainly of the VNC and CB, I also distinguished a small group of cells that due to its shape and nuclei size may be glia of the VNC tip and others close to the OL, as well as epithelial cells of the imaginal discs (Monastirioti et al., 1996; Roeder, 2005). Identify that role in the niche cells would not be uncommon since other studies show that OA can autoregulate its own release, as well as OA receptors their own expression in octopaminergic cells (Koon and Budnik, 2012; Koon et al., 2011). *Vmat* is the transporter of different trace amine molecules and also handle their release (Chen et al., 2013; Greer et al., 2005). This monoamine vesicle is used to identify monoaminergic cells of the larval CNS and, interestingly, it has been described in *Drosophila* BBB glia in adult brains (Croset et al., 2017; Greer et al., 2005). In addition, as I have mentioned before, the trace amine receptors are so related that they respond to different molecules of this family (Qi et al., 2017; Robb et al., 1994) and even their synthesis pathways are great interconnected (Roeder, 2005; Vömel and Wegener, 2008). Considering that tyrosine is the source for dopamine and OA synthesis, the key enzyme for dopamine production *DDC* (Huang et al., 2016; Livingstone and Tempel, 1983) has been postulated as a regulator of OA production as well, in a paracrine manner by compensatory or redundant behaviour (Chen et al., 2013; Roeder, 2005; Vömel and Wegener, 2008). In addition to the neurons, *DDC* has been described in glial cells of the CNS larval as well as cells in the imaginal discs; however, neither of the two cell types has been extensively characterised (Beall and Hirsh, 1987; Hodgetts and O'Keefe, 2006). Therefore, I wanted to observe a possible function of both the synthesis and the release of OA, in a direct or indirect manner, by both cells of the niche that also express their receptors. The down-regulation of *tβh*, *Vmat*, or *DDC* do not affect the larval development; even so, it would be necessary to observe what would happen with the sustained expression of OA during larval stages since, accordingly their receptors expression (El-Kholy et al., 2015), it is at that moment when its normal expression decreases. That does not occur in those cells since. Therefore, more knowledge in the regulation of the synthesis of OA in *c855a<sup>+</sup>* and *cg25c<sup>+</sup>* cells in an autocrine or paracrine manner is needed.

Lastly, I examined the OA receptor signalling pathway within the niche cells. Several studies describes that the OA signal stimulates through these receptors the intracellular accumulation of

cAMP and Ca<sup>2+</sup> (Balfanz et al., 2005; Han et al., 1998; Kim et al., 2013; Robb et al., 1994), and this activates the *CaMKII* and *Mmp2* enzymes which control the secretion of downstream effectors (Deady and Sun, 2015; Lee et al., 2009; Lim et al., 2014). Also it is known that the calcium-binding messenger protein *Cam* interacts with *CaMKII*, in the calcium signal transduction pathway (GuptaRoy et al., 1996; Xu et al., 1998). These signalling molecules have been described in both epithelial and glial cells (Deady and Sun, 2015; Lee et al., 2009; Lim et al., 2014; Ma et al., 2016) and therefore, I wanted to check them in the studied niche as well. In *c855a*<sup>+</sup> cells, down-regulation of *Mmp2* or *CaMKII* has no consequences in development; however, their overexpression causes lethality in the L1 stage and arrest in half of larvae at the early L3 stage, respectively. The first phenotype can be explained by a GOF at inappropriate time, while the second one as is essential in mediating multiple cellular responses needs to be studied more in detail. Also note that the *Cam* down-regulation in *c855a*<sup>+</sup> cells arrest larvae in late L3 stage for several days indicating an internal role of the calcium signalling pathway in those cells. Regarding intracellular signalling in the *cg25c*<sup>+</sup> cells, neither underexpression nor overexpression of the enzymes *CaMKII* and *Cam* affect the normal development of the organism. And about *Mmp2*, its up- and down-regulation produces the same phenotype as in its niche partner, so its function may be interpreted in the same way.

One question that remains to be discussed is the phenotypes in the L2-to-L3 transition of premature wandering observed by the down-regulation of several of the OA receptors. Several studies describes that OA from the larval CNS is be sufficient to enhance locomotor behaviour such as larval crawling (Chen et al., 2013; Fox et al., 2006; Saraswati et al., 2004). The whole larval expression of OA receptors tends to decrease during this stage but, interestingly, in late 3<sup>rd</sup> IL all these receptors increase their expression before a drastic reduction in the pupal stage, where OA is not expressed either (Ohhara et al., 2012). Furthermore, other studies define octopaminergic neurons and glia (apparently ALG) as locomotor behaviour modulator cells during development, through the visual motion pathway in the OL, since these cells contain OA receptors and enzymes that catabolism TA which has an antagonistic effect on OA in this function (Arenz et al., 2017; Ryglewski et al., 2017; Saraswati et al., 2004; Strother et al., 2017; Sujkowski et al., 2017; Tuthill et al., 2014). Therefore, perhaps the sudden and premature decline of the OA receptors anticipates that wandering behaviour prior to the larva-pupa transition. This interesting observation would be convenient to further studying.

In conclusion, the expression and functionality of OA receptors are time dependent but not cell type dependent. In such a way that the CNS cells of the niche studied in this thesis, both the NECs and the glia (Ma et al., 2016; Ryglewski et al., 2017; Schofield and Treherne, 1985), have an extreme importance in the OA signalling pathway. Both cell types are involved in this route through the expression of receptors and their ligands metabolization, and the dysfunction of them in the larval stage have consequences in the normal growth of the brain that derives in a development mismatch. The signalling pathways of OA together with its receptors are closely related to other neurohormones and neuromodulators in a network of communication and adaptation of the functions of other very complex (Chen et al., 2013; Davis et al., 2018; Deady and Sun, 2015; Faisal et al., 2014; Greer et al., 2005; Han et al., 1998; Li et al., 2016, 2017; Rewitz et al., 2013; Roeder, 2005; Schwaerzel et al., 2003; Vömel and Wegener, 2008). Even so, it is demonstrated that octopaminergic circuits mainly control the locomotion and survival of larvae (Chen et al., 2013), and also OA receptors have between themselves summatory or antagonistic activities in order to modulation these functions (Koon and Budnik, 2012; Koon et al., 2011; Sujkowski et al., 2017).

All in all, these exciting discoveries about OA receptors and their signalling pathways in a neuroepithelial-glial context have proved to be a highly interesting challenge. Therefore, despite the work done in this thesis, it is necessary to continue studying those receptors and their phenotypes in a global context of the organism in order to determine more specifically the mechanisms by which these niche cells control development in *Drosophila melanogaster*.





**CONCLUSIONS / CONCLUSIONES**





## **PART 1: Characterization of the neuroepithelial-glia niche**

1. The neuroepithelial promoter *c855a-Gal4* is continuously expressed in late 3<sup>rd</sup> IL brains, but in 2<sup>nd</sup> IL it is expressed in a discontinuous manner or may be activated depending on the moment of the neuroepithelial cell-cycle.
2. The collagen type IV  $\alpha 1$  chain protein (*Cg25c*) is synthesized in glial cells of the central nervous system during the larval stages.
3. The *cg25c-Gal4* promoter identifies cortex glial cells specific to the optic lobe which are a subset of the surface-associated *miR-8*<sup>+</sup> glia.
4. Down-regulation of the ligand Spitz in *cg25c*<sup>+</sup> glial cells results in brain growth because that underexpression causes in neuroepithelial cells from the OPC the opposite behaviour of that shown by *miR-8*<sup>+</sup> glial cells.

## **PART 2: Isolation of niche cells and transcriptomic analysis**

1. Labelling of progenitor cells, such as neuroepithelial cells, requires a short-lived fluorescent marker to overcome the phenomenon of perdurance and offspring tagging in the isolation by the FACS technique.
2. The use of a dual fluorescent labelling for cells sorted by FACS improves the precision of the isolation and the technique robustness.
3. The *in silico* approach by cell type allows for the identification of specific markers of both cell type (neuroepithelium and glia) and developmental stage (2<sup>nd</sup> IL and 3<sup>rd</sup> IL) from RNA-seq data.
4. The *in silico* approach by developmental stage allows for the identification of differentially expressed genes in different stages of development (2<sup>nd</sup> IL and 3<sup>rd</sup> IL) for each cell type from RNA-seq data.
5. The combination of different *in silico* screenings allows for the narrowing of the list of thousands of differentially expressed genes to a single list of 151 target genes.

## **PART 3: Validation of the target genes and their phenotypes**

1. *In vivo* validation reveals 51 genes of the 151 target genes which are important at different stages for proper growth and development of *Drosophila*.
2. The glial cells of the niche have implications in larval (e.g., *wg*, *Nrx-IV*, *Ret*, *mys*, *ed*, *trio*, *dpr2*, *dpr5*, *Dh44-R1*, *Wnt2*, *santa-maria*, *Egfr*, *spi*, *Oamb*, *Oct $\beta$ 1R*, and *Oct $\beta$ 3R*), pupal (e.g., *mys*, *dpr5*, and *5-HT2B*), and adult development (e.g., *SiFaR*, *baz*, *ine*, and *Egfr*).
3. Genetic dysregulations in the niche give rise to adult motor deficiencies that may be caused by neurodegenerative disorders (e.g., *stan*, *aos*, *mew*, *fz*, *Ten-a*, and *Ptp69D*).
4. The disruption of a gene causes different developmental anomalies depending on whether it is expressed in neuroepithelial or glial cells (e.g., *wg*, *Nrx-IV*, *mtt*, *mys*, and *ine*).
5. The neuroepithelial-glia interaction in the niche controls brain growth and development (e.g., *spi*, *ed*, *mys*, *Wnt2*, and *Oct $\beta$ 1R*).
6. Genetic dysregulation in neuroepithelial cells has non-cell autonomous effects on glial cells (e.g., *ed*, *mys*, and *nAChR $\alpha$ 3*), and vice versa (e.g., *mys*, *Wnt2*, *spi*, and *Oct $\beta$ 1R*).

7. Alterations of gene expression in *cg25c*<sup>+</sup> cells affect the development of this glial cell-type of the brain in a cell autonomous manner (e.g., *ed*, *mys*, *trio*, and *Octβ1R*).
8. Gene dysregulation in *c855a*<sup>+</sup> cells causes overproliferation and destructuration of neuroepithelial cells of the brain (e.g., *wg*, *bark*, *ptc*, *mtt*, *nAChRα3*, *ine*, *aos*, *Fas2*, and *Octβ3R*).
9. Gene dysregulation in the niche cells causes an increase in larval brain size (e.g., *wg*, *Nrx-IV*, *ptc*, *Burs*, *ed*, *mtt*, *mys*, *nAChRα3*, *otk2*, *Wnt2*, *unc-5*, *santa-maria*, *spi*, *aos*, *Fas2*, *Oamb*, *Octβ1R*, and *Octβ3R*).
10. Disruptions of genes during larval stages cause development of abnormal phenotypes in the brain that cause pupal lethality (e.g., *wg*, *bark*, *Nrx-IV*, *ptc*; *Burs*, *ed*, *mtt*, *mys*, *nAChRα3*, *otk2*, *wls*, *ine*, *aos*, *Fas2*, and *Oamb*).
11. Gene dysregulation in *c855a*<sup>+</sup> cells causes deregulation in the epithelial cells of the imaginal discs that has implications for the development of this tissue (e.g., *wg*, *bark*, *Pburs*, *mtt*, *Fas2*, and *Octβ3R*).
12. Gene dysregulation in the *cg25c*<sup>+</sup> cells of the fat body tissue may be involved in the onset of the innate immune response (e.g., *mtt*, *mys*, *Dh44-R1*, *Egfr*, *spi*, and *Oamb*).
13. Niche cells express receptors of neuropeptides, neuromodulators and neurohormones with important functions for organ growth and *Drosophila* development (e.g., *SIFaR*, *nAChRα3*, *5-HT2B*, *InR*, *Dh44-R1*, *ine*, *Oamb*, *Octβ1R*, and *Octβ3R*).
14. Genetic deregulations of the niche cause arrest in development in early larval stages and also in the central nervous system growth (e.g., *dpr2*, *Oamb*, *Octβ1R*, and *Octβ3R*).
15. The decrease in octopamine receptors anticipates the larval wandering behaviour prior to the larval-pupa transition (*Oamb*, and *Octβ1R*).

## **PART 4: The octopamine receptors in larval development**

1. The octopamine receptors *Oamb*, *Octβ1R*, and *Octβ3R* expressed in *c855a*<sup>+</sup> and *cg25c*<sup>+</sup> cells control larval development and central nervous system growth.
2. These three octopamine receptors are temporally regulated in larval niche cells, with higher expression in the brain in late 2<sup>nd</sup> IL than in late 3<sup>rd</sup> IL.
3. The *Oamb* gene is expressed in glial cells of the larval central nervous system.
4. Down-regulation of *Oamb* in *cg25c*<sup>+</sup>, *miR-8*<sup>+</sup> and *repo*<sup>+</sup> glial cells causes larval arrest in the 2<sup>nd</sup>-to-3<sup>rd</sup> instar transition, as well as arrest of their central nervous system.
5. Down-regulation of *Oamb* in *cg25c*<sup>+</sup> glial cells induces the death of a reduced neuronal group in the 2<sup>nd</sup> IL brain.
6. Deregulations of expression of *Oamb* in both *cg25c*<sup>+</sup> and *c855a*<sup>+</sup> cells cause larval arrest phenotypes in early 3<sup>rd</sup> instar.
7. Down-regulation of *Oamb* in the ring gland also causes an early larval arrest phenotype.
8. The *Octβ1R* gene is expressed in neuroepithelial and glial cells of the optic lobe of the larval brain.
9. Down-regulation in the expression of *Octβ1R* in both *cg25c*<sup>+</sup> and *c855a*<sup>+</sup> cells cause larval arrest phenotypes in early 3<sup>rd</sup> instar.
10. Down-regulation of *Octβ1R* in both *cg25c*<sup>+</sup> and *miR-8*<sup>+</sup> glial cells causes larval arrest in the 2<sup>nd</sup>-to-3<sup>rd</sup> instar transition, as well as arrest of their central nervous system.

11. The *Octβ3R* gene is expressed in the *cg25c*<sup>+</sup> cortex glia of the optic lobe.
12. Deregulation of *Octβ3R* expression in *cg25c*<sup>+</sup> cells causes larval arrest phenotypes in early 3<sup>rd</sup> instar while such deregulation in *c855a*<sup>+</sup> cells causes arrest in late 3<sup>rd</sup> instar.
13. Down-regulation of *Octβ3R* in the imaginal discs causes a larval arrest phenotype.
14. Down-regulation of *Octβ3R* in glial cells *cg25c*<sup>+</sup> and *miR-8*<sup>+</sup> causes larval arrest in the 2<sup>nd</sup>-to-3<sup>rd</sup> instar transition, as well as arrest of their central nervous system.
15. *c855a*<sup>+</sup> and *cg25c*<sup>+</sup> cells are not directly involved in the metabolic pathway of octopamine biosynthesis.
16. Down-regulation of *Calmodulin* in *c855a*<sup>+</sup> cells causes late larval arrest.





## **PARTE 1: Caracterización del nicho neuroepitelio-glía**

1. El promotor neuroepitelial *c855a-Gal4* es expresado continuamente en cerebros tardíos L3, pero en el estadio larval L2 se expresa de una manera discontinua o se activa dependiendo del momento del ciclo celular de la célula neuroepitelial.
2. La proteína de colágeno tipo IV con cadena  $\alpha 1$  (*Cg25c*) se sintetiza en células gliales del sistema nervioso central durante la etapa larval.
3. El promotor *cg25c-Gal4* identifica a células gliales del córtex específicas del lóbulo óptico y que son un subconjunto de la glía asociada a la superficie *miR-8*<sup>+</sup>.
4. Una disminución de la expresión del ligando Spitz en las células gliales *cg25c*<sup>+</sup> causa un comportamiento de las células neuroepiteliales del OPC contrario al mostrado por las células gliales *miR-8*<sup>+</sup> y que termina provocando un crecimiento del tamaño cerebral.

## **PARTE 2: Separación de las células del nicho y análisis transcriptómico**

1. Las células progenitoras, como las neuroepiteliales, requiere de un marcador fluorescente de corta vida para solventar el fenómeno de perduración y marcaje de su descendencia en la técnica de separación por FACS.
2. La utilización de un marcaje fluorescente dual para las células sorteadas por FACS añade precisión de separación y robustez a la técnica.
3. La aproximación *in silico* por tipo celular permite conocer marcadores específicos tanto de tipo celular (neuroepitelio y glía) como de etapa del desarrollo (L2 y L3) a partir de datos de RNA-seq.
4. La aproximación *in silico* por etapa de desarrollo permite conocer genes diferencialmente expresados en distintas etapas del desarrollo (L2 y L3) para cada tipo celular a partir de datos de RNA-seq.
5. La combinación de distintos cribajes *in silico* permite estrechar la lista de miles de genes diferencialmente expresados a una lista única de 151 genes diana.

## **PARTE 3: Validación de los genes diana y sus fenotipos**

1. La validación *in vivo* revela 51 genes, de los 151 genes diana, que son importantes en distintas etapas del crecimiento para un desarrollo adecuado de la *Drosophila*.
2. Las células gliales del nicho tienen implicaciones en el desarrollo en larva (e.g., *wg*, *Nrx-IV*, *Ret*, *mys*, *ed*, *trio*, *dpr2*, *dpr5*, *Dh44-R1*, *Wnt2*, *santa-maria*, *Egfr*, *spi*, *Oamb*, *Octβ1R*, y *Octβ3R*), pupa (e.g., *mys*, *dpr5*, y *5-HT2B*), y adulto (e.g., *SiFaR*, *baz*, *ine*, y *Egfr*).
3. Desregulaciones genéticas en el nicho dan lugar a deficiencias motoras en adulto que podrían ser causadas por desórdenes neurodegenerativos (e.g., *stan*, *aos*, *mew*, *fz*, *Ten-a*, y *Ptp69D*).
4. La alteración en la expresión de un mismo gen causa diferentes anomalías en el desarrollo dependiendo si está expresado en células neuroepiteliales o gliales (e.g., *wg*, *Nrx-IV*, *mtt*, *mys*, e *ine*).
5. La interacción neuroepitelio-glía en el nicho controla el crecimiento y desarrollo cerebral (e.g., *spi*, *ed*, *mys*, *Wnt2*, y *Octβ1R*).

6. La desregulación genética en las células neuroepiteliales tiene efectos celulares no autónomos en las células gliales (e.g., *ed*, *mys*, y *nAChRa3*), y viceversa (e.g., *mys*, *Wnt2*, *spi*, y *Octβ1R*).
7. Alteraciones en la expresión genética de las células *cg25c<sup>+</sup>* afectan directamente en el desarrollo de ésta glía del cerebro de una manera celular autónoma (e.g., *ed*, *mys*, *trio*, y *Octβ1R*).
8. La desregulación genética en las células *c855a<sup>+</sup>* causa una sobreproliferación y desestructuración de las células neuroepiteliales del cerebro (e.g., *wg*, *bark*, *ptc*, *mtt*, *nAChRa3*, *ine*, *aos*, *Fas2*, y *Octβ3R*).
9. La desregulación genética en las células del nicho causa un incremento del tamaño cerebral en larva (e.g., *wg*, *Nrx-IV*, *ptc*, *Burs*, *ed*, *mtt*, *mys*, *nAChRa3*, *otk2*, *Wnt2*, *unc-5*, *santa-maria*, *spi*, *aos*, *Fas2*, *Oamb*, *Octβ1R*, y *Octβ3R*).
10. La alteración de genes en la etapa larval desarrolla fenotipos anormales en el cerebro que causan letalidad en pupa (e.g., *wg*, *bark*, *Nrx-IV*, *ptc*; *Burs*, *ed*, *mtt*, *mys*, *nAChRa3*, *otk2*, *wls*, *ine*, *aos*, *Fas2*, y *Oamb*).
11. La desregulación genética en las células *c855a<sup>+</sup>* causa una desregulación en las células epiteliales de los discos imaginales que tiene implicaciones en el desarrollo de este tejido (e.g., *wg*, *bark*, *Pburs*, *mtt*, *Fas2*, y *Octβ3R*).
12. Genes alterados en las células *cg25c<sup>+</sup>* del tejido adiposo pueden estar implicados en iniciar la respuesta inmunológica innata (e.g., *mtt*, *mys*, *Dh44-R1*, *Egfr*, *spi*, y *Oamb*).
13. Las células del nicho expresan receptores de neuropeptidos, neuromoduladores y neurohormonas con funciones importantes para el crecimiento de órganos y desarrollo de *Drosophila* (e.g., *SIFaR*, *nAChRa3*, *5-HT2B*, *InR*, *Dh44-R1*, *ine*, *Oamb*, *Octβ1R*, y *Octβ3R*).
14. Desregulaciones genéticas del nicho causan arresto en etapas tempranas del desarrollo larval y del crecimiento del sistema nervioso central (e.g., *dpr2*, *Oamb*, *Octβ1R*, y *Octβ3R*).
15. La disminución de los receptores de octopamina anticipa el comportamiento larval de trepar previo a la transición larva-pupa (*Oamb*, y *Octβ1R*).

## **PARTE 4: Los receptores de octopamina en el desarrollo larval**

1. Los receptores de octopamina *Oamb*, *Octβ1R*, y *Octβ3R*, expresados en las células *c855a<sup>+</sup>* y *cg25c<sup>+</sup>* controlan el desarrollo de la etapa larval y el crecimiento del sistema nervioso central.
2. Esos tres receptores de octopamina se regulan temporalmente en las células del nicho larval, con una expresión cerebral más alta en L2 tardío que en L3 tardío.
3. El gen *Oamb* es expresado en células gliales del sistema nervioso central en larva.
4. La falta de expresión de *Oamb* en las células gliales *cg25c<sup>+</sup>*, *miR-8<sup>+</sup>* y *repo<sup>+</sup>* causa arresto larval en la transición L2-L3 así como de su sistema nervioso central.
5. La falta de expresión de *Oamb* en células gliales *cg25c<sup>+</sup>* induce la muerte de un reducido grupo neuronal en el cerebro en L2.
6. Desregulaciones en la expresión de *Oamb* tanto en las células *cg25c<sup>+</sup>* como las *c855a<sup>+</sup>* causan fenotipos de arresto larval en L3 temprano.
7. La falta de expresión de *Oamb* en tejidos como la glándula anular también causa un fenotipo de arresto larval temprano.
8. El gen *Octβ1R* es expresado en células neuroepiteliales y gliales del lóbulo óptico del cerebro larval.

9. La falta de expresión de *Octβ1R* tanto en las células *cg25c*<sup>+</sup> como las *c855a*<sup>+</sup> causan fenotipos de arresto larval en L3 temprano.
10. La falta de expresión de *Octβ1R* en las células gliales *cg25c*<sup>+</sup> y *miR-8*<sup>+</sup> causa arresto larval en la transición L2-L3 así como de su sistema nervioso central.
11. El gen *Octβ3R* es expresado en la glía del córtex *cg25c*<sup>+</sup> del lóbulo óptico.
12. Desregulaciones en la expresión de *Octβ3R* en las células *cg25c*<sup>+</sup> causa fenotipos de arresto larval en L3 temprano mientras que en las células *c855a*<sup>+</sup> ocurre en L3 tardío.
13. La falta de expresión de *Octβ3R* en los discos imaginales causa un fenotipo de arresto larval.
14. La falta de expresión de *Octβ3R* en las células gliales *cg25c*<sup>+</sup> y *miR-8*<sup>+</sup> causa arresto larval en la transición L2-L3 así como de su sistema nervioso central.
15. Las células *c855a*<sup>+</sup> y *cg25c*<sup>+</sup> no forman parte de la ruta metabólica de biosíntesis directa de octopamina.
16. La falta de expresión de *Calmodulina* en las células *c855a*<sup>+</sup> causa arresto larval tardío.









---

**APPENDIX I**  
***Supplementary figures***



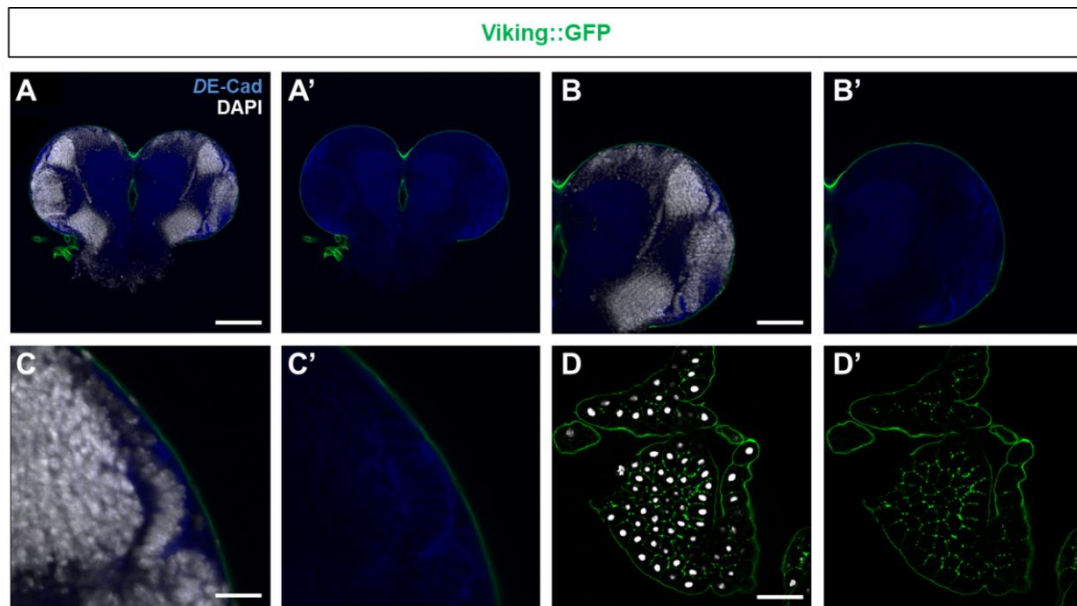


**Figure S1. Basement membrane in tissues where *cg25c-Gal4* is expressed during late L3 stage.** The extracellular matrix is revealed by one functional protein of the collagen IV components marked with fluorescence (Viking::GFP; Morin et al., 2001). The basement membrane (in green) is expressed on the tissue surface of the brain (A-C) and within individual cells in the fat body (D-D'). NECs and neuropil are marked with anti-DE-Cad antibody (blue); and DAPI (grey) stains cells' nuclei. Scale bars represent 100  $\mu\text{m}$  in (A), 50  $\mu\text{m}$  in (B), 20  $\mu\text{m}$  in (C) and 150  $\mu\text{m}$  in (D).

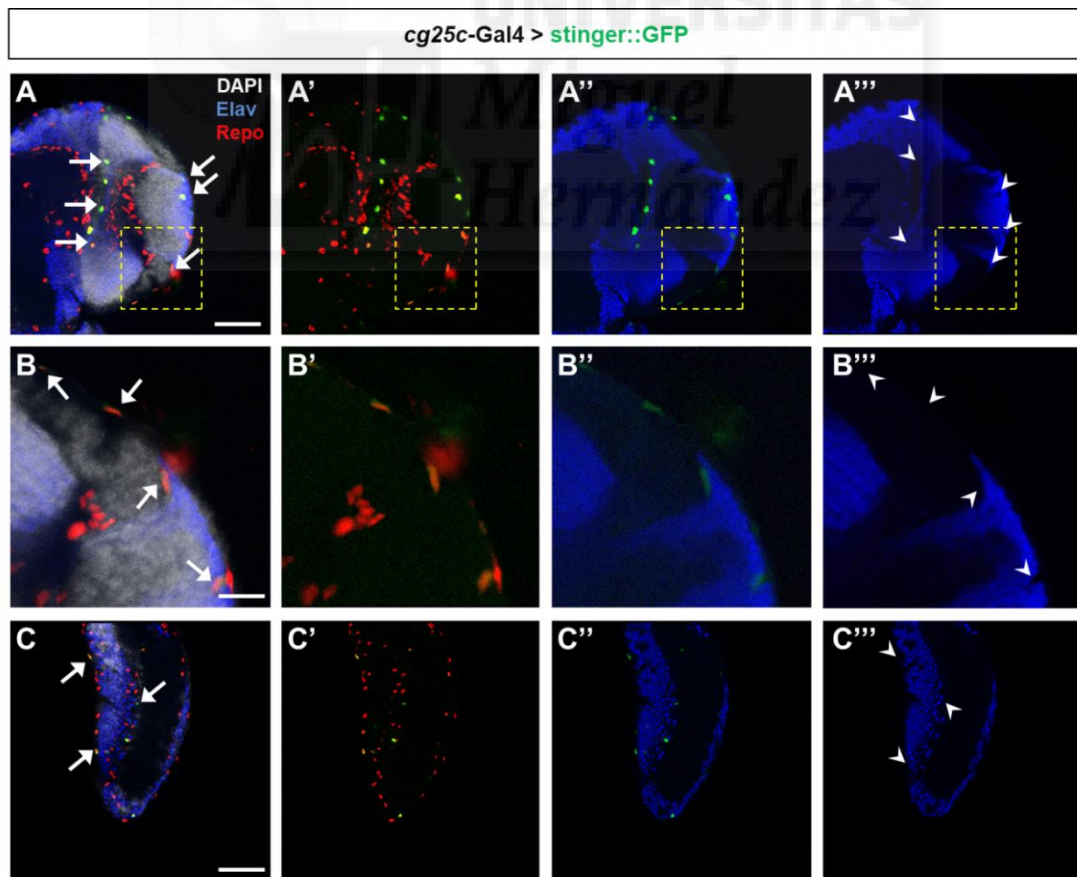


**Figure S2. *cg25c-Gal4* promoter is expressed in brain glia but not in neurons.** Confocal images of *cg25c-Gal4* driving the expression of nuclear fluorescent protein (UAS-*stinger::GFP*). In brain lobes (A-A'', B-B'') cells where the promoter is expressed (green) colocalise (arrows) with the glial antibody anti-Repo (red) but not with the neural (arrowheads) antibody anti-Elav (blue). (C-C'') The same happens in the ventral nerve cord. DAPI (grey) stains cells' nuclei. Lobes are from a late 3<sup>rd</sup>-IL (A,B) and the ventral nerve cord from early 3<sup>rd</sup>-IL (C). The yellow box in (A-A'') indicates the magnified OPC. Scale bars represent 50  $\mu\text{m}$  in (A), 20  $\mu\text{m}$  in (B) and 100  $\mu\text{m}$  in (C).

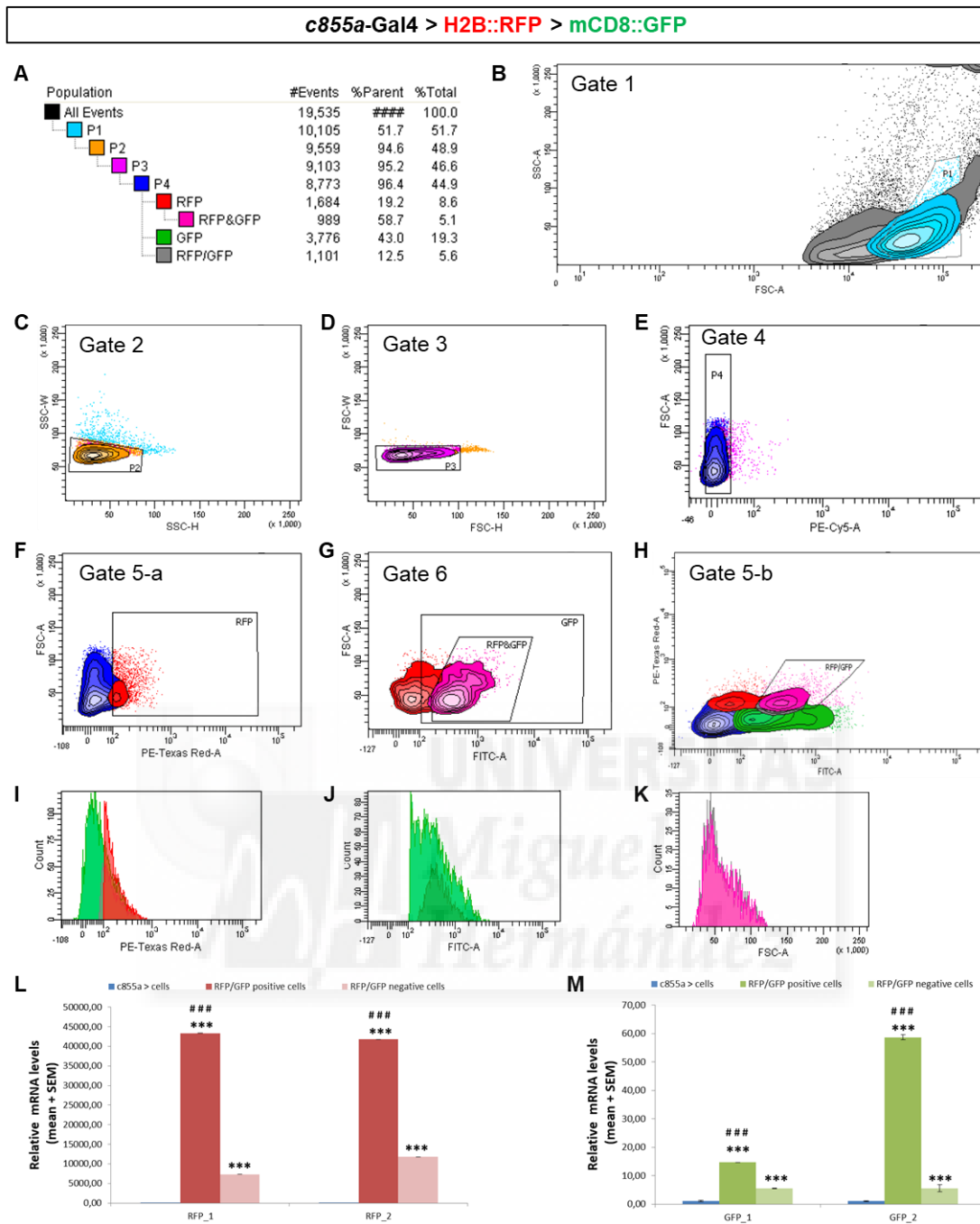


**Figure S3. Different approaches for identifying double fluorescent cells in FACS.** Populations of L3 lobe neuroepithelial cells (*c855a-Gal4*) expressing dual fluorescence in red (UAS-H2B::RFP) and green (UAS-mCD8::GFP) can be isolated by FACS. **(A)** Representative flow cytometry data to illustrate different gating strategies for purification of double fluorescent cells. **(B)** Total events plotted in side scatter area (SSC-A) and forward scatter area (FSC-A, log) allows for the discrimination of debris and cell clusters. Low SSC-A population allows for the definition of P1 (in cyan, Gate 1). **(C)** Plot of SSC width vs. height for P1 events, allowing the removal of complex cells and the visualisation of P2 (in orange, Gate 2). **(D)** P2 events plotted in FSC width vs. height discard cells by size and define P3 (in purple, Gate 3). **(E)** P3 events plotted in FSC-A and phycoerythrin (PE-Cy5, log) allows for the visualization of the incorporation of the marker 7-aminoactinomycin D (7-AAD) and permits discarding of dying or membrane-compromised positive cells. Then, individual living cells are defined in P4 (in blue, Gate 4). At this point two equivalent strategies of gating P4 fluorescent cells can be used. On one hand, **(F)** P4 can be plotted in FSC-A vs. RFP (PE-Texas Red-A, log) to pick up the RFP<sup>+</sup> population (in red, Gate 5-a); **(G)** then RFP<sup>+</sup> population is plotted in FSC-A vs. GFP (FITC-A) to distinguish the RFP<sup>+</sup>&GFP<sup>+</sup> population (in pink, Gate 6). Alternatively, **(H)** P4 may be plotted in a graph where RFP and GFP fluorescence are represented separately to distinguish the RFP<sup>+</sup>/GFP<sup>+</sup> population (in grey, Gate 5-b). Both strategies clearly gate the same double-fluorescent positive cells as shown by the fluorescent population in counts **(I, J)** and the superposition of both cell populations when counts vs. FSC-A is plotted in **(K)**. **(L, M)** Quantitative PCR is used as quality control for the sorted RFP<sup>+</sup>/GFP<sup>+</sup> population. mRNA levels for RFP and GFP show that both fluorescences are present and these mRNA levels are significantly higher than those for the control *c855a-Gal4* (\*\*\*) P-value < 0,001) and the fluorescent-negative population sorted (### P-value < 0,001).

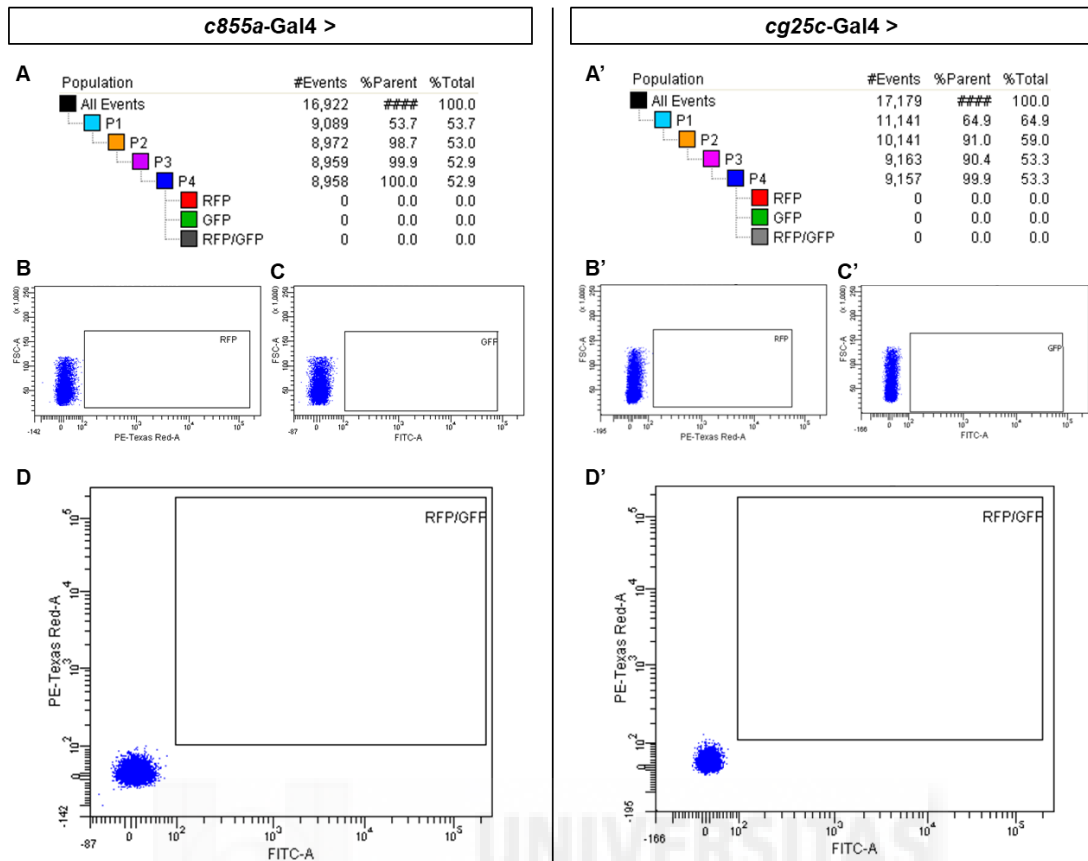


**Figure S4. FACS negative controls show that cells expressing only niche drivers do not present any autofluorescence.** Cell sorting for *c855a-Gal4* and *cg25c-Gal4* L3 brains reveals no autofluorescence caused by promoters. Gating (**A-A'**) by RFP (**B-B'**) and GFP (**C-C'**) fluorescence shows no natural emission of light by driving transgenes in sorted cells (**D-D'**). Graph axes are the same as in Figure S3.

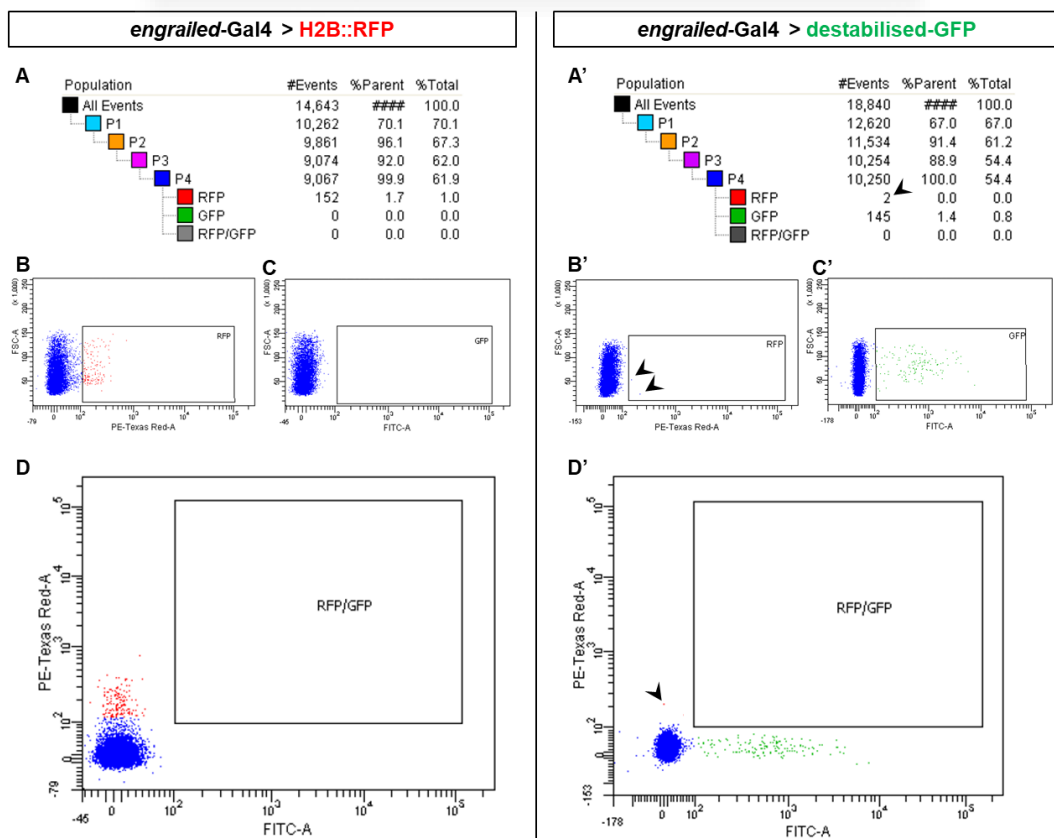


**Figure S5. FACS positive controls for reporter transgene expression with non-niche drivers.** Fluorescent sorting of cells in which the imaginal wing disc promoter *engrailed*-Gal4 drives the expression of red (UAS-H2B::RFP) and green (UAS-destabilised-GFP). Gating (A-A') with RFP (B-B') and GFP (C-C') fluorescence reveals the proper function of labelling proteins (D-D') using drivers other than those used in niche cells. Although some expression of crossing fluorescence may happen (arrowheads in *engrailed*>destabilised-GFP), this problem is solved with the dual fluorescence gating (D'). Graph axes are the same as in Figure S3.

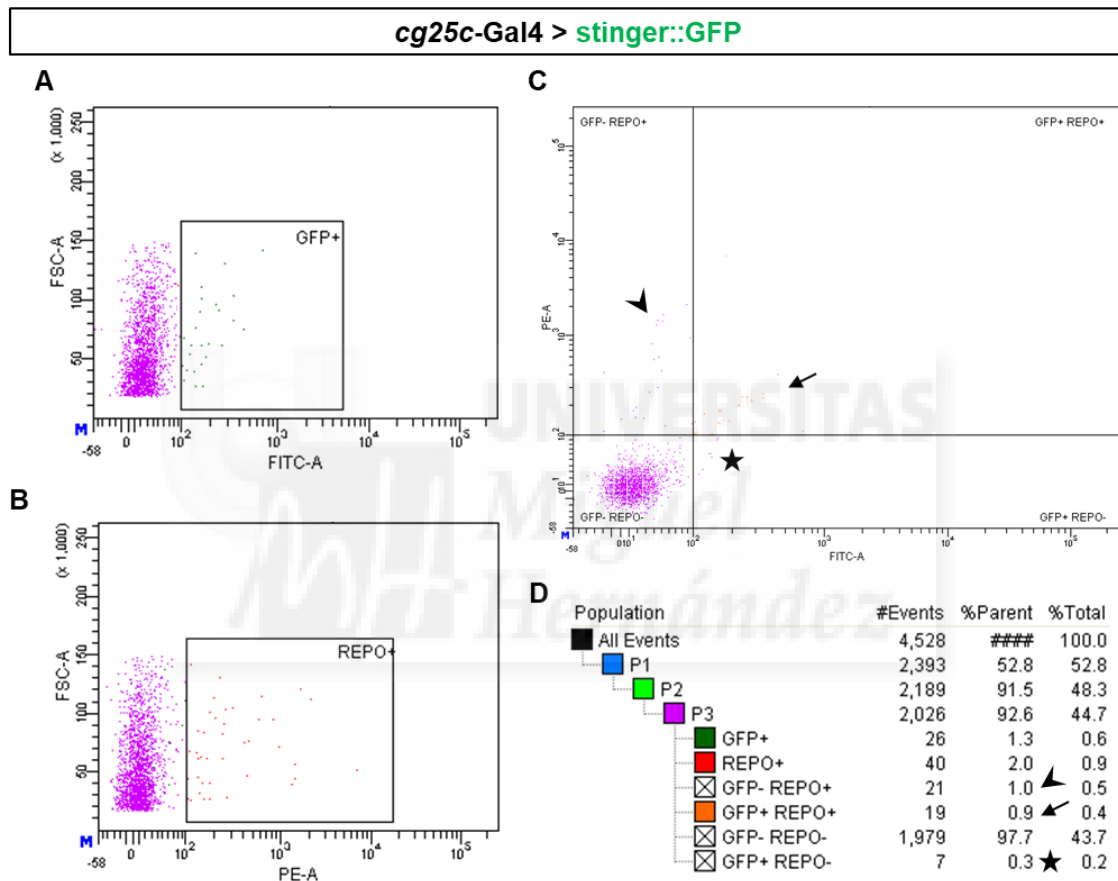
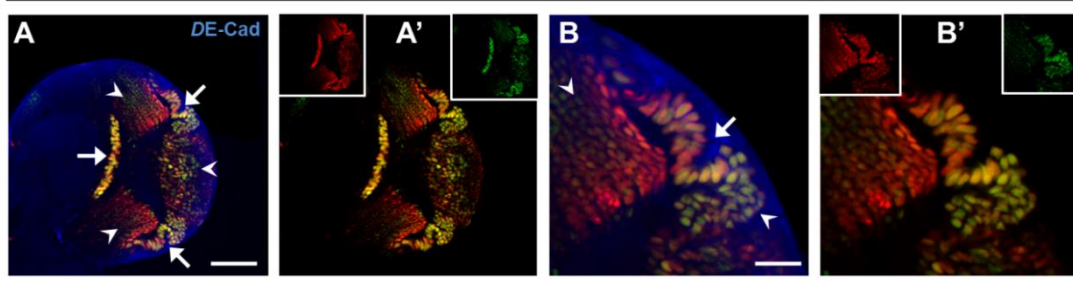
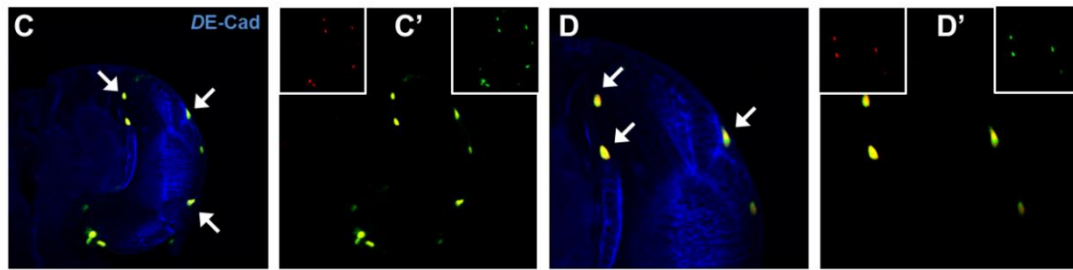


**Figure S6. Immunostaining of disaggregated brain lobes reveals glial cells standard in FACS.** Brain cells in suspension with the genotype *cg25c-Gal4*>*stinger::GFP* (A) are stained following a standard protocol with the glial antibody for Repo in red (B). (C,D) The majority of green fluorescent positive cells are also labelled with the glial marker (arrows); glial cells that are not *cg25c*<sup>+</sup> (arrowheads) and thus do not express the GFP are discarded. Cells that are positive for green fluorescence but not glial markers (asterisks) may be autofluorescent because of the immunostaining; in any case, those cells are not collected. Graph axes are the same as in Figure S3.

**c855a-Gal4 > H2B::RFP > stinger::GFP**



**cg25c-Gal4 > H2B::RFP > stinger::GFP**



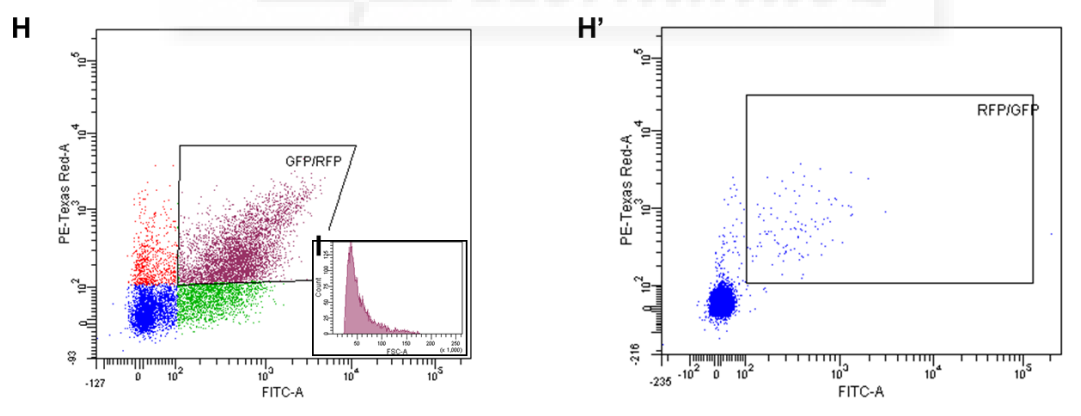
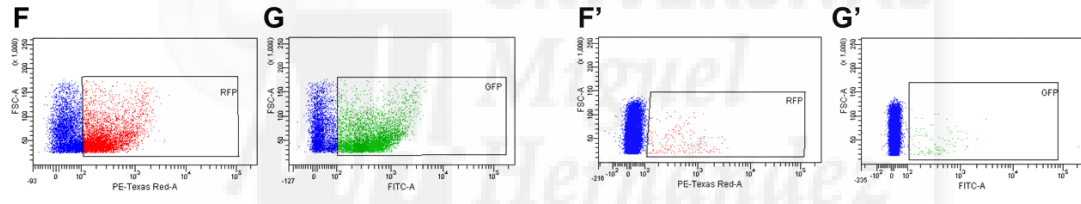
**c855a-Gal4 > H2B::RFP > stinger::GFP**

**cg25c-Gal4 > H2B::RFP > stinger::GFP**

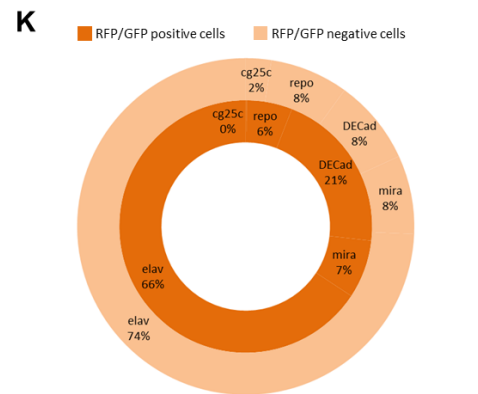
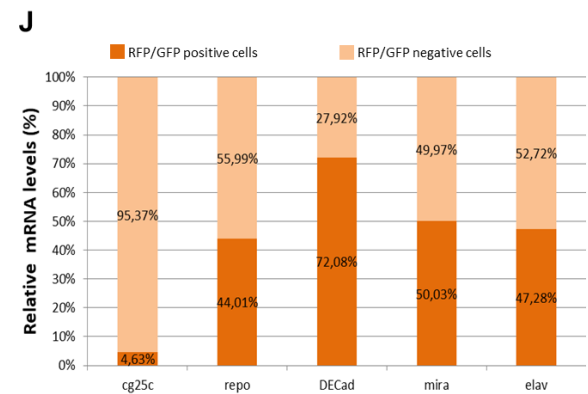
Population	#Events	%Parent	%Total
All Events	20,331	###	100.0
P1	11,671	57.4	57.4
P2	10,519	90.1	51.7
P3	10,070	95.7	49.5
P4	10,067	100.0	49.5
RFP	5,238	52.0	25.8
GFP	6,319	62.8	31.1
GFP/RFP	4,400	43.7	21.6

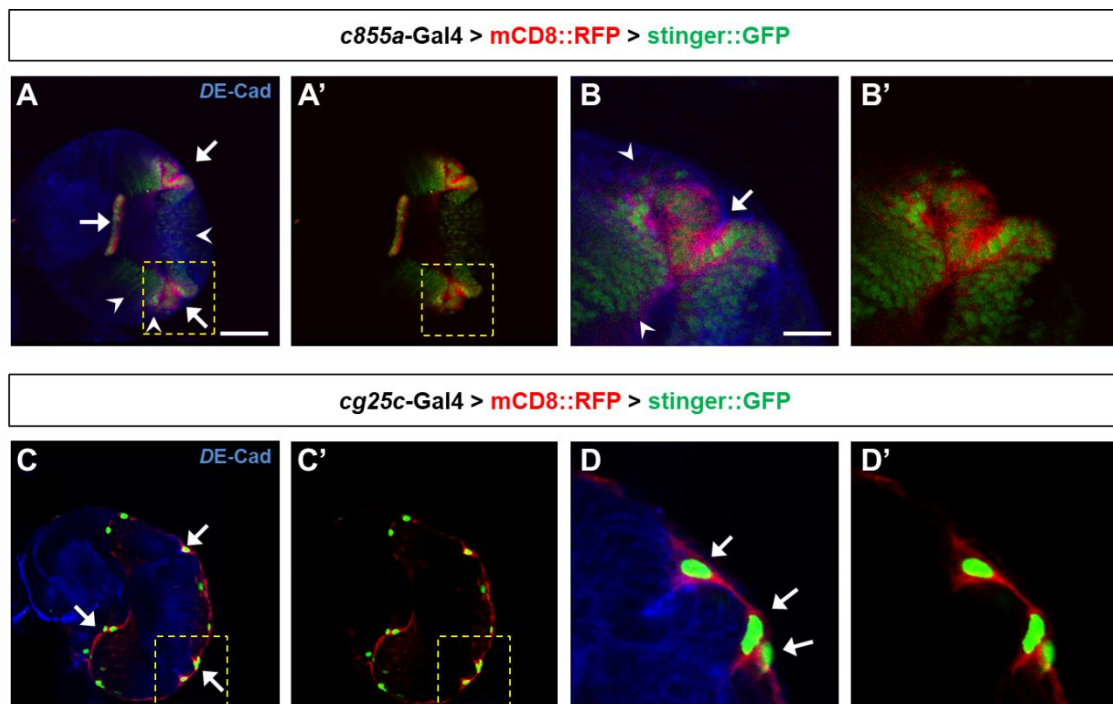
Population	#Events	%Parent	%Total
All Events	55,369	###	100.0
P1	35,613	64.3	64.3
P2	33,323	93.6	60.2
P3	30,645	92.0	55.3
P4	30,616	99.9	55.3
RFP	186	0.6	0.3
GFP	110	0.4	0.2
RFP/GFP	104	0.3	0.2



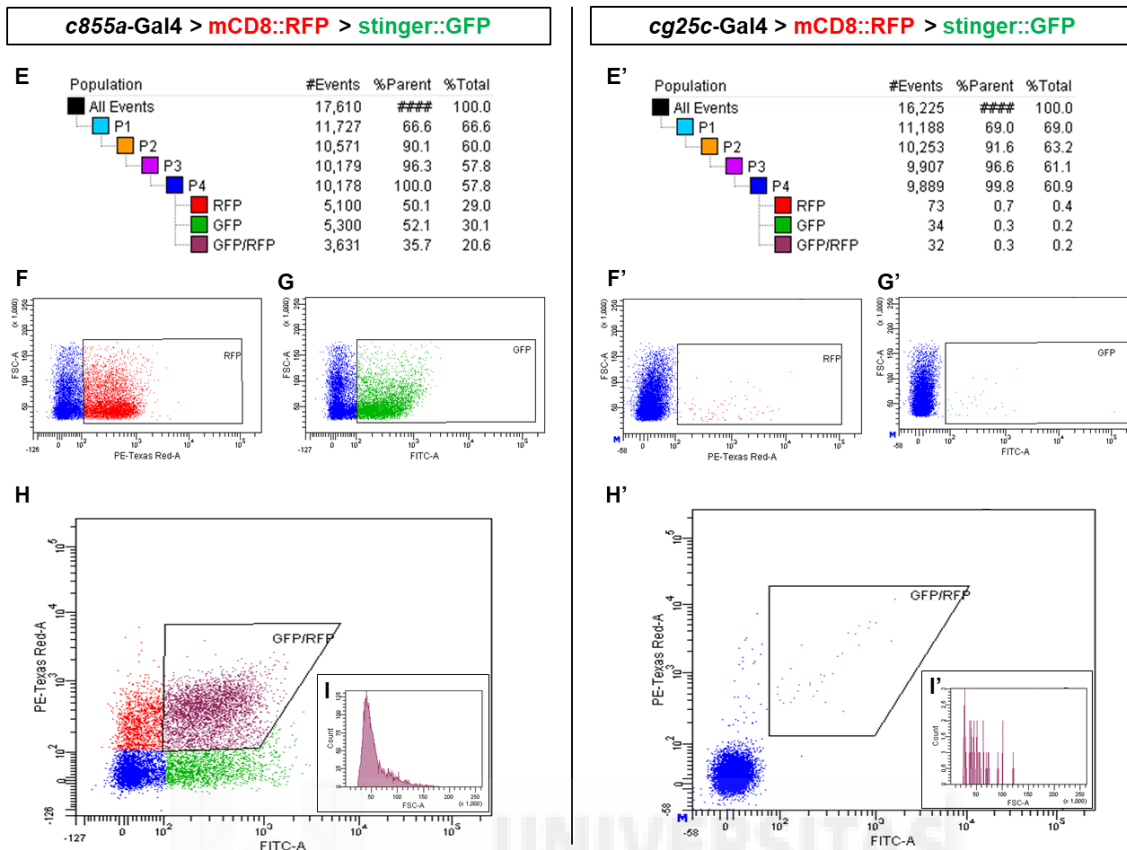
**c855a-Gal4 > H2B::RFP > stinger::GFP**



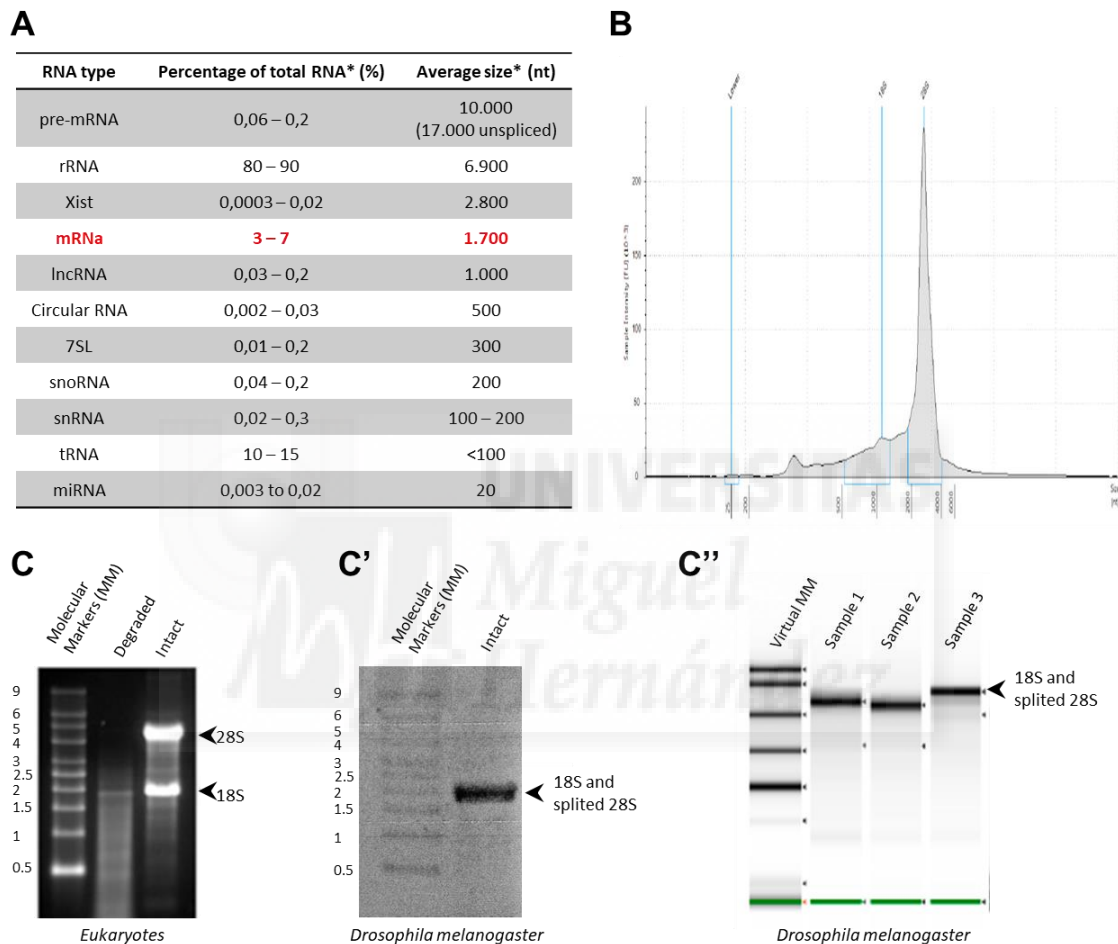
**Figure S7. Dual nuclear marker works for mature cells but not for progenitor cells in FACS.** (A-D) Confocal images of nuclear reporters double-fluorescent for red (UAS-H2B::RFP) and green (UAS-stinger::GFP) for the neuroepithelial driver *c855a-Gal4* and the glial driver *cg25c-Gal4* in the larval optic lobe. (A-A',B-B') Nuclear fluorescent markers label neuroepithelial cells (NECs, arrows) and their progeny (arrowheads) due to the perdurance phenomenon. (C-C',D-D') Those fluorescent reporters function properly in fully differentiated cells such as glia (arrows). NECs and neuropil are marked with anti-DE-Cad antibody (blue). Scale bars represent 50  $\mu\text{m}$  in (A) and 20  $\mu\text{m}$  in (B). Gating (E,E') nuclear reporters for UAS-H2B::RFP (F,F') and UAS-stinger::GFP (G,G') may be applied for the glial driver *cg25c-Gal4* (H') obtaining around 175 cells per larval brain (0,3%). However, with the neuroepithelial driver *c855a-Gal4* (H) the percentage of double fluorescent cells is high (43,7%) meaning the approximately 4.500 cells isolated per larval brain not only are progenitors but also all their progeny (I). Graph axes are the same as in Figure S3. (J-K) Quantitative PCR is used to identify the *c855a-Gal4* labelled population. (J) Relative mRNA levels in the positive and negative cells shows that the sorted population contain the mayor of neuroepithelial cells (*DECad*) but also a high number of neuroblasts (*mira*), neurons (*elav*) and glia (*repo*). However, *cg25c*<sup>+</sup> cells are correctly separated. (K) Inside the positive sorted population the majority of cells were neurons (66%), followed by neuroepithelial cells (21%), and finally neuroblasts (7%) and glia (6%). Thus, the double nuclear labelling is not suitable for the neuroepithelial driver.



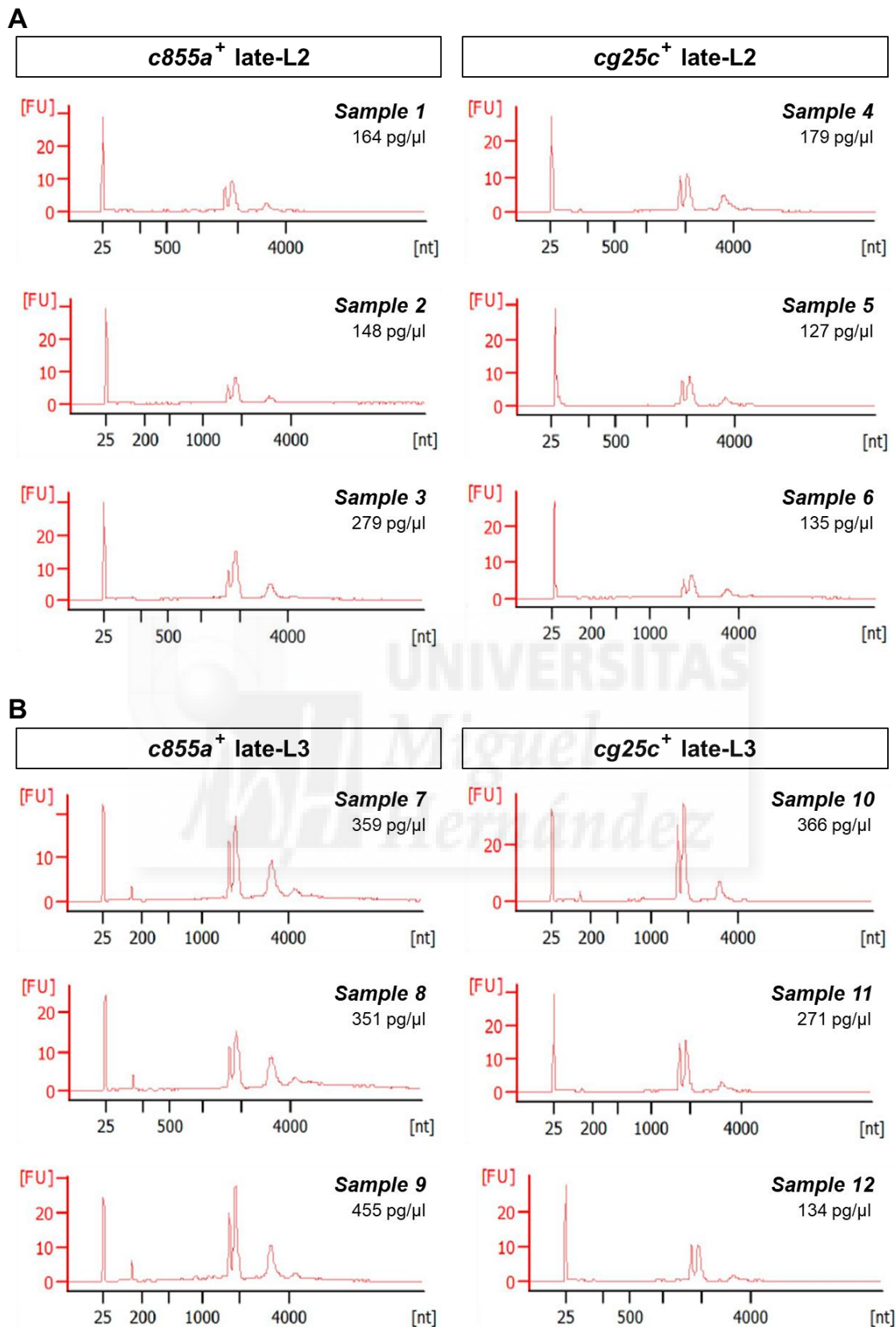




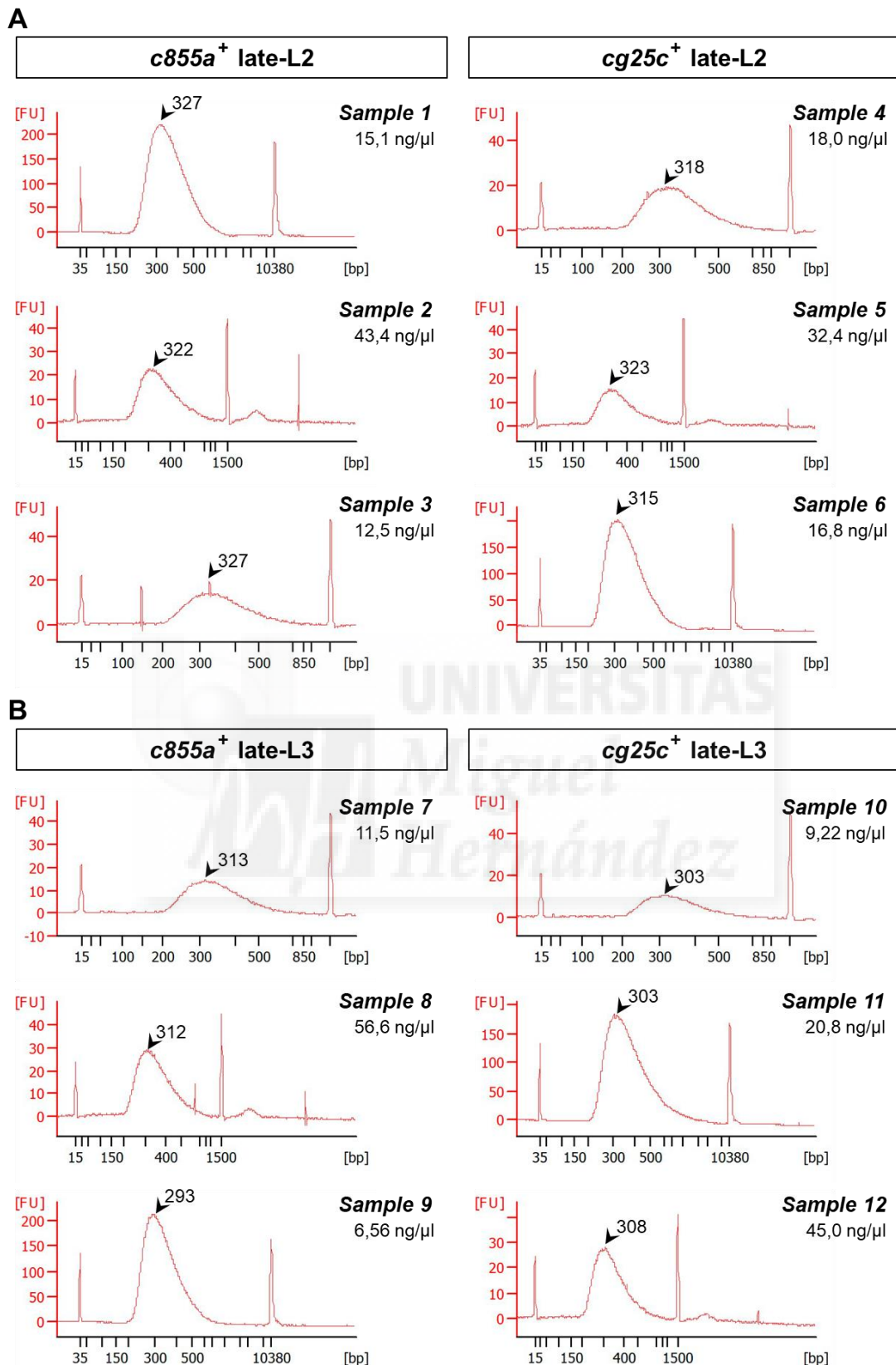
**Figure S8. Membranal and nuclear dual marker works for mature cells but not for progenitor cells in FACS.** (A-D) Confocal images of membranal (UAS-mCD8::RFP) and nuclear (UAS-stinger::GFP) fluorescent reporters for the neuroepithelial driver *c855a*-Gal4 and the glial driver *cg25c*-Gal4 from larval optic lobe. (A-A', B-B') Nuclear (green) and membranal (red) fluorescent markers label neuroepithelial cells (NECs, arrows) and their progeny (arrowheads) due to the perdurance phenomenon. (C-C', D-D') These fluorescent reporters work properly in fully differentiated cells such as glia (arrows). NECs and neuropil are marked with anti-DE-Cad antibody (blue). The yellow box in (A-A') and (C-C') indicates the magnified OPC. Scale bars represent 50  $\mu$ m in (A) and 20  $\mu$ m in (B). (E-H) FACS plots for the glial and the neuroepithelial drivers. Gating (E, E') using the membranal reporter UAS-CD8::RFP (F, F') and the nuclear reporter UAS-stinger::GFP (G, G') may be applied for the glial driver *cg25c*-Gal4 (H') obtaining a population with similar characteristics (I'). However, with the neuroepithelial driver *c855a*-Gal4 (H) the double fluorescent cells isolated are not only progenitors but also all their progeny (I). Thus, the double nuclear and membranal labelling is not suitable for the neuroepithelial driver. Graph axes are the same as in Figure S3.



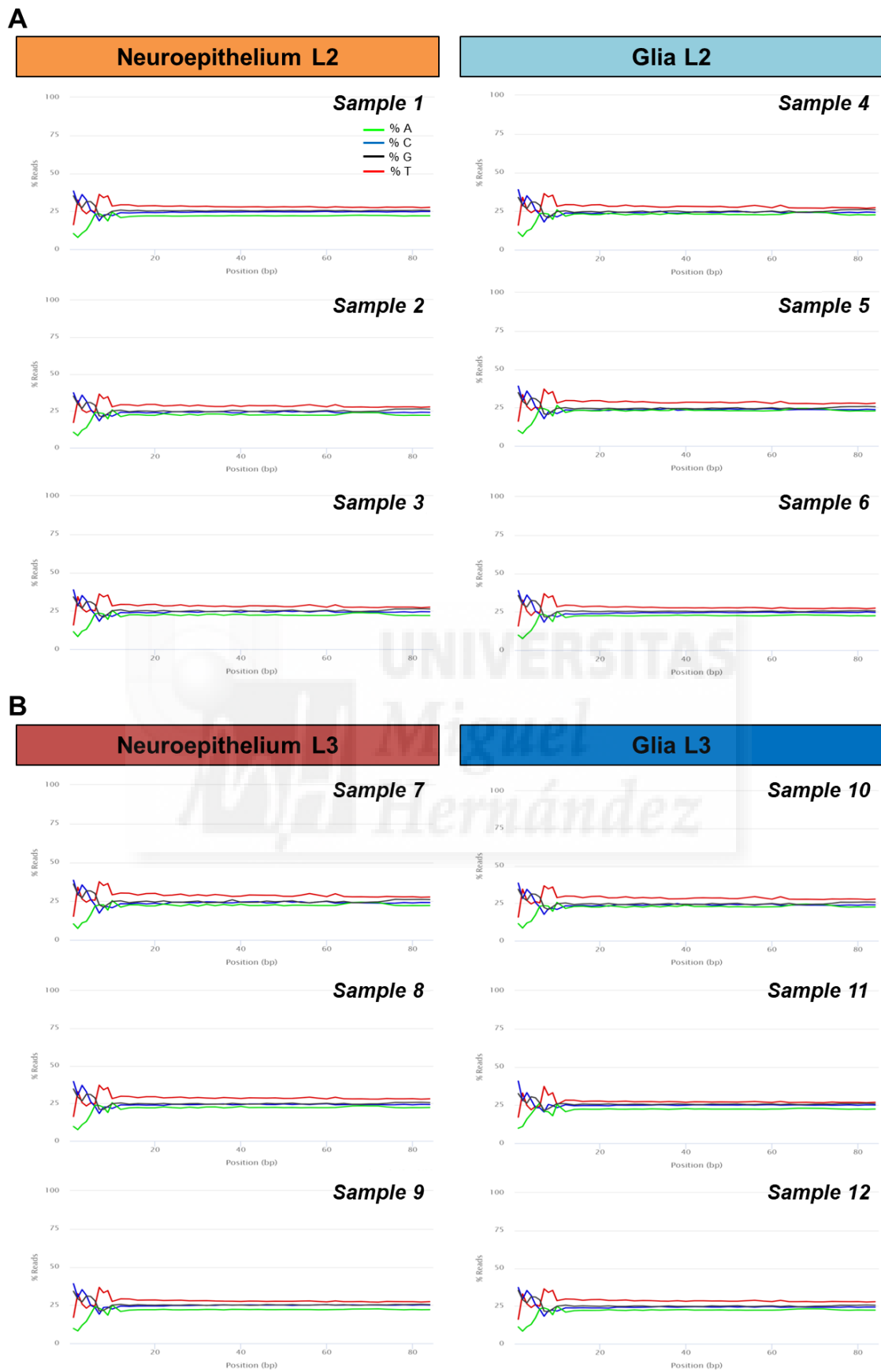
**Figure S9. RNA integrity evaluation in *Drosophila melanogaster*.** (A) Total eukaryotic RNA includes fragments of different lengths, ranging from 20 to thousands of nucleotides. Among these fragments is the messenger RNA (mRNA) polyA fragment used for cell expression profiling. (B) Graph of total *Drosophila* RNA fragments after whole larva RNA extraction measured by TapeStation 4200 (Agilent). (C-C'') Because mRNA comprises only ~3-7% of total RNA, it is difficult to detect in electrophoresis gel; ribosomal RNA (rRNA), which represents ~80-90%, is used instead for integrity. In eukaryotes (C) RNA is considered intact when two fragments of different molecular weights, 28S and 18S, are detected and the RIN ratio (28S:18S) is 2:1 (adapted from Thermo Fisher Scientific Protocols). However, in *Drosophila* (C'), it is not possible to use this ratio due to the fact that the 28S fragment splits into two fragments of similar weight to the 18S fragment and thus a single band appears on the gel. The virtual agarose gel (C'') performed in TapeStation also shows this. Other methodologies must be used to demonstrate RNA integrity.



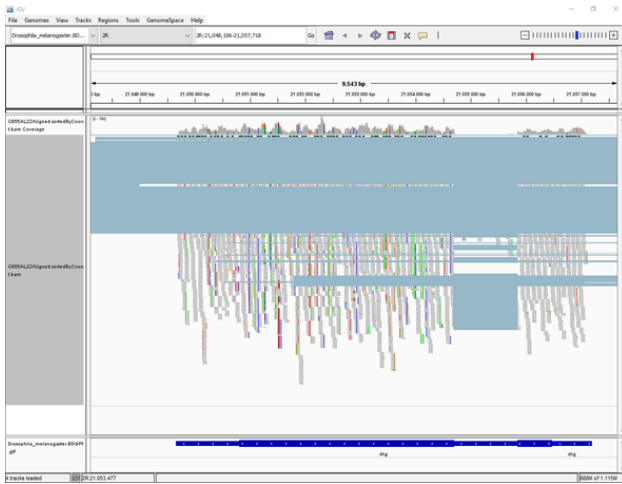
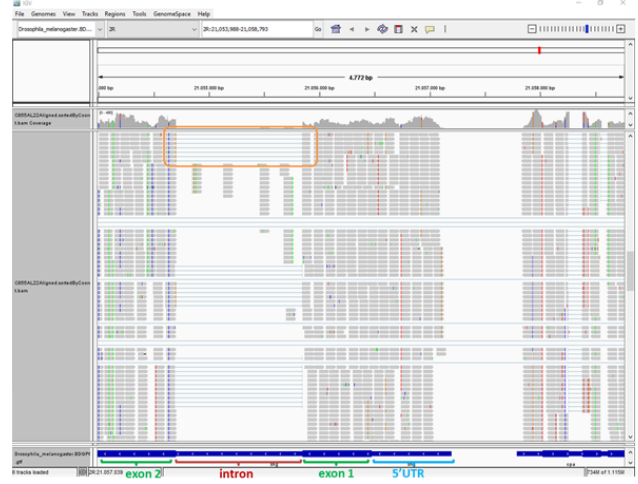
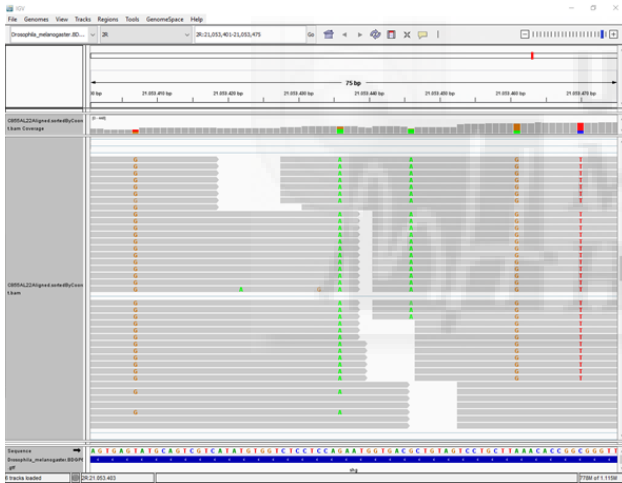
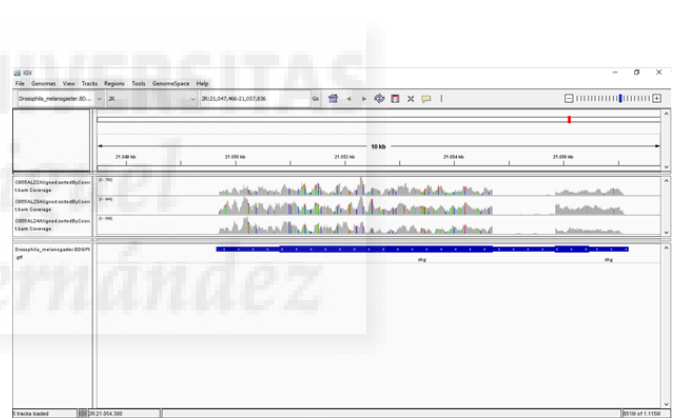
**Figure S10. RNA quality and quantity evaluation of FACS sorted population.** Total RNA amount and quality measurements from the 12 samples sorted in FACS. Peaks detected from the neuroepithelial (*c855a*<sup>+</sup>) and the glial (*cg25c*<sup>+</sup>) populations from late L2 (**A**) and late L3 (**B**) stages are of good quality and are concentrated enough to prepare the cDNA library. Three biological replicates per each condition are used. Concentration was obtained with a 2100 Bioanalyzer (Agilent Technologies) and also the electropherogram where the axes represent fluorescence intensity [FU] and fragment size [nt].



**Figure S11. Quality and quantity evaluation of cDNA library for pooling.** Total cDNA amount and quality measurements of the library constructed from the 12 samples of double-stranded cDNA. Peaks detected from the neuroepithelial (*c855a*<sup>+</sup>) and the glial (*cg25c*<sup>+</sup>) populations from late L2 (**A**) and late L3 (**B**) stages are of good quality and are concentrated enough for sequencing. Three biological replicates per each condition are used. The average fragment size (arrowhead) is given per each sample and has an average of 314 bp for pooling. The concentration was measured with a Qubit 2.0 fluorometer (Invitrogen) and the pool average was 8,78 ng/μl. The electropherogram was with a 2100 Bioanalyzer (Agilent Technologies) and the axes represent fluorescence intensity [FU] and fragment size [bp].



**Figure S12. RNA sequencing quality control per base sequence content.** Proportion in each base sequence position of the four DNA bases: adenine (A, in green), cytosine (C, in blue), guanine (G, in black), and thymine (T, in red). Either neuroepithelial or glial sequences from L2 (A) or L3 (B) stage maintain a proportion of the different bases (around 25% of the reads) as expected in a random library. Sample's colours by condition are the same in Figure 27. Graphs made with MultiQC software.

**A****B****C****D**

**Figure S13. Display of aligned sequences with the *Drosophila melanogaster* reference genome.** Example of *Sample 1* reads aligned with the fruit fly reference genome which matches with the *DE-Cad* gene (a.k.a. *shg*) shown in IGV viewer. **(A)** Gene coverage from the total amount of aligned fragments. **(B)** Reads directionality from 5'UTR are aligned into exons leaving mostly the intron uncovered. Circled reads belong to two exons due to sequence fragmentation. **(C)** A detailed visualisation of the reads at the nucleobase level reveals some base mismatching as a bias of the run sequencing. However, this does not disturb the downstream process. **(D)** Several biological replicates can be compared along the genome to overview their expression pattern.

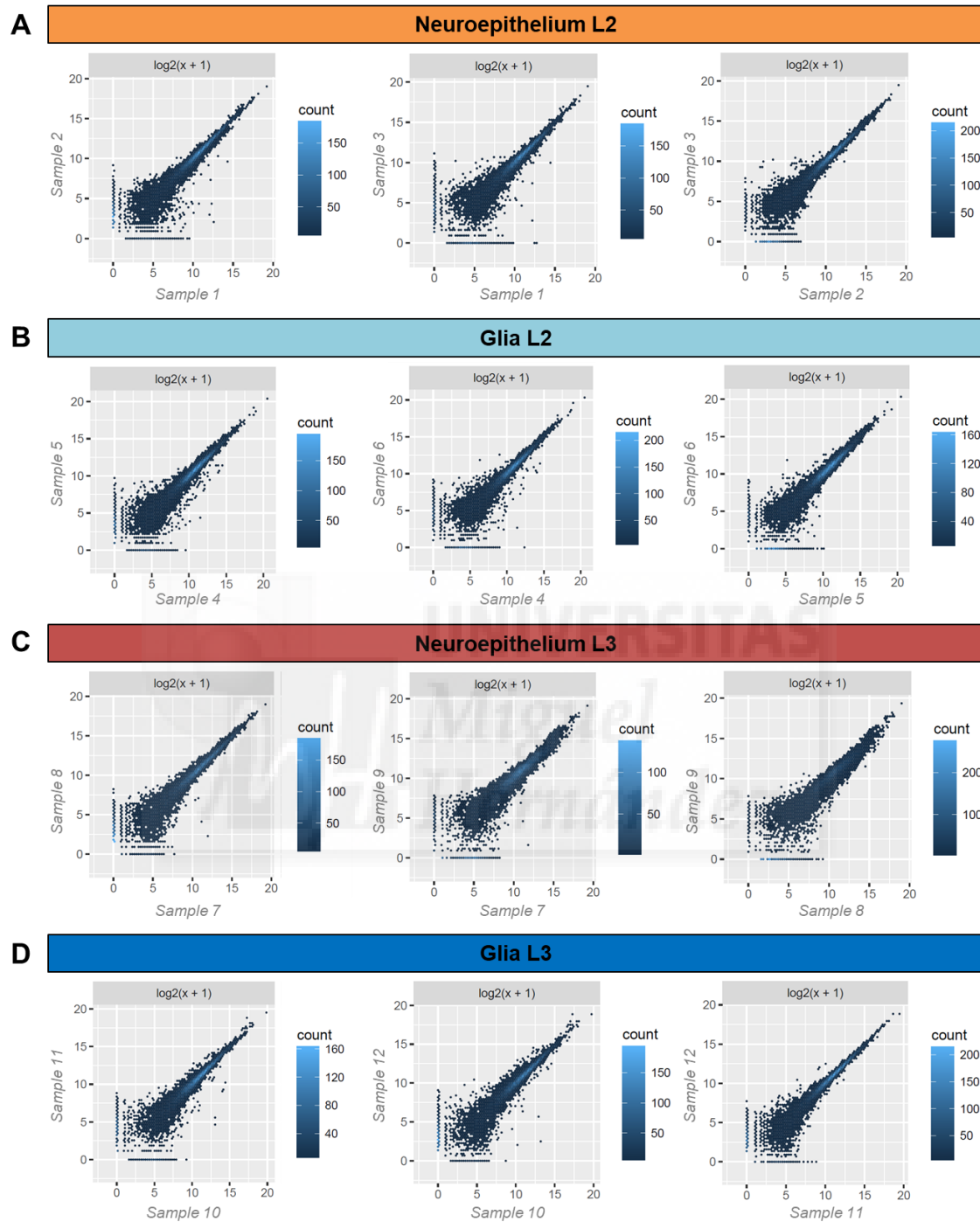
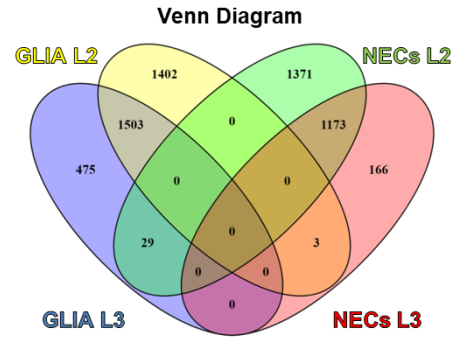


**Figure S14. Scatterplot of logarithmic normalised counts between two replicates from the same condition.** When plotting  $\log_2$  count values (after adding 1 to avoid the log of zero), the genes with lower counts are very variable. This issue is solved when the values are transformed with an  $r\log$  function. (A-D) Biological replicates from different larval periods are exposed for neuroepithelium and glia. Sample colours by condition are the same as in Figure 27.

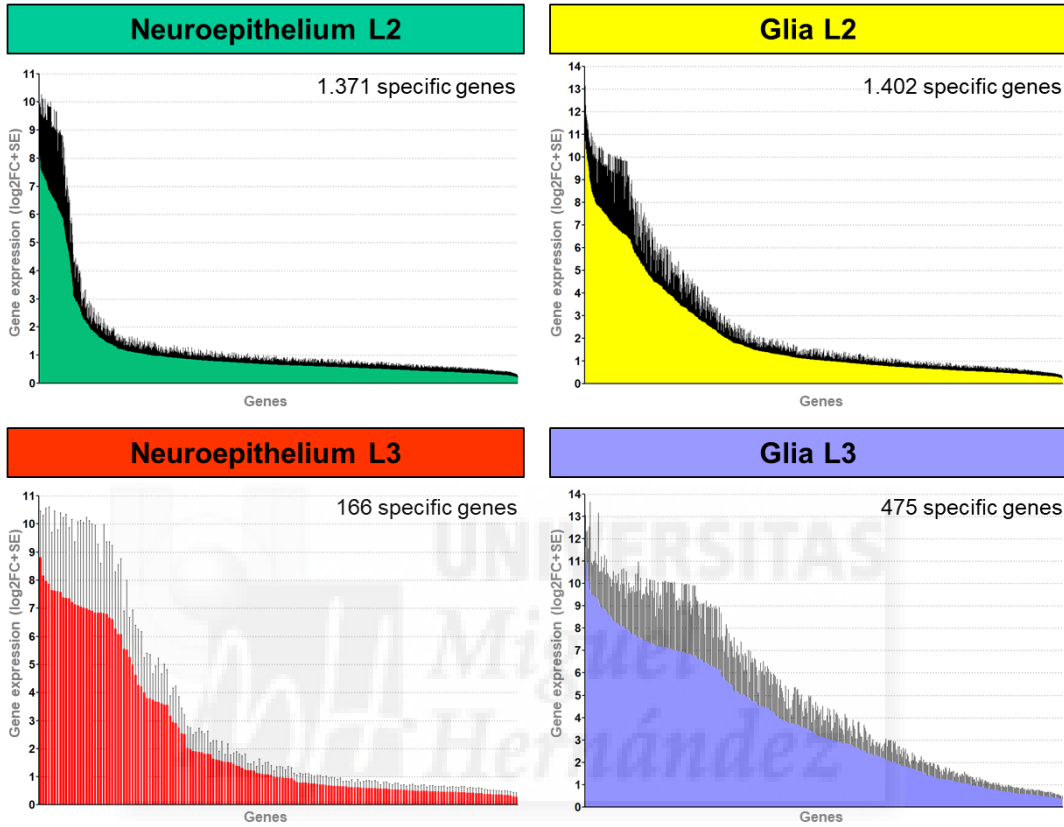
**A**

Input data analysed

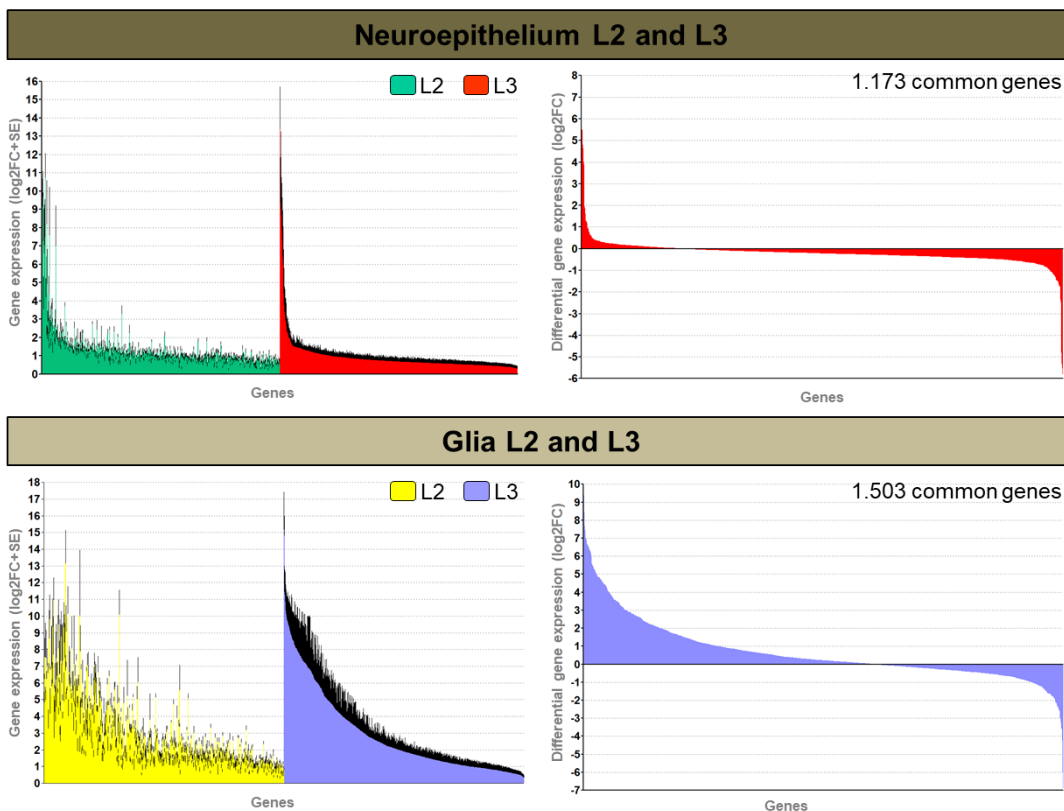
Condition	Number of DE genes	Total genes per stage	Overall number of unique genes
NECs L2	2.573	5.481	6.122
Glia L2	2.908		
NECs L3	1.342	3.349	
Glia L3	2.007		



**B**

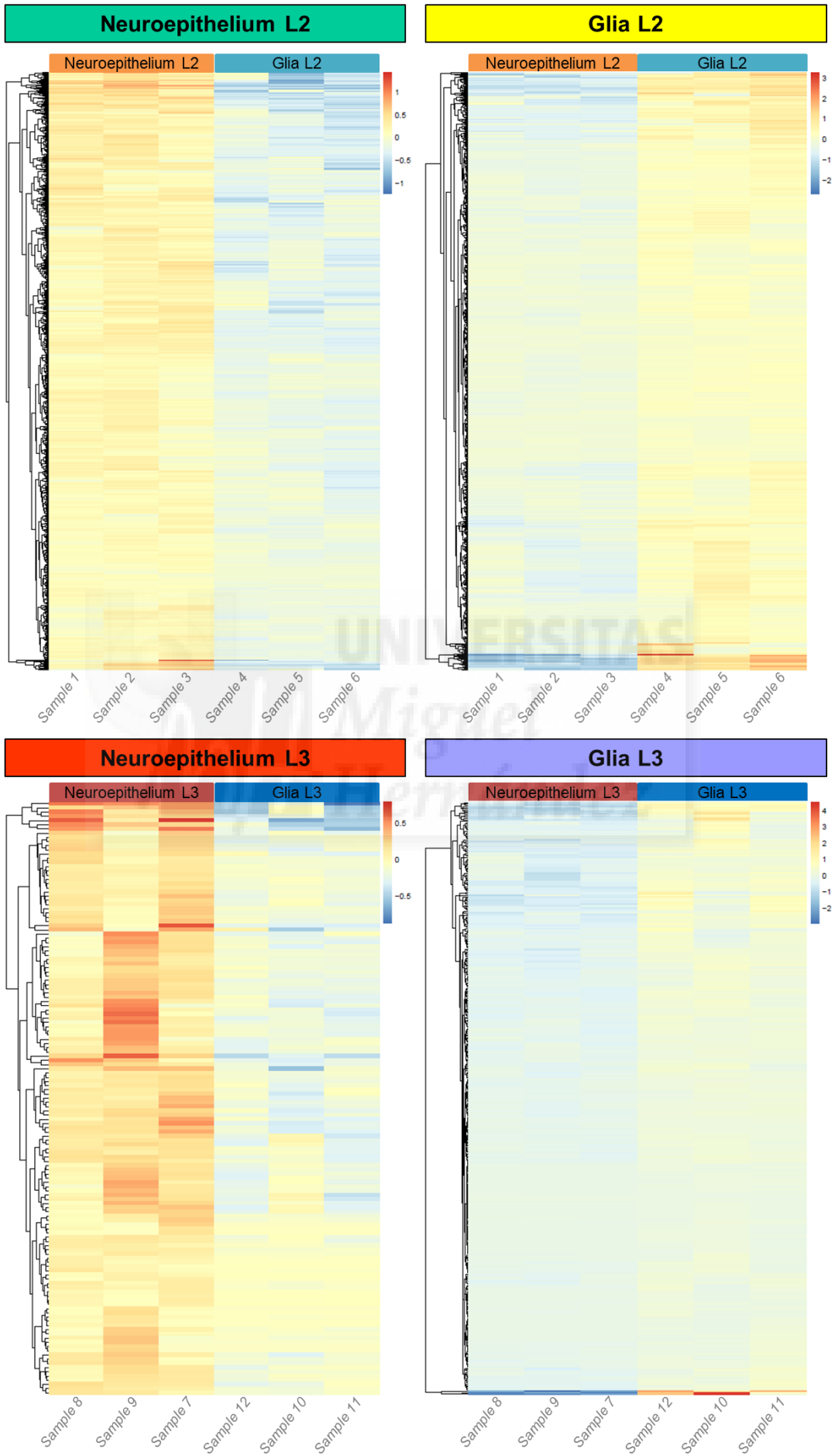


**C**





D



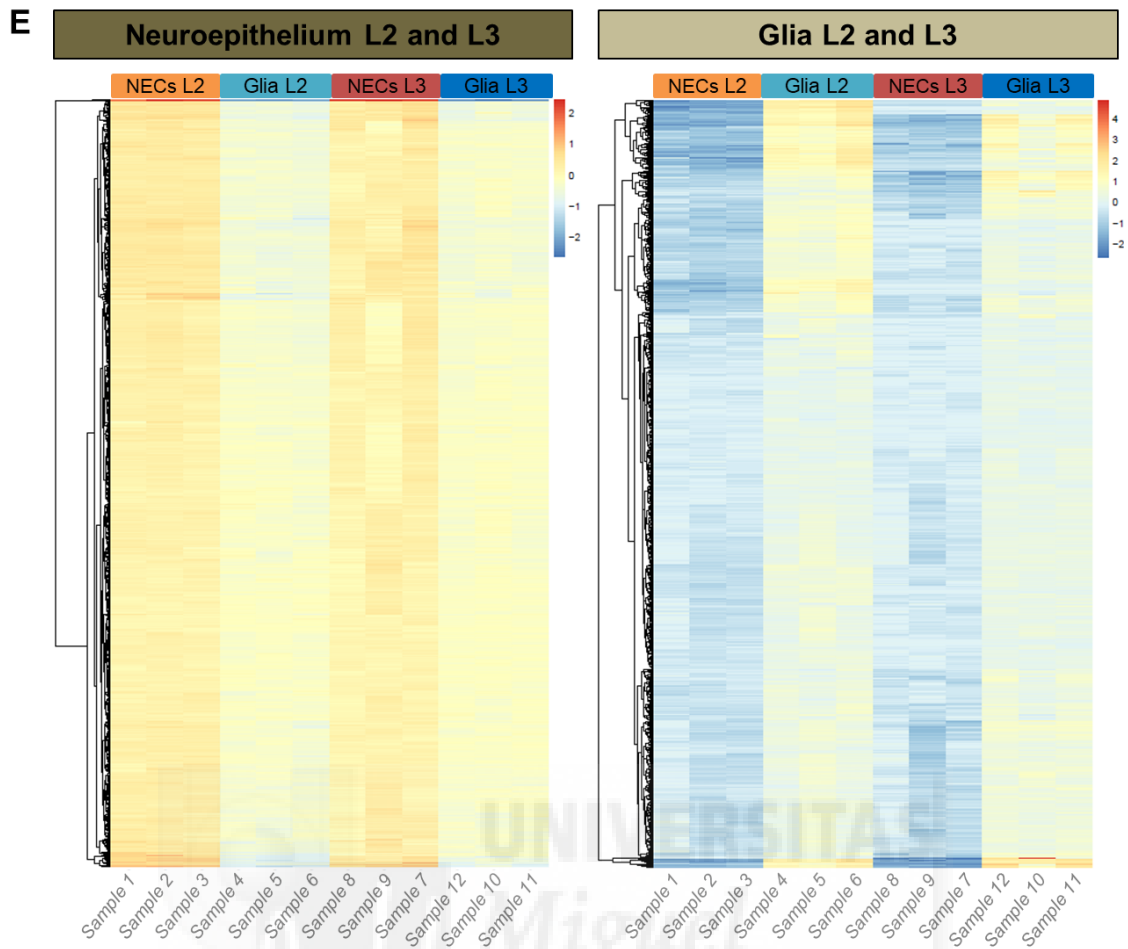


**Figure S15. Stage-specific gene expression by population on the cell type differential expression approach. (A)** Venn diagram shows all the possible relationships between the four conditions of differential gene expression. **(B)** Gene expression per each condition shows top specific genes which are potential markers. **(C)** Gene expression per cell type shows common specific genes which are potential cell-specific markers. Measuring their differential expression shows those which are more active in L2 (negative values) or in L3 (positive values), which indicates possible time specificity. **(D,E)** Gene clustering in heatmaps of Venn diagram groups reveals those genes with highest variance of relative *rlog*-transformed values across samples. Sample colours by condition are the same as in Figure 27. Grouped genes' colours are the same as in Venn diagram **(A)**.

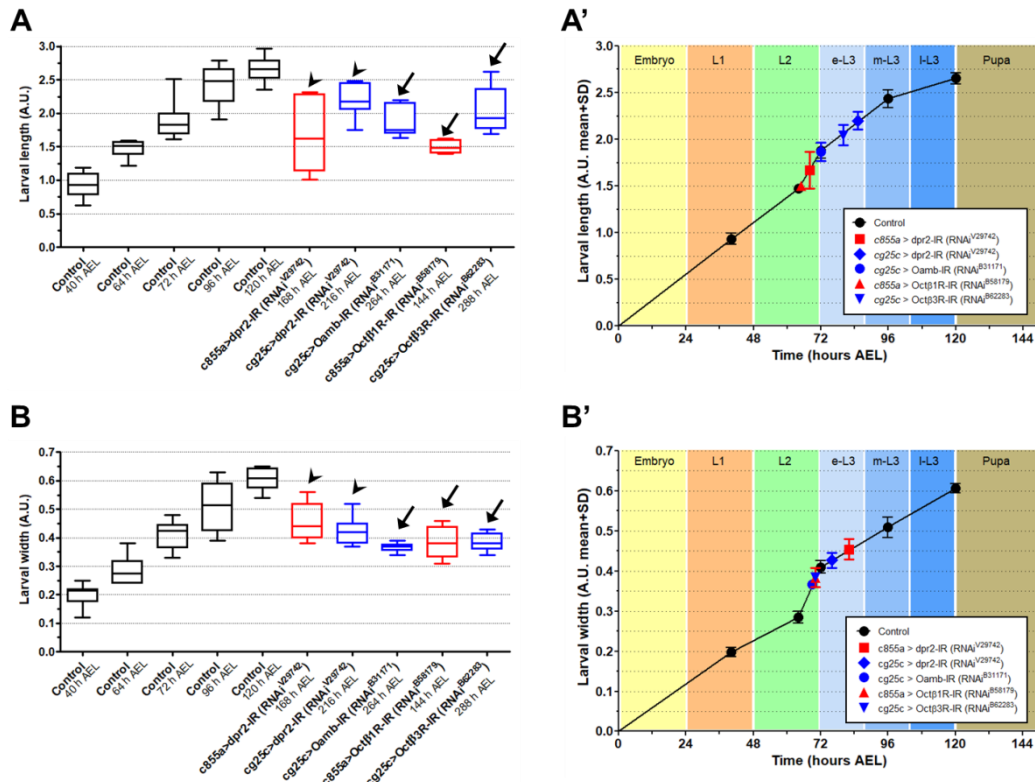


**Figure S16. Size of dysfunctional genes with arrested phenotype in larval stage.** Down-regulation of the genes *dpr2* (arrowheads) and octopamine receptors (*Oamb*, *Octβ1R* and *Octβ3R*; arrows) in *c855a*<sup>+</sup> (data in red) and *cg25c*<sup>+</sup> (data in blue) cells cause arrest during larval development. (A-B) Different size phenotypes are detected in those arrested larva when are compared by length (A-A') and width (B-B'). Underexpression of *dpr2* in niche cells causes different larval length but similar width. Larvae underexpressing octopamine receptors in niche cells shows similarities in arrested stage by length and width.

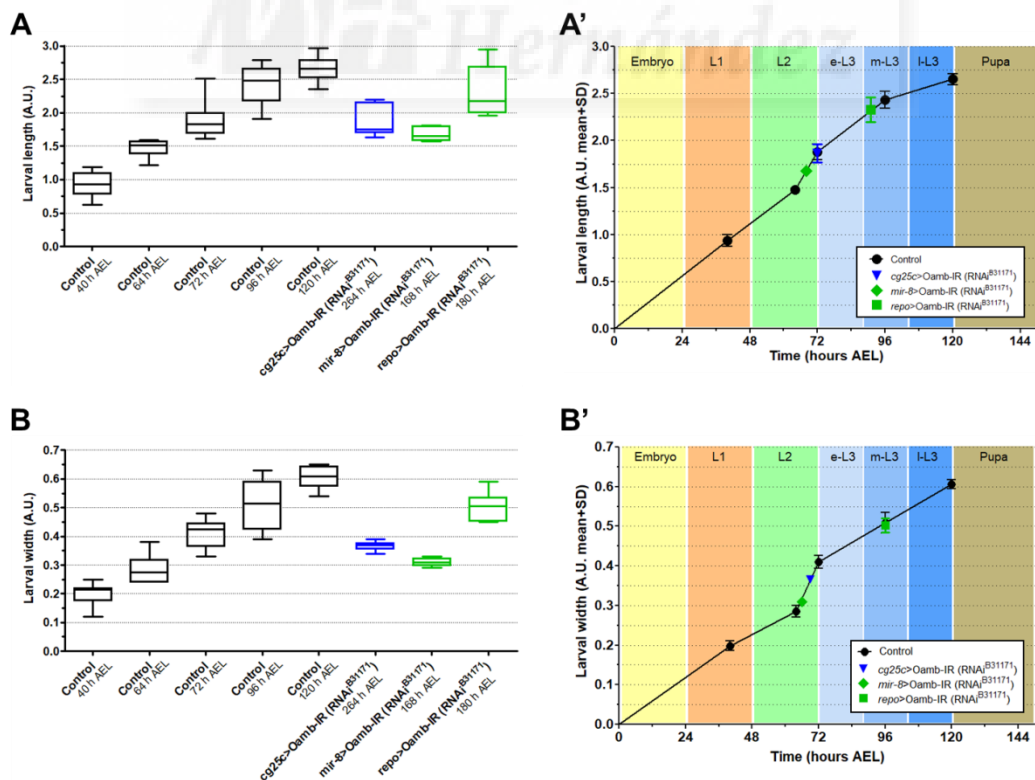


**Figure S17. Size of arrested larvae caused by dysfunctional *Oamb* expression in glia.** Down-regulation of the receptor *Oamb* in *miR-8*<sup>+</sup> and *repo*<sup>+</sup> glial cells (data in green) cause stage arrest during larval development as well as happens in *cg25c*<sup>+</sup> cells (data in blue). (A-B) Different size phenotypes are detected in those arrested larva when are compared by length (A-A') and width (B-B'). Underexpression of *Oamb* reveals larvae similarities when there are defects in *cg25c*<sup>+</sup> cells and *miR-8*<sup>+</sup> cells but differences in *repo*<sup>+</sup> cells.

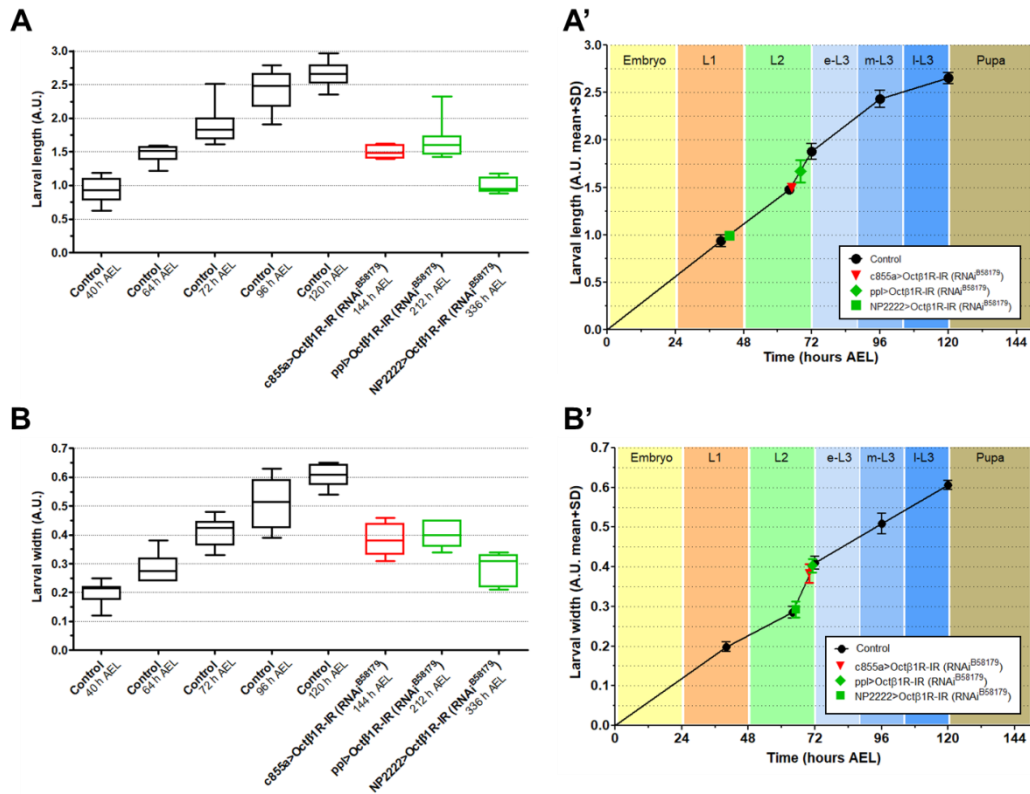


**Figure S18. Size of arrested larvae caused by dysfunctional *Octβ1R* expression.** Down-regulation of the receptor *Octβ1R* in *pp1*<sup>+</sup> fat body cells and *NP2222*<sup>+</sup> cortex glial cells (data in green) cause stage arrest during larval development as well as happens in *c855a*<sup>+</sup> neuroepithelial cells (data in red). (**A-B**) Different size phenotypes are detected in those arrested larva when are compared by length (**A-A'**) and width (**B-B'**). Underexpression of *Octβ1R* reveals larvae similarities when there are defects in *c855a*<sup>+</sup> and *pp1*<sup>+</sup> cells but differences in *NP2222*<sup>+</sup> cells.

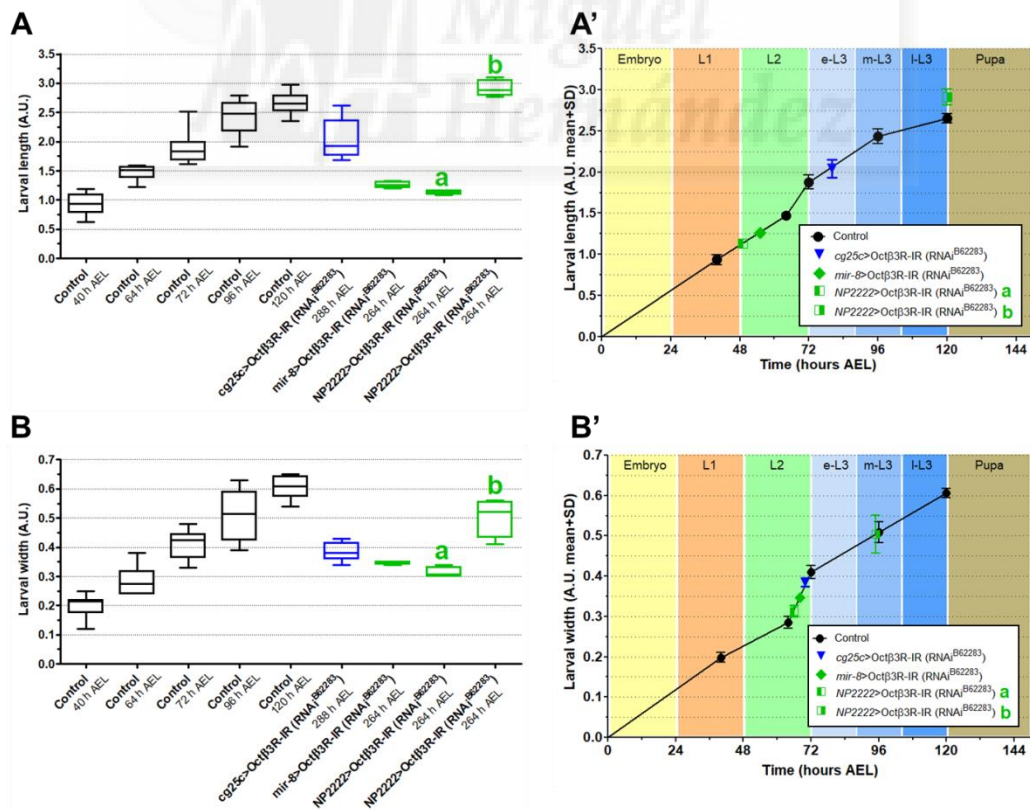


**Figure S19. Size of arrested larvae caused by dysfunctional *Octβ3R* expression in glia.** Down-regulation of the receptor *Octβ3R* in *mir-8*<sup>+</sup> and *NP2222*<sup>+</sup> glial cells (data in green) cause stage arrest during larval development as well as happens in *cg25c*<sup>+</sup> cells (data in blue). The driver *NP2222* cause a specific feature of arresting into two different larval times (**a** and **b**). (**A-B**) Different size phenotypes are detected in those arrested larva when are compared by length (**A-A'**) and width (**B-B'**). Underexpression of *Octβ1R* reveals larvae similarities when there are defects in *mir-8*<sup>+</sup> cells and *NP2222*<sup>-a</sup> cells but differences in *NP2222*<sup>-b</sup> cells. In between them, are located larvae with defects in *cg25c*<sup>+</sup> cells.

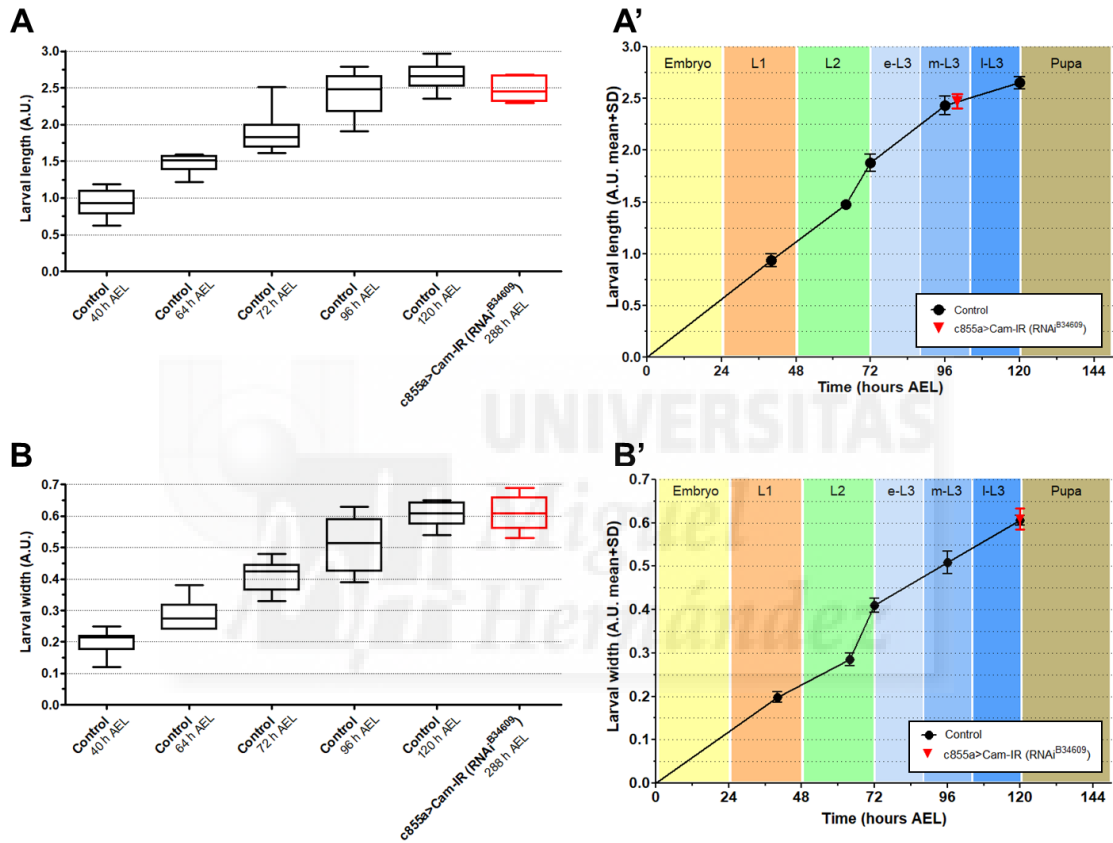


**Figure S20. Size of arrested larvae caused by dysfunctions in *Octβ3R* the OA receptor signalling pathway.** Downregulation of gene *calmodulin* (*Cam*), a downstream signal of octopamine receptors, in *c855a*<sup>+</sup> cells (data in red) cause stage arrest during larval development. (**A-B**) Different size phenotypes are detected in those arrested larva when are compared by length (**A-A'**) and width (**B-B'**). Malfunction of *Cam* in *c855a*<sup>+</sup> cells cause retain in larval size at late L3-like stage in a different amount of time.





---

**APPENDIX II**

***Supplementary tables***





Table S1. Packages used for the bioinformatics exploration.

Library	Version	Description
<b>acepack</b>	1.4.1	ACE and AVAS nonparametric methods for selecting multiple regression transformations
<b>annotate</b>	1.54.0	Annotation for microarrays
<b>AnnotationDbi</b>	1.38.0	Annotation database interface
<b>assertthat</b>	0.2.0	Easy pre- and post- assertions
<b>backports</b>	1.0.5	Reimplementation of functions introduced since R v3.0.0
<b>base</b>	3.4.0	Basic R functions
<b>base64enc</b>	0.1-3	Tools for base64 encoding
<b>BioBase</b>	2.36.2	Base functions for Bioconductor
<b>BiocGenerics</b>	0.22.0	S4 generic functions for Bioconductor
<b>BiocInstaller</b>	1.26.1	Install/update Bioconductor, CRAN, and Github packages
<b>BiocParallel</b>	1.10.1	Bioconductor facilities for parallel evaluation
<b>bitops</b>	1.0-6	Functions for bitwise operations on integer vectors
<b>caTools</b>	1.17.1	Tools: moving window statistics, GIF, Base64, ROC AUC, etc.
<b>checkmate</b>	1.8.2	Fast and versatile argument checks
<b>cluster</b>	2.0.6	Methods for cluster analysis based on (Kaufman and Rousseeuw, 1990)
<b>colorspace</b>	1.3-2	Colour space manipulation
<b>compiler</b>	3.4.0	The R compiler package
<b>data.table</b>	1.10.4	Extension of <b>data.frame</b> for matrices and lists
<b>datasets</b>	3.4.0	Base R datasets
<b>DBI</b>	0.6-1	R database interface
<b>DelayedArray</b>	0.2.7	Delayed operations on array-like objects
<b>DESeq2</b>	1.16.1	Differential analysis of count data (Love et al., 2014)
<b>devtools</b>	1.13.4	Tools for R scripts developing
<b>digest</b>	0.6.12	Create compact hash digests of R objects
<b>dplyr</b>	0.5.0	Data frame manipulation
<b>foreign</b>	0.8-67	Read data stored by minitab, S, SAS, SPSS, Stata, Systat, Weka, dBase, etc.
<b>Formula</b>	1.2-1	Extended model formulas
<b>gdata</b>	2.17.0	Various R programming tools for data manipulation
<b>genefilter</b>	1.58.1	Methods for filtering genes from high-throughput experiments
<b>geneplotter</b>	1.54.0	Functions for plotting genomic data
<b>GenomeInfoDb</b>	1.12.0	Utilities for manipulating chromosome and other 'seqname' identifiers
<b>GenomeInfoDbData</b>	0.99.0	Species and taxonomy ID look up tables used by <b>GenomeInfoDb</b>
<b>GenomicRanges</b>	1.28.3	Representation and manipulation of genomic intervals and variables defined along a genome
<b>ggplot</b>	3.0.1	Plotting
<b>ggplot2</b>	2.2.1	Plotting (Wickham, 2009)
<b>GO.db</b>	3.4.1	A set of annotation maps describing the entire Gene Ontology
<b>graphics</b>	3.4.0	R functions for base graphics
<b>grDevices</b>	3.4.0	R graphics devices and support for colours and fonts
<b>grid</b>	3.4.0	Graphics layout capabilities and support for interaction
<b>gridExtra</b>	2.2.1	Miscellaneous functions for <b>grid</b> graphics
<b>gtable</b>	0.2.0	Tools to work more easily with tables of 'grobs'
<b>gtools</b>	3.5.0	Various R programming tools
<b>Hmisc</b>	4.0-3	Many functions useful for data manipulation in R
<b>htmlTable</b>	1.9	Advanced tables for Markdown/HTML
<b>htmltools</b>	0.3.5	Tools for HTML generation and output
<b>htmlwidgets</b>	0.8	HTML widgets for R
<b>IRanges</b>	2.10.2	Infrastructure for manipulating intervals on sequences
<b>KernSmooth</b>	2.23-15	Functions for kernel smoothing (and density estimation) based on (Wand and Jones, 1995)
<b>knitr</b>	1.15.1	Provides a general-purpose tool for dynamic report generation in R using Literate Programming techniques.
<b>lattice</b>	0.20-35	Trellis graphics for R
<b>latticeExtra</b>	0.6-28	Extra graphical utilities for <b>Lattice</b>
<b>lazyeval</b>	0.2.0	Alternative approach to non-standard evaluation

<b>locfit</b>	1.5-9.1	Local regression, likelihood and density estimation
<b>magrittr</b>	1.5	A Forward-Pipe Operator for R
<b>Matrix</b>	1.2-8	Sparse and dense matrix classes and methods
<b>matrixStats</b>	0.52.2	High-performing functions operating on rows and columns of matrices
<b>memoise</b>	1.1.0	Memorisation of Functions
<b>methods</b>	3.4.0	Formally defined methods and classes for R objects
<b>mgsa</b>	1.24.0	Model-based gene set analysis (MGSA) is a Bayesian modelling approach for gene set enrichment which can be used with GO (Bauer et al., 2010)
<b>munsell</b>	0.4.3	Utilities for using Munsell colours
<b>nnet</b>	7.3-12	Feed-forward neural networks and multinomial Log-linear models
<b>org.Dm.eg.db</b>	3.4.1	Genome wide annotation for <i>Drosophila melanogaster</i>
<b>parallel</b>	3.4.0	Support for Parallel computation in R
<b>pheatmap</b>	1.0.8	Implementation for plotting heat maps
<b>plyr</b>	1.8.4	Data frame manipulation
<b>PoiClu</b>	1.0.2	Sample-to-sample distance based on a Poisson model (Witten, 2011)
<b>R6</b>	2.2.0	Creation of classes with reference semantics
<b>RColorBrewer</b>	1.1-2	Provides colour schemes for maps
<b>Rcpp</b>	0.12.10	Seamless R and C++ Integration
<b>RCurl</b>	1.95-4.8	General network (HTTP/FTP/...) client interface for R
<b>rpart</b>	4.1-11	Recursive partitioning and regression trees
<b>RSQLite</b>	1.1-2	'SQLite' interface for R
<b>S4Vectors</b>	0.14.3	S4 implementation of vectors and lists
<b>scales</b>	0.4.1	Scale functions for visualization
<b>splines</b>	3.4.0	Regression spline functions and classes
<b>stats</b>	3.4.0	The R stats package
<b>stats4</b>	3.4.0	Statistical functions using S4 classes
<b>stringi</b>	1.1.5	Character string processing facilities
<b>stringr</b>	1.2.0	Simple, consistent wrappers for common string operations
<b>SummarizedExperiment</b>	1.6.1	Contains one or more assays, each represented by a matrix-like object of numeric or other mode
<b>survival</b>	2.41-3	Core survival analysis routines
<b>tibble</b>	1.3.0	Simple data frames
<b>tools</b>	3.4.0	Tools for package development
<b>utils</b>	3.4.0	R utility functions
<b>withr</b>	1.0.2	Functions to run code 'with' safely and temporarily modified global state.
<b>XML</b>	3.98-1.6	Tools for Parsing and Generating XML Within R and S-Plus
<b>xtable</b>	1.8-2	Export Tables to LaTeX or HTML
<b>XVector</b>	0.16.0	Representation and manipulation of external sequences
<b>zlibbioc</b>	1.22.0	An R packaged zlib-1.2.5

Table S2. GO selected clusters for gene filtering in Screening 1.

GO ID	GO TERM	IN POPULATION	IN STUDY	ESTIMATE	STANDARD ERROR
<b>Glia up-regulated by BP – 1<sup>ST</sup> GO</b>					
GO:0007517	muscle organ development	149	31	0.4186984	0.0465874
GO:0007219	Notch signaling pathway	170	37	0.4135630	0.0460876
GO:0016358	dendrite development	247	60	0.2470288	0.0275196
GO:0048149	behavioral response to ethanol	55	17	0.2079688	0.0231936
GO:0035006	melanization defense response	47	12	0.1384178	0.0157278
GO:0016319	mushroom body development	78	21	0.1324816	0.0159196
GO:0045746	negative regulation of Notch signaling pathway	48	9	0.1217834	0.0137007
GO:0035218	leg disc development	105	27	0.1119876	0.0127798
GO:0002520	immune system development	99	26	0.1026038	0.0116491
<b>Glia up-regulated by CC – 1<sup>ST</sup> GO</b>					
GO:0005938	cell cortex	153	36	0.4525600	0.0503033
GO:0002116	semaphorin receptor complex	2	2	0.2787284	0.0288199

GO:0032992	protein-carbohydrate complex	3	2	0.1749552	0.0170630
GO:0070765	gamma-secretase complex	5	2	0.1154222	0.0117451
GO:0098552	side of membrane	61	13	0.1136634	0.0126376
<b>Glial up-regulated by MF – 1<sup>ST</sup> GO</b>					
GO:0005515	protein binding	3311	510	0.8000000	0.1333334
GO:0008289	lipid binding	193	29	0.1039242	0.0158436
<b>NECs up-regulated molecular partners by BP – 2<sup>ND</sup> GO</b>					
GO:0002009	morphogenesis of an epithelium	685	71	0.1749984	0.0052135
GO:0032870	cellular response to hormone stimulus	98	9	0.1618636	0.0017049
GO:0001708	cell fate specification	108	15	0.1292328	0.0018103
<b>NECs up-regulated molecular partners by CC – 2<sup>ND</sup> GO</b>					
GO:0030139	endocytic vesicle	27	4	0.5837716	0.0008846
GO:0005938	cell cortex	153	19	0.4956102	0.0012623
GO:0005911	cell-cell junction	95	11	0.4859630	0.0029297
GO:0098552	side of membrane	61	7	0.3167304	0.0012083
GO:0097610	cell surface furrow	33	4	0.2425996	0.0011368
GO:0009986	cell surface	127	6	0.1473204	0.0008251
GO:0089717	spanning component of membrane	5	1	0.1169090	0.0007726
GO:0030054	cell junction	219	16	0.1071508	0.0458651
<b>NECs up-regulated molecular partners by MF – 2<sup>ND</sup> GO</b>					
GO:0005515	protein binding	3311	176	0.4754582	0.1504014
GO:0005042	netrin receptor activity	2	1	0.1494818	0.0007413
GO:0005243	gap junction channel activity	8	1	0.1397584	0.0054360
GO:0017134	fibroblast growth factor binding	2	1	0.1394184	0.0006612
GO:0005164	tumor necrosis factor receptor binding	1	1	0.1366654	0.0006241
GO:0030547	receptor inhibitor activity	2	1	0.1302374	0.0009650
GO:0048019	receptor antagonist activity	2	1	0.1295202	0.0008488
<b>NECs up-regulated by BP – 1<sup>ST</sup> GO</b>					
GO:0030431	sleep	139	7	0.4560020	0.0016383
GO:0016197	endosomal transport	107	7	0.3237336	0.0025006
GO:0045454	cell redox homeostasis	54	4	0.3114390	0.0016805
GO:0007265	Ras protein signal transduction	188	8	0.2614172	0.0015562
GO:0009306	protein secretion	62	5	0.2146930	0.0020709
GO:0046467	membrane lipid biosynthetic process	55	4	0.2068296	0.0010767
GO:0010883	regulation of lipid storage	28	4	0.1843968	0.0020700
GO:0046578	regulation of Ras protein signal transduction	118	5	0.1166210	0.0007973
GO:0051607	defense response to virus	39	3	0.1021810	0.0008475
<b>NECs up-regulated by CC – 1<sup>ST</sup> GO</b>					
GO:0098797	plasma membrane protein complex	127	6	0.3257500	0.0011394
GO:0005938	cell cortex	153	5	0.1735672	0.0014573
GO:0044459	plasma membrane part	953	19	0.1143760	0.0008410
<b>NECs up-regulated by MF – 1<sup>ST</sup> GO</b>					
GO:0042277	peptide binding	69	5	0.4017364	0.0020493
GO:0017134	fibroblast growth factor binding	2	2	0.3562308	0.00141460
<b>Glial up-regulated molecular partners by BP – 2<sup>ND</sup> GO</b>					
GO:0016197	endosomal transport	107	5	0.3918896	0.0029997
GO:0007419	ventral cord development	84	4	0.2976478	0.0012624
GO:0032482	Rab protein signal transduction	46	3	0.1999848	0.0017215
GO:0035193	larval central nervous system remodeling	7	2	0.1681370	0.0012112
GO:0035265	organ growth	76	6	0.1351722	0.0017747
<b>Glial up-regulated molecular partners by CC – 2<sup>ND</sup> GO</b>					
GO:0005768	endosome	194	10	0.9720926	0.0006665
<b>Glial up-regulated molecular partners by MF – 2<sup>ND</sup> GO</b>					
GO:0004674	protein serine/threonine kinase activity	209	6	0.4967072	0.0054370
<b>Glial up-regulated molecular partners by CC – 3<sup>RD</sup> GO</b>					
GO:0005938	cell cortex	153	13	0.3241274	0.0026202
GO:0002116	semaphorin receptor complex	2	1	0.1963526	0.0011082
GO:0035230	cytoneme	7	1	0.1671072	0.0019671
GO:0051286	cell tip	2	1	0.1321640	0.0009493
GO:0005911	cell-cell junction	95	8	0.1188998	0.0030731
<b>Glial up-regulated molecular partners by MF – 3<sup>RD</sup> GO</b>					
GO:0019904	protein domain specific binding	81	5	0.7374972	0.0026566
GO:0005102	receptor binding	278	11	0.6928144	0.0052401
GO:0019198	transmembrane receptor protein phosphatase activity	7	2	0.2978136	0.0034500
GO:0019899	enzyme binding	375	11	0.2932610	0.0037548

\*GO clustered have an estimated  $p > 0.1$ .

\*\*Genes may belong to more than one GO group; thus, "unique geneID filtering" was done after clustering.

\*\*\*Sample colours by condition are the same as in Figure 27. Grouped genes' colours are the same as in Figure 24B Venn diagram.

**Table S3. GO selected clusters for gene filtering in Screening 2.**

GO ID	GO TERM	IN POPULATION	IN STUDY	ESTIMATE	STANDARD ERROR
<b>NECs &amp; Glia up-regulated by BP – 1<sup>st</sup> GO</b>					
GO:0048729	tissue morphogenesis	702	125	0.7756904	0.0021581
GO:0007417	central nervous system development	293	72	0.6058922	0.0062032
GO:0001708	cell fate specification	108	25	0.6017200	0.0045235
GO:0007167	enzyme linked receptor protein signaling pathway	286	46	0.3701930	0.0067840
GO:0007155	cell adhesion	292	51	0.3639422	0.0063325
GO:0030182	neuron differentiation	895	169	0.2043466	0.0044351
GO:0002009	morphogenesis of an epithelium	685	124	0.1723496	0.0016605
GO:0007422	peripheral nervous system development	95	21	0.1550222	0.0022614
GO:0060322	head development	168	40	0.1535470	0.0016380
GO:0007423	sensory organ development	496	99	0.1506360	0.0025554
GO:0030111	regulation of Wnt signaling pathway	93	21	0.1163546	0.0009667
<b>NECs &amp; Glia up-regulated by CC – 2<sup>nd</sup> GO</b>					
GO:0045177	apical part of cell	138	18	0.7706448	0.0027936
GO:0045202	synapse	357	21	0.6489738	0.0012888
GO:0071944	cell periphery	1637	96	0.5400240	0.0046835
GO:0030054	cell junction	219	31	0.3455104	0.0014438
GO:0097610	cell surface furrow	33	3	0.1174624	0.0009331

\*GO clustered have an estimated  $p > 0.1$ .

\*\*Genes may belong to more than one GO group; thus, “unique geneID filtering” was done after clustering.

\*\*\*Sample colours by condition are the same as in Figure 27. Grouped genes' colours are the same as in Figure 24B Venn diagram.

**Table S4. GO selected clusters for gene filtering in Screening 3.**

GO ID	GO TERM	IN POPULATION	IN STUDY	ESTIMATE	STANDARD ERROR
<b>NECs &amp; Glia down-regulated by BP – 1<sup>st</sup> GO</b>					
GO:0007186	G-protein coupled receptor signaling pathway	242	68	0.8000000	0.1333333
GO:0006811	ion transport	535	104	0.5053476	0.0844317
GO:0006836	neurotransmitter transport	154	26	0.3531978	0.0589468
GO:0034097	response to cytokine	11	5	0.2853322	0.0474289
GO:0045471	response to ethanol	78	17	0.2495252	0.0420705
GO:0040034	regulation of development, heterochronic	12	4	0.2088326	0.0348179
GO:0009593	detection of chemical stimulus	167	2	0.1970036	0.1313370
GO:0009581	detection of external stimulus	126	16	0.1423886	0.0237711
GO:0009582	detection of abiotic stimulus	126	16	0.1419596	0.0237151
GO:0071692	protein localization to extracellular region	2	2	0.1033260	0.0167304
<b>NECs &amp; Glia down-regulated by CC – 1<sup>st</sup> GO</b>					
GO:0005886	plasma membrane	1500	225	0.8973896	0.0997101
GO:0031012	extracellular matrix	221	29	0.8779708	0.0975536
GO:0045177	apical part of cell	138	23	0.6173298	0.0686451
GO:0044306	neuron projection terminus	61	14	0.2172128	0.0241380
GO:0043083	synaptic cleft	6	2	0.1061492	0.0109903
<b>NECs &amp; Glia down-regulated by BP – 2<sup>nd</sup> GO</b>					
GO:0007186	G-protein coupled receptor signaling pathway	242	39	1.0000000	0.0000000
GO:0050808	synapse organization	296	22	1.0000000	0.0000000
GO:0006836	neurotransmitter transport	154	23	0.9934160	0.0003487
GO:0098602	single organism cell adhesion	108	6	0.5202444	0.0036585
GO:0031589	cell-substrate adhesion	34	4	0.5148806	0.0028689
GO:0007602	phototransduction	69	6	0.3548370	0.0023668
GO:0055085	transmembrane transport	546	68	0.2133350	0.0076327
GO:0070633	transepithelial transport	19	4	0.2041962	0.0013118
GO:0007271	synaptic transmission, cholinergic	21	8	0.1640410	0.0015392
GO:0006858	extracellular transport	1	1	0.1480432	0.0012909
GO:0007185	transmembrane receptor protein tyrosine phosphatase signaling pathway	3	2	0.1433178	0.0008561
GO:0045465	R8 cell differentiation	22	3	0.1349516	0.0016790
GO:0008039	synaptic target recognition	46	4	0.1328014	0.0022597
GO:0035233	germ cell repulsion	2	1	0.1187066	0.0011666
GO:0015893	drug transport	7	2	0.1026526	0.0015817

<b>NECs &amp; Glia down-regulated by CC – 2<sup>ND</sup> GO</b>					
GO:0005887	integral component of plasma membrane	612	87	0.8270764	0.0016537
GO:0099503	secretory vesicle	84	14	0.8063346	0.0016383
GO:0034702	ion channel complex	104	26	0.5564180	0.0017918
GO:0043679	axon terminus	61	11	0.2437754	0.0010058
GO:0031395	bursicon neuropeptide hormone complex	2	1	0.1659814	0.0007031

\*GO clustered have an estimated  $p > 0.1$ .

\*\*Genes may belong in more than one GO group; thus, “unique geneID filtering” was done after clustering.

\*\*\*Sample's colours by condition are the same in Figure 27. Grouped genes colours are the same in Figure 24B Venn diagram.

**Table S5. List of top-hit genes differential expressed from RNA-seq bioinformatic screenings.**

GENE SYMBOL	FLYBASEID	NEC LOG2FC	NEC P-ADJ	GLIA LOG2FC	GLIA P-ADJ
<b>Neuroepithelial expressed unique genes</b>					
Abl	FBgn0000017	0,82	4,34E-03	-	-
aos	FBgn0004569	0,90	2,07E-02	-	-
CG3164	FBgn0025683	0,71	1,52E-04	-	-
egr	FBgn0033483	0,70	4,92E-05	-	-
fra	FBgn0011592	1,02	1,01E-04	-	-
fz3	FBgn0027343	-1,12	4,49E-02	-	-
llp8	FBgn0036690	-7,39	7,91E-03	-	-
InR	FBgn0283499	1,22	1,46E-03	-	-
Mmp2	FBgn0033438	1,50	1,10E-11	-	-
sog	FBgn0003463	-2,41	2,37E-03	-	-
spz	FBgn0003495	-1,94	9,42E-02	-	-
Tollo	FBgn0029114	-0,84	2,05E-02	-	-
<b>Glial expressed unique genes</b>					
baz	FBgn0000163	-	-	0,59	8,30E-03
Dab	FBgn0000414	-	-	0,50	1,12E-04
dpr6	FBgn0040823	-	-	-0,94	2,38E-03
Egfr	FBgn0003731	-	-	0,63	4,71E-02
fz2	FBgn0016797	-	-	0,59	1,50E-05
Grip	FBgn0029830	-	-	0,79	3,25E-02
kon	FBgn0032683	-	-	0,86	4,09E-02
nAChRa1	FBgn0000036	-	-	-0,45	3,28E-02
nAChRa6	FBgn0032151	-	-	-0,40	9,98E-02
Nrx-1	FBgn0038975	-	-	-0,73	1,29E-04
PlexA	FBgn0025741	-	-	0,58	3,46E-07
PlexB	FBgn0025740	-	-	0,82	1,04E-08
Ptp69D	FBgn0014007	-	-	0,55	6,99E-04
Ptp99A	FBgn0004369	-	-	0,32	5,55E-02
robo1	FBgn0005631	-	-	0,45	7,87E-03
sax	FBgn0003317	-	-	0,70	4,79E-06
scb	FBgn0003328	-	-	-0,81	3,06E-03
Sec8	FBgn0266672	-	-	0,45	6,76E-03

shg	FBgn0003391	-	-	0,37	1,97E-02
sli	FBgn0264089	-	-	0,88	3,43E-08
spi	FBgn0005672	-	-	0,34	1,40E-02
Ten-a	FBgn0267001	-	-	0,31	2,76E-02
Toll-6	FBgn0036494	-	-	-0,51	1,10E-02
trio	FBgn0024277	-	-	0,35	2,08E-02
Vang	FBgn0015838	-	-	0,37	5,80E-02
Wnt5	FBgn0010194	-	-	0,70	1,89E-05
<b>Neuroepithelial and glial common expressed genes</b>					
18w	FBgn0004364	1,54	4,22E-13	1,88	1,88E-19
5-HT1A	FBgn0004168	-1,51	3,33E-02	-1,43	7,24E-09
5-HT2B	FBgn0261929	-3,16	2,29E-02	-2,25	8,47E-06
AstA-R1	FBgn0266429	-3,31	3,87E-02	-2,38	2,36E-04
bark	FBgn0031571	-3,02	5,85E-06	-0,69	8,47E-02
Burs	FBgn0038901	-9,19	1,77E-07	-11,62	7,62E-19
CadN	FBgn0015609	1,19	2,97E-02	0,80	1,04E-08
CadN2	FBgn0262018	-2,80	2,41E-05	-2,22	1,22E-18
CapaR	FBgn0037100	-8,43	2,15E-05	-2,39	8,92E-03
CCHa2-R	FBgn0033058	-3,58	7,59E-03	-2,87	1,10E-07
CG31760	FBgn0051760	-2,37	3,20E-06	-1,63	1,64E-06
CG5758	FBgn0032666	-1,68	1,64E-02	-1,42	6,17E-11
Cow	FBgn0039054	-1,58	3,05E-03	-1,28	6,86E-11
crb	FBgn0259685	-2,78	1,94E-11	-0,98	1,60E-02
Dh31-R	FBgn0052843	-1,80	9,04E-03	-1,06	1,26E-02
Dh44-R1	FBgn0033932	-2,77	1,35E-03	-2,90	1,64E-14
dnt	FBgn0024245	0,60	7,07E-03	0,94	1,51E-04
Dop2R	FBgn0053517	-1,70	9,03E-04	-1,26	5,22E-06
DopEcR	FBgn0035538	-2,53	5,44E-16	-1,67	6,90E-12
dpr2	FBgn0261871	-2,55	1,76E-02	-1,97	5,47E-05
dpr3	FBgn0053516	-2,31	4,27E-02	-1,69	1,06E-08
dpr5	FBgn0037908	-3,82	2,11E-03	-1,81	1,90E-05
dpr9	FBgn0038282	-1,33	8,16E-03	-1,53	8,50E-11
dpr10	FBgn0052057	-1,64	5,28E-02	-0,83	3,03E-02
dpr13	FBgn0034286	-1,28	8,04E-02	-0,79	8,31E-03
dpr14	FBgn0029974	-0,90	2,69E-03	-0,92	1,59E-03
dpr17	FBgn0051361	-1,15	1,53E-02	-1,35	5,23E-05
dpr18	FBgn0030723	-2,89	3,21E-07	-2,02	3,39E-11
dpr20	FBgn0035170	-1,53	2,67E-02	-2,06	3,76E-08
Drep2	FBgn0028408	-1,08	6,17E-03	-1,27	5,34E-10
drl	FBgn0015380	0,39	7,75E-02	1,31	2,30E-16
Dscam2	FBgn0265296	2,13	9,77E-07	2,29	3,89E-89
Dscam3	FBgn0261046	2,54	5,58E-11	1,47	1,07E-11
Dscam4	FBgn0263219	1,67	6,23E-05	1,51	8,45E-14
eag	FBgn0000535	-1,19	7,28E-02	-0,55	3,81E-02
ebi	FBgn0263933	0,30	6,46E-02	0,42	1,85E-03

ed	FBgn0000547	0,73	2,54E-02	0,85	2,95E-10
Ephrin	FBgn0040324	0,90	7,84E-03	1,06	1,58E-15
ETHR	FBgn0038874	-4,82	7,48E-03	-3,68	2,28E-07
Fas2	FBgn0000635	1,02	1,87E-02	0,66	6,98E-06
FMRFaR	FBgn0035385	-4,82	4,95E-03	-1,88	6,35E-03
fz	FBgn0001085	1,30	1,14E-05	0,62	3,01E-04
Gfrl	FBgn0262869	-1,84	5,33E-03	-1,13	7,24E-05
GluRIA	FBgn0004619	-2,30	1,90E-05	-1,56	1,59E-05
GluRIB	FBgn0264000	-4,45	5,08E-02	-1,59	3,69E-02
gogo	FBgn0052227	1,41	1,72E-09	1,74	1,99E-21
Gp150	FBgn0013272	-1,47	2,26E-16	-0,75	5,54E-04
hbs	FBgn0029082	1,16	3,22E-03	1,33	1,65E-19
hig	FBgn0010114	-1,13	4,37E-06	-1,14	9,48E-08
ine	FBgn0011603	-3,11	3,33E-02	-3,74	1,70E-42
Inx3	FBgn0265274	0,44	3,65E-02	0,51	1,01E-02
ltgaPS5	FBgn0034880	1,17	6,25E-02	1,25	4,81E-03
Lgr3	FBgn0039354	-8,67	3,22E-06	-5,14	1,73E-07
mAChR-A	FBgn0000037	-1,56	2,30E-03	-1,45	2,00E-08
mav	FBgn0039914	0,97	3,48E-02	1,13	2,18E-05
mew	FBgn0004456	0,82	2,42E-03	1,60	1,14E-16
mGluR	FBgn0019985	-1,07	3,03E-02	-0,71	1,78E-02
moody	FBgn0025631	-1,53	1,76E-02	-1,75	9,69E-09
mtt	FBgn0050361	-1,81	1,59E-03	-1,81	9,11E-14
mys	FBgn0004657	0,58	4,05E-02	0,60	5,03E-04
nAChRa3	FBgn0015519	-1,25	7,44E-02	-0,66	1,50E-02
nAChRa5	FBgn0028875	-2,20	1,74E-05	-0,90	5,44E-07
nAChRa7	FBgn0086778	-1,54	1,44E-03	-0,49	7,66E-02
nAChRβ1	FBgn0000038	-1,04	1,24E-02	-1,86	9,96E-12
Nlg4	FBgn0083975	-2,51	9,35E-05	-1,26	7,13E-07
Nmdar1	FBgn0010399	-2,60	4,65E-04	-1,61	1,01E-07
NPFR	FBgn0037408	-1,84	3,58E-02	-3,04	8,94E-12
Nrk	FBgn0020391	0,93	5,92E-11	1,10	3,43E-08
Nrt	FBgn0004108	0,88	6,89E-12	1,24	2,24E-24
Nrx-IV	FBgn0013997	0,72	1,05E-02	1,18	6,35E-15
Oamb	FBgn0024944	-5,29	4,04E-07	-1,74	3,44E-04
Oct-TyrR	FBgn0004514	-6,03	2,42E-08	-3,19	3,07E-06
Octβ1R	FBgn0038980	-2,17	2,46E-03	-1,55	1,09E-10
Octβ2R	FBgn0038063	-4,30	1,35E-04	-2,17	2,65E-10
Octβ3R	FBgn0250910	-2,08	4,02E-04	-1,68	3,14E-07
otk	FBgn0004839	0,78	1,57E-02	1,62	1,60E-20
otk2	FBgn0267728	0,51	6,11E-02	1,16	3,46E-07
Pburs	FBgn0264810	-8,52	4,72E-05	-11,61	4,65E-18
PK2-R1	FBgn0038140	-5,17	2,55E-04	-2,45	2,35E-04
PK2-R2	FBgn0038139	-8,40	2,33E-05	-1,78	2,56E-02
Proc-R	FBgn0029723	-7,98	6,63E-08	-6,44	1,46E-127

<b>ptc</b>	FBgn0003892	0,52	1,09E-02	0,98	2,53E-07
<b>Rdl</b>	FBgn0004244	-3,27	2,55E-14	-2,28	4,81E-27
<b>Ret</b>	FBgn0011829	-6,75	2,40E-06	-5,68	1,98E-11
<b>robo3</b>	FBgn0041097	1,30	7,27E-03	0,76	8,29E-05
<b>Ror</b>	FBgn0010407	0,88	9,34E-09	1,28	2,51E-19
<b>rst</b>	FBgn0003285	0,76	8,46E-02	1,30	3,19E-08
<b>santa-maria</b>	FBgn0025697	-4,12	3,51E-02	-2,61	1,36E-04
<b>Sema1b</b>	FBgn0016059	0,54	1,53E-02	1,05	9,42E-12
<b>sev</b>	FBgn0003366	-1,61	2,79E-03	-2,28	1,95E-24
<b>shakB</b>	FBgn0085387	-3,03	8,18E-07	-1,85	8,26E-11
<b>SIFaR</b>	FBgn0038880	-5,15	1,45E-04	-3,13	8,04E-03
<b>smal</b>	FBgn0085409	1,01	4,99E-03	0,92	5,61E-18
<b>sns</b>	FBgn0024189	1,01	3,09E-03	1,03	4,94E-12
<b>SPR</b>	FBgn0029768	-3,51	1,11E-02	-1,32	6,89E-04
<b>stan</b>	FBgn0024836	1,12	1,96E-02	1,41	3,44E-23
<b>Ten-m</b>	FBgn0004449	0,88	6,38E-02	0,53	2,64E-04
<b>Tig</b>	FBgn0011722	-5,07	3,88E-13	-1,76	1,01E-06
<b>TkR86C</b>	FBgn0004841	-3,04	5,73E-02	-1,92	2,77E-05
<b>TI</b>	FBgn0262473	0,89	2,01E-02	0,75	1,08E-05
<b>Toll-7</b>	FBgn0034476	1,43	2,06E-07	1,01	7,33E-13
<b>TrissinR</b>	FBgn0085410	-3,30	3,06E-02	-1,52	2,04E-04
<b>TyrRII</b>	FBgn0038541	-8,70	1,41E-06	-3,78	1,37E-06
<b>unc-5</b>	FBgn0034013	1,03	2,67E-05	1,49	1,24E-38
<b>wg</b>	FBgn0284084	-1,01	4,27E-02	-1,12	7,48E-02
<b>wit</b>	FBgn0024179	1,39	3,44E-05	1,12	1,70E-06
<b>wls</b>	FBgn0036141	0,58	8,73E-03	1,09	1,21E-12
<b>Wnt2</b>	FBgn0004360	1,13	5,80E-04	1,52	9,09E-03
<b>Wnt4</b>	FBgn0010453	1,33	1,23E-16	0,86	3,68E-11
<b>Wnt6</b>	FBgn0031902	-3,26	5,29E-02	-2,82	6,69E-04
<b>Wnt10</b>	FBgn0031903	2,92	7,34E-07	1,50	7,39E-04
<b>wrapper</b>	FBgn0025878	-2,92	5,96E-06	-1,46	4,20E-02
<b>wun2</b>	FBgn0041087	-1,68	1,53E-03	-1,80	4,82E-12

\*Colours indicate up-regulated (**black**) and down-regulated (**red**) genes.

\*\*Gene expression is given by Log2FoldChange (Log2FC) and its probability by p-adjusted<0,1 (p-adj).



**Table S6. *Drosophila* lines with abnormal phenotype from gene validation.**

GENE SYMBOL	FLYBASEID	MUTANT TYPE	COLLECTION	STOCK NUMBER	FLYBASE GENOTYPE
<b>5-HT2B</b>	FBgn0261929	RNAi	BDSC	25874	y <sup>1</sup> v <sup>1</sup> ; P{TRiP.JF01913}attP2
<b>aos</b>	FBgn0004569	RNAi	BDSC	28383	y <sup>1</sup> v <sup>1</sup> ; P{TRiP.JF03020}attP2
			VDRC	3237	w <sup>1118</sup> ; P{GD1666}v3237
				3238	w <sup>1118</sup> ; P{GD1666}v3238/TM3
				47181	w <sup>1118</sup> ; P{GD16463}v47181
<b>bark</b>	FBgn0031571	RNAi	BDSC	67014	y <sup>1</sup> sc* v <sup>1</sup> ; P{TRiP.HMS05480}attP40
			VDRC	107348	P{KK103080}VIE-260B
<b>baz</b>	FBgn0000163	RNAi	VDRC	2914	w <sup>1118</sup> ; P{GD1384}v2914
<b>Burs</b>	FBgn0038901	RNAi	BDSC	26719	y <sup>1</sup> v <sup>1</sup> ; P{TRiP.JF02260}attP2
<b>crb</b>	FBgn0259685	UAS	BDSC	5544	w*; P{UAS-crb.wt}30.12e
<b>Dh44-R1</b>	FBgn0033932	RNAi	VDRC	110708	P{KK108591}VIE-260B
<b>dpr2</b>	FBgn0261871	RNAi	VDRC	29742	w <sup>1118</sup> ; P{GD15154}v29742
<b>dpr5</b>	FBgn0037908	RNAi	VDRC	102228	P{KK111180}VIE-260B
<b>dpr10</b>	FBgn0052057	RNAi	VDRC	103511	P{KK112452}VIE-260B
<b>Dscam4</b>	FBgn0263219	RNAi	BDSC	51508	y <sup>1</sup> sc* v <sup>1</sup> ; P{TRiP.HMC03277}attP2
<b>ebi</b>	FBgn0263933	RNAi	BDSC	8393	P{ebi.FRT}1, y <sup>1</sup> w <sup>1118</sup>
			BDSC	38209	y <sup>1</sup> sc* v <sup>1</sup> ; P{TRiP.GL00648}attP40
			VDRC	3087	w <sup>1118</sup> ; P{GD2575}v3087
104279	P{KK106928}VIE-260B				
<b>Egfr</b>	FBgn0003731	RNAi	BDSC	25781	y <sup>1</sup> v <sup>1</sup> ; P{TRiP.JF01368}attP2
<b>egr</b>	FBgn0033483	RNAi	VDRC	45253	w <sup>1118</sup> ; P{GD12658}v45253
<b>Fas2</b>	FBgn0000635	RNAi	BDSC	34084	y <sup>1</sup> sc* v <sup>1</sup> ; P{TRiP.HMS01098}attP2
<b>fz</b>	FBgn0001085	RNAi	BDSC	31036	y <sup>1</sup> v <sup>1</sup> ; P{TRiP.JF01481}attP2
<b>ine</b>	FBgn0011603	RNAi	BDSC	51919	y <sup>1</sup> sc* v <sup>1</sup> ; P{TRiP.HMS03378}attP2
<b>InR</b>	FBgn0283499	RNAi	BDSC	35251	y <sup>1</sup> sc* v <sup>1</sup> ; P{TRiP.GL00139}attP2
<b>Inx3</b>	FBgn0265274	RNAi	BDSC	30501	y <sup>1</sup> sc* v <sup>1</sup> ; P{TRiP.HM05245}attP2
			VDRC	39095	w <sup>1118</sup> ; P{GD14965}v39095
<b>mew</b>	FBgn0004456	RNAi	VDRC	109608	P{KK101081}VIE-260B
<b>Mmp2</b>	FBgn0033438	RNAi	BDSC	31371	y <sup>1</sup> v <sup>1</sup> ; P{TRiP.JF01337}attP2
<b>mtt</b>	FBgn0050361	RNAi	BDSC	44076	y <sup>1</sup> sc* v <sup>1</sup> ; P{TRiP.HMS02793}attP40
			BDSC	27735	y <sup>1</sup> v <sup>1</sup> ; P{TRiP.JF02819}attP2
			VDRC	29619	w <sup>1118</sup> ; P{GD15002}v29619
<b>mys</b>	FBgn0004657	RNAi	103704	P{KK100518}VIE-260B	
			BDSC	61225	y <sup>1</sup> v <sup>1</sup> ; P{TRiP.HMJ23004}attP40/CyO
<b>nAChRa3</b>	FBgn0015519	RNAi	BDSC	28715	y <sup>1</sup> v <sup>1</sup> ; P{TRiP.JF03142}attP2
			BDSC	8353	w <sup>1118</sup> ; P{GD2436}v8353
<b>Nrx-IV</b>	FBgn0013997	RNAi	VDRC	108128	P{KK102207}VIE-260B
			BDSC	31171	y <sup>1</sup> v <sup>1</sup> ; P{TRiP.JF01673}attP2
<b>Oamb</b>	FBgn0024944	RNAi	VDRC	2861	w <sup>1118</sup> ; P{GD696}v2861
			BDSC	68235	y <sup>1</sup> v <sup>1</sup> ; P{UAS-Oamb-Tango}attP2/TM3, Ser <sup>1</sup>
		UAS	BDSC	58179	y <sup>1</sup> v <sup>1</sup> ; P{TRiP.HMJ22156}attP40
<b>Octβ1R</b>	FBgn0038980	RNAi	BDSC	58179	y <sup>1</sup> v <sup>1</sup> ; P{TRiP.HMJ22156}attP40
<b>Octβ3R</b>	FBgn0250910	RNAi	BDSC	62283	y <sup>1</sup> v <sup>1</sup> ; P{TRiP.HMJ23640}attP40

<b>otk</b>	FBgn0004839	RNAi	VDRC	<b>30834</b>	w <sup>1118</sup> ; P{GD14399}v30834
<b>otk2</b>	FBgn0267728	RNAi	BDSC	<b>55892</b>	y <sup>1</sup> sc* v <sup>1</sup> ; P{TRiP.HMC04171}attP2
<b>Pburs</b>	FBgn0264810	RNAi	BDSC	<b>55924</b>	y <sup>1</sup> sc* v <sup>1</sup> ; P{TRiP.HMC04211}attP40
<b>ptc</b>	FBgn0003892	RNAi	BDSC	<b>28795</b>	y <sup>1</sup> v <sup>1</sup> ; P{TRiP.JF03223}attP2
				<b>55686</b>	y <sup>1</sup> sc* v <sup>1</sup> ; P{TRiP.HMC03872}attP40
<b>Ptp69D</b>	FBgn0014007	RNAi	BDSC	<b>29462</b>	y <sup>1</sup> v <sup>1</sup> ; P{TRiP.JF03399}attP2
<b>Ptp99A</b>	FBgn0004369	RNAi	BDSC	<b>25840</b>	y <sup>1</sup> v <sup>1</sup> ; P{TRiP.JF01858}attP2
<b>Ret</b>	FBgn0011829	UAS	BDSC	<b>59002</b>	y <sup>1</sup> w*; P{UAS-Ret.L}2/CyO
<b>santa-maria</b>	FBgn0025697	RNAi	BDSC	<b>29550</b>	y <sup>1</sup> v <sup>1</sup> ; P{TRiP.JF03227}attP2
		UAS	BDSC	<b>24519</b>	w*; santa-maria <sup>1</sup> ; P{UAS-santa-maria.W}3
<b>Sec8</b>	FBgn0266672	RNAi	VDRC	<b>105653</b>	P{KK101531}VIE-260B
<b>SIFaR</b>	FBgn0038880	RNAi	BDSC	<b>25831</b>	y <sup>1</sup> v <sup>1</sup> ; P{TRiP.JF01849}attP2
<b>sns</b>	FBgn0024189	RNAi	VDRC	<b>877</b>	w <sup>1118</sup> ; P{GD65}v877/TM3
<b>spi</b>	FBgn0005672	RNAi	VDRC	<b>3922</b>	w <sup>1118</sup> ; P{GD1779}v3922
<b>stan</b>	FBgn0024836	RNAi	VDRC	<b>107993</b>	P{KK100512}VIE-260B
<b>Ten-a</b>	FBgn0267001	RNAi	BDSC	<b>29439</b>	y <sup>1</sup> v <sup>1</sup> ; P{TRiP.JF03375}attP2
			VDRC	<b>103298</b>	P{KK112809}VIE-260B
<b>Ten-m</b>	FBgn0004449	RNAi	BDSC	<b>29390</b>	y <sup>1</sup> v <sup>1</sup> ; P{TRiP.JF03323}attP2
			VDRC	<b>51173</b>	<i>OUT OF VDRC COLLECTION</i>
<b>Tig</b>	FBgn0011722	RNAi	BDSC	<b>31570</b>	y <sup>1</sup> v <sup>1</sup> ; P{TRiP.JF01143}attP2
			VDRC	<b>100036</b>	P{KK103086}VIE-260B
<b>trio</b>	FBgn0024277	RNAi	BDSC	<b>43549</b>	y <sup>1</sup> sc* v <sup>1</sup> ; P{TRiP.HMS02690}attP2
<b>unc-5</b>	FBgn0034013	RNAi	BDSC	<b>33756</b>	y <sup>1</sup> sc* v <sup>1</sup> ; P{TRiP.HMS01099}attP2
<b>wg</b>	FBgn0284084	UAS	BDSC	5918	w*; P{UAS-wg.H.T:HA1}6C
			M.Domínguez	<b>717</b>	w <sup>1118</sup> ; UAS-wg
<b>wls</b>	FBgn0036141	RNAi	VDRC	<b>5214</b>	w <sup>1118</sup> ; P{GD2418}v5214
<b>Wnt2</b>	FBgn0004360	RNAi	VDRC	<b>38079</b>	w <sup>1118</sup> ; P{GD5736}v38079
<b>Wnt4</b>	FBgn0010453	RNAi	VDRC	<b>38010</b>	w <sup>1118</sup> ; P{GD5347}v38010
<b>Genes added to further explore phenotypes</b>					
<b>Cam</b>	FBgn0000253	RNAi	BDSC	<b>34609</b>	y <sup>1</sup> sc* v <sup>1</sup> ; P{TRiP.HMS01318}attP2
<b>CaMKII</b>	FBgn0264608	UAS	BDSC	<b>29664</b>	P{UAS-CaMKII.T287D}6B1
<b>Ddc</b>	FBgn0000422	RNAi	BDSC	<b>51462</b>	y <sup>1</sup> v <sup>1</sup> ; P{TRiP.HMC03200}attP40
<b>Mmp2</b>	FBgn0033438	UAS	BDSC	58705	w*; P{UAS-Mmp2.P}2
				58706	w*; P{UAS-Mmp2.P}3

\*Stock number colours indicate that the phenotype is observed in *c855a*<sup>+</sup> cells (red), *cg25c*<sup>+</sup> cells (blue) or in both cell types (black).



**BIBLIOGRAPHY**



## A

---

Adams, M.D., 1\* Susan E. Celniker, 2 Robert A. Holt, 1 Cheryl A. Evans, 1 Jeannine D. Gocayne, 1, Peter G. Amanatides, 1 Steven E. Scherer, 3 Peter W. Li, 1 Roger A. Hoskins, 2 Richard F. Galle, 2 Reed A. George, 2, Suzanna E. Lewis, 4 Stephen Richards, 2 Michael Ashburner, 5 Scott N. Henderson, 1 Granger G. Sutton, 1, Jennifer R. Wortman, 1 Mark D. Yandell, 1 Qing Zhang, 1 Lin X. Chen, 1 Rhonda C. Brandon, 1 Yu-Hui C. Rogers, 1, Robert G. Blazej, 2 Mark Champe, 2 Barret D. Pfeiffer, 2 Kenneth H. Wan, 2 Clare Doyle, 2 Evan G. Baxter, 2, Gregg Helt, 6 Catherine R. Nelson, 4 George L. Gabor Miklos, 7 Josep F. Abril, 8 Anna Agbayani, 2 Hui-Jin An, 1, Cynthia Andrews-Pfannkoch, 1 Danita Baldwin, 1 Richard M. Ballew, 1 Anand Basu, 1 James Baxendale, 1, Leyla Bayraktaroglu, 9 Ellen M. Beasley, 1 Karen Y. Beeson, 1 P. V. Benos, 10 Benjamin P. Berman, 2 Deepali Bhandari, 1, Slava Bolshakov, 11 Dana Borkova, 12 Michael R. Botchan, 13 John Bouck, 3 Peter Brokstein, 4 Phillipe Brottier, 14, et al. (2000). The genome sequence of *Drosophila melanogaster*. *Science*. 287, 2185–2195.

Alunni, A., and Bally-Cuif, L. (2016). A comparative view of regenerative neurogenesis in vertebrates. *Development* 143, 741–753.

Alvarez, E., Del Pino, F., Jara, L., and Godoy-Herrera, R. (2017). The genetics and development of mandibles and hypopharyngeal sclerite and cornua in larvae of *Drosophila gaucha*. *PLoS One* 12, 1–14.

Álvarez, J.-A., and Díaz-Benjumea, F.J. (2018). Origin and specification of type-II neuroblasts in the *Drosophila* embryo. *Development* 1, dev.158394.

Anders, S., Pyl, P.T., and Huber, W. (2015). HTSeq-A Python framework to work with high-throughput sequencing data. *Bioinformatics* 31, 166–169.

Antonello, Z. a, Reiff, T., Ballesta-Illan, E., and Dominguez, M. (2015). Robust intestinal homeostasis relies on cellular plasticity in enteroblasts mediated by miR-8-Escargot switch. *EMBO J.* 34, 2025–2041.

Apitz, H., and Salecker, I. (2014). A challenge of numbers and diversity: Neurogenesis in the *Drosophila* optic lobe. *J. Neurogenet.* 28, 233–249.

Apitz, H., and Salecker, I. (2015). A region-specific neurogenesis mode requires migratory progenitors in the *Drosophila* visual system. *Nat. Neurosci.* 18, 46–55.

Apitz, H., and Salecker, I. (2018). Spatiooral relays control layer identity of direction-selective neuron subtypes in *Drosophila*. *Nat. Commun.* 9, 1–16.

Arendt, D., and Nübler-Jung, K. (1999). Comparison of early nerve cord development in insects and vertebrates. *Development* 126, 2309–2325.

Arenz, A., Drews, M.S., Richter, F.G., Ammer, G., and Borst, A. (2017). The Temporal Tuning of the *Drosophila* Motion Detectors Is Determined by the Dynamics of Their Input Elements. *Curr. Biol.* 27, 929–944.

Atkins, M., Jiang, Y., Sansores-Garcia, L., Jusiak, B., Halder, G., and Mardon, G. (2013). Dynamic Rewiring of the *Drosophila* Retinal Determination Network Switches Its Function from Selector to Differentiation. *PLoS Genet.* 9, e1003731.

Avet-Rochex, A., Kaul, A.K., Gatt, A.P., McNeill, H., and Bateman, J.M. (2012). Concerted control of gliogenesis by InR/TOR and FGF signalling in the *Drosophila* post-embryonic brain. *Development* 139, 2763–2772.

Awasaki, T., and Lee, T. (2011). New Tools for the Analysis of Glial Cell Biology in *Drosophila* Takeshi. *Glia* 59, 1377–1386.

Awasaki, T., Lai, S.-L., Ito, K., and Lee, T. (2008). Organization and Postembryonic Development of Glial Cells in the Adult Central Brain of *Drosophila*. *J. Neurosci.* 28, 13742–13753.

## B

---

Bailey, A.P., Koster, G., Guillermier, C., Hirst, E.M.A., MacRae, J.I., Lechene, C.P., Postle, A.D., and Gould, A.P. (2015). Antioxidant Role for Lipid Droplets in a Stem Cell Niche of *Drosophila*. *Cell* 163, 340–353.

- Bainton, R.J., Tsai, L.T.Y., Schwabe, T., DeSalvo, M., Gaul, U., and Heberlein, U. (2005). *moody* encodes two GPCRs that regulate cocaine behaviors and blood-brain barrier permeability in *Drosophila*. *Cell* 123, 145–156.
- Balfanz, S., Strünker, T., Frings, S., and Baumann, A. (2005). A family of octapamine receptors that specifically induce cyclic AMP production or Ca<sup>2+</sup> release in *Drosophila melanogaster*. *J. Neurochem.* 93, 440–451.
- Ball, R.W., Warren-Paquin, M., Tsurudome, K., Liao, E.H., Elazzouzi, F., Cavanagh, C., An, B.S., Wang, T.T., White, J.H., and Haghighi, A.P. (2010). Retrograde BMP signaling controls synaptic growth at the nmj by regulating *trio* expression in motor neurons. *Neuron* 66, 536–549.
- Banerjee, S., Mino, R.E., Fisher, E.S., and Bhat, M.A. (2017). A versatile genetic tool to study midline glia function in the *Drosophila* CNS. *Dev. Biol.* 429, 35–43.
- Barolo, S., La, C., Gfp, P.J.W., and Barolo, S. (2000). GFP and  $\beta$ -Galactosidase Transformation Vectors for Promoter/Enhancer Analysis in *Drosophila*. *Biotechniques* 29, 726–732.
- Bartscherer, K., Pelte, N., Ingelfinger, D., and Boutros, M. (2006). Secretion of Wnt Ligands Requires Evi, a Conserved Transmembrane Protein. *Cell* 125, 523–533.
- Bauer, S., Gagneur, J., and Robinson, P.N. (2010). Going Bayesian: Model-based gene set analysis of genome-scale data. *Nucleic Acids Res.* 38, 3523–3532.
- Baumgardt, M., Miguel-Aliaga, I., Karlsson, D., Ekman, H., and Thor, S. (2007). Specification of neuronal identities by feedforward combinatorial coding. *PLoS Biol.* 5, 295–308.
- Baumgardt, M., Karlsson, D., Terriente, J., Díaz-Benjumea, F.J., and Thor, S. (2009). Neuronal Subtype Specification within a Lineage by Opposing Temporal Feed-Forward Loops. *Cell* 139, 969–982.
- Baumgartner, S., Littleton, J.T., Broadie, K., Bhat, M.A., Harbecke, R., Lengyel, J.A., Chiquet-Ehrismann, R., Prokop, A., and Bellen, H.J. (1996). A *Drosophila* *neurexin* is required for septate junction and blood-nerve barrier formation and function. *Cell* 87, 1059–1068.
- Bayraktar, O.A., and Doe, C.Q. (2013). Combinatorial temporal patterning in progenitors expands neural diversity. *Nature* 498, 449–455.
- Beall, C.J., and Hirsh, J. (1987). Regulation of the *Drosophila* *dopa* decarboxylase gene in neuronal and glial cells. *Genes Dev.* 1, 510–520.
- Bellen, H.J., Tong, C., and Tsuda, H. (2010). 100 years of *Drosophila* research and its impact on vertebrate neuroscience: a history lesson for the future.
- Berger, C., Harzer, H., Burkard, T.R., Steinmann, J., van der Horst, S., Laurenson, A.S., Novatchkova, M., Reichert, H., and Knoblich, J.A. (2012). FACS Purification and Transcriptome Analysis of *Drosophila* Neural Stem Cells Reveals a Role for *Klumpfuß* in Self-Renewal. *Cell Rep.* 2, 407–418.
- Bertet, C., Li, X., Erlik, T., Cavey, M., Wells, B., and Desplan, C. (2014). Temporal patterning of neuroblasts controls Notch-mediated cell survival through regulation of *Hid* or *Reaper*. *Cell* 158, 1173–1186.
- Beshel, J., Dubnau, J., and Zhong, Y. (2017). A Leptin Analog Locally Produced in the Brain Acts via a Conserved Neural Circuit to Modulate Obesity-Linked Behaviors in *Drosophila*. *Cell Metab.* 25, 208–217.
- Beumer, K.J., Rohrbough, J., Prokop, A., and Broadie, K. (1999). A role for PS integrins in morphological growth and synaptic function at the postembryonic neuromuscular junction of *Drosophila*. *Development* 126, 5833–5846.
- Bhat, M.A., Izaddoost, S., Lu, Y., Cho, K.O., Choi, K.W., and Bellen, H.J. (1999). *Discs lost*, a novel multi-PDZ domain protein, establishes and maintains epithelial polarity. *Cell* 96, 833–845.
- Bifari, F., Decimo, I., Pino, A., Llorens-Bobadilla, E., Zhao, S., Lange, C., Panuccio, G., Boeckx, B., Thienpont, B., Vinckier, S., et al. (2017). Neurogenic Radial Glia-like Cells in Meninges Migrate and Differentiate into Functionally Integrated Neurons in the Neonatal Cortex. *Cell Stem Cell* 20, 360–373.e7.
- Bivik, C., Bahrapour, S., Ulvko, C., Nilsson, P., Angel, A., Fransson, F., Lundin, E., Renhorn, J., and Thor, S. (2015). Novel genes involved in controlling specification of *Drosophila* *FMR*amide neuropeptide

cells. *Genetics* 200, 1229–1244.

Blenau, W., Daniel, S., Balfanz, S., Thamm, M., and Baumann, A. (2017). Dm5-HT2B: Pharmacological Characterization of the Fifth Serotonin Receptor Subtype of *Drosophila melanogaster*. *Front. Syst. Neurosci.* 11, 1–11.

Borowsky, B., Adham, N., Jones, K.A., Raddatz, R., Artymyshyn, R., Ogozalek, K.L., Durkin, M.M., Lakhani, P.P., Bonini, J.A., Pathirana, S., et al. (2001). Trace amines: Identification of a family of mammalian G protein-coupled receptors. *Proc. Natl. Acad. Sci.* 98, 8966–8971.

Borrell, V., and Götz, M. (2014). Role of radial glial cells in cerebral cortex folding. *Curr. Opin. Neurobiol.* 27, 39–46.

Brand, A.H., and Perrimon, N. (1993). Targeted gene expression as a means of altering cell fates and generating dominant phenotypes. *Development* 118, 401–415.

Brennecke, P., Anders, S., Kim, J.K., Kołodziejczyk, A.A., Zhang, X., Proserpio, V., Baying, B., Benes, V., Teichmann, S.A., Marioni, J.C., et al. (2013). Accounting for technical noise in single-cell RNA-seq experiments. *Nat. Methods* 10, 1093–1098.

Broadie, K., Baumgartner, S., and Prokop, A. (2011). Extracellular matrix and its receptors in *drosophila* neural development. *Dev. Neurobiol.* 71, 1102–1130.

Brody, T., and Cravchik, A. (2000). *Drosophila melanogaster* G protein-coupled receptors. *J. Cell Biol.* 150, 83–88.

Buchon, N., Broderick, N.A., Kuraishi, T., and Lemaitre, B. (2010). *Drosophila* EGFR pathway coordinates stem cell proliferation and gut remodeling following infection. *BMC Biol.* 8.

Bunch, T., Graner, M.W., Fessler, L.I., Fessler, J.H., Schneider, K.D., Kerschen, A., Choy, L.P., Burgess, B.W., and Brower, D.L. (1998). The PS2 integrin ligand tiggrin is required for proper muscle function in *Drosophila*. *Development* 125, 1679–1689.

Bunzow, J.R., Sonders, M.S., Arttamangkul, S., Harrison, L.M., Zhang, G., Quigley, D.I., Darland, T., Suchland, K.L., Pasumamula, S., Kennedy, J.L., et al. (2001). Amphetamine, 3,4-Methylenedioxymethamphetamine, Lysergic Acid Diethylamide, and Metabolites of the Catecholamine Neurotransmitters Are Agonists of a Rat Trace Amine Receptor. *Mol. Pharmacol.* 60, 1181–1188.

Busch, S., and Tanimoto, H. (2010). Cellular configuration of single octopamine neurons in *Drosophila*. *J. Comp. Neurol.* 518, 2355–2364.

Busch, S., Selcho, M., Ito, K., and Tanimoto, H. (2009). A map of octopaminergic neurons in the *Drosophila* brain. *J. Comp. Neurol.* 513, 643–667.

## C

---

Cajal, S.R. (1909). Nota sobre la estructura de la retina de la mosca (*Calliphora vomitoria*). *Trab. Lab. Inv. Biol.* 7.

Cajal, S.R., and Sánchez, D. (1915). Contribución al conocimiento de los centros nerviosos de los insectos. *Trab. Lab. Inv. Biol.* 13, 1–168.

Cannell, E., Dornan, A.J., Halberg, K.A., Terhzaz, S., Dow, J.A.T., and Davies, S. (2016). The corticotropin-releasing factor-like diuretic hormone 44 (DH44) and kinin neuropeptides modulate desiccation and starvation tolerance in *Drosophila melanogaster*. *Peptides* 80, 96–107.

Carrillo, R.A., Özkan, E., Menon, K.P., Nagarkar-Jaiswal, S., Lee, P.T., Jeon, M., Birnbaum, M.E., Bellen, H.J., Garcia, K.C., and Zinn, K. (2015). Control of Synaptic Connectivity by a Network of *Drosophila* IgSF Cell Surface Proteins. *Cell* 163, 1770–1782.

Carvalho, A.B. (2002). Origin and evolution of the *Drosophila* Y chromosome. *Curr. Opin. Genet. Dev.* 12, 664–668.

Caygill, E.E., and Brand, A.H. (2017). miR-7 Buffers Differentiation in the Developing *Drosophila* Visual System. *Cell Rep.* 20, 1255–1261.

Ceron, J., González, C., and Tejedor, F.J. (2001). Patterns of cell division and expression of asymmetric cell fate determinants in postembryonic neuroblast lineages of *Drosophila*. *Dev. Biol.* 230, 125–138.

Ceron, J., Tejedor, F.J., and Moya, F. (2006). A primary cell culture of *Drosophila* postembryonic larval neuroblasts to study cell cycle and asymmetric division. *Eur. J. Cell Biol.* 85, 567–575.

Chartier, A., Zaffran, S., Astier, M., Sémériva, M., and Gratecos, D. (2002). Pericardin, a *Drosophila* type IV collagen-like protein is involved in the morphogenesis and maintenance of the heart epithelium during dorsal ectoderm closure. *Development* 129, 3241–3253.

Chell, J.M., and Brand, A.H. (2010). Nutrition-responsive glia control exit of neural stem cells from quiescence. *Cell* 143, 1161–1173.

Chen, Y., and Struhl, G. (1996). Dual roles for patched in sequestering and transducing Hedgehog. *Cell* 87, 553–563.

Chen, A., Ng, F., Lebestky, T., Grygoruk, A., Djapri, C., Lawal, H.O., Zaveri, H.A., Mehanzel, F., Najibi, R., Seidman, G., et al. (2013). Dispensable, redundant, complementary, and cooperative roles of dopamine, octopamine, and serotonin in *Drosophila melanogaster*. *Genetics* 193, 159–176.

Chen, C.-L., Gajewski, K.M., Hamaratoglu, F., Bossuyt, W., Sansores-Garcia, L., Tao, C., and Halder, G. (2010). The apical-basal cell polarity determinant Crumbs regulates Hippo signaling in *Drosophila*. *Proc. Natl. Acad. Sci.* 107, 15810–15815.

Chen, C., Jack, J., and Garofalo, R.S. (1996). The *Drosophila* Insulin Receptor Is Required for Normal Growth. *Endocrinology* 137, 846–856.

Chen, X., Quan, Y., Wang, H., and Luo, H. (2014). Trehalase regulates neuroepithelial stem cell maintenance and differentiation in the *Drosophila* optic lobe. *PLoS One* 9, e101433.

Chen, Z., Del Valle Rodriguez, A., Li, X., Erlik, T., Fernandes, V.M., and Desplan, C. (2016). A Unique Class of Neural Progenitors in the *Drosophila* Optic Lobe Generates Both Migrating Neurons and Glia. *Cell Rep.* 15, 774–786.

Chotard, C., and Salecker, I. (2007). Glial cell development and function in the *Drosophila* visual system. *Neuron Glia Biol.* 3, 17–25.

Clark, M.C., Dever, T.E., Dever, J.J., Xu, P., Rehder, V., Sosa, M.A., and Baro, D.J. (2004). Arthropod 5-HT 2 Receptors: A Neurohormonal Receptor in Decapod Crustaceans That Displays Agonist Independent Activity Resulting from an Evolutionary Alteration to the DRY Motif. *J. Neurosci.* 24, 3421–3435.

Colombani, J., Raisin, S., Pantalacci, S., Radimerski, T., Montagne, J., and Léopold, P. (2003). A Nutrient Sensor Mechanism Controls *Drosophila* Growth. *Cell* 114, 739–749.

Colonques, J., Ceron, J., and Tejedor, F.J. (2007). Segregation of postembryonic neuronal and glial lineages inferred from a mosaic analysis of the *Drosophila* larval brain. *Mech. Dev.* 124, 327–340.

Colonques, J., Ceron, J., Reichert, H., and Tejedor, F.J. (2011). A transient expression of prospero promotes cell cycle exit of *drosophila* postembryonic neurons through the regulation of Dacapo. *PLoS One* 6, e19342.

Comber, K., Huelsmann, S., Evans, I., Sanchez-Sanchez, B.J., Chalmers, A., Reuter, R., Wood, W., and Martin-Bermudo, M.D. (2013). A dual role for the PS integrin myospheroid in mediating *Drosophila* embryonic macrophage migration. *J. Cell Sci.* 126, 3475–3484.

Couso, J.P., Bishop, S. a, and Martinez Arias, A. (1994). The wingless signalling pathway and the patterning of the wing margin in *Drosophila*. *Development* 120, 621–636.

Croset, V., Treiber, C.D., and Waddell, S. (2017). Cellular diversity in the *Drosophila* midbrain revealed by single-cell transcriptomics. *Elife* 4889–4896.

## D

---

Daines, B., Wang, H., Wang, L., Li, Y., Han, Y., Emmert, D., Gelbart, W., Wang, X., Li, W., Gibbs, R., et al. (2011). The *Drosophila melanogaster* transcriptome by paired-end RNA sequencing. *Genome Res.* 21, 315–324.



- Dani, N., and Lehtinen, M.K. (2016). CSF makes waves in the neural stem cell niche. *Cell Stem Cell* 19, 87–92.
- Das, A., Gupta, T., Davla, S., Godino Prieto, L.L., Diegelmann, S., Reddy, O.V., Vijayraghavan, K., Reichert, H., Lovick, J., and Hartenstein, V. (2013). Neuroblast lineage-specific origin of the neurons of the *Drosophila* larval olfactory system. *Dev. Biol.* 373, 322–337.
- Davis, F.P., Nern, A., Picard, S., Reiser, M.B., Rubin, G.M., Eddy, S.R., and Henry, G.L. (2018). A genetic, genomic, and computational resource for exploring neural circuit function. *BioRxiv*.
- Deady, L.D., and Sun, J. (2015). A Follicle Rupture Assay Reveals an Essential Role for Follicular Adrenergic Signaling in *Drosophila* Ovation. *PLoS Genet.* 11, 1–21.
- Delaunay, D., Kawaguchi, A., Dehay, C., and Matsuzaki, F. (2017). Division modes and physical asymmetry in cerebral cortex progenitors. *Curr. Opin. Neurobiol.* 42, 75–83.
- Delon, I., and Brown, N.H. (2009). The integrin adhesion complex changes its composition and function during morphogenesis of an epithelium. *J. Cell Sci.* 122, 4363–4374.
- Denno, M.E., Privman, E., and Venton, B.J. (2015). Analysis of neurotransmitter tissue content of *drosophila melanogaster* in different life stages. *ACS Chem. Neurosci.* 6, 117–123.
- Dentesano, G., Serratos, J., Tusell, J.M., Ramón, P., Valente, T., Saura, J., and Solà, C. (2014). CD200R1 and CD200 expression are regulated by PPAR- $\gamma$  in activated glial cells. *Glia* 62, 982–998.
- DeSalvo, M.K., Mayer, N., Mayer, F., and Bainton, R.J. (2011). Physiologic and Anatomic Characterization of the Brain Surface Glia Barrier of *Drosophila*. *Glia* 59, 1322–1340.
- DeSalvo, M.K., Hindle, S.J., Rusan, Z.M., Orng, S., Eddison, M., Halliwill, K., and Bainton, R.J. (2014). The *Drosophila* surface glia transcriptome: Evolutionary conserved blood-brain barrier processes. *Front. Neurosci.* 8, 1–22.
- Dewey, E.M., McNabb, S.L., Ewer, J., Kuo, G.R., Takanishi, C.L., Truman, J.W., and Honegger, H.-W. (2004). Identification of the Gene Encoding Bursicon, an Insect Neuropeptide Responsible for Cuticle Sclerotization and Wing Spreading. *Curr. Biol.* 14, 1208–1213.
- Diao, F., Ironfield, H., Luan, H., Diao, F., Shropshire, W.C., Ewer, J., Marr, E., Potter, C.J., Landgraf, M., and White, B.H. (2015). Plug-and-Play Genetic Access to *Drosophila* Cell Types Using Exchangeable Exon Cassettes. *Cell Rep.* 10, 1410–1421.
- Dillard, C., Narbonne-Reveau, K., Foppolo, S., Lanet, E., and Maurange, C. (2018). Two distinct mechanisms silence *chinmo* in *Drosophila* neuroblasts and neuroepithelial cells to limit their self-renewal. *Development* 145, dev154534.
- Ding, R., Weynans, K., Bossing, T., Barros, C.S., and Berger, C. (2016). The Hippo signalling pathway maintains quiescence in *Drosophila* neural stem cells. *Nat. Commun.* 7, 1–12.
- Dobin, A., Davis, C.A., Schlesinger, F., Drenkow, J., Zaleski, C., Jha, S., Batut, P., Chaisson, M., and Gingeras, T.R. (2013). STAR: Ultrafast universal RNA-seq aligner. *Bioinformatics* 29, 15–21.
- Doe, C.Q. (2017). Temporal Patterning in the *Drosophila* CNS. *Annu. Rev. Cell Dev. Biol.* 33, 219–240.
- Doherty, J., Logan, M.A., Tasdemir, O.E., and Freeman, M.R. (2009). Ensheathing Glia Function as Phagocytes in the Adult *Drosophila* Brain. *J. Neurosci.* 29, 4768–4781.
- Dong, X., Tsuda, L., Zavitz, K.H., Lin, M., Li, S., Carthew, R.W., and Zipursky, S.L. (1999). *ebi* regulates epidermal growth factor receptor signaling pathways in *Drosophila*. *Genes Dev.* 13, 954–965.
- Drosophila* 12 Genomes Consortium, Clark, A.G., Eisen, M.B., Smith, D.R., Bergman, C.M., Oliver, B., Markow, T.A., Kaufman, T.C., Kellis, M., Gelbart, W., et al. (2007). Evolution of genes and genomes on the *Drosophila* phylogeny. *Nature* 450, 203–218.
- Droujinine, I.A., and Perrimon, N. (2016). Interorgan Communication Pathways in Physiology: Focus on *Drosophila*. In *Annual Review of Genetics*, pp. 539–570.
- Du, L., Zhou, A., Patel, A., Rao, M., Anderson, K., and Roy, S. (2017). Unique patterns of organization and migration of FGF-expressing cells during *Drosophila* morphogenesis. *Dev. Biol.* 427, 35–48.

Dudoit, S., Yang, Y., Callow, M., and Speed, T. (2002). Statistical methods for identifying differentially expressed genes in replicated cDNA microarray experiments. *Stat. Sin.* 1–38.

Dupont, P., Besson, M.-T., Devaux, J., and Liévens, J.-C. (2012). Reducing canonical Wingless/Wnt signaling pathway confers protection against mutant Huntingtin toxicity in *Drosophila*. *Neurobiol. Dis.* 47, 237–247.

Duronio, R.J., and Xiong, Y. (2013). Signaling pathways that control cell proliferation. *Cold Spring Harb. Perspect. Biol.* 5, a008904.

Dutta, D., Xiang, J., and Edgar, B.A. (2013). RNA Expression Profiling from FACS-Isolated Cells of the *Drosophila* Intestine. *Curr. Protoc. Stem Cell Biol.* 2F.2, 1–12.

## E

---

Egger, B., Boone, J.Q., Stevens, N.R., Brand, A.H., and Doe, C.Q. (2007). Regulation of spindle orientation and neural stem cell fate in the *Drosophila* optic lobe. *Neural Dev.* 2, 1–14.

Egger, B., Gold, K.S., and Brand, A.H. (2010). Notch regulates the switch from symmetric to asymmetric neural stem cell division in the *Drosophila* optic lobe. *Development* 137, 2981–2987.

El-Kholy, S., Stephano, F., Li, Y., Bhandari, A., Fink, C., and Roeder, T. (2015). Expression analysis of octopamine and tyramine receptors in *Drosophila*. *Cell Tissue Res.* 361, 669–684.

Erclik, T., Li, X., Courgeon, M., Bertet, C., Chen, Z., Baumert, R., Ng, J., Koo, C., Arain, U., Behnia, R., et al. (2017). Integration of temporal and spatial patterning generates neural diversity. *Nature* 541, 365–370.

Erspamer, V. (1948). Active Substances in the Posterior Salivary Glands of Octopoda. I. Enteramine-like Substance. *Acta Pharmacol. Toxicol. (Copenh.)* 213–223.

Estrada, B., Gisselbrecht, S.S., and Michelson, A.M. (2007). The transmembrane protein Perdido interacts with Grip and integrins to mediate myotube projection and attachment in the *Drosophila* embryo. *Development* 134, 4469–4478.

Evans, P.D., and Maqueira, B. (2005). Insect octopamine receptors: A new classification scheme based on studies of cloned *Drosophila* G-protein coupled receptors. *Invertebr. Neurosci.* 5, 111–118.

Evans, C.J., Olson, J.M., Ngo, K.T., Kim, E., Lee, N.E., Kuoy, E., Patananan, A.N., Sitz, D., Tran, P.T., Do, M.T., et al. (2009). G-TRACE: Rapid Gal4-based cell lineage analysis in *Drosophila*. *Nat. Methods* 6, 603–605.

Ewels, P., Magnusson, M., Lundin, S., and Källér, M. (2016). MultiQC: Summarize analysis results for multiple tools and samples in a single report. *Bioinformatics* 32, 3047–3048.

Ewing, B., and Green, P. (1998). Base-Calling of Automated Sequencer Traces Using. *Genome Res.* 8, 186–197.

## F

---

Fabregat, A., Jupe, S., Matthews, L., Sidiropoulos, K., Gillespie, M., Garapati, P., Haw, R., Jassal, B., Korninger, F., May, B., et al. (2018). The Reactome Pathway Knowledgebase. *Nucleic Acids Res.* 46, D649–D655.

Faisal, M.N., Hoffmann, J., El-Kholy, S., Kallsen, K., Wagner, C., Bruchhaus, I., Fink, C., and Roeder, T. (2014). Transcriptional regionalization of the fruit fly's airway epithelium. *PLoS One* 9, e102534.

Fang, H., and Gough, J. (2013). DcGO: Database of domain-centric ontologies on functions, phenotypes, diseases and more. *Nucleic Acids Res.* 41, D536–D544.

Fernandes, V.M., Chen, Z., Rossi, A.M., Zipfel, J., and Desplan, C. (2017). Glia relay differentiation cues to coordinate neuronal development in *Drosophila*. *Science.* 357, 886–891.

Fernandez, R., Tabarini, D., Azpiazu, N., Frasch, M., and Schlessinger, J. (1995). The *Drosophila* insulin receptor homolog: a gene essential for embryonic development encodes two receptor isoforms with different signaling potential. *EMBO J.* 14, 3373–3384.

Fietz, S.A., Kelava, I., Vogt, J., Wilsch-Bräuninger, M., Stenzel, D., Fish, J.L., Corbeil, D., Riehn, A., Distler, W., Nitsch, R., et al. (2010). OSVZ progenitors of human and ferret neocortex are epithelial-like and expand by integrin signaling. *Nat. Neurosci.* 13, 690–699.

Fogerty, F.J., Fessler, L.I., Bunch, T. a, Yaron, Y., Parker, C.G., Nelson, R.E., Brower, D.L., Gullberg, D., and Fessler, J.H. (1994). Tiggrin, a novel *Drosophila* extracellular matrix protein that functions as a ligand for *Drosophila* alpha PS2 beta PS integrins. *Development* 120, 1747–1758.

Fontana, J.R., and Crews, S.T. (2012). Transcriptome Analysis of *Drosophila* CNS Midline Cells Reveals Diverse Peptidergic Properties and a Role for *castor* in Neuronal Differentiation. *Dev. Biol.* 372, 131–142.

Fox, L.E., Soll, D.R., and Wu, C.-F. (2006). Coordination and Modulation of Locomotion Pattern Generators in *Drosophila* Larvae: Effects of Altered Biogenic Amine Levels by the Tyramine beta Hydroxylase Mutation. *J. Neurosci.* 26, 1486–1498.

Freeman, M. (2002). A fly's eye view of EGF receptor signalling. *EMBO J.* 21, 6635–6642.

Freeman, M.R. (2015). *Drosophila* central nervous system glia. *Cold Spring Harb. Perspect. Biol.* 7, 1–14.

Freeman, M.R., and Doherty, J. (2006). Glial cell biology in *Drosophila* and vertebrates. *Trends Neurosci.* 29, 82–90.

Freeman, M.R., Delrow, J., Kim, J., Johnson, E., and Doe, C.Q. (2003). Unwrapping glial biology: *Gcm* target genes regulating glial development, diversification, and function. *Neuron* 38, 567–580.

## G

---

Gao, X.J., Potter, C.J., Gohl, D.M., Silies, M., Katsov, A.Y., Clandinin, T.R., and Luo, L. (2013). Specific Kinematics and Motor-Related Neurons for Aversive Chemotaxis in *Drosophila*. *Curr. Biol.* 23, 1163–1172.

Garelli, A., Gontijo, A.M., Miguela, V., Caparros, E., and Dominguez, M. (2012). Imaginal Discs Secrete Insulin-Like Peptide 8 to Mediate Plasticity of Growth and Maturation. *Science.* 336, 579–583.

Gaudet, P., Livstone, M.S., Lewis, S.E., and Thomas, P.D. (2011). Phylogenetic-based propagation of functional annotations within the Gene Ontology consortium. *Brief. Bioinform.* 12, 449–462.

Gay, L., Karfilis, K. V., Miller, M.R., Doe, C.Q., and Stankunas, K. (2014). Applying thiouracil tagging to mouse transcriptome analysis. *Nat. Protoc.* 9, 410–420.

Gentleman, R., Carey, V., Bates, D., Bolstad, B., Dettling, M., Dudoit, S., Ellis, B., Gautier, L., Ge, Y., Gentry, J., et al. (2004). Bioconductor: open software development for computational biology and bioinformatics. *Genome Biol.* 5, R80.

Gerstein, M.B., Rozowsky, J., Yan, K.K., Wang, D., Cheng, C., Brown, J.B., Davis, C.A., Hillier, L., Sisu, C., Li, J.J., et al. (2014). Comparative analysis of the transcriptome across distant species. *Nature* 512, 445–448.

Gnerer, J.P., Venken, K.J.T., and Dierick, H.A. (2015). Gene-specific cell labeling using MiMIC transposons. *Nucleic Acids Res.* 43, 1–13.

GO Consortium (2017). Expansion of the gene ontology knowledgebase and resources. *Nucleic Acids Res.* 45, D331–D338.

GO Consortium, Ashburner, M., Ball, C.A., Blake, J.A., Botstein, D., Butler, H., Cherry, J.M., Davis, A.P., Dolinski, K., Dwight, S.S., et al. (2000). Gene Ontology: tool for the unification of biology. *Nat. Genet.* 25, 25–29.

Gold, K.S., and Brand, A.H. (2014). Optix defines a neuroepithelial compartment in the optic lobe of the *Drosophila* brain. *Neural Dev.* 9, 1–16.

Gomez, J.M., Wang, Y., and Riechmann, V. (2012). Tao controls epithelial morphogenesis by promoting Fasciclin 2 endocytosis. *J. Cell Biol.* 199, 1131–1143.

Goodman, W.G., and Granger, N.A. (2005). The Juvenile Hormones. In *Comprehensive Molecular Insect Science*, pp. 319–408.

Gough, J., Karplus, K., Hughey, R., and Chothia, C. (2001). Assignment of homology to genome sequences using a library of hidden Markov models that represent all proteins of known structure. *J. Mol. Biol.* 313, 903–919.

Granger, N. a, Sturgis, S.L., Ebersohl, R., Geng, C., and Sparks, T.C. (1996). Dopaminergic control of corpora allata activity in the larval tobacco hornworm, *Manduca sexta*. *Arch. Insect Biochem. Physiol.* 32, 449–466.

Gratz, S.J., Cummings, A.M., Nguyen, J.N., Hamm, D.C., Donohue, L.K., Harrison, M.M., Wildonger, J., and O'connor-Giles, K.M. (2013). Genome engineering of *Drosophila* with the CRISPR RNA-guided Cas9 nuclease. *Genetics* 194, 1029–1035.

Greer, C.L., Grygoruk, A., Patton, D.E., Ley, B., Romero-Calderon, R., Chang, H.Y., Houshyar, R., Bainton, R.J., DiAntonio, A., and Krantz, D.E. (2005). A splice variant of the *Drosophila* vesicular monoamine transporter contains a conserved trafficking domain and functions in the storage of dopamine, serotonin, and octopamine. *J. Neurobiol.* 64, 239–258.

Grenningloh, G., Jay Rehm, E., and Goodman, C.S. (1991). Genetic analysis of growth cone guidance in *drosophila*: Fasciclin II functions as a neuronal recognition molecule. *Cell* 67, 45–57.

Guillermin, O., Perruchoud, B., Sprecher, S.G., and Egger, B. (2015). Characterization of tailless functions during *Drosophila* optic lobe formation. *Dev. Biol.* 405, 202–213.

Gulden, F.O., and Šestan, N. (2014). Neurobiology: Building a bigger brain. *Nature* 515, 206–207.

GuptaRoy, B., Beckingham, K., and Griffith, L.C. (1996). Functional Diversity of Alternatively Spliced Isoforms of *Drosophila* Ca<sup>2+</sup>/Calmodulin-Dependent Protein Kinase II. *J. Biol. Chem.* 271, 19846–19851.

## H

---

Hakeda-Suzuki, S., Takechi, H., Kawamura, H., and Suzuki, T. (2017). Two receptor tyrosine phosphatases dictate the depth of axonal stabilizing layer in the visual system. *Elife* 6, 1–25.

Hakes, A.E., Otsuki, L., and Brand, A.H. (2018). A newly discovered neural stem cell population is generated by the optic lobe neuroepithelium during embryogenesis in *Drosophila melanogaster*. *Development* 145, dev166207.

Han, K.-A., Millar, N.S., Grotewiel, M.S., and Davis, R.L. (1996). DAMB, a Novel Dopamine Receptor Expressed Specifically in *Drosophila* Mushroom Bodies. *Neuron* 16, 1127–1135.

Han, K.-A., Millar, N.S., and Davis, R.L. (1998). A novel octopamine receptor with preferential expression in *Drosophila* mushroom bodies. *J. Neurosci.* 18, 3650–3658.

Hartenstein, V. (2011). Morphological diversity and development of glia in *Drosophila*. *Glia* 59, 1237–1252.

Hartenstein, V., Younossi-Hartenstein, A., Lovick, J., Kong, A., Omoto, J., Ngo, K., and Viktorin, G. (2015). Lineage-associated tracts defining the anatomy of the *Drosophila* first instar larval brain. *Dev. Biol.* 406, 14–39.

Harzer, H., Berger, C., Conder, R., Schmauss, G., and Knoblich, J.A. (2013). FACS purification of *Drosophila* larval neuroblasts for next-generation sequencing. *Nat. Protoc.* 8, 1088–1099.

Hauser, F., Cazzamali, G., Williamson, M., Blenau, W., and Grimmelikhuijzen, C.J.P. (2006). A review of neurohormone GPCRs present in the fruitfly *Drosophila melanogaster* and the honey bee *Apis mellifera*. *Prog. Neurobiol.* 80, 1–19.

Herculano-Houzel, S. (2009). The human brain in numbers: a linearly scaled-up primate brain. *Front. Hum. Neurosci.* 3, 1–11.

Herr, P., and Basler, K. (2012). Porcupine-mediated lipidation is required for Wnt recognition by Wls. *Dev. Biol.* 361, 392–402.

Hewes, R.S., and Taghert, P.H. (2001). Neuropeptides and neuropeptide receptors in the *Drosophila melanogaster* genome. *Genome Res.* 11, 1126–1142.

Hidalgo, A., Kinrade, E.F. V, and Georgiou, M. (2001). The *Drosophila* Neuregulin Vein Maintains Glial

Survival during Axon Guidance in the CNS. *Dev. Cell* 1, 679–690.

Hildebrandt, A., Pflanz, R., Behr, M., Tarp, T., Riedel, D., and Schuh, R. (2015). Bark beetle controls epithelial morphogenesis by septate junction maturation in *Drosophila*. *Dev. Biol.* 400, 237–247.

Himmelreich, S., Masuho, I., Berry, J.A., MacMullen, C., Skamangas, N.K., Martemyanov, K.A., and Davis, R.L. (2017). Dopamine Receptor DAMB Signals via Gq to Mediate Forgetting in *Drosophila*. *Cell Rep.* 21, 2074–2081.

Hiruma, K., and Kaneko, Y. (2013). Hormonal Regulation of Insect Metamorphosis with Special Reference to Juvenile Hormone Biosynthesis. In *Current Topics in Developmental Biology*, pp. 73–100.

Hodgetts, R.B., and O’Keefe, S.L. (2006). DOPA DECARBOXYLASE: A Model Gene-Enzyme System for Studying Development, Behavior, and Systematics. *Annu. Rev. Entomol.* 51, 259–284.

Hofbauer, A., and Campos-Ortega, J.A. (1990). Proliferation pattern and early differentiation of the optic lobes in *Drosophila melanogaster*. *Roux’s Arch. Dev. Biol.* 198, 264–274.

Homem, C.C.F., and Knoblich, J.A. (2012). *Drosophila* neuroblasts: a model for stem cell biology. *Development* 139, 4297–4310.

Homem, C.C.F., Repic, M., and Knoblich, J.A. (2015). Proliferation control in neural stem and progenitor cells. *Nat. Rev. Neurosci.* 16, 647–659.

Honegger, H.W., Market, D., Pierce, L.A., Dewey, E.M., Kostron, B., Wilson, M., Choi, D., Klukas, K.A., and Mesce, K.A. (2002). Cellular localization of bursicon using antisera against partial peptide sequences of this insect cuticle-sclerotizing neurohormone. *J. Comp. Neurol.* 452, 163–177.

Hoppe, P.S., Coutu, D.L., and Schroeder, T. (2014). Single-cell technologies sharpen up mammalian stem cell research. *Nat. Cell Biol.* 16, 919–927.

Howell, K., and Hobert, O. (2016). Small Immunoglobulin Domain Proteins at Synapses and the Maintenance of Neuronal Features. *Neuron* 89, 239–241.

Hrdlicka, L., Gibson, M., Kiger, A., Micchelli, C., Schober, M., Schöck, F., and Perrimon, N. (2002). Analysis of twenty-four Gal4 lines in *Drosophila melanogaster*. *Genesis* 34, 51–57.

Huang, Z., and Kunes, S. (1996). Hedgehog, transmitted along retinal axons, triggers neurogenesis in the developing visual centers of the *Drosophila* brain. *Cell* 86, 411–422.

Huang, J., Liu, W., Qi, Y., Luo, J., and Montell, C. (2016). Neuromodulation of courtship drive through tyramine-responsive neurons in the *Drosophila* brain. *Curr. Biol.* 26, 2246–2256.

Huang, Z., Shilo, B.Z., and Kunes, S. (1998). A retinal axon fascicle uses Spitz, an EGF receptor ligand, to construct a synaptic cartridge in the brain of *Drosophila*. *Cell* 95, 693–703.

Huber, W., Carey, V.J., Gentleman, R., Anders, S., Carlson, M., Carvalho, B.S., Bravo, H.C., Davis, S., Gatto, L., Girke, T., et al. (2015). Orchestrating high-throughput genomic analysis with Bioconductor. *Nat. Methods* 12, 115–121.

Huelsmann, S., Hepper, C., Marchese, D., Knöll, C., and Reuter, R. (2006). The PDZ-GEF Dizzy regulates cell shape of migrating macrophages via Rap1 and integrins in the *Drosophila* embryo. *Development* 133, 2915–2924.

Hyun, S., Lee, J.H., Jin, H., Nam, J.W., Namkoong, B., Lee, G., Chung, J., and Kim, V.N. (2009). Conserved MicroRNA miR-8/miR-200 and Its Target USH/FOG2 Control Growth by Regulating PI3K. *Cell* 139, 1096–1108.

I

---

Isabella, A.J., and Horne-Badovinac, S. (2016). Building from the ground up: basement membranes in *Drosophila* development. *Curr. Top. Membr.* 76, 305–336.

Ito, K., Awano, W., Suzuki, K., Hiromi, Y., and Yamamoto, D. (1997). The *Drosophila* mushroom body is a quadruple structure of clonal units each of which contains a virtually identical set of neurones and glial cells. *Development* 124, 761–771.

## J

---

- Jacob, J., Maurange, C., and Gould, A.P. (2008). Temporal control of neuronal diversity: common regulatory principles in insects and vertebrates? *Development* 135, 3481–3489.
- Jaiswal, M., Sandoval, H., Zhang, K., Bayat, V., and Bellen, H.J. (2012). Probing Mechanisms That Underlie Human Neurodegenerative Diseases in *Drosophila*. *Annu. Rev. Genet.* 46, 371–396.
- Jakobs, R., Ahmadi, B., Houben, S., Gariepy, T.D., and Sinclair, B.J. (2017). Cold tolerance of third-instar *Drosophila suzukii* larvae. *J. Insect Physiol.* 96, 45–52.
- Jaszczak, J.S., and Halme, A. (2016). Arrested development: coordinating regeneration with development and growth in *Drosophila melanogaster*. *Curr. Opin. Genet. Dev.* 40, 87–94.
- Jefferis, G.S.X.E., Marin, E.C., Stocker, R.F., and Luo, L. (2001). Target neuron prespecification in the olfactory map of *Drosophila*. *Nature* 414, 204–208.
- Jenett, A., Rubin, G.M., Ngo, T.T.B., Shepherd, D., Murphy, C., Dionne, H., Pfeiffer, B.D., Cavallaro, A., Hall, D., Jeter, J., et al. (2012). A GAL4-Driver Line Resource for *Drosophila* Neurobiology. *Cell Rep.* 2, 991–1001.
- Jin, M.H., Sawamoto, K., Ito, M., and Okano, H. (2000). The Interaction between the *Drosophila* Secreted Protein Argos and the Epidermal Growth Factor Receptor Inhibits Dimerization of the Receptor and Binding of Secreted Spitz to the Receptor. *Mol. Cell. Biol.* 20, 2098–2107.
- Johnson, E.C., Bohn, L.M., and Taghert, P.H. (2004). *Drosophila* CG8422 encodes a functional diuretic hormone receptor. *J. Exp. Biol.* 207, 743–748.
- Jørgensen, L.M., Hauser, F., Cazzamali, G., Williamson, M., and Grimmelikhuijzen, C.J.P. (2006). Molecular identification of the first SIFamide receptor. *Biochem. Biophys. Res. Commun.* 340, 696–701.
- Juarez-Carreño, S., Morante, J., and Dominguez, M. (2018). Systemic signalling and local effectors in developmental stability, body symmetry, and size. *Cell Stress* 2, 340–361.

## K

---

- Kanai, M.I., Kim, M.J., Akiyama, T., Takemura, M., Wharton, K., O'Connor, M.B., and Nakato, H. (2018). Regulation of neuroblast proliferation by surface glia in the *Drosophila* larval brain. *Sci. Rep.* 8, 1–15.
- Karandikar, U.C., Jin, M., Jusiak, B., Kwak, S.J., Chen, R., and Mardon, G. (2014). *Drosophila* eyes absent is required for normal cone and pigment cell development. *PLoS One* 9, e102143.
- Kato, K., Forero, M.G., Fenton, J.C., and Hidalgo, A. (2011). The Glial Regenerative Response to Central Nervous System Injury Is Enabled by Pros-Notch and Pros-NF  $\kappa$  B Feedback. *PLoS Biol.* 9, 6–9.
- Kato, K., Losada-Perez, M., and Hidalgo, A. (2017). Gene network underlying the glial regenerative response to central nervous system injury. *Dev. Dyn.* 247, 85–93.
- Kaufman, T.C. (2017). A short history and description of *Drosophila melanogaster* classical genetics: Chromosome aberrations, forward genetic screens, and the nature of mutations. *Genetics* 206, 665–689.
- Kaufman, L., and Rousseeuw, P.J. (1990). *Finding Groups in Data* (New York, NY: John Wiley & Sons).
- Keightley, P.D., Trivedi, U., Thomson, M., Oliver, F., Kumar, S., and Blaxter, M.L. (2009). Analysis of the genome sequences of three *Drosophila melanogaster* spontaneous mutation accumulation lines. *Genome Res.* 19, 1195–1201.
- Kerr, K.S., Fuentes-Medel, Y., Brewer, C., Barria, R., Ashley, J., Abruzzi, K.C., Sheehan, A., Tasdemir-Yilmaz, O.E., Freeman, M.R., and Budnik, V. (2014). Glial Wingless/Wnt Regulates Glutamate Receptor Clustering and Synaptic Physiology at the *Drosophila* Neuromuscular Junction. *J. Neurosci.* 34, 2910–2920.
- Khadilkar, R.J., Ray, A., Chetan, D.R., Sinha, A.R., Magadi, S., Kulkarni, V., and Inamdar, M.S. (2017). Differential modulation of the cellular and humoral immune responses in *Drosophila* is mediated by the endosomal ARF1-Asrij axis. *Sci. Rep.* 7, 1–14.

Kim, M.D., Wen, Y., and Jan, Y. (2009). Patterning and Organization of Motor Neuron Dendrites in the *Drosophila* Larva. *Dev. Biol.* 336, 213–221.

Kim, Y.-C., Lee, H.-G., Lim, J., and Han, K.-A. (2013). Appetitive Learning Requires the Alpha1-Like Octopamine Receptor OAMB in the *Drosophila* Mushroom Body Neurons. *J. Neurosci.* 33, 1672–1677.

King, A.N., Barber, A.F., Smith, A.E., Nitabach, M.N., Cavanaugh, D.J., Sehgal, A., King, A.N., Barber, A.F., Smith, A.E., Dreyer, A.P., et al. (2017). A Peptidergic Circuit Links the Circadian Clock to Locomotor Activity. *Curr. Biol.* 27, 1915–1927.

Kiss, M., Kiss, A.A., Radics, M., Popovics, N., Hermes, E., Csiszár, K., and Mink, M. (2016). *Drosophila* type IV collagen mutation associates with immune system activation and intestinal dysfunction. *Matrix Biol.* 49, 120–131.

Klein, D.E., Nappi, V.M., Reeves, G.T., Shvartsman, S.Y., and Lemmon, M.A. (2004). Argos inhibits epidermal growth factor receptor signalling by ligand sequestration. *Nature* 430, 1040–1044.

Knibiehler, B., Mirre, C., Cecchini, J.P., and Le Parco, Y. (1987). Haemocytes accumulate collagen transcripts during *Drosophila melanogaster* metamorphosis. *Roux's Arch. Dev. Biol.* 196, 243–247.

Kohwi, M., and Doe, C.Q. (2013). Temporal fate specification and neural progenitor competence during development. *Nat. Rev. Neurosci.* 14, 823–838.

Kolodziejczyk, A.A., Kim, J.K., Svensson, V., Marioni, J.C., and Teichmann, S.A. (2015). The Technology and Biology of Single-Cell RNA Sequencing. *Mol. Cell* 58, 610–620.

Königshoff, M., Dumitrescu, R., Udaltov, S., Amarie, O.V., Reiter, R., Grimminger, F., Seeger, W., Schermuly, R.T., and Eickelberg, O. (2010). Increased expression of 5-hydroxytryptamine2A/B receptors in idiopathic pulmonary fibrosis: a rationale for therapeutic intervention. *Thorax* 65, 949–955.

Koniszewski, N.D.B., Kollmann, M., Bigham, M., Farnworth, M., He, B., Büscher, M., Hütteroth, W., Binzer, M., Schachtner, J., and Bucher, G. (2016). The insect central complex as model for heterochronic brain development—background, concepts, and tools. *Dev. Genes Evol.* 226, 209–219.

Koon, A.C., and Budnik, V. (2012). Inhibitory Control of Synaptic and Behavioral Plasticity by Octopaminergic Signaling. *J. Neurosci.* 32, 6312–6322.

Koon, A.C., Ashley, J., Barria, R., Dasgupta, S., Brain, R., Waddell, S., Alkema, M.J., and Budnik, V. (2011). Autoregulatory and paracrine control of synaptic and behavioral plasticity by octopaminergic signaling. *Nat. Neurosci.* 14, 190–201.

Korzelius, J., Naumann, S.K., Loza-Coll, M.A., Chan, J.S., Dutta, D., Oberheim, J., Gläßer, C., Southall, T.D., Brand, A.H., Jones, D.L., et al. (2014). Escargot maintains stemness and suppresses differentiation in *Drosophila* intestinal stem cells. *EMBO J.* 33, 2967–2982.

Kunitomo, H., Uesugi, H., Kohara, Y., and Iino, Y. (2005). Identification of ciliated sensory neuron-expressed genes in *Caenorhabditis elegans* using targeted pull-down of poly(A) tails. *Genome Biol.* 6, R17.

Kunz, T., Kraft, K.F., Technau, G.M., and Urbach, R. (2012). Origin of *Drosophila* mushroom body neuroblasts and generation of divergent embryonic lineages. *Development* 139, 2510–2522.

## L

---

Lai, S.L., and Lee, T. (2006). Genetic mosaic with dual binary transcriptional systems in *Drosophila*. *Nat. Neurosci.* 9, 703–709.

Landgraf, M., and Thor, S. (2006). Development and Structure of Motoneurons. *Int. Rev. Neurobiol.* 75, 33–53.

Lanet, E., Gould, A.P., and Maurange, C. (2013). Protection of Neuronal Diversity at the Expense of Neuronal Numbers during Nutrient Restriction in the *Drosophila* Visual System. *Cell Rep.* 3, 587–594.

Laplante, C. (2006). Differential expression of the adhesion molecule Echinoid drives epithelial morphogenesis in *Drosophila*. *Development* 133, 3255–3264.

- Larsen, C., Shy, D., Spindler, S.R., Fung, S., Pereanu, W., Younossi-Hartenstein, A., and Hartenstein, V. (2009). Patterns of growth, axonal extension and axonal arborization of neuronal lineages in the developing *Drosophila* brain. *Dev. Biol.* 335, 289–304.
- Lazareva, A.A., Roman, G., Mattox, W., Hardin, P.E., and Dauwalder, B. (2007). A role for the adult fat body in *Drosophila* male courtship behavior. *PLoS Genet.* 3, 0115–0122.
- Lee, T. (2017). Wiring the *Drosophila* Brain with Individually Tailored Neural Lineages. *Curr. Biol.* 27, R77–R82.
- Lee, T., and Luo, L. (1999). Mosaic analysis with a repressible neurotechnique cell marker for studies of gene function in neuronal morphogenesis. *Neuron* 22, 451–461.
- Lee, Y., and Sun, Y.H. (2015). Maintenance of Glia in the Optic Lamina Is Mediated by EGFR Signaling by Photoreceptors in Adult *Drosophila*. *PLoS Genet.* 11, 1–32.
- Lee, H.G., Seong, C.S., Kim, Y.C., Davis, R.L., and Han, K.A. (2003). Octopamine receptor OAMB is required for ovulation in *Drosophila melanogaster*. *Dev. Biol.* 264, 179–190.
- Lee, H.G., Rohila, S., and Han, K.A. (2009). The octopamine receptor OAMB mediates ovulation via Ca<sup>2+</sup>/calmodulin-dependent protein kinase II in the *Drosophila* oviduct epithelium. *PLoS One* 4, 1–9.
- Lee, P.T., Zirin, J., Kanca, O., Lin, W.W., Schulze, K.L., Li-Kroeger, D., Tao, R., Devereaux, C., Hu, Y., Chung, V., et al. (2018). A gene-specific T2A-GAL4 library for *drosophila*. *Elife* 7, 1–24.
- Lee, T., Lee, A., and Luo, L. (1999). Development of the *Drosophila* mushroom bodies: sequential generation of three distinct types of neurons from a neuroblast. *Development* 126, 4065–4076.
- van de Leemput, J., Boles, N.C., Kiehl, T.R., Corneo, B., Lederman, P., Menon, V., Lee, C., Martinez, R.A., Levi, B.P., Thompson, C.L., et al. (2014). CORTECON: A temporal transcriptome analysis of in vitro human cerebral cortex development from human embryonic stem cells. *Neuron* 83, 51–68.
- Levin, J.Z., Yassour, M., Adiconis, X., Nusbaun, C., Thompson, D.A., Friedman, N., Gnirke, A., and Regev, A. (2010). Comprehensive comparative analysis of strand specific RNA sequencing methods. *Nat. Methods* 7, 709–715.
- Li, X., and Wang, H. (2006). Non-neuronal nicotinic alpha 7 receptor , a new endothelial target for revascularization. *Life Sciences* 78, 1863–1870.
- Li, X., Erclik, T., Bertet, C., Chen, Z., Voutev, R., Venkatesh, S., Morante, J., Celik, A., and Desplan, C. (2013). Temporal patterning of *Drosophila* medulla neuroblasts controls neural fates. *Nature* 498, 456–462.
- Li, Y., Hoffmann, J., Li, Y., Stephano, F., Bruchhaus, I., Fink, C., and Roeder, T. (2016). Octopamine controls starvation resistance, life span and metabolic traits in *Drosophila*. *Sci. Rep.* 6, 1–11.
- Li, Y., Tiedemann, L., von Frieling, J., Nolte, S., El-Kholy, S., Stephano, F., Gelhaus, C., Bruchhaus, I., Fink, C., and Roeder, T. (2017). The Role of Monoaminergic Neurotransmission for Metabolic Control in the Fruit Fly *Drosophila Melanogaster*. *Front. Syst. Neurosci.* 11, 1–10.
- Lieber, T., Kidd, S., and Struhl, G. (2011). DSL-Notch signaling in the *Drosophila* brain in response to olfactory stimulation. *Neuron* 69, 468–481.
- Liebl, E.C., Forsthoefel, D.J., Franco, L.S., Sample, S.H., Hess, J.E., Cowger, J.A., Chandler, M.P., Shupert, A.M., and Seeger, M.A. (2000). Dosage-Sensitive, Reciprocal Genetic Interactions between the. *Interactions* 26, 107–118.
- Lim, J., Sabandal, P.R., Fernandez, A., Sabandal, J.M., Lee, H.G., Evans, P., and Han, K.A. (2014). The octopamine receptor Oct $\beta$ 2R regulates ovulation in *Drosophila melanogaster*. *PLoS One* 9, e104441.
- Lim, N.R., Shohayeb, B., Zaytseva, O., Mitchell, N., Millard, S.S., Ng, D.C.H., and Quinn, L.M. (2017). Glial-Specific Functions of Microcephaly Protein WDR62 and Interaction with the Mitotic Kinase AURKA Are Essential for *Drosophila* Brain Growth. *Stem Cell Reports* 9, 32–41.
- Lin, S., Kao, C.F., Yu, H.H., Huang, Y., and Lee, T. (2012). Lineage Analysis of *Drosophila* Lateral Antennal Lobe Neurons Reveals Notch-Dependent Binary Temporal Fate Decisions. *PLoS Biol.* 10, e1001425.



Lin, S., Marin, E.C., Yang, C.P., Kao, C.F., Apenteng, B.A., Huang, Y., O'Connor, M.B., Truman, J.W., and Lee, T. (2013). Extremes of lineage plasticity in the drosophila brain. *Curr. Biol.* 23, 1908–1913.

Lindsley, D.L., and Zimm, G.G. (1992). *The Genome of Drosophila Melanogaster*.

Linnemannstöns, K., Ripp, C., Honemann-Capito, M., Brechtel-Curth, K., Hedderich, M., and Wodarz, A. (2014). The PTK7-Related Transmembrane Proteins Off-track and Off-track 2 Are Co-receptors for Drosophila Wnt2 Required for Male Fertility. *PLoS Genet.* 10, e1004443.

Liu, L., MacKenzie, K.R., Putluri, N., Maletić-Savatić, M., and Bellen, H.J. (2017). The Glia-Neuron Lactate Shuttle and Elevated ROS Promote Lipid Synthesis in Neurons and Lipid Droplet Accumulation in Glia via APOE/D. *Cell Metab.* 26, 719–737.

Liu, Z., Yang, C.P., Sugino, K., Fu, C.C., Liu, L.Y., Yao, X., Lee, L.P., and Lee, T. (2015). Opposing intrinsic temporal gradients guide neural stem cell production of varied neuronal fates. *Science.* 350, 317–320.

Livingstone, M.S., and Tempel, B.L. (1983). Genetic dissection of monoamine neurotransmitter synthesis in Drosophila. *Nature* 303, 67–70.

Llorens-Bobadilla, E., Zhao, S., Baser, A., Saiz-Castro, G., Zwadlo, K., and Martin-Villalba, A. (2015). Single-Cell Transcriptomics Reveals a Population of Dormant Neural Stem Cells that Become Activated upon Brain Injury. *Cell Stem Cell* 17, 329–340.

Llorens, F., Hummel, M., Pastor, X., Ferrer, A., Pluvinet, R., Vivancos, A., Castillo, E., Iraola, S., Mosquera, A.M., González, E., et al. (2011). Multiple platform assessment of the EGF dependent transcriptome by microarray and deep tag sequencing analysis. *BMC Genomics* 12, 1–19.

Long, H., Yoshikawa, S., and Thomas, J.B. (2016). Equivalent Activities of Repulsive Axon Guidance Receptors. *J. Neurosci.* 36, 1140–1150.

Lopez-Atalaya, J.P., Askew, K.E., Sierra, A., and Gomez-Nicola, D. (2018). Development and maintenance of the brain's immune toolkit: Microglia and non-parenchymal brain macrophages. *Dev. Neurobiol.* 78, 561–579.

Love, M.I., Huber, W., and Anders, S. (2014). Moderated estimation of fold change and dispersion for RNA-seq data with DESeq2. *Genome Biol.* 15, 1–21.

Love, M.I., Anders, S., Kim, V., and Huber, W. (2015). RNA-Seq workflow: gene-level exploratory analysis and differential expression. *F1000Research* 4, 1–41.

Luan, Z., Quigley, C., and Li, H.S. (2015). The putative Na<sup>+</sup>/Cl<sup>-</sup>-dependent neurotransmitter/osmolyte transporter inebriated in the Drosophila hindgut is essential for the maintenance of systemic water homeostasis. *Sci. Rep.* 5, 1–9.

Lui, J.H., Nowakowski, T.J., Pollen, A.A., Javaherian, A., Kriegstein, A.R., and Oldham, M.C. (2014). Radial glia require PDGFR-β signalling in human but not mouse neocortex. *Nature* 515, 264–268.

Luo, C.-W., Dewey, E.M., Sudo, S., Ewer, J., Hsu, S.Y., Honegger, H.-W., and Hsueh, A.J.W. (2005). Bursicon, the insect cuticle-hardening hormone, is a heterodimeric cystine knot protein that activates G protein-coupled receptor LGR2. *Pnas* 102, 2820–2825.

## M

---

Ma, Z., Stork, T., Bergles, D.E., and Freeman, M.R. (2016). Neuromodulators signal through astrocytes to alter neural circuit activity and behavior. *Nature* 539, 428–432.

Macosko, E.Z., Basu, A., Satija, R., Nemesh, J., Shekhar, K., Goldman, M., Tirosh, I., Bialas, A.R., Kamitaki, N., Martersteck, E.M., et al. (2015). Highly parallel genome-wide expression profiling of individual cells using nanoliter droplets. *Cell* 161, 1202–1214.

Malartre, M. (2016). Regulatory mechanisms of EGFR signalling during Drosophila eye development. *Cell. Mol. Life Sci.*

Mann, D.A., and Oakley, F. (2013). Serotonin paracrine signaling in tissue fibrosis. *BBA - Mol. Basis Dis.* 1832, 905–910.

- Manning, L., and Doe, C.Q. (2017). Immunofluorescent antibody staining of intact *Drosophila* larvae. *Nat. Protoc.* *12*, 1–14.
- Manseau, L., Baradaran, A., Brower, D., Budhu, A., Elefant, F., Phan, H., Philp, A.V., Yang, M., Glover, D., Kaiser, K., et al. (1997). GAL4 enhancer traps expressed in the embryo, larval brain, imaginal discs, and ovary of *Drosophila*. *Dev. Dyn.* *209*, 310–322.
- Mao, Y., and Freeman, M. (2009). Fasciclin 2, the *Drosophila* orthologue of neural cell-adhesion molecule, inhibits EGF receptor signalling. *Development* *136*, 473–481.
- Maqueira, B., Chatwin, H., and Evans, P.D. (2005). Identification and characterization of a novel family of *Drosophila*  $\beta$ -adrenergic-like octopamine G-protein coupled receptors. *J. Neurochem.* *94*, 547–560.
- Matsumoto, K., Akio, T., and Oshima, Y. (1978). Genetic control of galactokinase synthesis in *Saccharomyces cerevisiae*: evidence for constitutive Genetic Control of Galactokinase Synthesis in *Saccharomyces cerevisiae*: Evidence for Constitutive Expression of the Positive Regulatory Gene *gal4*. *J. Bacteriol.* *134*, 446–457.
- Maurange, C., and Gould, A.P. (2005). Brainy but not too brainy: Starting and stopping neuroblast divisions in *Drosophila*. *Trends Neurosci.* *28*, 30–36.
- May Lim, R.S., Osato, M., and Kai, T. (2012). Isolation of undifferentiated female germline cells from adult *Drosophila* ovaries. *Curr. Protoc. Stem Cell Biol.* *2E.3*, 1–14.
- McCaffrey, L.M., and Macara, I.G. (2011). Epithelial organization, cell polarity and tumorigenesis. *Trends Cell Biol.* *21*, 727–735.
- McGuire, S.E., Le, P.T., Osborn, A.J., Matsumoto, K., and Davis, R.L. (2003). Spatiotemporal Rescue of Memory Dysfunction in *Drosophila*. *Science.* *302*, 1765–1768.
- Meinertzhagen, I.A., and Hanson, T.E. (1993). The Development of the Optic Lobe. In *The Development of Drosophila Melanogaster 2*, pp. 1363–1491.
- Meister, M., and Lagueux, M. (2003). *Drosophila* blood cells. *Cell. Microbiol.* 573–580.
- Mendive, F.M., Van Loy, T., Claeysen, S., Poels, J., Williamson, M., Hauser, F., Grimmelhuijzen, C.J.P., Vassart, G., and Vanden Broeck, J. (2005). *Drosophila* molting neurohormone bursicon is a heterodimer and the natural agonist of the orphan receptor DLGR2. *FEBS Lett.* *579*, 2171–2176.
- Meyer, S., Schmidt, I., and Kla, C. (2014). Glia ECM interactions are required to shape the *Drosophila* nervous system. *Mech. Dev.* *133*, 105–116.
- Miller, M.R., Robinson, K.J., Cleary, M.D., and Doe, C.Q. (2009). TU-tagging: Cell type-specific RNA isolation from intact complex tissues. *Nat. Methods* *6*, 439–441.
- Mirre, C., Le Parco, Y., and Knibiehler, B. (1992). Collagen IV is present in the developing CNS during *Drosophila* neurogenesis. *J. Neurosci. Res.* *31*, 146–155.
- Mitri, C., Parmentier, M., Pin, J., and Grau, Y. (2004). Divergent Evolution in Metabotropic Glutamate Receptors. A New Receptor Activated By An Endogenous Ligand Different From Glutamate In Insects. *J. Biol. Chem.* *279*, 9313–9320.
- Monastirioti, M., Gorczyca, M., Rapus, J., Eckert, M., White, K., and Budnik, V. (1995). Octopamine Immunoreactivity in the Fruit Fly *Drosophila melanogaster*. *J. Comp. Neurol.* *356*, 275–287.
- Monastirioti, M., Linn, E., and Ns, G. (1996). Tyramine-B-Hydroxylase Characterization of *Drosophila* Isolation of Mutant Flies Lacking Octopamine. *J. Neurosci.* *16*, 3900–3911.
- Monson, J.M., Natzle, J., Friedman, J., and McCarthy, B.J. (1982). Expression and novel structure of a collagen gene in *Drosophila*. *Proc. Natl. Acad. Sci. USA* *79*, 1761–1765.
- Mora, N., Oliva, C., Fiers, M., Ejsmont, R., Soldano, A., Zhang, T.T., Yan, J., Claeys, A., De Geest, N., and Hassan, B.A. (2018). A Temporal Transcriptional Switch Governs Stem Cell Division, Neuronal Numbers, and Maintenance of Differentiation. *Dev. Cell* *45*, 53–66.
- Morais-de-Sá, E., Mirouse, V., and St Johnston, D. (2010). aPKC Phosphorylation of Bazooka Defines the Apical/Lateral Border in *Drosophila* Epithelial Cells. *Cell* *141*, 509–523.

Morante, J., and Desplan, C. (2008). The Color-Vision Circuit in the Medulla of *Drosophila*. *Curr. Biol.* 18, 553–565.

Morante, J., and Desplan, C. (2011). Dissection and staining of *Drosophila* optic lobes at different stages of development. *Cold Spring Harb. Protoc.* 6, 652–656.

Morante, J., Vallejo, D.M., Desplan, C., and Dominguez, M. (2013). Conserved miR-8/miR-200 defines a glial niche that controls neuroepithelial expansion and neuroblast transition. *Dev. Cell* 27, 174–187.

Morin, X., Daneman, R., Zavortink, M., and Chia, W. (2001). A protein trap strategy to detect GFP-tagged proteins expressed from their endogenous loci in *Drosophila*. *Proc. Natl. Acad. Sci.* 98, 15050–15055.

Morrison, S.J., and Spradling, A.C. (2008). Stem Cells and Niches: Mechanisms That Promote Stem Cell Maintenance throughout Life. *Cell* 132, 598–611.

Mosca, T.J., and Luo, L. (2014). Synaptic organization of the *Drosophila* antennal lobe and its regulation by the Teneurins. *Elife* 3, e03726.

Murillo-Maldonado, J.M., Sánchez-Chávez, G., Salgado, L.M., Salceda, R., and Riesgo-Escovar, J.R. (2011). *Drosophila* Insulin Pathway Mutants Affect Visual Physiology and Brain Function Besides Growth, Lipid, and Carbohydrate Metabolism. *Diabetes* 60, 1632–1636.

## N

---

Nakamura, M., Baldwin, D., Hannaford, S., Palka, J., and Montell, C. (2002). Defective Proboscis Extension Response (DPR), a Member of the Ig Superfamily Required for the Gustatory Response to Salt. *J. Neurosci.* 22, 3463–3472.

Narbonne-Reveau, K., Lanet, E., Dillard, C., Foppolo, S., Chen, C.H., Parrinello, H., Rialle, S., Sokol, N.S., and Murainge, C. (2016). Neural stem cell-encoded temporal patterning delineates an early window of malignant susceptibility in *Drosophila*. *Elife* 5, 1–29.

Natzle, J.E., Monson, J.M., and McCarthy, B.J. (1982). Cytogenetic location and expression of collagen-like genes in *Drosophila*. *Nature* 296, 368–371.

Nave, K.A., Tzvetanova, I.D., and Schirmeier, S. (2017). Glial Cell Evolution: The Origins of a Lipid Store. *Cell Metab.* 26, 701–702.

Néric, N., and Desplan, C. (2016). From the Eye to the Brain. Development of the *Drosophila* Visual System. In *Current Topics in Developmental Biology*, pp. 247–271.

Ngo, K.T., Wang, J., Junker, M., Kriz, S., Vo, G., Asem, B., Olson, J.M., Banerjee, U., and Hartenstein, V. (2010). Concomitant requirement for Notch and Jak/Stat signaling during neuro-epithelial differentiation in the *Drosophila* optic lobe. *Dev. Biol.* 346, 284–295.

Ngo, K.T., Andrade, I., and Hartenstein, V. (2017). Spatio-temporal pattern of neuronal differentiation in the *Drosophila* visual system: A user's guide to the dynamic morphology of the developing optic lobe. *Dev. Biol.* 428, 1–24.

Nordstrom, W., Chen, P., Steller, H., and Abrams, J.M. (1996). Activation of the reaper Gene during Ectopic Cell Killing in *Drosophila*. *Dev. Biol.* 180, 213–226.

## O

---

Ohhara, Y., Kayashima, Y., Hayashi, Y., Kobayashi, S., and Yamakawa-Kobayashi, K. (2012). Expression of  $\beta$ -adrenergic-like Octopamine Receptors during *Drosophila* Development. *Zool. Sci.* 29, 83–89.

Ohshiro, T., Yagami, T., Zhang, C., and Matsuzaki, F. (2000). Role of cortical tumour-suppressor proteins in asymmetric division of *Drosophila* neuroblast. *Nature* 408, 593–596.

Okamoto, M., Miyata, T., Konno, D., Ueda, H.R., Kasukawa, T., Hashimoto, M., Matsuzaki, F., and Kawaguchi, A. (2016). Cell-cycle-independent transitions in temporal identity of mammalian neural progenitor cells. *Nat. Commun.* 7, 1–16.

Oliveros, J. (2009). Venny. An interactive tool for comparing lists with Venn's diagrams.

[Http://Bioinfofp.Cnb.Csic.Es/Tools/Venny/Index.Html](http://Bioinfofp.Cnb.Csic.Es/Tools/Venny/Index.Html) Accessed 2017-12-13.

Omoto, J.J., Yogi, P., and Hartenstein, V. (2015). Origin and development of neuropil glia of the *Drosophila* larval and adult brain: two distinct glial populations derived from separate progenitors. *Dev. Biol.* *404*, 2–20.

Organisti, C., Hein, I., Grunwald Kadow, I.C., and Suzuki, T. (2015). Flamingo, a seven-pass transmembrane cadherin, cooperates with Netrin/Frazzled in *Drosophila* midline guidance. *Genes to Cells* *20*, 50–67.

Osterwalder, T., Yoon, K.S., White, B.H., and Keshishian, H. (2001). A conditional tissue-specific transgene expression system using inducible GAL4. *Proc. Natl. Acad. Sci.* *98*, 12596–12601.

Otsuki, L., and Brand, A.H. (2017). The vasculature as a neural stem cell niche. *Neurobiol. Dis.* *107*, 4–14.

Otsuki, L., and Brand, A.H. (2018). Cell cycle heterogeneity directs the timing of neural stem cell activation from quiescence. *Science*. *360*, 99–102.

Ou, J., He, Y., Xiao, X., Yu, T.M., Chen, C., Gao, Z., and Ho, M.S. (2014). Glial cells in neuronal development: Recent advances and insights from *Drosophila melanogaster*. *Neurosci. Bull.* *30*, 584–594.

## P

---

Pallavi, S.K., and Shashidhara, L.S. (2003). Egfr / Ras pathway mediates interactions between peripodial and disc proper cells in *Drosophila* wing discs. *Development* *130*, 4931–4941.

Pandey, U.B., and Nichols, C.D. (2011). Human Disease Models in *Drosophila melanogaster* and the Role of the Fly in Therapeutic Drug Discovery. *Pharmacol. Rev.* *63*, 411–436.

Le Parco, Y., Knibiehler, B., Cecchini, J.P., and Mirre, C. (1986). Stage and tissue-specific expression of a collagen gene during *Drosophila melanogaster* development. *Exp. Cell Res.* *163*, 405–412.

Paridaen, J.T., and Huttner, W.B. (2014). Neurogenesis during development of the vertebrate central nervous system. *EMBO Rep.* *15*, 351–364.

Parkhomchuk, D., Borodina, T., Amstislavskiy, V., Banaru, M., Hallen, L., Krobitch, S., Lehrach, H., and Soldatov, A. (2009). Transcriptome analysis by strand-specific sequencing of complementary DNA. *Nucleic Acids Res.* *37*, 1–7.

Pastor-Pareja, J.C., and Xu, T. (2011). Shaping Cells and Organs in *Drosophila* by Opposing Roles of Fat Body-Secreted Collagen IV and Perlecan. *Dev. Cell* *21*, 245–256.

Patel, N.H., Schafer, B., Goodman, C.S., and Holmgren, R. (1989). The role of segment polarity genes during *Drosophila* neurogenesis. *Genes Dev.* *3*, 890–904.

Pereanu, W., Kumar, A., Jennett, A., Reichert, H., and Hartenstein, V. (2010). A development-based compartmentalization of the *Drosophila* central brain. *J. Comp. Neurol.* *518*, 2996–3023.

Perez-Gomez, R., Slovakova, J., Rives-Quinto, N., Krejci, A., and Carmena, A. (2013). A Serrate-Notch-Canoe complex mediates essential interactions between glia and neuroepithelial cells during *Drosophila* optic lobe development. *J. Cell Sci.* *126*, 4873–4884.

Pfeiffer, B.D., Ngo, T.T.B., Hibbard, K.L., Murphy, C., Jenett, A., Truman, J.W., and Rubin, G.M. (2010). Refinement of tools for targeted gene expression in *Drosophila*. *Genetics* *186*, 735–755.

Pinto-Teixeira, F., Koo, C., Rossi, A.M., Neriec, N., Bertet, C., Li, X., Del-Valle-Rodriguez, A., and Desplan, C. (2018). Development of Concurrent Retinotopic Maps in the Fly Motion Detection Circuit. *Cell* *173*, 485–498.

Pipes, G.C., Lin, Q., Riley, S.E., and Goodman, C.S. (2001). The Beat generation: a multigene family encoding IgSF proteins related to the Beat axon guidance molecule in *Drosophila*. *Development* *128*, 4545–4552.

Potter, C.J., Tasic, B., Russler, E. V., Liang, L., and Luo, L. (2010). The Q System: A Repressible Binary System for Transgene Expression, Lineage Tracing and Mosaic Analysis. *Cell* *141*, 536–548.

## Q

---

Qi, Y. xiang, Xu, G., Gu, G. xiang, Mao, F., Ye, G. yin, Liu, W., and Huang, J. (2017). A new *Drosophila* octopamine receptor responds to serotonin. *Insect Biochem. Mol. Biol.* *90*, 61–70.

## R

---

Ramon-Cañellas, P., Peterson, H.P., and Morante, J. (2019). From Early to Late Neurogenesis: Neural Progenitors and the Glial Niche from a Fly's Point of View. *Neuroscience* *399*, 39–52.

Rawlins, E.L. (2003). Echinoid facilitates Notch pathway signalling during *Drosophila* neurogenesis through functional interaction with Delta. *Development* *130*, 6475–6484.

Reddy, B.V.V.G., Rauskolb, C., and Irvine, K.D. (2010). Influence of Fat-Hippo and Notch signaling on the proliferation and differentiation of *Drosophila* optic neuroepithelia. *Development* *137*, 2397–2408.

Reiter, L.T., Potocki, L., Chien, S., Gribskov, M., and Bier, E. (2001). A Systematic Analysis of Human Disease-Associated Gene Sequences In *Drosophila melanogaster*. *Genome Res.* *11*, 1114–1125.

Reuter, J.A., Spacek, D. V., and Snyder, M.P. (2015). High-Throughput Sequencing Technologies. *Mol. Cell* *58*, 586–597.

Rewitz, K.F., Yamanaka, N., and O'Connor, M.B. (2013). Developmental Checkpoints and Feedback Circuits Time Insect Maturation. In *Current Topics in Developmental Biology*, pp. 1–33.

Rizki, M.T., and Rizki, R.M. (1959). Functional significance of the crystal cells in the larva of *Drosophila melanogaster*. *J. Biophys. Biochem. Cytol.* 235–240.

Robb, S., Cheek, T.R., Hannan, F.L., Haii, L.M., Midgley, J.M., and Evans, P.D. (1994). Agonist-specific coupling of a cloned *Drosophila* octopamine/tyramine receptor to multiple second messenger systems. *EMBO J.* *13*, 1325–1330.

Roberts, D.B. (1998). *Drosophila*, a practical approach. In Oxford, IRL Press, pp. 30–32.

Robinson, J.T., Thorvaldsdóttir, H., Winckler, W., Guttman, M., Lander, E.S., Getz, G., and Mesirov, J.P. (2011). Integrative Genomics Viewer. *Nat. Biotechnol.* *29*, 24–26.

Rodriguez, A., Zhou, Z., Tang, M.L., Meller, S., Chen, J., Bellen, H., and Kimbrell, D.A. (1996). Identification of immune system and response genes, and novel mutations causing melanotic tumor formation in *Drosophila melanogaster*. *Genetics* *143*, 929–940.

Roeder, T. (2005). TYRAMINE AND OCTOPAMINE: Ruling Behavior and Metabolism. *Annu. Rev. Entomol.* *50*, 447–477.

Rossi, A.M., and Fernandes, V.M. (2018). Wrapping Glial Morphogenesis and Signaling Control the Timing and Pattern of Neuronal Differentiation in the *Drosophila* Lamina. *J. Exp. Neurosci.* *12*, 1–6.

Rossi, A.M., Fernandes, V.M., and Desplan, C. (2017). Timing temporal transitions during brain development. *Curr. Opin. Neurobiol.* *42*, 84–92.

Roy, P.J., Stuart, J.M., Lund, J., and Kim, S.K. (2002). Chromosomal clustering of muscle-expressed genes in *Caenorhabditis elegans*. *Nature* *418*, 975–979.

Ryglewski, S., Duch, C., and Altenhein, B. (2017). Tyramine Actions on *Drosophila* Flight Behavior Are Affected by a Glial Dehydrogenase/Reductase. *Front. Syst. Neurosci.* *11*, 1–8.

## S

---

Saini, N., and Reichert, H. (2012). Neural stem cells in *drosophila*: Molecular genetic mechanisms underlying normal neural proliferation and abnormal brain tumor formation. *Stem Cells Int.* *2012*, 1–10.

Saraswati, S., Fox, L.E., Soll, D.R., and Wu, C.F. (2004). Tyramine and Octopamine Have Opposite Effects on the Locomotion of *Drosophila* Larvae. *J. Neurobiol.* *58*, 425–441.

- Sarov, M., Barz, C., Jambor, H., Hein, M.Y., Schmied, C., Suchold, D., Stender, B., Janosch, S., Vinay Vikas, K.J., Krishnan, R.T., et al. (2016). A genome-wide resource for the analysis of protein localisation in *Drosophila*. *Elife* 5, 1–38.
- Schneider, C.A., Rasband, W.S., and Eliceiri, K.W. (2012). NIH Image to ImageJ: 25 years of image analysis. *Nat. Methods* 9, 671–675.
- Schofield, P.K., and Treherne, J.E. (1985). Octopamine reduces potassium permeability of the glia that form the insect blood-brain barrier. *Brain Res.* 360, 344–348.
- Schulz, R., Sawruk, E., Mülhardt, C., Bertrand, S., Baumann, A., Phannavong, B., Betz, H., Bertrand, D., Gundelfinger, E.D., and Schmitt, B. (1998). D alpha3, a new functional alpha subunit of nicotinic acetylcholine receptors from *Drosophila*. *J. Neurochem.* 71, 853–862.
- Schwabe, T., Bainton, R.J., Fetter, R.D., Heberlein, U., and Gaul, U. (2005). GPCR signaling is required for blood-brain barrier formation in *Drosophila*. *Cell* 123, 133–144.
- Schwaerzel, M., Monastirioti, M., Scholz, H., Friggi-Grelin, F., Birman, S., and Heisenberg, M. (2003). Dopamine and Octopamine Differentiate between Aversive and Appetitive Olfactory Memories in *Drosophila*. *J. Neurosci.* 23, 10495–10502.
- Selcho, M., Pauls, D., Huser, A., Stocker, R.F., and Thum, A.S. (2014). Characterization of the octopaminergic and tyramineric neurons in the central brain of *Drosophila* larvae. *J. Comp. Neurol.* 522, 3485–3500.
- Shaikh, M.N., Gutierrez-Aviño, F., Colonques, J., Ceron, J., Hämmerle, B., and Tejedor, F.J. (2016). Minibrain drives the Dacapo-dependent cell cycle exit of neurons in the *Drosophila* brain by promoting *asense* and *prospero* expression. *Development* 143, 3195–3205.
- Shih, M.-F.M., Davis, F.P., Henry, G.L., and Dubnau, J. (2018). Nuclear Transcriptomes of the Seven Neuronal Cell Types That Constitute the *Drosophila* Mushroom Bodies. *G3 Genes|Genomes|Genetics* g3.200726.2018.
- Sidow, A. (1992). Diversification of the Wnt gene family on the ancestral lineage of vertebrates. *Proc. Natl. Acad. Sci. U. S. A.* 89, 5098–5102.
- Siegenthaler, J.A., and Pleasure, S.J. (2011). We have got you “covered”: How the meninges control brain development. *Curr. Opin. Genet. Dev.* 21, 249–255.
- Silva-Vargas, V., Maldonado-Soto, A.R., Mizrak, D., Codega, P., and Doetsch, F. (2016). Age-Dependent Niche Signals from the Choroid Plexus Regulate Adult Neural Stem Cells. *Cell Stem Cell* 19, 643–652.
- Slovakova, J., and Carmena, A. (2011). Canoe functions at the CNS midline glia in a complex with Shotgun and Wrapper-Nrx-IV during neuron-glia interactions. *Development* 138, 1563–1571.
- Soba, P., Han, C., Zheng, Y., Perea, D., Miguel-aliaga, I., Jan, L.Y., and Jan, Y.N. (2015). The Ret receptor regulates sensory neuron dendrite growth and integrin mediated adhesion. *Elife* 4, 1–21.
- Soehnge, H., Xi, H., Becker, M., Whitley, P., Conover, Di., and Stern, M. (1996). A neurotransmitter transporter encoded by the *Drosophila* *inebriated* gene. *Proc. Natl. Acad. Sci. USA* 93, 13262–13267.
- Sousa-Nunes, R., Cheng, L.Y., and Gould, A.P. (2010). Regulating neural proliferation in the *Drosophila* CNS. *Curr. Opin. Neurobiol.* 20, 50–57.
- Sousa-Nunes, R., Yee, L.L., and Gould, A.P. (2011). Fat cells reactivate quiescent neuroblasts via TOR and glial insulin relays in *Drosophila*. *Nature* 471, 508–513.
- Spéder, P., and Brand, A.H. (2018). Systemic and local cues drive neural stem cell niche remodelling during neurogenesis in *drosophila*. *Elife* 7, 1–16.
- Spencer, S. a, and Cagan, R.L. (2003). Echinoid is essential for regulation of Egfr signaling and R8 formation during *Drosophila* eye development. *Development* 130, 3725–3733.
- Steiner, F.A., Talbert, P.B., Kasinathan, S., Deal, R.B., and Henikoff, S. (2012). Cell-type-specific nuclei purification from whole animals for genome-wide expression and chromatin profiling. *Genome Res.* 22, 766–777.

Stork, T., Engelen, D., Krudewig, A., Silies, M., Bainton, R.J., and Klambt, C. (2008). Organization and Function of the Blood Brain Barrier in *Drosophila*. *J. Neurosci.* *28*, 587–597.

Stork, T., Bernardos, R., and Freeman, M.R. (2012). Analysis of Glial Cell Development and Function in *Drosophila*. *Cold Spring Harb. Protoc.* *1*, 1–17.

Strother, J.A., Wu, S.-T., Rogers, E.M., Eliason, J.L.M., Wong, A.M., Nern, A., and Reiser, M.B. (2017). Behavioral state modulates the ON visual motion pathway of *Drosophila*. *Proc. Natl. Acad. Sci.* E102–E111.

Struhl, G., and Basler, K. (1993). Organizing Activity of Wingless Protein in *Drosophila*. *Cell* *72*, 527–540.

Sugaya, R., Ishimaru, S., Hosoya, T., Saigo, K., and Emori, Y. (1994). A *Drosophila* homolog of human proto-oncogene *ret* transiently expressed in embryonic neuronal precursor cells including neuroblasts and CNS cells. *Mech. Dev.* *45*, 139–145.

Sujkowski, A., Ramesh, D., Brockmann, A., and Wessells, R. (2017). Octopamine drives endurance exercise adaptations in *Drosophila*. *Cell Rep.* *21*, 1809–1823.

Suzuki, T., Kaido, M., Takayama, R., and Sato, M. (2013). A temporal mechanism that produces neuronal diversity in the *Drosophila* visual center. *Dev. Biol.* *380*, 12–24.

Suzuki, T., Hasegawa, E., Nakai, Y., Kaido, M., Takayama, R., and Sato, M. (2016). Formation of Neuronal Circuits by Interactions between Neuronal Populations Derived from Different Origins in the *Drosophila* Visual Center. *Cell Rep.* *15*, 499–509.

Syed, M.H., Mark, B., and Doe, C.Q. (2017a). Steroid hormone induction of temporal gene expression in *drosophila* brain neuroblasts generates neuronal and glial diversity. *Elife* *6*, 1–23.

Syed, M.H., Mark, B., and Doe, C.Q. (2017b). Playing Well with Others: Extrinsic Cues Regulate Neural Progenitor Temporal Identity to Generate Neuronal Diversity. *Trends Genet.* *33*, 933–942.

## T

---

Tan, L., Zhang, K.X., Pecot, M.Y., Nagarkar-jaiswal, S., Takemura, S., Mcewen, J.M., Nern, A., Xu, S., Tadros, W., Chen, Z., et al. (2016). Ig Superfamily Ligand and Receptor Pairs Expressed in Synaptic Partners in *Drosophila*. *Cell* *163*, 1756–1769.

Tauc, H.M., Tasdogan, A., and Pandur, P. (2014). Isolating Intestinal Stem Cells from Adult *Drosophila* Midguts by FACS to Study Stem Cell Behavior During Aging. *J. Vis. Exp.* 1–11.

Technau, G.M. (2008). Brain development in *Drosophila melanogaster*. *Adv. Exp. Med. Biol.* *628*, 102–114.

Tepaß, U., and Knust, E. (1990). Phenotypic and developmental analysis of mutations at the *crumbs* locus, a gene required for the development of epithelia in *Drosophila melanogaster*. *Roux's Arch. Dev. Biol.* *199*, 189–206.

Terriente, J., and Pujades, C. (2015). Cell segregation in the vertebrate hindbrain: A matter of boundaries. *Cell. Mol. Life Sci.* *72*, 3721–3730.

Thorvaldsdóttir, H., Robinson, J.T., and Mesirov, J.P. (2012). Integrative Genomics Viewer (IGV): High-performance genomics data visualization and exploration. *Brief. Bioinform.* *14*, 178–192.

Tiberi, L., Vanderhaeghen, P., and van den Aemele, J. (2012). Cortical neurogenesis and morphogens: Diversity of cues, sources and functions. *Curr. Opin. Cell Biol.* *24*, 269–276.

Toledano, H., Alterio, C.D., Loza-coll, M., and Jones, D.L. (2012). Dual fluorescence detection of protein and RNA in *Drosophila* tissues. *Nat. Protoc.* *7*, 1808–1817.

Tuthill, J.C., Nern, A., Rubin, G.M., and Reiser, M.B. (2014). Wide-Field Feedback Neurons Dynamically Tune Early Visual Processing. *Neuron* *82*, 887–895.

## U

---

Ulvklo, C., MacDonald, R., Bivik, C., Baumgardt, M., Karlsson, D., and Thor, S. (2012). Control of neuronal cell fate and number by integration of distinct daughter cell proliferation modes with temporal progression. *Development* 139, 678–689.

Unhavaithaya, Y., and Orr-weaver, T.L. (2012). Polyploidization of glia in neural development links tissue growth to blood – brain barrier integrity. *Genes Dev.* 26, 31–36.

Urbach, R. (2007). A procephalic territory in *Drosophila* exhibiting similarities and dissimilarities compared to the vertebrate midbrain/hindbrain boundary region. *Neural Dev.* 2, 1–15.

## V

---

Vallejo, D.M., Juarez-Carreno, S., Bolivar, J., Morante, J., and Dominguez, M. (2015). A brain circuit that synchronizes growth and maturation revealed through Dilp8 binding to Lgr3. *Science.* 350, aaac6767.

Venken, K.J.T., Simpson, J.H., and Bellen, H.J. (2011). Genetic manipulation of genes and cells in the nervous system of the fruit fly. *Neuron* 72, 202–230.

Villegas, S.N., Gombos, R., García-López, L., Gutiérrez-Pérez, I., García-Castillo, J., Vallejo, D.M., Da Ros, V.G., Ballesta-Illán, E., Mihály, J., and Dominguez, M. (2018). PI3K/Akt Cooperates with Oncogenic Notch by Inducing Nitric Oxide-Dependent Inflammation. *Cell Rep.* 22, 2601–2614.

Vömel, M., and Wegener, C. (2008). Neuroarchitecture of aminergic systems in the larval ventral ganglion of *Drosophila melanogaster*. *PLoS One* 3, e1848.

## W

---

Wagner, A., Regev, A., and Yosef, N. (2016). Revealing the vectors of cellular identity with single-cell genomics. *Nat. Biotechnol.* 34, 1145–1160.

Wand, M.P., and Jones, M.C. (1995). *Kernel Smoothing* (London: Chapman and Hall).

Wang, H., Chen, X., He, T., Zhou, Y., and Luo, H. (2013). Evidence for tissue-specific JAK/STAT target genes in *Drosophila* optic lobe development. *Genetics* 195, 1291–1306.

Wang, L., Kounatidis, I., and Ligoxygakis, P. (2014). *Drosophila* as a model to study the role of blood cells in inflammation, innate immunity and cancer. *Front. Cell. Infect. Microbiol.* 3, 1–17.

Wang, T., Jiao, Y., and Montell, C. (2007). Dissection of the pathway required for generation of vitamin A and for *Drosophila* phototransduction. *J. Cell Biol.* 177, 305–316.

Wang, W., Liu, W., Wang, Y., Zhou, L., Tang, X., and Luo, H. (2011). Notch signaling regulates neuroepithelial stem cell maintenance and neuroblast formation in *Drosophila* optic lobe development. *Dev. Biol.* 350, 414–428.

Wang, Y., Pereira, E.F.R., Maus, A.D.J., Ostlie, N.S., Navaneetham, D., Lei, S., Albuquerque, E.X., and Conti-fine, B.M. (2001). Human Bronchial Epithelial and Endothelial Cells Express alpha 7 Nicotinic Acetylcholine Receptors. *Mol. Pharmacol.* 60, 1201–1209.

Wei, S.Y., Escudero, L.M., Yu, F., Chang, L.H., Chen, L.Y., Ho, Y.H., Lin, C.M., Chou, C.S., Chia, W., Modolell, J., et al. (2005). Echinoid is a component of adherens junctions that cooperates with DE-cadherin to mediate cell adhesion. *Dev. Cell* 8, 493–504.

Wickham, H. (2009). *ggplot2* (New York, NY: Springer).

Witten, D.M. (2011). Classification and clustering of sequencing data using a poisson model. *Ann. Appl. Stat.* 5, 2493–2518.

Wodarz, A., Ramrath, A., Kuchinke, U., and Knust, E. (1999). Bazooka provides an apical cue for inscuteable localization in *Drosophila* neuroblasts. *Nature* 402, 544–547.

## X

---

Xu, X.-Z.S., Wes, P.D., Chen, H., Li, H.-S., Yu, M., Morgan, S., Liu, Y., and Montell, C. (1998). Retinal



Targets for Calmodulin Include Proteins Implicated in Synaptic Transmission. *J. Biol. Chem.* 273, 31297–31307.

## Y

---

Yager, J., Richards, S., Hekmat-scafe, D.S., Hurd, D.D., Sundaresan, V., Caprette, D.R., Saxton, W.M., Carlson, J.R., and Stern, M. (2001). Control of *Drosophila* perineurial glial growth by interacting neurotransmitter-mediated signaling pathways. *Pnas* 98, 10445–10450.

Yamamoto, S., Jaiswal, M., Charng, W.L., Gambin, T., Karaca, E., Mirzaa, G., Wiszniewski, W., Sandoval, H., Haelterman, N.A., Xiong, B., et al. (2014). A *drosophila* genetic resource of mutants to study mechanisms underlying human genetic diseases. *Cell* 159, 200–214.

Yang, Z., Huang, R., Fu, X., Wang, G., Qi, W., Mao, D., Shi, Z., Shen, W.L., and Wang, L. (2018). A post-ingestive amino acid sensor promotes food consumption in *Drosophila*. *Cell Res.* 28, 1013–1025.

Yasothornsrikul, S., Davis, W.J., Cramer, G., Kimbrell, D.A., and Dearolf, C.R. (1997). viking: Identification and characterization of a second type IV collagen in *Drosophila*. *Gene* 198, 17–25.

Yasugi, T., Umetsu, D., Murakami, S., Sato, M., and Tabata, T. (2008). *Drosophila* optic lobe neuroblasts triggered by a wave of proneural gene expression that is negatively regulated by JAK/STAT. *Development* 135, 1471–1480.

Yasugi, T., Sugie, A., Umetsu, D., and Tabata, T. (2010). Coordinated sequential action of EGFR and Notch signaling pathways regulates proneural wave progression in the *Drosophila* optic lobe. *Development* 137, 3193–3203.

Yin, P., Wang, W., Zhang, Z., Bai, Y., Gao, J., and Zhao, C. (2018). Wnt signaling in human and mouse breast cancer: Focusing on Wnt ligands, receptors and antagonists. *Cancer Sci.* 109, 3368–3375.

Yoon, K.-J., Ming, G., and Song, H. (2018). Coupling Neurogenesis to Circuit Formation. *Cell* 173, 288–290.

Yu, H.H., Chen, C.H., Shi, L., Huang, Y., and Lee, T. (2009). Twin-spot MARCM to reveal the developmental origin and identity of neurons. *Nat. Neurosci.* 12, 947–953.

Yuan, Q., Lin, F., Zheng, X., and Sehgal, A. (2005). Serotonin Modulates Circadian Entrainment in *Drosophila*. *Neuron* 47, 115–127.

Yuan, Q., Joiner, W.J., and Sehgal, A. (2006). A Sleep-Promoting Role for the *Drosophila* Serotonin Receptor 1A. *Curr. Biol.* 16, 1051–1062.

Yue, T., Tian, A., and Jiang, J. (2012). The Cell Adhesion Molecule Echinoid Functions as a Tumor Suppressor and Upstream Regulator of the Hippo Signaling Pathway. *Dev. Cell* 22, 255–267.

## Z

---

Zeisel, A., Machado, A.B., Codeluppi, S., Lonnerberg, P., La Manno, G., Jureus, A., Marques, S., Munguba, H., He, L., Betsholtz, C., et al. (2015). Cell types in the mouse cortex and hippocampus revealed by single-cell RNA-seq. *Science.* 25, 279–284.

Zhao, S., Zhang, Y., Gordon, W., Quan, J., Xi, H., Du, S., von Schack, D., and Zhang, B. (2015). Comparison of stranded and non-stranded RNA-seq transcriptome profiling and investigation of gene overlap. *BMC Genomics* 16, 1–14.

Zhou, C., Rao, Y., and Rao, Y. (2008). A subset of octopaminergic neurons are important for *Drosophila* aggression. *Nat. Neurosci.* 11, 1059–1067.

Ziegenhain, C., Vieth, B., Parekh, S., Reinius, B., Guillaumet-Adkins, A., Smets, M., Leonhardt, H., Heyn, H., Hellmann, I., and Enard, W. (2017). Comparative Analysis of Single-Cell RNA Sequencing Methods. *Mol. Cell* 65, 631–643.

Zucchi, R., Chiellini, G., Scanlan, T.S., and Grandy, D.K. (2006). Trace amine-associated receptors and their ligands. *Br. J. Pharmacol.* 149, 967–978.



## NEUROSCIENCE FOREFRONT REVIEW

# From Early to Late Neurogenesis: Neural Progenitors and the Glial Niche from a Fly's Point of View

Pol Ramon-Cañellas, Hannah Payette Peterson and Javier Morante\*

Instituto de Neurociencias, Consejo Superior de Investigaciones Científicas (CSIC), and Universidad Miguel Hernández (UMH), Campus de Sant Joan, Apartado 18, 03550 Sant Joan, Alicante, Spain

\*Corresponding author.



*Neuroscience* 399 (2019) 39–52

(Received 6 October 2018, Accepted 12 December 2018)

(Available online 19 December 2018)

<https://doi.org/10.1016/j.neuroscience.2018.12.014>

0306-4522/© 2018 IBRO. Published by Elsevier Ltd. All rights reserved.



# From early to late neurogenesis: Neural progenitors and the glial niche from a fly's point of view

Pol Ramon-Cañellas<sup>a</sup>, Hannah Payette Peterson<sup>a</sup> and Javier Morante<sup>a,b</sup>

<sup>a</sup>Instituto de Neurociencias, Consejo Superior de Investigaciones Científicas (CSIC); and Universidad Miguel Hernandez (UMH), Campus de Sant Joan, Apartado 18, 03550 Sant Joan, Alicante, Spain.

<sup>b</sup>Corresponding author. E-mail: j.morante@umh.es (JM)

The authors declare no competing financial interests.

## Acknowledgements

We apologize to those whose work we did not cite due to focus and space limitations. We thank Stuart B. Ingham for helping with illustrations. This work was supported by the Ramon y Cajal Program (RyC-2010-07155), a Spanish National Grant (BFU2016-76295-R) co-financed by the European Regional Development Fund (ERDF), and the Severo Ochoa Program for Centres of Excellence in R&D (SEV-2017-0723) to Javier Morante. Pol Ramon-Cañellas is a FPI fellow (BES-2013-064947) from the Spanish Ministerio de Economía y Competitividad.

## Abstract

*Drosophila melanogaster* is an important model organism used to study the brain development of organisms ranging from insects to mammals. The central nervous system in fruit flies is formed primarily in two waves of neurogenesis, one of which occurs in the embryo and one of which occurs during larval stages. In order to understand neurogenesis, it is important to research the behaviour of progenitor cells that give rise to the neural networks which make up the adult nervous system. This behaviour has been shown to be influenced by different factors including interactions with other cells within the progenitor niche, or local tissue microenvironment. Glial cells form a crucial part of this niche and play an active role in the development of the brain. Although in the early years of neuroscience it was believed that glia were simply scaffolding for neurons and passive components of the nervous system, their importance is nowadays recognized. Recent discoveries in progenitors and niche cells have led to new understandings of how the developing brain shapes its diverse regions. In this review, we attempt to summarize the distinct neural progenitors and glia in the *Drosophila melanogaster* central nervous system, from embryo to late larval stages, and make note of homologous features in mammals. We also outline the recent advances in this field in order to define the impact that glial cells have on progenitor cell niches, and we finally emphasize the importance of communication between glia and progenitor cells for proper brain formation.

**KEYWORDS:** *Drosophila*, Central nervous system, Development, Neural progenitors, Glia, Niche.

**ABBREVIATIONS:** CNS: central nervous system; VZ: ventricular zone; SVZ: subventricular zone; NSCs: neural stem cells; NBs: neuroblasts; NECs: neuroepithelial cells; INPs: intermediate neural progenitors; GMCs: ganglion mother cells; TFs: transcription factors; VNC: ventral nerve cord; CB: central brain; OL: optic lobe.

## **Introduction**

Proper development of an organism's brain is crucial for successful communication between its organs and maintenance of their vital functions (Droujinine and Perrimon, 2016). *Drosophila melanogaster* has been instrumental in uncovering the molecular and cellular basis of fundamental developmental processes in metazoans, with research aided by an extensive range of genetic tools and reagents (Bellen et al., 2010). The fruit fly's transcriptome reveals that co-expression modules which are rich in developmental genes are shared across species (Gerstein et al., 2014), making it suitable for studying many biological principles in vertebrates (Ugur et al., 2016). Nowadays, studies of development are carried out in *Drosophila* from the early embryo until the late larval stage.

Neurogenesis in *Drosophila melanogaster* takes place in two waves. The embryonic phase, when the first wave of neurogenesis takes place, has been the model system where historically the majority of in-depth studies of cell fate specification (e.g., NB5-6 generation of Apterous neurons; Baumgardt et al., 2007; Bivik et al., 2015) and neuronal wiring (e.g., generation of RP1, 2, 3, 4, 5 and their innervation of specific single muscle fibres; Landgraf and Thor, 2006) have been carried out at single-lineage and single-cell resolution. Although it is during embryogenesis that researchers have most effectively studied the development of neural circuits and their versatility, recent research on larval development, when the second wave of neurogenesis takes place, has allowed scientists to gather novel insights into generic lineages that give rise to specialised cell populations (Baek and Mann, 2009; Clark et al., 2016; Couton et al., 2015; Heckscher et al., 2015; Kim et al., 2009).

Neural progenitors are multipotent, and thus can proliferate and differentiate into varied cell types in response to both intrinsic and extrinsic cues (Doe, 2017; Knoblich, 2008; Kohwi and Doe, 2013; Morante et al., 2013; Speder et al., 2011; Syed et al., 2017a). Though more is currently known about intrinsic than extrinsic cues (Paridaen and Huttner, 2014; Tiberi et al., 2012), an understanding of both is extremely important for describing the modulation of brain development within different stem cell niches. Niches are local tissue microenvironments that maintain and regulate stem cell capacity of cell division. Today, there is no doubt that the microenvironment of stem cells affects their development and behaviour (Lehtinen and Walsh, 2011; Lehtinen et al., 2011; Morrison and Spradling, 2008; Siegenthaler et al., 2009; Siegenthaler and Pleasure, 2011). It is clear that extrinsic cues received by stem cells need to be effectively interpreted to produce the correct intrinsic responses, but little is known about the specifics of these interactions.

In the nervous system, glial cells, like neurons, comprise a significant portion of the brain. However, in the early ages of brain science, glia were thought to serve only as scaffolding for neurons and to play a passive role in the nervous system. Nowadays, in contrast to what was initially believed, it is accepted that glia also play a relevant part in brain formation, and are important not only in structural development but also in controlling stem cell division (Awasaki et al., 2008; DeSalvo et al., 2014; Kanai et al., 2018; Kriegstein and Alvarez-Buylla, 2009; Okamoto and Nishimura, 2015; Ou et al., 2016). However, more knowledge of their interaction with precursor stem cells is needed. Since glia are so vital for brain growth and function, they have been thoroughly studied in organisms from *Drosophila* to vertebrates (Freeman, 2015; Freeman and Doherty, 2006; Hartenstein, 2011; Ou et al., 2014; Zuchero and Barres, 2015). In this review, we cover the interesting insights that the *Drosophila* central nervous system (CNS) has provided via studies carried out in stem cell niches (Banerjee et al., 2017; Berger et al., 2012) with vanguard systems of elementary genetic manipulation (Gratz et al., 2013; Manning and Doe, 2017; Sarov et al., 2016), and we attempt to contextualize the significance of these discoveries in the framework of vertebrates. To do so, we first provide an overview of the elements that constitute the stem cell niche, from embryonic (Figure 1) to larval (Figure 2 and Figure 3) progenitors and glia (Figure 4), and then explain their roles in the microenvironment they share. Finally, we end with the role that the glial niche may play in brain injuries and disease and emphasize the importance of future research on CNS development.

## **Drosophila neural stem cells**

*Drosophila* neural stem cells (NSCs), known as neuroblasts (NBs), are a useful model for studying the complexity of brain development from youth to adulthood (Clark et al., 2018; Enriquez et al., 2018; Ito et al., 2013; Jefferis et al., 2001; Marin et al., 2002; Sato et al., 2013; Yang et al., 2013; Yu et al., 2013; Figure 1 and Figure 2). Thus, the widely-understood temporal transition in the NBs of the fly brain (Baumgardt et al., 2009; Bayraktar and Doe, 2013; Brody and Odenwald, 2000; Doe, 2017; Grosskortenhau et al., 2005; Holguera and Desplan, 2018; Kambadur et al., 1998; Li et al., 2013; Maurange, 2012; Sato et al., 2013; Suzuki et al., 2013) has given insight into how similar sequential gene expression occurs in mammalian

corticogenesis (Delaunay et al., 2017; Holguera and Desplan, 2018), for instance in the independent cell-cycle progression (Okamoto et al., 2016) or to confer early temporal competence to retinal progenitor cells (Elliott et al., 2008).

NBs undergo distinct modes of cell division to shape different areas of the brain (Figure 1 and Figure 3). The behaviour of progenitors depends on three parameters: first, each cell's identity; second, each cell's intrinsic timer status; and finally, each cell's location, or immediate environment. Regarding the first parameter, for example, the nature of two classical types of fly NBs (type I and type II) has been broadly studied (Doe, 2017). These two subtypes mainly differ on whether or not neurogenesis is mediated by the intermediate neural progenitors (INPs) prior to the production of ganglion mother cells (GMCs; Bello et al., 2008; Boone and Doe, 2008; Bowman et al., 2008; Figure 1A-2 and Figure 3A). In contrast, type 0 NBs produce progeny that directly differentiate into neurons (Ulvklo et al., 2012; Figure 1C-2 and Figure 3B). The second parameter consists of the sequential expression of transcription factors (TFs) in progenitors, a phenomenon known as temporal patterning (Baumgardt et al., 2009; Brody and Odenwald, 2000; Doe, 2017; Grosskortenhaus et al., 2005; Kambadur et al., 1998; Li et al., 2013; Maurange, 2012; Sato et al., 2013; Suzuki et al., 2013), which is important for the generation of the neural diversity required in adults. The final parameter that influences progenitor behaviour is the place, or environment, in which each progenitor resides, as each progenitor is exposed to a varying set of extrinsic cues depending on its location (Ferraro et al., 2010; Morrison and Spradling, 2008). The effect of each NB's environment is evidenced by the fact that the same NB types may give rise to different neuronal populations depending on where they are located. For example, type 0 NBs have been described in late-embryonic ventral nerve cord (Baumgardt et al., 2014; Figure 1C-1) and larval optic lobe NB lineages (Bertet et al., 2014; Figure 2B-2). Some of the extrinsic cues involved in regulating cell division have been identified, as we will explain later. To make clear the progenitor types and their environments, we have divided them into the three main regions of the *Drosophila* CNS depending their origin: NBs of the central brain (CB; Figure 1A and Figure 2A), which delaminate from the embryonic procephalic neuroectoderm; NBs of the optic lobe (OL; Figure 1B and Figure 2B), which mostly delaminate from the postembryonic OL proliferative neuroepithelium derived from an embryonic optic placode; and NBs of the ventral nerve cord (VNC; Figure 1C and Figure 2C), which delaminate from the embryonic VNC neuroectoderm.

## **Embryonic progenitors**

Systematic studies of *Drosophila* embryonic NBs with single-lineage and single-cell resolution have elucidated the mechanisms controlling the generation of cellular diversity in the developing CNS, providing a detailed map of molecular markers of NBs in the early embryonic brain (Bossing et al., 1996; Doe, 2017; Schmidt et al., 1997; Urbach and Technau, 2004). Knowledge of the embryo also allows for the tracking of development from embryonic to larval stages and thus better contextualizes discoveries made in larvae. In this review, the terms VNC, CB and OL are used to refer to the parts of the embryonic CNS (Hakes et al., 2018) in order to maintain consistency with the terminology used in other stages of development.

The *Drosophila* VNC (Figure 1C), which is analogous to the spinal cord in vertebrates, is a region of the insect CNS in which temporal patterning of NBs was first observed (Baumgardt et al., 2009; Brody and Odenwald, 2000; Doe, 2017; Grosskortenhaus et al., 2005; Kambadur et al., 1998). In the VNC there are 30 NBs per bilateral hemisegment, arranged in rows and columns, which leads to their row/column naming scheme (e.g., NB5-6 is in row 5, column 6; Broadus et al., 1995; Hartenstein et al., 1994; Figure 1C-1). Most, if not all, VNC NBs begin in type I mode: they undergo several rounds of Notch-dependent asymmetric cell division to produce a self-renewed NB and a series of smaller GMCs that typically differentiate into a pair of neurons (Buescher et al., 1998; Figure 1C-2). Subsequently, many of these type I NBs switch to type 0 mode, and thus produce progeny that directly differentiate into neurons (Baumgardt et al., 2009; Monedero Cobeta et al., 2017; Ulvklo et al., 2012; Figure 1C-2). This switch is controlled by a temporal cascade, a series of five TFs (Hunchback (Hb), Krüppel (Kr), Pdm1/Pdm2 (Pdm), Castor (Cas) and Grainy head (Grh)) that are expressed sequentially during lineage development. Hb, Kr and Pdm promote type I proliferation and Cas and Grh promote type 0 proliferation and NB cell cycle exit (Bahrapour et al., 2017). The orphan nuclear receptor Seven-up (Svp) and the Pipsqueak domain proteins Dan and Danr promote the Hb to Kr switch by working synergistically to repress Hb transcription (Kanai et al., 2005; Kohwi et al., 2011; Mettler et al., 2006). Temporal factors control the competence of the NB, as demonstrated by the generation of different types of neurons and glia at different time points (Baumgardt et al., 2009; Grosskortenhaus et al., 2005; Isshiki et al., 2001; Moris-Sanz et al., 2014).

As in many species, the *Drosophila* brain undergoes even greater expansion than the VNC throughout development (Yaghmaeian Salmani et al., 2018). Like in the VNC, type I NBs are present in the embryonic

CB (Figure 1A-1), around 100 per hemisphere (Urbach et al., 2003; Urbach and Technau, 2004), although they do not switch to type 0 (Figure 1A-2). Recently, type II NBs have also been found to be present (Alvarez and Diaz-Benjumea, 2018; Walsh and Doe, 2017; Figure 1A-1 and Figure 1A-2). Mushroom body (MB) NBs are also found in the embryonic CB (Figure 1A-1), and divide in a mode similar to that of type I NBs, producing neurons via GMCs (Figure 1A-2); they eventually produce the Kenyon cells of the adult MB. Hence, there is a gradient of proliferation in the embryonic brain: there are a dozen hyperproliferative NBs (four MB NBs and eight type II NBs per brain lobe) while the rest of the brain's NBs exhibit exclusively type I behaviour (Alvarez and Diaz-Benjumea, 2018; Monedero Cobeta et al., 2017; Walsh and Doe, 2017; Yaghmaeian Salmani et al., 2018).

Although it was previously thought that OL development did not begin until larval stages, it was very recently discovered that in late embryogenesis, neuroepithelial cells (NECs) in the embryonic region that later gives rise to the OL delaminate into canonical NBs called embryonic optic neuroblasts (EONs; Hakes et al., 2018; Figure 1B-1). These EONs generate neurons and glia (Figure 1B-2).

At the end of embryogenesis, most of the remaining embryonic NBs in the entire CNS, except MB NBs (Kunz et al., 2012), enter into a quiescent state or are eliminated by apoptosis (Hakes et al., 2018; Truman and Bate, 1988; White et al., 1994). It is during the larval stage when they exit quiescence in a nutrition-dependent manner to start the second wave of neurogenesis (Chell and Brand, 2010; Lanet et al., 2013; Sousa-Nunes et al., 2011; Speder et al., 2011), generating the more complex CNS required for adult life.

## **Larval central brain and ventral nerve cord neuroblasts**

Unlike in the embryo, the VNC in larval stages consists of only type I NBs (Figure 2C and Figure 3C) while the larval CB has type I, type II, MB and antennal lobe (AL) NBs (Das et al., 2013; Doe, 2017; Homem and Knoblich, 2012; Sousa-Nunes et al., 2010; Figure 2A and Figure 3A). In larvae, type I NB cells, which are reactivated following the embryonic stage, are *Deadpan (Dpn)<sup>+</sup> Asense (Ase)<sup>+</sup> Pointed 1 (PntP1; Pnt)<sup>-</sup>* and produce GMCs that are *Dpn<sup>-</sup> Prospero (Pros)<sup>+</sup>* (Xie et al., 2016; Zhu et al., 2011). Unlike in the embryo, postembryonic type I NBs do not use *Hb*, *Kr* and *Pdm* to regulate temporal specification. In early larval stages, these NBs express *Cas* and give rise to a series of early-born neurons expressing the BTB transcription factor *Chronologically inappropriate morphogenesis (Chinmo)* and later-born neurons expressing *Broad (Br)* (Maurange et al., 2008; Zhu et al., 2006). *Svp* is re-expressed in larval NBs to trigger this temporal transition from *Chinmo* to *Br* expression by terminating *Cas* expression (Maurange et al., 2008).

As in the embryo, there are eight type II NBs per brain lobe (Figure 2A): six dorsal medial (DM1–6) and two dorsal lateral (DL1 and DL2). Type II NBs have a distinct molecular profile, which is *Dpn<sup>+</sup> Ase<sup>-</sup> PntP1<sup>+</sup>* (Doe, 2017; Homem and Knoblich, 2012; Sousa-Nunes et al., 2010). These NBs also temporally express a series of factors including *Dichaete (D)*, *Cas* and *Svp* (Bayraktar and Doe, 2013). As with neural progenitors in the human outer subventricular zone (SVZ; Doe, 2017; Fernandez et al., 2016; Homem and Knoblich, 2012), type II NBs asymmetrically divide to generate INPs with the molecular profile *Dpn<sup>+</sup> Ase<sup>+</sup>*. These INPs also sequentially express the TFs *D*, *Grh* and *Eyeless (Ey)* in order to each generate approximately six GMCs that are *Dpn<sup>-</sup> Ase<sup>+</sup>*, which then differentiate into distinct neural cell types (Bayraktar and Doe, 2013; Bello et al., 2008; Boone and Doe, 2008; Bowman et al., 2008; Izergina et al., 2009; Zhu et al., 2011; Figure 3A). Together, these expression patterns in NBs and INPs increase the neural diversity in the adult fruit fly CNS. The aforementioned factors, along with novel candidate temporal factors expressed by larval NBs (Ren et al., 2017; Syed et al., 2017b) including the *Ecdysone receptor (Syed et al., 2017b)*, were identified via the use of unbiased transcriptomic approaches. Further analysis will reveal the role of those potential novel temporal factors.

Also located in the larval CB are four MB NBs per hemisphere (Figure 2A), which emerge during the embryonic period and continuously divide during development until early adult stages without entering into quiescence (Kunz et al., 2012; Lee et al., 1999). Each give rise to three neuronal lineages, which together generate the adult centres for olfactory associative learning and cognitive functions (Lee et al., 1999). The cell division mode of MBs is similar to that of type I NBs: they produce MB neurons via GMCs (Figure 3A). Based on the age of the larva, two RNA-binding proteins, *IGF-II mRNA-binding protein (Imp)* and *Syncrin (Syp)*, display opposing temporal gradients: young NBs have high *Imp* and low *Syp* expression, middle-aged NBs express both, and old NBs have low *Imp* and high *Syp* expression (Liu et al., 2015). The expression of these proteins thus controls mushroom body lineages by regulating translation of the temporal transcription factor *Chinmo* (Liu et al., 2015; Narbonne-Reveau et al., 2016).



The ALs are an important part of the olfactory system in *Drosophila*. The functioning olfactory system in larvae is generated in the embryo (Marin et al., 2005; Yu et al., 2010), although knowledge of which specific embryonic progenitor cells give rise to the olfactory system is limited. In larvae, the system consists of 21 olfactory sensory neurons located in the antenno-maxillary complex which then form 21 subunits called glomeruli consisting of 21 projections and 21 local interneurons (Ramaekers et al., 2005). In each of the two larval ALs there are five NBs (Figure 2A), which are defined as anterodorsal (adNB/BAMv3), lateral (lNB/BAlc), ventral (vNB/BAla1), ventrolateral (vlNB/BAla2) and BAlp4 (Das et al., 2013). These AL NBs found in larvae give rise to the adult olfactory system, which is much more complex. Larval AL NBs undergo proliferation and can generate approximately 40 neuron types from a single hemilineage (Yu et al., 2010). GMCs descended from these larval AL NBs (Figure 3A) make daughter cells with distinct neuronal A/B fates due to a Notch-mediated binary sister fate decision. Notably, many CNS lineages exist as a lone hemilineage because one entire hemilineage may undergo premature cell death as a result of this binary decision (Lin et al., 2012; Lin et al., 2010; Yu et al., 2010). Using this neurogenic strategy, during larval stages AL NBs generate approximately 200 adult olfactory projection neurons and 100 local interneurons (Das et al., 2013; Das et al., 2008; Jefferis et al., 2001; Lai et al., 2008; Yu et al., 2013). AL NBs end proliferation around pupation. Within each adult AL, approximately 1300 olfactory receptor neurons expressing the same receptors make connections to two types of interneurons, projection neurons and local interneurons, forming approximately 50 glomeruli (Vosshall et al., 2000). Projection neurons extend their axons to higher brain centres in the MB and lateral horn (Jefferis et al., 2001). The behaviour of developmental progenitors in the OL is more complex, and will be discussed next.

## **Larval optic lobe progenitors**

The OL is the largest part of the *Drosophila* brain; it has four ganglia and is dedicated solely to vision, which reveals the importance of this sense for adult flies (Morante and Desplan, 2004). Neurons of the mature OL are produced during the larval and pupal periods (Hofbauer and Campos-Ortega, 1990).

Larval NECs delaminate into 800 OL NBs, which asymmetrically divide to self-renew and start neurogenesis and gliogenesis (Figure 2B and Figure 3B; Egger et al., 2007; Yasugi et al., 2008). This process resembles the behaviour of progenitors in the mammalian forebrain, which first divide symmetrically and then later divide asymmetrically to produce NSCs (Brand and Livesey, 2011; Gotz and Huttner, 2005; Kriegstein and Alvarez-Buylla, 2009). This region was thought to be unlike the rest of the fruit fly CNS, with most of the OL NBs being segregated from NECs beginning at the second-instar larval stage (Ceron et al., 2001; Egger et al., 2007). However, as previously discussed in the section "Embryonic progenitors", a recent study has challenged this view (Hakes et al., 2018), showing that embryonic OL NECs start to produce EONs during embryonic development (Figure 1B).

Characterization by molecular markers and morphology indicates that the four fly OL ganglia originate from two distinct neuroepithelial regions (Figure 2): the outer proliferation centre (OPC; Figure 2B-1 and Figure 2B-2), which gives rise to the medulla and lamina neuropils, and the inner proliferation centre (IPC; Figure 2B-3), which produces the lobula and lobula plate neurons (Apitz and Salecker, 2015; Hasegawa et al., 2011; Hofbauer and Campos-Ortega, 1990; Li et al., 2013; Meinertzhagen and Hanson, 1993; Mora et al., 2018; Morante and Desplan, 2004, 2011; Morante et al., 2011; Pinto-Teixeira et al., 2018). Although they originate in different parts of the brain, these neuron types have been found to interact with one another in order to establish the various neuropil compartments (Suzuki et al., 2016).

The OPC neuroepithelium (Figure 2B-1 and Figure 2B-2) is patterned into spatial domains along the anterior-posterior axis by expression of Visual system homeobox 1 (Vsx1), Optix, Decapentaplegic (Dpp) and Wingless (Wg; Erclik et al., 2008; Erclik et al., 2017; Gold and Brand, 2014) and is morphologically subdivided by the lamina furrow (LF), which separates the medial domain (m-OPC) and the lateral domain (l-OPC; Figure 2B-1). Differentiation of NBs from NECs in these regions is controlled at first by Notch, which maintains NECs, and then by JAK/STAT which negatively regulates proneural wave progression and thus triggers the switch from symmetric to asymmetric cell division (Egger et al., 2010; Ngo et al., 2010; Reddy et al., 2010; Yasugi et al., 2010; Yasugi et al., 2008). Later in development, Notch signalling remains active only in the m-OPC, which eventually gives rise to medulla neurons, while JAK/STAT signalling remains active only in the l-OPC, which gives rise to lamina neurons (Ngo et al., 2010). Apart from the ganglia they generate, these regions also differ in their distinct forms of neurogenesis, which we will discuss next.

In larval development in the m-OPC, dietary nutrients trigger insulin/PI3K/TOR signalling to regulate NEC proliferation (Lanet et al., 2013). The Fat-Hippo pathway also plays a role in regulation of growth through proliferation of NECs, and later arrests these cells in the G1 phase of the cell cycle before their conversion

to NBs (Reddy et al., 2010). In late larval stages, proliferation becomes insensitive to dietary nutrients and the steroid hormone Ecdysone becomes active. Ecdysone acts via Delta/Notch signalling to initiate the shift from symmetric/proliferative cell division to asymmetric/neurogenerative cell division (Lanet et al., 2013). Expression of the proneural protein Lethal-of-scute (L(1)sc), which is induced by epidermal growth factor (EGF) receptor signalling, also promotes the conversion of NECs to NBs (Egger et al., 2010; Morante et al., 2013; Yasugi et al., 2010; Yasugi et al., 2008; Figure 2B-1). The microRNA miR-7, along with other factors, is important for buffering this transition (Caygill and Brand, 2017). In type I NBs, temporal expression of six different TFs (Homothorax (Hth), Klumpfuss (Klu), Ey, Sloppy-paired (Slp), D and Tailless (Tll)) which triggers the differentiation of GMCs acts in tandem with Notch-dependent asymmetric cell division to control differentiation of the neuronal progeny (Doe, 2017; Li et al., 2013; Suzuki et al., 2013; Figure 3B). Overall, the integration of this temporal signalling with spatial cues is essential for generating neural diversity (Erclik et al., 2017).

In the m-OPC, there is a particular area located in the tip of the OPC (tip-OPC; Figure 2B-2) in which NB behaviour depends on two temporal windows. First, when the TF Distalless (Dll) is expressed, NBs divide in type 0 mode; type 0 NBs were originally described in the embryo and are the only postembryonic NBs which give rise to neuron progeny directly without further cell divisions (Bertet et al., 2014; Figure 3B). Later, when the TFs Ey, Slp and D are expressed, NBs switch to type I division mode, though half of their progeny is eliminated via apoptosis. This temporal expression of TFs contributes to the generation of diverse neural subtypes in the tip-OPC that innervate the medulla, lobula and lobula plate in adult flies (Bertet et al., 2014; Figure 3B).

Another type of progenitor, common progenitor cells (CPCs), delaminate from NECs of the tip-OPC (Chen et al., 2016; Figure 2B-2). CPCs do not express the canonical NB marker Dpn but do express Pros and Ase, and therefore more closely resemble GMCs. CPCs divide asymmetrically to generate two distinct precursor cell populations: lamina wide-field precursor cells (Lawf PCs) and glial precursor cells (GPCs; Figure 2B-2 and Figure 3B). Each one of the latter two precursor types divide symmetrically and respectively generate Lawf neurons and lamina glia (Chen et al., 2016; Figure 3B). This neurogliogenesis fate choice mediated by the Notch pathway resembles in many ways the role that Notch signalling plays in vertebrates in establishing neurogenic or gliogenic phases during development (Gaiano and Fishell, 2002; Rowitch and Kriegstein, 2010; Taylor et al., 2007). Finally, after the precursor cells differentiate into glia and Lawf neurons, both these cell types migrate to their position in the medulla (Chen et al., 2016).

NECs in the l-OPC (Figure 2B-1) generate non-NB cells in the G2-phase, which divide symmetrically to produce lamina neurons (Figure 3B). These posterior LF progenitors, called lamina precursor cells (LPC; Figure 2B-1), proliferate and differentiate in a manner regulated by sequential release of secreted factors by photoreceptors (PRs). First, PRs release Hedgehog to promote terminal divisions of NECs, and second they release Spitz/TGF- $\alpha$  and Fibroblast growth factor (FGF) which induce differentiation of lamina neurons (Fernandes et al., 2017; Franzdottir et al., 2009; Huang and Kunes, 1996, 1998; Huang et al., 1998; Selleck and Steller, 1991) in a process mediated by a glial relay (Fernandes et al., 2017).

The other proliferation centre, the IPC (Figure 2), consists of three domains, which are defined based on their location as surface, proximal and distal IPC (s-IPC, p-IPC and d-IPC, respectively; Apitz and Salecker, 2015). At the same time, the cells of the IPC belong to two proliferative zones: in the p-IPC region NECs divide symmetrically while the d-IPC is composed of NBs derived from the p-IPC cells (Figure 2B-3). Specifically, NECs in the p-IPC express either Dpp or Brinker (Brk), a negative regulator of Dpp target genes, which determines whether the NECs will give rise to either vertical or horizontal motion selective neurons (Apitz and Salecker, 2015; Pinto-Teixeira et al., 2018).

The IPC NECs then delaminate into migrating progenitors (MPs), which move from the p-IPC to the d-IPC (Apitz and Salecker, 2015; Figure 2B-3 and Figure 3B). This EMT-like mechanism is required for facilitating spatio-temporal matching of neurogenesis and neuronal connectivity, and resembles the migration of neurogenic radial glia-like cells from the meninges to the neonatal cortex of mice that then differentiate into functional integrated neurons (Bifari et al., 2017). Once MPs reach the d-IPC, they differentiate into NBs (Figure 2B-3 and Figure 3B) that sequentially express D and Ase and then Tll, Ato and Dac. These NBs first go through type I cell division orchestrated by Ase TFs to produce C- and T-neurons (Apitz and Salecker, 2015). When the NBs enter to the Ato temporal window they exclusively produce T4 and T5 neurons which respectively detect bright edge and dark edge motion (Apitz and Salecker, 2015; Oliva et al., 2014). Two conflicting models have been proposed for the production of T neurons. In the first model, Ato<sup>+</sup> NBs generated by either a horizontal or vertical progenitor undergo two sequential Notch-dependent divisions to produce matching sets of two T4 and two T5 neurons (Apitz and Salecker, 2018; Pinto-Teixeira et al., 2018). In the second model, a transient amplification of d-IPC NBs by symmetric cell division ensures that the correct number of T4 and T5 neurons is produced (Mora et al., 2018); the temporal transition in

proneural protein expression from Ase to Ato regulates the timing of the onset of this NB transient amplification. Although symmetric cell division in NBs has been previously described in mammals (Obernier et al., 2018), this is the first time it has been seen in *Drosophila*. Thus, these symmetrically dividing cells are categorised as type III NBs due to their initial self-propagation and subsequent loss of multipotency (Mora et al., 2018; Figure 2B-3 and Figure 3B).

## **Glial cells in the *Drosophila* central nervous system**

Glial cells in *Drosophila* are genetically similar to glia in mammals, and express many TF homologs such as the gene glial cells missing (*gcm*) which is responsible for glial cell fate (Freeman et al., 2003; Freeman and Doherty, 2006; Van De Bor and Giangrande, 2002). In the fruit fly, glial cells are derived from a small set of uniquely identifiable NBs (Figure 3). Glioblasts and neuroglioblasts, which are respectively named according to whether they give rise to only glia or both neurons and glia, delaminate from the neuroectoderm of the post-gastrulation embryo (Beckervordersandforth et al., 2008; Stork et al., 2012; von Hilchen et al., 2008). These cells increase in number at the third instar larval stage due to two mechanisms: division of differentiated glial cells (Colonques et al., 2007) and continued division of neuroglioblasts (Larsen et al., 2009; Omoto et al., 2015; Ren et al., 2017; Viktorin et al., 2013). Finally, the glial diversity in the adult CNS depends on embryonic and larval temporal patterning, and it is thus crucial to study glial development in order to fully understand the structure of the adult brain (Awasaki et al., 2008).

The embryonic *Drosophila* VNC contains around 25–30 glia per hemisegment. These glia can be divided into three main categories according to their location and morphology. The first category is surface glia (SG), made up of perineurial glia (PG) and subperineurial glia (SPG), which surround the CNS and peripheral nerves and contribute to the formation of the blood–brain barrier (BBB). The second category is cortex glia (CG), which ensheath neuronal cell bodies. The third category is neuropil glia (NG), which associate directly with the neuropil (Hartenstein et al., 1998; Ito et al., 1995; Poreanu et al., 2005). Apart from these three categories, midline glia are a small set of glia also present in the embryonic CNS; they play an important role in axon pathfinding at the CNS midline and commissure formation in the VNC (Jacobs, 2000). Midline glia later differentiate as ensheathing glia (Jacobs, 2000).

Though in past years there has been a significant effort to characterise glial cells in the larval *Drosophila* CNS (Figure 4), it has proved difficult (Awasaki and Lee, 2011); this has resulted in varied and broad terminology used to describe the diverse population of glia. Here, we categorize larval glia into the same three main groups as embryonic glia; these categories are defined by location, characteristics and function (Freeman, 2015; Hartenstein, 2011; Ou et al., 2014; Stork et al., 2012).

The first group, located in the outer part of the brain, is the SG; this glial type wraps the entire CNS (Figure 4) and is the gateway to the brain for particles carried within the hemolymph (the fluid analogous to blood in insects). In larvae as in the embryo, this cell population can be divided into PG, the first physical and chemical brain barrier for large particles, and SPG, which communicate amongst themselves via septate junctions and function as an evolutionarily conserved BBB (DeSalvo et al., 2011; Stork et al., 2008). SPG are also in contact with other glial subtypes through adherents or gap junctions (DeSalvo et al., 2011). Hundreds of PG are found per hemisphere and they are smaller in size and have an elongated cell body, while SPG are large with flattened nuclei and are very low in number, around twenty cells per larval hemisphere (Poreanu et al., 2005; Figure 4A and Figure 4B). Ultimately, SG serve as an important mediator between the exterior environment and the interior of the brain (DeSalvo et al., 2011).

A second main glial type, CG, is located underneath the SPG in the larval OLs and is characterised by the expression of the conserved microRNA miR-8 (Morante et al., 2013). In each OL approximately 140 miR-8<sup>+</sup> CG cells enwrap NECs, NBs, GMCs and neurons (Morante et al., 2013; Figure 4B). In the VNC and CB (Figure 4A and Figure 4C), CG also ensheathes NBs and their progeny and are required for regulating NB proliferation as well as maintaining energy homeostasis (Chell and Brand, 2010; Sousa-Nunes et al., 2011; Speder et al., 2011; Volkenhoff et al., 2015).

A third main glial type, NG, is located between the cortex and the neuropil in the VNC and CB. This glial cell population is the most diverse due to its variety of structures and expression of molecular markers (Poreanu et al., 2005). Although these cells can be named in many different manners depending on their location, they are mainly divided into two subtypes: ensheathing glia (EG) and astrocyte-like glia (ALG; Figure 4A and Figure 4C). EG surround parts of the neuropil whilst ALG manage neural remodelling through axon pruning and synaptic formation (Freeman, 2015; Peco et al., 2016; Tasdemir-Yilmaz and Freeman, 2014; Wu et al., 2017).

In the complexity of the OL, it is possible to distinguish different glial subtypes (Chotard and Salecker, 2007; Huang and Kunes, 1996; Figure 4B). A CG subtype, satellite glia (sg), ensheathes lamina neuron cell bodies. Two subtypes of NG, epithelial glia (eg) and marginal glia (mg), originate in GPC regions and share lineage with lamina neurons (Chen et al., 2016). Later on, both of these subtypes migrate respectively to above (eg) and below (mg) the lamina plexus, into the area where axons of PRs project from the eye imaginal discs (Chotard and Salecker, 2007). Other subtypes of NG are the medulla glia (meg), which are found in the first optic chiasm though their origin is uncertain, and the medulla neuropil glia (mng), which are mainly generated from neuroglioblasts of the OPC and migrate to the anterior cortex-neuropil interface (Li et al., 2013; Richier et al., 2017). Therefore, the wide variety of glial functions, the presence of glia across the entire CNS, and the complexity of glial development strongly suggest that glial cells play an essential role in the brain's regulation and are evolutionarily conserved across species.

## **Glial-neural progenitor interactions in the developing brain**

In recent years, glial cells have been found to play important roles in microenvironments where they can act directly on different biological processes. In adult mammals, the SVZ, where neurogenesis is maintained, receives external BBB inputs from diffusible morphogens, the blood or the cerebrospinal fluid (Dani and Lehtinen, 2016; Silva-Vargas et al., 2016). Similarly, in the larval insect brain, the BBB function of the SG layer highlights its importance as a member of a NSC microenvironment known as the neurovascular niche (Otsuki and Brand, 2017). SPG and CG cells are known to have large nuclei, as previously mentioned, and also are polyploid; this feature is required to maintain the integrity of the BBB as well as proper growth of SPG cells and the brain in general (Morante et al., 2013; Unhavaithaya and Orr-Weaver, 2012). Additionally, PG cells have been found to be involved in microenvironment signalling. Studies reveal that this SG subtype secretes two signals, Dally-like (Dlp), a heparan sulfate proteoglycan, and Glass bottom boat (Gbb), a BMP homologue, that directly communicate with NB cells and act as key cues for brain development (Kanai et al., 2018). These recent discoveries suggest that there is still more to be learned about the role of glia in the important processes of development.

Glial cells also act in the larval VNC and CB to reactivate quiescent embryological NBs, providing the source of *Drosophila* insulin-like peptides (dILPs) relevant for timely reactivation of NBs in response to nutrition (Chell and Brand, 2010; Lanet et al., 2013; Sousa-Nunes et al., 2011). As discovered recently, a VNC NB in the G2 cell cycle phase can enter into quiescence when induced by the evolutionarily conserved pseudokinase Tribbles (Otsuki and Brand, 2018), in contrast to the previously accepted belief that NBs could only arrest at G0. These arrested G2 cells can exit quiescence in the presence of dILP signalling originating from BBB glia, and these cells reactivate and regenerate neurons more quickly than arrested G0 NBs; this shows that the stage in which NSCs arrest affects the timing of their reactivation in response to external signals from the glial niche (Otsuki and Brand, 2018). Similarly, it has also been found that dILPs act in the *Drosophila* visual system as part of a signalling cascade involved in retinotopy. PRs communicate with lamina neurons by producing Spitz/TGF- $\alpha$  (Fernandes et al., 2017; Huang et al., 1998). PR Spitz/TGF- $\alpha$  then acts on EG, which in turn produce dILPs which induce LPC progenitors to differentiate into lamina neurons. The role of glia in this essential process demonstrates their importance in regulating spatiotemporal differentiation patterns across distinct brain regions (Fernandes et al., 2017; Rossi and Fernandes, 2018). Altogether, these conclusions reinforce the idea that glia have a decisive role in the precursor niche.

NECs are another type of progenitor in which it has been shown that glial ligand expression can significantly influence the development of the OL in the larval brain. Some examples of this impact on the regulation of NEC proliferation are, for example, the non-autonomous effect that the transmembrane protein Serrate from SPG produces in the Notch pathway (Perez-Gomez et al., 2013) and the influence that the release of Spitz/TGF- $\alpha$  from CG has on the EGF receptor pathway in NECs (Morante et al., 2013).

In addition to glia, NSCs can also send retrograde signals to glia and these local and systemic signals induce the remodelling of CG and help adapt the niche to their needs (Speder and Brand, 2018). The first step of this signalling cascade is the activation of the PI3k/Akt pathway in NSCs via nutritional cues, and this activation causes cortex glia to expand their membrane processes and begin to encase the NSCs. Then, NSCs exit quiescence and resume proliferation, which sends the signal to glial cells to alter the niche according to what is required to restart neurogenesis (Speder and Brand, 2018). In all, recent discoveries have helped elucidate the specific impacts that glial cells may have on neural stem cell niches. However, taking into consideration that glia have an active role in NSC niches, both glia-to-progenitor and progenitor-to-glia signalling must be further studied.

## The niche in brain injuries and future perspectives

As previously explained, temporal patterning is an essential mechanism for the development of the brain into such a complex organ. Dysregulation of the TFs important for the transition of neuronal precursors to neurons can lead to brain diseases including malignant tumour formation and loss of neural and glial identity (Maurange and Gould, 2005; Narbonne-Reveau et al., 2016). Additionally, defects in the cell polarity of neuroepithelial progenitors may have a direct impact on their offspring and may be involved in tumorigenesis (McCaffrey and Macara, 2011).

Glial cells not only are required for regulating NB proliferation (Chell and Brand, 2010; Lanet et al., 2013; Sousa-Nunes et al., 2011) but also protect NB proliferation in conditions of hypoxia and oxidative stress (Bailey et al., 2015). Dysfunction in glia and their non-autonomous effect on stem cell niches can cause severe problems in the *Drosophila* brain. It has recently been shown that a glial lineage-specific WDR62 depletion, the second most commonly mutated gene in primary microcephaly, significantly decreased brain volume (Lim et al., 2017). These examples show the importance of relevant function of glia within the stem cell niche.

In conclusion, although a significant amount is already known about progenitor niches and the functions of glial cells in the regulation of neural development, there remains much that has yet to be discovered and more research is required in this field. Scientists should take the opportunity to investigate not only development of each individual element of the stem cell niche but also interactions between the elements, examining the effects that one dysfunctional cell type may have on the other and consequently on the brain as a whole. By combining recent discoveries in *Drosophila melanogaster*, a powerful model organism, with new studies in mammals, researchers may soon be able to more fully describe the roles of each progenitor type in neurogenesis.

### Figures:

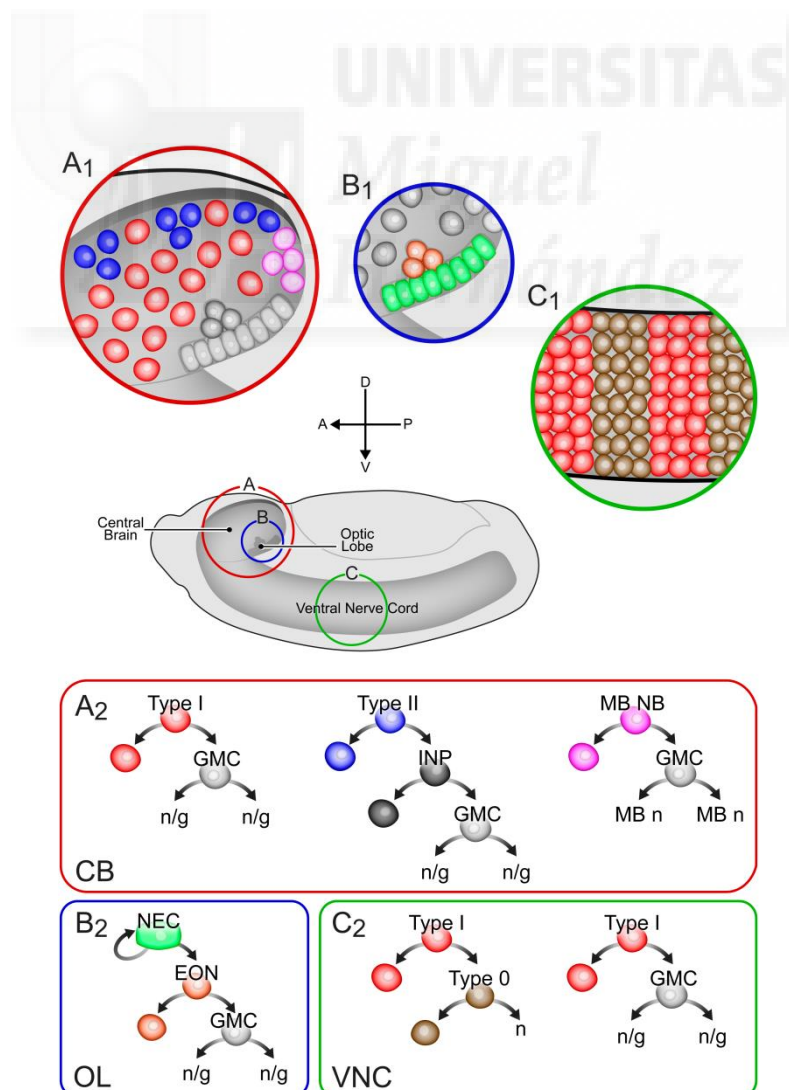


**Figure 1. Embryonic Neural Progenitors, Cell Division Modes and Progeny in *Drosophila melanogaster* CNS.** Diagram of neural progenitors and cell division modes described in the CNS of the late embryonic fruit fly. Progenitors and cell division modes are organised by CNS region: **(A)** the central brain (CB), framed in red; **(B)** the optic lobe (OL), framed in blue; and **(C)** the ventral nerve cord (VNC), framed in green. **(A1)** NBs of the CB: type I, type II (eight cells per hemisphere), and mushroom body (MB) NBs (four cells per hemisphere). **(B1)** Neuroepithelial cells (NECs) and embryonic optic neuroblasts (EONs) in the OL. **(C1)** NBs of the VNC: type I and type 0. **(A2), (B2)** and **(C2)** show cell division modes in each CNS region of the embryo. GMC: ganglion mother cell, INP: intermediate neural progenitor, n: neuron cell, g: glia cell, NB: neuroblast.

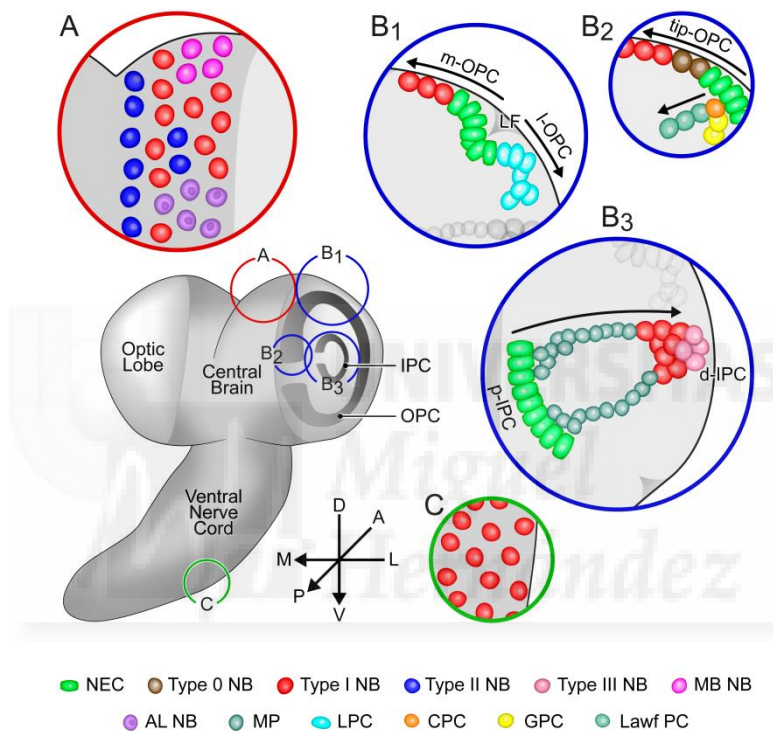


**Figure 2. Neural Progenitors in Larval CNS in *Drosophila melanogaster*.** Diagram of neural progenitors described in CNS of late larval fruit fly. **(A)** Circled in red, the four types of NBs located in the central brain: type I, type II (eight cells per hemisphere), mushroom body (MB) NBs (four cells per hemisphere), and antennal lobe (AL) NBs (five cells per hemisphere). **(B)** Circled in blue are the different types of progenitor cells which delaminate from neuroepithelial cells (NECs) of the optic lobe. **(B1)** shows the NECs of the outer proliferation centre (OPC), which delaminate into type I NBs and lamina precursor cells (LPCs). **(B2)** shows type 0 NBs of the tip-OPC and common progenitor cells (CPCs), which give rise to glial precursor cells (GPCs) and lamina wide-field precursor cells (Lawf PCs). This section of the figure is shown from a different angle. **(B3)** shows the NECs of the inner proliferation centre (IPC) that delaminate into migrating progenitors (MPs), which differentiate first into type I and finally into type III NBs. **(C)** Circled in green, the only NB type (type I) found in the ventral nerve cord. All views are frontal except for **(B2)**, which is seen from a dorsal perspective (for further points of view see figures in Ngo et al. 2017). Note that most of the NBs of the larval CNS originate during the first wave of neurogenesis in the embryonic stage. LF: lamina furrow, m-OPC: medial-OPC, l-OPC: lateral-OPC, p-IPC: proximal-IPC, d-IPC: distal-IPC.

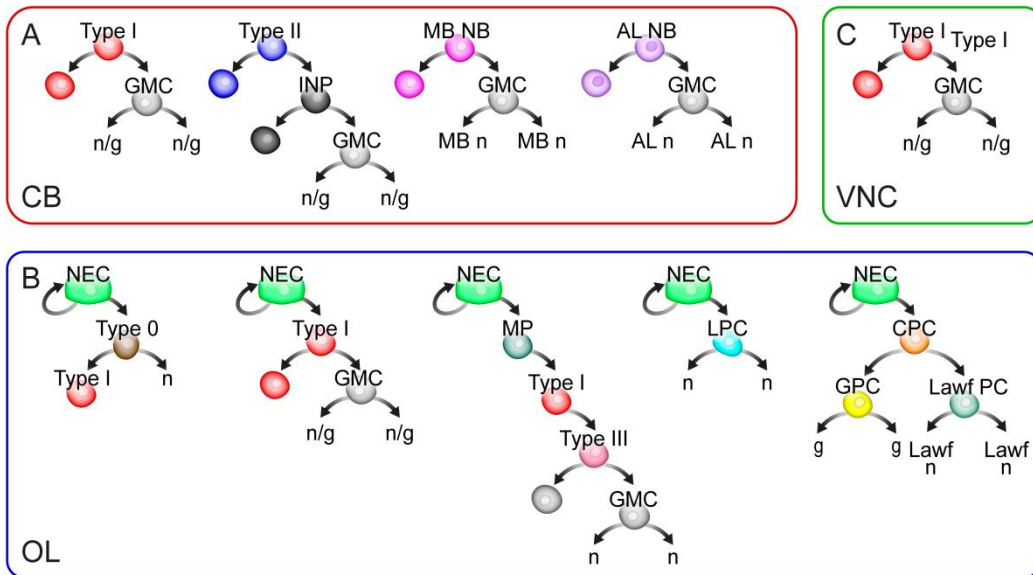


**Figure 3. Neural Progenitor Cell Division Modes and Progeny in Larval CNS in *Drosophila melanogaster*.** Representation of all types of NBs (type 0, I, II and III) and cell progenitors described in the CNS of the late larval fruit fly. The illustration indicates the type of cell division taking place (asymmetric or symmetric) by showing the offspring that each division generates. The progenitors are organized by the CNS region in which they are located: **(A)** the central brain (CB), framed in red; **(B)** the optic lobe (OL), framed in blue; and **(C)** the ventral nerve cord (VNC), framed in green. It is important to note that most NBs originate in the first wave of neurogenesis in the embryo. GMC: ganglion mother cell, INP: intermediate neural progenitor, n: neuron cell, g: glia cell, NB: neuroblast, MB: mushroom body, AL: antennal lobe, MP: migrating progenitor, LPC: lamina precursor cell, CPC: common progenitor cell, GPC: glia precursor cell, Lawf PC: lamina wide-field precursor cell, NEC: neuroepithelial cell.

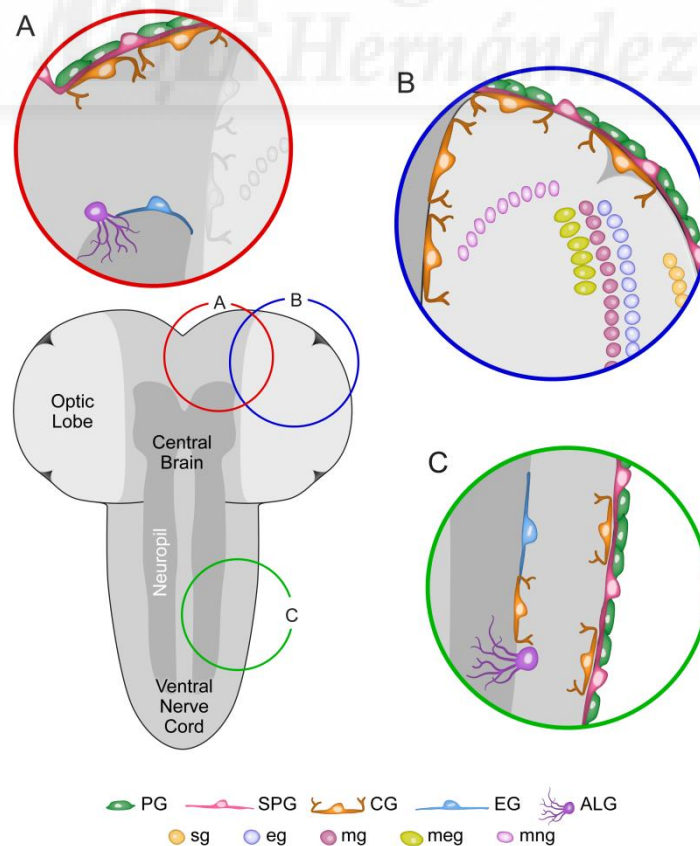


**Figure 4. Glial Cell Types in Larval CNS of *Drosophila melanogaster*.** Diagram of distinct glial cell types found in the CNS of the late larval fruit fly. **(A)** The types of glia found in the central brain, circled in red. The outer surface glia layers are classified as perineural glia (PG), subperineural glia (SPG) and miR8<sup>+</sup> surface-associated cortex glia (CG), and the neuropil glia (NG) are categorized as ensheathing glia (EG) and astrocyte-like glia (ALG). **(B)** The optic lobe, circled in blue. PG and SPG are the most external layers of glia, with the miR8<sup>+</sup> CG beneath them. Underneath those layers are a CG subtype, satellite glia (sg), and various NG subtypes: epithelial glia (eg), marginal glia (mg), medulla glia (meg) and medulla neuropil glia (mng). **(C)** Glia in the ventral nerve cord, circled in green. From the outside inward: PG, SPG, CG, EG and ALG.

## **References**

- Alvarez, J.A., and Diaz-Benjumea, F.J. (2018). Origin and specification of type II neuroblasts in the *Drosophila* embryo. *Development* 145.
- Apitz, H., and Salecker, I. (2015). A region-specific neurogenesis mode requires migratory progenitors in the *Drosophila* visual system. *Nat Neurosci* 18, 46-55.
- Apitz, H., and Salecker, I. (2018). Spatio-temporal relays control layer identity of direction-selective neuron subtypes in *Drosophila*. *Nature communications* 9, 2295.
- Awasaki, T., Lai, S.L., Ito, K., and Lee, T. (2008). Organization and postembryonic development of glial cells in the adult central brain of *Drosophila*. *J Neurosci* 28, 13742-13753.
- Awasaki, T., and Lee, T. (2011). New tools for the analysis of glial cell biology in *Drosophila*. *Glia* 59, 1377-1386.
- Baek, M., and Mann, R.S. (2009). Lineage and birth date specify motor neuron targeting and dendritic architecture in adult *Drosophila*. *J Neurosci* 29, 6904-6916.
- Bahrampour, S., Gunnar, E., Jonsson, C., Ekman, H., and Thor, S. (2017). Neural Lineage Progression Controlled by a Temporal Proliferation Program. *Dev Cell* 43, 332-348 e334.
- Bailey, A.P., Koster, G., Guillermer, C., Hirst, E.M., MacRae, J.I., Lechene, C.P., Postle, A.D., and Gould, A.P. (2015). Antioxidant Role for Lipid Droplets in a Stem Cell Niche of *Drosophila*. *Cell* 163, 340-353.
- Banerjee, S., Mino, R.E., Fisher, E.S., and Bhat, M.A. (2017). A versatile genetic tool to study midline glia function in the *Drosophila* CNS. *Dev Biol* 429, 35-43.
- Baumgardt, M., Karlsson, D., Salmani, B.Y., Bivik, C., MacDonald, R.B., Gunnar, E., and Thor, S. (2014). Global programmed switch in neural daughter cell proliferation mode triggered by a temporal gene cascade. *Dev Cell* 30, 192-208.
- Baumgardt, M., Karlsson, D., Terriente, J., Diaz-Benjumea, F.J., and Thor, S. (2009). Neuronal subtype specification within a lineage by opposing temporal feed-forward loops. *Cell* 139, 969-982.
- Baumgardt, M., Miguel-Aliaga, I., Karlsson, D., Ekman, H., and Thor, S. (2007). Specification of neuronal identities by feedforward combinatorial coding. *PLoS Biol* 5, e37.
- Bayraktar, O.A., and Doe, C.Q. (2013). Combinatorial temporal patterning in progenitors expands neural diversity. *Nature* 498, 449-455.
- Beckervordersandforth, R.M., Rickert, C., Altenhein, B., and Technau, G.M. (2008). Subtypes of glial cells in the *Drosophila* embryonic ventral nerve cord as related to lineage and gene expression. *Mech Dev* 125, 542-557.
- Bellen, H.J., Tong, C., and Tsuda, H. (2010). 100 years of *Drosophila* research and its impact on vertebrate neuroscience: a history lesson for the future. *Nature reviews Neuroscience* 11, 514-522.
- Bello, B.C., Izergina, N., Caussin, E., and Reichert, H. (2008). Amplification of neural stem cell proliferation by intermediate progenitor cells in *Drosophila* brain development. *Neural Develop* 3, 5.
- Berger, C., Harzer, H., Burkard, T.R., Steinmann, J., van der Horst, S., Laurenson, A.S., Novatchkova, M., Reichert, H., and Knoblich, J.A. (2012). FACS purification and transcriptome analysis of *drosophila* neural stem cells reveals a role for Klumpfuss in self-renewal. *Cell reports* 2, 407-418.



- Bertet, C., Li, X., Erclik, T., Cavey, M., Wells, B., and Desplan, C. (2014). Temporal patterning of neuroblasts controls Notch-mediated cell survival through regulation of Hid or Reaper. *Cell* 158, 1173-1186.
- Bifari, F., Decimo, I., Pino, A., Llorens-Bobadilla, E., Zhao, S., Lange, C., Panuccio, G., Boeckx, B., Thienpont, B., Vinckier, S., et al. (2017). Neurogenic Radial Glia-like Cells in Meninges Migrate and Differentiate into Functionally Integrated Neurons in the Neonatal Cortex. *Cell Stem Cell* 20, 360-373 e367.
- Bivik, C., Bahrapour, S., Ulvklo, C., Nilsson, P., Angel, A., Fransson, F., Lundin, E., Renhorn, J., and Thor, S. (2015). Novel Genes Involved in Controlling Specification of Drosophila FMRFamide Neuropeptide Cells. *Genetics* 200, 1229-1244.
- Boone, J.Q., and Doe, C.Q. (2008). Identification of Drosophila type II neuroblast lineages containing transit amplifying ganglion mother cells. *Dev Neurobiol* 68, 1185-1195.
- Bossing, T., Udolph, G., Doe, C.Q., and Technau, G.M. (1996). The embryonic central nervous system lineages of Drosophila melanogaster. I. Neuroblast lineages derived from the ventral half of the neuroectoderm. *Dev Biol* 179, 41-64.
- Bowman, S.K., Rolland, V., Betschinger, J., Kinsey, K.A., Emery, G., and Knoblich, J.A. (2008). The Tumor Suppressors Brat and Numb Regulate Transit-Amplifying Neuroblast Lineages in Drosophila. *Dev Cell*.
- Brand, A.H., and Livesey, F.J. (2011). Neural stem cell biology in vertebrates and invertebrates: more alike than different? *Neuron* 70, 719-729.
- Broadus, J., Skeath, J.B., Spana, E.P., Bossing, T., Technau, G., and Doe, C.Q. (1995). New neuroblast markers and the origin of the aCC/pCC neurons in the Drosophila central nervous system. *Mech Dev* 53, 393-402.
- Brody, T., and Odenwald, W.F. (2000). Programmed transformations in neuroblast gene expression during Drosophila CNS lineage development. *Dev Biol* 226, 34-44.
- Buescher, M., Yeo, S.L., Udolph, G., Zavortink, M., Yang, X., Tear, G., and Chia, W. (1998). Binary sibling neuronal cell fate decisions in the Drosophila embryonic central nervous system are nonstochastic and require inscuteable-mediated asymmetry of ganglion mother cells. *Genes Dev* 12, 1858-1870.
- Caygill, E.E., and Brand, A.H. (2017). miR-7 Buffers Differentiation in the Developing Drosophila Visual System. *Cell reports* 20, 1255-1261.
- Ceron, J., Gonzalez, C., and Tejedor, F.J. (2001). Patterns of cell division and expression of asymmetric cell fate determinants in postembryonic neuroblast lineages of Drosophila. *Dev Biol* 230, 125-138.
- Chell, J.M., and Brand, A.H. (2010). Nutrition-responsive glia control exit of neural stem cells from quiescence. *Cell* 143, 1161-1173.
- Chen, Z., Del Valle Rodriguez, A., Li, X., Erclik, T., Fernandes, V.M., and Desplan, C. (2016). A Unique Class of Neural Progenitors in the Drosophila Optic Lobe Generates Both Migrating Neurons and Glia. *Cell reports* 15, 774-786.
- Chotard, C., and Salecker, I. (2007). Glial cell development and function in the Drosophila visual system. *Neuron glia biology* 3, 17-25.
- Clark, M.Q., McCumsey, S.J., Lopez-Darwin, S., Heckscher, E.S., and Doe, C.Q. (2016). Functional Genetic Screen to Identify Interneurons Governing Behaviorally Distinct Aspects of Drosophila Larval Motor Programs. *G3 (Bethesda)* 6, 2023-2031.
- Clark, M.Q., Zarin, A.A., Carreira-Rosario, A., and Doe, C.Q. (2018). Neural circuits driving larval locomotion in Drosophila. *Neural Dev* 13, 6.
- Colonques, J., Ceron, J., and Tejedor, F.J. (2007). Segregation of postembryonic neuronal and glial lineages inferred from a mosaic analysis of the Drosophila larval brain. *Mech Dev* 124, 327-340.
- Couton, L., Mauss, A.S., Yunusov, T., Diegelmann, S., Evers, J.F., and Landgraf, M. (2015). Development of connectivity in a motoneuronal network in Drosophila larvae. *Curr Biol* 25, 568-576.
- Dani, N., and Lehtinen, M.K. (2016). CSF Makes Waves in the Neural Stem Cell Niche. *Cell Stem Cell* 19, 565-566.
- Das, A., Gupta, T., Davla, S., Prieto-Godino, L.L., Diegelmann, S., Reddy, O.V., Raghavan, K.V., Reichert, H., Lovick, J., and Hartenstein, V. (2013). Neuroblast lineage-specific origin of the neurons of the Drosophila larval olfactory system. *Dev Biol* 373, 322-337.

- Das, A., Sen, S., Lichtneckert, R., Okada, R., Ito, K., Rodrigues, V., and Reichert, H. (2008). *Drosophila* olfactory local interneurons and projection neurons derive from a common neuroblast lineage specified by the empty spiracles gene. *Neural Dev* 3, 33.
- Delaunay, D., Kawaguchi, A., Dehay, C., and Matsuzaki, F. (2017). Division modes and physical asymmetry in cerebral cortex progenitors. *Curr Opin Neurobiol* 42, 75-83.
- DeSalvo, M.K., Hindle, S.J., Rusan, Z.M., Orng, S., Eddison, M., Halliwill, K., and Bainton, R.J. (2014). The *Drosophila* surface glia transcriptome: evolutionary conserved blood-brain barrier processes. *Front Neurosci* 8, 346.
- DeSalvo, M.K., Mayer, N., Mayer, F., and Bainton, R.J. (2011). Physiologic and anatomic characterization of the brain surface glia barrier of *Drosophila*. *Glia* 59, 1322-1340.
- Doe, C.Q. (2017). Temporal Patterning in the *Drosophila* CNS. *Annu Rev Cell Dev Biol* 33, 219-240.
- Droujinine, I.A., and Perrimon, N. (2016). Interorgan Communication Pathways in Physiology: Focus on *Drosophila*. *Annu Rev Genet* 50, 539-570.
- Egger, B., Boone, J.Q., Stevens, N.R., Brand, A.H., and Doe, C.Q. (2007). Regulation of spindle orientation and neural stem cell fate in the *Drosophila* optic lobe. *Neural Develop* 2, 1.
- Egger, B., Gold, K.S., and Brand, A.H. (2010). Notch regulates the switch from symmetric to asymmetric neural stem cell division in the *Drosophila* optic lobe. *Development* 137, 2981-2987.
- Elliott, J., Jolicoeur, C., Ramamurthy, V., and Cayouette, M. (2008). Ikaros confers early temporal competence to mouse retinal progenitor cells. *Neuron* 60, 26-39.
- Enriquez, J., Rio, L.Q., Blazeski, R., Bellemin, S., Godement, P., Mason, C., and Mann, R.S. (2018). Differing Strategies Despite Shared Lineages of Motor Neurons and Glia to Achieve Robust Development of an Adult Neuropil in *Drosophila*. *Neuron* 97, 538-554 e535.
- Erlik, T., Hartenstein, V., Lipshitz, H.D., and McInnes, R.R. (2008). Conserved role of the *Vsx* genes supports a monophyletic origin for bilaterian visual systems. *Curr Biol* 18, 1278-1287.
- Erlik, T., Li, X., Courgeon, M., Bertet, C., Chen, Z., Baumert, R., Ng, J., Koo, C., Arain, U., Behnia, R., et al. (2017). Integration of temporal and spatial patterning generates neural diversity. *Nature* 541, 365-370.
- Fernandes, V.M., Chen, Z., Rossi, A.M., Zipfel, J., and Desplan, C. (2017). Glia relay differentiation cues to coordinate neuronal development in *Drosophila*. *Science* 357, 886-891.
- Fernandez, V., Llinares-Benadero, C., and Borrell, V. (2016). Cerebral cortex expansion and folding: what have we learned? *EMBO J* 35, 1021-1044.
- Ferraro, F., Celso, C.L., and Scadden, D. (2010). Adult stem cells and their niches. *Adv Exp Med Biol* 695, 155-168.
- Franzdottir, S.R., Engelen, D., Yuva-Aydemir, Y., Schmidt, I., Aho, A., and Klambt, C. (2009). Switch in FGF signalling initiates glial differentiation in the *Drosophila* eye. *Nature* 460, 758-761.
- Freeman, M.R. (2015). *Drosophila* Central Nervous System Glia. *Cold Spring Harb Perspect Biol* 7.
- Freeman, M.R., Delrow, J., Kim, J., Johnson, E., and Doe, C.Q. (2003). Unwrapping glial biology: *Gcm* target genes regulating glial development, diversification, and function. *Neuron* 38, 567-580.
- Freeman, M.R., and Doherty, J. (2006). Glial cell biology in *Drosophila* and vertebrates. *Trends Neurosci* 29, 82-90.
- Gaiano, N., and Fishell, G. (2002). The role of notch in promoting glial and neural stem cell fates. *Annu Rev Neurosci* 25, 471-490.
- Gerstein, M.B., Rozowsky, J., Yan, K.K., Wang, D., Cheng, C., Brown, J.B., Davis, C.A., Hillier, L., Sisu, C., Li, J.J., et al. (2014). Comparative analysis of the transcriptome across distant species. *Nature* 512, 445-448.
- Gold, K.S., and Brand, A.H. (2014). *Optix* defines a neuroepithelial compartment in the optic lobe of the *Drosophila* brain. *Neural Dev* 9, 18.
- Gotz, M., and Huttner, W.B. (2005). The cell biology of neurogenesis. *Nat Rev Mol Cell Biol* 6, 777-788.

- Gratz, S.J., Cummings, A.M., Nguyen, J.N., Hamm, D.C., Donohue, L.K., Harrison, M.M., Wildonger, J., and O'Connor-Giles, K.M. (2013). Genome engineering of *Drosophila* with the CRISPR RNA-guided Cas9 nuclease. *Genetics* 194, 1029-1035.
- Grosskortenhaus, R., Pearson, B.J., Marusich, A., and Doe, C.Q. (2005). Regulation of temporal identity transitions in *Drosophila* neuroblasts. *Dev Cell* 8, 193-202.
- Hakes, A.E., Otsuki, L., and Brand, A.H. (2018). A newly discovered neural stem cell population is generated by the optic lobe neuroepithelium during embryogenesis in *Drosophila melanogaster*. *Development* 145.
- Hartenstein, V. (2011). Morphological diversity and development of glia in *Drosophila*. *Glia* 59, 1237-1252.
- Hartenstein, V., Nassif, C., and Lekven, A. (1998). Embryonic development of the *Drosophila* brain. II. Pattern of glial cells. *J Comp Neurol* 402, 32-47.
- Hartenstein, V., Younossi-Hartenstein, A., and Lekven, A. (1994). Delamination and division in the *Drosophila* neuroectoderm: spatiotemporal pattern, cytoskeletal dynamics, and common control by neurogenic and segment polarity genes. *Dev Biol* 165, 480-499.
- Hasegawa, E., Kitada, Y., Kaido, M., Takayama, R., Awasaki, T., Tabata, T., and Sato, M. (2011). Concentric zones, cell migration and neuronal circuits in the *Drosophila* visual center. *Development* 138, 983-993.
- Heckscher, E.S., Zarin, A.A., Faumont, S., Clark, M.Q., Manning, L., Fushiki, A., Schneider-Mizell, C.M., Fetter, R.D., Truman, J.W., Zwart, M.F., et al. (2015). Even-Skipped(+) Interneurons Are Core Components of a Sensorimotor Circuit that Maintains Left-Right Symmetric Muscle Contraction Amplitude. *Neuron* 88, 314-329.
- Hofbauer, A., and Campos-Ortega, J.A. (1990). Proliferation pattern and early differentiation of the optic lobes in *Drosophila melanogaster*. *Roux's Arch Dev Biol* 198, 264-274.
- Holguera, I., and Desplan, C. (2018). Neuronal specification in space and time. *Science* 362, 176-180.
- Homem, C.C., and Knoblich, J.A. (2012). *Drosophila* neuroblasts: a model for stem cell biology. *Development* 139, 4297-4310.
- Huang, Z., and Kunes, S. (1996). Hedgehog, transmitted along retinal axons, triggers neurogenesis in the developing visual centers of the *Drosophila* brain. *Cell* 86, 411-422.
- Huang, Z., and Kunes, S. (1998). Signals transmitted along retinal axons in *Drosophila*: Hedgehog signal reception and the cell circuitry of lamina cartridge assembly. *Development* 125, 3753-3764.
- Huang, Z., Shilo, B.Z., and Kunes, S. (1998). A retinal axon fascicle uses spitz, an EGF receptor ligand, to construct a synaptic cartridge in the brain of *Drosophila*. *Cell* 95, 693-703.
- Isshiki, T., Pearson, B., Holbrook, S., and Doe, C.Q. (2001). *Drosophila* neuroblasts sequentially express transcription factors which specify the temporal identity of their neuronal progeny. *Cell* 106, 511-521.
- Ito, K., Urban, J., and Technau, G. (1995). Distribution, classification, and development of *Drosophila* glial cells in the late embryonic and early larval ventral nerve cord. *Roux's Archive in Developmental Biology* 204, 284-307.
- Ito, M., Masuda, N., Shinomiya, K., Endo, K., and Ito, K. (2013). Systematic analysis of neural projections reveals clonal composition of the *Drosophila* brain. *Curr Biol* 23, 644-655.
- Izergina, N., Balmer, J., Bello, B., and Reichert, H. (2009). Postembryonic development of transit amplifying neuroblast lineages in the *Drosophila* brain. *Neural Dev* 4, 44.
- Jacobs, J.R. (2000). The midline glia of *Drosophila*: a molecular genetic model for the developmental functions of glia. *Prog Neurobiol* 62, 475-508.
- Jefferis, G.S., Marin, E.C., Stocker, R.F., and Luo, L. (2001). Target neuron prespecification in the olfactory map of *Drosophila*. *Nature* 414, 204-208.
- Kambadur, R., Koizumi, K., Stivers, C., Nagle, J., Poole, S.J., and Odenwald, W.F. (1998). Regulation of POU genes by castor and hunchback establishes layered compartments in the *Drosophila* CNS. *Genes Dev* 12, 246-260.
- Kanai, M.I., Kim, M.J., Akiyama, T., Takemura, M., Wharton, K., O'Connor, M.B., and Nakato, H. (2018). Regulation of neuroblast proliferation by surface glia in the *Drosophila* larval brain. *Sci Rep* 8, 3730.

- Kanai, M.I., Okabe, M., and Hiromi, Y. (2005). seven-up Controls switching of transcription factors that specify temporal identities of *Drosophila* neuroblasts. *Dev Cell* 8, 203-213.
- Kim, M.D., Wen, Y., and Jan, Y.N. (2009). Patterning and organization of motor neuron dendrites in the *Drosophila* larva. *Dev Biol* 336, 213-221.
- Knoblich, J.A. (2008). Mechanisms of asymmetric stem cell division. *Cell* 132, 583-597.
- Kohwi, M., and Doe, C.Q. (2013). Temporal fate specification and neural progenitor competence during development. *Nature reviews Neuroscience* 14, 823-838.
- Kohwi, M., Hiebert, L.S., and Doe, C.Q. (2011). The pipsqueak-domain proteins Distal antenna and Distal antenna-related restrict Hunchback neuroblast expression and early-born neuronal identity. *Development* 138, 1727-1735.
- Kriegstein, A., and Alvarez-Buylla, A. (2009). The glial nature of embryonic and adult neural stem cells. *Annu Rev Neurosci* 32, 149-184.
- Kunz, T., Kraft, K.F., Technau, G.M., and Urbach, R. (2012). Origin of *Drosophila* mushroom body neuroblasts and generation of divergent embryonic lineages. *Development* 139, 2510-2522.
- Lai, S.L., Awasaki, T., Ito, K., and Lee, T. (2008). Clonal analysis of *Drosophila* antennal lobe neurons: diverse neuronal architectures in the lateral neuroblast lineage. *Development* 135, 2883-2893.
- Landgraf, M., and Thor, S. (2006). Development of *Drosophila* motoneurons: specification and morphology. *Semin Cell Dev Biol* 17, 3-11.
- Lanet, E., Gould, A.P., and Maurange, C. (2013). Protection of Neuronal Diversity at the Expense of Neuronal Numbers during Nutrient Restriction in the *Drosophila* Visual System. *Cell reports*.
- Larsen, C., Shy, D., Spindler, S.R., Fung, S., Pereanu, W., Younossi-Hartenstein, A., and Hartenstein, V. (2009). Patterns of growth, axonal extension and axonal arborization of neuronal lineages in the developing *Drosophila* brain. *Dev Biol* 335, 289-304.
- Lee, T., Lee, A., and Luo, L. (1999). Development of the *Drosophila* mushroom bodies: sequential generation of three distinct types of neurons from a neuroblast. *Development* 126, 4065-4076.
- Lehtinen, M.K., and Walsh, C.A. (2011). Neurogenesis at the brain-cerebrospinal fluid interface. *Annu Rev Cell Dev Biol* 27, 653-679.
- Lehtinen, M.K., Zappaterra, M.W., Chen, X., Yang, Y.J., Hill, A.D., Lun, M., Maynard, T., Gonzalez, D., Kim, S., Ye, P., et al. (2011). The cerebrospinal fluid provides a proliferative niche for neural progenitor cells. *Neuron* 69, 893-905.
- Li, X., Erclik, T., Bertet, C., Chen, Z., Voutev, R., Venkatesh, S., Morante, J., Celik, A., and Desplan, C. (2013). Temporal patterning of *Drosophila* medulla neuroblasts controls neural fates. *Nature* 498, 456-462.
- Lim, N.R., Shohayeb, B., Zaytseva, O., Mitchell, N., Millard, S.S., Ng, D.C.H., and Quinn, L.M. (2017). Glial-Specific Functions of Microcephaly Protein WDR62 and Interaction with the Mitotic Kinase AURKA Are Essential for *Drosophila* Brain Growth. *Stem Cell Reports* 9, 32-41.
- Lin, S., Kao, C.F., Yu, H.H., Huang, Y., and Lee, T. (2012). Lineage analysis of *Drosophila* lateral antennal lobe neurons reveals notch-dependent binary temporal fate decisions. *PLoS Biol* 10, e1001425.
- Lin, S., Lai, S.L., Yu, H.H., Chihara, T., Luo, L., and Lee, T. (2010). Lineage-specific effects of Notch/Numb signaling in post-embryonic development of the *Drosophila* brain. *Development* 137, 43-51.
- Liu, Z., Yang, C.P., Sugino, K., Fu, C.C., Liu, L.Y., Yao, X., Lee, L.P., and Lee, T. (2015). Opposing intrinsic temporal gradients guide neural stem cell production of varied neuronal fates. *Science* 350, 317-320.
- Manning, L., and Doe, C.Q. (2017). Immunofluorescent antibody staining of intact *Drosophila* larvae. *Nat Protoc* 12, 1-14.
- Marin, E.C., Jefferis, G.S., Komiyama, T., Zhu, H., and Luo, L. (2002). Representation of the glomerular olfactory map in the *Drosophila* brain. *Cell* 109, 243-255.
- Marin, E.C., Watts, R.J., Tanaka, N.K., Ito, K., and Luo, L. (2005). Developmentally programmed remodeling of the *Drosophila* olfactory circuit. *Development* 132, 725-737.

- Maurange, C. (2012). Temporal specification of neural stem cells: insights from *Drosophila* neuroblasts. *Curr Top Dev Biol* 98, 199-228.
- Maurange, C., Cheng, L., and Gould, A.P. (2008). Temporal transcription factors and their targets schedule the end of neural proliferation in *Drosophila*. *Cell* 133, 891-902.
- Maurange, C., and Gould, A.P. (2005). Brainy but not too brainy: starting and stopping neuroblast divisions in *Drosophila*. *Trends Neurosci* 28, 30-36.
- McCaffrey, L.M., and Macara, I.G. (2011). Epithelial organization, cell polarity and tumorigenesis. *Trends Cell Biol* 21, 727-735.
- Meinertzhagen, I.A., and Hanson, T.E. (1993). The Development of the Optic Lobe. *The Development of Drosophila melanogaster* 2, 1363-1491.
- Mettler, U., Vogler, G., and Urban, J. (2006). Timing of identity: spatiotemporal regulation of hunchback in neuroblast lineages of *Drosophila* by Seven-up and Prospero. *Development* 133, 429-437.
- Monedero Cobeta, I., Salmani, B.Y., and Thor, S. (2017). Anterior-Posterior Gradient in Neural Stem and Daughter Cell Proliferation Governed by Spatial and Temporal Hox Control. *Curr Biol* 27, 1161-1172.
- Mora, N., Oliva, C., Fiers, M., Ejsmont, R., Soldano, A., Zhang, T.T., Yan, J., Claeys, A., De Geest, N., and Hassan, B.A. (2018). A Temporal Transcriptional Switch Governs Stem Cell Division, Neuronal Numbers, and Maintenance of Differentiation. *Dev Cell* 45, 53-66 e55.
- Morante, J., and Desplan, C. (2004). Building a projection map for photoreceptor neurons in the *Drosophila* optic lobes. *Semin Cell Dev Biol* 15, 137-143.
- Morante, J., and Desplan, C. (2011). Dissection and staining of *Drosophila* optic lobes at different stages of development. *Cold Spring Harb Protoc* 2011, 652-656.
- Morante, J., Erclik, T., and Desplan, C. (2011). Cell migration in *Drosophila* optic lobe neurons is controlled by *eyeless/Pax6*. *Development* 138, 687-693.
- Morante, J., Vallejo, D.M., Desplan, C., and Dominguez, M. (2013). Conserved miR-8/miR-200 defines a glial niche that controls neuroepithelial expansion and neuroblast transition. *Dev Cell* 27, 174-187.
- Moris-Sanz, M., Estacio-Gomez, A., Alvarez-Rivero, J., and Diaz-Benjumea, F.J. (2014). Specification of neuronal subtypes by different levels of Hunchback. *Development* 141, 4366-4374.
- Morrison, S.J., and Spradling, A.C. (2008). Stem cells and niches: mechanisms that promote stem cell maintenance throughout life. *Cell* 132, 598-611.
- Narbonne-Reveau, K., Lanet, E., Dillard, C., Foppolo, S., Chen, C.H., Parrinello, H., Rialle, S., Sokol, N.S., and Maurange, C. (2016). Neural stem cell-encoded temporal patterning delineates an early window of malignant susceptibility in *Drosophila*. *eLife* 5.
- Ngo, K.T., Wang, J., Junker, M., Kriz, S., Vo, G., Asem, B., Olson, J.M., Banerjee, U., and Hartenstein, V. (2010). Concomitant requirement for Notch and Jak/Stat signaling during neuro-epithelial differentiation in the *Drosophila* optic lobe. *Dev Biol* 346, 284-295.
- Obernier, K., Cebrian-Silla, A., Thomson, M., Parraguez, J.I., Anderson, R., Guinto, C., Rodas Rodriguez, J., Garcia-Verdugo, J.M., and Alvarez-Buylla, A. (2018). Adult Neurogenesis Is Sustained by Symmetric Self-Renewal and Differentiation. *Cell Stem Cell* 22, 221-234 e228.
- Okamoto, M., Miyata, T., Konno, D., Ueda, H.R., Kasukawa, T., Hashimoto, M., Matsuzaki, F., and Kawaguchi, A. (2016). Cell-cycle-independent transitions in temporal identity of mammalian neural progenitor cells. *Nature communications* 7, 11349.
- Okamoto, N., and Nishimura, T. (2015). Signaling from Glia and Cholinergic Neurons Controls Nutrient-Dependent Production of an Insulin-like Peptide for *Drosophila* Body Growth. *Dev Cell* 35, 295-310.
- Oliva, C., Choi, C.M., Nicolai, L.J., Mora, N., De Geest, N., and Hassan, B.A. (2014). Proper connectivity of *Drosophila* motion detector neurons requires Atonal function in progenitor cells. *Neural Dev* 9, 4.
- Omoto, J.J., Yogi, P., and Hartenstein, V. (2015). Origin and development of neuropil glia of the *Drosophila* larval and adult brain: Two distinct glial populations derived from separate progenitors. *Dev Biol* 404, 2-20.

- Otsuki, L., and Brand, A.H. (2017). The vasculature as a neural stem cell niche. *Neurobiology of disease* 107, 4-14.
- Otsuki, L., and Brand, A.H. (2018). Cell cycle heterogeneity directs the timing of neural stem cell activation from quiescence. *Science* 360, 99-102.
- Ou, J., Gao, Z., Song, L., and Ho, M.S. (2016). Analysis of Glial Distribution in *Drosophila* Adult Brains. *Neurosci Bull* 32, 162-170.
- Ou, J., He, Y., Xiao, X., Yu, T.M., Chen, C., Gao, Z., and Ho, M.S. (2014). Glial cells in neuronal development: recent advances and insights from *Drosophila melanogaster*. *Neurosci Bull* 30, 584-594.
- Paridaen, J.T., and Huttner, W.B. (2014). Neurogenesis during development of the vertebrate central nervous system. *EMBO Rep* 15, 351-364.
- Peco, E., Davla, S., Camp, D., Stacey, S.M., Landgraf, M., and van Meyel, D.J. (2016). *Drosophila* astrocytes cover specific territories of the CNS neuropil and are instructed to differentiate by Prospero, a key effector of Notch. *Development* 143, 1170-1181.
- Pereanu, W., Shy, D., and Hartenstein, V. (2005). Morphogenesis and proliferation of the larval brain glia in *Drosophila*. *Dev Biol* 283, 191-203.
- Perez-Gomez, R., Slovakova, J., Rives-Quinto, N., Krejci, A., and Carmena, A. (2013). A Serrate-Notch-Canoe complex mediates essential interactions between glia and neuroepithelial cells during *Drosophila* optic lobe development. *J Cell Sci* 126, 4873-4884.
- Pinto-Teixeira, F., Koo, C., Rossi, A.M., Neriec, N., Bertet, C., Li, X., Del-Valle-Rodriguez, A., and Desplan, C. (2018). Development of Concurrent Retinotopic Maps in the Fly Motion Detection Circuit. *Cell* 173, 485-498 e411.
- Ramaekers, A., Magnenat, E., Marin, E.C., Gendre, N., Jefferis, G.S., Luo, L., and Stocker, R.F. (2005). Glomerular maps without cellular redundancy at successive levels of the *Drosophila* larval olfactory circuit. *Curr Biol* 15, 982-992.
- Reddy, B.V., Rauskolb, C., and Irvine, K.D. (2010). Influence of fat-hippo and notch signaling on the proliferation and differentiation of *Drosophila* optic neuroepithelia. *Development* 137, 2397-2408.
- Ren, Q., Yang, C.P., Liu, Z., Sugino, K., Mok, K., He, Y., Ito, M., Nern, A., Otsuna, H., and Lee, T. (2017). Stem Cell-Intrinsic, Seven-up-Triggered Temporal Factor Gradients Diversify Intermediate Neural Progenitors. *Curr Biol* 27, 1303-1313.
- Richier, B., Vijandi, C.M., Mackensen, S., and Salecker, I. (2017). Lapsyn controls branch extension and positioning of astrocyte-like glia in the *Drosophila* optic lobe. *Nature communications* 8, 317.
- Rossi, A.M., and Fernandes, V.M. (2018). Wrapping Glial Morphogenesis and Signaling Control the Timing and Pattern of Neuronal Differentiation in the *Drosophila* Lamina. *J Exp Neurosci* 12, 1179069518759294.
- Rowitch, D.H., and Kriegstein, A.R. (2010). Developmental genetics of vertebrate glial-cell specification. *Nature* 468, 214-222.
- Sarov, M., Barz, C., Jambor, H., Hein, M.Y., Schmied, C., Suchold, D., Stender, B., Janosch, S., K, J.V., Krishnan, R.T., et al. (2016). A genome-wide resource for the analysis of protein localisation in *Drosophila*. *eLife* 5, e12068.
- Sato, M., Suzuki, T., and Nakai, Y. (2013). Waves of differentiation in the fly visual system. *Dev Biol* 380, 1-11.
- Schmidt, H., Rickert, C., Bossing, T., Vef, O., Urban, J., and Technau, G.M. (1997). The embryonic central nervous system lineages of *Drosophila melanogaster*. II. Neuroblast lineages derived from the dorsal part of the neuroectoderm. *Dev Biol* 189, 186-204.
- Selleck, S.B., and Steller, H. (1991). The influence of retinal innervation on neurogenesis in the first optic ganglion of *Drosophila*. *Neuron* 6, 83-99.
- Siegenthaler, J.A., Ashique, A.M., Zarbališ, K., Patterson, K.P., Hecht, J.H., Kane, M.A., Folias, A.E., Choe, Y., May, S.R., Kume, T., et al. (2009). Retinoic acid from the meninges regulates cortical neuron generation. *Cell* 139, 597-609.
- Siegenthaler, J.A., and Pleasure, S.J. (2011). We have got you 'covered': how the meninges control brain development. *Curr Opin Genet Dev* 21, 249-255.
- Silva-Vargas, V., Maldonado-Soto, A.R., Mizrak, D., Codega, P., and Doetsch, F. (2016). Age-Dependent Niche Signals

from the Choroid Plexus Regulate Adult Neural Stem Cells. *Cell Stem Cell* 19, 643-652.

Sousa-Nunes, R., Cheng, L.Y., and Gould, A.P. (2010). Regulating neural proliferation in the *Drosophila* CNS. *Curr Opin Neurobiol* 20, 50-57.

Sousa-Nunes, R., Yee, L.L., and Gould, A.P. (2011). Fat cells reactivate quiescent neuroblasts via TOR and glial insulin relays in *Drosophila*. *Nature* 471, 508-512.

Speder, P., and Brand, A.H. (2018). Systemic and local cues drive neural stem cell niche remodelling during neurogenesis in *Drosophila*. *eLife* 7.

Speder, P., Liu, J., and Brand, A.H. (2011). Nutrient control of neural stem cells. *Curr Opin Cell Biol* 23, 724-729.

Stork, T., Bernardos, R., and Freeman, M.R. (2012). Analysis of glial cell development and function in *Drosophila*. *Cold Spring Harb Protoc* 2012, 1-17.

Stork, T., Engelen, D., Krudewig, A., Silies, M., Bainton, R.J., and Klambt, C. (2008). Organization and function of the blood-brain barrier in *Drosophila*. *J Neurosci* 28, 587-597.

Suzuki, T., Hasegawa, E., Nakai, Y., Kaido, M., Takayama, R., and Sato, M. (2016). Formation of Neuronal Circuits by Interactions between Neuronal Populations Derived from Different Origins in the *Drosophila* Visual Center. *Cell reports* 15, 499-509.

Suzuki, T., Kaido, M., Takayama, R., and Sato, M. (2013). A temporal mechanism that produces neuronal diversity in the *Drosophila* visual center. *Dev Biol* 380, 12-24.

Syed, M.H., Mark, B., and Doe, C.Q. (2017a). Playing Well with Others: Extrinsic Cues Regulate Neural Progenitor Temporal Identity to Generate Neuronal Diversity. *Trends Genet* 33, 933-942.

Syed, M.H., Mark, B., and Doe, C.Q. (2017b). Steroid hormone induction of temporal gene expression in *Drosophila* brain neuroblasts generates neuronal and glial diversity. *eLife* 6.

Tasdemir-Yilmaz, O.E., and Freeman, M.R. (2014). Astrocytes engage unique molecular programs to engulf pruned neuronal debris from distinct subsets of neurons. *Genes Dev* 28, 20-33.

Taylor, M.K., Yeager, K., and Morrison, S.J. (2007). Physiological Notch signaling promotes gliogenesis in the developing peripheral and central nervous systems. *Development* 134, 2435-2447.

Tiberi, L., Vanderhaeghen, P., and van den Aemele, J. (2012). Cortical neurogenesis and morphogens: diversity of cues, sources and functions. *Curr Opin Cell Biol* 24, 269-276.

Truman, J.W., and Bate, M. (1988). Spatial and temporal patterns of neurogenesis in the central nervous system of *Drosophila melanogaster*. *Dev Biol* 125, 145-157.

Ugur, B., Chen, K., and Bellen, H.J. (2016). *Drosophila* tools and assays for the study of human diseases. *Dis Model Mech* 9, 235-244.

Ulvklo, C., MacDonald, R., Bivik, C., Baumgardt, M., Karlsson, D., and Thor, S. (2012). Control of neuronal cell fate and number by integration of distinct daughter cell proliferation modes with temporal progression. *Development* 139, 678-689.

Unhavaithaya, Y., and Orr-Weaver, T.L. (2012). Polyploidization of glia in neural development links tissue growth to blood-brain barrier integrity. *Genes Dev* 26, 31-36.

Urbach, R., Schnabel, R., and Technau, G.M. (2003). The pattern of neuroblast formation, mitotic domains and proneural gene expression during early brain development in *Drosophila*. *Development* 130, 3589-3606.

Urbach, R., and Technau, G.M. (2004). Neuroblast formation and patterning during early brain development in *Drosophila*. *Bioessays* 26, 739-751.

Van De Bor, V., and Giangrande, A. (2002). *glide/gcm*: at the crossroads between neurons and glia. *Curr Opin Genet Dev* 12, 465-472.

Viktorin, G., Riebli, N., and Reichert, H. (2013). A multipotent transit-amplifying neuroblast lineage in the central brain gives rise to optic lobe glial cells in *Drosophila*. *Dev Biol* 379, 182-194.

- Volkenhoff, A., Weiler, A., Letzel, M., Stehling, M., Klambt, C., and Schirmeier, S. (2015). Glial Glycolysis Is Essential for Neuronal Survival in *Drosophila*. *Cell metabolism* 22, 437-447.
- von Hilchen, C.M., Beckervordersandforth, R.M., Rickert, C., Technau, G.M., and Altenhein, B. (2008). Identity, origin, and migration of peripheral glial cells in the *Drosophila* embryo. *Mech Dev* 125, 337-352.
- Vosshall, L.B., Wong, A.M., and Axel, R. (2000). An olfactory sensory map in the fly brain. *Cell* 102, 147-159.
- Walsh, K.T., and Doe, C.Q. (2017). *Drosophila* embryonic type II neuroblasts: origin, temporal patterning, and contribution to the adult central complex. *Development* 144, 4552-4562.
- White, K., Grether, M.E., Abrams, J.M., Young, L., Farrell, K., and Steller, H. (1994). Genetic control of programmed cell death in *Drosophila* [see comments]. *Science* 264, 677-683.
- Wu, B., Li, J., Chou, Y.H., Luginbuhl, D., and Luo, L. (2017). Fibroblast growth factor signaling instructs ensheathing glia wrapping of *Drosophila* olfactory glomeruli. *Proc Natl Acad Sci U S A* 114, 7505-7512.
- Xie, Y., Li, X., Deng, X., Hou, Y., O'Hara, K., Urso, A., Peng, Y., Chen, L., and Zhu, S. (2016). The Ets protein Pointed prevents both premature differentiation and dedifferentiation of *Drosophila* intermediate neural progenitors. *Development* 143, 3109-3118.
- Yaghmaeian Salmani, B., Monedero Cobeta, I., Rakar, J., Bauer, S., Curt, J.R., Starkenberg, A., and Thor, S. (2018). Evolutionarily conserved anterior expansion of the central nervous system promoted by a common PcG-Hox program. *Development* 145.
- Yang, J.S., Awasaki, T., Yu, H.H., He, Y., Ding, P., Kao, J.C., and Lee, T. (2013). Diverse neuronal lineages make stereotyped contributions to the *Drosophila* locomotor control center, the central complex. *J Comp Neurol* 521, 2645-2661.
- Yasugi, T., Sugie, A., Umetsu, D., and Tabata, T. (2010). Coordinated sequential action of EGFR and Notch signaling pathways regulates proneural wave progression in the *Drosophila* optic lobe. *Development* 137, 3193-3203.
- Yasugi, T., Umetsu, D., Murakami, S., Sato, M., and Tabata, T. (2008). *Drosophila* optic lobe neuroblasts triggered by a wave of proneural gene expression that is negatively regulated by JAK/STAT. *Development* 135, 1471-1480.
- Yu, H.H., Awasaki, T., Schroeder, M.D., Long, F., Yang, J.S., He, Y., Ding, P., Kao, J.C., Wu, G.Y., Peng, H., et al. (2013). Clonal development and organization of the adult *Drosophila* central brain. *Curr Biol* 23, 633-643.
- Yu, H.H., Kao, C.F., He, Y., Ding, P., Kao, J.C., and Lee, T. (2010). A complete developmental sequence of a *Drosophila* neuronal lineage as revealed by twin-spot MARCM. *PLoS Biol* 8.
- Zhu, S., Barshow, S., Wildonger, J., Jan, L.Y., and Jan, Y.N. (2011). Ets transcription factor Pointed promotes the generation of intermediate neural progenitors in *Drosophila* larval brains. *Proc Natl Acad Sci USA* 108, 20615-20620.
- Zhu, S., Lin, S., Kao, C.F., Awasaki, T., Chiang, A.S., and Lee, T. (2006). Gradients of the *Drosophila* Chinmo BTB-zinc finger protein govern neuronal temporal identity. *Cell* 127, 409-422.
- Zuchero, J.B., and Barres, B.A. (2015). Glia in mammalian development and disease. *Development* 142, 3805-3809.



